Nouvelles fonctions de p21Cip1 dans la dynamique cytosquelettique des cellules épithéliales mammaires humaines

Benjamin Bouchet

N° d'ordre 56-2010 Année 2010

THESE DE L'UNIVERSITE DE LYON

Délivrée par

L'UNIVERSITE CLAUDE BERNARD LYON 1

ECOLE DOCTORALE
Biologie Moléculaire Intégrative et Cellulaire

DIPLOME DE DOCTORAT
(arrêté du 7 août 2006)

soutenue publiquement le 5 Mai 2010

par

M. Benjamin BOUCHET

Nouvelles fonctions de $p21^{Cip1}$ dans la dynamique cytosquelettique des cellules épithéliales mammaires humaines

Directeur de thèse : Pr. Alain PUISIEUX
Co-encadrant : Dr. Carlos M. GALMARINI

JURY : Pr. Diane BRAGUER (président)
Dr. Sandrine ETIENNE-MANNEVILLE (rapporteur)
Dr. Ali BADACHE (rapporteur)
Dr. Ruth RIMOKH (examinateur)
Pr. Alain PUISIEUX (directeur)
Dr. Carlos M. GALMARINI (co-encadrant)

UNIVERSITE CLAUDE BERNARD - LYON 1

Président de l'Université	**M. le Professeur L. Collet**
Vice-président du Conseil Scientifique	M. le Professeur J-F. Mornex
Vice-président du Conseil d'Administration	M. le Professeur G. Annat
Vice-président du Conseil des Etudes et de la Vie Universitaire	M. le Professeur D. Simon
Secrétaire Général	M. G. Gay

COMPOSANTES SANTE

Faculté de Médecine Lyon Est – Claude Bernard	Directeur : M. le Professeur J. Etienne
Faculté de Médecine Lyon Sud – Charles Mérieux	Directeur : M. le Professeur F-N. Gilly
UFR d'Odontologie	Directeur : M. le Professeur D. Bourgeois
Institut des Sciences Pharmaceutiques et Biologiques	Directeur : M. le Professeur F. Locher
Institut des Sciences et Techniques de Réadaptation	Directeur : M. le Professeur Y. Matillon
Département de Formation et Centre de Recherche en Biologie Humaine	Directeur : M. le Professeur P. Farge

COMPOSANTES SCIENCES ET TECHNOLOGIE

Faculté des Sciences et Technologies	Directeur : M. Le Professeur F. Gieres
UFR Sciences et Techniques des Activités Physiques et Sportives	Directeur : M. C. Collignon
Observatoire de Lyon	Directeur : M. B. Guiderdoni
Institut des Sciences et des Techniques de l'Ingénieur de Lyon	Directeur : M. le Professeur J. Lieto
Institut Universitaire de Technologie A	Directeur : M. le Professeur C. Coulet
Institut Universitaire de Technologie B	Directeur : M. le Professeur R. Lamartine
Institut de Science Financière et d'Assurance	Directeur : M. le Professeur J-C. Augros
Institut Universitaire de Formation des Maîtres	Directeur : M R. Bernard

RESUMÉ

Le gène *CDKN1A* a été initialement décrit comme une cible transcriptionnelle de la protéine oncosuppressive p53. Son produit, $p21^{Cip1}$ (p21), supprime l'activité des kinases dépendantes des cyclines et de la protéine PCNA, ce qui en fait un puissant inhibiteur du cycle et de la prolifération cellulaires. En outre, p21 est fréquemment inactivée dans les cancers épithéliaux. Or, la progression de ces tumeurs est associée à l'altération de l'organisation tissulaire, au processus invasif et à la dissémination métastatique. Ces phénomènes résultent des modifications cytosquelettiques conduisant à la transformation des propriétés d'adhésion et de migration cellulaires. Pourtant, le rôle de p21 dans la dynamique cytosquelettique des cellules épithéliales humaines n'a jamais été adressé. Nous montrons ici que p21 contribue à l'adhésion et la migration normale des cellules épithéliales mammaires non transformées. Nos résultats montrent également que l'inactivation de p21 provoque la suppression de l'adhésion focale et des fibres de stress. Ce phénotype est caractérisé par l'inactivation de la GTPase Rho et l'activation de la cofiline, facteur de dépolymérisation de l'actine. En outre, la suppression de p21 provoque une désacétylation des microtubules associée à une déstabilisation microtubulaire globale. La réduction de l'instabilité dynamique, par inhibition de la désacétylase HDAC6, restaure partiellement l'étalement cellulaire et l'adhésion focale altérés par l'inactivation de p21. L'ensemble de nos données démontre que la régulation de la dynamique cytosquelettique par p21 est nécessaire au contrôle de l'adhésion des cellules épithéliales humaines non tumorales.

TITLE : New functions of $p21^{Cip1}$ in cytoskeletal dynamics of human mammary epithelial cells

ABSTRACT

CDKN1A gene was initially identified as a target of the tumor suppressor p53. The ability to inhibit cyclin-dependant kinase and PCNA activities confers to its product, $p21^{Cip1}$ (p21), strong anti-proliferative properties. Moreover, p21 is frequently inactivated in epithelial cancers. Progression of these malignancies is also associated with disorganized tissue architecture, invasion and metastatic dissemination. These processes involve major cytoskeletal reorganization associated with transformation of adhesion and migration properties. Still, the role of p21 in cytoskeletal dynamics in normal epithelial cell has never been addressed. Here we show that p21 contributes to normal adhesion and migration in untransformed human mammary epithelial cells (HMEC). We also demonstrate that p21 inactivation in HMEC suppresses focal adhesion and stress fiber assembly. p21 depletion is also associated with inactivation of Rho GTPase and activation of the F-actin severing factor cofilin. In addition, p21 silencing provokes microtubule hypoacetylation associated with increased dynamic instability. We find that forced microtubule stabilization by HDAC6 inhibition partially restore cell spreading and focal adhesion in p21-depleted cells. Collectively, our data show that regulation of cytoskeletal dynamics by p21 is required for adhesion control in untransformed human epithelial cells.

DISCIPLINE : Biologie cellulaire

MOTS-CLES : p21, adhésion, cytosquelette, actine, microtubules, cancer du sein
KEYWORDS : p21, adhesion, cytoskeleton, actin, microtubules, breast cancer

INTITULE ET ADRESSE DE L'U.F.R. OU DU LABORATOIRE :

Unité INSERM 590
Centre Léon Bérard, Cheney D
28 rue Laennec, 69373 Lyon Cedex 08

REMERCIEMENTS

Je tiens d'abord à remercier le Pr. Alain Puisieux pour m'avoir permis de débuter mon apprentissage scientifique, il y a maintenant plus de six ans, au sein de son laboratoire. Alain, je te suis profondément reconnaissant pour m'avoir offert des moyens exceptionnels pour la poursuite de mes travaux. Tu m'as autorisé à développer ces projets en dehors du cadre thématique de ton équipe et, malgré mon éloignement, tu m'as renouvelé ton soutien, ta confiance et ton écoute, tout au long de ces années. Ta rencontre, d'abord comme professeur puis comme directeur, a été décisive à bien des égards. Je ne l'oublierai pas.

Je tiens également à remercier le Dr. Carlos M. Galmarini qui a initié la plupart des travaux présentés ici. Carlos, je te dois mon initiation à la biologie du cytosquelette et la découverte de nombreux travaux qui sont devenus pour moi des références. En me transmettant ta passion, tu m'as appris beaucoup et tu m'as donné confiance en moi. Ta vision de la science ne sert aucun dogme, aucune mode, elle se nourrit de l'originalité et de l'excellence, et discuter avec toi est toujours aussi inspirant. Je veux aussi rendre hommage ici à ton intégrité et à ta générosité. Sois assuré de ma gratitude et de mon amitié.

Je remercie le Pr. Diane Braguer pour avoir accepté la direction de mon jury de thèse et pour sa bienveillance et son intérêt au cours de ces dernières années. Le fait d'avoir pu bénéficier de votre expertise, à l'occasion de nos différentes rencontres, a été crucial pour la réalisation de mon projet doctoral. Veuillez trouver ici l'expression de ma reconnaissance et de mon profond respect.

Je tiens aussi à remercier tout particulièrement le Dr. Sandrine Etienne-Manneville et le Dr. Ali Badache pour avoir accepté d'être rapporteurs de ce travail. Vos travaux sont pour moi un modèle d'excellence et une source d'inspiration. Je suis donc très honoré de votre participation à l'évaluation de mes résultats. Je vous suis également reconnaissant pour votre patience et pour m'avoir accordé la possibilité d'améliorer le présent manuscrit.

Je remercie le Dr. Ruth Rimokh pour sa participation à l'évaluation de ce projet, pour son intérêt constant et ses encouragements particulièrement motivants.

***

Je remercie les anciens membres de l'équipe du Dr. Galmarini. Merci au Dr. Jacques Bertholon pour avoir partagé sa passion et ses connaissances dans le domaine du cytosquelette avec moi. Je garde un souvenir ému de nos discussions à trois ; sur le plan scientifique, elles furent probablement les plus stimulantes que j'ai eues au cours de ces dernières années. Merci au Dr. Nicole Falette pour son soutien et sa gentillesse constante. Merci à Christelle Lamblot pour son aide technique. Je tiens à remercier tout spécialement Carole Audoynaud pour son enseignement technique et sa fidélité qui a toujours beaucoup compté (et puis Blondie, on s'est bien marré non ?).

Je remercie les membres des équipes du département de Biologie Génétique du Centre Léon Bérard, dirigées par le Dr. Qing Wang, le Dr. Olga Sinilnikova et le Dr. Valérie Combaret, pour leur aide occasionnelle et leur contribution à mon intégration dans le laboratoire : Jessie Auclair, Claudine Navarro, Elisabeth Garin, Mélanie Léone, Laure Barjhoux, Chantal Ghaemmaghami, Carole Pierre et Stéphanie Bréjon. Un merci spécial aux gars pour leur soutien viril : Gilles Montmain, Eric Ruano et Cyril Lafaye. Un merci tout particulier à Isabelle "Zaza" Iacono : tu as un sens de l'humour inoxydable, une grande générosité et tu apportes beaucoup d'humanité à ce laboratoire.

Je remercie l'équipe d'Eric Gilson, UMR 5239 CNRS/ENS, et plus particulièrement ses doctorants qui m'ont permis d'utiliser leurs étuves. Merci à Christophe Chamot, à Claire Lionnet et aux autres membres du PLATIM, ENS, pour leur arsenal impressionnant de microscopes, pour leur aide technique et leur expertise précieuse dans le domaine de l'imagerie cellulaire. Je remercie également le Dr. Anne Béghin et les membres du CCQ, Domaine Rockefeller, pour leur collaboration aux mises au point des techniques d'imagerie utilisées pour ce travail. Merci au Dr. Stéphane Honoré, UMR INSERM 911, Centre de Recherche en Oncologie Biologique et Oncopharmacologie, Marseille, pour ses conseils concernant l'analyse de la dynamique microtubulaire. Merci au

Pr. Joel Lachuer et aux membres de ProfileXpert pour leur collaboration aux expériences d'étude transcriptomique.

Je remercie tous les chercheurs, les techniciens et les étudiants de l'unité INSERM 590 qui m'ont accordé leur aide et leur sympathie durant toutes ces années. Même si je ne peux pas citer tout le monde, que chacun trouve ici l'expression de ma sincère reconnaissance. Merci au Dr. Claude Caron de Fromentel pour m'avoir conseillé pendant la préparation de mon premier projet de thèse. Merci à Julie Pourchet et Joëlle Genève pour leur aide inestimable. Merci à Nathalie Borel et Jessica Vuillod pour leur disponibilité et leur dévouement. Merci au duo d'étudiantes Marjory Lièvre-Clémence Thomas pour avoir égayé notre quotidien, il y a quelques années, dans les pièces de culture de notre bon vieux Cheney B. Merci à Clémence pour son soutien constant et son intérêt pour les discussions scientifiques. Merci au Dr. Jérémy Bastid pour sa classe, son humour et pour avoir perpétué la tradition de l'unique étudiant de sa promotion de Pharmacie qui poursuit la filière Recherche. Merci à Frédérique Fauvet pour son enthousiasme et sa disponibilité au cours de notre collaboration. Merci aux Drs. Amandine Chatagnon et Delphine Perrin pour leur bonne humeur et leur adhésion aux déjeuners de 11h30. Merci à Laury Perriaud pour son humour et son soutien précieux. Merci au Dr. Stéphanie Courtois-Cox et au noyau du Team SHAFT récemment arrivé : le Dr. David Bernard a.k.a. Dadoo, Arnaud Augert a.k.a. Nono a.k.a. Augie Kid a.k.a. Houndzie et le Dr. Delphine Gitenay a.k.a. Mireille pour l'ambiance en culture et aux déjeuners.

Je remercie chaleureusement le Dr. Abdelkader Selmi a.k.a. Bulli a.k.a. Wullit. Sans toi je ne connaitrais pas Santa Susanna, le rayon frais de la zone étudiant, la division par deux comme geste de survie et nous n'aurions pas pu inventer les Business Pauses. Tu as aussi été un collaborateur précieux lors de la dernière expédition en haut de l'étagère du Grand Office. Je n'étais pas sans ignorer ta capacité à rebondir mais ce que tu as réalisé depuis la fin de ta thèse est un petit clin d'œil du destin qui me ravit. Bonne chance pour la suite.

Merci au Dr. Gaël Grelier a.k.a. Mitch. Mitch, mon frère d'armes, nous avons tellement partagé pendant nos thèses respectives, qu'évidemment je ne détaillerai pas ta contribution à mon épanouissement dans le laboratoire. Ceux qui ne connaissent pas ton histoire et ta valeur peuvent m'interroger à ce sujet, je répondrai volontiers. Je dirai simplement ici que ce fut un véritable bonheur de travailler à tes côtés pendant toutes ces années. Tu m'as toujours aidé à surmonter les problèmes techniques et humains. En me persuadant qu'aucune manip n'est impossible, tu m'as appris le B-A-BA de la paillasse et tu m'as aidé à prendre confiance en moi. Je te suis reconnaissant pour tout ça et t'assure de mon amitié.

***

Je remercie Romain Rotival, Jean-Daniel Kaiser et Pierre Collange (je n'ai pas la place ici pour préciser leurs multiples identités) pour leur amitié sans faille et pour avoir supporté que beaucoup de nos conversations depuis quatre ans finissent invariablement par se focaliser sur mon projet de thèse. Les filles, je dirai seulement ceci : bravo les gras.

Je remercie toute ma famille pour son soutien. Merci en particulier à mes deux grand-mères pour leur affection et leur intérêt indéfectible pour mes études. Merci à ma petite sœur Pauline pour le bonheur que m'apporte chacune de nos conversations et pour le réconfort qu'elle me dispense (et aussi Tanguy). Merci à mes parents. C'est bien peu, mais cette thèse vous est dédiée. Merci de continuer à être présents quand j'en ai besoin. Merci infiniment à Marie-May pour m'avoir supporté pendant toutes ces années. Tu apportes la paix dans mon cœur et le bonheur dans ma vie.

TABLE DES MATIERES

TABLE DES ILLUSTRATIONS

ABREVIATIONS UTILISEES

ACTB	Actine, beta
ADN	Acide désoxyribonucléique
ADN pol	ADN polymérase
ADNc	ADN complémentaire
ADP	Adénosine diphosphate
AF	Adhésion focale
AKT	RAC-alpha serine/threonine-protein kinase
Apc	Adenomatosis Polyposis Coli protein
aPKC	PKC atypique
ARHGAP19	Rho GTPase activating protein 19
ARN	Acide RiboNucléique
ARNi	Interférence ARN
ARNm	ARN messager
ASK1	Apoptosis Signal regulating Kinase 1
Atm	Ataxia telangiectasia mutated
ATP	Adénosine triphosphate
ATP6AP1	ATPase, H+ transporting, lysosomal accessory protein 1
BCCIP	BRCA2 and CDKN1A interacting protein
BCL2	B-cell CLL/lymphoma 2 protein
BIRC5	Baculoviral IAP repeat-containing 5
B-Myb	MYB-related protein B; v-myb avian myeloblastosis viral oncogene homolog-like 2
BSA	Bovine serum albumin
C/EBPα	CCAAT/enhancer binding protein alpha
C8a	Proteasome (prosome, macropain) subunit, alpha type, 3
CASP3	Caspase-3
Cdc42	Cell division control protein 42 homolog
CDC42BP	CDC42-binding protein kinase
CDK	Cyclin-dependent kinase
CDKN1A	Cyclin-dependent kinase inhibitor 1A
CDT2	Denticleless protein homolog
CFL1	Cofilin 1 (non-muscle)
Cip1	CDK-interacting protein 1
CK2	Casein kinase II subunit alpha
c-Myc	Myc proto-oncogene protein
CRIK	Citron Rho-interacting kinase

$CRL4^{CDT2}$	CUL4B–DDB1–CDT2
CRYAB	Crystallin, alpha B
ctp.	Localisation cytoplasmique
CUL1	Cullin 1
CUL4B	Cullin 4B
Cy	Domaine cycline
DAPK3	Death-associated protein kinase 3
DDB1	DNA damage-binding protein 1
dgd.	Dégradation
DIAPH	Protein diaphanous homolog
DMSO	Dimethyl sulfoxide
DNMT1	DNA (cytosine-5-)-methyltransferase 1
DTT	Dithiothreitol
E2F1	E2F transcription factor 1
ECM	Extracellular Matrix
EGF	Epidermal growth factor
EGTA	Ethylene glycol-bis(2-aminoethylether)-N,N,N',N'-tetraacetic acid
EMT	Epithelilal-Mesenchymal Transition
ERBB	Receptor tyrosine-protein kinase erbB
ESM	Erreur standard de la moyenne
EST	Expressed sequence tag
évt.	Evénement
F-actine	Actine filamenteuse
FAK	Focal adhesion kinase
FBS	Fetal bovine serum
FEN-1	Flap structure-specific endonuclease 1
FERMT3	Fermitin family homolog 3
FITC	Fluorescein IsoThioCyanate
FKBPL	FK506 binding protein like
FRET	Fluorescence Resonance Energy Transfer
FS	Fibre de stress
GADD45	Growth Arrest and DNA damage-inducible protein 45
GAP	GTPase-activating protein
GAPDH	Glyceraldehyde-3-phosphate dehydrogenase
GDP	Guanosine diphosphate
GEF	Guanine-exchange factor
GFP	Green fluorescent protein
GP-hMEC	GFP-paxilline hTMEC

GSK3β	Glycogen synthase kinase 3 beta
GT-hMEC	GFP-tubuline hTMEC
GTP	Guanosine triphosphate
GUSB	Glucuronidase, beta
h	Heure
HDAC6	Histone deacetylase 6
HMEC	Human mammary epithelial cell
HPRT1	Hypoxanthine phosphoribosyltransferase 1
HPV-16	Human papilloma virus type 16
Hras1	Homologue de l'oncogene viral du sarcome d'Harvey, gène murin
hTERT	Human telomerase reverse transcriptase
hTMEC	hTERT HMEC
Ig	Immunoglobuline
JNK	C-jun-amino-terminal kinase
KD	Knock-down
kDa	Kilo Dalton
LIMK	LIM domain kinase
MAP3K5	Mitogen-activated protein kinase kinase kinase 5
MAPK9	Mitogen-activated protein kinase 9
MDM2	E3 ubiquitin-protein ligase Mdm2
MEBM	Mammary Epithelial Basal Medium
MEC	Matrice extracellulaire
min	Minute
MLCK	Myosin light chain kinase, smooth muscle
MLCP	Myosin light chain phosphatase
MRCK	Myotonic dystrophy kinase-related CDC42-binding kinase alpha
MT	Microtubule
MTOC	Microtubule organizing center
MYBL2	V-myb myeloblastosis viral oncogene homolog (avian)-like
MYPT1	Myosin phosphatase-targeting subunit 1
NA	Numerical aperture
Nb	Nombre
NF-kB	Nuclear factor-kappa B
NLS	Nuclear localization signal
NRK	Nicotinamide riboside kinase 1
NT	Non targeting
N-WASP	Neural Wiskott-Aldrich syndrome protein
p21KD	Knock-down p21

PAK1	p21-activated kinase 1
PARP-1	Poly (ADP-ribose) polymerase 1
PBS	Phosphate buffered saline
PCNA	Proliferating Cell Nuclear Antigen
PCR	Polymerase chain reaction
PGK1	Phosphoglycerate kinase 1
Pi	Phosphate inorganique
PIM1	Proto-oncogene serine/threonine-protein kinase Pim-1
PIP2	Phosphatidylinositol-4,5-bisphosphate
PKC	Protein kinase C
PKCμ	Protein kinase C m
PLCγ	Phospholipase C, gamma 1
PP1	Protein phosphatase 1
PP2	Protein phosphatase 2
PPIB	Peptidylprolyl isomerase B (cyclophilin B)
PRKD1	Protein kinase D1
pS3	phospho-Ser 3
pS744/8	phospho-Ser 744/8
pS978	phospho-Ser 978
pT508/5	phospho-Thr 505/8
PVDF	PolyVinyliDene Fluoride
PXN	Paxillin
pY397	Phospho-Tyr 397
pY416	Phospho-Tyr 416
qRT-PCR	Quantitative real-time PCR
Rac1	Ras-related C3 botulinum toxin substrate 1
Ras	Homologue de l'oncogene viral du sarcome d'Harvey chez le rat
Rb	Retinoblastoma-associated protein
RFC1	Replication factor C subunit 1
Rho	Ras homolog gene family, member A/B/C protein
ROCK	Rho-associated protein kinase
ROCK1	Rho-associated, coiled-coil containing protein kinase 1
SAPK	Stress activated protein kinase
SCF^{SKP2}	SKP1–CUL1-SKP2
sec	Seconde
SET	Suppressor of variegation, Enhancer of zeste and Trithorax; SET nuclear oncogene
shRNA	Short hairpin RNA

siCT	SiRNA contrôle
siRNA	Small interfering RNA
SKP1	S-phase kinase-associated protein 1
SKP2	S-phase kinase-associated protein 2
Src	Proto-oncogene tyrosine-protein kinase Src
SSH1	Slingshot homolog 1 (Drosophila)
SSH1L	Protein phosphatase slingshot homolog 1
STAT3	Signal transducer and activator of transcription 3
stb.	Stabilisation
TBP	TATA box binding protein
TBS	Tris-buffered saline
TBST	TBS Triton X-100
TESK	Dual specificity testis-specific protein kinase 1
test t	Test de Student
TFRC	Transferrin receptor (p90, CD71)
Thr	Thréonine
TK1	Thymidine kinase
TRAIL	Tumor necrosis factor (ligand) superfamily, member 10
TRITC	Tetramethylrhodamine isothiocyanate
TSC	Tampon de stabilisation du cytosquelette
TSMT	Tampon de stabilisation des MT
TUBA1C	Tubulin, alpha 1c
TUBB2A	Tubulin, beta 2A
TUBB2B	Tubulin, beta 2B
TUBB3	Tubulin, beta 3
ua	Unité arbitraire
UBB	Ubiquitin B
VASP	Vasodilator-stimulated phosphoprotein
WAF1	Wild-type p53-activated fragment 1
ZIPK	ZIP-kinase

A) INTRODUCTION

A.1) Fonctions de p21 et implication dans la tumorigenèse humaine

A.1.a) Identification et fonctions primordiales de p21

La protéine $p21^{Cip1}$ (CDK-interacting protein 1 ou WAF1, Wild-type p53-Activated Fragment 1 ; *CDKN1A*, cyclin-dependent kinase inhibitor 1A, GeneID: 1026) fut identifiée en 1993 et initialement décrite comme un inhibiteur du cycle cellulaire et médiateur potentiel du rôle oncosuppresseur de p53 (*TP53*, 1-3). Un effort intense fut consacré à l'élucidation des fonctions de p21 responsables de l'inhibition du cycle et de la prolifération cellulaire, en particulier dans les conditions de son activation transcriptionnelle par p53. L'identification de deux types de motifs protéiques impliqués respectivement dans l'inhibition des complexes cyclines -kinases dépendantes des cyclines (CDK) et de PCNA (Proliferating Cell Nuclear Antigen) constitua une étape cruciale dans ce domaine (Fig. A.1, 4, 5). L'activité séquentielle des CDK, régulée par la stabilité de leurs substrats, les cyclines, est nécessaire à la progression du cycle cellulaire et elle est inhibée, entre autres, par les CKI (CDK inhibitors) de la famille Cip/Kip qui inclue p21, $p27^{Kip1}$ (p27) et $p57^{Kip2}$ (p57, 6, 7). En outre, PCNA est une protéine majeure des complexes de réplication de l'ADN réalisée au cours de la phase S du cycle (8). Sa capacité à inactiver les complexes cycline-CDK et PCNA fait donc de p21 un puissant inhibiteur du cycle cellulaire (Fig. A.1, Fig. A.2). Par ailleurs, l'inhibition du cycle et de la prolifération, en particulier lors de l'activation de p53, fut décrite comme un mécanisme essentiel de sauvegarde de l'homéostasie cellulaire, s'opposant à la transformation maligne (9-12). Ces premières données ont donc permis d'envisager que p21 puisse être un nouveau suppresseur de tumeur.

A.1.b) Expression dans les cancers et activité oncosuppressive de p21

Le rôle oncosuppresseur de p21 fut clairement établi par l'observation d'une augmentation de la tumorigenèse spontanée chez les souris présentant un knock-out (KO) de *Cdkn1a* (13). Néanmoins, bien que le spectre des tumeurs observé chez ces souris soit comparable à celui observé chez les

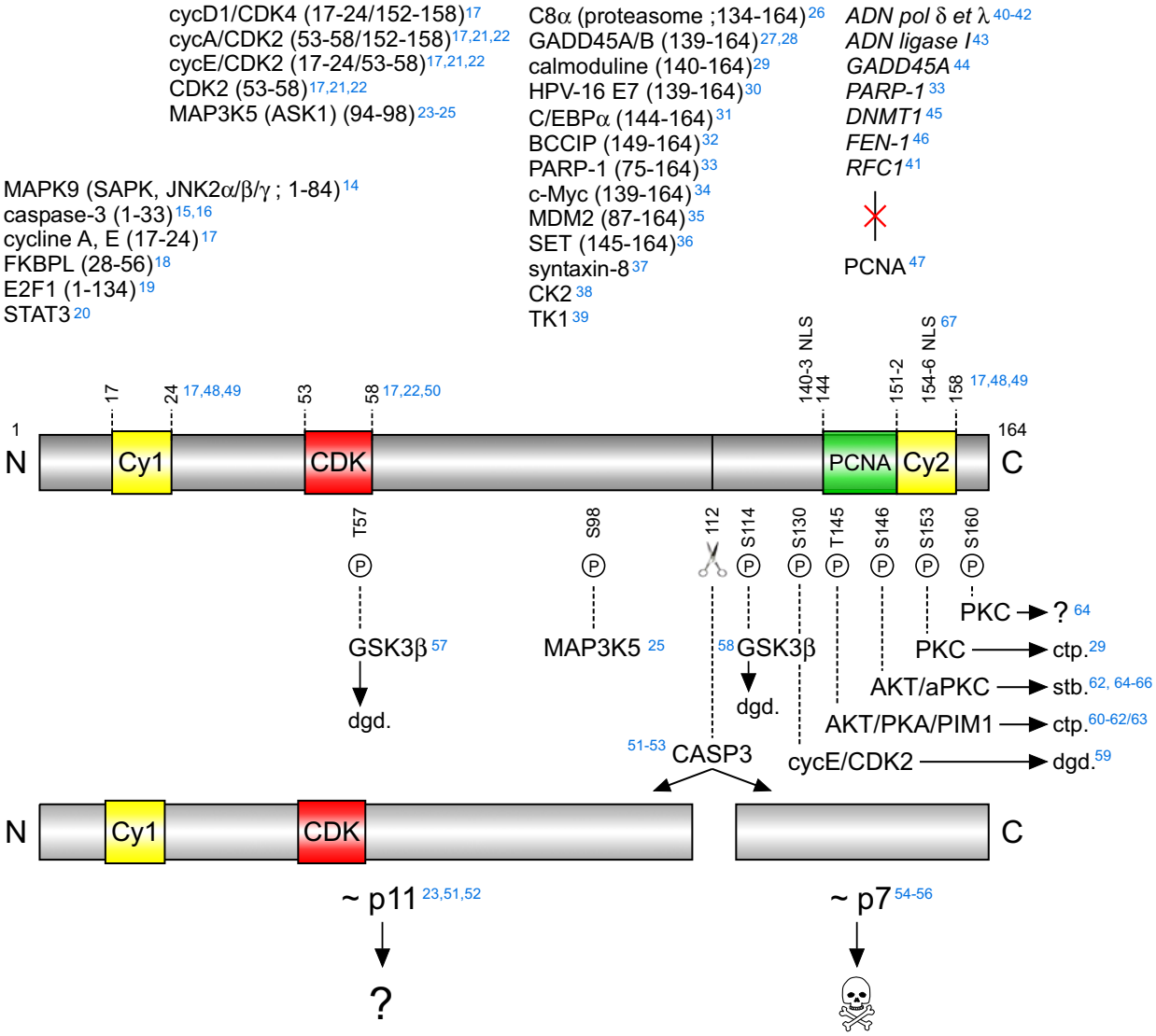

Figure A.1. Interactions, domaines fonctionnels et modifications post-traductionnelles de p21. N et C, acides aminés en position N- et C-terminale. En jaune (Cy1, Cy2), domaines d'interaction avec les cyclines. En rouge et vert, respectivement domaines d'interaction avec les CDK et PCNA. cyc, cycline ; aPKC, PKC atypiques ; dgd., dégradation ; stb., stabilisation ; ctp., localisation cytoplasmique ; CASP3, caspase-3 ; ?, fonction inconnue ; ✂, clivage ; ⊣, perte d'interaction ; Ⓟ, phosphorylation ; →, conséquences ; ☠ apoptose. Entre paranthèses, position des acides aminés correspondant aux domaines de p21 impliqués dans l'interaction ; en italique, protéines en compétition avec p21 pour l'interaction avec PCNA ; en bleu, références.

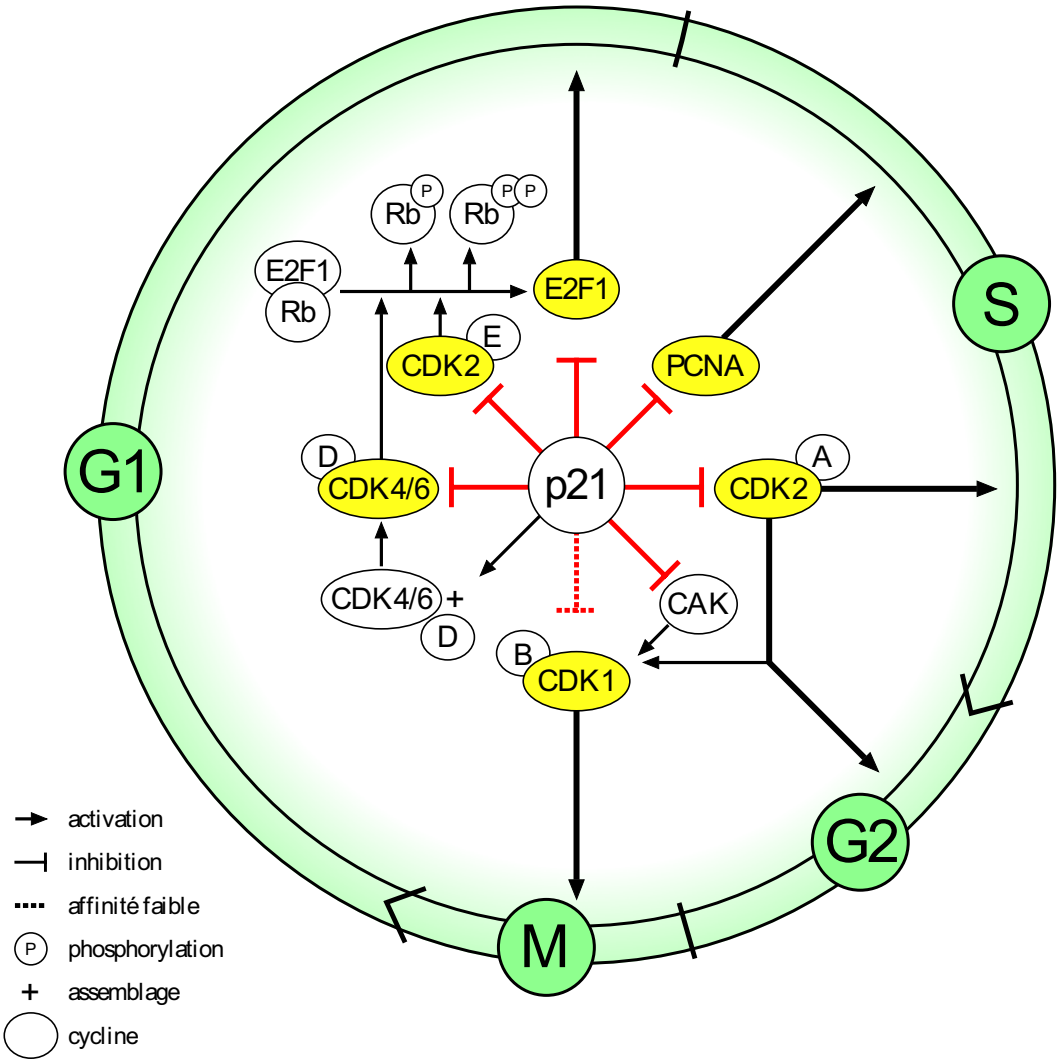

Figure A.2. Régulation du cycle cellulaire par p21. CAK, CDK-activating kinase. (68-72).

souris présentant un KO de *Trp53*, qui code pour la forme murine de p53, leur latence est beaucoup plus grande (13, 73). Ce résultat indique que les fonctions de p21 ne suffisent pas à résumer l'activité oncosuppressive globale exercée par p53. D'autre part, d'autres travaux montrèrent que l'inactivation de p21 favorisait la tumorigenèse, par exemple lors de la perte spécifique des fonctions apoptotiques de p53, l'inactivation d'*Atm*, d'*Apc* ou lors de l'activation oncogénique de *Hras1* (74-77). Par ailleurs, de nombreuses études rapportèrent, en accord avec les premiers travaux, que l'expression de p21 était diminuée dans un certain nombre de types tumoraux (78-86).

En plus des études d'expression, diverses données indiquent que p21 est la cible de mécanismes d'inactivation dans les cancers. La transcription de *CDKN1A* a fait l'objet de très nombreuses études qui ont montré, entre autres, que son inhibition peut être la conséquence d'altérations couramment identifiées dans les cancers humains, incluant l'inactivation de p53 et l'activation de c-Myc (13, 72, 87-94). En outre, d'autres données suggèrent que la dégradation protéique pourrait également être un mode d'inactivation de p21 dans les tumeurs. En effet, certaines protéines impliquées dans la dégradation de p21, telles que MDM2, les protéines des complexes SCF^{SKP2} et $CRL4^{CDT2}$ et 14-3-3τ, sont surexprimées dans les cancers humains (35, 95-100). Par ailleurs, le rôle oncosuppresseur de p21 peut, comme nous le verrons plus loin, être dénaturé par des modifications post-traductionnelles aberrantes, notamment sous l'influence de l'oncogène ERBB2 (61).

Il faut noter que plusieurs travaux ont suggéré que la capacité de p21 à induire l'apoptose contribue à son rôle suppresseur de tumeur (101-106). Bien que l'activité pro-apoptotique potentielle de p21 soit encore assez mal comprise, plusieurs mécanismes candidats ont été proposés. La portion C-terminale de p21, qui est libérée lors de son clivage par la caspase-3, pourrait avoir une activité pro-apoptotique intrinsèque (54-56). L'inhibition par p21 du programme transcriptionnel dépendant des facteurs de transcriptions STAT3 et NF-κB a également été proposée comme un facteur pro-apoptotique (20, 107, 108). En outre, les études transcriptomiques relatives au statut de p21 ont permis d'identifier certains gènes codant pour des protéines anti-apoptotiques et réprimés par p21, tels que *BIRC5*, *MYBL2* et *CRYAB*, codant respectivement pour la survivine, B-MyB et l'α B-crystalline (105, 109, 110). Néanmoins, il apparait que les fonctions de régulation du transcriptome par p21 et les éventuelles propriétés pro-apoptotiques associées sont fortement dépendantes du contexte cellulaire.

A.1.c) Potentiel oncogénique de p21

Comme nous l'avons vu précédemment, de nombreux travaux ont montré que l'expression de p21 est réduite dans certains types tumoraux (A.1.b). Cependant, cette analyse d'expression suggère également que le rôle de p21 au cours de la progression tumorale est plus ambigu que ne le laissait supposer l'identification initiale de son activité oncosupressive (72). Ainsi, plusieurs études révèlent que p21 est surexprimée dans certains cancers et que ce phénomène peut être de surcroît un marqueur de mauvais pronostic, associé notamment à l'apparition de métastases (111-118). Notons que le maintien de l'expression de p21 dans les tissus tumoraux peut aussi être corrélée à sa localisation cytoplasmique aberrante qui est, comme nous le verrons, un facteur d'oncogénicité (61, 118-122).

De nombreux travaux indiquent que l'inhibition du cycle cellulaire par p21 participe à la protection vis-à-vis de l'apoptose induite par différents stress (123). Cependant, cette propriété est fortement dépendante de l'intégrité des systèmes de sauvegarde cellulaire. Aussi, dans un contexte de transformation et de progression tumorale, le niveau d'altération de ces systèmes détermine les conséquences, éventuellement antagonistes, du blocage du cycle cellulaire par p21 vis-à-vis de l'apoptose. En revanche, un nombre croissant de données vient indiquer que des fonctions alternatives de p21 pourraient participer directement à la progression tumorale. Depuis l'identification initiale des domaines Cy1/2, CDK et PCNA de p21, une investigation intensive à permis de découvrir de nombreux partenaires de p21 ainsi que les domaines impliqués dans leur interaction (Fig. A.1). Or, il a été proposé que les conséquences fonctionnelles ces interactions puissent, dans certains cas, participer au processus tumoral. De même que la modulation de l'activité de p21 par sa modification post-traductionnelle a révélé que ses fonctions peuvent être détournées au profit de la progression tumorale. Un certain nombre de travaux ont donc été consacré à l'évaluation de ces fonctions alternatives.

Un exemple bien décrit de modification de l'activité de p21 potentiellement impliquée dans la progression tumorale est celui de son altération lors de la surexpression de l'oncogène ERBB2 dans les cancers du sein. En effet, la surexpression d'ERBB2 dans ces cancers fut corrélée à la séquestration

cytoplasmique de p21 due à sa phosphorylation au niveau de la thréonine 145 (Thr45) par la voie PI3K-AKT, activée en aval d'ERBB2 (61, 119, 121). En outre, cette phosphorylation, notamment sous l'influence d'AKT et PIM1, fut décrite comme un facteur décisif dans la modulation des fonctions de p21. Ainsi, non seulement la forme phospho-thréonine 145 de p21 semble incapable d'interagir avec PCNA, mais elle se localise majoritairement au niveau cytoplasmique (60-63). Or, un certain nombre de partenaires cytoplasmiques de p21 ont permis de proposer un modèle selon lequel cette localisation lui confèrerait des propriétés oncogéniques (124). Plusieurs études ont établi que la forme cytoplasmique de p21 était capable d'interagir directement avec MAP3K5 (ASK1) et MAPK9 (SAPK), et de réduire leur participation à la transduction des signaux pro-apoptotiques (14, 23-25). De la même manière, il fut démontré que p21 interagissait avec la caspase-3 et inhibait son activation (15, 16). Il a également été montré que p21 inhibait l'activation des caspases-8 et -10 lors de l'apoptose induite par le récepteur de TRAIL, DR4 (125). De façon alternative, l'activité de régulateur transcriptionnel de p21 semble aussi être impliquée dans l'inactivation de l'apoptose, en inhibant, par interaction directe avec c-Myc et E2F1, le programme pro-apoptotique (19, 34, 108). Enfin, l'éventuel rôle pro-apoptotique des CDK dans divers modèles a permis de suggérer que leur inhibition par p21 pourrait contribuer à l'inhibition de l'apoptose, en particulier dans les cellules tumorales (126-129). Notons d'ailleurs que la forme cytoplasmique de p21 favorise l'assemblage des complexes cycline-CDK et pourrait, dans ce cas, en plus d'inhiber l'apoptose, promouvoir la prolifération par activation du cycle cellulaire (71).

Enfin, il a été décrit que la forme cytoplasmique de p21, dans des cellules transformées, était capable d'interagir directement avec ROCK1 et ainsi d'inhiber la voie ROCK-LIMK qui promeut normalement la formation des fibres de stress par inhibition de la cofiline, un facteur de dislocation de l'actine (130, 131). Le modèle proposé par ces derniers travaux indique que p21 activerait la migration et l'invasion en favorisant l'activation de la cofiline et le renouvellement des fibres d'actine, malgré l'activation de Ras et Rho (124, 131, 132).

L'ensemble de ces données permet donc d'envisager que le maintien de l'expression de p21 participe, dans certains cas, à la tumorigenèse et à la progression tumorale, par inhibition de l'apoptose, activation de la prolifération et promotion de la motilité. Ces travaux mettent également en

exergue que les fonctions parfois antagonistes de p21 sont clairement dépendantes du contexte cellulaire et de l'intégrité des systèmes régulateurs de l'apoptose et du cycle cellulaire.

A.2) Adhésion focale et dynamique cytosquelettique

L'adhésion des cellules à la matrice extracellulaire (MEC) est une propriété essentielle pour la morphogenèse et l'homéostasie tissulaire (133). Cette propriété implique la coordination dynamique des structures majeures du cytosquelette que sont les filaments d'actine et les microtubules (134, 135). Plus précisément, la morphogenèse cellulaire résulte des forces physiques et des voies de signalisation complexes transduites grâce à l'interaction de ces fibres avec les membranes et les structures d'adhésion (135-138). Parmi ces dernières, les podosomes et les invadopodes, furent identifiés comme des structures riches en fibres d'actine, associées à la dégradation de la MEC, et caractérisant le phénomène d'invasion dans certains contextes physiologiques ou pathologies (139). Nous nous intéresserons ici à un type de structures d'adhésion plus fréquentes, appelées adhésions focales. Ces structures caractérisent le principal mode d'adhésion des cellules motiles non transformées et sont intégrées dans un modèle d'assemblage progressif. Ce modèle comprend leur forme précoce - le complexe focal, et une forme mature alternative se différenciant par sa morphologie allongée, sa localisation centrale au sein de l'aire d'adhesion et sa composition moléculaire - l'adhésion fibrillaire (pour revues : 140, 141). Tout en abordant leur modèle d'assemblage, nous ne détaillerons pas ici les différences entre les adhésions focales et leurs précurseurs ou leurs dérivés. Le chapitre suivant est donc consacré à la présentation des caractéristiques générales des adhésions focales matures ou en cours de maturation. En outre, dans les chapitres A.2.b.3 et A.2.c.5, nous aborderons plus en détail les mécanismes dépendant de l'actine et des microtubules impliqués dans la maturation ou le désassemblage des adhésions focales.

A.2.a) Adhésion focale

Les adhésions focales sont des complexes macromoléculaires composés de plus d'une centaine de protéines identifiées et fonctionnant comme des plateformes de signalisation situées à l'interface

entre le cytosquelette et la MEC (140). Leur assemblage est contrôlé par les récepteurs transmembranaires majeurs que sont les hétérodimères d'intégrines α et β (142-144). A ce jour, les nombreux travaux consacrés à leur caractérisation moléculaire ont permis de proposer un modèle simplifié de leur dynamique d'assemblage. D'abord, les intégrines sont activées par liaison de leur domaine extracellulaire à un ligand de la MEC ou l'interaction de leur domaine intracellulaire avec une protéine effectrice (142, 145-148). La conformation active des intégrines conduit, par l'intermédiaire de leur domaine cytoplasmique, au recrutement de protéines adaptatrices de type taline, paxilline, vinculine ou zyxine (144, 149, 150). A ce stade, les sites d'adhésions correspondent à des structures occupant une aire réduite (généralement inférieure à 1 μm^2 dans un modèle d'adhésion bidimensionnelle sur un support associé à la fibronectine) et assemblées au niveau du lamellipode des cellules migrantes (138). Ces structures d'adhésion, appelées complexes focaux, sont corrélées à une polymérisation active de l'actine sous une forme dite « branchée », essentiellement dépendante, comme nous le verrons plus loin, des GTPases Cdc42 et Rac1 (138, 151-155). Les complexes focaux, pouvant être classés en deux catégories : les complexes focaux précoces et tardifs, subissent un processus de renouvellement très actif. Les complexes tardifs se distinguent essentiellement des complexes précoces par le recrutement de la kinase FAK et de certaines protéines de couplage à l'actine évoqués ci-dessous (141). Il faut noter que le phosphatidylinositol biphosphate (PIP2 ; phospholipide membranaire) permet de localiser certains acteurs essentiels des complexe focaux tels que la taline, la vinculine et l'actinine α, au niveau des sites d'adhésion (150, 156, 157). L'engagement de ce complexe protéique va à son tour promouvoir l'agglomération focale des intégrines et ainsi potentialiser la maturation des complexes focaux et leur interaction avec l'actine (144). Cette dernière est réalisée, entre autre, grâce à des facteurs tels que la taline, la vinculine et l'actinine α, qui interagissent directement avec l'actine filamenteuse (F-actine, 140, 157). Cette étape initie le couplage physique entre la MEC et les forces intracellulaires exercées par le cytosquelette. Elle va permettre la transformation des complexes focaux persistants en adhésions focales précoces puis matures. La maturation de ces structures est corrélée à l'avancée du front de migration et à leur relocalisation vers l'intérieur de la lamella (158). Comme nous le verrons également dans le chapitre consacré à la dynamique de l'actine, cette zone est caractérisée, notamment sous l'influence de la GTPase Rho, par la transition du mode d'assemblage de l'actine branchée vers un assemblage de

structures supérieures contractiles. Il faut noter que la nécessité d'une immobilisation des ligands d'intégrines pour la formation des adhésions focales indique clairement que les complexes focaux sont des structures mécano-sensibles précoces dans l'interface cellule-environnement (150).

Une étape essentielle de la formation des adhésions focales à partir des complexes focaux réside dans le recrutement de nombreux facteurs de signalisation. Ces facteurs incluent les kinases FAK et Src, la protéine adaptatrice BCAR1 (p130cas) et plusieurs facteurs régulant l'activité des GTPases de la famille Rho (GEF, Guanine-exchange factor : facteurs activateurs ; GAP, GTPase-activating protein : facteurs inhibiteurs, 159). Sous la forme d'un complexe avec Src et grâce à son interaction à la fois avec les intégrines et des protéines associées à l'actine (*e.g.* taline), FAK fonctionne comme un intégrateur des signaux mécaniques provenant à la fois du cytosquelette et de la MEC (157). Le complexe FAK-Src possède de très nombreuses cibles qui lui permettent de réguler finement la dynamique des adhésions focales en contrôlant à la fois l'assemblage des fibres cytosquelettiques et la focalisation des intégrines (158). Ainsi la localisation fonctionnelle et la phosphorylation de cibles telles que la paxilline, l'actinine α, BCAR1 ou la filamine participe à l'équilibre dynamique de l'adhésion focale (158). Nous verrons plus loin en quoi FAK participe plus particulièrement à la dynamique de l'actine en régulant notamment l'activité des GTPases Rho. Schématiquement, l'adhésion focale mature se compose donc d'un module récepteur, d'un module de couplage intégrine-F-actine, d'un module de régulation de l'assemblage de la F-actine et d'un module de signalisation (Fig. A.3, 158). Nous verrons qu'elle est également impliquée dans un processus d'interrégulation avec les microtubules. Aussi, l'intégration des signaux provenant à la fois de la MEC et du cytosquelette font des adhésions focales des complexes mécano-sensibles très dynamiques au cours de la morphogenèse et de la migration cellulaire (158, 160). Enfin, au-delà de son rôle dans la morphogenèse et l'homéostasie cytosquelettique, il faut noter que l'adhésion focale a été décrite comme un facteur de régulation de la prolifération et de la mort cellulaire (161-166).

A.2.b) Dynamique de l'actine et adhésion focale

A.2.b.1) Dynamique de l'actine

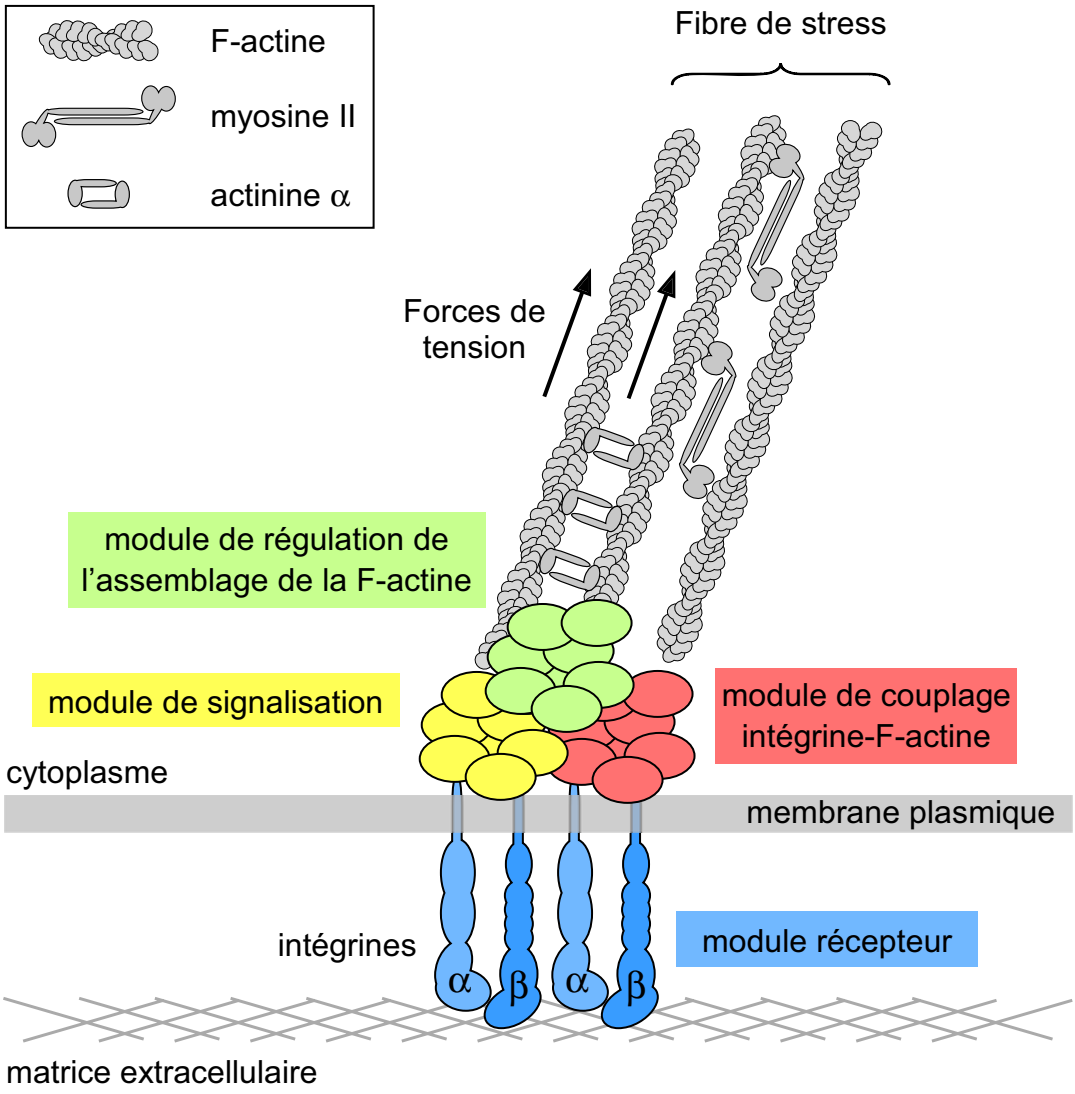

Figure A.3. Principe de l'adhésion focale. D'après Humphries *et al.* (143) et Geiger *et al.* (158).

La dynamique de l'actine est définie par l'ensemble des phénomènes dynamiques qui caractérisent sa polymérisation sous la forme de filaments ou F-actine. La F-actine correspond à l'assemblage non covalent de sous-unités dites monomériques (G-actine ; ~ 6,7 x 4,0 x 3,7 nm ; MM, 43 kDa) selon une conformation en double hélice d'un demi-pas d'environ 37 nm (Fig. A.4A, B, 167). Chaque demi-pas comprend 12 à 14 monomères et confère au filament un diamètre de 9 à 10 nm (167). Les études *in vitro* ont permis de proposer un modèle selon lequel la polymérisation de l'actine débute avec la nucléation d'un trimère de G-actine qui sert de matrice minimale pour l'élongation du filament (167). Le modèle de double hélice est fondé sur l'idée que l'affinité monomère-monomère au sein d'un brin est supérieure à l'affinité inter-brins (168). Notons également que, bien que l'actine fonctionne comme une ATPase, l'hydrolyse de l'ATP n'est pas directement corrélée à sa polymérisation (167). En effet, la G-actine est incorporée dans le filament d'actine en cours d'assemblage sous sa forme liée à l'ATP, qui est sa forme majoritaire *in vivo*. Ensuite, la transformation de la F-actine-ATP en F-actine-ADP-Pi (Pi, phosphate inorganique) survient rapidement. Néanmoins, la libération du Pi qui génère la forme F-actine-ADP est beaucoup plus lente (169, 170). Par ailleurs, il est important de signaler que la G-actine est incapable de régénérer l'ATP à partir de l'ADP et du Pi ; elle doit donc subir un échange nucléotidique afin de recouvrer sa forme liée à l'ATP (171). En présence d'ATP et sans systèmes protéiques associés, l'extrémité F-actine-ADP nécessite une concentration minimum de monomères, ou concentration critique, nettement supérieure à celle requise par l'extrémité F-actine-ATP pour la néo-polymérisation (167). La concentration critique de l'extrémité F-actine-ADP a été estimée douze à quinze fois supérieure à celle de l'extrémité F-actine-ATP en conditions physiologiques (172). A l'état d'équilibre la concentration en monomères est nettement inférieure à la concentration critique de l'extrémité F-actine-ADP (138). Par conséquent, la polymérisation est donc principalement réalisée à l'extrémité F-actine-ATP et la dépolymérisation à l'extrémité F-actine-ADP. Cette polarité structurale est un facteur essentiel dans la régulation de la dynamique de l'actine. Celle-ci conduit au renouvellement progressif des segments d'actine grâce à la croissance de l'extrémité positive et au désassemblage concomitant de l'extrémité négative, selon un modèle dit de « tapis roulant » (Fig. A.5A, 138). Ce phénomène est le vecteur principal des forces protrusives du lamellipode au cours de l'étalement et de la migration cellulaires. Notons que, en fonction de la conformation spatiale du domaine exposé, l'extrémité F-actine-ATP, site principal d'assemblage, est

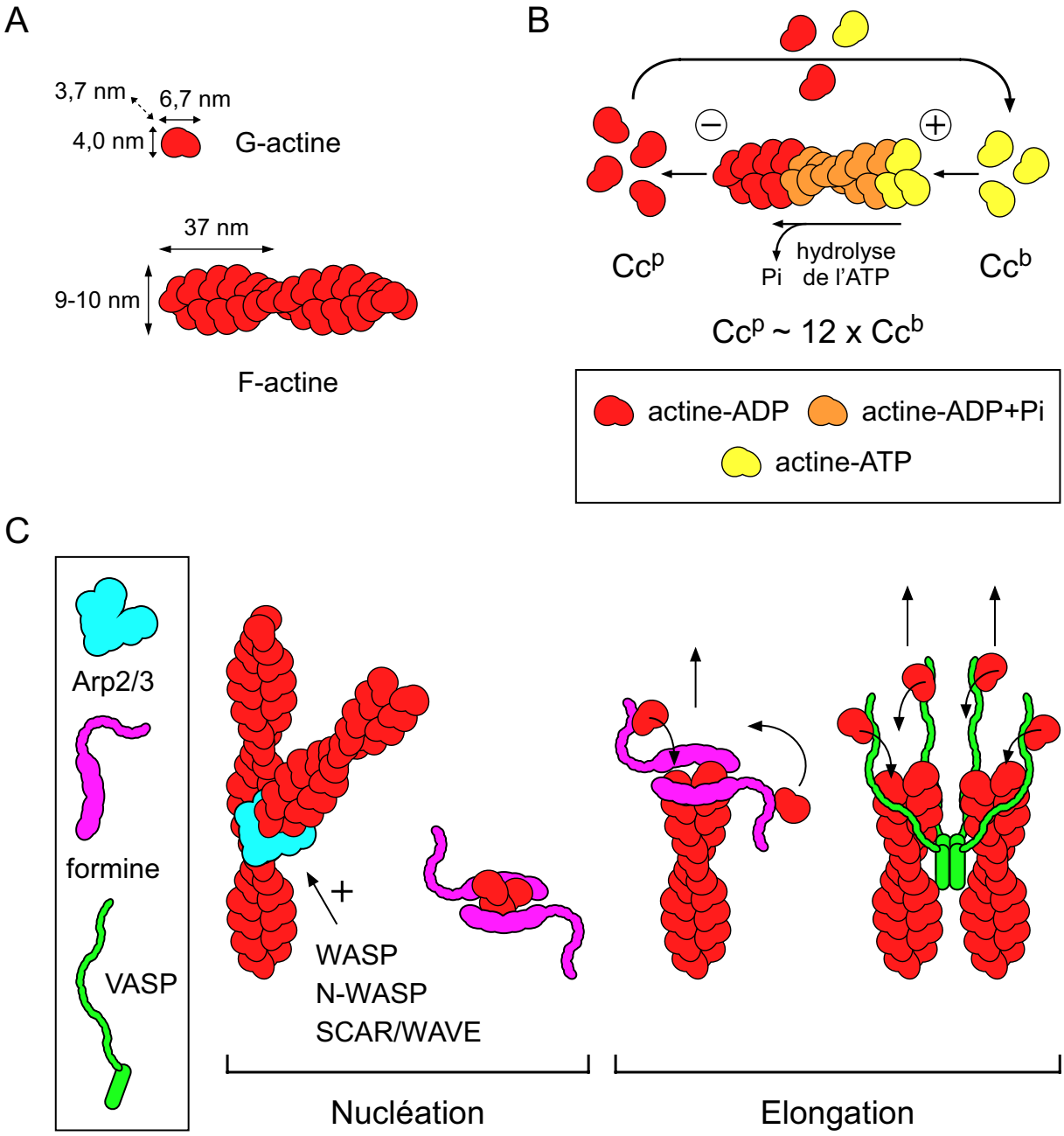

Figure A.4. Actine et principe d'assemblage. (A) Monomère d'actine (G-actine) et actine filamenteuse (F-actine). (B) Assemblage de l'actine. -, extrémité pointue ; +, extrémité barbelée ; Cc^p, concentration critique de l'extrémité pointue ; Cc^b, concentration critique de l'extrémité barbelée ; Pi, phosphate inorganique. (C) Principales modalités de nucléation et d'élongation de la F-actine. +, activation ; flèche verticale, sens de l'élongation de la F-actine. D'après Dos Remedios (167) et Chesarone (173).

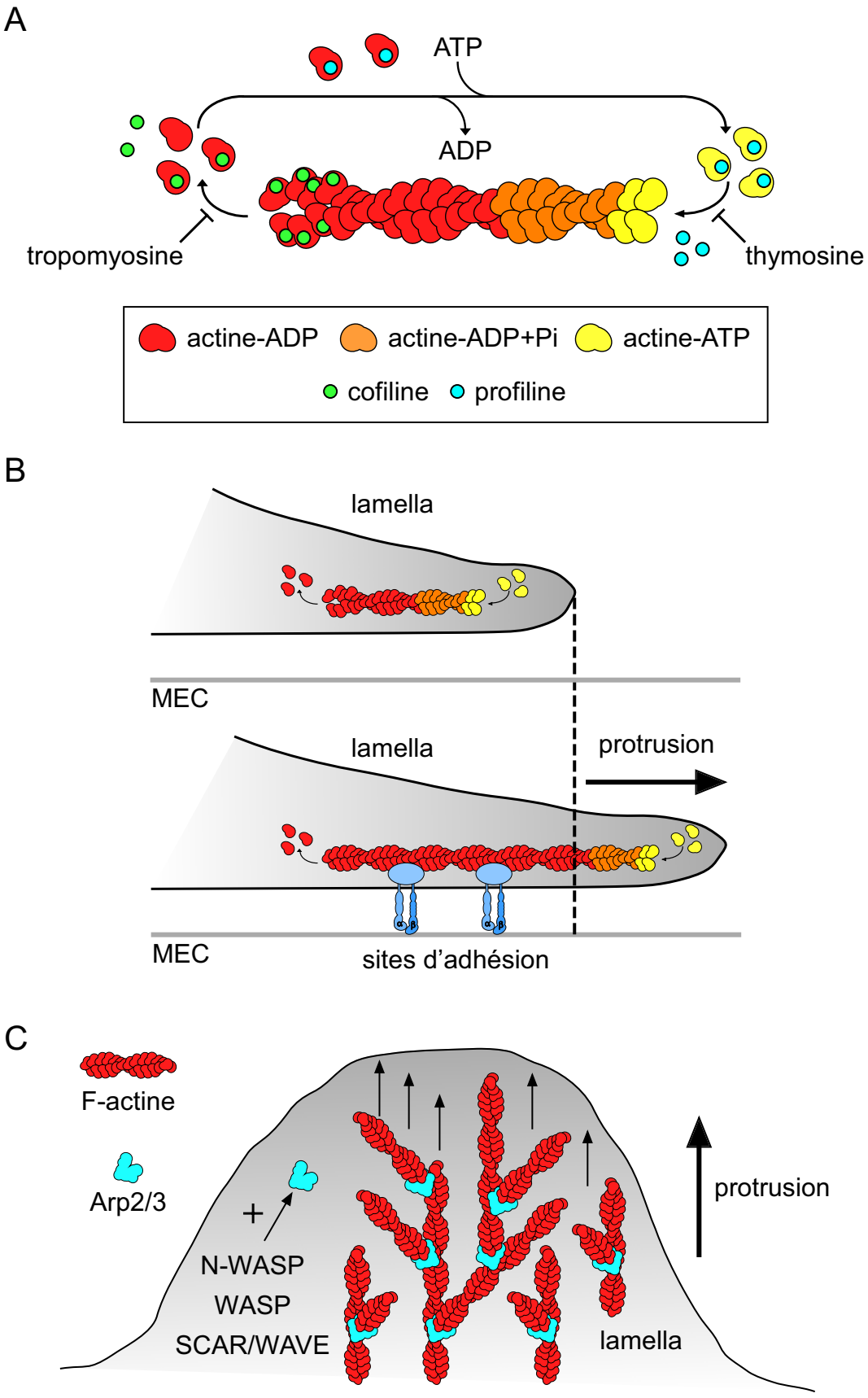

Figure A.5. Principe des forces protrusives exercées par la F-actine au cours de l'extension du lamellipode. A. Renouvellement de la F-actine selon le modèle du "tapis roulant". B. Principe de l'ancrage de la F-actine pour l'exercice des forces protrusives. MEC, matrice extracellulaire. C. Principe d'activation lamellaire de Arp2/3 pour la formation du réseau d'actine branchée au cours de la protrusion. D'après Le Clainche et Carlier (138).

dite extrémité « barbelée » ou positive (barbed end), et l'extrémité F-actine-ADP est dite extrémité « pointue » ou négative (pointed end).

La dynamique de l'actine *in vivo* est principalement contrôlée par les facteurs qui régulent sa nucléation et son assemblage (Fig. A.4C). Parmi ces facteurs, le complexe Arp2/3 est responsable de la nucléation de l'actine le long de filaments préexistants, donnant lieu à une polymérisation dite « branchée » (173). L'initiation de ce type de polymérisation requiert l'activation d'Arp2/3 par des facteurs généralement membranaires, tels que les protéines WASP, N-WASP, SCAR/WAVE ou encore la cortactine (138). La nucléation par les formines (DIAPH1 et 2) permet, quant à elle, le néo-assemblage de filaments linéaires, vraisemblablement à partir du seul noyau de trimère de G-actine (173, 174). Des facteurs de nucléation présentant un mode d'action alternatif ont également été identifiés. Néanmoins, l'activité de ces facteurs, qui incluent Spire, Cobl et Lmod, n'a pas encore été clairement adressée dans les cellules humaines (175-177). Par ailleurs, la stabilité de la F-actine est régulé par un complexe de coiffe localisé à l'extrémité barbelée (138). Cette coiffe limite l'adjonction de nouveaux monomères, favorisant ainsi l'augmentation de la quantité de G-actine disponible, issue des extrémités pointues, et la croissance rapide des extrémités barbelées non coiffées (138). Certains facteurs du complexe de coiffe ont été identifiés, comme l'hétérodimère CPα/β, CAPG, la tensine ou la gelsoline (138, 167). Des facteurs prévenant la formation des complexes de coiffe et favorisant ainsi la croissance des extrémités barbelées ont également été décrits. Ces facteurs d'élongation, comprenant les formines et la protéine VASP, restent associés à l'extrémité positive du filament d'actine pendant sa progression au cours de la polymérisation (173, 174, 178, 179). La concentration de facteurs de polymérisation associés aux membranes plasmiques fait de la lamella un site d'assemblage de l'actine très actif. L'adjonction de monomères aux extrémités barbelées des filaments libres génère un flux rétrograde continu d'actine entretenu par le désassemblage au niveau des extrémités pointues (138, 180). Ce flux rétrograde est le support de forces à faible rendement pour l'extension membranaire caractérisant les protrusions, car la terminaison des filaments animés par ce flux est sensiblement stationnaire (Fig. A.5B, 180). En revanche, l'ancrage de la F-actine au niveau de sites d'adhésion va permettre aux filaments de générer des forces plus importantes, participant ainsi de manière efficace au processus protrusif et l'extension lamellaire (138, 180). Notons d'ailleurs que

l'extension lamellaire des cellules migrantes se caractérise principalement par deux types de structures protrusives :

• le lamellipode qui, selon un mode d'adhésion bidimensionnel, correspond à une projection membranaire aplatie, essentiellement caractérisée par un flux rétrograde et un réseau d'actine branché très dynamique, site privilégié d'assemblage des complexes focaux (Fig. A.5C, 138),

• le filopode qui est une projection membranaire filamenteuse contenant un faisceau de 10 à 20 filaments d'actine dont les terminaisons barbelées sont orientées vers l'extrémité de la projection (138).

Une autre famille de protéines jouant un rôle prépondérant dans la dynamique de l'actine est celle des GTPases de la famille Rho (GTPases Rho). Dans les cellules mammifères, il existe plus d'une vingtaine de GTPases Rho qui se localisent majoritairement au niveau des membranes et qui régulent la dynamique cytosquelettique associée (181). Les GTPases Rho les plus étudiées sont Rho (RhoA, B, C), Rac (Rac1, 2, 3) et Cdc42. L'identification du rôle primordial de ces GTPases dans la dynamique de l'actine vient de l'observation qu'elles activent toutes les trois son assemblage, en particulier au niveau des extensions membranaires des cellules migrantes (151, 182-184). Les protéines de cette famille peuvent lier le GTP et le GDP, et possèdent une activité GTPase intrinsèque (185-187). Il existe donc un équilibre entre les formes associées au GTP, dites actives, qui peuvent interagir avec leurs cibles et les activer, et les formes associées au GDP, dites inactives. L'activité des GTPases Rho est promue par des facteurs d'échanges (guanine nucleotide exchange factors, GEF) qui stimulent le désengagement du GDP au profit du GTP (181). Inversement, les GTPases Rho sont inactivées par l'action de facteurs favorisant l'hydrolyse du GTP en GDP (GTPase-activating proteins, GAP). Des mécanismes de régulation alternatifs consistent à moduler leur capacité d'interaction avec les membranes par modification post-traductionnelle (prénylation, palmitoylation, phosphorylation) ou association avec des facteurs inhibiteurs (guanine nucleotide dissociation inhibitors, GDI, 181). Les GTPases Rho activent directement des molécules qui stimulent la polymérisation de l'actine telles que les protéines WASP, N-WASP, SCAR/WAVE et les formines (DIAPH1-3, 181, 188-193). Comme nous le verrons plus loin, Rho et Rac1 inhibe également l'action d'un facteur de dépolymérisation de l'actine, la cofiline, et favorise la stabilité et la contractilité de structures supérieures composées de filaments d'actine, les fibres de stress.

La polymérisation des filaments d'actine et la progression de leur extrémité positive fournissent les forces physiques nécessaires à la fois à l'établissement de l'adhésion focale et à la protrusion des membranes au cours de l'étalement cellulaire et de la migration (194). L'équilibre dynamique entre la croissance des extrémités barbelées et le raccourcissement des extrémités pointues est sous la dépendance de deux facteurs majeurs : la profiline et la cofiline (Fig. A.5A). La profiline interagit avec la G-actine et promeut l'échange nucléotidique nécessaire à la production de la forme G-actine-ATP (195). La forme G-actine-ATP-profiline se localise au niveau des extrémités positives et libère la profiline lorsque la G-actine-ATP est intégrée au filament en cours d'élongation. En outre, la profiline inhibe l'hydrolyse de l'ATP, favorisant ainsi la mise à disposition de monomères polymérisables au niveau de l'extrémité positive. Cependant, il fut également observé que le taux de dépolymérisation, au niveau des extrémités barbelées, était quatre à dix fois supérieur en présence de profiline (196-198). Le modèle actuel propose donc que la profiline soit à la fois un facteur de polymérisation mais aussi, lors de son désengagement de certaines liaisons - par exemple avec PIP2, Arp2/3, VASP, ENAH (MENA) - un facteur de dépolymérisation (195). En outre, son action entre en compétition directe avec une autre protéine qui interagit avec l'actine monomérique, la thymosine, qui fonctionne comme un inhibiteur de la polymérisation en empêchant l'échange nucléotidique (167). Il faut retenir que la profiline promeut l'assemblage et accélère la dynamique de l'actine ce qui en fait un acteur clé de la réorganisation rapide du réseau d'actine.

La cofiline est une protéine qui appartient à la famille des facteurs de dépolymérisation de l'actine qui comprend également la protéine ADF. Une partie de son activité consiste à lier latéralement les segments d'actine composés de F-actine-ADP et à modifier leur structure de manière à favoriser la dépolymérisation au niveau des extrémités pointues (167). Le pool de G-actine libérée promeut ainsi la croissance des extrémités barbelées. La liaison de la cofiline à la F-actine peut également conduire à la rupture du filament, réduisant ainsi sa longueur de deux à trois fois (199, 200). Cette liaison entre d'ailleurs en compétition avec celle de la tropomyosine qui agit comme un facteur stabilisateur de la F-actine mais également comme un inhibiteur de la nucléation par Arp2/3 et la polymérisation branchée (167, 201). La cofiline génère donc de nouvelles extrémités barbelées disponibles pour la néo-polymérisation. L'activité de la cofiline est régulée par quatre mécanismes (Fig. A.6) :

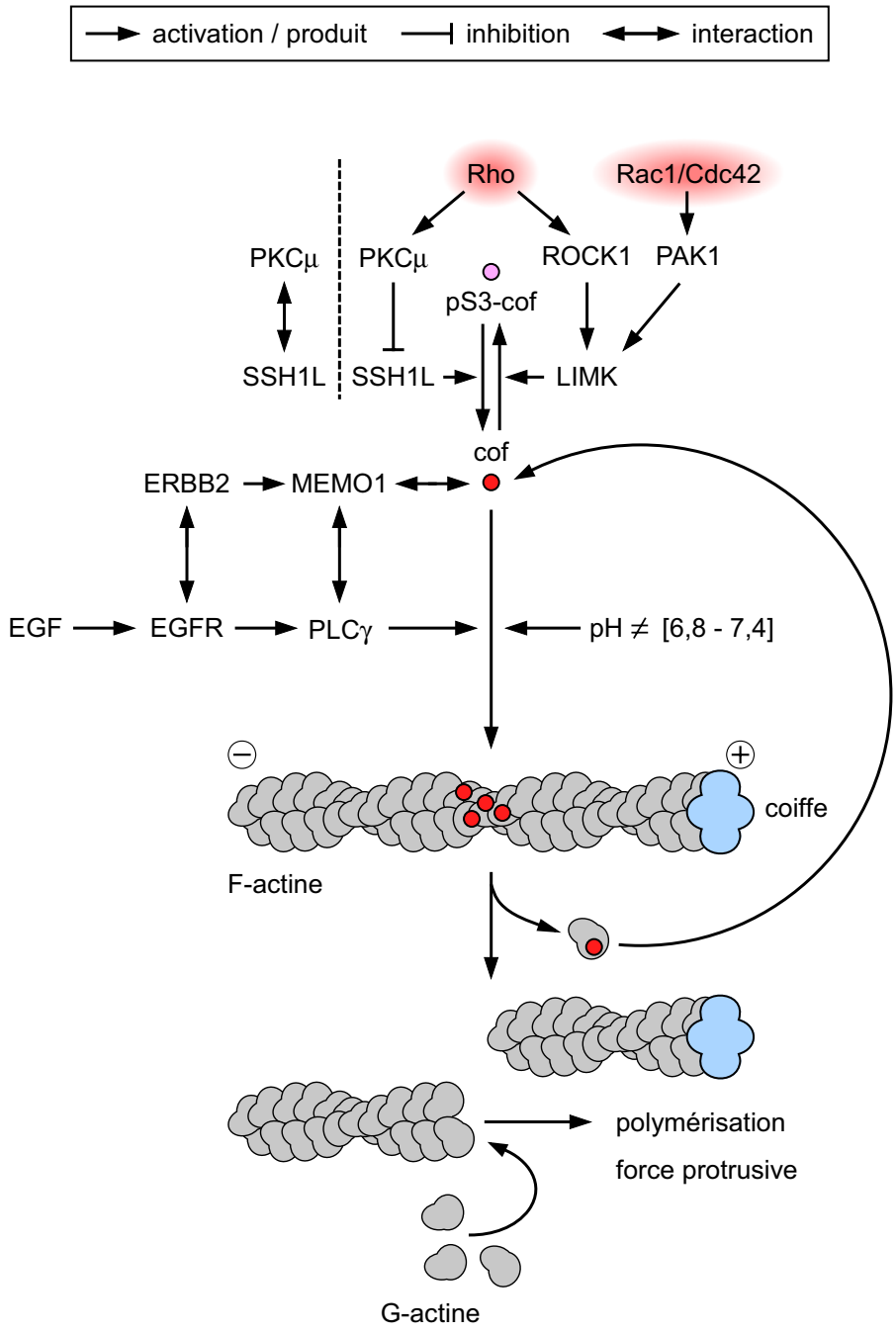

Figure A.6. Régulation de la cofiline et rôle dans la production d'extrémités barbelées libres au cours de la protrusion. pS3-cof, phospho-sérine 3 cofiline (inactive, mauve) ; cof, cofiline (rouge). +, extrémité barbelée ; -, extrémité pointue. En bleu, complexe de coiffe. D'après Wang *et al.* (202) et Meira *et al.* (209).

• La cofiline n'exerce son activité que sous sa forme déphosphorylée au niveau de la sérine 3. Cette phosphorylation est positivement régulée par les kinases LIMK1/2 (LIMK), NRK et TESK1/2 (202). Les LIMK sont, entre autres, activées par la voie de signalisation Rho-ROCK que nous détaillerons plus loin.

• La forme phospho-sérine 3 est inhibée par les phosphatases PP1, PP2A/B, chronophine et SSH1L, qui agissent donc comme des activateurs de la cofiline (202). SSH1L est inactivée par la voie de signalisation Rho-PKCμ qui sera également abordée plus loin.

• La cofiline est liée au phospholipide membranaire PIP2 et ne peut exercer son activité que lorsque celui-ci est hydrolysé par la phospholipase Cγ (PLCγ ou PLCγ1, 203-206). Ce mécanisme fait de l'activation de la cofiline un phénomène dépendant du microenvironnement. En effet, l'EGF, par l'intermédiaire de son récepteur EGFR pouvant former des hétérodimères avec ERBB2 ou ERBB3, catalyse l'hydrolyse de PIP2 par activation de PLCγ lors de la formation de la lamella (206-208). De plus, de récents travaux ont montré que l'effecteur d'ERBB2 MEMO1 interagit avec PLCγ et la cofiline (209). Il semble que MEMO1 lie à la fois la forme phosphorylée et déphosphorylée de la cofiline pour contribuer à sa localisation au niveau du lamellipode. Enfin, cette étude indique que MEMO1 promeut l'activité de dépolymérisation de l'actine exercée par la cofiline lors de l'activation d'ERBB2. Ainsi, l'ensemble de ces données montre que l'EGF provoque l'activation locale de la cofiline, en particulier au niveau de la lamella, pour favoriser la production de nouvelles extrémités barbelées. De cette façon, le renouvellement du réseau d'actine lamellaire fournit les forces physiques impliquées dans la protrusion membranaire.

• Un pH différent des valeurs physiologiques moyennes (6,8 - 7,4) favorise l'activité de la cofiline sous sa forme déphosphorylée (210-212). Ce mode de régulation de la cofiline explique en partie l'importance du pH dans la migration cellulaire, en particulier dans les cellules épithéliales humaines (213-215).

Il faut noter que l'activité de la cofiline est également soumise, selon différentes modalités, à un contrôle par les GTPases Rho (Fig. A.6). En effet, celles-ci participent à l'activation des LIMK, qui inhibent à leur tour la cofiline par phosphorylation. Plus précisément Rho et Rac1/Cdc42 favorisent la phosphorylation activatrice des LIMK par l'intermédiaire respectivement des kinases effectrices ROCK et PAK (216-219). En outre, il a été démontré récemment que Rho contribue à l'inhibition locale de la

cofiline en inactivant la phosphatase SSH1L, associée au réseau d'actine périphérique, par l'intermédiaire de la protéine kinase C atypique PKCμ (220). Rho active PKCμ qui à son tour phosphoryle SSH1L, inhibe son interaction avec le réseau d'actine et favorise sa séquestration cytoplasmique par les protéines 14-3-3β/ζ (220, 221). La cofiline est donc un régulateur crucial de l'assemblage des structures d'actine, notamment dans les cellules migrantes. Elle agit comme un facteur déstabilisateur de l'actine, tout en favorisant localement l'établissement de nouveaux sites de polymérisation requis pour l'extension membranaire au cours de l'étalement cellulaire et de la migration.

A.2.b.2) Fibre de stress

Les fibres de stress correspondent à l'assemblage longitudinal de filaments d'actine (10 à 30) au sein de structures supérieures présentant des propriétés contractiles requises pour la morphogenèse et la motilité cellulaire (222, 223). Ces fibres sont un marqueur de la dynamique de l'actine car leur formation nécessite la polymérisation et la stabilité des filaments d'actine qui les constituent. Elles possèdent de nombreuses protéines associées qui contrôlent leur assemblage, leur contractilité et leur interaction avec d'autres formations cytosquelettiques, telles que les adhésions focales (224).

Au sein des fibres de stress, les filaments d'actine sont principalement reliés entre eux par une protéine de liaison, l'actinine α, bien que d'autres protéines candidates à cette fonction aient été détectées dans ces structures (fascine, espine, filamine, Fig. A.7A, 223, 225, 226). L'actinine α correspond à un dimère antiparallèle dont les extrémités sont chacune composées d'un domaine de liaison à l'actine et dont l'exposition est favorisée par liaison au PIP2 (227). En outre, la contractilité des fibres de stress est assurée par la connexion des filaments de F-actine par des dimères antiparallèles de myosine non-musculaire de type II (myosine II), complexe multipeptidique doté d'une activité motrice couplée à l'hydrolyse de l'ATP (228, 229). La myosine II est composée de deux chaines lourdes, deux chaines légères régulatrices (myosin light chain, MLC) qui régulent son activité et deux chaines légères stabilisatrices des chaînes lourdes (essential light chain, ELC, 229). L'activité ATPase de la myosine II connectant deux filaments d'actine permet son changement conformationnel, provoquant ainsi le déplacement antiparallèle des deux filaments interconnectés (229). De plus, la

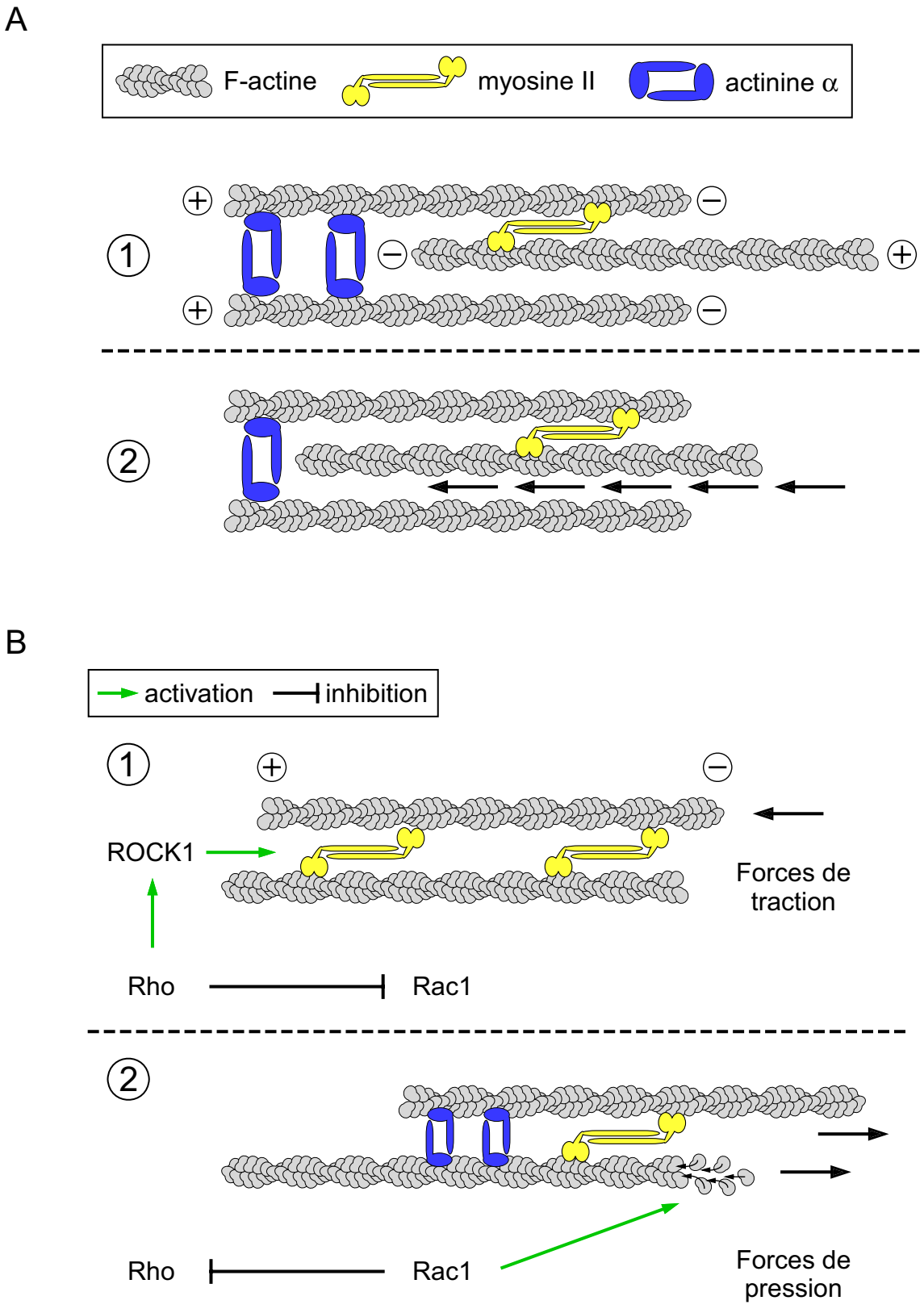

Figure A.7. Fibres de stress et régulation des forces associées par Rho et Rac1. (A) Principe d'assemblage et de contraction de la fibre de stress. +, extrémité barbelée ; -, extrémité pointue. 1, fibre de stress non contractée ; 2, contraction ; flèches, sens de déplacement. (B) Principe de l'alternance des forces exercées par les fibres de stress sous le contrôle du couple Rho/Rac1. 1, Contractilité activée par la voie Rho-ROCK1-myosine II: forces de traction. 2, Relaxation de la fibre de stress par inhibition de Rho et promotion de l'asemblage de la F-actine par Rac1, forces de pression. Flèche noire, direction des forces. D'après Pellegrin et Mellor (223).

contraction des fibres de stress induit le désengagement de l'actinine α, ce qui facilite probablement la progression de la myosine II (Fig. A.7A, 230). Au sein des fibres de stress des cellules motiles, l'orientation des filaments est graduelle. Au centre, des filaments parallèles et antiparallèles confèrent une orientation mixte, associée à l'interpénétration de segments au cours de la contraction. Aux extrémités, l'orientation est généralement uniforme, avec des terminaisons barbelées orientées vers l'extérieur de la fibre (222, 223).

Il faut remarquer ici que deux types d'effecteur de la GTPase RhoA ont été identifiés comme des régulateurs essentiels des fibres de stress : la kinase ROCK1 et la formine DIAPH1. D'abord, comme nous l'avons évoqué précédemment, Rho active les LIMK par l'intermédiaire des ROCK (A.2.b.1). Plusieurs travaux ont suggéré que la voie ROCK-LIMK favorisait la stabilité des fibres de stress en induisant la phosphorylation inactivatrice de la cofiline (231-233). Cependant, les ROCK promeuvent aussi la contractilité des fibres de stress en phosphorylant directement MLC (234, 235). De plus, ROCK1 fut décrite comme un inhibiteur de MYPT1, la sous-unité régulatrice d'une phosphatase (MLC phosphatase, MLCP) qui inactive la myosine II (236, 237). MLC est par ailleurs l'objet d'une régulation complexe qui fait intervenir son activation par plusieurs kinases dont MLCK, CRIK (Citron Rho-interacting kinase), DAPK3 (ZIPK) et CDC42BP (MRCK, 237). Enfin, plusieurs travaux ont montré que le facteur de nucléation DIAH1 était requis pour l'assemblage correct des fibres stress (238-240).

Notons enfin que, bien que les fibres de stress soient, comme nous allons le voir, à l'origine des forces de traction nécessaires à la migration cellulaire, leur impact sur le phénotype motile est dépendant du contexte cellulaire. En effet, alors que de nombreux travaux indiquent que leur contractilité est requise pour la migration, d'autres travaux, utilisant en particulier des fibroblastes, suggèrent qu'elles pourraient avoir un effet inhibiteur sur celle-ci (194, 241, 242).

A.2.b.3) Interaction actine-adhésion focale et conséquences

L'adhésion focale est un site privilégié d'interaction avec la F-actine (A.2.a). Cette association permet d'ancrer les fibres d'actine pour générer à la fois les forces de protrusion et les forces de traction des cellules motiles (194). Les extrémités en cours d'assemblage peuvent ainsi

exercer une pression au niveau du front de migration qui abouti à la protrusion membranaire (138, 194). Les forces de traction proviennent elles de la contraction des fibres de stress qui participe à l'extension et la maturation des adhésions focales au front migration et à leur déplacement ou leur dissociation au niveau du front de rétraction (136, 158). Comme nous allons le voir, l'adhésion focale et les fibres de stress sont interrégulés.

L'interaction adhésion focale-F-actine fut démontrée grâce à l'injection d'actine monomérique fluorescente dans des cellules vivantes et l'observation de sa polymérisation au niveau des sites d'adhésion (243, 244). Ces expériences ne permirent pas de déterminer si ces sites étaient plus enclins à initier la nucléation de l'actine ou au contraire, à capturer l'extrémité libre de filaments préexistants. Néanmoins, de nombreux travaux indiquent clairement que les sites d'adhésion sont associés à l'assemblage de l'actine. Ce phénomène est sous la dépendance des quatre modules associés aux adhésions focales et cités précédemment (A.2.a, 158) :

- un module récepteur (intégrines),
- un module de couplage intégrine-F-actine (*e.g.* taline, FERMT3 (kindline 3), paxilline, vinculine),
- un module de régulation de l'assemblage de la F-actine (*e.g.* tensine, VASP, Arp2/3, DIAPH1),
- un module de signalisation (*e.g.* ILK, FAK, Src, Rho, Rac1).

L'inhibition expérimentale du flux rétrograde conduit à la disparition des adhésions focales naissantes, et les extrémités barbelées non-coiffées sont particulièrement bien corrélées aux sites d'activation de l'intégrine β1 (245, 246). Ces observations renforcent l'idée selon laquelle l'assemblage de l'actine est couplé à celui des adhésions focales. Même si son activité au niveau des sites d'adhésions n'a pas été établie, la localisation cytoplasmique du facteur de nucléation N-WASP est favorisée par FAK et pourrait contribuer à la nucléation de l'actine associé à l'adhésion focale (247). D'autre part, il a été montré que le complexe de nucléation Arp2/3, grâce à son interaction avec la vinculine, se localise au niveau du lamellipode des cellules motiles (248). Dans ce cas, il semble que, malgré l'incapacité de la vinculine à activer Arp2/3, leur interaction est néanmoins requise pour l'extension lamellaire et l'étalement cellulaire correct. Plus directement, il a été démontré que la forme non-phosphorylée de FAK recrute et active Arp2/3 au niveau des sites d'adhésion, et que le domaine de FAK impliqué dans ce processus promeut l'assemblage des fibres de stress (249). Ce résultat

indique que la nucléation de l'actine est une étape précoce de l'assemblage de l'adhésion focale. Notons que les formines sont également impliquées dans la nucléation de l'actine au niveau des adhésions focales et qu'elles pourraient participer à leur mécano-sensibilité (240, 250-252). Le facteur d'élongation VASP se localise aussi au niveau des adhésions focales, précocement au cours de leur assemblage et probablement sous l'influence de sa liaison à la zyxine (154, 253, 254). D'ailleurs, la zyxine semble être un facteur de mécano-sensibilité crucial puisque son association aux adhésions focales est dépendante des forces de traction exercée par l'actine (255, 256).

Comme nous l'avons évoqué précédemment, le module de signalisation associé aux adhésions focales est caractérisé par de nombreux acteurs qui intègrent les signaux provenant à la fois des intégrines et du cytosquelette (A.2.a). Une famille de protéines est plus particulièrement impliquée dans la régulation dynamique des fibres de stress dépendante de l'adhésion focale et du complexe FAK-Src, celle des GTPases Rho. Plusieurs travaux ont établi, grâce à la technique de FRET (Fluorescence Resonance Energy Transfer), que l'activité des GTPases Rho, dans les cellules migrantes, est principalement localisée au niveau des sites d'interaction dynamique actine-adhésion focale (257-260). En outre, RhoA et Rac1 semblent exercer une activité inhibitrice réciproque au cours de ce processus (261-263). Cette interrégulation négative permet de distinguer l'alternance deux types de mécanismes (Fig. A.7B) :

• Rac1 et Cdc42 favorisent la nucléation et la polymérisation des fibres d'actine branchées par activation de Arp2/3, en même temps que Rac1 inhibe la contractilité dépendante de Rho (159, 264-267) - ce mécanisme conduit à la croissance et au relâchement des fibres de stress et génère ainsi les forces de « pression » au niveau des membranes, au cours de l'extension lamellaire ;

• RhoA favorise la contractilité des fibres de stress et inhibe la genèse de nouvelles extrémités barbelées dépendante de la cofiline - ce mécanisme a pour conséquences d'augmenter les forces de « traction » au niveau des adhésions focales, favorisant ainsi leur déplacement ou leur dissociation au front de rétraction et contribuant aussi à leur maturation au front de migration (194, 267).

L'activité des GTPases Rho est gouvernée par des facteurs activateurs (GEF) et inhibiteurs (GAP) qui favorisent respectivement les formes liées au GTP ou au GDP (A.2.b.1). Or, le complexe FAK-Src, en coordonnant l'action de plusieurs de ces facteurs, va fonctionner comme un modulateur

alternatif de Rho et Rac1 pour contrôler l'équilibre pression/traction des fibres de stress associées aux adhésions focales (Fig. A.8, 267). En effet, le complexe FAK-Src active, par l'intermédiaire de BCAR1, le complexe DOCK1-ELMO1 qui fonctionne comme un GEF pour Rac1 (268-270). De plus, bien que l'activité de ces facteurs reste discutée, les GEF de Rac1 et Cdc42, GIT2 et ARHGEF7 (βPIX), sont recrutés au niveau des adhésions focales et possiblement activés par le complexe FAK-Src via la paxilline (271-274). Outre l'activation de Rac1 et Cdc42, le complexe FAK-Src est aussi capable d''inhiber transitoirement RhoA pour favoriser les forces protrusives, en activant GRLF1 (p190ARhoGAP, ARHGAP35) via RASA1 (p120RasGAP) et ARHGAP26 (GRAF, 275, 276). Alternativement, il a été proposé que l'activité de RhoA soit promue au cours des phases tardives de l'extension lamellaire ou au front de rétraction, grâce à l'activation de GEF tells que ARHGEF1 (p115RhoGEF), ARHGEF12 (LARG), RGNEF (p190RhoGEF, 277, 278). FAK interagit directement avec ARHGEF12 et RGNEF, et pourrait ainsi promouvoir la contractilité au niveau des deux fronts opposés des cellules migrantes (278, 279). Enfin, des travaux récents ont montré que RhoA exerçait des fonctions spécifiques, indépendantes de des effecteurs ROCK, mais en rapport avec l'activité de DIAPH1, pour l'initiation des adhésions focales de la lamella des cellules migrantes. Cette régulation spatio-temporelle subtile de l'activité de RhoA contrôle la localisation de facteurs d'assemblage et de liaison de la F-actine, et est sous le contrôle d'ERBB2 via MEMO1 (207, 280).

Alors que l'adhésion focale initie et supporte l'assemblage de l'actine, sa mécano-sensibilité permet aussi aux fibres de stress de développer les forces de tension au cours des différentes étapes de l'étalement et de la migration cellulaires (138). Au cours de ce processus le module de couplage adhésion focale-actine joue un rôle crucial, notamment sous l'influence de la taline et des kindlines. En effet, ces deux types de protéine présentent la particularité d'interagir directement avec l'actine et d'activer simultanément les intégrines (147, 281-284). Le lien entre les intégrines et le cytosquelette est renforcé, en particulier sous le contrôle de la vinculine qui, une fois recrutée par la taline, va contribuer à leur focalisation tout en conservant son interaction directe avec l'actine (285, 286). A ce stade là, plusieurs observations indiquent que l'interaction de l'actine avec les adhésions focales est régulée par la mécano-sensibilité de ces dernières. D'abord, la myosine II est requise pour le recrutement de la vinculine, la zyxine, l'actinine α et FAK, l'activation de la paxilline et l'assemblage

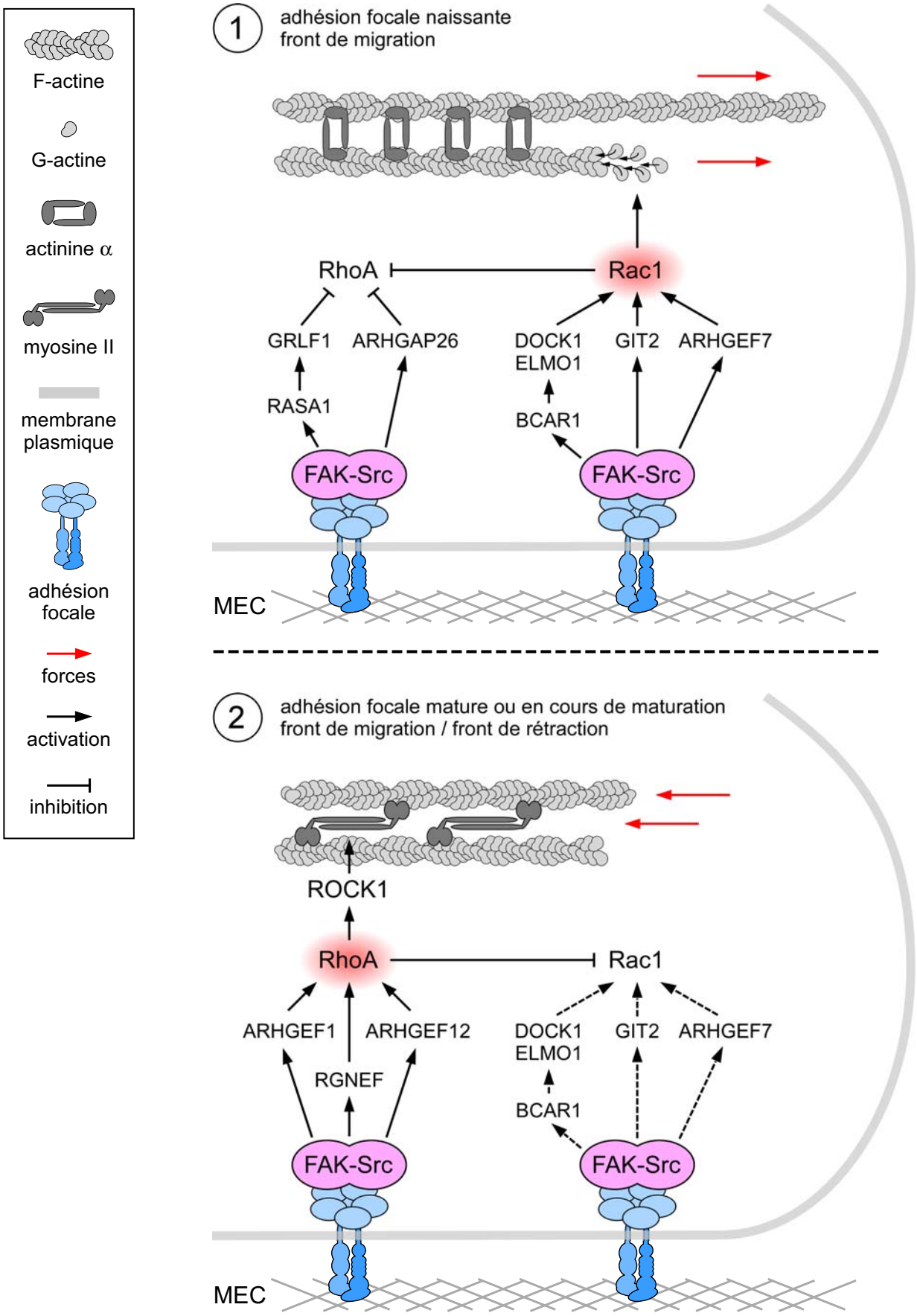

Figure A.8. Régulation de l'activité de RhoA et Rac1 par le complexe FAK-Src pour le contrôle des forces associées à l'interface actine-adhésion focale. MEC, matrice extracellulaire ; pointillés, signalisation minoritaire. D'après Huveneers et Danen (159), et Tomar et Schlaepfer (267).

complet des adhésions focales (246, 287-291). Ces données démontrent que la contractilité des fibres de stress participe à la maturation des adhésions focales (246, 287-291). Notons que le mode d'activation de la myosine II, notamment par ROCK1 et MLCK, ainsi que son effet sur la morphométrie des adhésions focales présentent des différences spatio-temporelles relatives au phénomène de migration cellulaire (292). En outre, la protéine de couplage intégrine-F-actine BCAR1 peut modifier sa conformation en réponse à une extension mécanique, de façon à exposer ses sites de phosphorylation et ainsi augmenter sa susceptibilité à être activée (293). Le modèle proposé ici indique que BCAR1, en réponse à une tension, va provoquer la polymérisation de l'actine via Rac1 pour renforcer la connexion intégrine-actine (Fig. A.8).

En résumé, l'assemblage et la maturation des adhésions focales requiert la polymérisation de l'actine et la contractilité associée aux fibres de stress. Inversement, l'adhésion focale est un promoteur essentiel de l'assemblage et de l'intégrité du réseau d'actine.

A.2.c) Dynamique microtubulaire et adhésion focale

A.2.c.1) Dynamique microtubulaire

Les microtubules résultent de la polymérisation de dimères de tubuline α-β (294). Comme nous le verrons plus loin, bien que cette polymérisation se produise spontanément, de nombreux facteurs permettent de l'activer *in vivo*. La tubuline (MM, ~50 kDa ; diamètre, 4 nm) fonctionne comme une GTPase, cependant, au sein des dimères α-β, seule la tubuline β est susceptible de subir un échange de GDP au profit du GTP puis d'hydrolyser celui-ci (Fig. A.9A, 295). En effet, la tubuline α voit son site nucléotidique masqué par la formation du dimère α-β et reste liée au GTP non hydrolysé (295). Par ailleurs, l'hétérodimérisation des tubulines nécessite leur mise en conformation par l'intermédiaire de cofacteurs (296-299). La polarité des dimères α-β détermine leur mode d'assemblage en tête-à-queue, au sein de protofilaments qui sont par conséquent polarisés (294). Selon le modèle actuel, l'échange de GDP contre le GTP permettrai un changement conformationnel des dimères conduisant à un alignement progressif des monomères qui les constituent, favorisant ainsi l'interaction dimère-dimère au sein des protofilaments (300). De plus, l'assemblage des dimères et oligomères provoque

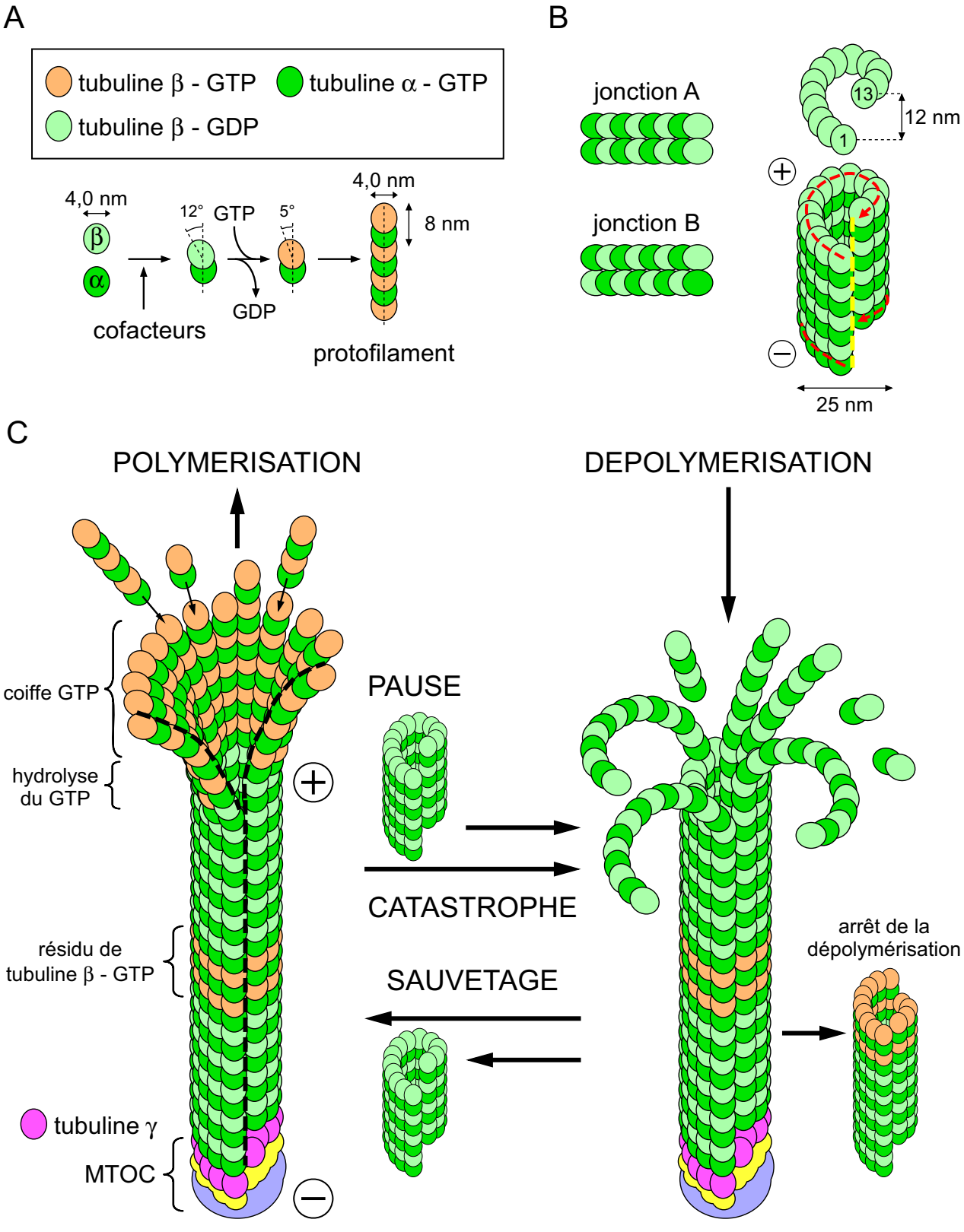

Figure A.9. Tubuline et principe d'assemblage des microtubules. (A) Assemblage des protofilaments de tubuline. Pointillés, axe des monomères. (B) Module de base du microtubule. Pointillés rouges, trajet hélicoïdal des monomères homologues appariés; pointillés jaunes, ligne de fermeture. (C) Assemblage du microtubule et instabilité dynamique. Pointillés noirs, limite du feuillet de protofilaments. -, extrémité négative ; +, extrémité positive. MTOC, Microtubule Organizing Center. Références, A.2.c.1.

l'alignement des monomères pour conférer aux protofilaments leur caractère rectiligne (301-303). L'intégration des protofilaments au microtubule va finaliser ce processus (304). Notons qu'au début de l'assemblage du microtubule, l'interaction latérale des protofilaments est réalisée par contact entre monomères homologues (α/α, β/β) pour former un feuillet continu (jonctions A, Fig. A.9B, 305, 306).

L'assemblage, ou polymérisation, d'un microtubule correspond à la formation d'un tube de 25 nm de diamètre, constitué par fermeture d'un feuillet de 13 protofilaments de tubuline selon une jonction longitudinale. Par rapport à l'axe du microtubule, l'appariement de monomères homologues, à chaque jonction de protofilaments, se fait selon un décalage sensible (295). Autrement dit, les monomères des protofilaments adjacents ne sont pas parfaitement alignés. De ce fait, la paroi cylindrique des microtubules présente des rangées de monomères homologues organisés en hélices d'un pas de 12 nm (Fig. A.9B, 295). Le long d'un segment microtubulaire de 12 nm, trois hélices parallèles de monomères homologues sont enroulées selon cette configuration. La combinaison du pas de 12 nm et du motif de dimère α-β de 8 nm conduit à la formation d'une ligne de « fermeture » du feuillet de protofilaments où les monomères sont appariés de manière non-homologue (contact α/β ; jonctions B, Fig. A.9B, 295). Cette fermeture est associée à l'hydrolyse du GTP des sous-unités β des dimères déjà intégrés dans le protofilament et consécutivement à leur interaction avec les sous-unités α des dimères entrants (295). On suppose que le recouvrement de la courbure des dimères, au cours de ce processus, sensibilise les protofilaments à la dépolymérisation sous l'effet de la contrainte structurale ainsi générée (300, 307). Lorsque l'hydrolyse du GTP est retardée, le maintien de sous-unités β-GTP à l'extrémité positive d'un microtubule peut constituer une coiffe stabilisatrice qui, selon un modèle dynamique, progresse en même temps que l'extrémité supportant la polymérisation (Fig. A.9C, 308, 309). En outre, les sous-unités β-GTP peuvent également persister au sein d'un segment de microtubule et semble fonctionner dépolymérisation (310).

Les microtubules sont polarisés du fait du mode d'assemblage imposé par les dimères de tubuline. Les sous-unités de tubuline β sont exposées à l'extrémité « positive », qui supporte l'adjonction de nouveaux dimères et oligomères, et les sous-unités de tubuline α sont exposées à l'extrémité opposée, dite « négative » (311). Cette dernière est protégée de la dépolymérisation par l'ancrage à un centre d'organisation des microtubules (MTOC, Microtubule Organizing Center) qui

contient, parmi diverses protéines, la tubuline γ, facteur majeur de nucléation des microtubules (312). Ce type structure peut contenir la tubuline γ sous forme d'un complexe de deux sous-unités (γTuSC, γ-Tubulin Small Complex) ou d'un assemblage plus étendu et, en fonction du modèle, formant un anneau ou un protofilament (γTuRC, γ-Tubulin Ring Complex, 312). Dans les cellules eucaryotes, les MTOC sont principalement associés aux centrosomes, cependant, il existe aussi des sites d'ancrage non-centrosomiques permettant la formation de MTOC, tels que l'appareil de Golgi (313-315). En outre, bien qu'elle soit le facteur dominant de nucléation des microtubules, plusieurs données indiquent que des mécanismes de nucléation et de stabilisation des extrémités négatives indépendants de la tubuline γ existent *in vivo* (314, 316, 317).

La tubuline purifiée peut, *in vitro*, se polymériser spontanément en filaments caractérisés par un comportement dynamique à leurs deux extrémités (318). Néanmoins, alors que l'extrémité négative des microtubules présente, en conditions physiologiques, une certaine stabilité, notamment grâce à son engagement dans le MTOC, l'extrémité positive fut décrite comme un site d'assemblage et de désassemblage bien plus actif (319-321). En effet, cette extrémité subit l'alternance rapide de phases de polymérisation (croissance) et de dépolymérisation (raccourcissement), séparées par des phases de transition appelées pauses ou atténuations. Ce phénomène est appelé instabilité dynamique (Fig. A.9C, 322). La survenue d'une phase de dépolymérisation après une pause ou une phase de polymérisation est appelée catastrophe. Inversement, l'initiation d'une phase de polymérisation ou de pause après une phase de dépolymérisation est appelée sauvetage. La dynamique microtubulaire est donc définie par quatre paramètres principaux :

- la vitesse de croissance
- la vitesse de raccourcissement
- la fréquence des catastrophes
- la fréquence des sauvetages.

Ce comportement dynamique est un facteur fondamental des fonctions microtubulaires car il conditionne l'interaction des microtubules avec les structures cellulaires essentielles qu'ils régulent. En effet, le comportement de « recherche et capture » des extrémités positives des microtubules dynamiques vis-à-vis de ces structures est impliqué dans diverses fonctions. Il concerne par exemple la ségrégation chromosomique au cours de la mitose, l'assemblage de l'appareil de Golgi, l'interaction

avec le cortex cellulaire pour le positionnement des centrosomes, les jonctions cellulaires ou encore, comme nous le verrons, la formation des adhésions focales (136, 323-326). La dynamique microtubulaire est régulée par deux types de facteurs : les facteurs stabilisateurs et déstabilisateurs. La stabilisation peut être obtenues par inhibition des catastrophes, sauvetage des microtubules en cours de dépolymérisation ou réduction de la vitesse de raccourcissement (322). Inversement, la déstabilisation peut être obtenue par augmentation des catastrophes, inhibition des sauvetages et augmentation de la vitesse de raccourcissement. Il faut remarquer que si l'augmentation de la vitesse de croissance peut participer à la stabilité des microtubules, elle peut également les sensibiliser aux catastrophes. Cette régulation est sous l'influence de trois principales familles de facteurs : les protéines associées aux microtubules, la modification post-traductionnelle des tubulines et la représentation relative des différentes isoformes (Fig. A.10). Nous nous intéresserons plus particulièrement aux conséquences fonctionnelles de l'interaction des microtubules avec les adhésions focales au cours de l'étalement cellulaire et de la migration.

A.2.c.2) Protéines associées aux microtubules

De nombreuses protéines interagissent avec les microtubules. Ces interactions peuvent faire des microtubules le vecteur de fonctions spécialisées comme le transport vésiculaire centrifuge et centripète assuré respectivement par certaines kinésines motiles et dynéines (327). Cependant de nombreuses protéines associées aux microtubules (MAP, Microtubule Associated Proteins) régulent leur stabilité à l'interface avec leurs structures cibles. Elles sont l'objet de multiples modes de régulation incluant leur interaction au sein de complexes associés aux microtubules et leur contrôle par des protéines effectrices telles que les kinases MARK ou GSK3β (328). Ainsi, certaines protéines stabilisent les microtubules pour leurs fonctions mitotiques, comme par exemple la protéine centromérique CENPE qui permet la capture des extrémités positives des microtubules par les kinétochores (329). De la même manière les protéines TPX2, TACC et NuMA associées aux pôles du fuseau mitotique participent à la stabilisation des extrémités négatives des microubules (330). Les MAP dites classiques, incluant MAP1, les isoformes de MAP2 et MAP4, Tau (MAPT) et MAP6 (F- et N-STOP), peuvent lier latéralement les microtubules et sont généralement des facteurs stabilisateurs

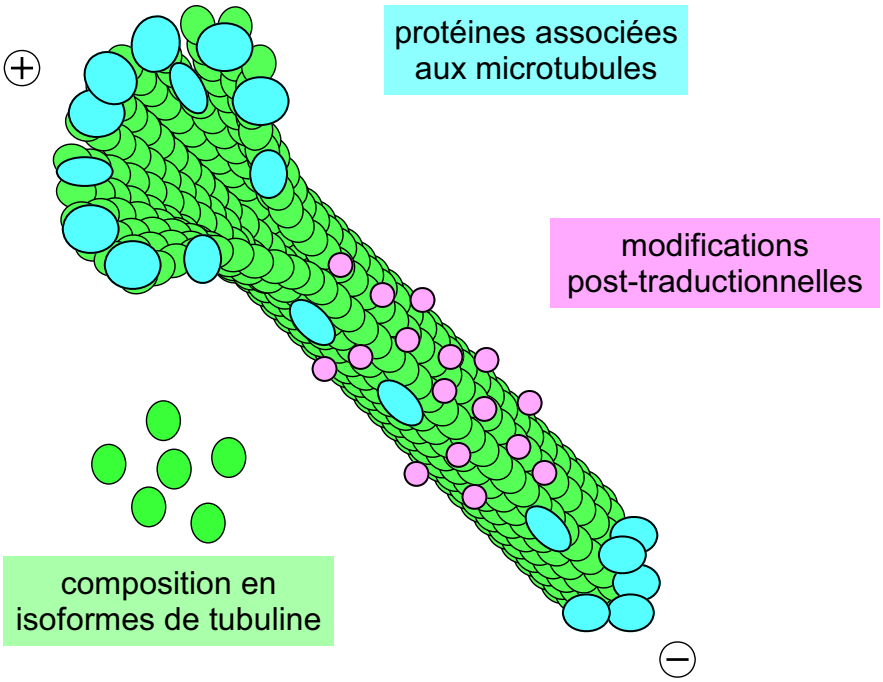

Figure A.10. Principaux modes de régulation de la dynamique microtubulaire. -, extrémité négative ; +, extrémité positive

(331-335). Par ailleurs, les protéines interagissant avec les extrémités positives sont aujourd'hui reconnues comme des facteurs majeurs de régulation la dynamique microtubulaire (+TIP, Plus-end tracking proteins). Les +TIP intègrent de nombreux signaux comprenant l'organisation des structures interagissant avec les extrémités positives et la signalisation induite par divers facteurs intra- et extracellulaires (336). Parmi ces protéines, on dénombre principalement cinq catégories structurales :

• les protéines de la famille EB (End-binding family proteins) : EB1, 2, 3,

• les protéines de la famille CAP-Gly (Cytoskeleton-associated protein Gly-rich proteins) : CLIP170, CLIP115, la sous-unité de la dynactine $p150^{Glued}$,

• les protéines à séquences basiques et riches en sérine : CLASP1/2, ACF7, APC, STIM1,

• les protéines à motifs HEAT et WD40 : LIS1, XMAP215 (*homo sapiens*, CKAP5 ou chTOG),

• les protéines motrices : KIF2C (MCAK) et d'autres kinésines identifiées chez la levure et la drosophile.

Les protéines EB, et notamment EB1, sont des régulateurs majeurs de la dynamique microtubulaire et contrôlent la formation des complexes de +TIP (328, 337). Ces protéines interagissent de façon autonome avec les extrémités positives (338). En outre, elles contiennent un motif d'interaction avec les microtubules qui agit comme un signal de localisation aux extrémités positives, partagé par d'autres +TIP et permettant leur activité stabilisatrice (339-341). EB1 interagit avec plusieurs +TIP, ce qui la place au centre d'intégration du complexe qui coiffe l'extrémité positive des microtubules (337). Néanmoins, il apparait que l'engagement d'EB1 dans ce complexe et sa concentration aux extrémités positives sont des facteurs déterminants pour son action finale sur la stabilité microtubulaire (339, 341). Les protéines de la famille CLIP stabilisent les microtubules en activant leur sauvetage (342, 343). ACF7 et CLASP (CLASP1/2) fonctionnent aussi comme des promoteurs du sauvetage et des stabilisateurs des extrémités positives au niveau du cortex cellulaire (343, 344). Notons d'ailleurs que les protéines CLASP ont également été identifiées comme des facteurs d'assemblage des microtubules ancrés spécifiquement au niveau de l'appareil de Golgi et impliqués dans la migration directionnelle (315). La protéine ACF7 est une protéine cruciale car elle permet la liaison des microtubules avec la F-actine et l'adressage de leurs extrémités positives aux adhésions focales (344, 345). Il faut souligner ici que, bien qu'ils soient des stabilisateurs et/ou des promoteurs de l'assemblage, des protéines telles que EB1/3, les CLASP et ACF7 peuvent aussi

participer à l'augmentation de la fréquence des catastrophes (339, 341, 343, 344). Quant à la protéine oncosuppressive APC, son rôle spécifique consiste à inhiber les catastrophes et à promouvoir la polymérisation au niveau des sites de protrusion (346, 347). La protéine STIM1 permet de coupler la croissance des extrémités positives avec le remodelage du réticulum endoplasmique (348). De plus, bien que son activité soit, comme pour EB1, dépendante de sa concentration et de la composition du complexe +TIP, la protéine XMAP215 (chTOG chez l'homme) est un des plus puissants promoteurs de l'assemblage des microtubules identifiés (322). Son action est assimilée à celle d'une polymérase microtubulaire (349). Notons enfin que les formines (DIAPH1/2), effecteurs de Rho (A.2.b.1), interagissent avec les microtubules et les stabilisent, indépendamment de leurs fonctions régulatrices de la F-actine et possiblement via un mécanisme dépendant de EB1 et APC (350-353).

Comme évoqué plus haut, le contrôle de l'association de plusieurs MAP avec les microtubules par GSK3β font de cette kinase un régulateur majeur de la dynamique microtubulaire (Fig. A.11). Il faut remarquer ici qu'elle participe à l'augmentation de la dynamique microtubulaire selon différentes modalités. Par exemple, elle inactive la protéine CRMP-2 qui promeut l'assemblage des microtubules en interagissant directement avec les hétérodimères de tubuline (354). En outre, elle inhibe par phosphorylation la liaison de MAP stabilisatrices avec les microtubules, dont MAP1B, MAP2C et Tau (355-360). Néanmoins, GSK3β peut aussi favoriser l'action stabilisatrice de certaines MAP, notamment par inhibition des kinases MARK qui empêchent l'interaction de MAP2C, MAP4 et Tau avec les microtubules (361-364). De plus, GSK3β déstabilise les microtubules en inhibant l'association d'APC avec les extrémités positives (365). Cette activité est spécifiquement inhibée pour stabiliser les microtubules au niveau des protrusions par Cdc42 via le complexe Par6-PKCζ (366). En outre, il semble qu'un gradient spatio-temporel de l'activité de GSK3β module également l'association biphasique des CLASP avec les microtubules, récemment décrite dans les cellules migrantes. En effet, alors qu'elles se comportent comme des +TIP au niveau du corps cellulaire, les CLASP se localisent préférentiellement le long des microtubules de la lamella (367). Cette relocalisation est dépendante de l'activité de GSK3β et participe au contrôle de la dynamique microtubulaire de la lamella (368, 369).

Enfin, alors que plusieurs kinésines ont été identifiées chez la levure ou la drosophile comme étant des facteurs déstabilisateurs des microtubules, l'une d'entre elles a été plus particulièrement étudiée dans les cellules mammifères : MCAK (370). Il semble que cette protéine favorise les

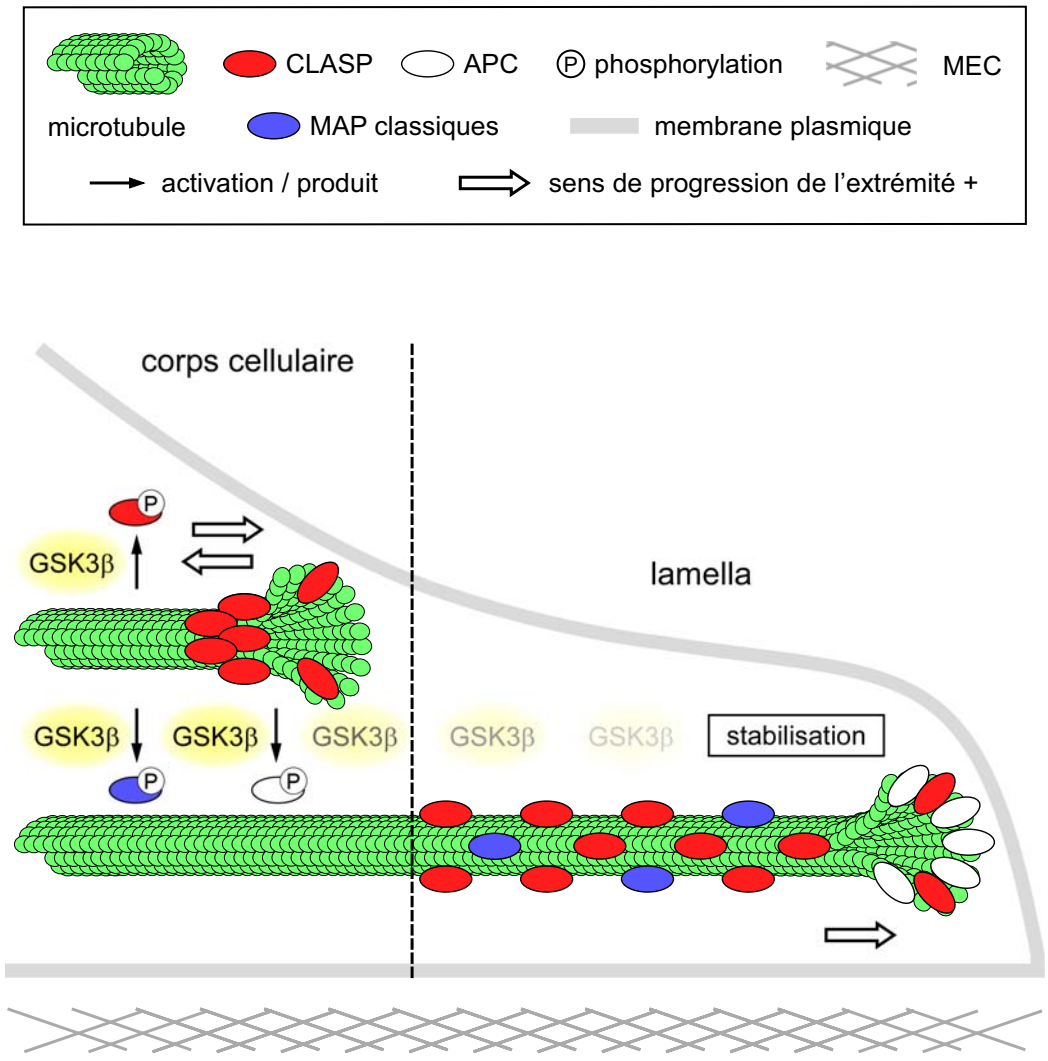

Figure A.11. Modèle de régulation de l'interaction des MAP classiques, des CLASP et d'APC avec les microtubules par GSK3β. Références, A.2.c.2.

catastrophes en s'associant préférentiellement aux protofilaments présentant une courbure proche de celle observée lors de la dépolymérisation (371, 372). Cette affinité structurale, qui s'exerce à la fois aux extrémités négatives et positives, serait donc à l'origine de son activité déstabilisatrice. Alternativement, la stathmine est également un inhibiteur fort de la polymérisation, entravant celle-ci par séquestration des sous-unités de tubuline sous une forme non-assimilable par les protofilaments (322, 373).

A.2.c.3) Modifications post-traductionnelles des microtubules

Les sous-unités de tubuline assemblées au sein des microtubules sont l'objet de différents types de modifications post-traductionnelles réversibles qui régulent potentiellement leurs propriétés physiques et leur pour certaines des protéines évoquées précédemment. Nous évoquerons ici les quatre types majeurs de modifications qui comprennent la polyglycylation, la polyglutamylation, la tyrosination et l'acétylation, sans aborder la déglutamylation de la tubuline détyrosinées (tubuline $\Delta 2$), la phosphorylation et la palmitoylation donc les fonctions sont encore peu étudiées.

• la polyglycylation

Cette modification consiste en l'adjonction d'une chaine de glycines au niveau de résidus glutamate des extrémités C-terminales des tubulines α et β par un mécanisme encore inconnu (374). Elle a été essentiellement étudiée dans le modèle de la Tetrahymena et semble être requise pour la ciliogenèse correcte et la cytokinèse (375, 376).

• la polyglutamylation

Cette modification consiste en l'adjonction d'une chaine de glutamates au niveau de résidus glutamate des extrémités C-terminales des tubulines α et β. Elle est réalisée par les polyglutamylases qui appartiennent à la famille récemment identifiées des TTLL (Tubulin Tyrosin Ligase Like, 377). La polyglutamylation semble réguler l'association de certaines MAP aux microtubules et serait impliquée dans la ciliogenèse, l'assemblage des centrioles, la mitose et les fonctions synaptiques (378-381).

• la tyrosination

Cette modification consiste en l'adjonction d'une tyrosine en position C-terminale de la tubuline α. Cette modification est régulée par un cycle de tyrosination/détyrosination sous l'influence de deux

enzymes : TTCP (tubulin tyrosine carboxypeptidase) qui supprime le résidu tyrosine C-terminal natif de la plupart des tubulines α, et TTL (tubulin tyrosine ligase) qui restore ce groupement (382-384). La déglutamylation de la tubuline détyrosinées (tubuline $\Delta 2$) est réalisée par un mécanisme inconnu et rend la tubuline réfractaire à la tyrosination (374). Il a été montré que la détyrosination n'était pas, à elle seule, suffisante pour stabiliser les microtubules, bien qu'elle soit associée *in vivo* aux microtubules stables (385). Elle semble néanmoins nécessaire à l'interaction de la kinésine-1 avec les microtubules (386, 387). Il a également été montré que la tyrosination était essentielle à la localisation fonctionelle de +TIP de la famille CAP-Gly telles que CLIP170 (388-390). Ces données indiquent donc que la tyrosination pourrait indirectement participer à la stabilisation des microtubules en favorisant le recrutement de +TIP stabilisatrices.

• l'acétylation

Cette modification consiste en l'acétylation de la plupart des tubulines α au niveau de la lysine 40 en position N-terminale après leur intégration au sein des microtubules (374). Bien que son rôle soit encore mal compris, l'acétylation caractérise essentiellement les microtubules stables (391, 392). Des expériences d'acétylation de tubuline purifiée *in vitro* ont montré que cette modification n'avait pas d'influence significative sur l'assemblage des microtubules (393). Elle fut cependant décrite comme un facteur d'association de la kinésine-1 aux microtubules (387, 394). En outre, ce n'est que récemment que le complexe Elongator chez la levure fut proposé comme facteur d'acétylation de la tubuline (395). La réaction inverse, la désacétylation, fut attribuée à l'action de deux enzymes à activité désacétylase : SIRT2 et HDAC6 (396-398). Le niveau d'acétylation est particulièrement sensible à l'activité d'HDAC6 (397, 399-401). De plus, l'acétylation fut associée à la stabilisation des microtubules et à l'inhibition de la motilité (397). Néanmoins, il a été proposé que la désacétylation ne soit pas suffisante par elle-même pour promouvoir la motilité (402). Plus récemment, des expériences d'inhibition de l'activité d'HDAC6 ont d'avantage montré que l'interaction de la forme inactive d'HDAC6 avec les microtubules était probablement un facteur de stabilisation, plus que l'acétylation elle-même (403). Ces travaux ont suggéré qu'HDAC6 pouvait participer à la régulation de la dynamique microtubulaire par interaction avec des +TIP telles que EB1. Par ailleurs, d'autres travaux permirent d'associer la présence d'une forme active d'HDAC6 à la réduction de l'adhésion focale en rapport avec la déstabilisation des microtubules (404).

A.2.c.4) Isoformes de tubuline

Les tubulines α et β qui participent à l'assemblage des microtubules existent sous différentes isoformes (405, 406). A ce jour, il n'existe que peu de données concernant l'influence respective des différentes isoformes de tubuline α. Ces résultats montrent que l'isoforme de tubuline α Tub1 chez la levure, accélère la dynamique microtubulaire en augmentant la vitesse de raccourcissement et la fréquence des catastrophes (407). Dans le même modèle, l'isoforme de tubuline α Tub3 agit de manière opposée sur la dynamique microtubulaire.

L'influence des isoformes de tubuline β fut en revanche plus étudiée, notamment pour son implication dans la chimiosensibilité des tumeurs humaines (406). Le développement d'anticorps monoclonaux contre les isoformes de tubulines β, qui comprennent les formes βI, βII, βIII, βIVa/b et βV, a permis d'adresser *in vitro* le rôle de certaines d'entre elles dans la stabilité microtubulaire. Il fut ainsi montré que la déplétion de la tubuline βIII augmentait la vitesse d'assemblage des microtubules, notamment en présence de MAP telles que MAP2 ou Tau (408). Des résultats similaires furent obtenus avec la déplétion de la tubuline βII (408). L'assemblage à partir de tubuline βII, tubuline βIII et tubuline βIV se révéla plus rapide que celui à partir de tubuline non fractionnée (409, 410). En outre, l'assemblage des filaments assemblés à partir de tubuline βIII purifiée fut initialement décrit comme plus lent que celui obtenu avec les formes βII et βIV (410). Cependant, d'autres travaux ont montré que les filaments résultant exclusivement d'un assemblage à partir de dimères contenant la tubuline βIII sont plus dynamiques avec, en particulier, une instabilité dynamique augmentée au niveau des extrémités positives (411). Enfin, les filaments assemblés à partir de tubuline βII, βIII ou βIV purifiés sont moins sensibles que des filaments assemblés à partir de tubuline non fractionnée à l'action du paclitaxel (412). De plus, alors qu'il fut démontré que le paclitaxel modifiait la dynamique microtubulaire *in vivo*, la modification de celle-ci fut associée à la résistance à ce composé dans les cellules tumorales (413, 414). Enfin, l'augmentation de l'expression de certaines isoformes fut observée dans les lignées tumorales et les cancers, et associée à la résistance aux agents anti-microtubulaires (406, 415, 416). Ces résultats ont donc permis de proposer que la composition relative en isoformes de tubuline β soit un facteur de régulation de la dynamique microtubulaire et de

la chimiosensibilité aux composés anti-microtubulaires. Notons que les modifications de la composition relative en isoformes des tubulines, éventuellement associée à un changement de la dynamique microtubulaire, n'a jamais été corrélée à la transformation des propriétés d'adhésion.

A.2.c.5) Interaction microtubule-adhésion focale et conséquences

De nombreux travaux ont permis d'identifier l'adhésion focale comme un site d'interaction privilégié avec les extrémités positives des microtubules. Il apparait que ces deux structures exercent un influence réciproque, mais l'adhésion focale a également été décrite comme un site d'interrégulation des fibres d'actine et des microtubules (134). Les premières données dans ce domaine ont rapporté que la déstabilisation des microtubules conduisait au renforcement des adhésions focales, notamment par un mécanisme dépendant de l'activation de Rho (417, 418). Ces résultats permirent d'envisager un mécanisme inhibiteur de l'adhésion focale induit par les microtubules. L'interaction des microtubules dynamiques avec les adhésions focales dans les cellules vivantes fut établie en 1998 (419). Ces travaux ont montré que les extrémités positives des microtubules ciblent les adhésions focales au niveau desquelles ils expérimentent de courtes phases de pause. Dans les cellules migrantes, cette interaction est généralement suivie de la dissociation des adhésions focales au niveau du front de rétraction et leur relaxation au niveau du front de migration (420). Plusieurs mécanismes ont été proposés pour expliquer ces phénomènes (Fig. A.12). Le facteur de relaxation des fibres de stress ABL2 (ARG), qui inhibe Rho via GRLF1 (p190ARhoGAP) et atténue la formation des adhésions focales, est associé aux microtubules (421). Similairement, des travaux ont suggéré que les microtubules pouvaient délivrer au niveau des adhésions focales des facteurs de protéolyse impliqués dans la dissociation des fibres de stress (422). Alternativement, certains GEF ont été identifiés comme des protéines associées aux microtubules (423-425). Ces travaux ont permis de proposer un modèle selon lequel les microtubules libèrent, lors de leur dépolymérisation, des GEF qui activent l'assemblage et la contractilité des fibres de stress dépendante de Rho et suppriment ainsi leur liaison aux adhésions focales (Fig. A.12).

Comme nous l'avons vu, certaines données ont indiqué que le renforcement des adhésions focales pouvait survenir consécutivement à la dépolymérisation forcée des microtubules (417, 418,

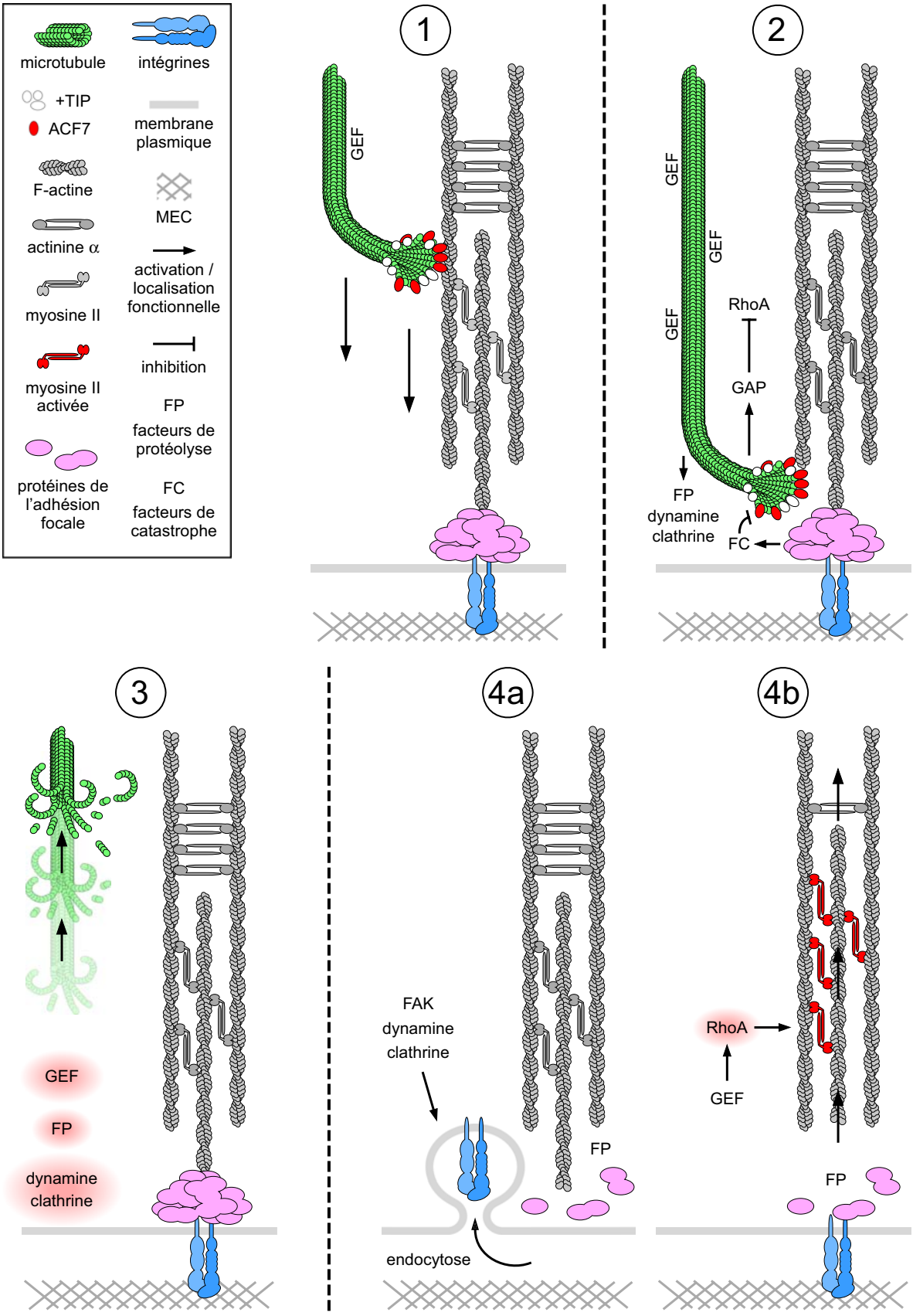

Figure A.12. Principe de dissociation des adhésions focales induite par les microtubules. 1, adressage de l'extrémité positive des microtubules aux adhésions focales via les filaments d'actine et grâce à la protéine de liaison ACF7 ; 2, localisation fonctionnelle de GAP, de facteurs de protéolyse, de la dynamine et de la clathrine au niveau des adhésions focales via les microtubules et activation de facteurs de catastrophe par contact microtubule-adhésion focale ; 3, catastrophe microtubulaire et libération des GEF ; 4a, endocytose des intégrines dépendante de FAK, la dynamine et la clathrine ; 4b, désengagement des fibres de stress dû à l'activation de la contractilité par RhoA. En fonction de leur localisation et de leur niveau de maturation, l'activation de RhoA par contact des microtubules peut également conduire au renforcement des adhésions focales. Références, A.2.c.5.

426). D'autres travaux ont proposé un mécanisme indépendant de Rho et Rac1 mais nécessitant FAK et la dynamine, et conduisant à la dissociation des adhésions focales après recouvrement de la dynamique microtubulaire normale (427). Ce phénomène implique en fait l'endocytose des intégrines par un mécanisme dépendant de la clathrine localisée au niveau des adhésions focales (Fig. A.12 (428). En outre, une étude a montré que la stabilisation forcée des microtubules par une forme inactive d'HDAC6 conduit aussi au renforcement des adhésions focales et à l'inhibition de leur renouvellement (404). L'ensemble de ces résultats démontre que le comportement dynamique normal des microtubules est requis pour la dissociation des adhésions focales et leur renouvellement pendant l'étalement cellulaire et la migration.

Il faut signaler que parallèlement à leur rôle déstabilisateur évoqué ci-dessous, les microtubules sont vraisemblablement, dans certaines situations, des activateurs de l'assemblage des adhésions focales. En effet, les microtubules, par leur capacité à activer Rac1, semblent promouvoir le néo-assemblage des adhésions focales au niveau des protrusions (Fig. A.13, 429, 430). Ce mécanisme pourrait être gouverné par le facteur d'activation de Rac1 et Cdc42, ARHGEF4 (Asef), qui interagit avec la +TIP APC (431, 432). Réciproquement, Rac1 promeut l'assemblage et la stabilité des microtubules au cours de la protrusion au front de migration, possiblement par inhibition du facteur déstabilisateur stathmine, via PAK1 (433, 434). Cdc42 fut également décrite comme un facteur de stabilisation des microtubules, au cour de la protrusion, par sa capacité à promouvoir l'association d'APC aux extrémités positives par inhibition de GSK3β via le complexe Par6-PKCζ (365, 366).

Enfin, les adhésions focales et la signalisation qui leur est associée, notamment impliquée dans de le contrôle de la F-actine, régulent la dynamique microtubulaire. En effet, il a été montré récemment que les adhésions focales induisaient les catastrophes microtubulaires selon un mécanisme dépendant de la paxilline (435). D'après ces données, il semble que la paxilline permette la localisation de facteurs de catastrophe microtubulaire au niveau des adhésions focales (Fig. A.12). Inversement, une signalisation dépendante de FAK et des intégrines a été décrite comme un facteur stabilisateur des microtubules au front de migration par l'intermédiaire de la voie RhoA-DIAPH1/2 (350, 351, 353, 436). Ces travaux indiquent que les formines pourraient participer à la stabilisation microtubulaire grâce à leur capacité à interagir avec les +TIP EB1 et APC (Fig. A.13). Enfin, il a été montré que les filaments d'actine servent de guides pour l'accession des extrémités positives des

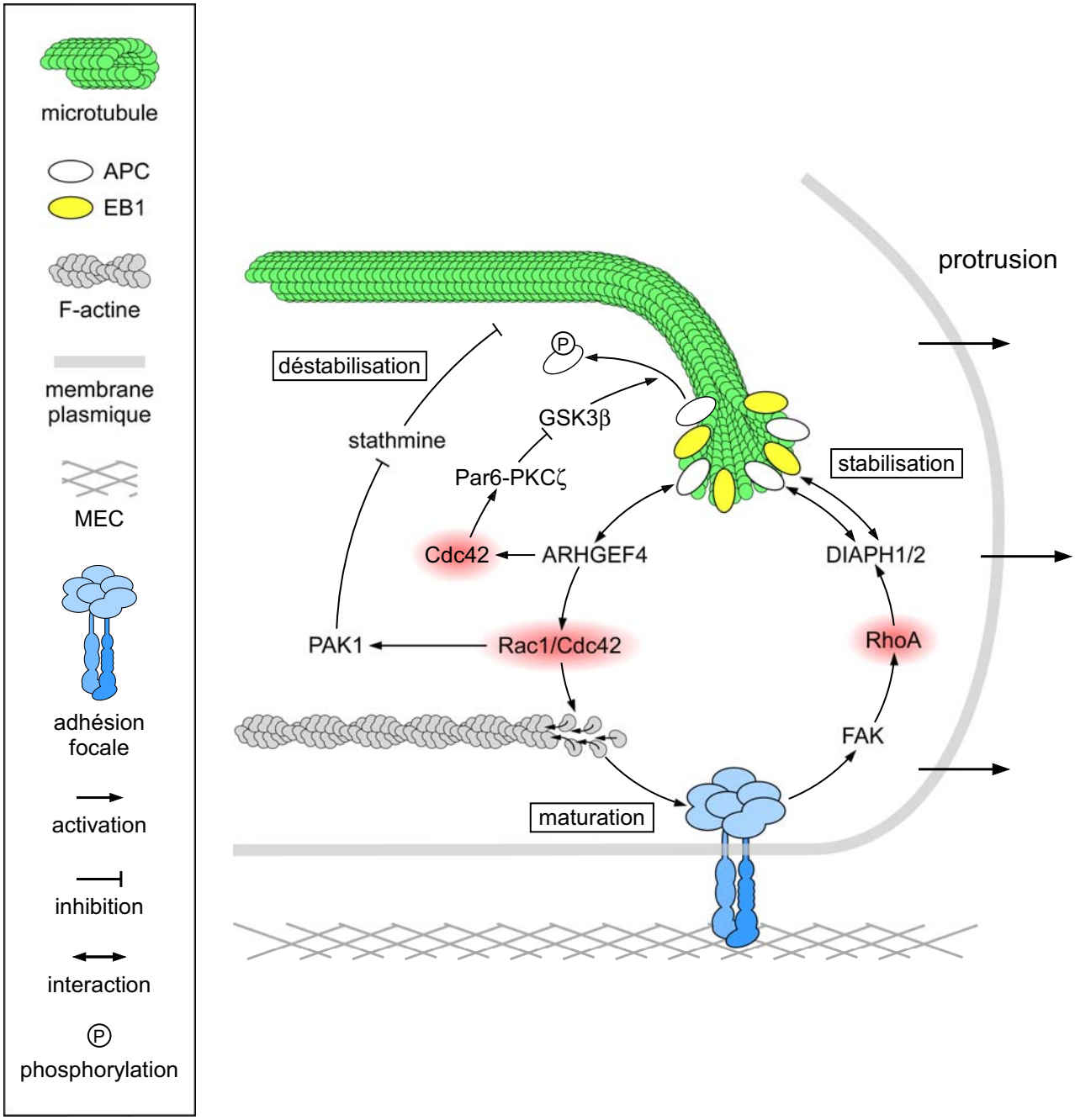

Figure A.13. Stabilisation réciproque des microtubules et des adhésions focales de la lamella. Références, A.2.c.5.

microtubules aux adhésions focales, notamment grâce à la +TIP ACF7 qui sert ici de protéine de liaison (Fig. 8bis, 344, 345, 437). Ce modèle suppose que la stabilité de l'actine et son interaction avec l'adhésion focale sont nécessaires pour la régulation de cette dernière par les microtubules.

A.3) Dynamique cytosquelettique et CKI

Plusieurs travaux, concernant en particulier p27 et p57, indiquent clairement que, outre leurs activités régulatrices du cycle cellulaire, les CKI pourraient être des acteurs clés de la régulation du cytosquelette. En effet, certaines données montrent que p27 et p57 régulent la signalisation dépendante de Rho (124). p57 fut notamment décrite comme un régulateur de la formation des fibres de stress en aval de Rho, via le contrôle des LIMK (438, 439). Cependant, les données contradictoires de ces travaux ne permettent pas encore d'attribuer clairement à p57 un rôle inhibiteur ou activateur au cours de ce processus. En effet, alors que les travaux de Yokoo *et al.* proposent que p57 inhibe LIMK1 par séquestration nucléaire, Vlachos *et al.* montrent au contraire que l'activité de LIMK1 et les fibres de stress sont promues par p57 au niveau cytoplasmique (438, 439). Notons également, que plusieurs études ont montré que p27 était un activateur de la migration, éventuellement associé à l'acquisition de propriétés invasives (440-442). Plus précisément les travaux de Besson *et al.* ont montré que p27 interagissait directement avec RhoA et inhibait son activité et la formation des fibres de stress (442). Cependant, il semble que les conséquences de cette activité sur la migration soient subtilement dépendantes du niveau d'inhibition de Rho et du contexte cellulaire (132, 443). En effet, les cellules tumorales particulièrement présentent une grande hétérogénéité dans les modalités d'acquisition d'un phénotype migratoire (444).

Les premiers travaux évoquant une activité potentielle de p21 sur le cytosquelette ont d'abord été consacrés à la démonstration que p21 est un régulateur de l'assemblage et de la duplication des centrosomes (445-448). Des travaux récents ont également montré que p21, sous l'influence de p53, participe à un point de contrôle en phase G1, sensible à l'intégrité centrosomique (449, 450). Enfin, comme évoqué plus haut, il a été proposé que p21 soit, grâce à sa localisation cytoplasmique et l'inhibition de ROCK1, un promoteur de la migration par inhibition de la formation des fibres de stress dans des fibroblastes transformés par Ras (130, 131). Alternativement, des travaux récents ont

montré que p21 inhibe la migration associée à la transition épithélio-mésenchymateuse (EMT) dans les cellules épithéliales mammaires (451).

B) OBJECTIFS ET PRESENTATION DES TRAVAUX

p21 est fréquemment inactivée dans les cancers épithéliaux. En outre, la progression des tumeurs épithéliales est généralement caractérisée par une désorganisation de l'architecture tissulaire associée éventuellement aux phénomènes d'invasion et de dissémination métastatique (160). Or ces altérations nécessitent la modification de la dynamique cytosquelettique conduisant à la transformation des propriétés d'adhésion et de migration cellulaires (452-454). Au cours de travaux antérieurs à l'étude présentée ici, notre équipe a montré que l'inactivation de p53 conduit à la déstabilisation des microtubules dans les cellules épithéliales mammaires tumorales (416). Par ailleurs, d'autres travaux réalisés précédemment nous ont permis d'établir un lien entre l'inactivation de p21 dans les cellules épithéliales mammaires non transformées et la résistance à un agent anti-microtubulaire, le paclitaxel (H.2, 455).

L'objectif du travail, présenté ici dans le chapitre RESULTATS ET DISCUSSION (C.), est d'examiner le lien possible entre p21 et la dynamique cytosquelettique, et de déterminer son importance dans le contrôle de l'adhésion des cellules épithéliales non transformées (Fig. A.14). Ces résultats ont fait l'objet de la rédaction d'un article actuellement soumis à publication (MANUSCRIT 1, G.). Le chapitre ANNEXES (H.) comprend (i) un manuscrit non publié, trois articles et deux revues publiés concernant des travaux antérieurs à ce projet de thèse, relatifs aux mécanismes de chimiorésistance dans les cancers, et (ii) deux articles publiés, relatifs aux mécanismes d'inactivation des systèmes de sauvegarde cellulaire au cours de la progression tumorale et réalisés en collaboration.

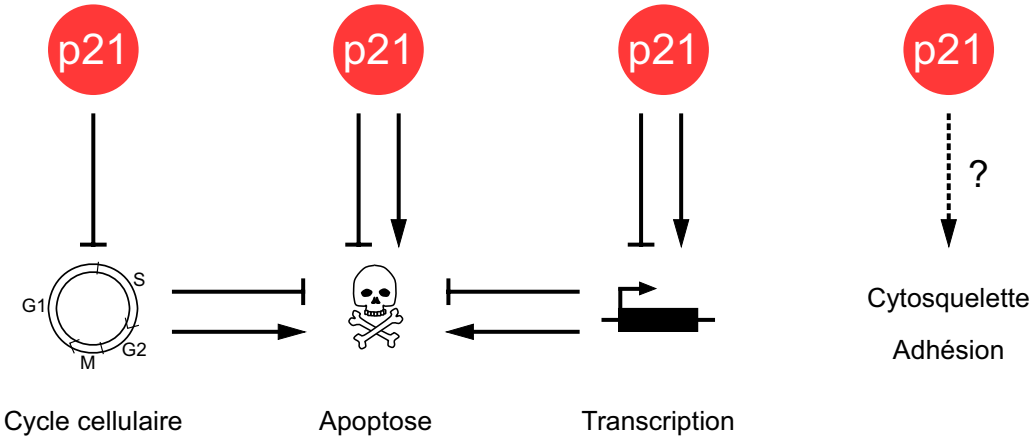

Figure A.14. Résumé des fonctions identifiées de p21.

C) RESULTATS ET DISCUSSION

C.1) p21 est requise pour la morphogenèse bidimensionnelle et la migration normale des cellules épithéliales mammaires non transformées

L'établissement de la morphologie cellulaire implique la coordination dynamique des mécanismes qui régulent l'assemblage et l'organisation spatiale des filaments d'actine et des microtubules. Plus précisément, comme nous l'avons vu, cette morphogenèse est contrôlée par les forces physiques et les voies de signalisation complexes associées à l'interaction de ces fibres avec les membranes et les structures d'adhésion des zones motiles (136-138). Aussi, afin d'identifier une éventuelle influence de p21 sur la dynamique globale du cytosquelette, nous avons d'abord choisi d'analyser les conséquences de son inactivation sur la morphogenèse cellulaire. Pour cela, nous avons utilisé des cellules épithéliales mammaires non transformées. En effet, la transformation maligne, notamment dans les cellules épithéliales, est généralement caractérisée par l'altération de nombreuses voies de signalisation impliquées dans l'homéostasie cytosquelettique (453, 456, 457). L'EMT est un exemple frappant de transformation du cytosquelette associé à la progression tumorale (454). Au cours de ce phénomène, les cellules épithéliales acquièrent un phénotype motile qui s'oppose à leur engagement dans le tissu normal caractérisé par une cohésion cellulaire forte. Aussi, l'utilisation de cellules épithéliales non transformées permet de s'affranchir des altérations cytosquelettiques caractérisant la plupart des lignées cellulaires disponibles, généralement tumorales, et qui peuvent compromettre partiellement l'interprétation des résultats.

Nous avons utilisé des cellules épithéliales mammaires non transformées préalablement immortalisées par transduction virale de la sous-unité catalytique de la télomérase, hTERT (hTMEC ; hTERT-human Mammary Epithelial Cells). Pour des raisons pratiques, nous avons limité les expériences utilisant des cellules épithéliales mammaires non immortalisées (HMEC ; Human Mammary Epithelial Cells). En effet, celles-ci ne se cultivent que durant un temps limité par la sénescence réplicative qu'elles expérimentent généralement au bout de 17 à 18 doublements de population. La transduction lentivirale de deux shRNA différents, ciblant *CDKN1A*, a permis l'obtention,

à la fois dans les hTMEC et dans les HMEC, de deux modèles indépendants d'inactivation stable de p21 (p21KD5, p21KD6, Fig. B.1).

Nous avons observé, de manière préliminaire, une augmentation sensible de la prolifération des cellules p21KD comparées aux cellules contrôles (NT, données non présentées). Cette observation est cohérente avec le rôle antiprolifératif très documenté de p21 (72). Néanmoins, nous avons remarqué que la phosphorylation de Rb reste inchangée par l'inactivation de p21 (Fig. B.1). Ce résultat semble en désaccord avec le modèle selon lequel p21 inhibe le cycle cellulaire en empêchant la phosphorylation de Rb par les CDK2/4/6 et qui prévoit une augmentation de celle-ci en réponse à l'inactivation de p21 (70). Plusieurs travaux antérieurs suggèrent cependant que p21 participe à l'assemblage et la localisation nucléaire des complexes contenant les cyclines de type D associées à CDK4/6 (71, 124). Or, il a été proposé que les complexes contenant CDK4/6 puissent titrer les CKI localisés dans le noyau et favoriser ainsi l'activité des complexes contenant CDK2 (124, 458). Cette hypothèse est renforcée par l'observation d'une activité de CDK2 réduite chez les souris présentant un knock-out des cyclines de type D (459). Donc, dans les cellules p21KD, la perte de l'effet inhibiteur de p21 sur CDK2 pourrait être partiellement compensée par la diminution de la localisation des complexes contenant CDK4/6 et l'augmentation du pool de p27 disponible pour l'inhibition de CDK2. Nous pensons que d'autres phénomènes de compensation, mettant notamment en jeu la modulation de l'expression des CKI, pourraient conduire au maintien de la l'hypophosphorylation de Rb, malgré l'inactivation de p21. Ces données suggèrent également que la perte d'inhibition de PCNA par p21 est ici suffisante pour augmenter significativement la prolifération. Il serait donc intéressant d'explorer la redistribution des localisations et activités des complexes cycline-CDK lorsque p21 est inactivée dans des cellules non-transformées.

Nous avons donc examiné la morphologie des cellules p21KD, cultivées sur support plastique, comparées aux cellules contrôles (Fig. B.2A, C). L'analyse montre que l'inactivation de p21, à la fois dans les hTMEC et les HMEC, a pour conséquence de réduire de 60 à 70% la surface occupée par les cellules (Fig. B.2B, D). Afin de vérifier si cette différence d'étalement était due à un défaut constitutif de l'adhésion, nous avons analysé par vidéomicroscopie le ré-étalement de ces cellules après ensemencement (Fig. B.3A). La mesure de la vitesse d'étalement montre que les cellules p21KD sont

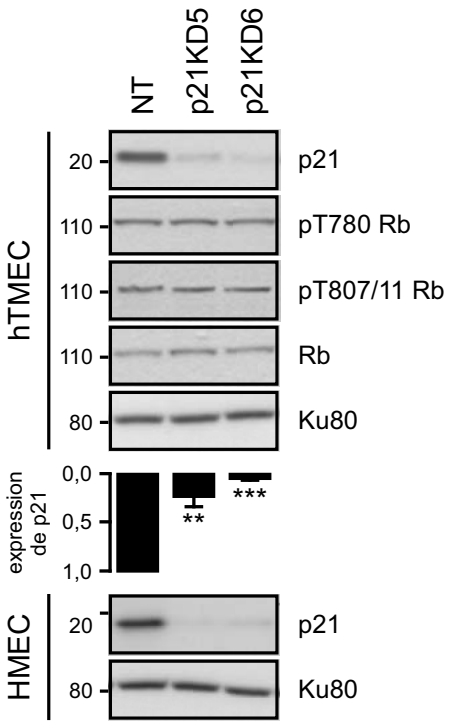

Figure B.1. Inactivation stable de p21 dans les cellules épithéliales mammaires non transformées. Analyse de l'expression de p21, de Rb et de sa phosphorylation au niveau des thréonines 780 et 807/811 de Rb (pT780 Rb, pT807/811 Rb) par western blot dans les cellules épithéliales mammaires immortalisées (hTMEC) transduites pour le shRNA contrôle (NT) ou les shRNA ciblant *CDKN1A* (p21KD5, p21KD6). L'expression de p21 est représentée en unités arbitraires. Analyse de l'expression de p21 par western blot dans les cellules épithéliales mammaires non immortalisées (HMEC) et transduites pour les mêmes vecteurs. Expression de Ku80, contrôle de chargement ; poids moléculaires en kDa. Barre d'erreur, écart type sur trois expériences indépendantes. **, P < 0,005 ; ***, P < 0,001 (test *t*).

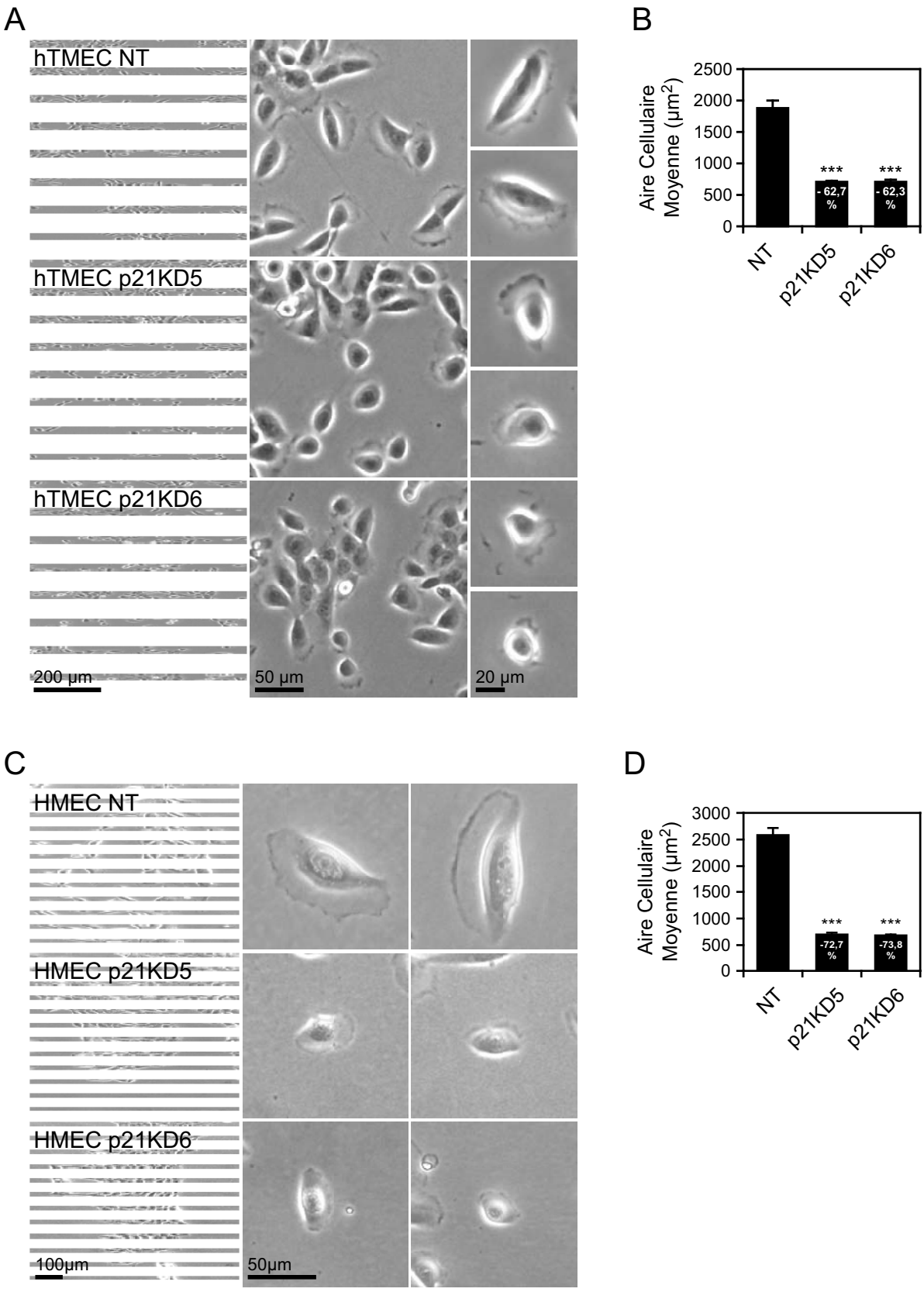

Figure B.2. Conséquences morphologiques de l'inactivation de p21 dans les cellules épithéliales mammaires non transformées. Images acquises en microscopie par contraste de phase de hTMEC (A) ou HMEC (C), contrôles (NT) ou présentant une inactivation stable de p21 (p21KD5, p21KD6). (B) Aire moyenne des hTMEC NT (n = 30), p21KD5 (n = 30) et p21KD6 (n = 30). (D) Aire moyenne des HMEC NT (n = 50), p21KD5 (n = 50) et p21KD6 (n = 50). Le pourcentage de diminution d'aire cellulaire moyenne est indiqué, le cas échéant, sur les graphiques. Barre d'erreur, ESM. ***, P < 0,001 (test t).

Figure B.3. Conséquences de l'inactivation de p21 sur l'adhésion des cellules épithéliales mammaires. (A) Séquence d'images issue d'un enregistrement vidéo représentatif de l'adhésion des cellules NT et p21KD6, 24 h après ensemencement. Barre, 20 µm. (B) Vitesse moyenne d'étalement des cellules NT (*n* = 29), p21KD5 (*n* = 30) et p21KD6 (*n* = 34). Barre d'erreur, ESM. ***, P < 0,001 (test *t*).

plus de deux fois moins aptes à s'étaler que les cellules NT (Fig. B.3A, B). Ceci démontre que l'inactivation de p21 dans les cellules épithéliales mammaires humaines est effectivement associée à un défaut constitutif d'adhésion (Fig. B.3A, B). Notons que cette différence de morphologie fut également observée entre les cellules NT et p21KD, synchronisées en G1 après double-bloc thymidine, ce qui indique clairement que l'effet de l'inactivation de p21 n'est pas relatif à un défaut du cycle cellulaire (données non présentées).

Enfin, pour savoir si le défaut d'adhésion des cellules p21KD a une influence sur leur capacité migratoire, nous avons analysé par vidéomicroscopie leur déplacement individuel, sur support plastique, comparé à celui des cellules contrôles. Nous avons d'abord constaté que, alors que les cellules épithéliales mammaires humaines sont capables de se déplacer sur le support choisi, leur migration isolée est limitée à une zone d'environ 3500 à 4000 μm^2 autour de l'emplacement initial de ré-adhésion après ensemencement. Cette observation est cohérente avec le fait que les capacités migratoires des cellules épithéliales non transformées sont généralement décrites comme relativement limitées, comparativement à leur contrepartie transformée et éventuellement métastatique (460). Cependant, nous avons quand même pu constater que la vélocité des cellules p21KD est diminuée d'environ 50% par rapport aux cellules contrôles (Fig. B.4A, B). Du fait de la faible amplitude de leur déplacement, la persistance directionnelle des cellules épithéliales mammaires migrantes a été calculée à partir de séquences de migration de courte durée (35 min, Fig. B.4A, C). Ainsi, nous avons déterminé que la capacité des hTMEC à conserver une persistance directionnelle au cours de leur mouvement est significativement altérée par l'inactivation de p21 (Fig. B.4A, C).

Par ailleurs, on sait aujourd'hui que les cellules épithéliales qui conservent les propriétés de cohésion intercellulaire forte caractérisant leur tissu d'origine, peuvent néanmoins présenter des propriétés migratoires collectives quantifiables, et éventuellement altérées (461). Les modifications de la migration épithéliale collective peuvent ainsi être observées *in vitro* pendant la cicatrisation d'une blessure artificiellement provoquée sur un tapis cellulaire monocouche (452, 456, 462). Ce test appliqué aux cellules p21KD, comparées aux cellules contrôles, révèle que la migration épithéliale collective est réduite par l'inactivation de p21, de façon cohérente avec l'altération de l'adhésion et de la migration individuelle observées précédemment (Fig. B.4D). Toutes ces données indiquent donc

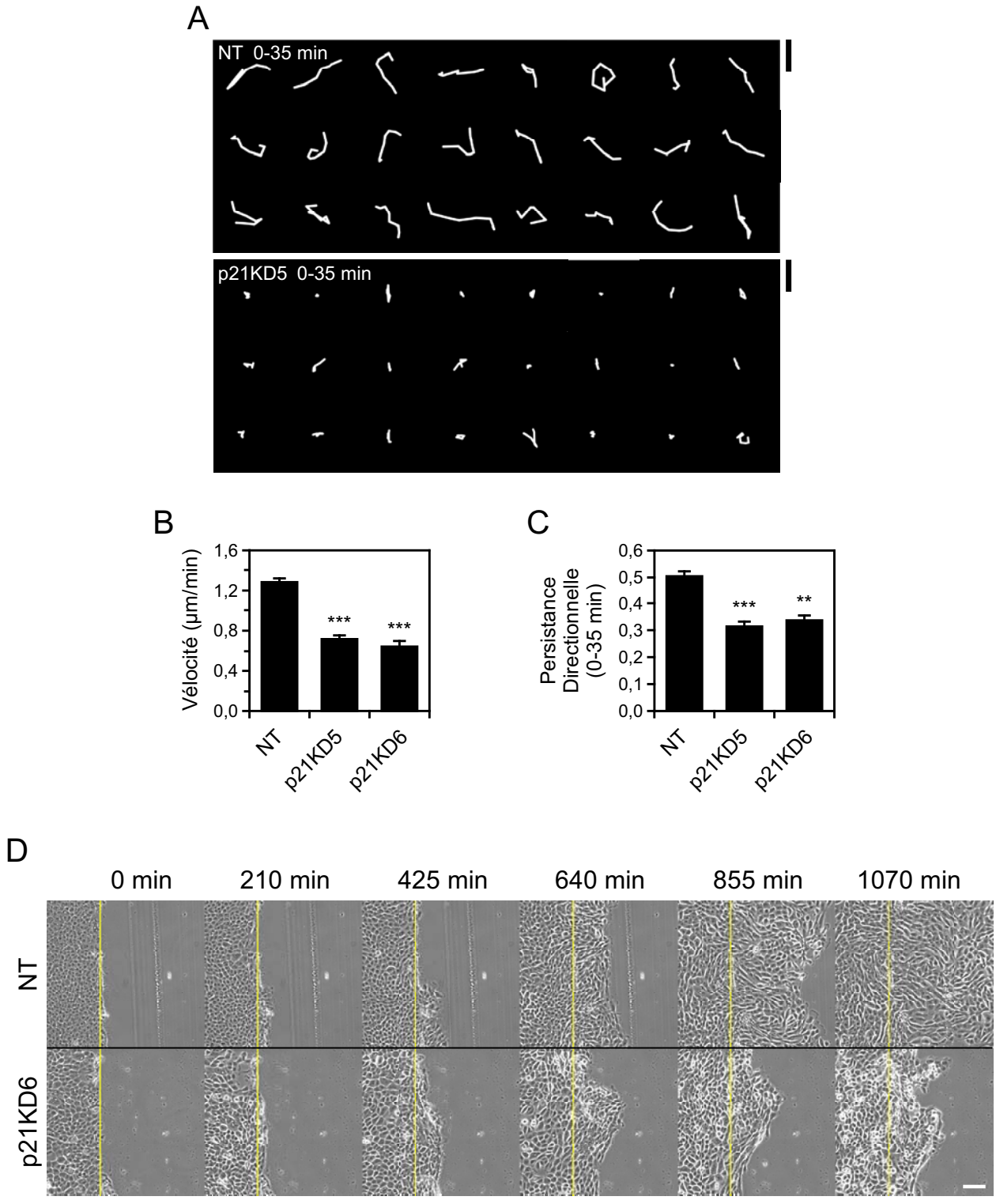

Figure B.4. Conséquences de l'inactivation de p21 sur la migration des cellules épithéliales mammaires. (A) Représentation du déplacement cellulaire obtenu à partir d'enregistrements vidéo en microscopie par contraste de phase de la migration des cellules NT and p21KD5. Barre, 50 µm. (B) Vélocité moyenne des cellules NT (*n* = 35), p21KD5 (*n* = 61) et p21KD6 (*n* = 41), basée sur l'analyse de séquences de migration de 90 min obtenues selon la méthode décrite en (A). (C) Persistance directionnelle calculée à partir de séquences de migration de 35 min pour les cellules NT (*n* = 56), p21KD5 (*n* = 60), p21KD6 (*n* = 40). (D) Séquence d'images acquises en microscopie par contraste de phase et issues d'un enregistrement vidéo de la migration cellulaire au cours d'un test de cicatrisation de blessure sur les cellules NT et p21KD6. Barre, 100 µm. Barre d'erreur, ESM. **, P < 0,005 ; ***, P < 0,001 (test *t*).

que p21 est nécessaire pour la morphogenèse, l'adhésion et la migration normale des cellules épithéliales mammaires humaines non transformées.

C.2) p21 contribue à la formation de l'adhésion focale

Afin de mieux comprendre l'origine du défaut d'adhésion provoqué par l'inactivation de p21, nous avons décidé d'examiner l'adhésion focale dans les cellules p21KD. Pour cela, nous avons mis au point un modèle d'hTMEC p21KD et contrôles, exprimant stablement la protéine de fusion GFP-paxilline (GP-hMEC, Fig. B.5A). La paxilline est une protéine essentielle des structures d'adhésion incluant les complexes focaux, les adhésions focales qui en sont dérivées et les adhésions fibrillaires qui représentent une forme d'adhésion focale alternative (141). Les GP-hMEC permettent donc d'observer, par microscopie à fluorescence, la formation et la dynamique de ces structures d'adhésion dans les cellules vivantes (463-465). La classification de ces structures est essentiellement basée sur leur morphologie et leur composition moléculaire (A.2). Cette caractérisation a été réalisée sur des cellules - généralement des fibroblastes - cultivées sur un support contenant des éléments facilitant l'assemblage des adhésions focales, comme la fibronectine. En outre, il a été montré que la fibronectine peut également favoriser l'EMT des cellules épithéliales mammaires (466). Nous avons ici utilisé le modèle des cellules épithéliales mammaires humaines sur support plastique ou verre. Par ailleurs, nous pensons que l'utilisation des ces supports ne permet pas de se référer directement à la classification des structures précédemment évoquée, notamment en terme de surface d'adhésion. Aussi, bien que nous adressions la question de l'aire des structures marquées par la paxilline-GFP, nous les désignons ici, de façon simplifiée, par le terme d' « adhésions focales », indépendamment de leur taille, de leur localisation ou de leur dynamique. La quantification des adhésions focales a ainsi montré que l'inactivation de p21 diminue de plus de moitié leur nombre (Fig. B.5B). De plus, l'aire des adhésions focales dans les cellules p21KD est significativement diminuée par rapport aux cellules contrôles (Fig. B.5C).

En outre, comme évoqué ci-dessus, les adhésions focales des cellules migrantes présentent une hétérogénéité de taille due aux différents stades de maturation et à leurs localisations fonctionnelles (136, 141, 467-469). Nous n'avons pas fait ici la distinction morphologique et moléculaire entre ces

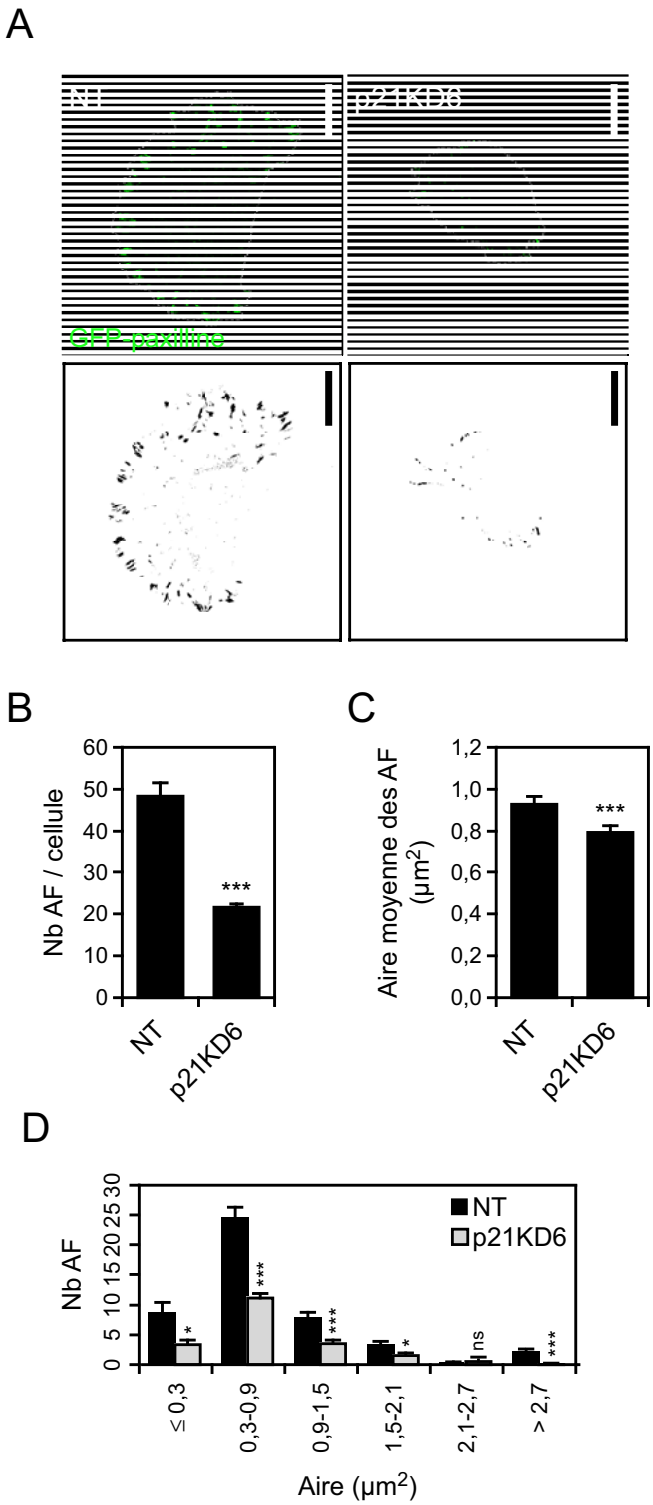

Figure B.5. Conséquences de l'inactivation de p21 sur l'adhésion focale. (A) Images de GP-hMEC NT et p21KD6 vivantes, obtenues en microscopie à fluorescence (haut) et images binaires correspondantes (bas). Ligne pointillée grise, contour cellulaire. (B) Nombre moyen (Nb) de structures d'adhésion focale (AF) dans les cellules NT (*n* = 13) et p21KD6 (*n* = 13). (C) Aire moyenne des AF dans les cellules NT (13 cellules, 629 AF) et p21KD6 (13 cellules, 282 AF). (D) Distribution de l'aire des AF dans les cellules NT (*n* = 13) et p21KD6 (*n* = 13). Barre, 20 µm. Barre d'erreur, ESM. *, P < 0,05 ; ***, P < 0,001 ; ns, non significatif (test *t*).

différents types de structure dans les cellules épithéliales mammaires cultivées sur support plastique ou verre. Pourtant, nous avons voulu connaître la distribution de l'aire des adhésions focales dans les cellules p21KD comparées aux cellules contrôles. Cette analyse a montré que la diminution de leur taille moyenne n'est pas due à l'altération d'une sous-population mais concerne en fait toutes les adhésions focales (Fig. B.5D). L'analyse par vidéomicroscopie à fluorescence des GP-hMEC montre en outre que la fréquence d'assemblage des adhésions focales est fortement diminuée par l'inactivation de p21 (Fig. B.6A, B).

Enfin, dans le but de mieux caractériser l'altération des adhésions focales dans les cellules p21KD, nous avons exploré la phosphorylation de FAK et Src qui sont deux régulateurs essentiels de leur assemblage (A.2.a, A.2.b.3). Alors que la phosphorylation de Src n'est pas altérée, la phosphorylation de FAK subit une forte diminution suite à la perte de p21 (Fig. B.6C). Ce résultat suggère que, malgré un maintien partiel des étapes primordiales d'assemblage de l'adhésion focale, l'activation de FAK reste limitée dans les cellules p21KD. L'ensemble de ces données démontre que p21 est requise pour la dynamique normale de l'adhésion focale dans les cellules épithéliales mammaires humaines non transformées.

C.3) p21 régule l'assemblage des fibres de stress

L'interrégulation des adhésions focales et des structures d'actine est un élément fondamental de la dynamique d'adhésion et de la morphogenèse cellulaire. Comme nous l'avons vu, les fibres de stress participent à la maturation des adhésions focales mais également à leur renouvellement (A.2.b.3). Réciproquement, les adhésions focales, en particulier via le complexe FAK-Src, participe à la fois à la polymérisation de l'actine, l'assemblage des fibres de stress et leur contractilité. Du fait du défaut majeur d'adhésion focale observé dans les cellules p21KD, nous avons décidé d'explorer les conséquences de l'inactivation de p21 sur l'assemblage des fibres de stress. De manière frappante, notre analyse montre que la formation des fibres de stress est sévèrement altérée par l'inactivation de p21 (Fig. B.7A, B). Néanmoins, la quantité totale de F-actine est inchangée par l'inactivation de p21 (Fig. B.7C). Ces résultats indiquent que, malgré le maintien de la polymérisation de l'actine,

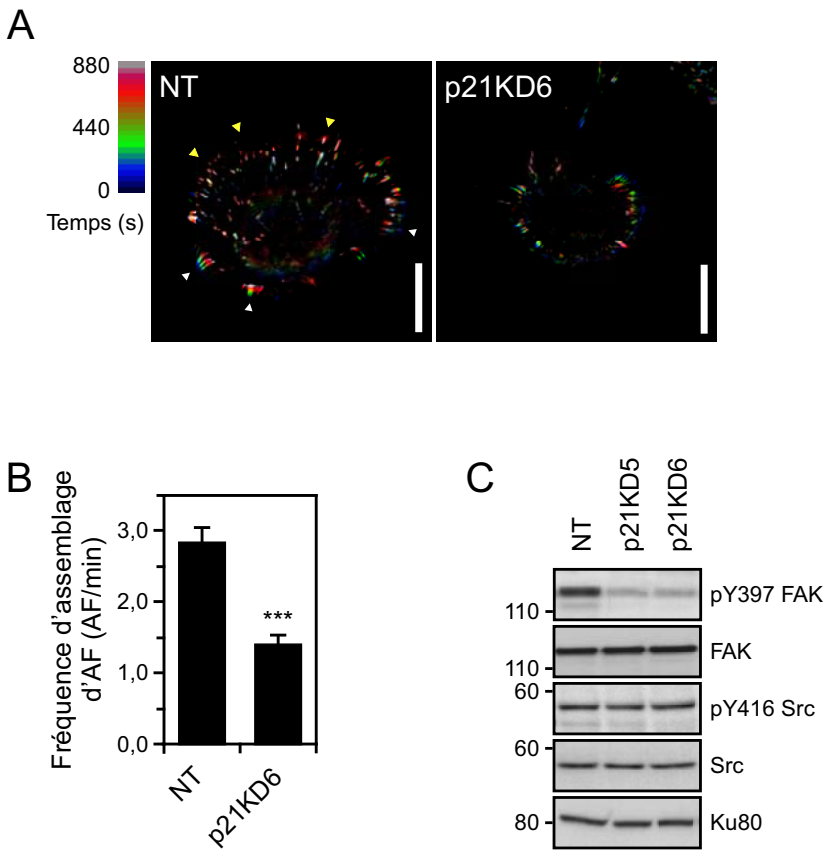

Figure B.6. Conséquences de l'inactivation de p21 sur la dynamique d'assemblage de l'adhésion focale (AF) et son activation. (A) Représentation de la dynamique d'AF basée sur la superposition d'images d'une même séquence de vidéomicroscopie à fluorescence réalisée sur les cellules GP-hMEC NT et p21KD6 vivantes, et un codage temporel par le spectre de couleur présenté à gauche. Les flèches jaunes indiquent les AF néoformées dans la zone lamellaire du front de migration. Les flèches blanches indiquent les AF "glissantes" dans la zone de rétraction. Barre, 20 µm. (B) Fréquence d'assemblage d'AF dans les cellules NT (n = 6) et p21KD6 (n = 6). (C) Analyse par western blot de la phosphorylation de FAK (pY397) et de Src (pY416) comparées à l'expression de FAK et Src totales dans les cellules NT, p21KD5, p21KD6. Expression de Ku80, contrôle de chargement ; poids moléculaires en kDa. Barre, 20 µm. Barre d'erreur, ESM. ***, P < 0,001 ; ns, non significatif (test t).

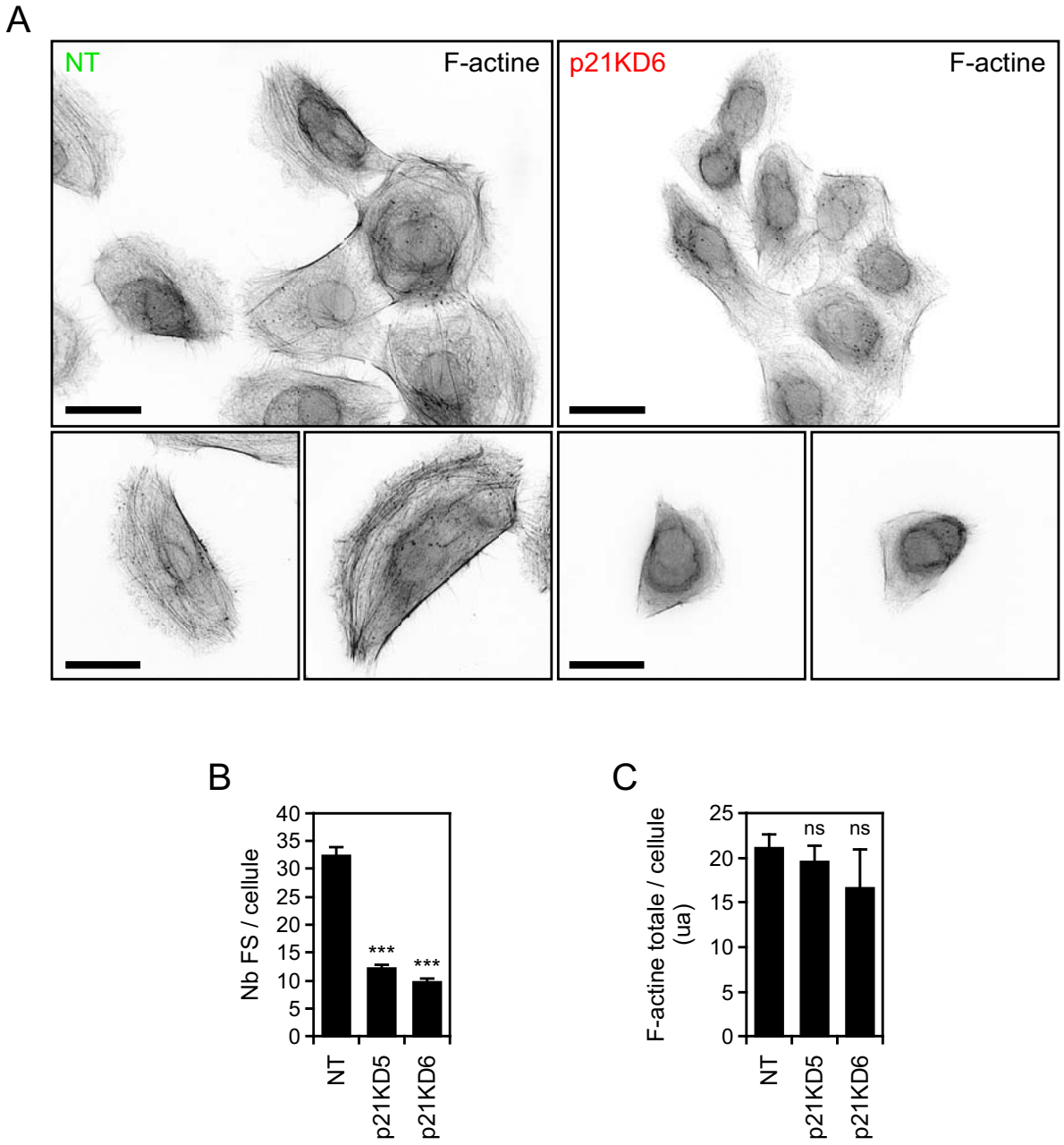

Figure B.7. Conséquences de l'inactivation de p21 sur la formation des fibres des stress. (A) Visualisation de la F-actine dans les cellules NT et p21KD6 par marquage avec la phalloïdine couplée au TRITC. Les images sont traitées comme indiqué dans la section D. Barre, 20 µm. (B) Numération (Nb) des fibres de stress (FS) dans les cellules NT (*n* = 34), p21KD5 (*n* = 30) et p21KD6 (*n* = 31). (C) Quantification de la F-actine totale par mesure de la fluorescence totale dans les cellules NT (*n* = 45), p21KD5 (*n* = 45) et p21KD6 (*n* = 44) marquées comme en (A), et exprimée en unités arbitraires (ua). Barre d'erreur, ESM. ***, P < 0,001 ; ns, non significatif (test *t*).

l'inactivation de p21 compromet l'intégrité des filaments et/ou leurs systèmes de liaison pour empêcher l'assemblage des fibres de stress.

C.4) p21 régule l'activité de la GTPase Rho et de la cofiline

C.4.a) Activités des Rho GTPases et de la cofiline dans les cellules p21KD

Du fait de l'altération majeure du réseau d'actine consécutive à l'inactivation de p21, nous avons décidé d'analyser l'activité des GTPases RhoA/B/C (Rho), Rac1 et Cdc42. En effet, ces GTPases sont des régulateurs pléiotropiques de la dynamique et de l'organisation des filaments d'actine (A.2.b.1). Nos résultats montrent que les activités de Rac1 et Cdc42 ne sont pas significativement modifiées, alors que l'activité de Rho est fortement diminuée par la déplétion de p21 (Fig. B.8A). En suite, nous avons souhaité examiner l'éventuel lien entre cette altération et le défaut d'assemblage des fibres de stress dans les cellules p21KD. Pour cela, nous avons choisi d'explorer certaines voies de signalisation modulées par Rho et régulant la formation des fibres de stress. Nous nous sommes plus particulièrement intéressés à l'activité de la cofiline qui agit comme un effecteur commun des voies ROCK-LIMK et PKCμ-SSH1L pour réguler la polymérisation et l'organisation de l'actine (A.2.b.1, Fig. A.6).

Lorsqu'elle est hypophosphorylée, la cofiline agit comme un facteur de dislocation des filaments d'actine, favorisant le désassemblage et le renouvellement des fibres de stress. Or, la phosphorylation de la cofiline est considérablement diminuée par la perte de p21, à la fois dans les hTMEC et les HMEC (Fig. B.8B). Comme nous l'avons vu précédemment, la cofiline permet la production de nouvelles extrémités barbelées afin d'activer la polymérisation dans les zones de protrusion (A.2.b.1). L'activité protrusive du lamellipode est donc hautement dépendante de la dynamique de l'actine dépendante de la cofiline. Aussi, affin de mieux comprendre les conséquences de l'hypophosphorylation de la cofiline sur la dynamique de l'actine dans les cellules p21KD, nous avons choisi d'étudier la formation des protrusions par vidéomicroscopie (Fig. B.9). Cette analyse a montré que l'inactivation de p21 est accompagnée d'une altération profonde de la dynamique protrusive caractérisée par une augmentation de la persistance, une vélocité diminuée et une fréquence de protrusion près de trois

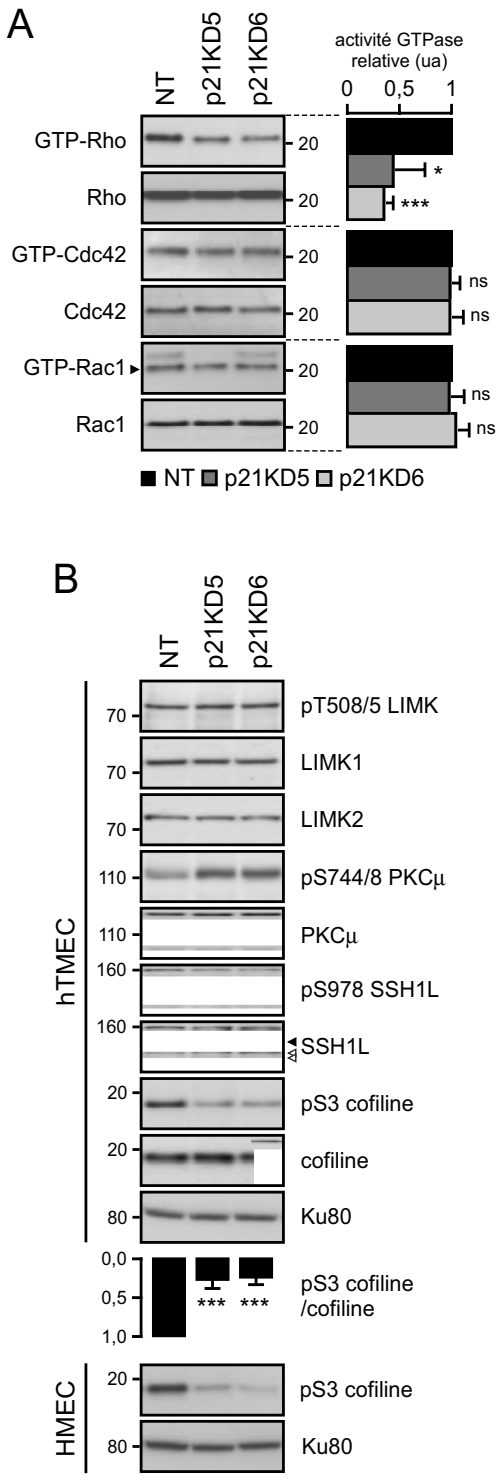

Figure B.8. Conséquences de l'inactivation de p21 sur la signalisation contrôlée par la GTPase Rho. (A) Quantification de l'activité des GTPases RhoA/B/C (Rho), Rac1 et Cdc42 dans les cellules NT et p21KD. L'activité GTPase relative a été déterminée selon trois expériences indépendantes comme indiqué dans la section D, et est exprimée en unités arbitraires (ua). Barres d'erreur, écart type. Flèche noire, signal spécifique de Rac1. (B) Analyse par western blot de l'expression de pT508/5 LIMK, LIMK1 et LIMK2 totales, pS744/8 PKCμ, PKCμ totale, pS978 SSH1L, SSH1L totale (flèche noire, forme phosphorylée; flèches blanches, formes hypophosphorylées), la pS3 cofiline et la cofiline totale dans les hTMEC NT, p21KD et p21KD6 ; analyse par western blot de l'expression de la pS3 cofiline dans les HMEC NT, p21KD et p21KD6. Le niveau relatif de phosphorylation de la cofiline (pS3 cofiline/cofiline) est exprimé en unités arbitraires. Expression de Ku80, contrôle de chargement ; poids moléculaires en kDa. Barre d'erreur, écart type (trois expériences indépendantes). *, $P < 0,05$; ***, $P < 0,001$; ns, non significatif (test *t*).

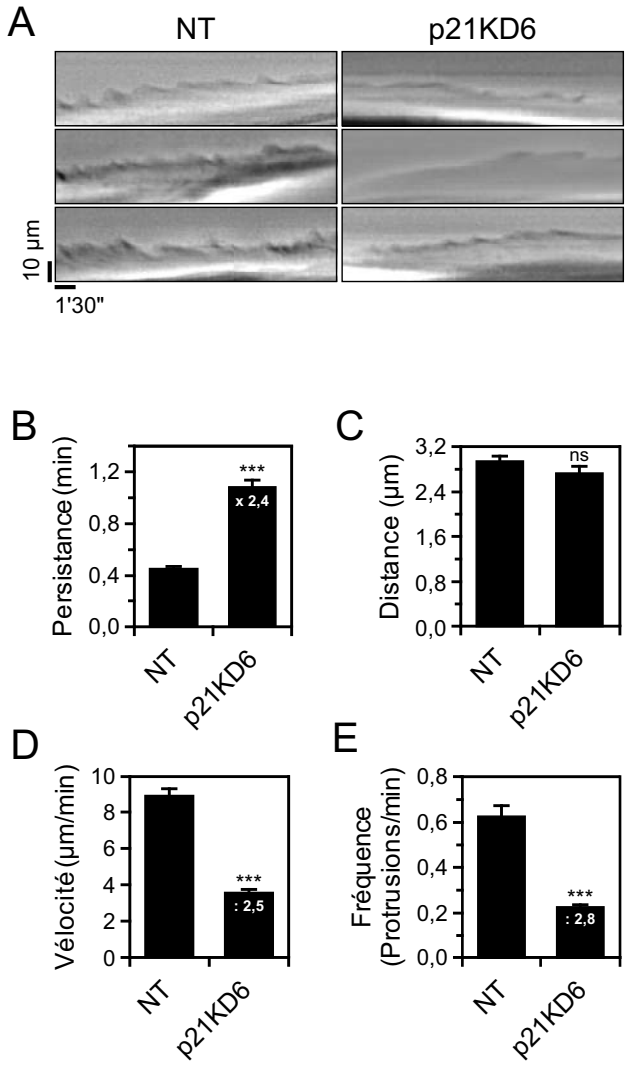

Figure B.9. Conséquences de l'inactivation de p21 sur la dynamique de protrusion. (A) Présentation kymographique de la position du bord de la lamella dans les hTMEC NT et p21KD6 en fonction du temps. Barre verticale, 10 µm; barre horizontale bar, 1 min 30 s. Les graphiques en (B), (C), (D) et (E) présentent respectivement la persistance, la distance, la vélocité et la fréquence de protrusion dans les hTMEC NT (16 cellules, 200 mesures) et p21KD6 (39 cellules, 174 mesures). Le facteur d'augmentation ou de diminution est indiqué, le cas échéant, sur les graphiques. Barre d'erreur, ESM. ***, P < 0,001 ; ns, non significatif (test *t*).

fois moins élevée que dans les cellules contrôles (Fig. B.9A-E). L'ensemble de ces données suggèrent donc que la cofiline est hyperactive dans les cellules dépourvues de p21, conduisant ainsi à la dislocation continue des filaments d'actine et entravant l'assemblage des fibres de stress, la formation des protrusions et l'étalement cellulaire.

C.4.b) Activité de la voie ROCK-LIMK dans les cellules p21KD

En aval de Rho, la voie de signalisation ROCK-LIMK conduit à l'inhibition de la cofiline par phosphorylation de la serine 3 (A.2.b.1, Fig. A.6). Nous avons donc supposé que l'inactivation de cette voie pouvait être à l'origine de l'hypophosphorylation de la cofiline observée dans les cellules p21KD. Mais, nous n'avons pas détecté de diminution de la phosphorylation des LIMK, marqueur d'activation de la voie ROCK-LIMK (Fig. B.8B). Pourtant, l'inhibition spécifique des ROCK par l'Y-27632 réduit considérablement la phosphorylation des LIMK et de la cofiline, de même que l'inhibition spécifique des LIMK par le peptide S3 conduit à une diminution de la phosphorylation de la cofiline (Fig. B.10A). Par ailleurs, l'inhibition spécifique de Rho par l'exoenzyme C3 inhibe la phosphorylation de la cofiline mais ne modifie pas celle des LIMK (Fig. B.10B). Donc, d'après ces données, bien que la voie ROCK-LIMK-cofiline soit fonctionnelle, il semble que l'inactivation de Rho ne soit pas suffisante pour altérer l'activation des LIMK par ROCK dans les cellules épithéliales mammaires non transformées.

Notons que des études précédentes ont montré que, dans des cellules transformées, la forme cytoplasmique de p21 supprime la phosphorylation de la cofiline en inhibant, par interaction directe, ROCK1 (130, 131). Le modèle proposé par ces travaux prévoit que l'inactivation de p21 soit associée à une augmentation de la phosphorylation de la cofiline. Notre étude montre, au contraire que l'inactivation de p21 provoque une réduction de la phospho-cofiline. Cependant, il faut remarquer que ces études ont été réalisées dans des cellules hautement transformées (fibroblastes NIH/3T3 transformés par Ras, cellules de neuroblastome N1E-115 et 293T) dans lesquelles la forme cytoplasmique de p21 est fortement favorisée, en particulier après phosphorylation par AKT en réponse à l'activation oncogénique de la voie H-RAS-PI3K (130, 131). Cependant ces travaux n'adressent pas les effets de p21 sur la voie ROCK-LIMK-cofiline en conditions physiologiques. Par ailleurs, les lignées utilisées présentent de nombreuses altérations, notamment génétiques, qui les

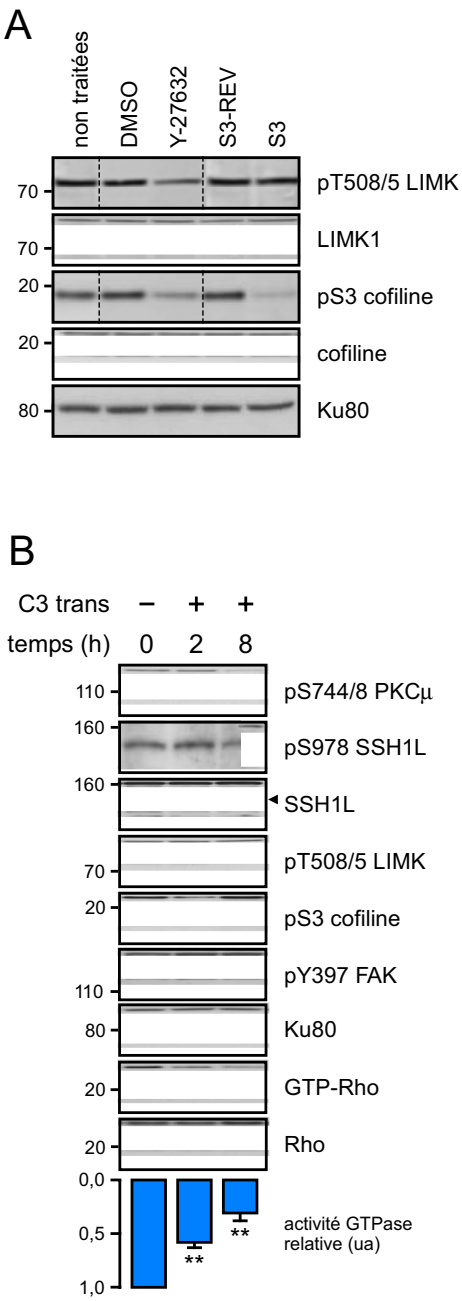

Figure B.10. Dépendance des voies de signalisation ROCK-LIMK et PKCμ-SSH1L vis-à-vis de la GTPase Rho dans les cellules épithéliales mammaires non transformées. (A) Analyse par western blot de l'expression de pT508/5 LIMK, LIMK1 totale, la pS3 cofiline et la cofiline totale dans les hTMEC non traitées, ou traitées pendant 12 h avec l'inhibiteur de ROCK Y-27632 (20 μM; contrôle, DMSO) ou le peptide S3, inhibiteur de LIMK (40 μg/mL; contrôle, peptide S3-REV). Les lignes pointillées verticales délimitent les blots issus de gels indépendants. (B) Analyse par western blot de l'expression de pS744/8 PKCμ, pS978 SSH1L, SSH1L totale, pT508/5 LIMK, la pS3 cofiline, pY397 FAK, GTP-Rho et Rho total dans les hTMEC non traitées, ou traitées pendant 2 ou 8 h avec l'inhibiteur spécifique de Rho, l'exoenzyme C3 transferase (C3 trans, 0,5 μg/mL). L'activité GTPase de Rho a été quantifiée selon trois expériences indépendantes comme indiqué dans la section D, et est exprimée en unités arbitraires (ua). Barre d'erreur, écart type. **, P < 0,005 (test *t*).

rendent moins pertinentes que les HMEC pour comprendre la régulation du cytosquelette des cellules épithéliales humaines. Néanmoins, il serait tout à fait judicieux, pour compléter notre étude, de vérifier si l'interaction de p21 et ROCK1 existe dans les cellules épithéliales mammaires humaines et si elle influence réellement l'activité de la voie ROCK-LIMK dans des cellules épithéliales non transformées.

La phosphorylation de la cofiline par les LIMK a été décrite comme un phénomène dépendant du cycle cellulaire (470, 471). L'analyse de la phosphorylation de la cofiline dans les cellules NT et p21KD synchronisées par double-bloc thymidine montre, de façon cohérente avec les travaux antérieurs, que celle-ci est effectivement éteinte après la mitose et similairement à la phosphorylation de LIMK (données non présentées). Néanmoins, nous avons observé que l'hypophosphorylation de la cofiline dans les cellules p21KD comparées aux cellules contrôles, était maintenue tout au long du cycle cellulaire. Ceci indique clairement que le défaut de phosphorylation de la cofiline dans les cellules p21KD n'est pas dû à un défaut du cycle provoqué par la perte de p21, mais qu'il correspond plutôt à la suppression d'une fonction de p21 indépendante du cycle.

C.4.c) Activité de la voie PKCμ-SSH1L dans les cellules p21KD

Sous sa forme hypophosphorylée et associée à la F-actine, SSH1L est un activateur de la cofiline, grâce à son activité phosphatase ciblée sur la sérine 3 (A.2.b.1, Fig. A.6, 220, 221, 472-474). Or, nous avons observé une hypophosphorylation significative de SSH1L dans les cellules p21KD (Fig. B.8B). Un modèle proposé récemment suggère que la kinase PKCμ recrute la forme hypophosphorylée de SSH1L au niveau de la F-actine périphérique, permettant ainsi l'activation de la cofiline par déphosphorylation. En revanche, en condition d'activation par Rho, PKCμ phosphoryle SSH1L qui est dissociée de la F-actine et se localise au niveau cytoplasmique sous sa forme inactive, associée aux protéines 14-3-3β/ζ (220, 221). La phosphorylation de PKCμ est généralement considérée comme un marqueur de son activité, et du fait de l'inactivation de Rho dans les cellules p21KD, nous nous attendions à observer une diminution de celle-ci. Mais c'est au contraire une augmentation de la phosphorylation de PKCμ que nous avons détectée dans les cellules p21KD (Fig. B.8B). En considérant l'hypophosphorylation de SSH1L dans ces cellules, nous pensons que PKCμ ne peut pas phosphoryler

SSH1L, possiblement du fait de la déstabilisation importante du réseau d'actine, empêchant leur colocalisation fonctionnelle (220). Pour tester cette hypothèse, il faudrait explorer par immunomarquage et immunoprécipitation, dans les cellules p21KD, la capacité de PKCμ à interagir avec SSH1L. De même, des expériences de précipitation spécifique de la F-actine pourraient être réalisées pour quantifier la proportion relative de PKCμ et SSH1L interagissant avec celle-ci dans les cellules p21KD. Nous n'excluons pas que les cellules p21KD présentent une activation anormale de phosphatases contribuant à l'hypophosphorylation de SSH1L. Néanmoins, le système impliqué dans la déphosphorylation de SSH1L n'ayant pas encore été clairement identifié, son implication dans le phénotype des cellules p21KD n'a pas pu être adressée ici.

Il a été montré que l'activation de la voie EGF-PLCγ-PKC conduisait à la phosphorylation de PKCμ (475). Donc l'hyperphosphorylation de PKCμ pourrait être due à l'activité de cette voie. Comme nous l'avons vu, l'EGF participe à l'activation de la cofiline. La voie EGF-PLCγ-PIP2 pourrait donc potentialiser l'activation de la cofiline dans les cellules p21KD qui sont, comme les cellules contrôles, cultivées en présence d'EGF (B.4.a, 208, 220). De plus, des données non présentées ici, issues d'une étude transcriptionnelle nous permettent d'envisager la possibilité que la surexpression de l'EGFR participe également à la suractivation de la cofiline et la phosphorylation de PKCμ.

Nous montrons, d'autre part, que l'inhibition transitoire de Rho pendant 2h par l'exoenzyme C3 est suffisante pour diminuer la phosphorylation de la cofiline (Fig. B.10B). Cependant, cette expérience montre qu'après 8h de traitement, la phospho-cofiline recouvre son niveau normal, malgré une inactivation de Rho accrue. Ceci indique que la phosphorylation de la cofiline est un phénomène tamponné, vraisemblablement du fait des nombreuses voies de signalisation impliquées dans sa régulation. De plus, cette expérience montre aussi que l'inhibition transitoire de Rho pendant 2 à 8h n'est pas suffisante pour modifier la phosphorylation de SSH1L, tandis que celle de PKCμ diminue, mais seulement après 8h de traitement (Fig. B.10B). Ces résultats suggèrent d'abord que l'hypophosphorylation de SSH1L n'est pas une conséquence directe de l'inactivation de Rho dans les cellules p21KD. Cependant, à ce stade, nous ne pouvons pas exclure que cette altération participe au maintien de la cofiline sous sa forme hypophosphorylée. En outre, l'hypophosphorylation de SSH1L dans les cellules p21KD peut être due à la perturbation à long terme du réseau d'actine qui prévient son interaction avec PKCμ (220). Cette altération peut aussi être la conséquence de l'activation de

phosphatases spécifiquement activées par la perte de p21. Ces deux hypothèses ne sont d'ailleurs pas exclusives. De plus, nous confirmons ici la dépendance de la phosphorylation de PKCμ vis-à-vis de Rho. Cependant, nos résultats montrent que sa diminution n'est pas un événement impliqué directement dans la diminution de la phospho-cofiline lors de l'inactivation de Rho. Nous ne pouvons pas d'avantage exclure que l'hyperphosphorylation de PKCμ, observée dans les cellules p21KD, soit provoqué par un mécanisme relatif à l'altération du réseau d'actine. L'ensemble de ces résultats montrent que la phosphorylation des protéines PKCμ et SSH1L est altérée par l'inactivation de p21. Cependant, nous n'avons pas pu mettre en évidence un lien entre ces altérations, l'activité de ces protéines et l'inactivation de Rho dans les cellules p21KD. Des expériences supplémentaires devraient donc viser à (i) préciser le contrôle de l'activité de PKCμ et SSH1L par Rho et (ii) déterminer de quelle manière la voie PKCμ-SSH1L participe au contrôle de la cofiline dépendant de Rho, en conditions physiologiques. Par exemple, l'analyse des phosphorylations de PKCμ et SSH1L lors d'expériences de réactivation de Rho dans les cellules p21KD devrait permettre de spécifier le lien entre leur altération et l'inhibition de Rho dans ces cellules.

C.4.d) L'inactivation transitoire de Rho n'est pas suffisante pour inactiver FAK

Il est intéressant de noter qu'au cours de l'expérience d'inhibition transitoire de Rho par l'exoenzyme C3, la phosphorylation de FAK est augmentée (Fig. B.10B). Ce résultat semble incohérent avec les nombreux travaux qui montrent que l'activité de Rho et la contractilité des fibres d'actine sont nécessaires à l'assemblage complet des adhésions focales (134, 138, 191, 476). Cependant, comme présenté en A.2.b.3, le complexe FAK-Src fonctionne comme un module d'activation de Rho au cours des phases de maturation de ces structures. Par ailleurs certains travaux indiquent que leur maturation est associée à la déphosphorylation de certaines protéines qui les constituent, telles que la paxilline (155). Par conséquent, on peut imaginer ici que la déstabilisation des fibres d'actine conduit à l'activation de FAK du fait d'un retour des adhésions focales à un niveau de maturation intermédiaire. La perturbation de l'équilibre des facteurs d'échange et d'activation qui régule Rho joue probablement un rôle essentiel dans cette réponse précoce à l'inhibition de Rho. Nous présumons, par ailleurs, que l'inactivation stable de Rho, comme dans les cellules p21KD, est requise pour entraver durablement

l'activation de FAK et contribuer à un niveau d'adhésions focales constitutivement réduit. Il est également envisageable que des altérations, relatives à l'inactivation de p21 et indépendantes de Rho, contribuent à la suppression de la phosphorylation de FAK dans les cellules p21KD.

C.4.e) Conséquences de l'inactivation de PKCμ dans les cellules contrôles

Puisque SSH1L est hypophosphorylée dans les cellules p21KD, et malgré l'hyperphosphorylation de PKCμ, nous avons choisi de tester l'hypothèse d'une interruption de la signalisation PKCμ-SSH1L dans les cellules p21KD. Pour cela, nous avons décidé d'explorer les conséquences de l'inactivation de PKCμ par ARNi dans les cellules contrôles (Fig. B.11A). Bien que la phosphorylation de SSH1L ne soit pas significativement modifiée, la phosphorylation de la cofiline est effectivement inhibée par l'inactivation transitoire de PKCμ, à un niveau comparable à celui observé dans les cellules p21KD (Fig. B.11A). Ce résultat renforce l'idée que l'inactivation de PKCμ est suffisante pour conduire à l'hypophosphorylation de la cofiline dans les cellules p21KD. Il est d'ailleurs frappant de constater que le phénotype des cellules présentant une inactivation de PKCμ résume partiellement les altérations précédemment observées dans les cellules p21KD, incluant l'hypophosphorylation de FAK, la réduction de l'étalement cellulaire, la diminution du nombre et de l'aire des adhésions focales et l'inhibition de la formation des fibres de stress (Fig. B.11B-E). Ce résultat est aussi en faveur de l'hypothèse d'une perte de modulation de la cofiline par PKCμ dans les cellules p21KD, même si elle n'est probablement pas une conséquence directe de l'inactivation de Rho (Fig. B.10B). En revanche, le fait que la phospho-SSH1L ne soit pas modifiée par le knock-down de PKCμ suggère que l'éventuelle inactivation de PKCμ dans les cellules p21KD n'est pas non plus directement responsable de l'hypophosphorylation de SSH1L dans ces cellules.

C.4.f) Conséquences de l'inactivation de SSH1L dans les cellules p21KD

De nombreux travaux rapportent que la forme hypophosphorylée de SSH1L est un activateur majeur de la cofiline (472, 477). Nos résultats précédents n'ont pas permis d'établir un lien entre l'hypophosphorylation de SSH1L et l'inactivation de Rho et/ou de PKCμ. Cependant, à ce stade, nous

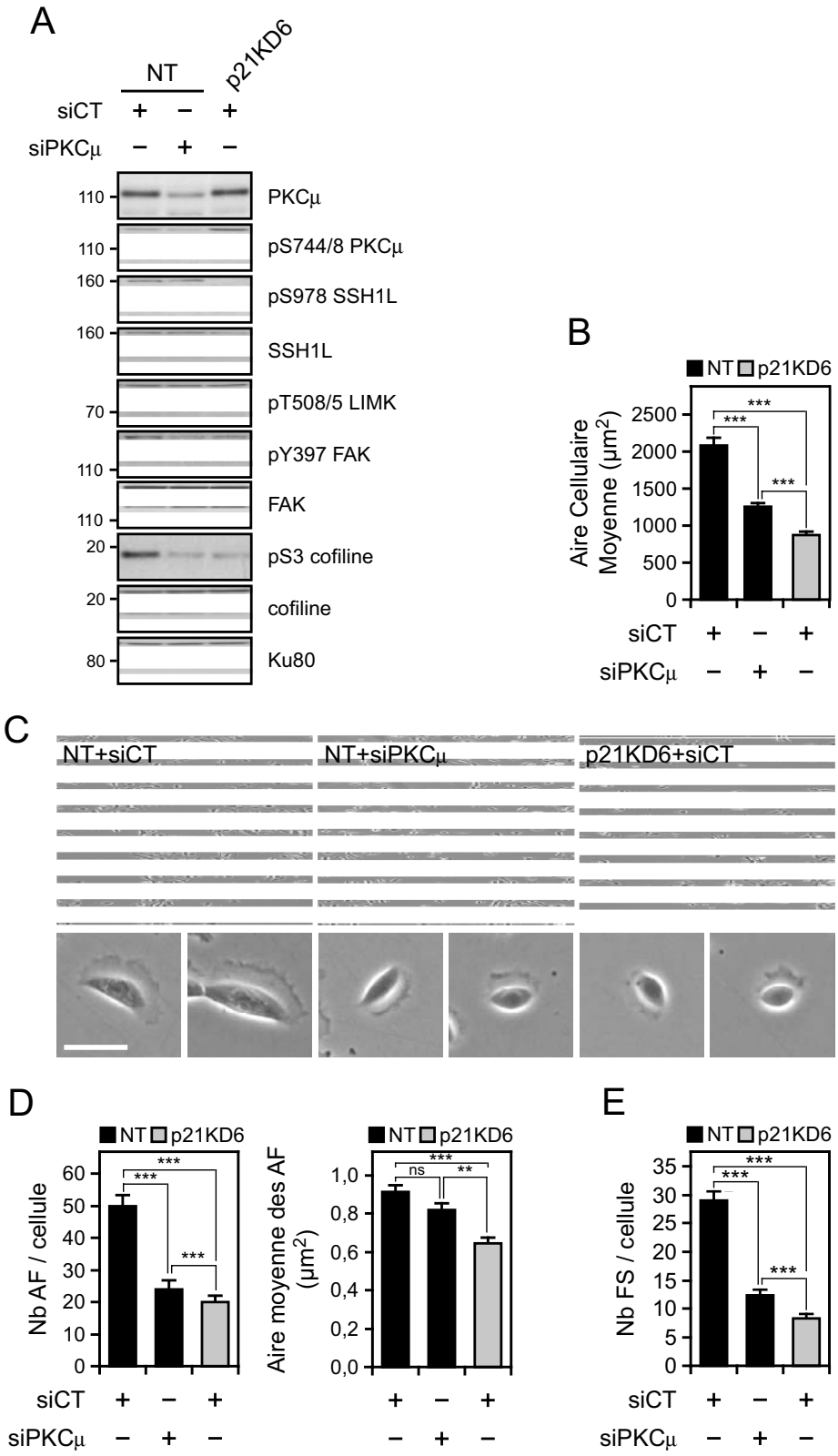

Figure B.11. Conséquences de l'inactivation de PKCμ sur la phosphorylation de la cofiline, la morphologie, l'adhésion focale et la formation des fibres des stress dans les cellules épithéliales mammaires. (A) Analyse par western blot de l'expression de PKCμ, pS744/8 PKCμ, pS978 SSH1L, SSH1L totale, pT508/5 LIMK, pY397 FAK, FAK totale, la pS3 cofiline et la cofiline totale dans les cellules NT, 72 h après transfection d'un pool de siRNA contrôle (siCT) ou d'un pool de siRNA ciblant *PRKD1* (siPKCμ) et les cellules p21KD6, après transfection du pool de siRNA contrôle. (B) Mesure de l'aire moyenne des cellules NT et p21KD6 traitées comme en (A)(NT+siCT, *n* = 75 ; NT+siPKCμ, *n* = 75 ; p21KD6+siCT, *n* = 75). (C) Images acquises en microscopie par contraste de phase des cellules NT et p21KD6 traitées comme en (A). Barre, 100 μm (haut) et 50 μm (bas). (D) Quantité (Nb) et aire moyennes des structures d'AF dans les cellules NT et p21KD6 traitées comme indiqué en (A). (E) Quantité moyenne de fibres de stress dans les cellules NT et p21KD6 traitées comme en (A). (NT+siCT, *n* = 15; NT+siPKCμ, *n* = 15; p21KD6+siCT, *n* = 15). Expression de Ku80, contrôle de chargement ; poids moléculaires en kDa. Barre d'erreur, ESM. ***, P < 0,001 ; **, P < 0,005 ; ns, non significatif (test *t*).

n'avons pas encore déterminé si SSH1L participe à l'hypophosphorylationd de la cofiline dans les cellules p21KD. Pour tester cette hypothèse, nous avons analysé les conséquences de l'inactivation de SSH1L par ARNi dans les cellules p21KD (Fig. B.12A). Nous avons pensé que si la cofiline était effectivement hypophosphorylée en réponse à une suractivation de SSH1L dans ces cellules, l'inhibition de cette dernière devrait restaurer la phosphorylation de la première. Cette hypothèse fut confirmée par la restauration partielle de la phospho-cofiline suite au knock-down de SSH1L dans les cellules p21KD (Fig. B.12A). Ceci indique que SSH1L contribue à l'hypophosphorylation de la cofiline dans les cellules p21KD. Cependant, le niveau de phospho-cofiline n'est pas rétabli au niveau de celui observé dans les cellules contrôles. D'autre part, loin de limiter le défaut d'adhésion, la perte de SSH1L conduit au contraire à une altération accentuée de l'adhésion et de la morphogenèse des cellules p21KD (Fig. B.12B). Ce phénotype est caractérisé par l'aggravation de l'hypophosphorylation de FAK, une réduction accrue de la quantité d'adhésions focales et un réseau d'actine complètement désorganisé et presque exempt de fibres de stress (Fig. B.12A, Fig. B.13A, B). Un phénotype similaire fut obtenu dans les cellules contrôles, ce qui suggère, en accord avec de récents travaux, que SSH1L est un facteur essentiel de la dynamique d'adhésion focale (données non présentées, 478).

Toutes ces données montrent que p21 régule la dynamique de l'actine et qu'elle module l'activité de la cofiline. Bien que nos résultats montrent que p21 régule également Rho, nous n'avons pas réussi à identifier clairement la ou les voies effectrices dont l'altération conduit à la suractivation de la cofiline. Si nos données montrent que SSH1L est probablement impliquée dans ce phénomène, nous ne savons pas encore si l'activité de cette phosphatase est effectivement altérée en réponse à l'inactivation de Rho. Par ailleurs plusieurs phosphatase et kinases ont également été décrites comme des facteurs de régulation de la phosphorylation de la cofiline (A.2.b.1). Il serait donc intéressant de connaître (i) leur activité dans les cellules épithéliales mammaires, et notamment leur implication dans le contrôle de la phospho-cofiline et (ii) leur dépendance vis-à-vis de p21.

C.5) p21 régule l'expression d'*ARHGAP19*

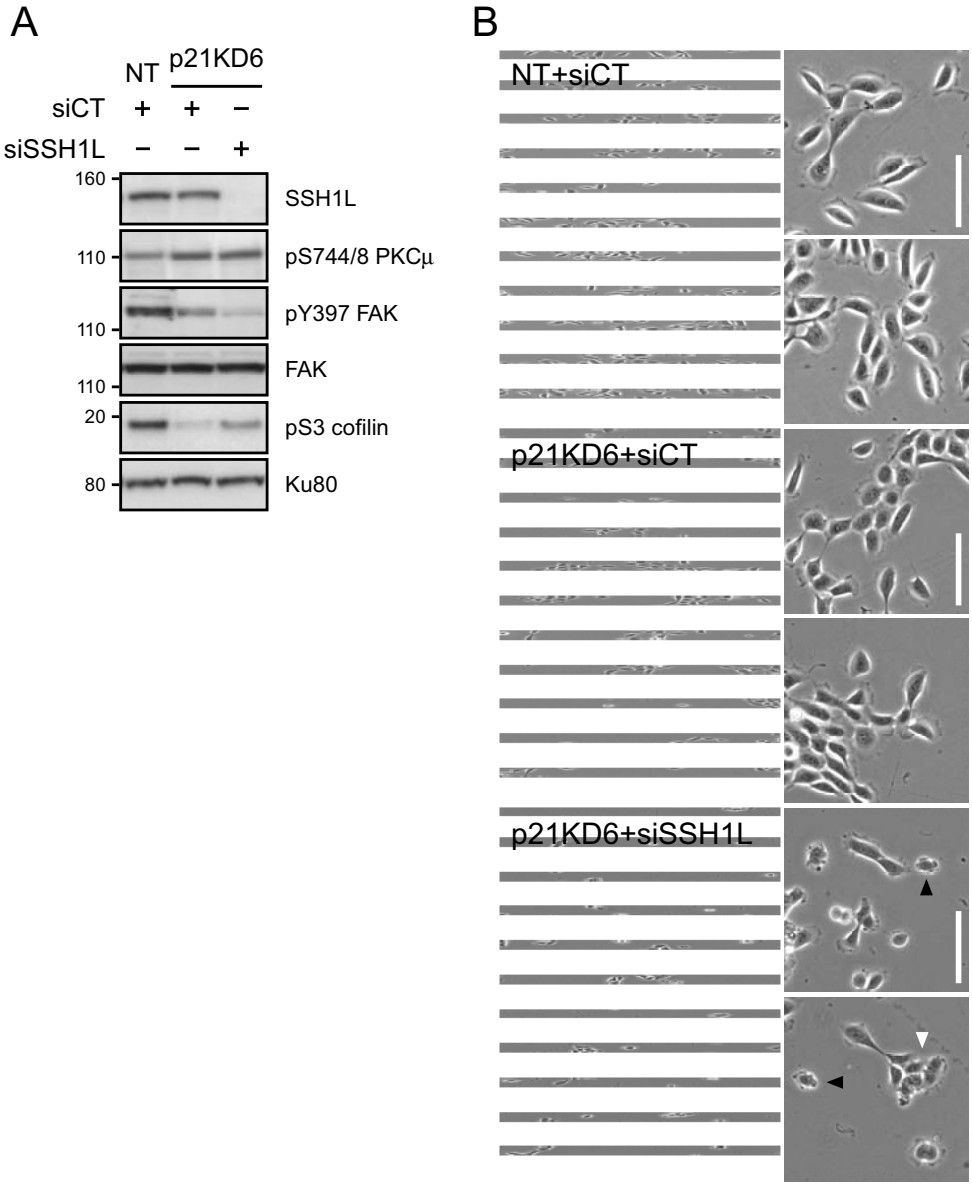

Figure B.12. Conséquences morphologiques de l'inactivation de SSH1L dans les hTMEC p21KD. (A) Analyse par western blot de l'expression de SSH1L totale, pS744/7448 PKCμ, pY397 FAK, FAK totale, la pS3 cofiline dans les hTMEC NT, 72 h après transfection d'un pool de siRNA contrôle (siCT) et dans les hTMEC p21KD6, après transfection du pool de siRNA contrôle ou d'un pool de siRNA ciblant *SSH1* (siSSH1L). Expression de Ku80, contrôle de chargement ; poids moléculaires en kDa. (B) Images acquises en microscopie par contraste de phase des hTMEC NT et p21KD6 traitées comme indiqué en (A). Les flèches noires et blanches indiquent la morphologie altérée des cellules transfectées avec le siRNA siSSH1L et respectivement isolées ou en groupe. Barre, 100 μm.

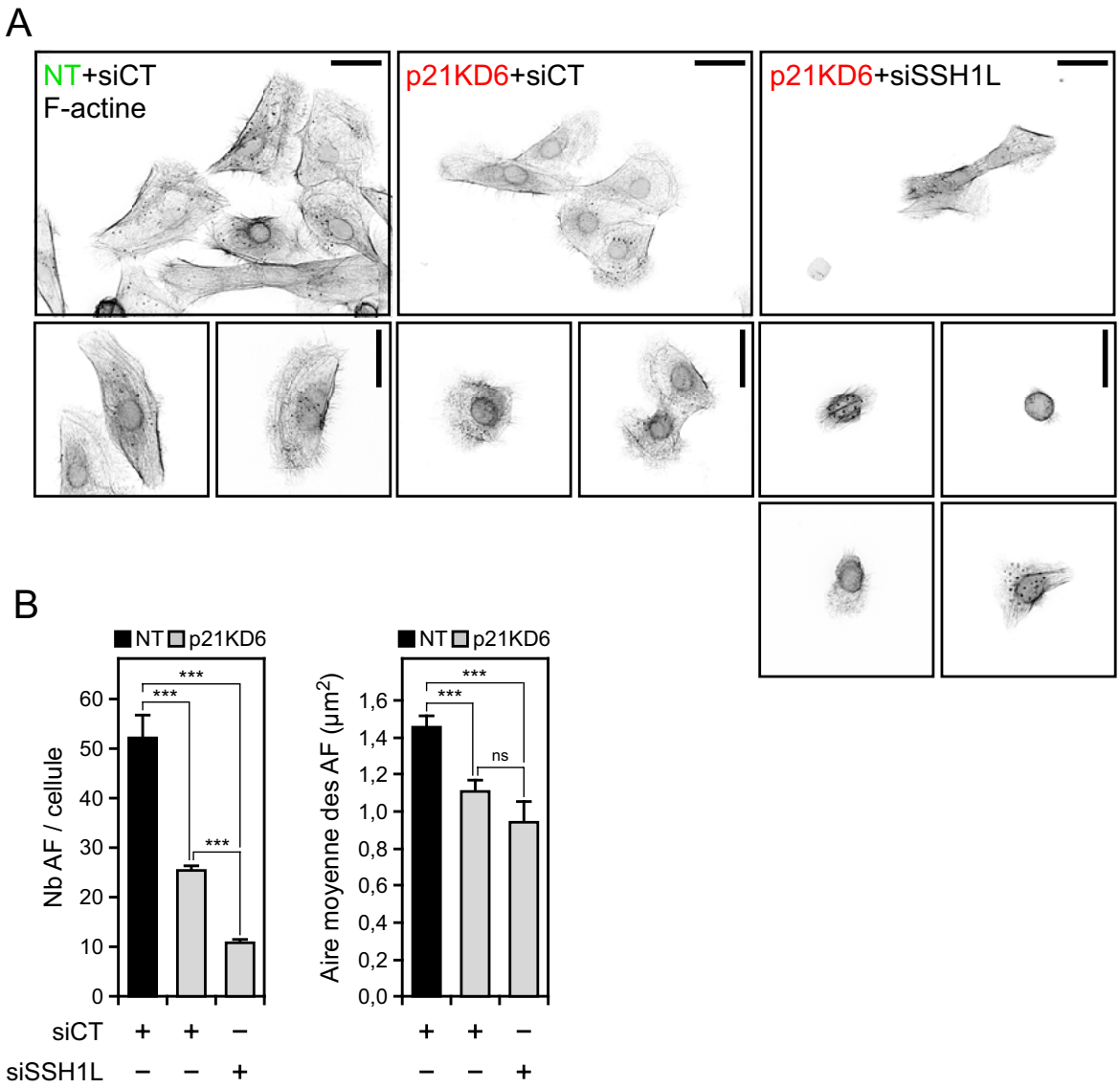

Figure B.13. Conséquences de l'inactivation de SSH1L sur la formation des fibres des stress et l'adhésion focale des hTMEC p21KD. (A) Visualisation de la F-actine dans les hTMEC NT, 72 h après transfection d'un pool de siRNA contrôle (+siCT) et dans les hTMEC p21KD6, après transfection du pool de siRNA contrôle ou d'un pool de siRNA ciblant SSH1 (+siSSH1L). Barre, 20 µm. (B) Nombre moyen (Nb) de structures d'AF dans les cellules NT et p21KD6 traitées comme indiqué en (A) (NT+siCT, 10 cellules, 520 AF ; p21KD6+siCT, 10 cellules, 251 AF ; p21KD6+siSSH1L, 10 cellules, 106 AF). Barre d'erreur, ESM. ***, P < 0,001 ; ns, non significatif (test *t*).

Plusieurs travaux ont montré que p21 est un régulateur de la transcription dans les cellules humaines (72, 110, 451, 479). Or, à ce jour, aucune activité connue de p21, y compris son rôle de CKI, ne permet d'établir un lien direct entre elle et la régulation de l'activité de Rho. Nous avons donc pensé que la diminution de cette activité, ainsi que les défauts d'adhésion focale et du réseau d'actine dans les cellules p21KD pouvaient être provoqués par la modification d'expression de gènes codant pour des protéines intervenant dans leur régulation. Pour vérifier cette hypothèse, nous avons réalisé une analyse du transcriptome des cellules présentant une inactivation transitoire de p21, 48h après transfection d'un siRNA contrôle (siCT) ou de siRNA ciblant *CDKN1A*, et correspondant aux séquences des sh5 et sh6 (si5, si6). L'extinction de l'ARNm de *CDKN1A* fut contrôlée par qRT-PCR, dans les trois expériences indépendantes utilisées pour l'hybridation des puces, et la perte d'expression de p21 fut validée par western blot (données non présentées).

Selon les critères de modification commune aux échantillons si5 et si6 comparés aux échantillons siCT, et de facteur de modification supérieur à 1,3, nous avons déterminé que l'inactivation de p21 conduisait à la surexpression de 119 et la sous-expression de 384 ARNm. Parmi les gènes correspondant à ces transcrits, un classement par voie de signalisation (logiciel IPA), combiné à une analyse bibliographique pour chaque gène candidat, a été réalisé. Cette sélection nous a permis d'établir une liste de 11 transcrits surexprimés et 29 transcrits sous-exprimés en réponse à l'inactivation transitoire de p21 et codant pour des régulateurs putatifs ou caractérisés du cytosquelette (Table 1). Nous n'avons, à ce jour, réalisé la validation d'expression que de 11 transcrits. Parmi ces 11 transcrits, seuls 3 ont montré une modification significative d'expression après invalidation stable de *CDKN1A* : *PPP2R1B*, *ARHGAP19* et *ARHGAP5* (Table 1).

Le gène *ARHGAP19* (GeneID: 84986) nous a semblé un excellent candidat pour expliquer l'altération de l'activité de Rho dans les cellules p21KD. En effet, il code pour un membre putatif de la famille des facteurs d'activation de Rho (GAP), qui incluent p190BRhoGAP (*ARHGAP5*), et son niveau de surexpression est parmi les plus élevés dans les cellules p21KD (480). Nous avons donc spéculé que la surexpression de RhoGAP19 puisse participer à l'inactivation globale de Rho dans les cellules p21KD (Fig. B.14A). En accord avec cette hypothèse, le knock-down d'*ARHGAP19* par ARNi dans les cellules a fait remonter le niveau d'activation de Rho à un niveau comparable à celui observé dans les

Description	Référence genbank	Nom	Facteur de modification		Confirmation qPCR siRNA	test *t*	Confirmation qPCR shRNA Facteur de modification (sh5 ; sh6)	test *t*
			si5/siCT	**si6/siCT**				
protein phosphatase 2 (formerly 2A), regulatory subunit A (PR 65), beta isoform	NM_002716	*PPP2R1B*	2,97	2,59	oui	*	oui (1,6 ; 2,3)	*
Rho GTPase activating protein 19	AW068242	*ARHGAP19*	5,56	1,83	oui	*	oui (3,6 ; 9,0)	*
Rho GTPase activating protein 5	AU138284	*ARHGAP5*	1,97	1,54	oui	*	oui (2,9 ; 2,5)	*
Src homology 3 domain-containing guanine nucleotide exchange factor	NM_015595	*SGEF*	4,47	4,18	oui	*	non	
cyclin-dependent kinase inhibitor 1C (p57, Kip2)	NM_000076	*CDKN1C*	3,35	5,93				
Integrin, beta-like 1 (with EGF-like repeat domains)	CD677332	*ITGBL1*	3,44	2,33				
Ras-related GTP binding D	NM_021244	*RRAGD*	2,18	2,23				
Family with sequence similarity 33, member A	CB053681	*SKA2*	2,70	2,05				
ankyrin repeat domain 47	NM_198471	*ANKRD47*	1,98	1,99				
NIMA (never in mitosis gene a)-related kinase 7	AA309645	*NEK7*	2,29	1,89				
sema domain, immunoglobulin domain (Ig), transmembrane domain (TM) and short cytoplasmic	NM_006378	*SEMA4D*	2,03	1,78				
			siCT/si5	**siCT/si6**				
parvin, beta	NM_013327	*PARVB*	2,45	1,54	oui	*	non	
leupaxin	NM_004811	*LPXN*	5,69	5,57	oui	*	non	
podoplanin	NM_006474	*PDPN*	2,58	2,68	oui	*	non	
laminin, gamma 2	NM_005562	*LAMC2*	2,98	3,71	oui	*		
filamin B, beta (actin binding protein 278)	NM_001457	*FLNB*	1,90	1,52	oui	-		
MAP/microtubule affinity-regulating kinase 1	NM_018650	*MARK1*	1,96	1,73	oui	-		
microtubule associated monoxygenase, calponin and LIM domain containing 1	NM_022765	*MICAL1*	1,73	1,62	non			
S100 calcium binding protein A8 (calgranulin A)	NM_002964	*S100A8*	16,73	19,45				
serpin peptidase inhibitor,clade E (nexin, plasminogen activator inhibitor type 1), member 1	NM_000602	*SERPINE1*	5,60	3,29				
Myosin, light polypeptide kinase	AA327512	*MYLK*	4,66	1,69				
S100 calcium binding protein A9 (calgranulin B)	AA318707	*S100A9*	3,56	8,53				
Rap guanine nucleotide exchange factor (GEF)-like 1	NM_016339	*RAPGEFL1*	2,99	1,46				
actin binding LIM protein 1	NM_002313	*ABLIM1*	2,82	1,44				
adipocyte-specific adhesion molecule	NM_024769	*ASAM*	2,74	2,25				
syndecan 1	NM_002997	*SDC1*	2,57	1,70				
myosin VIIA	NM_000260	*MYO7A*	2,48	2,22				
tetraspanin 13	NM_014399	*TSPAN13*	2,46	2,54				
tubulin, alpha 3	NM_006009	*TUBA1A*	2,34	2,54				
RAB38, member RAS oncogene family	NM_022337	*RAB38*	2,32	2,31				
Metastasis suppressor 1	CB178032	*MTSS1*	2,28	1,77				
RAB31, member RAS oncogene family	NM_006868	*RAB31*	2,28	2,57				
RAP1, GTP-GDP dissociation stimulator 1	NM_021159	*RAP1GDS1*	2,09	1,71				
coronin, actin binding protein, 1A	NM_007074	*CORO1A*	2,06	1,85				
Tubulin tyrosine ligase	BM794270	*TTL*	2,00	2,82				
dynactin 5 (p25)	NM_032486	*DCTN5*	1,96	1,65				
coronin, actin binding protein, 2A	NM_003389	*CORO2A*	1,87	2,28				
serine/threonine kinase 38	NM_007271	*STK38*	1,61	1,90				
actin related protein 2/3 complex, subunit 1B, 41kDa	NM_005720	*ARPC1B*	1,60	2,01				
coactosin-like 1 (Dictyostelium)	NM_021149	*COTL1*	1,57	1,88				

Table B.1. Gènes dont la transcription est modifiée par l'inactivation de p21 et codant pour des régulateurs caractérisés ou supposés du cytosquelette. Les références genbank correspondent à la nomenclature d'identification des transcrits et EST de la puce CodeLink Human Whole Genome. Les noms de gènes ont été vérifiés et mis à jours si nécessaire. Les facteurs de modifications sont : le rapport du signal moyen obtenu pour les expériences de si5 et 6 sur le signal obtenu pour les expériences de siRNA contrôle, lorsque le transcrit est surexprimé (si5/CT, si6/CT) ; le rapport du signal moyen obtenu pour les expériences siRNA contrôle sur le signal moyen obtenu pour les expériences de si5 et 6, lorsque le transcrit est sous-exprimé (siCT/si5 ; siCT/si6). La confirmation en qRT-PCR a été réalisée à partir des ADNc correspondants aux trois expériences utilisées pour l'hybridation des puces (qPCR siRNA). La confirmation en qRT-PCR de la modification transcriptionnelle a ensuite été réalisée à partir de trois ADNc des cellules NT, p21KD5 et p21KD6, préparés indépendamment. Les facteurs de modifications ont été calculés comme précédemment. *, $P < 0,05$ (test *t*).

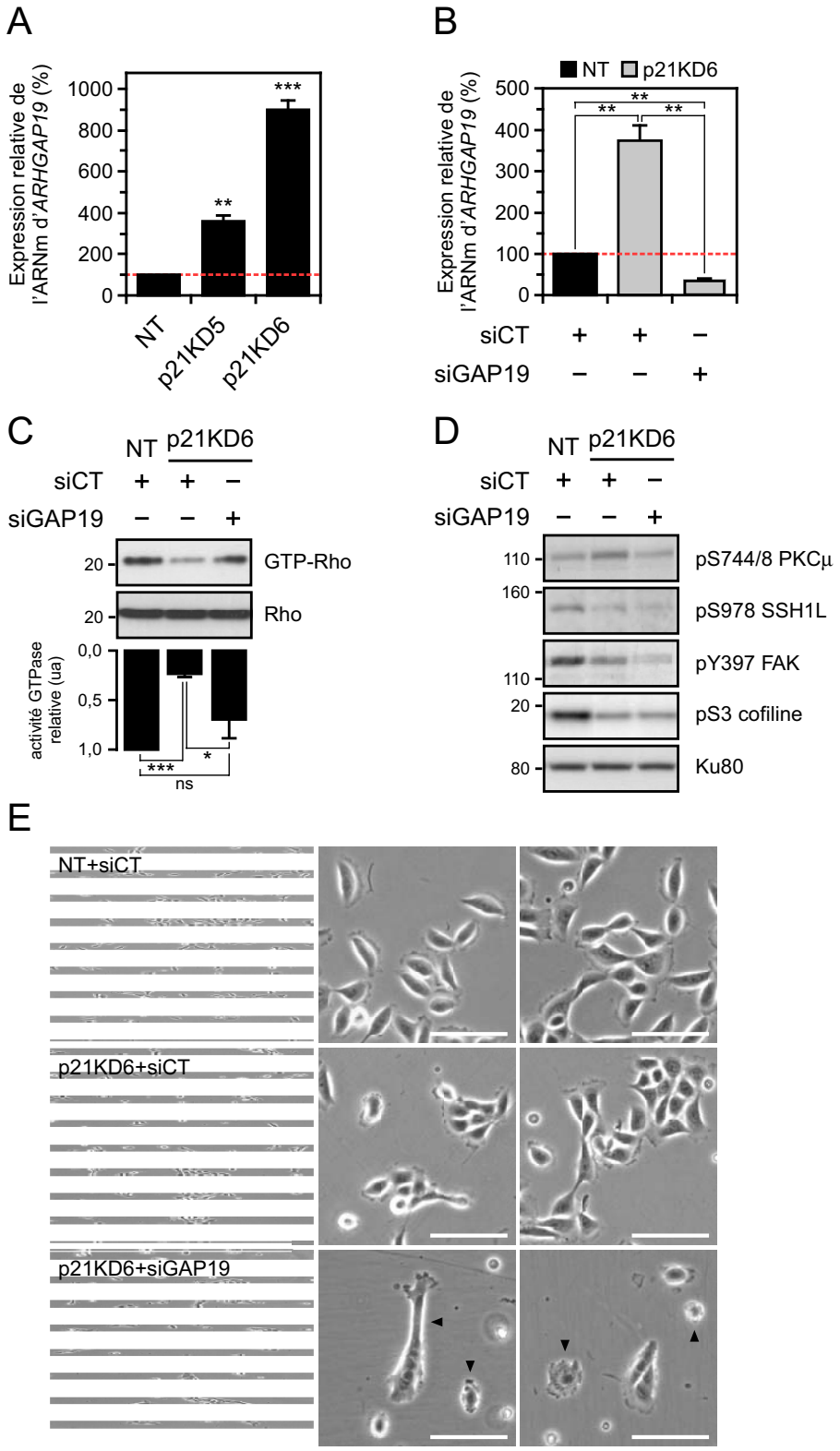

Figure B.14. Transcription d'*ARHGAP19* et implication dans la régulation de Rho et la morphologie des cellules p21KD. (A) Quantification relative de la transcription d'*ARHGAP19* dans les hTMEC NT, p21KD5 et p21KD6. Ligne rouge pointillée, 100% de la transcription d'*ARHGAP19* dans les cellules NT. (B) Quantification relative de la transcription d'*ARHGAP19* dans les GP-hMEC NT, 72 h après transfection d'un pool de siRNA contrôle (siCT) ou et dans les GP-hMEC p21KD6, après transfection du pool de siRNA contrôle ou d'un pool de siRNA ciblant *ARHGAP19* (siGAP19). Des résultats similaires furent obtenues dans chaque lignées NT et p21KD6 dérivées des hTMEC. Ligne rouge pointillée, 100% de la transcription d'*ARHGAP19* dans les cellules NT transfectées avec le pool de siRNA contrôle. (C) Quantification de l'activité GTPase de Rho dans les cellules NT et p21KD6 traitées comme en (B). (D) Analyse par western blot de l'expression de pS744/8 PKCμ, pS978 SSH1L, pY397 FAK, la pS3 cofiline dans les cellules NT et p21KD6 traitées comme en (B). (E) Images acquises en microscopie par contraste de phase des cellules NT et p21KD6 traitées comme en (B). Flèches noires, morphologie représentative. Barre, 100 μm. Expression de Ku80, contrôle de chargement ; poids moléculaires en kDa. Barre d'erreur, écart type (trois expériences indépendantes). *, P < 0,05 ; **, P < 0,005 ; ***, P < 0,001 ; ns, non significatif (test *t*).

cellules NT (Fig. B.14B, C). Cependant la restauration transitoire de l'activité de Rho n'est pas suffisante, dans les cellules p21KD, pour normaliser la phosphorylation de SSH1L et la cofiline (Fig. B.14D). De plus, l'inhibition de RhoGAP19 accentue les défauts d'étalement cellulaire, caractérisés par une morphologie fortement altérée montrant des extensions aberrantes et un bord cellulaire hautement irrégulier (Fig. B.14E). Enfin, le knock-down d'*ARHGAP19* se caractérise aussi par des défauts d'assemblage de la F-actine encore plus sévères que ceux observés dans les cellules p21KD contrôles (Fig. B.15A). En effet, ces cellules montrent un niveau d'assemblage de filaments de F-actine supérieur à celui des cellules p21KD contrôles, mais anormalement aggloméré et désorganisé, empêchant même la quantification des fibres de stress (Fig. B.15A). Par ailleurs, de manière frappante, l'inhibition de RhoGAP19 abolit presque totalement la formation des adhésions focales (Fig. B.15BC). Toutes ces aberrations furent également observées dans les cellules NT présentant un knock-down d'*ARHGAP19* (données non présentées). Ces données révèlent donc que le facteur d'échange RhoGAP19 est un nouveau régulateur de l'adhésion focale et de l'assemblage de l'actine dans les cellules épithéliales mammaires humaines.

L'ensemble de ces résultats montrent que RhoGAP19 est possiblement impliquée dans l'inactivation de Rho dans les cellules p21KD mais qu'elle est aussi nécessaire à la formation de l'adhésion focale. Ceci permet d'envisager que RhoGAP19 puisse agir, de la même manière que certains membres de la famille des GAP, dans la régulation locale de l'activité de Rho, nécessaire à la dynamique d'assemblage des adhésions focales (159, 267). Il faut noter en outre que, bien que nous ne l'ayons pas évalué fonctionnellement, la transcription d'*ARHGAP5* est aussi augmentée, ce qui suggère que p21 régule au niveau transcriptionnel plusieurs acteurs de la formation des adhésions focales associés au contrôle de Rho (Table 1, 267, 481, 482).

C.6) p21 régule la dynamique microtubulaire

Comme nous l'avons vu dans l'introduction, de nombreux travaux ont montré que les microtubules sont impliqués dans la régulation de l'adhésion focale et que celle-ci est un site privilégié d'interrégulation entre les filaments d'actine et les microtubules (A.2.c.5). Nous avons donc supposé

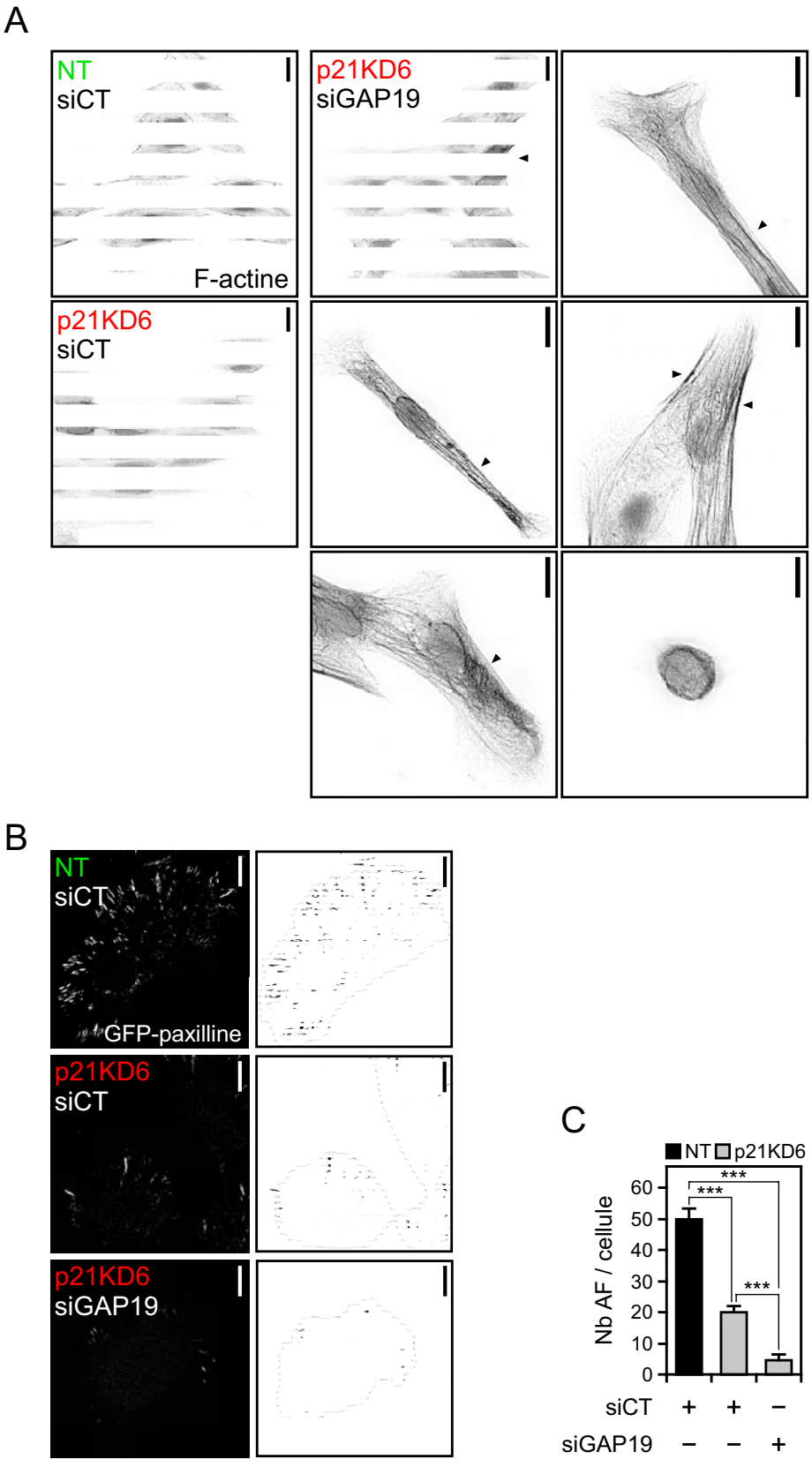

Figure B.15. Implication de RhoGAP19 dans la formation des fibres de stress et l'adhésion focale. (A) Visualisation de la F-actine dans les cellules NT, 72 h après transfection d'un pool de siRNA contrôle (siCT) ou et dans les cellules p21KD6, après transfection du pool de siRNA contrôle ou d'un pool de siRNA ciblant *ARHGAP19* (siGAP19). Flèches noires, structures aberrantes de F-actine. (B) Images de GP-hMEC NT et p21KD6 vivantes traitées comme en (A), obtenues en microscopie à fluorescence (gauche) et images binaires correspondantes (droite). Ligne pointillée grise, contour cellulaire. (C) Nombre moyen (Nb) de structures d'adhésion focale (AF) dans les cellules NT et p21KD6 traitées comme en (A) (NT+siCT, *n* = 14 ; p21KD6+siCT, *n* = 14 ; p21KD6+siGAP19, *n* = 17). Barre, 10 µm. Barre d'erreur, ESM. ***, P < 0,001 (test *t*).

que les défauts majeurs d'adhésion et d'assemblage de l'actine des cellules p21KD pouvaient être associés à, voire partiellement causés par une altération de la dynamique microtubulaire consécutive à la perte de p21. Pour tester cette hypothèse, nous avons mis au point des lignées clonales issues de hTMEC exprimant stablement la protéine de fusion GFP-tubuline α (GT-hMEC), permettant d'analyser, par vidéomicroscopie à fluorescence sur cellules vivantes, la dynamique microtubulaire. L'observation en temps réel des microtubules permet de mesurer les paramètres de l'instabilité dynamique définis dans le chapitre A.2.c.1 (320, 483). Les GT-hMEC furent, comme précédemment, transformées pour présenter une inactivation stable de p21 (p21KD), et comparées à des GT-hMEC contrôles (NT).

L'analyse de la dynamique microtubulaire montre clairement que l'inactivation de p21 provoque une modification de l'instabilité dynamique des microtubules de la lamella (Fig. B.16A). En effet, les microtubules des cellules p21KD sont caractérisées par une augmentation de la vitesse moyenne de croissance (NT, 13,91±0,23 µm/min ; p21KD6, 16,03±0,31 µm/min ; P<0,001), de la vitesse moyenne de raccourcissement (NT, 20,97±0,54 µm/min ; p21KD6, 23,66±0,62 µm/min ; P<0,005) et de la fréquence de catastrophe (NT, 1,97±0,09/min ; p21KD6, 2,44±0,11/min ; P<0,001). En outre, les microtubules des cellules p21KD présentent un temps passé en pause réduit en faveur des phases de croissance et de rétrécissement (NT, pause, 66,3±1,2% ; p21KD6, pause, 56,6±1,4% ; P<0,001). Nous avons également observé une fréquence de sauvetage réduite dans les cellules p21KD (NT, 12,44±0,29/min ; p21KD6, 10,96±0,31/min ; P<0,001). Enfin, la dynamicité moyenne qui est définie par la vélocité des phases dynamiques est, de façon cohérente avec les données précédentes, augmentée par l'inactivation de p21 (NT, 6,13±0,30 µm/min ; p21KD6, 8,99±0,39 µm/min ; +31,8% ; P<0,001). En outre, nous avons remarqué, à la fois sur cellules fixées et d'après les observations en temps réel, que les microtubules dynamiques des cellules NT peuvent croitre stablement selon une disposition parallèle, le long de la lamella (Fig. B.16E). Au contraire, dans les cellules p21KD, nous avons observé un réseau dense de microtubules dynamiques qui ciblent généralement, avec une faible persistance, la frontière lamellaire selon un angle sensiblement perpendiculaire (Fig. B.16E). Ces données montrent que p21 est requise pour la dynamique microtubulaire normale dans les cellules épithéliales mammaires humaines.

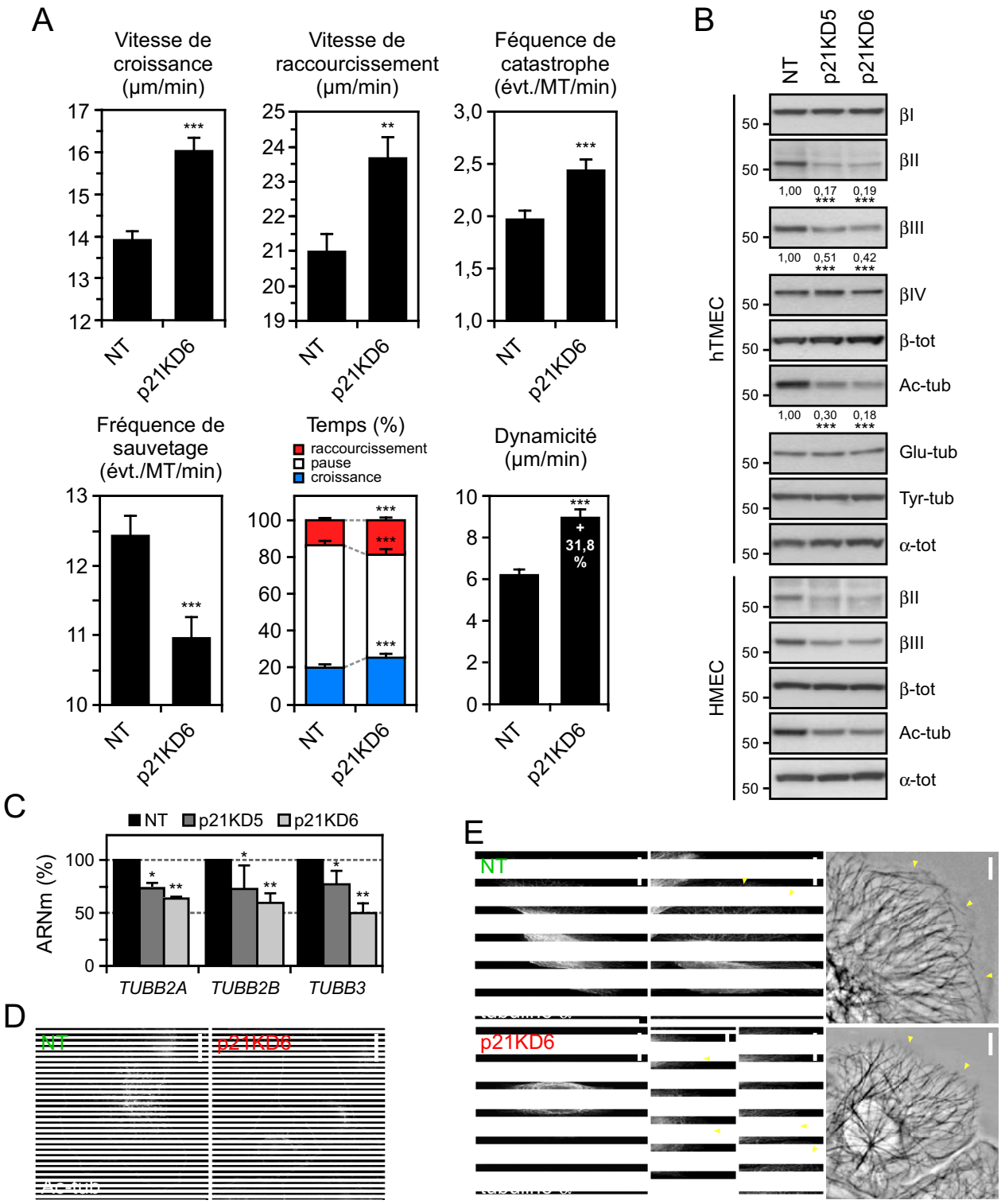

Figure B.16. Conséquences de l'inactivation de p21 sur la dynamique et la composition des microtubules. (A) Paramètres de l'instabilité dynamique des microtubules mesurés dans les GT-hMEC NT (70 MT ; 14 cellules) et p21KD6 GT-hMEC (65 MT ; 20 cellules). Barre d'erreur sur le graphique de distribution du temps en fonction des phases, intervalle de confiance à 95% ; pourcentage d'augmentation de la dynamicité indiqué ; évt., événement. (B) Analyse par western blot de l'expression des tubulines βI (βI), βII (βII), βIII (βIII), βIV (βIV), de la tubuline β totale (β-tot), de la tubuline acétylée (Ac-tub), de la tubuline polyglutamylée (Glu-tub), de la tubuline tyrosinylée (Tyr-tub) et de la tubuline α totale dans les hTMEC NT, p21KD5 et p21KD6 ; analyse par western blot de l'expression des tubulines βII, βIII, de la tubuline β totale, de la tubuline acétylée et de la tubuline α totale dans les HMEC NT, p21KD5 et p21KD6. La quantification relative de l'expression déterminée à partir de trois western blots indépendants est indiquée. (C) Quantification relative de la transcription de *TUBB2A*, *TUBB2B* et *TUBB3* dans les hTMEC NT, p21KD5 et p21KD6. Barre d'erreur, écart type (trois expériences indépendantes). (D) Marquage par immunofluorescence de la tubuline acétylée (Ac-tub) dans les cellules NT et p21KD6. Ligne pointillée grise, contour cellulaire. (E) Marquage par immunofluorescence de la tubuline α totale (gauche et milieu) et GFP-tubuline α (droite) dans les cellules NT et p21KD6. Flèches jaunes, MT de la lamella. Sauf indication, la barre d'erreur représente l'ESM. Poids moléculaires en kDa. Barre, 10 µm. *, P < 0,05 ; **, P < 0,005 ; ***, P < 0,001 (test *t*).

Nous avons expliqué précédemment en quoi l'expression de certaines isoformes et les modifications post-traductionnelles des tubulines peuvent influencer les propriétés dynamiques des microtubules (A.2.c.3-4). Nous avons donc choisi d'examiner certains de ces paramètres en fonction du statut de p21. Nous avons d'abord remarqué une forte inhibition de l'expression des tubulines βII et βIII, consécutive à l'inactivation de p21, à la fois dans les hTMEC et les HMEC (Fig. B.16A). Nous avons en outre pu établir que cette inhibition était associée à une diminution de la transcription des gènes des tubulines βII (*TUBB2A*, *TUBB2B*) et βIII (*TUBB3*) dans les cellules p21KD (Fig. B.16C). De plus, nous avons déterminé, par expérience de synchronisation par double-bloc thymidine, que l'expression des tubulines βII et βIII n'était pas dépendante du cycle (données non présentées). Ces données suggèrent donc que p21, indépendamment de ses fonctions de régulateur du cycle, est requise pour l'expression normale des gènes des tubulines βII et βIII dans les cellules épithéliales mammaires humaines. Cependant, les conséquences de l'altération d'expression de ces isoformes sur la dynamique microtubulaire restent à déterminer. En effet, à ce stade, nous ne savons pas si la diminution d'expression des tubulines βII et/ou βIII est suffisante pour provoquer les défauts d'instabilité dynamique observés dans les cellules p21KD. L'analyse des effets de l'inactivation par ARNi sélective ou combinée de ces isoformes sur la dynamique microtubulaire des cellules contrôles devrait apporter des éléments de réponse à ce sujet.

Par ailleurs, nous avons observé que les microtubules des cellules présentant une inactivation de p21 (hTMEC et HMEC) subissaient une sévère diminution de l'acétylation comparativement aux cellules contrôles (Fig. B.16B, D). Cette modification post-traductionnelle de la tubuline α est généralement observée dans les microtubules stables et fut proposée comme un facteur inhibiteur de la dynamique, favorisant l'étalement cellulaire et la maturation des adhésions focales (403, 404). L'acétylation de la tubuline est en grande partie réprimée par la désacétylase HDAC6. Or, l'association directe de sa forme inactive avec les microtubules, plus que l'acétylation *per se*, fut proposée comme le principal vecteur de stabilisation microtubulaire lors des expériences utilisant un inhibiteur spécifique, la tubacine (374, 403). Cette molécule permet donc de stabiliser expérimentalement les microtubules par inhibition d'HDAC6, tout en en contrôlant, par analyse de l'acétylation, l'activité de celle-ci. Cette manipulation nous permet donc d'adresser la possibilité que la déstabilisation des microtubules participe à l'altération des propriétés d'adhésion dans les cellules p21KD. Ainsi, nous

avons analysé les effets de la stabilisation microtubulaire par la tubacine, sur les cellules p21KD comparées aux cellules NT et p21KD traitées par la niltubacine, l'analogue inactif de la tubacine.

D'abord, les conditions de traitement par la tubacine furent mises au point de façon à restaurer l'acétylation de la tubuline dans les cellules p21KD au même niveau que celle observée dans les cellules NT (Fig. B.17A). Si l'on considère ce paramètre comme un marqueur et non comme un facteur de stabilisation microtubulaire, le recouvrement d'un niveau d'acétylation normale permet d'envisager que la tubacine rectifie la dynamique microtubulaire dans les cellules p21KD. L'analyse détaillée des paramètres de l'instabilité dynamique a confirmé cette hypothèse. De façon tout à fait remarquable, le traitement par la tubacine est accompagné d'une normalisation quasi totale de l'instabilité dynamique dans les cellules p21KD, à l'exception de la fréquence de catastrophe, partiellement inhibée, et du temps passé en croissance, excessivement inhibé (Fig. B.17B). Nous avons ensuite constaté que l'inhibition d'HDAC6 dans les cellules p21KD, provoque une restauration partielle de la phosphorylation de FAK, de même que l'adhésion focale et l'étalement cellulaire furent partiellement rétablis (Fig. B.17A, Fig. 18A-C).

Comme nous l'avons vu dans le chapitre A.2.c.5, il a été proposé que certains facteurs d'échanges (GEF) interagissant avec les microtubules soient capables d'activer localement l'activité de Rho pour promouvoir la contractilité des fibres de stress et la dislocation des adhésions focales (136, 423-425, 484). Considérant l'inactivation de Rho observée dans les cellules p21KD, nous spéculons que l'interaction des GEF avec les microtubules pourrait être corrompue dans ces cellules. Cette idée est renforcée par l'augmentation sensible de la phospho-cofiline après traitement par la tubacine qui suggère une activation locale de Rho après stabilisation des microtubules (Fig. B.17A). De récents travaux indiquent que l'inactivation locale de la cofiline participe à la maturation et au renouvellement des adhésions focales (478, 485). Ceci nous permet de supposer que la stabilisation microtubulaire contribue ici à une meilleure association des GEF avec les microtubules, favorisant leur meilleure distribution au niveau des adhésions focales et une augmentation locale de la phospho-cofiline dépendante de Rho. Une imagerie microscopique par FRET de l'activation de Rho serait un excellent moyen de savoir si l'activation de Rho est restaurée au niveau des adhésions focales, après traitement par la tubacine (260). Par ailleurs, notons que les résultats présentés ici sont en accord avec les effets déjà décrits de l'inhibition d'HDAC6 sur l'adhésion focale et l'étalement cellulaire (404). Ils suggèrent

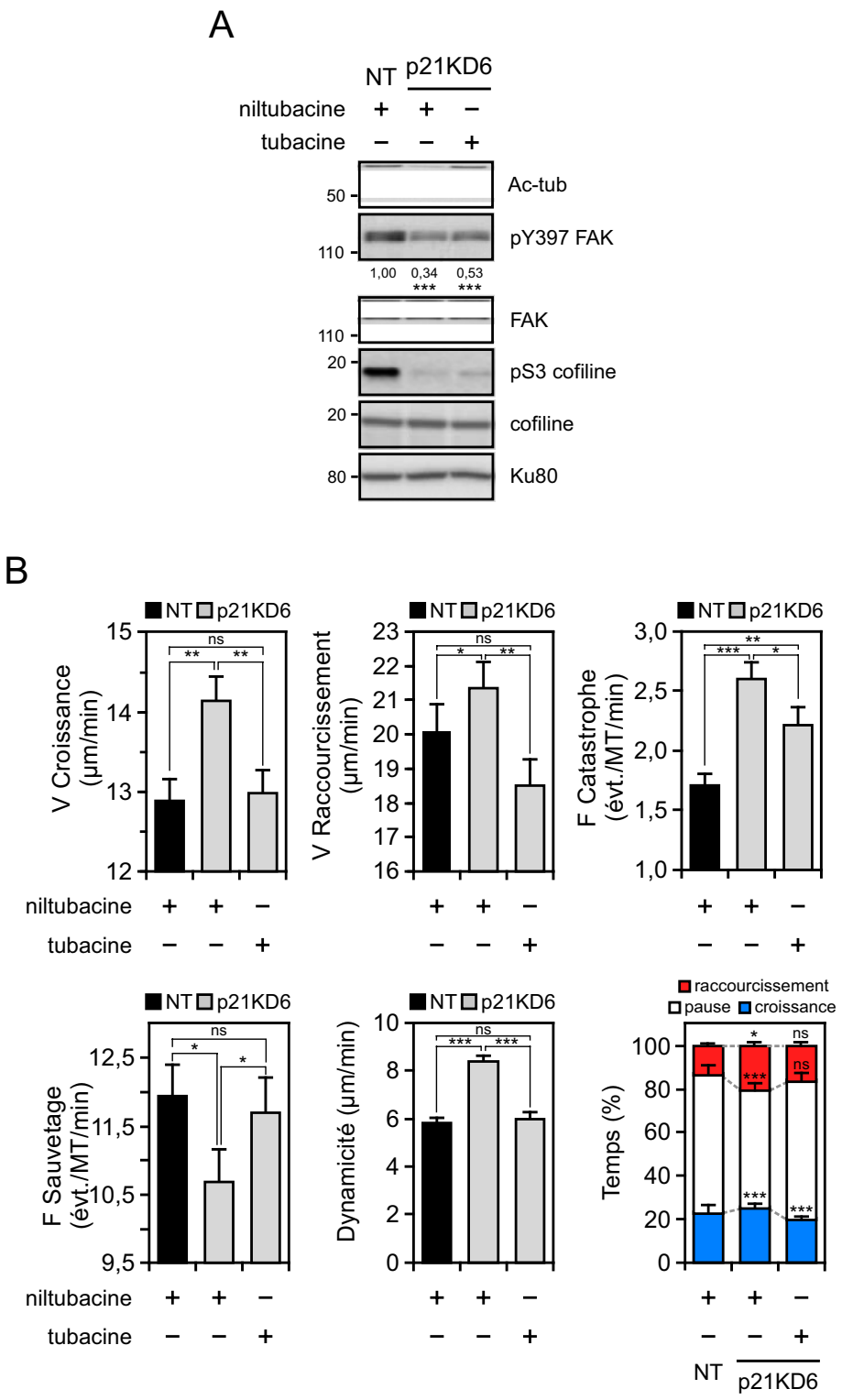

Figure B.17. Effets de l'inhibition d'HDAC6 sur la dynamique microtubulaire des cellules p21KD. (A) Analyse par western blot de l'expression de la tubuline acétylée, pY397 FAK, FAK totale, la pS3 cofiline et la cofiline totale dans les GT-hMEC NT traitées pendant 24 h avec la niltubacine (NLT ; 0,4 µM) et les GT-hMEC p21KD6 traitées pendant 24 h avec la niltubacine (0,4 µM) ou la tubacine (TUB ; 0,4 µM). La quantification relative de la phosphorylation (Y397) de FAK déterminé à partir de trois western blots indépendants est indiqué. Expression de Ku80, contrôle de chargement ; poids moléculaires en kDa. (B) Paramètres de l'instabilité dynamique microtubulaire mesurés dans les GT-hMEC NT et p21KD6 traitées comme en (A) (NT+NLT, 43 MT, 10 cellules ; p21KD6+NLT, 30 MT, 11 cellules ; p21KD6+TUB, 30 MT, 11 cellules). V, vitesse ; F, fréquence ; évt., événement. Barre d'erreur sur le graphique de distribution du temps en fonction des phases, intervalle de confiance à 95%. Les autres barres d'erreur représentent l'ESM. *, P < 0,05 ; **, P < 0,005 ; ***, P < 0,001; ns, non significatif (test *t*).

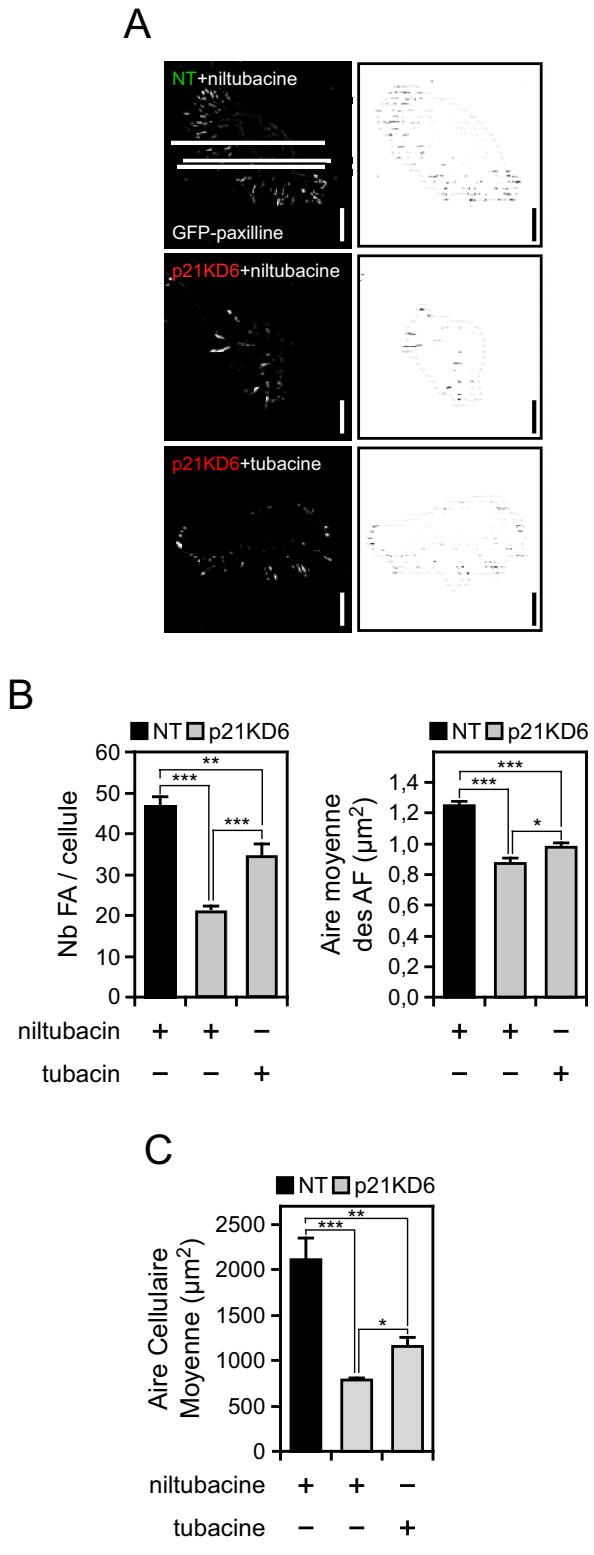

Figure B.18. Effets de l'inhibition d'HDAC6 sur l'adhésion des cellules p21KD. (A) Images de GP-hMEC NT traitées pendant 24 h avec la niltubacine (NLT ; 0,4 µM) et les GP-hMEC p21KD6 traitées pendant 24 h avec la niltubacine (0,4 µM) ou la tubacine (TUB ; 0,4 µM) obtenues en microscopie à fluorescence (gauche) et images binaires correspondantes (droite). Ligne pointillée grise, contour cellulaire. Barre, 10 µm. (B) Nombre moyen (Nb) et aire moyenne des structures d'AF dans les cellules NT et p21KD6 traitées comme en (A)(NT+NLT, 13 cellules, 612 AF ; p21KD6+NLT, 14 cellules, 299 AF ; p21KD6+TUB, 13 cellules, 491 AF). (C) Aire moyenne des cellules NT et p21KD6 traitées comme en (A)(NT+NLT, *n* = 30 ; p21KD6+NLT, *n* = 30 ; p21KD6+TUB, *n* = 30). Barre d'erreur, ESM. *, P < 0,05 ; **, P < 0,005 ; ***, P < 0,001 (test *t*).

aussi que la perte d'inhibition d'HDAC6 pourrait être une des causes majeures des défauts d'adhésion résultant de l'inactivation de p21.

D) CONCLUSION

Les travaux présentés indiquent pour la première fois que p21 contribue à la régulation de la dynamique du cytosquelette au cours de l'adhésion des cellules épithéliales mammaires humaines (Fig. B.19). En effet, nous montrons d'abord que p21 est requise pour l'étalement cellulaire normal, la formation et le renouvellement de l'adhésion focale. De plus, notre étude démontre que p21 est requise pour l'assemblage normal des fibres de stress, vraisemblablement en participant au contrôle de la GTPase Rho et de la cofiline. Nous montrons également que l'activité de régulation transcriptomique associée à p21 pourrait jouer un rôle important dans cette fonction, en modulant notamment l'expression de certains facteurs d'activation de Rho (RhoGAP19, RhoGAP5). Enfin, notre étude révèle que p21 est nécessaire à la stabilisation microtubulaire, possiblement via l'inhibition d'HDAC6, et que cette fonction est, au moins partiellement impliquée, dans le contrôle de l'adhésion. De notre point de vue, ce travail relativement préliminaire soulève plusieurs questions quant au rôle exact de p21 dans la régulation du cytosquelette :

1) Est-ce que le contrôle d'expression de facteurs de régulation suffit à expliquer la modulation de l'activité de Rho par p21 ? Si ce n'est pas le cas, est-ce que p21 pourrait, par interaction directe, modifier l'activité de facteurs de régulation de Rho ?

2) Nous montrons ici, que l'inactivation d'*ARHGAP19* provoque une altération majeure de la formation de l'adhésion focale (Fig. B.14, Fig. B.15). Ce résultat nous permet de proposer RhoGAP19 comme un nouveau facteur de régulation de Rho au cours de la formation de l'adhésion focale. Cependant, pour adresser plus complètement la responsabilité de RhoGAP19 dans l'inactivation de Rho il serait intéressant d'évaluer aussi l'activité des autres GAP déjà connus pour leur rôle dans l'adhésion focale (159, 267).

3) Quelle est exactement l'origine de l'hyperactivation de la cofiline dans les cellules p21KD ? S'agit-il uniquement de l'altération de la voie dépendante de PKCμ ou est-ce que d'autres voies de régulation, notamment au niveau de l'adhésion focale, sont impliquées dans ce phénomène ?

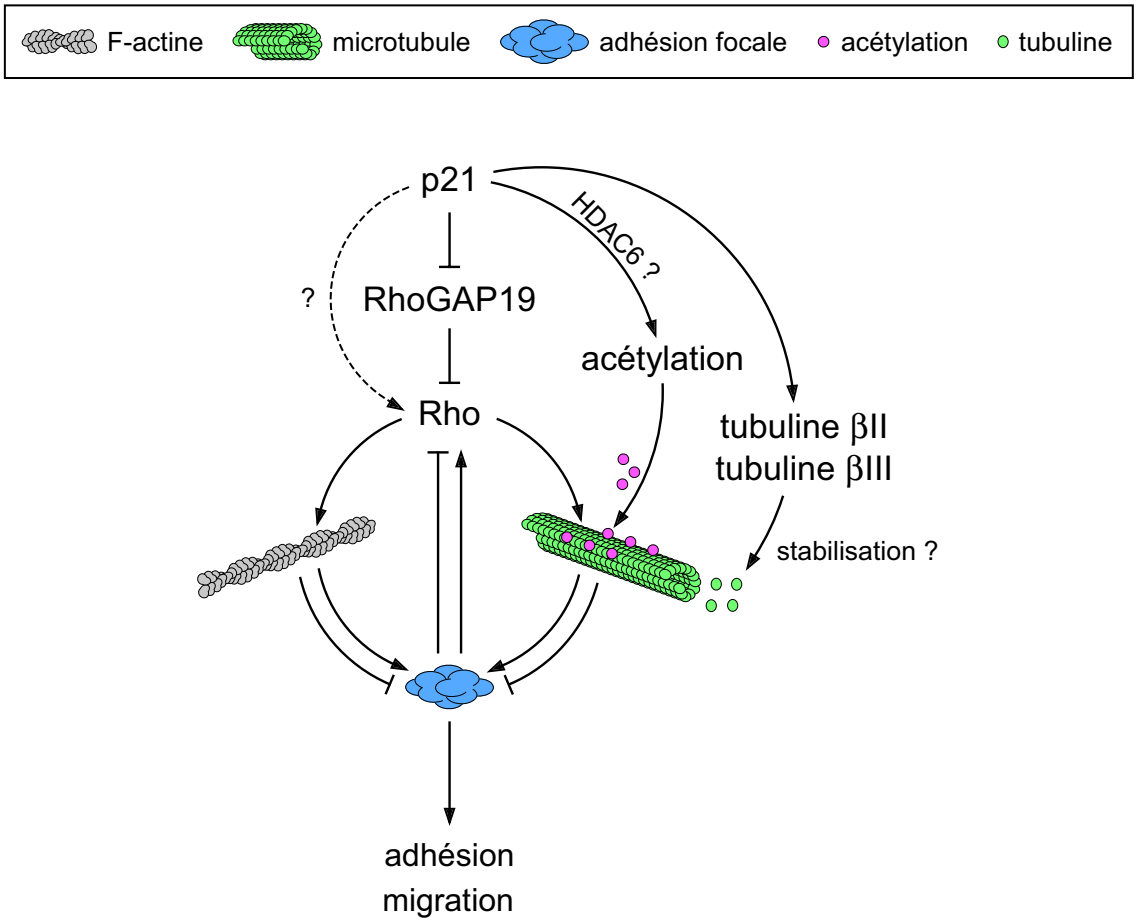

Figure B.19. Modèle de régulation du cytosquelette par p21 pour le contrôle de l'adhésion.

4) De quelle manière l'interrégulation de Rho et des adhésions focales est modifiée dans les cellules p21KD ?

5) Sachant que les assemblages de l'actine et des microtubules sont également interrégulés, de quelle manière les défauts de l'un modifient la dynamique de l'autre lors de l'inactivation de p21 ?

6) Pourquoi la déplétion de p21 dans les cellules non transformées semble ne pas modifier l'activité des LIMK alors que des travaux antérieurs ont montré qu'elles sont inhibées par la forme cytoplasmique de p21 (130, 131) ? Notre analyse du transcriptome montre que p57 pourrait être surexprimée dans les cellules dépourvues de p21 (Table 1). Or, plusieurs travaux ont montré qu'elle interagit avec LIMK1 (438, 439). Néanmoins, l'effet de p57 sur la dynamique de l'actine n'est pas encore totalement compris, bien que les derniers travaux en date proposent que p57 soit un activateur des LIMK et donc un promoteur des fibres de stress (439). Cependant l'absence de modifications de la phosphorylation des LIMK dans les cellules p21KD suggère que, si leur activité est modifiée en l'absence de p21, il s'agit d'un phénomène indépendant de leur phosphorylation par les ROCK. Caractériser l'équilibre entre les différents CKI dans le contrôle de l'actine, dans les cellules humaines non transformées, sera donc crucial pour mieux comprendre les conséquences de leur inactivation au cours du processus tumoral.

7) Est-ce que l'inactivation des tubulines βII et βIII due à la suppression de p21 participe à la déstabilisation des microtubules dans ces cellules ? Comment leur expression est-elle contrôlée par p21 ?

8) Est-ce que l'hypoacétylation de la tubuline dans les cellules p21KD est due à la perte d'inhibition d'HDAC6 ? Si c'est le cas, est-ce que p21 inhibe HDAC6 par interaction directe avec celle-ci ou un complexe régulateur, ou module-t-elle l'expression de facteurs encore non identifiés et contrôlant son activité ? Sinon, quelles voies alternatives régulant l'acétylation de la tubuline sont altérées en réponse à l'inactivation de p21 ?

L'ensemble de ces questions devra faire l'objet d'une étude plus approfondie afin de préciser le rôle de p21 dans le contrôle du cytosquelette. Les perspectives de ce projet devraient permettre de mieux comprendre en quoi l'altération de p21 au cours du processus tumoral mammaire peut participer aux altérations du cytosquelette qui contribuent notamment aux phénomènes d'invasion et de métastase. De nombreuses stratégies thérapeutiques ont pour cible la modification de la dynamique microtubulaire, en particulier celles employées pour la chimiothérapie des cancers du sein. Il sera donc de première importance de définir en quoi p21 peut éventuellement être un facteur prédictif de réponse à ce type de traitement.

E) MATERIELS ET METHODES

E.1) Plasmides et siRNA

Le plasmide pAcGFP1-Tubulin a été fourni par Clontech. La séquence codante du gène de la paxillin, *PXN* a été amplifiée par PCR à partir de l'ADNc total de la lignée épithéliale mammaire non tumorale HME-1 grâce aux amorces suivantes :

Sens : 5'-TAATTGGTACCATGGACGACCTCGACGCCCTGCTGGCGGACTT

Antisens : 5'-TAACGCAGATCTCTAGCAGAAGAGCTTGAGGAAGCAGTTCTGACAG.

Le produit de purification de cette PCR a été digéré par les enzymes KpnI et BglII, et cloné dans le vecteur pEGFP-C1 (Clontech) digéré par KpnI et BamHI afin de générer le vecteur pGFP-PXN. Le vecteur rétroviral pQC-GPXN a été construit en clonant le produit de digestion de pGFP-PXN par AgeI et BamHI dans le vecteur pQCXIN (Clontech).

Les différents vecteurs lentiviraux (pLKO.1) codant pour un shRNA ciblant *CDKN1A* ont été achetés chez Sigma-Aldrich (TRCN0000040123-7). La position sur l'ARNm de *CDKN1A* du premier nucléotide de la séquence cible du shRNA (sh) a été utilisée pour désigner les vecteurs correspondants. La transduction des vecteurs pLKO.1 sh5 et pLKO.1 sh6 a permis la meilleure inhibition de l'expression de p21 et fut utilisée dans toutes les expériences nécessitant l'invalidation stable par interférence ARN (ARNi ; knock-down, KD) de *CDKN1A*. La transduction du vecteur pLKO.1 codant pour un shRNA ne ciblant aucun ARNm identifié chez l'humain (NT, non targeting) (Sigma) fut utilisé comme contrôle au cours de ces expériences.

Un pool de quatre siRNA (siGENOME SMARTpool, Dharmacon) fut utilisé au cours des expériences d'invalidation transitoire par interférence ARN de *SSH1*, *PRKD1* et *ARHGAP19*, afin d'inhiber respectivement les expressions de SSH1L (protein phosphatase slingshot homolog 1), PKCμ et RhoGAP19. Les siRNA individuels ciblant p21 et correspondant aux séquences des sh5 et sh6 (si5 and si6) furent également commandées chez Dharmacon. Un pool de quatre siRNA ne ciblant aucun ARNm identifié chez l'humain (siCONTROL Non-Targeting siRNA Pool #2, Dharmacon) fut utilisé comme contrôle au cours de ces expériences.

E.2) Culture cellulaire, transfection de plasmides et infection

Les cellules épithéliales mammaires humaines (HMEC) ont été fournies par Lonza. Les cellules épithéliales mammaires humaines immortalisées après transduction de hTERT et à faible passage ont été obtenues auprès de R. A. Weinberg (Whitehead Institute, Cambrige, USA) et appelées hTMEC. Les lignées dérivées des HMEC et hTMEC ont été cultivées dans le milieu de base pour cellules épithéliales mammaires MEBM (Lonza) complétées avec de l'EGF (10 ng/mL), de l'insuline humaine (5 µg/mL), de l'hydrocortisone (0,5 µg/mL), 0,4% d'extrait pituitaire bovin, de la gentamycine (50 µg/mL) et de l'amphotéricine B (50 ng/mL).

La transfection de plasmides dans les hTMEC a été réalisée grâce au FuGENE HD (Roche) et un ratio agent de transfection/ADN de 6:2. La production rétrovirale a été réalisée par les cellules Phoenix Ampho (SD 3443, ATCC) et la production lentivirale par les cellules 293FT (Invitrogen) co-transfectée par le vecteur pCMV∆R8.91 (D. Trono, EPFL, Lausanne, Switzerland) et le vecteur phCMV-G (F.-L. Cosset, ENS, Lyon, France). Les cellules transfectées par pAcGFP1-Tubulin et transduites pour pQC-GPXN, appelées respectivement GT-hMEC and GP-hMEC, furent sélectionnées par un traitement à la généticine à 100 µg/mL. Les sous-clones obtenus par dilution limite (3,33 cellules/mL ; plaque 96 puits ; 100 µL/puit) furent sélectionnés selon des critères de similarité morphologique bidimensionnelle avec le phénotype dominant de la lignée mère, l'expression optimale des protéines chimères fluorescentes (GFP-tubuline, GFP-paxilline) et leur croissance. La validation des lignées exprimant une protéine chimère fluorescente fut réalisée par imagerie sur cellules vivantes et fixées. Les lignées transduites pour les vecteurs pLKO.1 furent sélectionnées par un traitement à la puromycine à 0,5 µg/mL. Les lignées transduites pour pLKO.1 sh5, sh6 et NT furent respectivement désignées p21KD5, p21KD6 et NT. La présentation des données obtenues avec un modèle cellulaire présentant un knock-down stable de *CDKN1A* indique que des résultats similaires ont été obtenus avec un deuxième modèle indépendant si celui-ci n'est pas présenté.

La transfection de siRNA (10-30 nM) dans les cellules dérivées de hTMEC fut réalisée en utilisant la Lipofectamine RNAiMAX (Invitrogen).

E.3) Anticorps et réactifs

Anticorps	Espèce	Clone	Fabricant
Cdc42	souris	-	Millipore
cofiline	lapin		Cell Signaling Technology
cycline B1	souris	GNS3	Millipore
FAK	lapin	-	Cell Signaling Technology
Ig murines / conjugué TRITC	lapin	-	DAKO
Ku80	souris	7/Ku80	BD Biosciences
LIMK1	lapin	-	Cell Signaling Technology
LIMK2	lapin	-	Cell Signaling Technology
p21	souris	CP36-CP74	Millipore
paxilline	souris	349/Paxillin	BD Biosciences
PKCμ	lapin	-	Cell Signaling Technology
pT508/5 LIMK	lapin	-	Cell Signaling Technology
pS3 cofiline	lapin	77G2	Cell Signaling Technology
pS744/748 PKCμ	lapin	-	Cell Signaling Technology
pS978 SSH1L	lapin	-	K. Mizuno (Graduate School of Life Sciences, Sendai, Japan)
pT780 Rb	lapin	-	Cell Signaling Technology
pT807/811 Rb	lapin	-	Cell Signaling Technology
pY397 FAK	lapin	-	Cell Signaling Technology
pY416 Src	lapin	-	Cell Signaling Technology
Rac1	souris	102	BD Biosciences
Rb	souris	4H1	Cell Signaling Technology
RhoA/B/C	souris	55	Millipore
Src	souris	L4A1	Cell Signaling Technology
SSH1L	lapin	-	Bethyl Laboratories
tubuline α totale	souris	B-5-1-2	Sigma
tubuline α totale / conjugué FITC	souris	DM1A	Sigma
tubuline acétylée	souris	6-11B-1	Sigma
tubuline glutamylée	souris	B3	Sigma
tubuline tyrosinylée	souris	TUB-1A2	Sigma
tubuline β totale	souris	TUB 2.1	Sigma
tubuline βI	souris	SAP.4G5	Sigma
tubuline βII	souris	7B9	Novus
tubuline βIII	souris	SDL.3D10	Sigma
tubuline βIV	souris	ONS.1A6	Sigma

Le colorant Hoechst 33258, la thymidine, la désoxycytidine, la RNAse, l'iodure de propidium, le paclitaxel et la mitomycine C ont été achetées chez Sigma. L'inhibiteur de ROCK, Y-27632, a été fourni par Calbiochem. Le peptide S3, inhibiteur de LIMK, et son analogue inactif S3-REV ont été synthétisés chez Eurogentec selon les séquences suivantes :

S3: H2N- MASGVAVSDGVIKVFNRQIKIWFQNRRMKWKK-COOH

S3-REV: H2N-NFV KIVGDSVAVGSAMRQIKIWFQNRRMKWKK-COOH.

L'exoenzyme C3 transférase utilisée pour l'inhibition spécifique des RhoGTPAses A, B et C, a été achetée chez Cytoskeleton. La solution de neutralisation de la trypsine fut achetée chez Lonza et l'oxyrase chez Oxyrase, Inc. L'inhibiteur spécifique de HDAC6, la tubacine, et son analogue inactif, la niltubacine, ont été gracieusement fournies par R. Mazitschek (Massachusetts General Hospital, Boston, USA).

E.4) Extraction de protéines

L'extraction de protéines totales fut réalisée par lyse, à 4°C, de culots cellulaires par le tampon de lyse TEB150 (HEPES (50 mM), NaCl (150 mM), MgCl2 (2 mM), EGTA (5 mM), DTT (1 mM), 0,5% Triton X-100 (0,5%), 10% glycerol (10%), orthovanadate de sodium (1 mM) activé extemporanément, PIC (1X) (Protease Inhibitor Cocktail 25X (1 comprimé / 2 mL eau), Roche). Après centrifugation (14000 rpm, 20 min, 4°C) les protéines totales contenues dans le surnageant furent dosées par lecture spectrophotométrique de la réaction obtenue avec Protein Assay (Biorad ; Coomassie Brilliant Blue G-250).

E.5) Western blot

L'analyse d'expression des protéines par western blot a été réalisée à l'aide de gel précoulé Criterion (XT Bis-Tris, gradient 4-12% ; Tris-HCl, 15%), en utilisant, pour les migrations sur gels gradients, le tampon XT MOPS pour les protéines de taille supérieure à 100 kDa et le tampon XT MES pour les protéines de taille inférieure à 100 kDa. En général, 50 μg de protéines, mélangées extemporanément au tampon de dépôt (agent de réduction XT et tampon de chargement XT (Biorad))

et dénaturées pendant 5 min à 95°C, furent déposés et résolus. Tous les transferts ont été réalisés sur membranes PVDF (0,22 μm) ou nitrocellulose (0,45 μm) de 8 x 13,5 cm, dans le tampon de transfert (Tris (48 mM), glycine (39 mM), 20% de méthanol), sur appareil de transfert semi-sec Trans-blot (Biorad) pendant 30-45 min (20 V ; 325 mA). Les membranes furent saturées avec les solutions adéquates (TBS-Tween 0,05% contenant 5% de lait écrémé ou de BSA).

E.6) Quantification de l'activité des GTPases Rho, Rac1 et Cdc42

La quantification de l'activité GTPase de RhoA/B/C (Rho), Rac1 et Cdc42 a été réalisée grâce aux kits Rho et Rac1/Cdc42 Activation Assay (Millipore). Brièvement, les GTPases Rho et Rac1/Cdc42 sous leur forme liée au GTP furent précipitées par pull-down à partir de 1 mg de protéines totales d'un lysat frais et à l'aide, respectivement, de 30 μg de GST-Rhotekin RBD et 15 μg de GST-PAK1 PBD liées à des billes de glutathion-agarose. Une pré-incubation du lysat avec du GTPγS ou du GDP fut utilisée respectivement comme contrôle positif et négatif. Après 1h30 à 2h d'incubation à 4°C, les billes furent lavées et 15 µL du mélange billes/tampon de chargement furent résolus, pour chaque échantillon, sur gel Bis-Tris, le résultat transféré sur membrane PVDF 0,22 µm et les membranes incubées avec les anticorps appropriés. Après détection par chimioluminescence, l'activité relative des GTPases fut évaluée par quantification du signal obtenu avec les formes liées au GTP issues du pull-down rapporté au signal obtenu avec les GTPases respectives dans le lysat protéique total de la même origine.

E.7) Extraction d'ARN

L'extraction d'ARN total fut réalisée par lyse de culots cellulaires par le TRI Reagent (Sigma) puis séparation en chloroforme (500 µL / million de cellules) sur tubes Phase Lock Gel (Eppendorf). La précipitation des ARN fut obtenue par ajout d'isopropanol. Les culots résultant de la précipitation furent lavés dans de l' l'éthanol à 75%, séchés et repris dans de l'eau stérile. Les ARN furent dosés et vérifiés sur Nanodrop ND-1000.

E.8) Analyse transcriptomique

L'ARN total correspondant à trois expériences indépendantes, incluant les hTMEC non traitées ou transfectées (48 h) avec un pool de siRNA contrôle (siCT) ou des siRNA ciblant p21 (si5 et si6), fut extrait sur colonnes, traité par la DNase, quantifié sur Nanodrop (Thermo Scientific) et vérifié sur Bioanalyzer 2100 (Agilent). Un microgramme de chaque ARN total fut amplifié sous forme d'ARN complémentaire ou antisens (ARNc, ARNa) à l'aide du kit d'amplification d'ARNa MessageAmp II (Ambion), dosé et vérifié. Dix microgrammes de chaque ARNc furent fragmentés puis hybridés sur puce CodeLink Human Whole Genome (Applied Microarrays), environ 57000 ARNm et EST (expression tagged sequences)). Les signaux obtenus après hybridation furent scannés à l'aide d'un scanner Genepix 4000B (Molecular Devices). Les résultats ont ensuite été filtrés en utilisant le logiciel d'analyse Genespring (Agilent). Seuls les transcrits présentant un facteur de modification supérieur ou égal à 1,3, en terme de sous- ou surexpression, à la fois dans les échantillons si5 et si6, comparés aux échantillons siCT, furent sélectionnés. Les données correspondant aux cellules non traitées furent utilisées comme contrôle d'expression pour la validation des échantillons siCT. Le logiciel IPA (Ingenuity Systems), combiné à une analyse bibliographique, fut utilisé pour la sélection finale des gènes codant pour des protéines caractérisées ou potentielles régulatrices du cytosquelette, et présentant une transcription significativement modifiée par l'inactivation de p21.

E.9) PCR quantitative en temps réel (qRT-PCR)

Les analyses de transcription ont été réalisées sur des ADNc totaux obtenus, selon les conseils du fabricant, par rétrotranscription d'1 à 2 µg d'ARN totaux par la transcriptase inverse du virus de la leucémie murine de Moloney (MoMLV) (kit First-Strand cDNA Synthesis (GE Healthcare)). Les qRT-PCR ont été préparées en capillaires, dans une solution de réaction comprenant 0,067 µL d'amorces (sens et antisens ; 200 nM), 0,067 µL de sonde (100 nM), 1,33 µL du mélange du kit LightCycler TaqMan Master (Roche Applied Science) contenant l'ADN polymérase FastStart Taq, 1,67 µL de cDNA (1/60) et de l'eau qsp 6,67 µL. Les réactions ont été réalisées sur LightCycler 2.0 System (Roche Applied Science) selon le programme suivant : 10 min à 95°C puis 40 cycles de 10 sec à 95°C, 30 sec à 59°C,

1 sec at 72°C. L'analyse a été réalisée sur LightCycler 2.0 System (Roche Applied Science). Les Cp (crossing point ; cycle de sortie) ont été enregistrés sur feuille Excel.

Les études de transcription ont toutes été réalisées par quantification relative de l'expression des ARNm d'intérêts par rapport à une combinaison de deux gènes choisis pour leur stabilité, selon une analyse combinée par les algorithmes NormFinder et geNorm, parmi les gènes de ménages candidats suivants : *ACTB*, *ATP6AP1*, *CFL1*, *GAPDH*, *GUSB*, *HPRT1*, *PGK1*, *PPIB*, *TBP*, *TFRC*, *TUBA1C* et *UBB* (486, 487). Les amorces et sondes correspondantes ont été choisies grâce au logiciel ProbeFinder 2.45 (Roche Applied Science) de façon à ce que toutes les amplifications chevauchent un intron, excluant ainsi les amplifications à partir d'ADN génomique contaminant. Les références de chaque qRT-PCR sont listées ci-dessous.

Gène	**ARNm cible (RefSeq NCBI)**	**Amorces**	**Séquence**	**Sonde UPL**
ACTB	NM_001101.2	sens	attggcaatgagcggttc	#11
		antisens	ggatgccacaggactccat	
ARHGAP19	NM_032900.4	sens	acgtcctgtggccaaaaa	#2
		antisens	agccatcccactgtttaacttt	
ARHGAP5	NM_001030055.1	sens	ctgccagatcctttaattcca	#38
	NM_001173.2	antisens	aaggcatgaagacgttctgttt	
ATP6AP1	NM_001183.4	sens	tgcagctctctacctacttagatcc	#1
		antisens	ctgtgaaatcctcaatgctcag	
CDKN1A	NM_078467.1	sens	tcactgtcttgtacccttgtgc	#32
	NM_000389.3	antisens	ggcgtttggagtggtagaaa	
CFL1	NM_005507.2	sens	gtgccctctccttttcgttt	#5
		antisens	ttgaacaccttgatgacaccat	
FLNB	NM_001457.2	sens	gaggaggcaccggtaaatg	#81
		antisens	gtcactcactgggacataggc	
GAPDH	NM_002046.3	sens	agccacatcgctcagacac	#60
		antisens	gcccaatacgaccaaatcc	
GUSB	NM_000181.2	sens	cgccctgcctatctgtattc	#57
		antisens	tccccacagggagtgtgtag	
HPRT1	NM_000194.1	sens	tgaccttgatttattttgcatacc	#73
		antisens	cgagcaagacgttcagtcct	
LAMC2	NM_005562.2	sens	ctcagcccaacgactagacc	#51
	NM_018891.2	antisens	tcacctgttgattcccaaga	
LPXN	NM_004811.1	sens	caatatccaggagctcaatgtct	#77

		antisens	tgagctcatccaactgagca	
MARK1	NM_018650.3	sens	tgaagaaattattagtcctgaatccaa	#34
		antisens	acattcatccatcgatctttca	
MICAL1	NM_022765.2	sens	ccccagacagaccacaaaa	#8
		antisens	ctggtggcatgctattctca	
PARVB	NM_001003828.1	sens	gctgcagaagctcttggaa	#30
	NM_013327.3	antisens	tgccctatttcggactgtgt	
PDPN	NM_001006624.1	sens	aaagtccaagcgccacag	#49
	NM_001006625.1	antisens	tgtctgtgtgtctccatccac	
	NM_006474.4			
	NM_198389.2			
PGK1	NM_000291.2	sens	ctgtggcttctggcatacct	#42
		antisens	cttgctgctttcaggacca	
PPIB	NM_000942.4	sens	acttcaccaggggagatgg	#20
		antisens	agccgttggtgtctttgc	
PPP2R1B	NM_002716.4	sens	agtgggaggtcctgactttg	#16
		antisens	tctcttccacagttgccaga	
SGEF	NM_015595.3	sens	ctctgcggtgaaaagaaagg	#79
		antisens	tcagaggatatgacttcaaagatagc	
TUBA1C	NM_032704.2	sens	ccccttcaagttctagtcatgc	#58
		antisens	cattgccaatctggacacc	
TUBB2A	NM_001069.2	sens	cacaggcagttaccatggag	#78
		antisens	cgaggtacatatttgttaccagca	
TUBB2B	NM_178012.4	sens	ttgcagctggagagaatcaa	#50
		antisens	acctaaccgaatccatcgtg	
TUBB3	NM_006086.2	sens	gcaactacgtgggcgact	#78
		antisens	cgaggcacgtacttgtgaga	
UBB	NM_018955.2	sens	aggatcctggtatccgctaac	#39
		antisens	tcacattttcgatggtgtcact	

E.10) Synchronisation et analyse du cycle cellulaire

La synchronisation des lignées issues de la lignée mère hTMEC a été réalisée par la technique de double-bloc thymidine. Brièvement, les cellules ont été traitées par de la thymidine (2 mM) pendant 16 h puis remises en présence de milieu frais contenant de la désoxycytidine (24 µM) et récoltées à chaque point-temps pendant 14 h. Le cycle cellulaire fut analysé de façon préliminaire par

cytométrie de flux. Les cellules récoltées ont été lavées en PBS, fixées dans de l'éthanol à 70 % et stockées à 4°C. Avant l'analyse, les cellules ont été réhydratées dans du PBS et resuspendues en présence de 1 mg/mL de RNAse A et 5 µg/mL d'iodure de propidium. La distribution du cycle cellulaire fut analysée sur un cytomètre de flux FACS Calibur (Becton Dickinson).

E.11) Microscopie et marquage fluorescent sur cellules fixées

Le marquage de la F-actine a été réalisé sur cellules extraites pendant 1 min à 37°C dans le Tampon de Stabilisation du Cytosquelette (TSC ; HEPES (20 mM), KCl (138 mM), MgCl2 (4 mM), EGTA (3 mM)) complété avec 0,1% de Triton X-100, 1% de BSA, de l'ATP (1 mM) et de la phalloïdine (3 µM)). Après un lavage en TBS complété par 0,1% de Triton X-100 (TBST), les cellules ont été fixées dans du TSC contenant 4% de PFA et 10% de sucrose. Ensuite, les cellules furent perméabilisées dans du TSC contenant 0,5% de Triton X-100 et 1% de BSA puis saturées pendant 20 min dans du TBST complété avec 3% de BSA et and 3% de FBS. Enfin, les cellules furent incubées avec de la phalloïdine conjuguée au TRITC (1/100) pendant 20 min à température ambiante et colorées avec du Hoechst 33258 (1 μg/mL) pendant 10 minutes.

Le marquage de la tubuline acétylée a été réalisé sur des cellules extraites à température ambiante pendant 1 min dans le Tampon de Stabilisation des microtubules (TSMT; PIPES (60 mM ; pH 6,8), HEPES (20 mM), $MgCl_2$ (1mM), EGTA (4mM)) complété par 0,04% de Triton X-100 et du paclitaxel (0.25 nM)). Les cellules ont été fixées dans du TSMT contenant 4% de PFA et 10% de sucrose, perméabilisées dans du TSMT complété par 0,5% Triton X-100 et saturées pendant 20 min dans du TBST complété avec 3% de BSA et 3% de FBS. Les cellules furent ensuite incubées avec l'anticorps anti-tubuline acétylée (1/1000) à température ambiante pendant 2 h puis avec l'anticorps anti-Ig murines conjugué au TRITC (1/100) à température ambiante pendant 1 h et colorées avec du Hoechst 33258 (1 µg/mL) pendant 10 minutes.

Le marquage de la tubuline α totale a été réalisé sur des cellules extraites à température ambiante pendant 1 min dans le TSMT complété par 0,04% de Triton X-100 et du paclitaxel (0,25 nM). Les cellules furent fixées dans du méthanol 100% pendant 15 min à -20°C, brièvement déshydratées et saturées pendant 20 min dans du TBST complété avec 3% de BSA et 3% de FBS. Les

cellules furent ensuite incubées avec l'anticorps anti-tubuline α totale conjugué au FITC (1/100) pendant 1 h à température ambiante pendant 1 h et colorées avec du Hoechst 33258 (1 µg/mL) pendant 10 minutes.

Le marquage de la paxilline a été réalisé sur des cellules fixées avec du TSC contenant 4% de PFA pendant 20 min à température ambiante puis perméabilisées avec du TBS complété par 1% de Triton X-100 pendant 15 min, dans les mêmes conditions. Les cellules furent ensuite incubées avec l'anticorps anti-paxilline (1/500) à température ambiante pendant 1 h puis avec l'anticorps anti-Ig murines conjugué au TRITC (1/100) à température ambiante pendant 1 h et colorées avec du Hoechst 33258 (1 μg/mL) pendant 10 minutes.

L'imagerie microscopique des marquages fluorescents a été réalisée sur un microscope Axioplan 2 à l'aide d'objectifs 100x/1.4 NA Plan-Apochromat et 63x/1.4 NA Plan-Apochromat, et l'acquisition fut automatisée grâce au logiciel MetaMorph (7.5.6.0). Les images du marquage de F-actine ont été acquises en séries de z (0,2 μm entre chaque plan) et la fluorescence totale a été quantifiée à partir d'images non traitées correspondant à la projection des images acquises en séries de z et selon leur intensité maximum. Pour le comptage des fibres de stress, leur mesure et leur présentation, les couleurs des images acquises ont été inversées, le bruit de fond supprimé, et les images résultantes traitées avec une matrice de convolution 5x5 et soumises à un filtre d'amélioration de l'acutance. Les images de marquage microtubulaire ont été acquises en séries de z (0,2 μm entre chaque plan) et traitées de la même manière que les images du marquage de F-actine.

E.12) Imagerie sur cellules vivantes et analyse

Les cellules vivantes ont été visualisées à l'aide d'un microscope Axiovert 100M (Zeiss) thermostaté à 37°C équipé d'une caméra CCD refroidie (CoolSNAP HQ monochrome; Photometrics). Les expériences ont été réalisées sur des cellules poussant dans des boîtes en plastique ou possédant un fond en verre (MatTek) maintenues par des inserts thermostatés et sous une atmosphère humidifiée contenant 5% de CO_2. Toutes les acquisitions ont été automatisées grâce au logiciel MetaMorph 7.5.6.0 (Molecular Devices).

L'imagerie en contraste de phase des phénomènes d'adhésion et de migration a été conduite avec un objectif A-Plan 10x/0.25 Ph1 (Zeiss) sur des cellules cultivées en MEBM complet et ensemencées en boîtes à fond plastique ou verre. L'adhésion a été filmée sur une solution de 5.10^3 cellules/mL complétée avec de la solution de neutralisation de la trypsine, 15 min après la récolte, selon 5 min d'intervalle, avec une exposition de 10 ms et pendant 24 h. L'aire des cellules a été mesurée manuellement à l'aide du logiciel ImageJ 1.42q.

La migration des cellules isolées a été analysée selon la même procédure, 24 à 36 h après ensemencement. La persistance directionnelle a été déterminée à partir d'enregistrement de 8 images successives comme le ratio de la distance à l'origine de la position de la cellule à la fin de la séquence par rapport à la distance totale parcourue. Le suivi de déplacements pendant plus de 35 min ne s'est pas avéré informatif de la persistance directionnelle, à la fois dans les cellules NT et p21KD. En effet, sur un support en plastique, celles-ci présentent des capacités de migration limitées à une zone de faible surface, centrée sur la position d'adhésion initiale. Cette observation est cohérente avec le fait que les cellules épithéliales mammaires ont été décrites comme des cellules présentant des propriétés migratoires limitées lorsqu'elles sont comparées à leur contrepartie transformée et métastatique.

Les tests de cicatrisation *in vitro* furent réalisés par enregistrement, dans les mêmes conditions, de la migration cellulaire, après retrait sur une zone rectiligne et à l'aide d'une pointe de pipette, d'une monocouche de cellules adhérentes et confluentes.

La dynamique protrusive a été analysée à partir d'images réalisées en contraste de phase à l'aide d'un objectif A-Plan 10x/0.25 Ph1, selon 6 sec d'intervalle et durant 20 min. Au moins trois enregistrements kymographiques par cellule furent utilisés pour évaluer les paramètres de la dynamique protrusive (488, 489). La fréquence de protrusion est exprimée en µm/min.

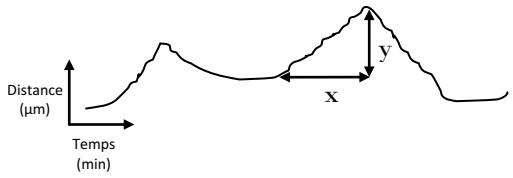

$\mathbf{x}$ = persistance

$\mathbf{y}$ = distance

$\mathbf{y/x}$ = vélocité

L'imagerie fluorescente des microtubules a été réalisée avec les objectifs 100x/1.4 NA Plan-Apochromat ou 63x/1.4 NA Plan-Apochromat (Zeiss), et une lampe à vapeur de mercure et arc court (120W ; X-Cite 120PC Q; EXFO) sur des cellules cultivées en MEBM sans rouge phénol contenant 5-10 µL/mL d'oxyrase (Oxyrase, Inc.) utilisée pour réduire le stress oxydatif consécutif au photoblanchiment des molécules de GFP. Les acquisitions ont été réalisées selon un focus optimal dans la région lamellaire, à 3,5 s d'intervalle, avec 350 ms d'exposition et pendant un minimum de 2,5 min. L'enregistrement de la position de l'extrémité libre des microtubules, repérée manuellement, a été réalisé à l'aide du logiciel ImageJ 1.42q (http://rsb.info.nih.gov/ij/) et du plugin MTrackJ (Erik Meijering; http://www.imagescience.org/meijering/software/mtrackj/). Pour l'analyse et la présentation, les séquences d'images assemblées en séries ont subi une inversion de couleurs, une suppression du bruit de fond, une correction du photoblanchiment, un traitement par un filtre FFT passe-bande et une augmentation de contraste. La mesure de distance entre l'extrémité libre et un point fixe sur le corps du MT a été utilisée pour évaluer les changements de longueur et la vélocité entre chaque point temps. Seuls les changements de longueur ≥ 0.4 µm entre deux images consécutives furent considérés comme des événements de croissance ou de raccourcissement. De la même manière, les changements < 0.4 µm furent considérés comme des pauses. Au cours de l'analyse, des événements uniques ou consécutifs de croissance, raccourcissement ou pause furent respectivement considérés comme des phases de croissance, raccourcissement ou pause. Les taux moyens de croissance ou de raccourcissement furent calculés comme la moyenne des vélocités microtubulaire dans chacune des phases, à l'aide d'une macro Excel écrite à cet effet. La variation de longueur microtubulaire totale de chaque phase fut calculée par le produit du taux moyen de croissance ou de raccourcissement par la durée totale de la phase. Les catastrophes (transitions d'une phase de croissance ou de pause à un raccourcissement) et les sauvetages (transitions d'une phase de raccourcissement à une pause ou une croissance) furent comptés à l'aide d'une macro Excel. La fréquence de catastrophes fut calculée en divisant le nombre de catastrophes par la somme du temps passé en croissance ou pause. De même que la fréquence de sauvetage fut calculée en divisant le nombre de sauvetages par le temps passé en croissance. La dynamicité microtubulaire fut mesurée comme la longueur acquise en phase de croissance ajoutée à celle perdue par raccourcissement et divisée par la durée de vie totale du microtubule. La dynamicité moyenne fut calculée comme la

moyenne des dynamicités microtubulaires. Pour chaque condition, nous avons analysé un minimum de 60 microtubules dans 10 cellules.

L'imagerie fluorescente des plaques d'adhésion focale a été réalisée à l'aide d'un objectif 63x/1.4 NA Plan-Apochromat (Zeiss) selon les mêmes conditions d'excitation et de culture que pour l'imagerie des microtubules. Chaque acquisition fut réalisée en série de z (0,2 µm entre chaque plan) en utilisant une exposition de 300 à 500 ms. Les acquisitions cinétiques furent réalisées avec un intervalle de 40 sec et pendant 15-25 min. Les enregistrements ont été traités par le plugin Smart Projector d'ImageJ afin d'obtenir, pour chaque séquence, une projection en z optimal. Les séquences finales furent soumises à une inversion de couleurs, une suppression du bruit de fond, une correction du photoblanchiment, un traitement par des filtres FFT passe-bande et d'amélioration de l'acutance. La numération et la mesure des aires d'adhésion focale furent réalisées sur les images issues du traitement précédent, soumises à un seuillage et converties en images binaires.

F) BIBLIOGRAPHIE

(1) Zhang, H., Xiong, Y., and Beach, D. Proliferating cell nuclear antigen and p21 are components of multiple cell cycle kinase complexes. *Mol.Biol.Cell*. 4(9): 897-906, 1993.

(2) Harper, J.W., Adami, G.R., Wei, N., Keyomarsi, K., and Elledge, S.J. The p21 Cdk-interacting protein Cip1 is a potent inhibitor of G1 cyclin-dependent kinases. *Cell*. 75(4): 805-16, 1993.

(3) el-Deiry, W.S., Tokino, T., Velculescu, V.E., Levy, D.B., Parsons, R., Trent, J.M., Lin, D., Mercer, W.E., Kinzler, K.W., and Vogelstein, B. WAF1, a potential mediator of p53 tumor suppression. *Cell*. 75(4): 817-25, 1993.

(4) Luo, Y., Hurwitz, J., and Massague, J. Cell-cycle inhibition by independent CDK and PCNA binding domains in p21Cip1. *Nature*. 375(6527): 159-61, 1995.

(5) Chen, J., Jackson, P.K., Kirschner, M.W., and Dutta, A. Separate domains of p21 involved in the inhibition of Cdk kinase and PCNA. *Nature*. 374(6520): 386-8, 1995.

(6) Koepp, D.M., Harper, J.W., and Elledge, S.J. How the cyclin became a cyclin: regulated proteolysis in the cell cycle. *Cell*. 97(4): 431-4, 1999.

(7) Obaya, A.J. and Sedivy, J.M. Regulation of cyclin-Cdk activity in mammalian cells. *Cell Mol.Life Sci.* 59(1): 126-42, 2002.

(8) Moldovan, G.L., Pfander, B., and Jentsch, S. PCNA, the maestro of the replication fork. *Cell*. 129(4): 665-79, 2007.

(9) Lowe, S.W., Cepero, E., and Evan, G. Intrinsic tumour suppression. *Nature*. 432(7015): 307-15, 2004.

(10) Bartkova, J., Horejsi, Z., Koed, K., Kramer, A., Tort, F., Zieger, K., Guldberg, P., Sehested, M., Nesland, J.M., Lukas, C., Orntoft, T., Lukas, J., and Bartek, J. DNA damage response as a candidate anti-cancer barrier in early human tumorigenesis. *Nature*. 434(7035): 864-70, 2005.

(11) Gorgoulis, V.G., Vassiliou, L.V., Karakaidos, P., Zacharatos, P., Kotsinas, A., Liloglou, T., Venere, M., DiTullio, R.A., Jr., Kastrinakis, N.G., Levy, B., Kletsas, D., Yoneta, A., Herlyn, M., Kittas, C., and Halazonetis, T.D. Activation of the DNA damage checkpoint and genomic instability in human precancerous lesions. *Nature*. 434(7035): 907-13, 2005.

(12) Bartkova, J., Rezaei, N., Liontos, M., Karakaidos, P., Kletsas, D., Issaeva, N., Vassiliou, L.V., Kolettas, E., Niforou, K., Zoumpourlis, V.C., Takaoka, M., Nakagawa, H., Tort, F., Fugger, K., Johansson, F., Sehested, M., Andersen, C.L., Dyrskjot, L., Orntoft, T., Lukas, J., Kittas, C.,

Helleday, T., Halazonetis, T.D., Bartek, J., and Gorgoulis, V.G. Oncogene-induced senescence is part of the tumorigenesis barrier imposed by DNA damage checkpoints. *Nature*. 444(7119): 633-7, 2006.

(13) Martin-Caballero, J., Flores, J.M., Garcia-Palencia, P., and Serrano, M. Tumor susceptibility of p21(Waf1/Cip1)-deficient mice. *Cancer Res.* 61(16): 6234-8, 2001.

(14) Shim, J., Lee, H., Park, J., Kim, H., and Choi, E.J. A non-enzymatic p21 protein inhibitor of stress-activated protein kinases. *Nature*. 381(6585): 804-6, 1996.

(15) Suzuki, A., Tsutomi, Y., Miura, M., and Akahane, K. Caspase 3 inactivation to suppress Fas-mediated apoptosis: identification of binding domain with p21 and ILP and inactivation machinery by p21. *Oncogene*. 18(5): 1239-44, 1999.

(16) Suzuki, A., Kawano, H., Hayashida, M., Hayasaki, Y., Tsutomi, Y., and Akahane, K. Procaspase 3/p21 complex formation to resist fas-mediated cell death is initiated as a result of the phosphorylation of p21 by protein kinase A. *Cell Death.Differ.* 7(8): 721-8, 2000.

(17) Chen, J., Saha, P., Kornbluth, S., Dynlacht, B.D., and Dutta, A. Cyclin-binding motifs are essential for the function of p21CIP1. *Mol.Cell Biol.* 16(9): 4673-82, 1996.

(18) Jascur, T., Brickner, H., Salles-Passador, I., Barbier, V., El, K.A., Smith, B., Fotedar, R., and Fotedar, A. Regulation of p21(WAF1/CIP1) stability by WISp39, a Hsp90 binding TPR protein. *Mol.Cell*. 17(2): 237-49, 2005.

(19) Delavaine, L. and La Thangue, N.B. Control of E2F activity by p21Waf1/Cip1. *Oncogene*. 18(39): 5381-92, 1999.

(20) Coqueret, O. and Gascan, H. Functional interaction of STAT3 transcription factor with the cell cycle inhibitor p21WAF1/CIP1/SDI1. *J.Biol.Chem.* 275(25): 18794-800, 2000.

(21) Goubin, F. and Ducommun, B. Identification of binding domains on the p21Cip1 cyclin-dependent kinase inhibitor. *Oncogene*. 10(12): 2281-7, 1995.

(22) Nakanishi, M., Robetorye, R.S., Adami, G.R., Pereira-Smith, O.M., and Smith, J.R. Identification of the active region of the DNA synthesis inhibitory gene p21Sdi1/CIP1/WAF1. *EMBO J.* 14(3): 555-63, 1995.

(23) Asada, M., Yamada, T., Ichijo, H., Delia, D., Miyazono, K., Fukumuro, K., and Mizutani, S. Apoptosis inhibitory activity of cytoplasmic p21(Cip1/WAF1) in monocytic differentiation. *EMBO J.* 18(5): 1223-34, 1999.

(24) Huang, S., Shu, L., Dilling, M.B., Easton, J., Harwood, F.C., Ichijo, H., and Houghton, P.J. Sustained activation of the JNK cascade and rapamycin-induced apoptosis are suppressed by p53/p21(Cip1). *Mol.Cell.* 11(6): 1491-501, 2003.

(25) Zhan, J., Easton, J.B., Huang, S., Mishra, A., Xiao, L., Lacy, E.R., Kriwacki, R.W., and Houghton, P.J. Negative regulation of ASK1 by p21Cip1 involves a small domain that includes Serine 98 that is phosphorylated by ASK1 in vivo. *Mol.Cell Biol.* 27(9): 3530-41, 2007.

(26) Touitou, R., Richardson, J., Bose, S., Nakanishi, M., Rivett, J., and Allday, M.J. A degradation signal located in the C-terminus of p21WAF1/CIP1 is a binding site for the C8 alpha-subunit of the 20S proteasome. *EMBO J.* 20(10): 2367-75, 2001.

(27) Kearsey, J.M., Coates, P.J., Prescott, A.R., Warbrick, E., and Hall, P.A. Gadd45 is a nuclear cell cycle regulated protein which interacts with p21Cip1. *Oncogene*. 11(9): 1675-83, 1995.

(28) Vairapandi, M., Balliet, A.G., Fornace, A.J., Jr., Hoffman, B., and Liebermann, D.A. The differentiation primary response gene MyD118, related to GADD45, encodes for a nuclear protein which interacts with PCNA and p21WAF1/CIP1. *Oncogene*. 12(12): 2579-94, 1996.

(29) Rodriguez-Vilarrupla, A., Jaumot, M., Abella, N., Canela, N., Brun, S., Diaz, C., Estanyol, J.M., Bachs, O., and Agell, N. Binding of calmodulin to the carboxy-terminal region of p21 induces nuclear accumulation via inhibition of protein kinase C-mediated phosphorylation of Ser153. *Mol.Cell Biol.* 25(16): 7364-74, 2005.

(30) Funk, J.O., Waga, S., Harry, J.B., Espling, E., Stillman, B., and Galloway, D.A. Inhibition of CDK activity and PCNA-dependent DNA replication by p21 is blocked by interaction with the HPV-16 E7 oncoprotein. *Genes Dev.* 11(16): 2090-100, 1997.

(31) Harris, T.E., Albrecht, J.H., Nakanishi, M., and Darlington, G.J. CCAAT/enhancer-binding protein-alpha cooperates with p21 to inhibit cyclin-dependent kinase-2 activity and induces growth arrest independent of DNA binding. *J.Biol.Chem.* 276(31): 29200-9, 2001.

(32) Ono, T., Kitaura, H., Ugai, H., Murata, T., Yokoyama, K.K., Iguchi-Ariga, S.M., and Ariga, H. TOK-1, a novel p21Cip1-binding protein that cooperatively enhances p21-dependent inhibitory activity toward CDK2 kinase. *J.Biol.Chem.* 275(40): 31145-54, 2000.

(33) Frouin, I., Maga, G., Denegri, M., Riva, F., Savio, M., Spadari, S., Prosperi, E., and Scovassi, A.I. Human proliferating cell nuclear antigen, poly(ADP-ribose) polymerase-1, and p21waf1/cip1. A dynamic exchange of partners. *J.Biol.Chem.* 278(41): 39265-8, 2003.

(34) Kitaura, H., Shinshi, M., Uchikoshi, Y., Ono, T., Iguchi-Ariga, S.M., and Ariga, H. Reciprocal regulation via protein-protein interaction between c-Myc and p21(cip1/waf1/sdi1) in DNA replication and transcription. *J.Biol.Chem.* 275(14): 10477-83, 2000.

(35) Jin, Y., Lee, H., Zeng, S.X., Dai, M.S., and Lu, H. MDM2 promotes p21waf1/cip1 proteasomal turnover independently of ubiquitylation. *EMBO J.* 22(23): 6365-77, 2003.

(36) Estanyol, J.M., Jaumot, M., Casanovas, O., Rodriguez-Vilarrupla, A., Agell, N., and Bachs, O. The protein SET regulates the inhibitory effect of p21(Cip1) on cyclin E-cyclin-dependent kinase 2 activity. *J.Biol.Chem.* 274(46): 33161-5, 1999.

(37) McShea, A., Samuel, T., Eppel, J.T., Galloway, D.A., and Funk, J.O. Identification of CIP-1-associated regulator of cyclin B (CARB), a novel p21-binding protein acting in the G2 phase of the cell cycle. *J.Biol.Chem.* 275(30): 23181-6, 2000.

(38) Gotz, C., Wagner, P., Issinger, O.G., and Montenarh, M. p21WAF1/CIP1 interacts with protein kinase CK2. *Oncogene*. 13(2): 391-8, 1996.

(39) Huang, D.Y. and Chang, Z.F. Interaction of human thymidine kinase 1 with p21(Waf1). *Biochem.J.* 356(Pt 3): 829-34, 2001.

(40) Waga, S. and Stillman, B. Cyclin-dependent kinase inhibitor p21 modulates the DNA primer-template recognition complex. *Mol.Cell Biol.* 18(7): 4177-87, 1998.

(41) Oku, T., Ikeda, S., Sasaki, H., Fukuda, K., Morioka, H., Ohtsuka, E., Yoshikawa, H., and Tsurimoto, T. Functional sites of human PCNA which interact with p21 (Cip1/Waf1), DNA polymerase delta and replication factor C. *Genes Cells*. 3(6): 357-69, 1998.

(42) Maga, G., Ramadan, K., Locatelli, G.A., Shevelev, I., Spadari, S., and Hubscher, U. DNA elongation by the human DNA polymerase lambda polymerase and terminal transferase activities are differentially coordinated by proliferating cell nuclear antigen and replication protein A. *J.Biol.Chem.* 280(3): 1971-81, 2005.

(43) Levin, D.S., Bai, W., Yao, N., O'Donnell, M., and Tomkinson, A.E. An interaction between DNA ligase I and proliferating cell nuclear antigen: implications for Okazaki fragment synthesis and joining. *Proc.Natl.Acad.Sci.U.S.A*. 94(24): 12863-8, 1997.

(44) Chen, I.T., Smith, M.L., O'Connor, P.M., and Fornace, A.J., Jr. Direct interaction of Gadd45 with PCNA and evidence for competitive interaction of Gadd45 and p21Waf1/Cip1 with PCNA. *Oncogene*. 11(10): 1931-7, 1995.

(45) Chuang, L.S., Ian, H.I., Koh, T.W., Ng, H.H., Xu, G., and Li, B.F. Human DNA-(cytosine-5) methyltransferase-PCNA complex as a target for p21WAF1. *Science*. 277(5334): 1996-2000, 1997.

(46) Warbrick, E., Lane, D.P., Glover, D.M., and Cox, L.S. Homologous regions of Fen1 and p21Cip1 compete for binding to the same site on PCNA: a potential mechanism to co-ordinate DNA replication and repair. *Oncogene*. 14(19): 2313-21, 1997.

(47) Warbrick, E., Lane, D.P., Glover, D.M., and Cox, L.S. A small peptide inhibitor of DNA replication defines the site of interaction between the cyclin-dependent kinase inhibitor p21WAF1 and proliferating cell nuclear antigen. *Curr.Biol.* 5(3): 275-82, 1995.

(48) Adams, P.D., Sellers, W.R., Sharma, S.K., Wu, A.D., Nalin, C.M., and Kaelin, W.G., Jr. Identification of a cyclin-cdk2 recognition motif present in substrates and p21-like cyclin-dependent kinase inhibitors. *Mol.Cell Biol.* 16(12): 6623-33, 1996.

(49) Ball, K.L., Lain, S., Fahraeus, R., Smythe, C., and Lane, D.P. Cell-cycle arrest and inhibition of Cdk4 activity by small peptides based on the carboxy-terminal domain of p21WAF1. *Curr.Biol.* 7(1): 71-80, 1997.

(50) Lin, J., Reichner, C., Wu, X., and Levine, A.J. Analysis of wild-type and mutant p21WAF-1 gene activities. *Mol.Cell Biol.* 16(4): 1786-93, 1996.

(51) Levkau, B., Koyama, H., Raines, E.W., Clurman, B.E., Herren, B., Orth, K., Roberts, J.M., and Ross, R. Cleavage of p21Cip1/Waf1 and p27Kip1 mediates apoptosis in endothelial cells through activation of Cdk2: role of a caspase cascade. *Mol.Cell*. 1(4): 553-63, 1998.

(52) Gervais, J.L., Seth, P., and Zhang, H. Cleavage of CDK inhibitor p21(Cip1/Waf1) by caspases is an early event during DNA damage-induced apoptosis. *J.Biol.Chem.* 273(30): 19207-12, 1998.

(53) Jin, Y.H., Yoo, K.J., Lee, Y.H., and Lee, S.K. Caspase 3-mediated cleavage of p21WAF1/CIP1 associated with the cyclin A-cyclin-dependent kinase 2 complex is a prerequisite for apoptosis in SK-HEP-1 cells. *J.Biol.Chem.* 275(39): 30256-63, 2000.

(54) Mutoh, M., Lung, F.D., Long, Y.Q., Roller, P.P., Sikorski, R.S., and O'Connor, P.M. A p21(Waf1/Cip1)carboxyl-terminal peptide exhibited cyclin-dependent kinase-inhibitory activity and cytotoxicity when introduced into human cells. *Cancer Res.* 59(14): 3480-8, 1999.

(55) Dong, C., Lyu, S.C., Krensky, A.M., and Clayberger, C. DQ 65-79, a peptide derived from HLA class II, mimics p21 to block T cell proliferation. *J.Immunol.* 171(10): 5064-70, 2003.

(56) Dong, C., Li, Q., Lyu, S.C., Krensky, A.M., and Clayberger, C. A novel apoptosis pathway activated by the carboxyl terminus of p21. *Blood*. 105(3): 1187-94, 2005.

(57) Rossig, L., Badorff, C., Holzmann, Y., Zeiher, A.M., and Dimmeler, S. Glycogen synthase kinase-3 couples AKT-dependent signaling to the regulation of p21Cip1 degradation. *J.Biol.Chem.* 277(12): 9684-9, 2002.

(58) Lee, J.Y., Yu, S.J., Park, Y.G., Kim, J., and Sohn, J. Glycogen synthase kinase 3beta phosphorylates p21WAF1/CIP1 for proteasomal degradation after UV irradiation. *Mol.Cell Biol.* 27(8): 3187-98, 2007.

(59) Bornstein, G., Bloom, J., Sitry-Shevah, D., Nakayama, K., Pagano, M., and Hershko, A. Role of the SCFSkp2 ubiquitin ligase in the degradation of p21Cip1 in S phase. *J.Biol.Chem.* 278(28): 25752-7, 2003.

(60) Rossig, L., Jadidi, A.S., Urbich, C., Badorff, C., Zeiher, A.M., and Dimmeler, S. Akt-dependent phosphorylation of p21(Cip1) regulates PCNA binding and proliferation of endothelial cells. *Mol.Cell Biol.* 21(16): 5644-57, 2001.

(61) Zhou, B.P., Liao, Y., Xia, W., Spohn, B., Lee, M.H., and Hung, M.C. Cytoplasmic localization of p21Cip1/WAF1 by Akt-induced phosphorylation in HER-2/neu-overexpressing cells. *Nat.Cell Biol.* 3(3): 245-52, 2001.

(62) Li, Y., Dowbenko, D., and Lasky, L.A. AKT/PKB phosphorylation of p21Cip/WAF1 enhances protein stability of p21Cip/WAF1 and promotes cell survival. *J.Biol.Chem.* 277(13): 11352-61, 2002.

(63) Wang, Z., Bhattacharya, N., Mixter, P.F., Wei, W., Sedivy, J., and Magnuson, N.S. Phosphorylation of the cell cycle inhibitor p21Cip1/WAF1 by Pim-1 kinase. *Biochim.Biophys.Acta*. 1593(1): 45-55, 2002.

(64) Scott, M.T., Morrice, N., and Ball, K.L. Reversible phosphorylation at the C-terminal regulatory domain of p21(Waf1/Cip1) modulates proliferating cell nuclear antigen binding. *J.Biol.Chem.* 275(15): 11529-37, 2000.

(65) Scott, M.T., Ingram, A., and Ball, K.L. PDK1-dependent activation of atypical PKC leads to degradation of the p21 tumour modifier protein. *EMBO J.* 21(24): 6771-80, 2002.

(66) Oh, Y.T., Chun, K.H., Park, B.D., Choi, J.S., and Lee, S.K. Regulation of cyclin-dependent kinase inhibitor p21WAF1/CIP1 by protein kinase Cdelta-mediated phosphorylation. *Apoptosis.* 12(7): 1339-47, 2007.

(67) Rodriguez-Vilarrupla, A., Diaz, C., Canela, N., Rahn, H.P., Bachs, O., and Agell, N. Identification of the nuclear localization signal of p21(cip1) and consequences of its mutation on cell proliferation. *FEBS Lett.* 531(2): 319-23, 2002.

(68) Guadagno, T.M. and Newport, J.W. Cdk2 kinase is required for entry into mitosis as a positive regulator of Cdc2-cyclin B kinase activity. *Cell*. 84(1): 73-82, 1996.

(69) Mandal, M., Bandyopadhyay, D., Goepfert, T.M., and Kumar, R. Interferon-induces expression of cyclin-dependent kinase-inhibitors p21WAF1 and p27Kip1 that prevent activation of cyclin-dependent kinase by CDK-activating kinase (CAK). *Oncogene*. 16(2): 217-25, 1998.

(70) Sherr, C.J. and Roberts, J.M. CDK inhibitors: positive and negative regulators of G1-phase progression. *Genes Dev.* 13(12): 1501-12, 1999.

(71) Coqueret, O. New roles for p21 and p27 cell-cycle inhibitors: a function for each cell compartment? *Trends Cell Biol.* 13(2): 65-70, 2003.

(72) Abbas, T. and Dutta, A. p21 in cancer: intricate networks and multiple activities. *Nat.Rev.Cancer*. 9(6): 400-14, 2009.

(73) Donehower, L.A., Harvey, M., Slagle, B.L., McArthur, M.J., Montgomery, C.A., Jr., Butel, J.S., and Bradley, A. Mice deficient for p53 are developmentally normal but susceptible to spontaneous tumours. *Nature*. 356(6366): 215-21, 1992.

(74) Efeyan, A., Collado, M., Velasco-Miguel, S., and Serrano, M. Genetic dissection of the role of p21Cip1/Waf1 in p53-mediated tumour suppression. *Oncogene*. 26(11): 1645-9, 2007.

(75) Shen, K.C., Heng, H., Wang, Y., Lu, S., Liu, G., Deng, C.X., Brooks, S.C., and Wang, Y.A. ATM and p21 cooperate to suppress aneuploidy and subsequent tumor development. *Cancer Res.* 65(19): 8747-53, 2005.

(76) Yang, W.C., Mathew, J., Velcich, A., Edelmann, W., Kucherlapati, R., Lipkin, M., Yang, K., and Augenlicht, L.H. Targeted inactivation of the p21(WAF1/cip1) gene enhances Apc-initiated tumor formation and the tumor-promoting activity of a Western-style high-risk diet by altering cell maturation in the intestinal mucosal. *Cancer Res.* 61(2): 565-9, 2001.

(77) Bearss, D.J., Lee, R.J., Troyer, D.A., Pestell, R.G., and Windle, J.J. Differential effects of p21(WAF1/CIP1) deficiency on MMTV-ras and MMTV-myc mammary tumor properties. *Cancer Res.* 62(7): 2077-84, 2002.

(78) Balbin, M., Hannon, G.J., Pendas, A.M., Ferrando, A.A., Vizoso, F., Fueyo, A., and Lopez-Otin, C. Functional analysis of a p21WAF1,CIP1,SDI1 mutant (Arg94 --> Trp) identified in a human

breast carcinoma. Evidence that the mutation impairs the ability of p21 to inhibit cyclin-dependent kinases. *J.Biol.Chem.* 271(26): 15782-6, 1996.

(79) Caffo, O., Doglioni, C., Veronese, S., Bonzanini, M., Marchetti, A., Buttitta, F., Fina, P., Leek, R., Morelli, L., Palma, P.D., Harris, A.L., and Barbareschi, M. Prognostic value of p21(WAF1) and p53 expression in breast carcinoma: an immunohistochemical study in 261 patients with long-term follow-up. *Clin.Cancer Res.* 2(9): 1591-9, 1996.

(80) Polyak, K., Hamilton, S.R., Vogelstein, B., and Kinzler, K.W. Early alteration of cell-cycle-regulated gene expression in colorectal neoplasia. *Am.J.Pathol.* 149(2): 381-7, 1996.

(81) Lu, X., Toki, T., Konishi, I., Nikaido, T., and Fujii, S. Expression of p21WAF1/CIP1 in adenocarcinoma of the uterine cervix: a possible immunohistochemical marker of a favorable prognosis. *Cancer*. 82(12): 2409-17, 1998.

(82) Anttila, M.A., Kosma, V.M., Hongxiu, J., Puolakka, J., Juhola, M., Saarikoski, S., and Syrjanen, K. p21/WAF1 expression as related to p53, cell proliferation and prognosis in epithelial ovarian cancer. *Br.J.Cancer*. 79(11-12): 1870-8, 1999.

(83) Zirbes, T.K., Baldus, S.E., Moenig, S.P., Nolden, S., Kunze, D., Shafizadeh, S.T., Schneider, P.M., Thiele, J., Hoelscher, A.H., and Dienes, H.P. Prognostic impact of p21/waf1/cip1 in colorectal cancer. *Int.J.Cancer*. 89(1): 14-8, 2000.

(84) Kapranos, N., Stathopoulos, G.P., Manolopoulos, L., Kokka, E., Papadimitriou, C., Bibas, A., Yiotakis, J., and Adamopoulos, G. p53, p21 and p27 protein expression in head and neck cancer and their prognostic value. *Anticancer Res.* 21(1B): 521-8, 2001.

(85) Mitomi, H., Mori, A., Kanazawa, H., Nishiyama, Y., Ihara, A., Otani, Y., Sada, M., Kobayashi, K., and Igarashi, M. Venous invasion and down-regulation of p21(WAF1/CIP1) are associated with metastasis in colorectal carcinomas. *Hepatogastroenterology*. 52(65): 1421-6, 2005.

(86) Ogino, S., Kawasaki, T., Kirkner, G.J., Ogawa, A., Dorfman, I., Loda, M., and Fuchs, C.S. Down-regulation of p21 (CDKN1A/CIP1) is inversely associated with microsatellite instability and CpG island methylator phenotype (CIMP) in colorectal cancer. *J.Pathol.* 210(2): 147-54, 2006.

(87) Deng, C., Zhang, P., Harper, J.W., Elledge, S.J., and Leder, P. Mice lacking p21CIP1/WAF1 undergo normal development, but are defective in G1 checkpoint control. *Cell*. 82(4): 675-84, 1995.

(88) Brugarolas, J., Chandrasekaran, C., Gordon, J.I., Beach, D., Jacks, T., and Hannon, G.J. Radiation-induced cell cycle arrest compromised by p21 deficiency. *Nature*. 377(6549): 552-7, 1995.

(89) Macleod, K.F., Sherry, N., Hannon, G., Beach, D., Tokino, T., Kinzler, K., Vogelstein, B., and Jacks, T. p53-dependent and independent expression of p21 during cell growth, differentiation, and DNA damage. *Genes Dev.* 9(8): 935-44, 1995.

(90) van de Wetering, M., Sancho, E., Verweij, C., de, L.W., Oving, I., Hurlstone, A., van der Horn, K., Batlle, E., Coudreuse, D., Haramis, A.P., Tjon-Pon-Fong, M., Moerer, P., van den Born, M., Soete, G., Pals, S., Eilers, M., Medema, R., and Clevers, H. The beta-catenin/TCF-4 complex imposes a crypt progenitor phenotype on colorectal cancer cells. *Cell*. 111(2): 241-50, 2002.

(91) Mukherjee, S. and Conrad, S.E. c-Myc suppresses p21WAF1/CIP1 expression during estrogen signaling and antiestrogen resistance in human breast cancer cells. *J.Biol.Chem.* 280(18): 17617-25, 2005.

(92) Jung, P., Menssen, A., Mayr, D., and Hermeking, H. AP4 encodes a c-MYC-inducible repressor of p21. *Proc.Natl.Acad.Sci.U.S.A*. 105(39): 15046-51, 2008.

(93) Gartel, A.L. and Tyner, A.L. Transcriptional regulation of the p21((WAF1/CIP1)) gene. *Exp.Cell Res.* 246(2): 280-9, 1999.

(94) Gartel, A.L. and Radhakrishnan, S.K. Lost in transcription: p21 repression, mechanisms, and consequences. *Cancer Res.* 65(10): 3980-5, 2005.

(95) Zhang, Z., Wang, H., Li, M., Agrawal, S., Chen, X., and Zhang, R. MDM2 is a negative regulator of p21WAF1/CIP1, independent of p53. *J.Biol.Chem.* 279(16): 16000-6, 2004.

(96) Onel, K. and Cordon-Cardo, C. MDM2 and prognosis. *Mol.Cancer Res.* 2(1): 1-8, 2004.

(97) Frescas, D. and Pagano, M. Deregulated proteolysis by the F-box proteins SKP2 and beta-TrCP: tipping the scales of cancer. *Nat.Rev.Cancer*. 8(6): 438-49, 2008.

(98) Chen, L.C., Manjeshwar, S., Lu, Y., Moore, D., Ljung, B.M., Kuo, W.L., Dairkee, S.H., Wernick, M., Collins, C., and Smith, H.S. The human homologue for the Caenorhabditis elegans cul-4 gene is amplified and overexpressed in primary breast cancers. *Cancer Res.* 58(16): 3677-83, 1998.

(99) Kim, Y., Starostina, N.G., and Kipreos, E.T. The CRL4Cdt2 ubiquitin ligase targets the degradation of p21Cip1 to control replication licensing. *Genes Dev.* 22(18): 2507-19, 2008.

(100) Wang, B., Liu, K., Lin, H.Y., Bellam, N., Ling, S., and Lin, W.C. 14-3-3Tau regulates ubiquitin-independent proteasomal degradation of p21, a novel mechanism of p21 downregulation in breast cancer. *Mol.Cell Biol.* 30(6): 1508-27, 2010.

(101) Fotedar, R., Brickner, H., Saadatmandi, N., Rousselle, T., Diederich, L., Munshi, A., Jung, B., Reed, J.C., and Fotedar, A. Effect of p21waf1/cip1 transgene on radiation induced apoptosis in T cells. *Oncogene*. 18(24): 3652-8, 1999.

(102) Lincet, H., Poulain, L., Remy, J.S., Deslandes, E., Duigou, F., Gauduchon, P., and Staedel, C. The p21(cip1/waf1) cyclin-dependent kinase inhibitor enhances the cytotoxic effect of cisplatin in human ovarian carcinoma cells. *Cancer Lett.* 161(1): 17-26, 2000.

(103) Prabhu, N.S., Blagosklonny, M.V., Zeng, Y.X., Wu, G.S., Waldman, T., and el-Deiry, W.S. Suppression of cancer cell growth by adenovirus expressing p21(WAF1/CIP1) deficient in PCNA interaction. *Clin.Cancer Res.* 2(7): 1221-9, 1996.

(104) Ramondetta, L., Mills, G.B., Burke, T.W., and Wolf, J.K. Adenovirus-mediated expression of p53 or p21 in a papillary serous endometrial carcinoma cell line (SPEC-2) results in both growth inhibition and apoptotic cell death: potential application of gene therapy to endometrial cancer. *Clin.Cancer Res.* 6(1): 278-84, 2000.

(105) Wu, Q., Kirschmeier, P., Hockenberry, T., Yang, T.Y., Brassard, D.L., Wang, L., McClanahan, T., Black, S., Rizzi, G., Musco, M.L., Mirza, A., and Liu, S. Transcriptional regulation during p21WAF1/CIP1-induced apoptosis in human ovarian cancer cells. *J.Biol.Chem.* 277(39): 36329-37, 2002.

(106) Tsao, Y.P., Huang, S.J., Chang, J.L., Hsieh, J.T., Pong, R.C., and Chen, S.L. Adenovirus-mediated p21((WAF1/SDII/CIP1)) gene transfer induces apoptosis of human cervical cancer cell lines. *J.Virol.* 73(6): 4983-90, 1999.

(107) Khanna, A.K., Plummer, M., Nilakantan, V., and Pieper, G.M. Recombinant p21 protein inhibits lymphocyte proliferation and transcription factors. *J.Immunol.* 174(12): 7610-7, 2005.

(108) Janicke, R.U., Sohn, D., Essmann, F., and Schulze-Osthoff, K. The multiple battles fought by anti-apoptotic p21. *Cell Cycle*. 6(4): 407-13, 2007.

(109) Lohr, K., Moritz, C., Contente, A., and Dobbelstein, M. p21/CDKN1A mediates negative regulation of transcription by p53. *J.Biol.Chem.* 278(35): 32507-16, 2003.

(110) Chang, B.D., Watanabe, K., Broude, E.V., Fang, J., Poole, J.C., Kalinichenko, T.V., and Roninson, I.B. Effects of p21Waf1/Cip1/Sdi1 on cellular gene expression: implications for

carcinogenesis, senescence, and age-related diseases. *Proc.Natl.Acad.Sci.U.S.A*. 97(8): 4291-6, 2000.

(111) Korkolopoulou, P., Konstantinidou, A.E., Thomas-Tsagli, E., Christodoulou, P., Kapralos, P., and Davaris, P. WAF1/p21 protein expression is an independent prognostic indicator in superficial and invasive bladder cancer. *Appl.Immunohistochem.Mol.Morphol.* 8(4): 285-92, 2000.

(112) Zhang, W., Kornblau, S.M., Kobayashi, T., Gambel, A., Claxton, D., and Deisseroth, A.B. High levels of constitutive WAF1/Cip1 protein are associated with chemoresistance in acute myelogenous leukemia. *Clin.Cancer Res.* 1(9): 1051-7, 1995.

(113) Jung, J.M., Bruner, J.M., Ruan, S., Langford, L.A., Kyritsis, A.P., Kobayashi, T., Levin, V.A., and Zhang, W. Increased levels of p21WAF1/Cip1 in human brain tumors. *Oncogene*. 11(10): 2021-8, 1995.

(114) Baretton, G.B., Klenk, U., Diebold, J., Schmeller, N., and Lohrs, U. Proliferation- and apoptosis-associated factors in advanced prostatic carcinomas before and after androgen deprivation therapy: prognostic significance of p21/WAF1/CIP1 expression. *Br.J.Cancer*. 80(3-4): 546-55, 1999.

(115) Cheung, T.H., Lo, K.W., Yu, M.M., Yim, S.F., Poon, C.S., Chung, T.K., and Wong, Y.F. Aberrant expression of p21(WAF1/CIP1) and p27(KIP1) in cervical carcinoma. *Cancer Lett.* 172(1): 93-8, 2001.

(116) Ferrandina, G., Stoler, A., Fagotti, A., Fanfani, F., Sacco, R., De, P.A., Mancuso, S., and Scambia, G. p21WAF1/CIP1 protein expression in primary ovarian cancer. *Int.J.Oncol.* 17(6): 1231-5, 2000.

(117) Sarbia, M., Stahl, M., zur, H.A., Zimmermann, K., Wang, L., Fink, U., Heep, H., Dutkowski, P., Willers, R., Muller, W., Seeber, S., and Gabbert, H.E. Expression of p21WAF1 predicts outcome of esophageal cancer patients treated by surgery alone or by combined therapy modalities. *Clin.Cancer Res.* 4(11): 2615-23, 1998.

(118) Winters, Z.E., Hunt, N.C., Bradburn, M.J., Royds, J.A., Turley, H., Harris, A.L., and Norbury, C.J. Subcellular localisation of cyclin B, Cdc2 and p21(WAF1/CIP1) in breast cancer. association with prognosis. *Eur.J.Cancer*. 37(18): 2405-12, 2001.

(119) Winters, Z.E., Leek, R.D., Bradburn, M.J., Norbury, C.J., and Harris, A.L. Cytoplasmic p21WAF1/CIP1 expression is correlated with HER-2/ neu in breast cancer and is an independent predictor of prognosis. *Breast Cancer Res.* 5(6): R242-R249, 2003.

(120) Ping, B., He, X., Xia, W., Lee, D.F., Wei, Y., Yu, D., Mills, G., Shi, D., and Hung, M.C. Cytoplasmic expression of p21CIP1/WAF1 is correlated with IKKbeta overexpression in human breast cancers. *Int.J.Oncol.* 29(5): 1103-10, 2006.

(121) Xia, W., Chen, J.S., Zhou, X., Sun, P.R., Lee, D.F., Liao, Y., Zhou, B.P., and Hung, M.C. Phosphorylation/cytoplasmic localization of p21Cip1/WAF1 is associated with HER2/neu overexpression and provides a novel combination predictor for poor prognosis in breast cancer patients. *Clin.Cancer Res.* 10(11): 3815-24, 2004.

(122) Shiraki, K. and Wagayama, H. Cytoplasmic p21(WAF1/CIP1) expression in human hepatocellular carcinomas. *Liver Int.* 26(8): 1018-9, 2006.

(123) Gartel, A.L. and Tyner, A.L. The role of the cyclin-dependent kinase inhibitor p21 in apoptosis. *Mol.Cancer Ther.* 1(8): 639-49, 2002.

(124) Besson, A., Dowdy, S.F., and Roberts, J.M. CDK inhibitors: cell cycle regulators and beyond. *Dev.Cell*. 14(2): 159-69, 2008.

(125) Xu, S.Q. and el-Deiry, W.S. p21(WAF1/CIP1) inhibits initiator caspase cleavage by TRAIL death receptor DR4. *Biochem.Biophys.Res.Commun.* 269(1): 179-90, 2000.

(126) Zhou, B.B., Li, H., Yuan, J., and Kirschner, M.W. Caspase-dependent activation of cyclin-dependent kinases during Fas-induced apoptosis in Jurkat cells. *Proc.Natl.Acad.Sci.U.S.A*. 95(12): 6785-90, 1998.

(127) Hakem, A., Sasaki, T., Kozieradzki, I., and Penninger, J.M. The cyclin-dependent kinase Cdk2 regulates thymocyte apoptosis. *J.Exp.Med.* 189(6): 957-68, 1999.

(128) Sohn, D., Essmann, F., Schulze-Osthoff, K., and Janicke, R.U. p21 blocks irradiation-induced apoptosis downstream of mitochondria by inhibition of cyclin-dependent kinase-mediated caspase-9 activation. *Cancer Res.* 66(23): 11254-62, 2006.

(129) Harvey, K.J., Lukovic, D., and Ucker, D.S. Caspase-dependent Cdk activity is a requisite effector of apoptotic death events. *J.Cell Biol.* 148(1): 59-72, 2000.

(130) Tanaka, H., Yamashita, T., Asada, M., Mizutani, S., Yoshikawa, H., and Tohyama, M. Cytoplasmic p21(Cip1/WAF1) regulates neurite remodeling by inhibiting Rho-kinase activity. *J.Cell Biol.* 158(2): 321-9, 2002.

(131) Lee, S. and Helfman, D.M. Cytoplasmic p21Cip1 is involved in Ras-induced inhibition of the ROCK/LIMK/cofilin pathway. *J.Biol.Chem.* 279(3): 1885-91, 2004.

(132) Besson, A., Assoian, R.K., and Roberts, J.M. Regulation of the cytoskeleton: an oncogenic function for CDK inhibitors? *Nat.Rev.Cancer*. 4(12): 948-55, 2004.

(133) Gumbiner, B.M. Cell adhesion: the molecular basis of tissue architecture and morphogenesis. *Cell*. 84(3): 345-57, 1996.

(134) Etienne-Manneville, S. Actin and microtubules in cell motility: which one is in control? *Traffic.* 5(7): 470-7, 2004.

(135) Mogilner, A. and Keren, K. The shape of motile cells. *Curr.Biol.* 19(17): R762-R771, 2009.

(136) Broussard, J.A., Webb, D.J., and Kaverina, I. Asymmetric focal adhesion disassembly in motile cells. *Curr.Opin.Cell Biol.* 20(1): 85-90, 2008.

(137) Small, J.V. and Kaverina, I. Microtubules meet substrate adhesions to arrange cell polarity. *Curr.Opin.Cell Biol.* 15(1): 40-7, 2003.

(138) Le, C.C. and Carlier, M.F. Regulation of actin assembly associated with protrusion and adhesion in cell migration. *Physiol Rev.* 88(2): 489-513, 2008.

(139) Buccione, R., Orth, J.D., and McNiven, M.A. Foot and mouth: podosomes, invadopodia and circular dorsal ruffles. *Nat.Rev.Mol.Cell Biol.* 5(8): 647-57, 2004.

(140) Zamir, E. and Geiger, B. Molecular complexity and dynamics of cell-matrix adhesions. *J.Cell Sci.* 114(Pt 20): 3583-90, 2001.

(141) Zaidel-Bar, R., Cohen, M., Addadi, L., and Geiger, B. Hierarchical assembly of cell-matrix adhesion complexes. *Biochem.Soc.Trans.* 32(Pt3): 416-20, 2004.

(142) Hynes, R.O. Integrins: bidirectional, allosteric signaling machines. *Cell*. 110(6): 673-87, 2002.

(143) Humphries, M.J., McEwan, P.A., Barton, S.J., Buckley, P.A., Bella, J., and Mould, A.P. Integrin structure: heady advances in ligand binding, but activation still makes the knees wobble. *Trends Biochem.Sci.* 28(6): 313-20, 2003.

(144) Lock, J.G., Wehrle-Haller, B., and Stromblad, S. Cell-matrix adhesion complexes: master control machinery of cell migration. *Semin.Cancer Biol.* 18(1): 65-76, 2008.

(145) Takagi, J., Petre, B.M., Walz, T., and Springer, T.A. Global conformational rearrangements in integrin extracellular domains in outside-in and inside-out signaling. *Cell*. 110(5): 599-11, 2002.

(146) Vinogradova, O., Velyvis, A., Velyviene, A., Hu, B., Haas, T., Plow, E., and Qin, J. A structural mechanism of integrin alpha(IIb)beta(3) "inside-out" activation as regulated by its cytoplasmic face. *Cell*. 110(5): 587-97, 2002.

(147) Tadokoro, S., Shattil, S.J., Eto, K., Tai, V., Liddington, R.C., de Pereda, J.M., Ginsberg, M.H., and Calderwood, D.A. Talin binding to integrin beta tails: a final common step in integrin activation. *Science*. 302(5642): 103-6, 2003.

(148) Askari, J.A., Tynan, C.J., Webb, S.E., Martin-Fernandez, M.L., Ballestrem, C., and Humphries, M.J. Focal adhesions are sites of integrin extension. *J.Cell Biol.* 188(6): 891-903, 2010.

(149) Clark, E.A., King, W.G., Brugge, J.S., Symons, M., and Hynes, R.O. Integrin-mediated signals regulated by members of the rho family of GTPases. *J.Cell Biol.* 142(2): 573-86, 1998.

(150) Cluzel, C., Saltel, F., Lussi, J., Paulhe, F., Imhof, B.A., and Wehrle-Haller, B. The mechanisms and dynamics of (alpha)v(beta)3 integrin clustering in living cells. *J.Cell Biol.* 171(2): 383-92, 2005.

(151) Nobes, C.D. and Hall, A. Rho, rac, and cdc42 GTPases regulate the assembly of multimolecular focal complexes associated with actin stress fibers, lamellipodia, and filopodia. *Cell*. 81(1): 53-62, 1995.

(152) Rottner, K., Hall, A., and Small, J.V. Interplay between Rac and Rho in the control of substrate contact dynamics. *Curr.Biol.* 9(12): 640-8, 1999.

(153) Webb, D.J., Parsons, J.T., and Horwitz, A.F. Adhesion assembly, disassembly and turnover in migrating cells -- over and over and over again. *Nat.Cell Biol.* 4(4): E97-100, 2002.

(154) Zaidel-Bar, R., Ballestrem, C., Kam, Z., and Geiger, B. Early molecular events in the assembly of matrix adhesions at the leading edge of migrating cells. *J.Cell Sci.* 116(Pt 22): 4605-13, 2003.

(155) Zaidel-Bar, R., Milo, R., Kam, Z., and Geiger, B. A paxillin tyrosine phosphorylation switch regulates the assembly and form of cell-matrix adhesions. *J.Cell Sci.* 120(Pt 1): 137-48, 2007.

(156) Fukami, K., Endo, T., Imamura, M., and Takenawa, T. alpha-Actinin and vinculin are PIP2-binding proteins involved in signaling by tyrosine kinase. *J.Biol.Chem.* 269(2): 1518-22, 1994.

(157) Mitra, S.K., Hanson, D.A., and Schlaepfer, D.D. Focal adhesion kinase: in command and control of cell motility. *Nat.Rev.Mol.Cell Biol.* 6(1): 56-68, 2005.

(158) Geiger, B., Spatz, J.P., and Bershadsky, A.D. Environmental sensing through focal adhesions. *Nat.Rev.Mol.Cell Biol.* 10(1): 21-33, 2009.

(159) Huveneers, S. and Danen, E.H. Adhesion signaling - crosstalk between integrins, Src and Rho. *J.Cell Sci.* 122(Pt 8): 1059-69, 2009.

(160) Debnath, J. and Brugge, J.S. Modelling glandular epithelial cancers in three-dimensional cultures. *Nat.Rev.Cancer*. 5(9): 675-88, 2005.

(161) Frisch, S.M., Vuori, K., Ruoslahti, E., and Chan-Hui, P.Y. Control of adhesion-dependent cell survival by focal adhesion kinase. *J.Cell Biol.* 134(3): 793-9, 1996.

(162) Ilic, D., Almeida, E.A., Schlaepfer, D.D., Dazin, P., Aizawa, S., and Damsky, C.H. Extracellular matrix survival signals transduced by focal adhesion kinase suppress p53-mediated apoptosis. *J.Cell Biol.* 143(2): 547-60, 1998.

(163) Golubovskaya, V.M., Finch, R., and Cance, W.G. Direct interaction of the N-terminal domain of focal adhesion kinase with the N-terminal transactivation domain of p53. *J.Biol.Chem.* 280(26): 25008-21, 2005.

(164) Westhoff, M.A., Serrels, B., Fincham, V.J., Frame, M.C., and Carragher, N.O. SRC-mediated phosphorylation of focal adhesion kinase couples actin and adhesion dynamics to survival signaling. *Mol.Cell Biol.* 24(18): 8113-33, 2004.

(165) Ding, Q., Grammer, J.R., Nelson, M.A., Guan, J.L., Stewart, J.E., Jr., and Gladson, C.L. p27Kip1 and cyclin D1 are necessary for focal adhesion kinase regulation of cell cycle progression in glioblastoma cells propagated in vitro and in vivo in the scid mouse brain. *J.Biol.Chem.* 280(8): 6802-15, 2005.

(166) Oktay, M., Wary, K.K., Dans, M., Birge, R.B., and Giancotti, F.G. Integrin-mediated activation of focal adhesion kinase is required for signaling to Jun NH2-terminal kinase and progression through the G1 phase of the cell cycle. *J.Cell Biol.* 145(7): 1461-9, 1999.

(167) Dos Remedios, C.G., Chhabra, D., Kekic, M., Dedova, I.V., Tsubakihara, M., Berry, D.A., and Nosworthy, N.J. Actin binding proteins: regulation of cytoskeletal microfilaments. *Physiol Rev.* 83(2): 433-73, 2003.

(168) Holmes, K.C., Popp, D., Gebhard, W., and Kabsch, W. Atomic model of the actin filament. *Nature*. 347(6288): 44-9, 1990.

(169) Carlier, M.F. and Pantaloni, D. Direct evidence for ADP-Pi-F-actin as the major intermediate in ATP-actin polymerization. Rate of dissociation of Pi from actin filaments. *Biochemistry*. 25(24): 7789-92, 1986.

(170) Carlier, M.F., Pantaloni, D., and Korn, E.D. The mechanisms of ATP hydrolysis accompanying the polymerization of Mg-actin and Ca-actin. *J.Biol.Chem.* 262(7): 3052-9, 1987.

(171) Carlier, M.F., Pantaloni, D., Evans, J.A., Lambooy, P.K., Korn, E.D., and Webb, M.R. The hydrolysis of ATP that accompanies actin polymerization is essentially irreversible. *FEBS Lett.* 235(1-2): 211-4, 1988.

(172) Wegner, A. and Isenberg, G. 12-fold difference between the critical monomer concentrations of the two ends of actin filaments in physiological salt conditions. *Proc.Natl.Acad.Sci.U.S.A.* 80(16): 4922-5, 1983.

(173) Chesarone, M.A. and Goode, B.L. Actin nucleation and elongation factors: mechanisms and interplay. *Curr.Opin.Cell Biol.* 21(1): 28-37, 2009.

(174) Pruyne, D., Evangelista, M., Yang, C., Bi, E., Zigmond, S., Bretscher, A., and Boone, C. Role of formins in actin assembly: nucleation and barbed-end association. *Science*. 297(5581): 612-5, 2002.

(175) Quinlan, M.E., Heuser, J.E., Kerkhoff, E., and Mullins, R.D. Drosophila Spire is an actin nucleation factor. *Nature*. 433(7024): 382-8, 2005.

(176) Ahuja, R., Pinyol, R., Reichenbach, N., Custer, L., Klingensmith, J., Kessels, M.M., and Qualmann, B. Cordon-bleu is an actin nucleation factor and controls neuronal morphology. *Cell*. 131(2): 337-50, 2007.

(177) Chereau, D., Boczkowska, M., Skwarek-Maruszewska, A., Fujiwara, I., Hayes, D.B., Rebowski, G., Lappalainen, P., Pollard, T.D., and Dominguez, R. Leiomodin is an actin filament nucleator in muscle cells. *Science*. 320(5873): 239-43, 2008.

(178) Ferron, F., Rebowski, G., Lee, S.H., and Dominguez, R. Structural basis for the recruitment of profilin-actin complexes during filament elongation by Ena/VASP. *EMBO J.* 26(21): 4597-606, 2007.

(179) Kuhnel, K., Jarchau, T., Wolf, E., Schlichting, I., Walter, U., Wittinghofer, A., and Strelkov, S.V. The VASP tetramerization domain is a right-handed coiled coil based on a 15-residue repeat. *Proc.Natl.Acad.Sci.U.S.A.* 101(49): 17027-32, 2004.

(180) Ponti, A., Machacek, M., Gupton, S.L., Waterman-Storer, C.M., and Danuser, G. Two distinct actin networks drive the protrusion of migrating cells. *Science*. 305(5691): 1782-6, 2004.

(181) Ridley, A.J. Rho GTPases and actin dynamics in membrane protrusions and vesicle trafficking. *Trends Cell Biol.* 16(10): 522-9, 2006.

(182) Ridley, A.J. and Hall, A. The small GTP-binding protein rho regulates the assembly of focal adhesions and actin stress fibers in response to growth factors. *Cell*. 70(3): 389-99, 1992.

(183) Ridley, A.J., Paterson, H.F., Johnston, C.L., Diekmann, D., and Hall, A. The small GTP-binding protein rac regulates growth factor-induced membrane ruffling. *Cell*. 70(3): 401-10, 1992.

(184) Kozma, R., Ahmed, S., Best, A., and Lim, L. The Ras-related protein Cdc42Hs and bradykinin promote formation of peripheral actin microspikes and filopodia in Swiss 3T3 fibroblasts. *Mol.Cell Biol.* 15(4): 1942-52, 1995.

(185) Barbacid, M. ras genes. *Annu.Rev.Biochem.* 56(779-827, 1987.

(186) Garrett, M.D., Self, A.J., van, O.C., and Hall, A. Identification of distinct cytoplasmic targets for ras/R-ras and rho regulatory proteins. *J.Biol.Chem.* 264(1): 10-3, 1989.

(187) Garrett, M.D., Major, G.N., Totty, N., and Hall, A. Purification and N-terminal sequence of the p21rho GTPase-activating protein, rho GAP. *Biochem.J.* 276 (Pt 3)(833-6, 1991.

(188) Kim, A.S., Kakalis, L.T., Abdul-Manan, N., Liu, G.A., and Rosen, M.K. Autoinhibition and activation mechanisms of the Wiskott-Aldrich syndrome protein. *Nature*. 404(6774): 151-8, 2000.

(189) Takenawa, T. and Miki, H. WASP and WAVE family proteins: key molecules for rapid rearrangement of cortical actin filaments and cell movement. *J.Cell Sci.* 114(Pt 10): 1801-9, 2001.

(190) Suetsugu, S., Kurisu, S., Oikawa, T., Yamazaki, D., Oda, A., and Takenawa, T. Optimization of WAVE2 complex-induced actin polymerization by membrane-bound IRSp53, PIP(3), and Rac. *J.Cell Biol.* 173(4): 571-85, 2006.

(191) Watanabe, N., Kato, T., Fujita, A., Ishizaki, T., and Narumiya, S. Cooperation between mDia1 and ROCK in Rho-induced actin reorganization. *Nat.Cell Biol.* 1(3): 136-43, 1999.

(192) Alberts, A.S., Bouquin, N., Johnston, L.H., and Treisman, R. Analysis of RhoA-binding proteins reveals an interaction domain conserved in heterotrimeric G protein beta subunits and the yeast response regulator protein Skn7. *J.Biol.Chem.* 273(15): 8616-22, 1998.

(193) Higgs, H.N. Formin proteins: a domain-based approach. *Trends Biochem.Sci.* 30(6): 342-53, 2005.

(194) Ridley, A.J., Schwartz, M.A., Burridge, K., Firtel, R.A., Ginsberg, M.H., Borisy, G., Parsons, J.T., and Horwitz, A.R. Cell migration: integrating signals from front to back. *Science*. 302(5651): 1704-9, 2003.

(195) Yarmola, E.G. and Bubb, M.R. Profilin: emerging concepts and lingering misconceptions. *Trends Biochem.Sci.* 31(4): 197-205, 2006.

(196) Kinosian, H.J., Selden, L.A., Gershman, L.C., and Estes, J.E. Actin filament barbed end elongation with nonmuscle MgATP-actin and MgADP-actin in the presence of profilin. *Biochemistry*. 41(21): 6734-43, 2002.

(197) Bubb, M.R., Yarmola, E.G., Gibson, B.G., and Southwick, F.S. Depolymerization of actin filaments by profilin. Effects of profilin on capping protein function. *J.Biol.Chem.* 278(27): 24629-35, 2003.

(198) Yarmola, E.G. and Bubb, M.R. Effects of profilin and thymosin beta4 on the critical concentration of actin demonstrated in vitro and in cell extracts with a novel direct assay. *J.Biol.Chem.* 279(32): 33519-27, 2004.

(199) Maciver, S.K., Zot, H.G., and Pollard, T.D. Characterization of actin filament severing by actophorin from Acanthamoeba castellanii. *J.Cell Biol.* 115(6): 1611-20, 1991.

(200) Carlier, M.F., Laurent, V., Santolini, J., Melki, R., Didry, D., Xia, G.X., Hong, Y., Chua, N.H., and Pantaloni, D. Actin depolymerizing factor (ADF/cofilin) enhances the rate of filament turnover: implication in actin-based motility. *J.Cell Biol.* 136(6): 1307-22, 1997.

(201) Blanchoin, L., Pollard, T.D., and Hitchcock-DeGregori, S.E. Inhibition of the Arp2/3 complex-nucleated actin polymerization and branch formation by tropomyosin. *Curr.Biol.* 11(16): 1300-4, 2001.

(202) Wang, W., Eddy, R., and Condeelis, J. The cofilin pathway in breast cancer invasion and metastasis. *Nat.Rev.Cancer*. 7(6): 429-40, 2007.

(203) Yonezawa, N., Nishida, E., Iida, K., Yahara, I., and Sakai, H. Inhibition of the interactions of cofilin, destrin, and deoxyribonuclease I with actin by phosphoinositides. *J.Biol.Chem.* 265(15): 8382-6, 1990.

(204) Yonezawa, N., Homma, Y., Yahara, I., Sakai, H., and Nishida, E. A short sequence responsible for both phosphoinositide binding and actin binding activities of cofilin. *J.Biol.Chem.* 266(26): 17218-21, 1991.

(205) Mouneimne, G., Soon, L., Desmarais, V., Sidani, M., Song, X., Yip, S.C., Ghosh, M., Eddy, R., Backer, J.M., and Condeelis, J. Phospholipase C and cofilin are required for carcinoma cell directionality in response to EGF stimulation. *J.Cell Biol.* 166(5): 697-708, 2004.

(206) Mouneimne, G., Desmarais, V., Sidani, M., Scemes, E., Wang, W., Song, X., Eddy, R., and Condeelis, J. Spatial and temporal control of cofilin activity is required for directional sensing during chemotaxis. *Curr.Biol.* 16(22): 2193-205, 2006.

(207) Marone, R., Hess, D., Dankort, D., Muller, W.J., Hynes, N.E., and Badache, A. Memo mediates ErbB2-driven cell motility. *Nat.Cell Biol.* 6(6): 515-22, 2004.

(208) van, R.J., Song, X., van, R.W., Cammer, M., Chen, X., Desmarais, V., Yip, S.C., Backer, J.M., Eddy, R.J., and Condeelis, J.S. EGF-induced PIP2 hydrolysis releases and activates cofilin locally in carcinoma cells. *J.Cell Biol.* 179(6): 1247-59, 2007.

(209) Meira, M., Masson, R., Stagljar, I., Lienhard, S., Maurer, F., Boulay, A., and Hynes, N.E. Memo is a cofilin-interacting protein that influences PLCgamma1 and cofilin activities, and is essential for maintaining directionality during ErbB2-induced tumor-cell migration. *J.Cell Sci.* 122(Pt 6): 787-97, 2009.

(210) Bernstein, B.W., Painter, W.B., Chen, H., Minamide, L.S., Abe, H., and Bamburg, J.R. Intracellular pH modulation of ADF/cofilin proteins. *Cell Motil.Cytoskeleton*. 47(4): 319-36, 2000.

(211) Srivastava, J., Barber, D.L., and Jacobson, M.P. Intracellular pH sensors: design principles and functional significance. *Physiology.(Bethesda.)*. 22(30-9, 2007.

(212) Frantz, C., Barreiro, G., Dominguez, L., Chen, X., Eddy, R., Condeelis, J., Kelly, M.J., Jacobson, M.P., and Barber, D.L. Cofilin is a pH sensor for actin free barbed end formation: role of phosphoinositide binding. *J.Cell Biol.* 183(5): 865-79, 2008.

(213) Klein, M., Seeger, P., Schuricht, B., Alper, S.L., and Schwab, A. Polarization of Na(+)/H(+) and Cl(-)/HCO (3)(-) exchangers in migrating renal epithelial cells. *J.Gen.Physiol*. 115(5): 599-608, 2000.

(214) Denker, S.P. and Barber, D.L. Cell migration requires both ion translocation and cytoskeletal anchoring by the Na-H exchanger NHE1. *J.Cell Biol.* 159(6): 1087-96, 2002.

(215) Stock, C., Gassner, B., Hauck, C.R., Arnold, H., Mally, S., Eble, J.A., Dieterich, P., and Schwab, A. Migration of human melanoma cells depends on extracellular pH and Na+/H+ exchange. *J.Physiol*. 567(Pt 1): 225-38, 2005.

(216) Arber, S., Barbayannis, F.A., Hanser, H., Schneider, C., Stanyon, C.A., Bernard, O., and Caroni, P. Regulation of actin dynamics through phosphorylation of cofilin by LIM-kinase. *Nature*. 393(6687): 805-9, 1998.

(217) Geneste, O., Copeland, J.W., and Treisman, R. LIM kinase and Diaphanous cooperate to regulate serum response factor and actin dynamics. *J.Cell Biol.* 157(5): 831-8, 2002.

(218) Yang, N., Higuchi, O., Ohashi, K., Nagata, K., Wada, A., Kangawa, K., Nishida, E., and Mizuno, K. Cofilin phosphorylation by LIM-kinase 1 and its role in Rac-mediated actin reorganization. *Nature*. 393(6687): 809-12, 1998.

(219) Edwards, D.C., Sanders, L.C., Bokoch, G.M., and Gill, G.N. Activation of LIM-kinase by Pak1 couples Rac/Cdc42 GTPase signalling to actin cytoskeletal dynamics. *Nat.Cell Biol.* 1(5): 253-9, 1999.

(220) Eiseler, T., Doppler, H., Yan, I.K., Kitatani, K., Mizuno, K., and Storz, P. Protein kinase D1 regulates cofilin-mediated F-actin reorganization and cell motility through slingshot. *Nat.Cell Biol.* 11(5): 545-56, 2009.

(221) Nagata-Ohashi, K., Ohta, Y., Goto, K., Chiba, S., Mori, R., Nishita, M., Ohashi, K., Kousaka, K., Iwamatsu, A., Niwa, R., Uemura, T., and Mizuno, K. A pathway of neuregulin-induced activation of cofilin-phosphatase Slingshot and cofilin in lamellipodia. *J.Cell Biol.* 165(4): 465-71, 2004.

(222) Cramer, L.P., Siebert, M., and Mitchison, T.J. Identification of novel graded polarity actin filament bundles in locomoting heart fibroblasts: implications for the generation of motile force. *J.Cell Biol.* 136(6): 1287-305, 1997.

(223) Pellegrin, S. and Mellor, H. Actin stress fibres. *J.Cell Sci.* 120(Pt 20): 3491-9, 2007.

(224) Naumanen, P., Lappalainen, P., and Hotulainen, P. Mechanisms of actin stress fibre assembly. *J.Microsc.* 231(3): 446-54, 2008.

(225) Lazarides, E. and Burridge, K. Alpha-actinin: immunofluorescent localization of a muscle structural protein in nonmuscle cells. *Cell*. 6(3): 289-98, 1975.

(226) Langanger, G., De, M.J., Moeremans, M., Daneels, G., de, B.M., and Small, J.V. Ultrastructural localization of alpha-actinin and filamin in cultured cells with the immunogold staining (IGS) method. *J.Cell Biol.* 99(4 Pt 1): 1324-34, 1984.

(227) Sjoblom, B., Salmazo, A., and Djinovic-Carugo, K. Alpha-actinin structure and regulation. *Cell Mol.Life Sci.* 65(17): 2688-701, 2008.

(228) Weber, K. and Groeschel-Stewart, U. Antibody to myosin: the specific visualization of myosin-containing filaments in nonmuscle cells. *Proc.Natl.Acad.Sci.U.S.A*. 71(11): 4561-4, 1974.

(229) Vicente-Manzanares, M., Ma, X., Adelstein, R.S., and Horwitz, A.R. Non-muscle myosin II takes centre stage in cell adhesion and migration. *Nat.Rev.Mol.Cell Biol.* 10(11): 778-90, 2009.

(230) Peterson, L.J., Rajfur, Z., Maddox, A.S., Freel, C.D., Chen, Y., Edlund, M., Otey, C., and Burridge, K. Simultaneous stretching and contraction of stress fibers in vivo. *Mol.Biol.Cell*. 15(7): 3497-508, 2004.

(231) Maekawa, M., Ishizaki, T., Boku, S., Watanabe, N., Fujita, A., Iwamatsu, A., Obinata, T., Ohashi, K., Mizuno, K., and Narumiya, S. Signaling from Rho to the actin cytoskeleton through protein kinases ROCK and LIM-kinase. *Science*. 285(5429): 895-8, 1999.

(232) Amano, T., Tanabe, K., Eto, T., Narumiya, S., and Mizuno, K. LIM-kinase 2 induces formation of stress fibres, focal adhesions and membrane blebs, dependent on its activation by Rho-associated kinase-catalysed phosphorylation at threonine-505. *Biochem.J.* 354(Pt 1): 149-59, 2001.

(233) Pritchard, C.A., Hayes, L., Wojnowski, L., Zimmer, A., Marais, R.M., and Norman, J.C. B-Raf acts via the ROCKII/LIMK/cofilin pathway to maintain actin stress fibers in fibroblasts. *Mol.Cell Biol.* 24(13): 5937-52, 2004.

(234) Amano, M., Ito, M., Kimura, K., Fukata, Y., Chihara, K., Nakano, T., Matsuura, Y., and Kaibuchi, K. Phosphorylation and activation of myosin by Rho-associated kinase (Rho-kinase). *J.Biol.Chem.* 271(34): 20246-9, 1996.

(235) Katoh, K., Kano, Y., Amano, M., Onishi, H., Kaibuchi, K., and Fujiwara, K. Rho-kinase--mediated contraction of isolated stress fibers. *J.Cell Biol.* 153(3): 569-84, 2001.

(236) Kimura, K., Ito, M., Amano, M., Chihara, K., Fukata, Y., Nakafuku, M., Yamamori, B., Feng, J., Nakano, T., Okawa, K., Iwamatsu, A., and Kaibuchi, K. Regulation of myosin phosphatase by Rho and Rho-associated kinase (Rho-kinase). *Science*. 273(5272): 245-8, 1996.

(237) Somlyo, A.P. and Somlyo, A.V. Ca2+ sensitivity of smooth muscle and nonmuscle myosin II: modulated by G proteins, kinases, and myosin phosphatase. *Physiol Rev.* 83(4): 1325-58, 2003.

(238) Higashida, C., Miyoshi, T., Fujita, A., Oceguera-Yanez, F., Monypenny, J., Andou, Y., Narumiya, S., and Watanabe, N. Actin polymerization-driven molecular movement of mDia1 in living cells. *Science*. 303(5666): 2007-10, 2004.

(239) Peng, J., Wallar, B.J., Flanders, A., Swiatek, P.J., and Alberts, A.S. Disruption of the Diaphanous-related formin Drf1 gene encoding mDia1 reveals a role for Drf3 as an effector for Cdc42. *Curr.Biol.* 13(7): 534-45, 2003.

(240) Hotulainen, P. and Lappalainen, P. Stress fibers are generated by two distinct actin assembly mechanisms in motile cells. *J.Cell Biol.* 173(3): 383-94, 2006.

(241) Couchman, J.R. and Rees, D.A. The behaviour of fibroblasts migrating from chick heart explants: changes in adhesion, locomotion and growth, and in the distribution of actomyosin and fibronectin. *J.Cell Sci.* 39(149-65, 1979.

(242) Sahai, E., Olson, M.F., and Marshall, C.J. Cross-talk between Ras and Rho signalling pathways in transformation favours proliferation and increased motility. *EMBO J.* 20(4): 755-66, 2001.

(243) Glacy, S.D. Subcellular distribution of rhodamine-actin microinjected into living fibroblastic cells. *J.Cell Biol.* 97(4): 1207-13, 1983.

(244) Wang, Y.L. Reorganization of actin filament bundles in living fibroblasts. *J.Cell Biol.* 99(4 Pt 1): 1478-85, 1984.

(245) Alexandrova, A.Y., Arnold, K., Schaub, S., Vasiliev, J.M., Meister, J.J., Bershadsky, A.D., and Verkhovsky, A.B. Comparative dynamics of retrograde actin flow and focal adhesions: formation of nascent adhesions triggers transition from fast to slow flow. *PLoS.One.* 3(9): e3234, 2008.

(246) Choi, C.K., Vicente-Manzanares, M., Zareno, J., Whitmore, L.A., Mogilner, A., and Horwitz, A.R. Actin and alpha-actinin orchestrate the assembly and maturation of nascent adhesions in a myosin II motor-independent manner. *Nat.Cell Biol.* 10(9): 1039-50, 2008.

(247) Wu, X., Suetsugu, S., Cooper, L.A., Takenawa, T., and Guan, J.L. Focal adhesion kinase regulation of N-WASP subcellular localization and function. *J.Biol.Chem.* 279(10): 9565-76, 2004.

(248) DeMali, K.A., Barlow, C.A., and Burridge, K. Recruitment of the Arp2/3 complex to vinculin: coupling membrane protrusion to matrix adhesion. *J.Cell Biol.* 159(5): 881-91, 2002.

(249) Serrels, B., Serrels, A., Brunton, V.G., Holt, M., McLean, G.W., Gray, C.H., Jones, G.E., and Frame, M.C. Focal adhesion kinase controls actin assembly via a FERM-mediated interaction with the Arp2/3 complex. *Nat.Cell Biol.* 9(9): 1046-56, 2007.

(250) Butler, B., Gao, C., Mersich, A.T., and Blystone, S.D. Purified integrin adhesion complexes exhibit actin-polymerization activity. *Curr.Biol.* 16(3): 242-51, 2006.

(251) Gupton, S.L., Eisenmann, K., Alberts, A.S., and Waterman-Storer, C.M. mDia2 regulates actin and focal adhesion dynamics and organization in the lamella for efficient epithelial cell migration. *J.Cell Sci.* 120(Pt 19): 3475-87, 2007.

(252) Kozlov, M.M. and Bershadsky, A.D. Processive capping by formin suggests a force-driven mechanism of actin polymerization. *J.Cell Biol.* 167(6): 1011-7, 2004.

(253) Hoffman, L.M., Jensen, C.C., Kloeker, S., Wang, C.L., Yoshigi, M., and Beckerle, M.C. Genetic ablation of zyxin causes Mena/VASP mislocalization, increased motility, and deficits in actin remodeling. *J.Cell Biol.* 172(5): 771-82, 2006.

(254) Golsteyn, R.M., Beckerle, M.C., Koay, T., and Friederich, E. Structural and functional similarities between the human cytoskeletal protein zyxin and the ActA protein of Listeria monocytogenes. *J.Cell Sci.* 110 (Pt 16)(1893-906, 1997.

(255) Yoshigi, M., Hoffman, L.M., Jensen, C.C., Yost, H.J., and Beckerle, M.C. Mechanical force mobilizes zyxin from focal adhesions to actin filaments and regulates cytoskeletal reinforcement. *J.Cell Biol.* 171(2): 209-15, 2005.

(256) Lele, T.P., Pendse, J., Kumar, S., Salanga, M., Karavitis, J., and Ingber, D.E. Mechanical forces alter zyxin unbinding kinetics within focal adhesions of living cells. *J.Cell Physiol*. 207(1): 187-94, 2006.

(257) Itoh, R.E., Kurokawa, K., Ohba, Y., Yoshizaki, H., Mochizuki, N., and Matsuda, M. Activation of rac and cdc42 video imaged by fluorescent resonance energy transfer-based single-molecule probes in the membrane of living cells. *Mol.Cell Biol.* 22(18): 6582-91, 2002.

(258) Yoshizaki, H., Ohba, Y., Kurokawa, K., Itoh, R.E., Nakamura, T., Mochizuki, N., Nagashima, K., and Matsuda, M. Activity of Rho-family GTPases during cell division as visualized with FRET-based probes. *J.Cell Biol.* 162(2): 223-32, 2003.

(259) Pertz, O., Hodgson, L., Klemke, R.L., and Hahn, K.M. Spatiotemporal dynamics of RhoA activity in migrating cells. *Nature*. 440(7087): 1069-72, 2006.

(260) Yamada, S. and Nelson, W.J. Localized zones of Rho and Rac activities drive initiation and expansion of epithelial cell-cell adhesion. *J.Cell Biol.* 178(3): 517-27, 2007.

(261) Ohta, Y., Hartwig, J.H., and Stossel, T.P. FilGAP, a Rho- and ROCK-regulated GAP for Rac binds filamin A to control actin remodelling. *Nat.Cell Biol.* 8(8): 803-14, 2006.

(262) Nimnual, A.S., Taylor, L.J., and Bar-Sagi, D. Redox-dependent downregulation of Rho by Rac. *Nat.Cell Biol.* 5(3): 236-41, 2003.

(263) Wildenberg, G.A., Dohn, M.R., Carnahan, R.H., Davis, M.A., Lobdell, N.A., Settleman, J., and Reynolds, A.B. p120-catenin and p190RhoGAP regulate cell-cell adhesion by coordinating antagonism between Rac and Rho. *Cell*. 127(5): 1027-39, 2006.

(264) Miki, H., Suetsugu, S., and Takenawa, T. WAVE, a novel WASP-family protein involved in actin reorganization induced by Rac. *EMBO J.* 17(23): 6932-41, 1998.

(265) Rohatgi, R., Ma, L., Miki, H., Lopez, M., Kirchhausen, T., Takenawa, T., and Kirschner, M.W. The interaction between N-WASP and the Arp2/3 complex links Cdc42-dependent signals to actin assembly. *Cell*. 97(2): 221-31, 1999.

(266) Egile, C., Loisel, T.P., Laurent, V., Li, R., Pantaloni, D., Sansonetti, P.J., and Carlier, M.F. Activation of the CDC42 effector N-WASP by the Shigella flexneri IcsA protein promotes actin nucleation by Arp2/3 complex and bacterial actin-based motility. *J.Cell Biol.* 146(6): 1319-32, 1999.

(267) Tomar, A. and Schlaepfer, D.D. Focal adhesion kinase: switching between GAPs and GEFs in the regulation of cell motility. *Curr.Opin.Cell Biol.* 21(5): 676-83, 2009.

(268) Kiyokawa, E., Hashimoto, Y., Kobayashi, S., Sugimura, H., Kurata, T., and Matsuda, M. Activation of Rac1 by a Crk SH3-binding protein, DOCK180. *Genes Dev.* 12(21): 3331-6, 1998.

(269) Brugnera, E., Haney, L., Grimsley, C., Lu, M., Walk, S.F., Tosello-Trampont, A.C., Macara, I.G., Madhani, H., Fink, G.R., and Ravichandran, K.S. Unconventional Rac-GEF activity is mediated through the Dock180-ELMO complex. *Nat.Cell Biol.* 4(8): 574-82, 2002.

(270) Chodniewicz, D. and Klemke, R.L. Regulation of integrin-mediated cellular responses through assembly of a CAS/Crk scaffold. *Biochim.Biophys.Acta*. 1692(2-3): 63-76, 2004.

(271) West, K.A., Zhang, H., Brown, M.C., Nikolopoulos, S.N., Riedy, M.C., Horwitz, A.F., and Turner, C.E. The LD4 motif of paxillin regulates cell spreading and motility through an interaction with paxillin kinase linker (PKL). *J.Cell Biol.* 154(1): 161-76, 2001.

(272) ten Klooster, J.P., Jaffer, Z.M., Chernoff, J., and Hordijk, P.L. Targeting and activation of Rac1 are mediated by the exchange factor beta-Pix. *J.Cell Biol.* 172(5): 759-69, 2006.

(273) Schober, M., Raghavan, S., Nikolova, M., Polak, L., Pasolli, H.A., Beggs, H.E., Reichardt, L.F., and Fuchs, E. Focal adhesion kinase modulates tension signaling to control actin and focal adhesion dynamics. *J.Cell Biol.* 176(5): 667-80, 2007.

(274) Frank, S.R., Adelstein, M.R., and Hansen, S.H. GIT2 represses Crk- and Rac1-regulated cell spreading and Cdc42-mediated focal adhesion turnover. *EMBO J.* 25(9): 1848-59, 2006.

(275) Tomar, A., Lim, S.T., Lim, Y., and Schlaepfer, D.D. A FAK-p120RasGAP-p190RhoGAP complex regulates polarity in migrating cells. *J.Cell Sci.* 122(Pt 11): 1852-62, 2009.

(276) Hildebrand, J.D., Taylor, J.M., and Parsons, J.T. An SH3 domain-containing GTPase-activating protein for Rho and Cdc42 associates with focal adhesion kinase. *Mol.Cell Biol.* 16(6): 3169-78, 1996.

(277) Dubash, A.D., Wennerberg, K., Garcia-Mata, R., Menold, M.M., Arthur, W.T., and Burridge, K. A novel role for Lsc/p115 RhoGEF and LARG in regulating RhoA activity downstream of adhesion to fibronectin. *J.Cell Sci.* 120(Pt 22): 3989-98, 2007.

(278) Lim, Y., Lim, S.T., Tomar, A., Gardel, M., Bernard-Trifilo, J.A., Chen, X.L., Uryu, S.A., Canete-Soler, R., Zhai, J., Lin, H., Schlaepfer, W.W., Nalbant, P., Bokoch, G., Ilic, D., Waterman-Storer, C., and Schlaepfer, D.D. PyK2 and FAK connections to p190Rho guanine nucleotide exchange factor regulate RhoA activity, focal adhesion formation, and cell motility. *J.Cell Biol.* 180(1): 187-203, 2008.

(279) Iwanicki, M.P., Vomastek, T., Tilghman, R.W., Martin, K.H., Banerjee, J., Wedegaertner, P.B., and Parsons, J.T. FAK, PDZ-RhoGEF and ROCKII cooperate to regulate adhesion movement and trailing-edge retraction in fibroblasts. *J.Cell Sci.* 121(Pt 6): 895-905, 2008.

(280) Zaoui, K., Honore, S., Isnardon, D., Braguer, D., and Badache, A. Memo-RhoA-mDia1 signaling controls microtubules, the actin network, and adhesion site formation in migrating cells. *J.Cell Biol.* 183(3): 401-8, 2008.

(281) Tanentzapf, G. and Brown, N.H. An interaction between integrin and the talin FERM domain mediates integrin activation but not linkage to the cytoskeleton. *Nat.Cell Biol.* 8(6): 601-6, 2006.

(282) Wegener, K.L., Partridge, A.W., Han, J., Pickford, A.R., Liddington, R.C., Ginsberg, M.H., and Campbell, I.D. Structural basis of integrin activation by talin. *Cell.* 128(1): 171-82, 2007.

(283) Montanez, E., Ussar, S., Schifferer, M., Bosl, M., Zent, R., Moser, M., and Fassler, R. Kindlin-2 controls bidirectional signaling of integrins. *Genes Dev.* 22(10): 1325-30, 2008.

(284) Ma, Y.Q., Qin, J., Wu, C., and Plow, E.F. Kindlin-2 (Mig-2): a co-activator of beta3 integrins. *J.Cell Biol.* 181(3): 439-46, 2008.

(285) Galbraith, C.G., Yamada, K.M., and Sheetz, M.P. The relationship between force and focal complex development. *J.Cell Biol.* 159(4): 695-705, 2002.

(286) Humphries, J.D., Wang, P., Streuli, C., Geiger, B., Humphries, M.J., and Ballestrem, C. Vinculin controls focal adhesion formation by direct interactions with talin and actin. *J.Cell Biol.* 179(5): 1043-57, 2007.

(287) Vicente-Manzanares, M., Zareno, J., Whitmore, L., Choi, C.K., and Horwitz, A.F. Regulation of protrusion, adhesion dynamics, and polarity by myosins IIA and IIB in migrating cells. *J.Cell Biol.* 176(5): 573-80, 2007.

(288) Vicente-Manzanares, M., Koach, M.A., Whitmore, L., Lamers, M.L., and Horwitz, A.F. Segregation and activation of myosin IIB creates a rear in migrating cells. *J.Cell Biol.* 183(3): 543-54, 2008.

(289) Even-Ram, S., Doyle, A.D., Conti, M.A., Matsumoto, K., Adelstein, R.S., and Yamada, K.M. Myosin IIA regulates cell motility and actomyosin-microtubule crosstalk. *Nat.Cell Biol.* 9(3): 299-309, 2007.

(290) Giannone, G., Dubin-Thaler, B.J., Rossier, O., Cai, Y., Chaga, O., Jiang, G., Beaver, W., Dobereiner, H.G., Freund, Y., Borisy, G., and Sheetz, M.P. Lamellipodial actin mechanically links myosin activity with adhesion-site formation. *Cell*. 128(3): 561-75, 2007.

(291) Pasapera, A.M., Schneider, I.C., Rericha, E., Schlaepfer, D.D., and Waterman, C.M. Myosin II activity regulates vinculin recruitment to focal adhesions through FAK-mediated paxillin phosphorylation. *J.Cell Biol.* 188(6): 877-90, 2010.

(292) Totsukawa, G., Wu, Y., Sasaki, Y., Hartshorne, D.J., Yamakita, Y., Yamashiro, S., and Matsumura, F. Distinct roles of MLCK and ROCK in the regulation of membrane protrusions and focal adhesion dynamics during cell migration of fibroblasts. *J.Cell Biol.* 164(3): 427-39, 2004.

(293) Sawada, Y., Tamada, M., Dubin-Thaler, B.J., Cherniavskaya, O., Sakai, R., Tanaka, S., and Sheetz, M.P. Force sensing by mechanical extension of the Src family kinase substrate p130Cas. *Cell*. 127(5): 1015-26, 2006.

(294) Desai, A. and Mitchison, T.J. Microtubule polymerization dynamics. *Annu.Rev.Cell Dev.Biol.* 13(83-117, 1997.

(295) Amos, L.A. and Schlieper, D. Microtubules and maps. *Adv.Protein Chem.* 71(257-98, 2005.

(296) Tian, G., Lewis, S.A., Feierbach, B., Stearns, T., Rommelaere, H., Ampe, C., and Cowan, N.J. Tubulin subunits exist in an activated conformational state generated and maintained by protein cofactors. *J.Cell Biol.* 138(4): 821-32, 1997.

(297) Lopez-Fanarraga, M., Avila, J., Guasch, A., Coll, M., and Zabala, J.C. Review: postchaperonin tubulin folding cofactors and their role in microtubule dynamics. *J.Struct.Biol.* 135(2): 219-29, 2001.

(298) Cowan, N.J. and Lewis, S.A. Type II chaperonins, prefoldin, and the tubulin-specific chaperones. *Adv.Protein Chem.* 59(73-104, 2001.

(299) Beghin, A., Galmarini, C.M., and Dumontet, C. Tubulin folding pathways: implication in the regulation of microtubule dynamics. *Curr.Cancer Drug Targets.* 7(8): 697-703, 2007.

(300) Nogales, E. and Wang, H.W. Structural mechanisms underlying nucleotide-dependent self-assembly of tubulin and its relatives. *Curr.Opin.Struct.Biol.* 16(2): 221-9, 2006.

(301) Wang, H.W. and Nogales, E. Nucleotide-dependent bending flexibility of tubulin regulates microtubule assembly. *Nature*. 435(7044): 911-5, 2005.

(302) Nogales, E. and Wang, H.W. Structural intermediates in microtubule assembly and disassembly: how and why? *Curr.Opin.Cell Biol.* 18(2): 179-84, 2006.

(303) Mozziconacci, J., Sandblad, L., Wachsmuth, M., Brunner, D., and Karsenti, E. Tubulin dimers oligomerize before their incorporation into microtubules. *PLoS.One.* 3(11): e3821, 2008.

(304) Rice, L.M., Montabana, E.A., and Agard, D.A. The lattice as allosteric effector: structural studies of alphabeta- and gamma-tubulin clarify the role of GTP in microtubule assembly. *Proc.Natl.Acad.Sci.U.S.A*. 105(14): 5378-83, 2008.

(305) Amos, L. and Klug, A. Arrangement of subunits in flagellar microtubules. *J.Cell Sci.* 14(3): 523-49, 1974.

(306) Chretien, D., Fuller, S.D., and Karsenti, E. Structure of growing microtubule ends: two-dimensional sheets close into tubes at variable rates. *J.Cell Biol.* 129(5): 1311-28, 1995.

(307) Caplow, M., Ruhlen, R.L., and Shanks, J. The free energy for hydrolysis of a microtubule-bound nucleotide triphosphate is near zero: all of the free energy for hydrolysis is stored in the microtubule lattice. *J.Cell Biol.* 127(3): 779-88, 1994.

(308) Gardner, M.K., Hunt, A.J., Goodson, H.V., and Odde, D.J. Microtubule assembly dynamics: new insights at the nanoscale. *Curr.Opin.Cell Biol.* 20(1): 64-70, 2008.

(309) Howard, J. and Hyman, A.A. Growth, fluctuation and switching at microtubule plus ends. *Nat.Rev.Mol.Cell Biol.* 10(8): 569-74, 2009.

(310) Dimitrov, A., Quesnoit, M., Moutel, S., Cantaloube, I., Pous, C., and Perez, F. Detection of GTP-tubulin conformation in vivo reveals a role for GTP remnants in microtubule rescues. *Science*. 322(5906): 1353-6, 2008.

(311) Howard, J. and Hyman, A.A. Dynamics and mechanics of the microtubule plus end. *Nature*. 422(6933): 753-8, 2003.

(312) Raynaud-Messina, B. and Merdes, A. Gamma-tubulin complexes and microtubule organization. *Curr.Opin.Cell Biol.* 19(1): 24-30, 2007.

(313) Luders, J. and Stearns, T. Microtubule-organizing centres: a re-evaluation. *Nat.Rev.Mol.Cell Biol.* 8(2): 161-7, 2007.

(314) Bartolini, F. and Gundersen, G.G. Generation of noncentrosomal microtubule arrays. *J.Cell Sci.* 119(Pt 20): 4155-63, 2006.

(315) Efimov, A., Kharitonov, A., Efimova, N., Loncarek, J., Miller, P.M., Andreyeva, N., Gleeson, P., Galjart, N., Maia, A.R., McLeod, I.X., Yates, J.R., III, Maiato, H., Khodjakov, A., Akhmanova, A., and Kaverina, I. Asymmetric CLASP-dependent nucleation of noncentrosomal microtubules at the trans-Golgi network. *Dev.Cell*. 12(6): 917-30, 2007.

(316) Job, D., Valiron, O., and Oakley, B. Microtubule nucleation. *Curr.Opin.Cell Biol.* 15(1): 111-7, 2003.

(317) Wiese, C. and Zheng, Y. Microtubule nucleation: gamma-tubulin and beyond. *J.Cell Sci.* 119(Pt 20): 4143-53, 2006.

(318) Lee, J.C. and Timasheff, S.N. The reconstitution of microtubules from purified calf brain tubulin. *Biochemistry*. 14(23): 5183-7, 1975.

(319) Mitchison, T. and Kirschner, M. Dynamic instability of microtubule growth. *Nature*. 312(5991): 237-42, 1984.

(320) Cassimeris, L., Pryer, N.K., and Salmon, E.D. Real-time observations of microtubule dynamic instability in living cells. *J.Cell Biol.* 107(6 Pt 1): 2223-31, 1988.

(321) Kinoshita, K., Arnal, I., Desai, A., Drechsel, D.N., and Hyman, A.A. Reconstitution of physiological microtubule dynamics using purified components. *Science*. 294(5545): 1340-3, 2001.

(322) van, d., V, Akhmanova, A., and Straube, A. Regulation of microtubule dynamic instability. *Biochem.Soc.Trans.* 37(Pt 5): 1007-13, 2009.

(323) Dumont, S. and Mitchison, T.J. Force and length in the mitotic spindle. *Curr.Biol.* 19(17): R749-R761, 2009.

(324) Miller, P.M., Folkmann, A.W., Maia, A.R., Efimova, N., Efimov, A., and Kaverina, I. Golgi-derived CLASP-dependent microtubules control Golgi organization and polarized trafficking in motile cells. *Nat.Cell Biol.* 11(9): 1069-80, 2009.

(325) Manneville, J.B. and Etienne-Manneville, S. Positioning centrosomes and spindle poles: looking at the periphery to find the centre. *Biol.Cell.* 98(9): 557-65, 2006.

(326) Akhmanova, A., Stehbens, S.J., and Yap, A.S. Touch, grasp, deliver and control: functional cross-talk between microtubules and cell adhesions. *Traffic.* 10(3): 268-74, 2009.

(327) Ross, J.L., Ali, M.Y., and Warshaw, D.M. Cargo transport: molecular motors navigate a complex cytoskeleton. *Curr.Opin.Cell Biol.* 20(1): 41-7, 2008.

(328) Etienne-Manneville, S. From signaling pathways to microtubule dynamics: the key players. *Curr.Opin.Cell Biol.* 2009.

(329) Yao, X., Anderson, K.L., and Cleveland, D.W. The microtubule-dependent motor centromere-associated protein E (CENP-E) is an integral component of kinetochore corona fibers that link centromeres to spindle microtubules. *J.Cell Biol.* 139(2): 435-47, 1997.

(330) Fant, X., Merdes, A., and Haren, L. Cell and molecular biology of spindle poles and NuMA. *Int.Rev.Cytol.* 238(1-57, 2004.

(331) Faller, E.M., Villeneuve, T.S., and Brown, D.L. MAP1a associated light chain 3 increases microtubule stability by suppressing microtubule dynamics. *Mol.Cell Neurosci.* 41(1): 85-93, 2009.

(332) Dehmelt, L. and Halpain, S. The MAP2/Tau family of microtubule-associated proteins. *Genome Biol.* 6(1): 204, 2005.

(333) Denarier, E., Fourest-Lieuvin, A., Bosc, C., Pirollet, F., Chapel, A., Margolis, R.L., and Job, D. Nonneuronal isoforms of STOP protein are responsible for microtubule cold stability in mammalian fibroblasts. *Proc.Natl.Acad.Sci.U.S.A.* 95(11): 6055-60, 1998.

(334) Guillaud, L., Bosc, C., Fourest-Lieuvin, A., Denarier, E., Pirollet, F., Lafanechere, L., and Job, D. STOP proteins are responsible for the high degree of microtubule stabilization observed in neuronal cells. *J.Cell Biol.* 142(1): 167-79, 1998.

(335) Lyle, K., Kumar, P., and Wittmann, T. SnapShot: Microtubule regulators II. *Cell.* 136(3): 566, 566, 2009.

(336) Akhmanova, A. and Hoogenraad, C.C. Microtubule plus-end-tracking proteins: mechanisms and functions. *Curr.Opin.Cell Biol.* 17(1): 47-54, 2005.

(337) Akhmanova, A. and Steinmetz, M.O. Tracking the ends: a dynamic protein network controls the fate of microtubule tips. *Nat.Rev.Mol.Cell Biol.* 9(4): 309-22, 2008.

(338) Bieling, P., Laan, L., Schek, H., Munteanu, E.L., Sandblad, L., Dogterom, M., Brunner, D., and Surrey, T. Reconstitution of a microtubule plus-end tracking system in vitro. *Nature*. 450(7172): 1100-5, 2007.

(339) Vitre, B., Coquelle, F.M., Heichette, C., Garnier, C., Chretien, D., and Arnal, I. EB1 regulates microtubule dynamics and tubulin sheet closure in vitro. *Nat.Cell Biol.* 10(4): 415-21, 2008.

(340) Honnappa, S., Gouveia, S.M., Weisbrich, A., Damberger, F.F., Bhavesh, N.S., Jawhari, H., Grigoriev, I., van Rijssel, F.J., Buey, R.M., Lawera, A., Jelesarov, I., Winkler, F.K., Wuthrich, K., Akhmanova, A., and Steinmetz, M.O. An EB1-binding motif acts as a microtubule tip localization signal. *Cell*. 138(2): 366-76, 2009.

(341) Komarova, Y., De Groot, C.O., Grigoriev, I., Gouveia, S.M., Munteanu, E.L., Schober, J.M., Honnappa, S., Buey, R.M., Hoogenraad, C.C., Dogterom, M., Borisy, G.G., Steinmetz, M.O., and Akhmanova, A. Mammalian end binding proteins control persistent microtubule growth. *J.Cell Biol.* 184(5): 691-706, 2009.

(342) Komarova, Y.A., Akhmanova, A.S., Kojima, S., Galjart, N., and Borisy, G.G. Cytoplasmic linker proteins promote microtubule rescue in vivo. *J.Cell Biol.* 159(4): 589-99, 2002.

(343) Mimori-Kiyosue, Y., Grigoriev, I., Lansbergen, G., Sasaki, H., Matsui, C., Severin, F., Galjart, N., Grosveld, F., Vorobjev, I., Tsukita, S., and Akhmanova, A. CLASP1 and CLASP2 bind to EB1 and regulate microtubule plus-end dynamics at the cell cortex. *J.Cell Biol.* 168(1): 141-53, 2005.

(344) Kodama, A., Karakesisoglou, I., Wong, E., Vaezi, A., and Fuchs, E. ACF7: an essential integrator of microtubule dynamics. *Cell*. 115(3): 343-54, 2003.

(345) Wu, X., Kodama, A., and Fuchs, E. ACF7 regulates cytoskeletal-focal adhesion dynamics and migration and has ATPase activity. *Cell*. 135(1): 137-48, 2008.

(346) Mogensen, M.M., Tucker, J.B., Mackie, J.B., Prescott, A.R., and Nathke, I.S. The adenomatous polyposis coli protein unambiguously localizes to microtubule plus ends and is involved in establishing parallel arrays of microtubule bundles in highly polarized epithelial cells. *J.Cell Biol.* 157(6): 1041-8, 2002.

(347) Kita, K., Wittmann, T., Nathke, I.S., and Waterman-Storer, C.M. Adenomatous polyposis coli on microtubule plus ends in cell extensions can promote microtubule net growth with or without EB1. *Mol.Biol.Cell.* 17(5): 2331-45, 2006.

(348) Grigoriev, I., Gouveia, S.M., van, d., V, Demmers, J., Smyth, J.T., Honnappa, S., Splinter, D., Steinmetz, M.O., Putney, J.W., Jr., Hoogenraad, C.C., and Akhmanova, A. STIM1 is a MT-plus-end-tracking protein involved in remodeling of the ER. *Curr.Biol.* 18(3): 177-82, 2008.

(349) Brouhard, G.J., Stear, J.H., Noetzel, T.L., Al-Bassam, J., Kinoshita, K., Harrison, S.C., Howard, J., and Hyman, A.A. XMAP215 is a processive microtubule polymerase. *Cell.* 132(1): 79-88, 2008.

(350) Palazzo, A.F., Cook, T.A., Alberts, A.S., and Gundersen, G.G. mDia mediates Rho-regulated formation and orientation of stable microtubules. *Nat.Cell Biol.* 3(8): 723-9, 2001.

(351) Wen, Y., Eng, C.H., Schmoranzer, J., Cabrera-Poch, N., Morris, E.J., Chen, M., Wallar, B.J., Alberts, A.S., and Gundersen, G.G. EB1 and APC bind to mDia to stabilize microtubules downstream of Rho and promote cell migration. *Nat.Cell Biol.* 6(9): 820-30, 2004.

(352) Bartolini, F., Moseley, J.B., Schmoranzer, J., Cassimeris, L., Goode, B.L., and Gundersen, G.G. The formin mDia2 stabilizes microtubules independently of its actin nucleation activity. *J.Cell Biol.* 181(3): 523-36, 2008.

(353) DeWard, A.D. and Alberts, A.S. Microtubule stabilization: formins assert their independence. *Curr.Biol.* 18(14): R605-R608, 2008.

(354) Yoshimura, T., Kawano, Y., Arimura, N., Kawabata, S., Kikuchi, A., and Kaibuchi, K. GSK-3beta regulates phosphorylation of CRMP-2 and neuronal polarity. *Cell.* 120(1): 137-49, 2005.

(355) Goold, R.G., Owen, R., and Gordon-Weeks, P.R. Glycogen synthase kinase 3beta phosphorylation of microtubule-associated protein 1B regulates the stability of microtubules in growth cones. *J.Cell Sci.* 112 (Pt 19)(3373-84, 1999.

(356) Scales, T.M., Lin, S., Kraus, M., Goold, R.G., and Gordon-Weeks, P.R. Nonprimed and DYRK1A-primed GSK3 beta-phosphorylation sites on MAP1B regulate microtubule dynamics in growing axons. *J.Cell Sci.* 122(Pt 14): 2424-35, 2009.

(357) Sanchez, C., Perez, M., and Avila, J. GSK3beta-mediated phosphorylation of the microtubule-associated protein 2C (MAP2C) prevents microtubule bundling. *Eur.J.Cell Biol.* 79(4): 252-60, 2000.

(358) Sun, W., Qureshi, H.Y., Cafferty, P.W., Sobue, K., Agarwal-Mawal, A., Neufield, K.D., and Paudel, H.K. Glycogen synthase kinase-3beta is complexed with tau protein in brain microtubules. *J.Biol.Chem.* 277(14): 11933-40, 2002.

(359) Agarwal-Mawal, A., Qureshi, H.Y., Cafferty, P.W., Yuan, Z., Han, D., Lin, R., and Paudel, H.K. 14-3-3 connects glycogen synthase kinase-3 beta to tau within a brain microtubule-associated tau phosphorylation complex. *J.Biol.Chem.* 278(15): 12722-8, 2003.

(360) Yuan, Z., Agarwal-Mawal, A., and Paudel, H.K. 14-3-3 binds to and mediates phosphorylation of microtubule-associated tau protein by Ser9-phosphorylated glycogen synthase kinase 3beta in the brain. *J.Biol.Chem.* 279(25): 26105-14, 2004.

(361) Illenberger, S., Drewes, G., Trinczek, B., Biernat, J., Meyer, H.E., Olmsted, J.B., Mandelkow, E.M., and Mandelkow, E. Phosphorylation of microtubule-associated proteins MAP2 and MAP4 by the protein kinase p110mark. Phosphorylation sites and regulation of microtubule dynamics. *J.Biol.Chem.* 271(18): 10834-43, 1996.

(362) Drewes, G., Ebneth, A., Preuss, U., Mandelkow, E.M., and Mandelkow, E. MARK, a novel family of protein kinases that phosphorylate microtubule-associated proteins and trigger microtubule disruption. *Cell*. 89(2): 297-308, 1997.

(363) Ebneth, A., Drewes, G., Mandelkow, E.M., and Mandelkow, E. Phosphorylation of MAP2c and MAP4 by MARK kinases leads to the destabilization of microtubules in cells. *Cell Motil.Cytoskeleton*. 44(3): 209-24, 1999.

(364) Timm, T., Balusamy, K., Li, X., Biernat, J., Mandelkow, E., and Mandelkow, E.M. Glycogen synthase kinase (GSK) 3beta directly phosphorylates Serine 212 in the regulatory loop and inhibits microtubule affinity-regulating kinase (MARK) 2. *J.Biol.Chem.* 283(27): 18873-82, 2008.

(365) Zumbrunn, J., Kinoshita, K., Hyman, A.A., and Nathke, I.S. Binding of the adenomatous polyposis coli protein to microtubules increases microtubule stability and is regulated by GSK3 beta phosphorylation. *Curr.Biol.* 11(1): 44-9, 2001.

(366) Etienne-Manneville, S. and Hall, A. Cdc42 regulates GSK-3beta and adenomatous polyposis coli to control cell polarity. *Nature*. 421(6924): 753-6, 2003.

(367) Wittmann, T. and Waterman-Storer, C.M. Spatial regulation of CLASP affinity for microtubules by Rac1 and GSK3beta in migrating epithelial cells. *J.Cell Biol.* 169(6): 929-39, 2005.

(368) Akhmanova, A., Hoogenraad, C.C., Drabek, K., Stepanova, T., Dortland, B., Verkerk, T., Vermeulen, W., Burgering, B.M., De Zeeuw, C.I., Grosveld, F., and Galjart, N. Clasps are CLIP-

115 and -170 associating proteins involved in the regional regulation of microtubule dynamics in motile fibroblasts. *Cell*. 104(6): 923-35, 2001.

(369) Kumar, P., Lyle, K.S., Gierke, S., Matov, A., Danuser, G., and Wittmann, T. GSK3beta phosphorylation modulates CLASP-microtubule association and lamella microtubule attachment. *J.Cell Biol.* 184(6): 895-908, 2009.

(370) Wordeman, L. Microtubule-depolymerizing kinesins. *Curr.Opin.Cell Biol.* 17(1): 82-8, 2005.

(371) Moores, C.A., Yu, M., Guo, J., Beraud, C., Sakowicz, R., and Milligan, R.A. A mechanism for microtubule depolymerization by KinI kinesins. *Mol.Cell*. 9(4): 903-9, 2002.

(372) Hertzer, K.M. and Walczak, C.E. The C-termini of tubulin and the specific geometry of tubulin substrates influence the depolymerization activity of MCAK. *Cell Cycle*. 7(17): 2727-37, 2008.

(373) Steinmetz, M.O. Structure and thermodynamics of the tubulin-stathmin interaction. *J.Struct.Biol.* 158(2): 137-47, 2007.

(374) Westermann, S. and Weber, K. Post-translational modifications regulate microtubule function. *Nat.Rev.Mol.Cell Biol.* 4(12): 938-47, 2003.

(375) Xia, L., Hai, B., Gao, Y., Burnette, D., Thazhath, R., Duan, J., Bre, M.H., Levilliers, N., Gorovsky, M.A., and Gaertig, J. Polyglycylation of tubulin is essential and affects cell motility and division in Tetrahymena thermophila. *J.Cell Biol.* 149(5): 1097-106, 2000.

(376) Thazhath, R., Liu, C., and Gaertig, J. Polyglycylation domain of beta-tubulin maintains axonemal architecture and affects cytokinesis in Tetrahymena. *Nat.Cell Biol.* 4(3): 256-9, 2002.

(377) Janke, C., Rogowski, K., Wloga, D., Regnard, C., Kajava, A.V., Strub, J.M., Temurak, N., van, D.J., Boucher, D., van, D.A., Suryavanshi, S., Gaertig, J., and Edde, B. Tubulin polyglutamylase enzymes are members of the TTL domain protein family. *Science*. 308(5729): 1758-62, 2005.

(378) Larcher, J.C., Boucher, D., Lazereg, S., Gros, F., and Denoulet, P. Interaction of kinesin motor domains with alpha- and beta-tubulin subunits at a tau-independent binding site. Regulation by polyglutamylation. *J.Biol.Chem.* 271(36): 22117-24, 1996.

(379) Bonnet, C., Boucher, D., Lazereg, S., Pedrotti, B., Islam, K., Denoulet, P., and Larcher, J.C. Differential binding regulation of microtubule-associated proteins MAP1A, MAP1B, and MAP2 by tubulin polyglutamylation. *J.Biol.Chem.* 276(16): 12839-48, 2001.

(380) Ikegami, K., Heier, R.L., Taruishi, M., Takagi, H., Mukai, M., Shimma, S., Taira, S., Hatanaka, K., Morone, N., Yao, I., Campbell, P.K., Yuasa, S., Janke, C., Macgregor, G.R., and Setou, M. Loss of alpha-tubulin polyglutamylation in ROSA22 mice is associated with abnormal targeting of KIF1A and modulated synaptic function. *Proc.Natl.Acad.Sci.U.S.A.* 104(9): 3213-8, 2007.

(381) Hammond, J.W., Cai, D., and Verhey, K.J. Tubulin modifications and their cellular functions. *Curr.Opin.Cell Biol.* 20(1): 71-6, 2008.

(382) Argarana, C.E., Barra, H.S., and Caputto, R. Release of [14C]tyrosine from tubulinyl-[14C]tyrosine by brain extract. Separation of a carboxypeptidase from tubulin-tyrosine ligase. *Mol.Cell Biochem.* 19(1): 17-21, 1978.

(383) Barra, H.S., Rodriguez, J.A., Arce, C.A., and Caputto, R. A soluble preparation from rat brain that incorporates into its own proteins (14 C)arginine by a ribonuclease-sensitive system and (14 C)tyrosine by a ribonuclease-insensitive system. *J.Neurochem.* 20(1): 97-108, 1973.

(384) Argarana, C.E., Arce, C.A., Barra, H.S., and Caputto, R. In vivo incorporation of [14C]tyrosine into the C-terminal position of the alpha subunit of tubulin. *Arch.Biochem.Biophys.* 180(2): 264-8, 1977.

(385) Webster, D.R., Wehland, J., Weber, K., and Borisy, G.G. Detyrosination of alpha tubulin does not stabilize microtubules in vivo. *J.Cell Biol.* 111(1): 113-22, 1990.

(386) Liao, G. and Gundersen, G.G. Kinesin is a candidate for cross-bridging microtubules and intermediate filaments. Selective binding of kinesin to detyrosinated tubulin and vimentin. *J.Biol.Chem.* 273(16): 9797-803, 1998.

(387) Reed, N.A., Cai, D., Blasius, T.L., Jih, G.T., Meyhofer, E., Gaertig, J., and Verhey, K.J. Microtubule acetylation promotes kinesin-1 binding and transport. *Curr.Biol.* 16(21): 2166-72, 2006.

(388) Badin-Larcon, A.C., Boscheron, C., Soleilhac, J.M., Piel, M., Mann, C., Denarier, E., Fourest-Lieuvin, A., Lafanechere, L., Bornens, M., and Job, D. Suppression of nuclear oscillations in Saccharomyces cerevisiae expressing Glu tubulin. *Proc.Natl.Acad.Sci.U.S.A.* 101(15): 5577-82, 2004.

(389) Erck, C., Peris, L., Andrieux, A., Meissirel, C., Gruber, A.D., Vernet, M., Schweitzer, A., Saoudi, Y., Pointu, H., Bosc, C., Salin, P.A., Job, D., and Wehland, J. A vital role of tubulin-tyrosine-ligase for neuronal organization. *Proc.Natl.Acad.Sci.U.S.A.* 102(22): 7853-8, 2005.

(390) Peris, L., Thery, M., Faure, J., Saoudi, Y., Lafanechere, L., Chilton, J.K., Gordon-Weeks, P., Galjart, N., Bornens, M., Wordeman, L., Wehland, J., Andrieux, A., and Job, D. Tubulin

tyrosination is a major factor affecting the recruitment of CAP-Gly proteins at microtubule plus ends. *J.Cell Biol.* 174(6): 839-49, 2006.

(391) Piperno, G., LeDizet, M., and Chang, X.J. Microtubules containing acetylated alpha-tubulin in mammalian cells in culture. *J.Cell Biol.* 104(2): 289-302, 1987.

(392) Webster, D.R. and Borisy, G.G. Microtubules are acetylated in domains that turn over slowly. *J.Cell Sci.* 92 (Pt 1)(57-65, 1989.

(393) Maruta, H., Greer, K., and Rosenbaum, J.L. The acetylation of alpha-tubulin and its relationship to the assembly and disassembly of microtubules. *J.Cell Biol.* 103(2): 571-9, 1986.

(394) Dompierre, J.P., Godin, J.D., Charrin, B.C., Cordelieres, F.P., King, S.J., Humbert, S., and Saudou, F. Histone deacetylase 6 inhibition compensates for the transport deficit in Huntington's disease by increasing tubulin acetylation. *J.Neurosci.* 27(13): 3571-83, 2007.

(395) Creppe, C., Malinouskaya, L., Volvert, M.L., Gillard, M., Close, P., Malaise, O., Laguesse, S., Cornez, I., Rahmouni, S., Ormenese, S., Belachew, S., Malgrange, B., Chapelle, J.P., Siebenlist, U., Moonen, G., Chariot, A., and Nguyen, L. Elongator controls the migration and differentiation of cortical neurons through acetylation of alpha-tubulin. *Cell*. 136(3): 551-64, 2009.

(396) North, B.J., Marshall, B.L., Borra, M.T., Denu, J.M., and Verdin, E. The human Sir2 ortholog, SIRT2, is an NAD+-dependent tubulin deacetylase. *Mol.Cell*. 11(2): 437-44, 2003.

(397) Hubbert, C., Guardiola, A., Shao, R., Kawaguchi, Y., Ito, A., Nixon, A., Yoshida, M., Wang, X.F., and Yao, T.P. HDAC6 is a microtubule-associated deacetylase. *Nature*. 417(6887): 455-8, 2002.

(398) Zhang, Y., Li, N., Caron, C., Matthias, G., Hess, D., Khochbin, S., and Matthias, P. HDAC-6 interacts with and deacetylates tubulin and microtubules in vivo. *EMBO J.* 22(5): 1168-79, 2003.

(399) Haggarty, S.J., Koeller, K.M., Wong, J.C., Grozinger, C.M., and Schreiber, S.L. Domain-selective small-molecule inhibitor of histone deacetylase 6 (HDAC6)-mediated tubulin deacetylation. *Proc.Natl.Acad.Sci.U.S.A*. 100(8): 4389-94, 2003.

(400) Matsuyama, A., Shimazu, T., Sumida, Y., Saito, A., Yoshimatsu, Y., Seigneurin-Berny, D., Osada, H., Komatsu, Y., Nishino, N., Khochbin, S., Horinouchi, S., and Yoshida, M. In vivo destabilization of dynamic microtubules by HDAC6-mediated deacetylation. *EMBO J.* 21(24): 6820-31, 2002.

(401) Zhang, Y., Kwon, S., Yamaguchi, T., Cubizolles, F., Rousseaux, S., Kneissel, M., Cao, C., Li, N., Cheng, H.L., Chua, K., Lombard, D., Mizeracki, A., Matthias, G., Alt, F.W., Khochbin, S., and Matthias, P. Mice lacking histone deacetylase 6 have hyperacetylated tubulin but are viable and develop normally. *Mol.Cell Biol.* 28(5): 1688-701, 2008.

(402) Palazzo, A., Ackerman, B., and Gundersen, G.G. Cell biology: Tubulin acetylation and cell motility. *Nature*. 421(6920): 230, 2003.

(403) Zilberman, Y., Ballestrem, C., Carramusa, L., Mazitschek, R., Khochbin, S., and Bershadsky, A. Regulation of microtubule dynamics by inhibition of the tubulin deacetylase HDAC6. *J.Cell Sci.* 122(Pt 19): 3531-41, 2009.

(404) Tran, A.D., Marmo, T.P., Salam, A.A., Che, S., Finkelstein, E., Kabarriti, R., Xenias, H.S., Mazitschek, R., Hubbert, C., Kawaguchi, Y., Sheetz, M.P., Yao, T.P., and Bulinski, J.C. HDAC6 deacetylation of tubulin modulates dynamics of cellular adhesions. *J.Cell Sci.* 120(Pt 8): 1469-79, 2007.

(405) Luduena, R.F. Multiple forms of tubulin: different gene products and covalent modifications. *Int.Rev.Cytol.* 178(207-75, 1998.

(406) Burkhart, C.A., Kavallaris, M., and Band, H.S. The role of beta-tubulin isotypes in resistance to antimitotic drugs. *Biochim.Biophys.Acta*. 1471(2): O1-O9, 2001.

(407) Bode, C.J., Gupta, M.L., Suprenant, K.A., and Himes, R.H. The two alpha-tubulin isotypes in budding yeast have opposing effects on microtubule dynamics in vitro. *EMBO Rep.* 4(1): 94-9, 2003.

(408) Banerjee, A., Roach, M.C., Trcka, P., and Luduena, R.F. Increased microtubule assembly in bovine brain tubulin lacking the type III isotype of beta-tubulin. *J.Biol.Chem.* 265(3): 1794-9, 1990.

(409) Banerjee, A., Roach, M.C., Trcka, P., and Luduena, R.F. Preparation of a monoclonal antibody specific for the class IV isotype of beta-tubulin. Purification and assembly of alpha beta II, alpha beta III, and alpha beta IV tubulin dimers from bovine brain. *J.Biol.Chem.* 267(8): 5625-30, 1992.

(410) Lu, Q. and Luduena, R.F. In vitro analysis of microtubule assembly of isotypically pure tubulin dimers. Intrinsic differences in the assembly properties of alpha beta II, alpha beta III, and alpha beta IV tubulin dimers in the absence of microtubule-associated proteins. *J.Biol.Chem.* 269(3): 2041-7, 1994.

(411) Panda, D., Miller, H.P., Banerjee, A., Luduena, R.F., and Wilson, L. Microtubule dynamics in vitro are regulated by the tubulin isotype composition. *Proc.Natl.Acad.Sci.U.S.A.* 91(24): 11358-62, 1994.

(412) Derry, W.B., Wilson, L., Khan, I.A., Luduena, R.F., and Jordan, M.A. Taxol differentially modulates the dynamics of microtubules assembled from unfractionated and purified beta-tubulin isotypes. *Biochemistry*. 36(12): 3554-62, 1997.

(413) Yvon, A.M., Wadsworth, P., and Jordan, M.A. Taxol suppresses dynamics of individual microtubules in living human tumor cells. *Mol.Biol.Cell.* 10(4): 947-59, 1999.

(414) Goncalves, A., Braguer, D., Kamath, K., Martello, L., Briand, C., Horwitz, S., Wilson, L., and Jordan, M.A. Resistance to Taxol in lung cancer cells associated with increased microtubule dynamics. *Proc.Natl.Acad.Sci.U.S.A.* 98(20): 11737-42, 2001.

(415) Carles, G., Braguer, D., Dumontet, C., Bourgarel, V., Goncalves, A., Sarrazin, M., Rognoni, J.B., and Briand, C. Differentiation of human colon cancer cells changes the expression of beta-tubulin isotypes and MAPs. *Br.J.Cancer*. 80(8): 1162-8, 1999.

(416) Galmarini, C.M., Kamath, K., Vanier-Viornery, A., Hervieu, V., Peiller, E., Falette, N., Puisieux, A., Ann, J.M., and Dumontet, C. Drug resistance associated with loss of p53 involves extensive alterations in microtubule composition and dynamics. *Br.J.Cancer*. 88(11): 1793-9, 2003.

(417) Bershadsky, A., Chausovsky, A., Becker, E., Lyubimova, A., and Geiger, B. Involvement of microtubules in the control of adhesion-dependent signal transduction. *Curr.Biol.* 6(10): 1279-89, 1996.

(418) Liu, B.P., Chrzanowska-Wodnicka, M., and Burridge, K. Microtubule depolymerization induces stress fibers, focal adhesions, and DNA synthesis via the GTP-binding protein Rho. *Cell Adhes.Commun.* 5(4): 249-55, 1998.

(419) Kaverina, I., Rottner, K., and Small, J.V. Targeting, capture, and stabilization of microtubules at early focal adhesions. *J.Cell Biol.* 142(1): 181-90, 1998.

(420) Kaverina, I., Krylyshkina, O., and Small, J.V. Microtubule targeting of substrate contacts promotes their relaxation and dissociation. *J.Cell Biol.* 146(5): 1033-44, 1999.

(421) Peacock, J.G., Miller, A.L., Bradley, W.D., Rodriguez, O.C., Webb, D.J., and Koleske, A.J. The Abl-related gene tyrosine kinase acts through p190RhoGAP to inhibit actomyosin contractility and regulate focal adhesion dynamics upon adhesion to fibronectin. *Mol.Biol.Cell.* 18(10): 3860-72, 2007.

(422) Bhatt, A., Kaverina, I., Otey, C., and Huttenlocher, A. Regulation of focal complex composition and disassembly by the calcium-dependent protease calpain. *J.Cell Sci.* 115(Pt 17): 3415-25, 2002.

(423) Glaven, J.A., Whitehead, I., Bagrodia, S., Kay, R., and Cerione, R.A. The Dbl-related protein, Lfc, localizes to microtubules and mediates the activation of Rac signaling pathways in cells. *J.Biol.Chem.* 274(4): 2279-85, 1999.

(424) Krendel, M., Zenke, F.T., and Bokoch, G.M. Nucleotide exchange factor GEF-H1 mediates cross-talk between microtubules and the actin cytoskeleton. *Nat.Cell Biol.* 4(4): 294-301, 2002.

(425) Kwan, K.M. and Kirschner, M.W. A microtubule-binding Rho-GEF controls cell morphology during convergent extension of Xenopus laevis. *Development*. 132(20): 4599-610, 2005.

(426) Ren, X.D., Kiosses, W.B., and Schwartz, M.A. Regulation of the small GTP-binding protein Rho by cell adhesion and the cytoskeleton. *EMBO J.* 18(3): 578-85, 1999.

(427) Ezratty, E.J., Partridge, M.A., and Gundersen, G.G. Microtubule-induced focal adhesion disassembly is mediated by dynamin and focal adhesion kinase. *Nat.Cell Biol.* 7(6): 581-90, 2005.

(428) Ezratty, E.J., Bertaux, C., Marcantonio, E.E., and Gundersen, G.G. Clathrin mediates integrin endocytosis for focal adhesion disassembly in migrating cells. *J.Cell Biol.* 187(5): 733-47, 2009.

(429) Waterman-Storer, C.M. and Salmon, E.D. Actomyosin-based retrograde flow of microtubules in the lamella of migrating epithelial cells influences microtubule dynamic instability and turnover and is associated with microtubule breakage and treadmilling. *J.Cell Biol.* 139(2): 417-34, 1997.

(430) Waterman-Storer, C.M., Worthylake, R.A., Liu, B.P., Burridge, K., and Salmon, E.D. Microtubule growth activates Rac1 to promote lamellipodial protrusion in fibroblasts. *Nat.Cell Biol.* 1(1): 45-50, 1999.

(431) Kawasaki, Y., Senda, T., Ishidate, T., Koyama, R., Morishita, T., Iwayama, Y., Higuchi, O., and Akiyama, T. Asef, a link between the tumor suppressor APC and G-protein signaling. *Science*. 289(5482): 1194-7, 2000.

(432) Kawasaki, Y., Sagara, M., Shibata, Y., Shirouzu, M., Yokoyama, S., and Akiyama, T. Identification and characterization of Asef2, a guanine-nucleotide exchange factor specific for Rac1 and Cdc42. *Oncogene*. 26(55): 7620-267, 2007.

(433) Wittmann, T., Bokoch, G.M., and Waterman-Storer, C.M. Regulation of leading edge microtubule and actin dynamics downstream of Rac1. *J.Cell Biol.* 161(5): 845-51, 2003.

(434) Wittmann, T., Bokoch, G.M., and Waterman-Storer, C.M. Regulation of microtubule destabilizing activity of Op18/stathmin downstream of Rac1. *J.Biol.Chem.* 279(7): 6196-203, 2004.

(435) Efimov, A., Schiefermeier, N., Grigoriev, I., Ohi, R., Brown, M.C., Turner, C.E., Small, J.V., and Kaverina, I. Paxillin-dependent stimulation of microtubule catastrophes at focal adhesion sites. *J.Cell Sci.* 121(Pt 2): 196-204, 2008.

(436) Palazzo, A.F., Eng, C.H., Schlaepfer, D.D., Marcantonio, E.E., and Gundersen, G.G. Localized stabilization of microtubules by integrin- and FAK-facilitated Rho signaling. *Science*. 303(5659): 836-9, 2004.

(437) Krylyshkina, O., Anderson, K.I., Kaverina, I., Upmann, I., Manstein, D.J., Small, J.V., and Toomre, D.K. Nanometer targeting of microtubules to focal adhesions. *J.Cell Biol.* 161(5): 853-9, 2003.

(438) Yokoo, T., Toyoshima, H., Miura, M., Wang, Y., Iida, K.T., Suzuki, H., Sone, H., Shimano, H., Gotoda, T., Nishimori, S., Tanaka, K., and Yamada, N. p57Kip2 regulates actin dynamics by binding and translocating LIM-kinase 1 to the nucleus. *J.Biol.Chem.* 278(52): 52919-23, 2003.

(439) Vlachos, P. and Joseph, B. The Cdk inhibitor p57(Kip2) controls LIM-kinase 1 activity and regulates actin cytoskeleton dynamics. *Oncogene*. 28(47): 4175-88, 2009.

(440) Nagahara, H., Vocero-Akbani, A.M., Snyder, E.L., Ho, A., Latham, D.G., Lissy, N.A., Becker-Hapak, M., Ezhevsky, S.A., and Dowdy, S.F. Transduction of full-length TAT fusion proteins into mammalian cells: TAT-p27Kip1 induces cell migration. *Nat.Med.* 4(12): 1449-52, 1998.

(441) McAllister, S.S., Becker-Hapak, M., Pintucci, G., Pagano, M., and Dowdy, S.F. Novel p27(kip1) C-terminal scatter domain mediates Rac-dependent cell migration independent of cell cycle arrest functions. *Mol.Cell Biol.* 23(1): 216-28, 2003.

(442) Besson, A., Gurian-West, M., Schmidt, A., Hall, A., and Roberts, J.M. p27Kip1 modulates cell migration through the regulation of RhoA activation. *Genes Dev.* 18(8): 862-76, 2004.

(443) Diez-Juan, A. and Andres, V. Coordinate control of proliferation and migration by the p27Kip1/cyclin-dependent kinase/retinoblastoma pathway in vascular smooth muscle cells and fibroblasts. *Circ.Res.* 92(4): 402-10, 2003.

(444) Friedl, P. and Wolf, K. Plasticity of cell migration: a multiscale tuning model. *J.Cell Biol.* 2010.

(445) Mantel, C., Braun, S.E., Reid, S., Henegariu, O., Liu, L., Hangoc, G., and Broxmeyer, H.E. p21(cip-1/waf-1) deficiency causes deformed nuclear architecture, centriole overduplication, polyploidy, and relaxed microtubule damage checkpoints in human hematopoietic cells. *Blood*. 93(4): 1390-8, 1999.

(446) Lacey, K.R., Jackson, P.K., and Stearns, T. Cyclin-dependent kinase control of centrosome duplication. *Proc.Natl.Acad.Sci.U.S.A*. 96(6): 2817-22, 1999.

(447) Tarapore, P., Horn, H.F., Tokuyama, Y., and Fukasawa, K. Direct regulation of the centrosome duplication cycle by the p53-p21Waf1/Cip1 pathway. *Oncogene*. 20(25): 3173-84, 2001.

(448) Duensing, A., Ghanem, L., Steinman, R.A., Liu, Y., and Duensing, S. p21(Waf1/Cip1) deficiency stimulates centriole overduplication. *Cell Cycle*. 5(24): 2899-902, 2006.

(449) Srsen, V., Gnadt, N., Dammermann, A., and Merdes, A. Inhibition of centrosome protein assembly leads to p53-dependent exit from the cell cycle. *J.Cell Biol.* 174(5): 625-30, 2006.

(450) Mikule, K., Delaval, B., Kaldis, P., Jurcyzk, A., Hergert, P., and Doxsey, S. Loss of centrosome integrity induces p38-p53-p21-dependent G1-S arrest. *Nat.Cell Biol.* 9(2): 160-70, 2007.

(451) Liu, M., Casimiro, M.C., Wang, C., Shirley, L.A., Jiao, X., Katiyar, S., Ju, X., Li, Z., Yu, Z., Zhou, J., Johnson, M., Fortina, P., Hyslop, T., Windle, J.J., and Pestell, R.G. p21CIP1 attenuates Ras- and c-Myc-dependent breast tumor epithelial mesenchymal transition and cancer stem cell-like gene expression in vivo. *Proc.Natl.Acad.Sci.U.S.A*. 106(45): 19035-9, 2009.

(452) Friedl, P. Prespecification and plasticity: shifting mechanisms of cell migration. *Curr.Opin.Cell Biol.* 16(1): 14-23, 2004.

(453) Kedrin, D., van, R.J., Hernandez, L., Condeelis, J., and Segall, J.E. Cell motility and cytoskeletal regulation in invasion and metastasis. *J.Mammary.Gland.Biol.Neoplasia.* 12(2-3): 143-52, 2007.

(454) Yilmaz, M. and Christofori, G. EMT, the cytoskeleton, and cancer cell invasion. *Cancer Metastasis Rev.* 28(1-2): 15-33, 2009.

(455) Galmarini, C.M., Bouchet, B.P., Audoynaud, C., Lamblot, C., Falette, N., Bertholon, J., Wang, Q., Beghin, A., Dumontet, C., and Puisieux, A. A p21/WAF1 mutation favors the appearance of drug resistance to paclitaxel in human noncancerous epithelial mammary cells. *Int.J.Cancer*. 119(1): 60-6, 2006.

(456) Hall, A. The cytoskeleton and cancer. *Cancer Metastasis Rev.* 28(1-2): 5-14, 2009.

(457) Karlsson, R., Pedersen, E.D., Wang, Z., and Brakebusch, C. Rho GTPase function in tumorigenesis. *Biochim.Biophys.Acta*. 1796(2): 91-8, 2009.

(458) Perez-Roger, I., Kim, S.H., Griffiths, B., Sewing, A., and Land, H. Cyclins D1 and D2 mediate myc-induced proliferation via sequestration of p27(Kip1) and p21(Cip1). *EMBO J.* 18(19): 5310-20, 1999.

(459) Geng, Y., Yu, Q., Sicinska, E., Das, M., Bronson, R.T., and Sicinski, P. Deletion of the p27Kip1 gene restores normal development in cyclin D1-deficient mice. *Proc.Natl.Acad.Sci.U.S.A*. 98(1): 194-9, 2001.

(460) Yang, J. and Weinberg, R.A. Epithelial-mesenchymal transition: at the crossroads of development and tumor metastasis. *Dev.Cell*. 14(6): 818-29, 2008.

(461) Revenu, C. and Gilmour, D. EMT 2.0: shaping epithelia through collective migration. *Curr.Opin.Genet.Dev.* 19(4): 338-42, 2009.

(462) Nobes, C.D. and Hall, A. Rho GTPases control polarity, protrusion, and adhesion during cell movement. *J.Cell Biol.* 144(6): 1235-44, 1999.

(463) Turner, C.E., Brown, M.C., Perrotta, J.A., Riedy, M.C., Nikolopoulos, S.N., McDonald, A.R., Bagrodia, S., Thomas, S., and Leventhal, P.S. Paxillin LD4 motif binds PAK and PIX through a novel 95-kD ankyrin repeat, ARF-GAP protein: A role in cytoskeletal remodeling. *J.Cell Biol.* 145(4): 851-63, 1999.

(464) Zamir, E., Katz, M., Posen, Y., Erez, N., Yamada, K.M., Katz, B.Z., Lin, S., Lin, D.C., Bershadsky, A., Kam, Z., and Geiger, B. Dynamics and segregation of cell-matrix adhesions in cultured fibroblasts. *Nat.Cell Biol.* 2(4): 191-6, 2000.

(465) Laukaitis, C.M., Webb, D.J., Donais, K., and Horwitz, A.F. Differential dynamics of alpha 5 integrin, paxillin, and alpha-actinin during formation and disassembly of adhesions in migrating cells. *J.Cell Biol.* 153(7): 1427-40, 2001.

(466) Prunier, C. and Howe, P.H. Disabled-2 (Dab2) is required for transforming growth factor beta-induced epithelial to mesenchymal transition (EMT). *J.Biol.Chem.* 280(17): 17540-8, 2005.

(467) Rid, R., Schiefermeier, N., Grigoriev, I., Small, J.V., and Kaverina, I. The last but not the least: the origin and significance of trailing adhesions in fibroblastic cells. *Cell Motil.Cytoskeleton*. 61(3): 161-71, 2005.

(468) Gupton, S.L. and Waterman-Storer, C.M. Spatiotemporal feedback between actomyosin and focal-adhesion systems optimizes rapid cell migration. *Cell*. 125(7): 1361-74, 2006.

(469) Hu, K., Ji, L., Applegate, K.T., Danuser, G., and Waterman-Storer, C.M. Differential transmission of actin motion within focal adhesions. *Science*. 315(5808): 111-5, 2007.

(470) Amano, T., Kaji, N., Ohashi, K., and Mizuno, K. Mitosis-specific activation of LIM motif-containing protein kinase and roles of cofilin phosphorylation and dephosphorylation in mitosis. *J.Biol.Chem.* 277(24): 22093-102, 2002.

(471) Kaji, N., Ohashi, K., Shuin, M., Niwa, R., Uemura, T., and Mizuno, K. Cell cycle-associated changes in Slingshot phosphatase activity and roles in cytokinesis in animal cells. *J.Biol.Chem.* 278(35): 33450-5, 2003.

(472) Niwa, R., Nagata-Ohashi, K., Takeichi, M., Mizuno, K., and Uemura, T. Control of actin reorganization by Slingshot, a family of phosphatases that dephosphorylate ADF/cofilin. *Cell*. 108(2): 233-46, 2002.

(473) Nishita, M., Tomizawa, C., Yamamoto, M., Horita, Y., Ohashi, K., and Mizuno, K. Spatial and temporal regulation of cofilin activity by LIM kinase and Slingshot is critical for directional cell migration. *J.Cell Biol.* 171(2): 349-59, 2005.

(474) Soosairajah, J., Maiti, S., Wiggan, O., Sarmiere, P., Moussi, N., Sarcevic, B., Sampath, R., Bamburg, J.R., and Bernard, O. Interplay between components of a novel LIM kinase-slingshot phosphatase complex regulates cofilin. *EMBO J.* 24(3): 473-86, 2005.

(475) Yuan, J., Slice, L.W., and Rozengurt, E. Activation of protein kinase D by signaling through Rho and the alpha subunit of the heterotrimeric G protein G13. *J.Biol.Chem.* 276(42): 38619-27, 2001.

(476) Flinn, H.M. and Ridley, A.J. Rho stimulates tyrosine phosphorylation of focal adhesion kinase, p130 and paxillin. *J.Cell Sci.* 109 (Pt 5)(1133-41, 1996.

(477) Huang, T.Y., DerMardirossian, C., and Bokoch, G.M. Cofilin phosphatases and regulation of actin dynamics. *Curr.Opin.Cell Biol.* 18(1): 26-31, 2006.

(478) Marshall, T.W., Aloor, H.L., and Bear, J.E. Coronin 2A regulates a subset of focal-adhesion-turnover events through the cofilin pathway. *J.Cell Sci.* 122(Pt 17): 3061-9, 2009.

(479) Perkins, N.D. Not just a CDK inhibitor: regulation of transcription by p21(WAF1/CIP1/SDI1). *Cell Cycle*. 1(1): 39-41, 2002.

(480) Moon, S.Y. and Zheng, Y. Rho GTPase-activating proteins in cell regulation. *Trends Cell Biol.* 13(1): 13-22, 2003.

(481) Burbelo, P.D., Miyamoto, S., Utani, A., Brill, S., Yamada, K.M., Hall, A., and Yamada, Y. p190-B, a new member of the Rho GAP family, and Rho are induced to cluster after integrin cross-linking. *J.Biol.Chem.* 270(52): 30919-26, 1995.

(482) Gen, Y., Yasui, K., Zen, K., Nakajima, T., Tsuji, K., Endo, M., Mitsuyoshi, H., Minami, M., Itoh, Y., Tanaka, S., Taniwaki, M., Arii, S., Okanoue, T., and Yoshikawa, T. A novel amplification target, ARHGAP5, promotes cell spreading and migration by negatively regulating RhoA in Huh-7 hepatocellular carcinoma cells. *Cancer Lett.* 275(1): 27-34, 2009.

(483) Rusan, N.M., Fagerstrom, C.J., Yvon, A.M., and Wadsworth, P. Cell cycle-dependent changes in microtubule dynamics in living cells expressing green fluorescent protein-alpha tubulin. *Mol.Biol.Cell*. 12(4): 971-80, 2001.

(484) Zenke, F.T., Krendel, M., DerMardirossian, C., King, C.C., Bohl, B.P., and Bokoch, G.M. p21-activated kinase 1 phosphorylates and regulates 14-3-3 binding to GEF-H1, a microtubule-localized Rho exchange factor. *J.Biol.Chem.* 279(18): 18392-400, 2004.

(485) Kim, Y.B., Choi, S., Choi, M.C., Oh, M.A., Lee, S.A., Cho, M., Mizuno, K., Kim, S.H., and Lee, J.W. Cell adhesion-dependent cofilin serine 3 phosphorylation by the integrin-linked kinase.c-Src complex. *J.Biol.Chem.* 283(15): 10089-96, 2008.

(486) Andersen, C.L., Jensen, J.L., and Orntoft, T.F. Normalization of real-time quantitative reverse transcription-PCR data: a model-based variance estimation approach to identify genes suited for normalization, applied to bladder and colon cancer data sets. *Cancer Res.* 64(15): 5245-50, 2004.

(487) Vandesompele, J., De, P.K., Pattyn, F., Poppe, B., Van, R.N., De, P.A., and Speleman, F. Accurate normalization of real-time quantitative RT-PCR data by geometric averaging of multiple internal control genes. *Genome Biol.* 3(7): RESEARCH0034, 2002.

(488) Bryce, N.S., Clark, E.S., Leysath, J.L., Currie, J.D., Webb, D.J., and Weaver, A.M. Cortactin promotes cell motility by enhancing lamellipodial persistence. *Curr.Biol.* 15(14): 1276-85, 2005.

(489) Sidani, M., Wessels, D., Mouneimne, G., Ghosh, M., Goswami, S., Sarmiento, C., Wang, W., Kuhl, S., El-Sibai, M., Backer, J.M., Eddy, R., Soll, D., and Condeelis, J. Cofilin determines the migration behavior and turning frequency of metastatic cancer cells. *J.Cell Biol.* 179(4): 777-91, 2007.

G) MANUSCRIT 1

$p21^{Cip1}$ regulates actin and microtubule dynamics in untransformed epithelial cells

Benjamin Pierre Bouchet[1,2,*], Frédérique Fauvet[3], Gaël Grelier[1,2], George Hinkal[1,2], Carlos María Galmarini[4,5,‡] and Alain Puisieux[1,2,3,*]

1 INSERM U590, Centre LEON BERARD, Lyon, F-69008, France

2 Université Lyon 1, ISPB, IFR62, Lyon, F-69008, France

3 Unité d'Oncologie Moléculaire, Centre LEON BERARD Lyon, F-69373, France

4 ENS-CNRS UMR 5239, Ecole Normale Supérieure de Lyon, Lyon, F-69364, France

5 Université Lyon 1, UFR de Médecine Lyon-Sud, IFR128, Oullins, F-69921, France

* Authors for correspondence (bouchetb@lyon.fnclcc.fr ; puisieux@lyon.fnclcc.fr)

‡ Current address: PharmaMar, S.A., Colmenar Viejo (Madrid), E-28770 Spain

Short title: p21 regulates overall cytoskeletal dynamics

Keywords: p21, focal adhesion, actin, microtubule, migration, mammary epithelial cells

Summary

Despite its frequent inactivation during epithelial tumor progression, the requirement of $p21^{Cip1}$ (p21) for cytoskeletal dynamics in normal epithelial cells has never been addressed. Here, we investigate the role of p21 in adhesion, actin and microtubule dynamics in untransformed human mammary epithelial cells. Firstly, we find that p21 is required for normal cell adhesion and migration. Depletion of p21 suppresses focal adhesions, stress fibers and Rho activity. Additionally, p21-depleted cells show strong dephosphorylation of cofilin correlating with altered protrusion dynamics and PKCμ-SSH1L signaling. PKCμ silencing largely recapitulates adhesion and actin defects found in p21-depleted cells. Moreover, *ARHGAP19*, which encodes a putative Rho inhibitor, is upregulated in p21-depleted cells and its knockdown restores Rho activity. Finally, we show that microtubules are severely destabilized and deacetylated by p21 loss. Restoration of normal microtubule dynamics by HDAC6 inhibition partially reverses cell spreading and focal adhesion defects. Collectively, these data

reveal a new role for p21 which consists in promoting overall cytoskeleton stability to ensure normal adhesion in untransformed epithelial cells.

Introduction

$p21^{Cip1}$ (p21) was initially identified as an inhibitor of the activity of cyclin-dependent kinases (CDK)-cyclin complexes and PCNA-dependent DNA synthesis (Chen et al., 1995; el-Deiry et al., 1993; Harper et al., 1993; Luo et al., 1995; Xiong et al., 1993). Since its discovery, it has been extensively studied as a key player in the G1/S checkpoint due to its ability to inhibit cell cycle progression and cellular proliferation (Abbas and Dutta, 2009). p53-dependent transactivation of CDKN1A, the gene encoding p21, was described as a factor of tumor suppression (Brugarolas et al., 1995; Deng et al., 1995; Macleod et al., 1995; Martin-Caballero et al., 2001). Of note, while numerous binding partners of p21 were identified, apart from cell cycle inhibition, very few alternative functions were clearly described (Abbas and Dutta, 2009). Several works have proposed that cytoplasmic p21 could exhibit anti-apoptotic activity by inhibiting caspase-3, MAP3K5 (ASK1) and MAPK9 (SAPK) through direct binding to these proteins (Asada et al., 1999; Huang et al., 2003; Shim et al., 1996; Suzuki et al., 1999; Suzuki et al., 2000; Zhan et al., 2007). Other studies have revealed that p21 could regulate gene transcription, notably by interacting directly with transcription factors, such as c-Myc and E2F1 (Chang et al., 2000; Delavaine and La Thangue, 1999; Janicke et al., 2007; Kitaura et al., 2000; Lohr et al., 2003; Wu et al., 2002). However, the consequences of transcriptome modulation by p21 in proliferation and apoptosis are still poorly understood and seem to be highly dependent upon cellular context (Abbas and Dutta, 2009; Janicke et al., 2007).

Multiple mechanisms of p21 inactivation have been proposed in human cancers including loss of CDKN1A transactivators (e.g. p53), c-Myc activation, increased degradation and aberrant cytoplasmic localization related to ERBB2 activation (Abbas and Dutta, 2009; Jung et al., 2008; Mukherjee and Conrad, 2005; van de Wetering et al., 2002; Zhou et al., 2001). More specifically, functional inactivation of p21 is frequently observed in epithelial tumors (Anttila et al., 1999; Balbin et al., 1996; Caffo et al., 1996; Lu et al., 1998; Polyak et al., 1996). Despite their histological diversity, tumor progression of these malignancies is generally associated with disorganized tissue architecture,

invasion and metastatic dissemination (Debnath and Brugge, 2005). Moreover, it is well documented that these processes involve major reorganization of the cytoskeleton associated with transformation of adhesion and migration properties (Friedl, 2004; Hall, 2009; Kedrin et al., 2007; Yilmaz and Christofori, 2009).

A first link between p21 and cytoskeleton was established by identifying its role in regulating centrosome assembly and duplication through its control of cyclin-CDK activity (Duensing et al., 2006; Lacey et al., 1999; Tarapore et al., 2001). p21 was also described as the effector of a p53-dependent G1 checkpoint that controls centrosome integrity (Mikule et al., 2007; Srsen et al., 2006). Furthermore, studies in transformed cells have claimed that cytoplasmic p21 inactivates the downstream Rho pathway ROCK-LIM kinases (LIMK) which stabilizes stress fiber by inhibiting the actin depolymerizing factor cofilin (Lee and Helfman, 2004; Tanaka et al., 2002). These works concluded that cytoplasmic p21 promotes migration in specific context (neuronal differentiation, Ras-induced transformation) by impeding stress fiber assembly. Alternatively, recent data have proposed that total p21 inhibits cell migration associated with Ras- and c-Myc-induced epithelial-mesenchymal transition (EMT) in human mammary epithelial cells (Liu et al., 2009). Altogether, these results suggest that the role of p21 in migration is dependent on cellular context and point out the necessity to address this question in untransformed human epithelial cells.

Hence, we have investigated the role of p21 in the adhesion, cell migration and cytoskeletal dynamics of untransformed human mammary epithelial cells. Our results show for the first time that p21 is required for normal adhesion and migration in untransformed epithelial cells. We also find that p21 physiologically promotes the assembly of focal adhesions and stress fibers, Rho activity and cofilin inactivation. Finally, the present study provides evidence that p21 mediates microtubule stability required for normal adhesion in untransformed epithelial cells. Our findings could have major implications in understanding epithelial tumorigenesis because we demonstrate that p21, which is a frequent target of tumor progression, is also a crucial regulator of cytoskeletal homeostasis in normal cells.

Results

p21 mediates cell spreading and adhesion

Two-dimensional (2D) cell shape results from mechanical forces provided by cytoskeleton, including actin filaments and microtubules, and their interaction with adhesion structures (Broussard et al., 2008; Le and Carlier, 2008; Mogilner and Keren, 2009). Thus, to identify an eventual role of p21 in cytoskeleton dynamics, we firstly analyzed 2D morphological consequences of stable shRNA-mediated depletion of p21 in both mortal and hTERT-immortalized human mammary epithelial cells (mortal HMECs, hTMECs; Fig. 1A,B,C). In accord with its well described anti-proliferative activity, preliminary observations indicated that p21 depletion was accompanied by increased proliferation in both mortal HMECs and hTMECs (data not shown). Remarkably, the physical 2D area occupied by p21-knockdowned (p21KD) cells was strongly reduced when compared with control cells expressing the non-targeting shRNA (NT) cells (Fig. 1B-E). Time-lapse imaging of re-adhesion showed that 2D morphological alteration of p21KD cells was related to defective adhesion affecting primary steps of cells spreading (Fig. 1F,G; supplementary material Movie 1). Of note, similar results obtained by comparing synchronized NT and p21KD cells indicate that adhesion defects in p21KD cells are unlikely to be caused by loss of a cell cycle-related function of p21 (data not shown).

Because 2D migration properties are closely related to adhesion in motile cells, we next examined migration in p21KD cells compared with NT cells (Mogilner and Keren, 2009). In accordance with previous works, our preliminary observations showed that isolated HMECs, grown on 2D uncoated polystyrene support, migrated in a limited zone around initial spreading location (supplementary material Movie 2)(Maheshwari et al., 2001). The velocity of migrating p21KD cells was found to be reduced nearly 50% when compared with NT cells (supplementary material Movie 2 and Fig. S1A,B). Similar results were obtained by analyzing collective cell migration, during 2D wound closure, in p21KD cells compared to control cells (Fig. S1D). Directional migration is a feature of numerous human cell types in vivo and untransformed epithelial cells are characterized by their ability to initiate persistent migration. Here we found that directional persistence of isolated migrating cells was also impeded by p21 silencing (supplementary material Fig. S1C). Collectively, these data demonstrate that p21 is required for normal adhesion and migration in untransformed human epithelial cells.

p21 promotes focal adhesion assembly

Focal adhesions are involved in extracellular matrix (ECM) interaction with the cytoskeleton and the physical transduction of forces that govern adhesion and migration (Geiger et al., 2009; Le and Carlier, 2008; Mogilner and Keren, 2009). To understand the origin of the cell spreading defect related to p21 inactivation, we aimed to quantify focal adhesions in p21KD cells. For this purpose, we established at least two clonal hTMEC-derived cell lines stably expressing a GFP-tagged component of focal adhesions, paxillin (GP-hMECs), which allowed live imaging of focal adhesion morphometry and dynamics (Laukaitis et al., 2001; Turner et al., 1999; Zamir et al., 2000). GP-hMECs were transformed as previously described to harbor stable p21 knockdown. We observed that focal adhesions in p21KD cells were dramatically reduced in number when compared with NT cells (Fig. 2A,B). Also, mean focal adhesion area was diminished in p21KD cells (Fig. 2B). Because focal adhesions in migrating cells exhibit function-related size heterogeneity, we examined this parameter in NT and p21KD cells (Fig. 2C) (Broussard et al., 2008; Zaoui et al., 2008). Our data showed that focal adhesion depletion in p21KD cells was not size-specific (Fig. 2C).

Focal adhesion turnover in motile cells is required for proper adhesion dynamics during migration (Broussard et al., 2008; Tomar and Schlaepfer, 2009). To further document the focal adhesion defect due to p21 loss, we evaluated frequency of focal adhesion assembly by time-lapse imaging. Focal adhesion assembly was found to be significantly less frequent in p21-depleted cells than in control cells, consistently with their reduced migration (Fig. 2D,E; supplementary material Movie 3). Lastly, we investigated phosphorylation of FAK and Src which are primary factors of focal adhesion assembly (Huveneers and Danen, 2009). Phosphorylation of FAK at tyrosine 397 is essential for the formation of the FAK-Src complex that governs focal adhesion formation and maturation (Mitra and Schlaepfer, 2006). We found that, while Src phosphorylation was unchanged, phosphorylation of FAK at tyrosine 397 was strongly reduced by p21 depletion (Fig. 2F). This implies that the early steps of focal adhesion assembly are impeded by p21 loss. Together, these data demonstrate that p21 is required for proper assembly and dynamics of focal adhesion in untransformed human epithelial cells.

p21 is required for sustained stress fiber assembly, Rho activity and cofilin phosphorylation

Coordination of focal adhesion and actin filament assembly is essential in adhesion formation and maturation (Choi et al., 2008; Le and Carlier, 2008). Having demonstrated that p21 inactivation was associated with major cell spreading and focal adhesion defect, it was still unclear how actin filaments may be affected. Hence, we aimed to examine whether p21 silencing was also associated with alteration of actin polymerization. F-actin staining showed that stress fiber assembly was reduced over 60% in p21KD cells relative to control cells (Fig. 3A,B). Notably, total F-actin content was not significantly modified by p21 depletion, indicating that primary steps of actin polymerization were not inhibited (Fig. 3C). We next examined the effect of knocking down p21 on the activity of Rho GTPases which have been described as pleiotropic regulators of actin dynamics (Etienne-Manneville and Hall, 2002; Heasman and Ridley, 2008). We found that, while Cdc42 and Rac1 activities were not affected by p21 depletion, RhoA/B/C (Rho) activity was strongly reduced (Fig. 3D).

Acting downstream Rho, ROCK-LIM kinase (LIMK) and PKCμ-SSH1L signalings have been shown to regulate cofilin as a common effector in actin polymerization and organization (Eiseler et al., 2009; Wang et al., 2007). While LIMK inactivates cofilin via phosphorylation, SSH1L phosphatase enhances its activity. When hypophosphorylated, cofilin acts as an F-actin severing factor, favoring stress fiber disassembly and actin filament turnover (Wang et al., 2007). Therefore, we next investigated the cofilin phosphorylation status in p21KD and NT cells. Phospho-serine 3 cofilin (pS3 cofilin) was found to be strongly reduced by p21 depletion in mortal HMECs and hTMECs (Fig. 3E). Noticeably, cofilin was previously shown to be a key factor in protrusion dynamics (van Rheenen et al., 2007). We thus analysed protrusion in p21KD cells. Protrusion dynamics was found severely altered by p21 depletion, due to higher persistence, and decreased velocity and frequency (Supplementary material Fig. S2A-E and Movie 4). This clearly suggests that cycle of cofilin activation-inactivation is highly disrupted by p21 inactivation, preventing stable polymerization required for protrusion. Altogether, our results imply that p21 physiologically promotes Rho activation and actin stability in untransformed human epithelial cells.

p21 is dispensable for LIMK activation by ROCK but is required for PKCμ-SSH1L signaling

The ROCK-LIMK pathway acts downstream Rho to inhibit cofilin through phosphorylation (Arber et al., 1998; Wang et al., 2007; Yang et al., 1998). Because we observed Rho inactivation, we

hypothesized that the lack of cofilin phosphorylation in p21-depleted cells could be caused by a reduced activation of LIMK by ROCK. However, ROCK-dependent phosphorylation of LIMK was found unchanged in these cells (Fig. 3E). Still, specific inhibition of ROCK by the small molecule Y-27632 reduced both LIMK and cofilin phosphorylation, and treatment with S3 peptide, which is effective competitive inhibitor of LIMK1, led to reduced cofilin phosphorylation (Fig. 4A). Additionally, specific Rho inhibition by the C3 exoenzyme decreased cofilin phosphorylation but did not modify ROCK-dependent LIMK phosphorylation (Fig. 4B). Thus, though the ROCK-LIMK-cofilin pathway is active in HMECs, Rho inactivation is not sufficient to impede its activity. These results also imply that p21 does not control cofilin phosphorylation through ROCK-dependent activation of LIMK.

When hypophosphorylated, SSH1L activates cofilin via dephosphorylation (Eiseler et al., 2009; Nagata-Ohashi et al., 2004; Nishita et al., 2005; Niwa et al., 2002). Here we found SSH1L to be hypophosphorylated at serine 978 in p21KD cells, which suggests that it is involved in cofilin hyperactivation in these cells (Fig. 3E). It has been shown that cofilin dephosphorylation by SSH1L requires inactive PKCμ (Eiseler et al., 2009; Nagata-Ohashi et al., 2004). When activated by Rho, PKCμ inhibits SSH1L by phosphorylation (Eiseler et al., 2009; Nagata-Ohashi et al., 2004). Because Rho activity and SSH1L phosphorylation were found downregulated in p21KD cells, we speculated that PKCμ should be inactive in these cells. But, surprisingly, phosphorylation of PKCμ at serines 744/748 was found to be increased in p21KD cells (Fig. 3E). This indicates that PKCμ phosphorylation in p21KD cells is likely to be uncoupled from its capacity to phosphorylate and inactivate SSH1L.

Next, we sought to verify whether PKCμ phosphorylation was linked to basal Rho activity in HMECs. Inhibition of Rho by C3 exoenzyme led to PKCμ dephosphorylation 8 h after treatment, which indicates that PKCμ's basal activation indeed depends on Rho activity (Fig. 4B). However, this modification arose after an earlier drop in phosphorylated cofilin at 2 hours after treatment, which suggests that cofilin hyperactivation is not directly related to loss of Rho-dependent PKCμ activation (Fig. 4B). Additionally, SSH1L phosphorylation was found unchanged by C3 treatment at any time point (Fig. 4B). Thus, if SSH1L is involved in early cofilin dephosphorylation due to basal Rho inhibition, this process is not caused by loss of PKCμ-mediated phosphorylation. Moreover, it must be emphasized that at the 8 hour time point when PKCμ was dephosphorylated due to Rho inhibition, cofilin phosphorylation had returned to normal high levels (Fig. 4B). This signals a possible feedback

loop targeting cofilin. Collectively, these results demonstrate that p21 is required for normal PKCμ-SSH1L signaling. Our data also reveal that basal Rho inactivation is not sufficient per se to induce the alterations of PKCμ and SSH1L phosphorylation observed in p21-depleted cells.

To further test the hypothesis that the PKCμ inactivation contributes to cofilin hyperactivation in p21-depleted cells, we analyzed the consequences of PKCμ depletion by transient RNA interference (RNAi) in control cells. Strikingly, PKCμ silencing partially recapitulated alterations related to p21 depletion, including FAK and cofilin hypophosphorylation, the decrease in cell spreading, and the inhibition of stress fiber and focal adhesion assembly (supplementary material Fig. S3A-E). This argues for functional inactivation of PKCμ as a possible factor of adhesion, actin and cofilin defects found in p21KD cells. Of note, PKCμ depletion did not modify SSH1L phosphorylation (supplementary material Fig. S3A). Thus, if SSH1L is involved in cofilin activation during the PKCμ depletion experiment, this process is not caused by loss of PKCμ-mediated phosphorylation. The combination of long-term Rho inactivity with adhesion and actin alteration could be necessary to induce the stable SSH1L hypophosphorylated state we observed in p21KD cells.

Next, we reasoned that if SSH1L activity contributes to cofilin hypophosphorylation and activation in p21-depleted cells, its silencing should reverse this alteration. Hence, we analyzed consequences of SSH1L depletion by RNAi in p21KD cells. As expected, we found that cofilin phosphorylation was increased by SSH1L depletion (supplementary material Fig. S4A). Thus, SSH1L is partially responsible for cofilin hyperactivation in p21-depleted cells. Of note, SSH1L silencing also induced, in both NT and p21KD cells, major alteration of cell spreading and adhesion as well as suppression of focal adhesion and FAK phosphorylation, and disruption of actin network (data not shown; supplementary material Fig. S4A-E). These data further suggest that SSH1L controls focal adhesion stability in normal cells.

p21 controls Rho activation possibly through regulation of RhoGAP19 expression

Several works illustrate the role of p21 as a regulator of gene transcription (Abbas and Dutta, 2009; Besson et al., 2008; Chang et al., 2000; Liu et al., 2009; Perkins, 2002). Thus we have hypothesized that cytoskeletal defects found in p21-depleted cells could arise partially from deregulated expression of genes coding for cytoskeleton regulators. In order to identify these eventual p21-modulated genes, we performed a whole genome microarray analysis of the

transcriptome of hTMECs 48 h after transfection with CDKN1A-targeting (si5, si6) or non-specific (siCT) siRNA. Our cut-off selection criteria used was a minimum of 1.3-fold change of mRNA expression in si5 and si6 samples versus the siCT control. We identified 119 up-regulated and 384 down-regulated mRNAs as a consequence of p21 silencing (data available upon request). From these data, we identified 11 up-regulated and 29 down-regulated mRNAs coding for characterized or putative cytoskeleton regulators. We further analyzed this subset for candidates of Rho regulation and identified *ARHGAP19* mRNA (NM_032900.4) that was strongly overexpressed in p21-depleted cells, as confirmed by qRT-PCR (p21KD5, 3.6±0.3 fold, $P<0.05$; p21KD6, 9.0±0.5 fold, $P<0.001$; Fig. 5A). *ARHGAP19* (GeneID: 84986) codes for a putative member of the Rho GTPase activating protein (GAP) family, including p190-B/RhoGAP5 and corresponding to Rho inhibitors. We thus reasoned that overexpression of *ARHGAP19* product (RhoGAP19) could participate in Rho inactivation related to p21 depletion. Consistently, we found that *ARHGAP19* knockdown in p21KD cells was sufficient to restore Rho activity similar to that detected in NT cells (Fig. 5B,C). However, SSH1L and cofilin phosphorylation were found unchanged, cell spreading defects and aberrant F-actin pattern were aggravated and focal adhesion mostly abolished in p21KD cells knocked down for RhoGAP19, as compared to p21KD cells with intact RhoGAP19 (Fig. 5E-G). Same alterations were observed in NT cells knocked down for RhoGAP19 (data not shown). Thus, RhoGAP19 is an important player in focal adhesion assembly in untransformed cells. Furthermore, the present data clearly suggest that p21 could physiologically promote Rho activity in untransformed human epithelial cells by participating in repression of RhoGAP19 expression.

p21 contributes to focal adhesion assembly through regulation of microtubule dynamics

Microtubules and focal adhesions have been shown to be interregulated in motile cells (Broussard et al., 2008; Efimov et al., 2008; Kaverina et al., 1999; Palazzo et al., 2004). Moreover, several mechanisms associated with focal adhesion are involved in cross-linking actin and microtubule assembly (Palazzo et al., 2001; Rodriguez et al., 2003; Wen et al., 2004). We have just shown that p21 silencing induces suppression of focal adhesion and actin assembly. Hence, we reasoned that these alterations could also be associated with modified microtubule dynamics. To test this hypothesis, we aimed to analyze consequences of p21 depletion in overall microtubule dynamics of

HMECs. For this purpose, at least two clonal hTMEC-derived cell lines stably expressing GFP-α-tubulin (GT-hMECs) and allowing live imaging of microtubule dynamics were transformed as previously described to harbor stable p21 knockdown (Rusan et al., 2001). p21 depletion was found to strongly affect lamella microtubule dynamics, showing increased growth (NT, 13.91±0.23 μm/min; p21KD6, 16.03±0,31; P<0.001) and shortening rate (NT, 20.97±0.54 μm/min; p21KD6, 23.66±0.62 μm/min; P<0.005) as well as frequency of catastrophe (NT, 1.97±0.09/min; p21KD6, 2.44±0.11/min; P<0.001; Fig. 6A). Time spent in pause was reduced in favor of time spent in growth and shortening, in p21KD cells (NT, pause, 66.3±1.2%; p21KD6, pause, 56.6±1.4%; P<0.001; Fig. 6A). Rescue frequency was decreased while mean dynamicity was increased of 31.8% in same cells (Fig. 6A). Microtubules in NT cells were prone to produce stable longitudinal growth along the lamellar edge (Fig. 6B and supplementary material Movie 5). In contrast, p21KD cells exhibit a dense microtubule array where weakly persistent microtubules mainly targeted lamellar edge under a near-perpendicular angle (Fig. 6B and supplementary material Movie 5). Together, these data demonstrate that p21 mediates overall microtubule stability in untransformed epithelial cells.

In order to test the possibility that dynamic instability defects seen in p21KD cells could arise from intrinsic microtubule modifications, we next assayed β-tubulin isoforms expression and tubulin post-translational modifications which are known to modulate microtubule dynamics (Derry et al., 1997; Galmarini et al., 2003; Panda et al., 1994; Westermann and Weber, 2003). Singularly, both p21KD hTMECs and mortal HMECs showed a strong reduction of βII- and βIII-tubulin expression (Fig. 6C). We further found that transcription of genes coding for βII- (*TUBB2A*, *TUBB2B*) and βIII- tubulin (*TUBB3*) was inhibited in p21KD cells, suggesting a physiological role for p21 in transactivating those genes (Fig. 6D).

Additionally, p21KD cells showed a dramatic reduction of tubulin acetylation (Fig. 6C,E). This post-translational modification found in stable microtubules is inhibited by both SIRT2 and HDAC6 deacetylases (Hubbert et al., 2002; North et al., 2003; Westermann and Weber, 2003). In addition, tubulin acetylation has been shown to be a sensitive marker of HDAC6 activity (Haggarty et al., 2003; Hubbert et al., 2002; Matsuyama et al., 2002; Zhang et al., 2008). It was proposed that the inactive form of HDAC6, rather than tubulin acetylation per se, stabilizes microtubules and favors focal adhesion enlargement and cell spreading (Tran et al., 2007; Zilberman et al., 2009). Therefore, we

sought to determine the contribution of microtubule destabilization in the suppression of focal adhesion assembly in p21-depleted cells. To this aim, we have tested whether forced microtubule stabilization by specific inhibition of HDAC6 with tubacin (Haggarty et al., 2003), in p21-depleted cells, was sufficient to reverse focal adhesion and cell spreading defects. We found that, concomitantly with restoring tubulin acetylation, HDAC6 inhibition in p21KD cells fully normalized almost all microtubule dynamic instability features except catastrophe frequency, which was only partially restored, and time spent in growth, which was further inhibited (Fig. 7A,B). Furthermore, this treatment in p21KD cells partially rescued FAK phosphorylation, as well as focal adhesion area and cell spreading (Fig. 7C-E). This demonstrates that microtubule destabilization in p21KD cells contributes to adhesion defects. Altogether, our data suggest that p21-dependent regulation of microtubule dynamics participates in control of focal adhesion. Whether this function consists in HDAC6 inhibition by p21 is still unknown but p21 is unlikely to inhibit HDAC6 transactivation because we did not observed the upregulation of HDAC6 mRNA in the transcriptome of p21KD cells (data not shown).

Discussion

Cytoskeletal regulation by CKIs of the Cip/Kip family (p21, p27, p57) has recently emerged as an important issue in understanding tumor cell behavior. However, this specific question has never been addressed in untransformed cells relevant to modeling epithelial carcinogenesis. Elucidation of cytoskeletal functions involved in adhesion and their implications in cell plasticity are essential for understanding epithelial tumor progression. Moreover, functional inactivation of p21 is frequent in breast cancers. Hence, in the present study, we aimed to investigate whether p21 regulates primary cytoskeletal functions controlling adhesion in untransformed human mammary epithelial cells. For this purpose, we have analyzed focal adhesion, actin and microtubule dynamics in HMECs harboring stable p21 depletion. We show here that p21 inactivation provokes suppression of cell spreading and focal adhesions which associates with overall destabilization of actin and microtubule dynamics.

We found that p21 depletion in HMECs leads to defective spreading and migration related to reduction of focal adhesion and stress fiber assembly. Moreover, our data clearly show that p21 is required for physiological Rho activity, possibly by repressing expression of the GAP family member

RhoGAP19. The mechanism by which p21 inhibits *ARHGAP19* transcription is still unknown. However, several transactivators directly inhibited by p21 could be responsible for *ARHGAP19* overexpression in p21-depleted cells, including c-Myc, E2F1 and STAT3 (Coqueret and Gascan, 2000; Delavaine and La Thangue, 1999; Janicke et al., 2007; Kitaura et al., 2000). If the primary activity of p21 in modulating Rho consists in transcriptional control of its regulators, further studies should clearly define the p21 partners involved in this function. In addition, we found that RhoGAP19 silencing suppresses focal adhesion, putatively supporting Rho as a downstream target of p21. Thus, future investigations should focus on how RhoGAP19 regulates focal adhesion assembly and its requirement for Rho modulation in normal epithelial cells.

Interestingly, previous works have shown that p27 silencing in MEFs leads to defective migration but is associated with increased Rho activity and focal adhesion (Besson et al., 2004b). Nevertheless, MEFs and HMECs are distinct polarized migrating cell type in which spatio-temporal regulation of Rho and focal adhesion is, in many aspects, dissimilar (Mogilner and Keren, 2009). As well, investigation of p27 role in Rho modulation and adhesion in HMECs should document this point. Besides, there is no demonstration that p21 and p27, in the same cell model, share homologous functions in regulating actin and migration. Indeed, Besson et al. showed that migration of p21-/- MEFs was not modified when compared to wild-type MEFs in contrast to their p27-/- MEF data (Besson et al., 2004b). Still, further cytoskeleton studies in p21-/- MEFs should definitively address this question. Investigating the role of p21 in cytoskeletal dynamics of cells that have undergone EMT could also be highly informative about its differential activity in epithelial and fibroblastic context. At this point, it must be noted that, while p21-/- mice are viable and develop normally, they experiment spontaneous tumorigenesis, notably in epithelial tissues (Brugarolas et al., 1995; Martin-Caballero et al., 2001). These data suggest that loss of cytoskeletal functions of p21 has no crucial effect in development but could synergize with cell cycle alteration to promote tumorigenesis.

Our results also indicate that activity of the F-actin depolymerizing factor cofilin is enhanced by loss of p21. Alternatively, previous works, performed in Ras-transformed NIH/3T3 fibroblasts, N1E-115 neuroblastoma cells and 293T cells, have claimed that cytoplasmic p21 interacts with and inhibits ROCK1 which normally inactivates cofilin via LIMK (Lee and Helfman, 2004; Tanaka et al., 2002). The main goal of our study was to evaluate the global requirement of p21 in adhesion and cytoskeleton

dynamics of untransformed cells. Moreover, contrarily to transformed cells used in previous studies, p21 is largely nuclear in untransformed HMECs. We show that depletion of total p21 does not enhance ROCK-dependent LIMK phosphorylation. Thus, we assume that total p21 is not sufficient to inhibit basal ROCK-induced LIMK activation. Still, if the previously described p21-dependent inhibition of ROCK1 is released by p21 depletion, it could be compensated by an unidentified mechanism (Lee and Helfman, 2004; Tanaka et al., 2002). Similarly, we show that transient inhibition of Rho induces cofilin hypophosphorylation but has no effect on ROCK-dependent LIMK phosphorylation. This reinforces the idea that cofilin hypophosphorylation in p21-depleted cells is unlikely to be caused by suppression of ROCK-dependent LIMK activation. Of note, ROCK-independent mechanisms involved in both activation and inactivation of LIMK have been previously described by others (Vlachos and Joseph, 2009; Yokoo et al., 2003). Thus, we cannot exclude that these mechanisms could be modified in response to p21 loss. Noticeably, whether ROCK is downregulated due to Rho inactivation in p21-depleted cells was not investigated. ROCK controls stress fiber contractility and force transduction depending on myosin II, and loss of this function could strongly contribute to suppression of stress fiber formation as well as spreading and motility in these cells (Amano et al., 1996; Kimura et al., 1996; Pellegrin and Mellor, 2007).

It was recently suggested that Rho activates PKCμ which in turn inhibits the cofilin activator SSH1L by phosphorylation (Eiseler et al., 2009). Accordingly, the present data show that Rho inactivation is correlated with cofilin activation in p21-depleted cells. Additionally, SSH1L was found hypophosphorylated in the same cells. However, we show that these alterations are unrelated to reduced PKCμ phosphorylation. We assume that ability of PKCμ to interact with SSH1L is impeded in this context, despite its sustained phosphorylation. Actually, we establish that basal SSH1L phosphorylation is not directly dependent on Rho and PKCμ□because their respective transient inactivation had no effect on this modification in normal cells. Thus, induction of stable SSH1L hypophosphorylation, as seen in p21-depleted cells, probably requires the combination of long-term inactivation of Rho, focal adhesion and actin assembly, and prevention of the PKCμ/SSH1L interaction (Eiseler et al., 2009; van Rheenen et al., 2007; Wang et al., 2007). Notably, EGF was described as an activator of phosphatidylinositol 4,5-bisphosphate (PIP2) production via the phospholipase Cγ (PLCγ) (Mouneimne et al., 2004; van Rheenen et al., 2007). Furthermore, PIP2 production was found to

transduce both cofilin activation and PKCμ phosphorylation (van Rheenen et al., 2007; Yuan et al., 2001). As HMECs are grown in EGF, we speculate that active EGF-PLCγ-PIP2 signaling participates in both cofilin hyperactivation and PKCμ hyperphosphorylation in p21KD cells.

We also provide here the first demonstration that p21 is required for normal microtubule dynamics in untransformed human epithelial cells. Depletion of p21 in HMECs induces strong destabilization of microtubules accompanied by alteration of tubulin isoforms expression and acetylation. Of note, we have previously found that p53 is involved in microtubule dynamics regulation in human mammary epithelial cells (Galmarini et al., 2003). Strikingly, these previous data showed an increase of dynamicity caused by p53 inactivation similar to that observed here in p21-depleted cells. Thus, it is tempting to speculate that p21 could be a major effector of p53 in microtubule regulation. Though, the patterns of tubulin isoform expression and post-translational modifications observed as a consequence of stable p53 inactivation in MCF7 cells are different from those we found here (Galmarini et al., 2003). We suspect this could partially arise from the marked difference of cell models used - transformed and untransformed cells. Additional investigation in untransformed cells should help to identify p21-dependent and -independent functions of p53 in microtubule dynamics. The present work can also be linked to previous data showing association of p21 inactivation, in untransformed HMECs, with resistance to the microtubule stabilizing drug, paclitaxel (Galmarini et al., 2006). Although, whether microtubule destabilization due to p21 silencing is a factor of resistance to paclitaxel is still unknown.

In addition, it is noteworthy that, while we observed major hypoacetylation of tubulin in p21-depleted cells, inhibition of the acetylase activity of HDAC6 in these cells largely restored both microtubule dynamic instability and adhesion. More specifically, HDAC6 inhibition in p21KD cells increased cell spreading and focal adhesion, in line with previous works linking HDAC6 activity to reduced adhesion (Tran et al., 2007). However, these previous data have also indicated that HDAC6 inhibition leads to reduced focal adhesion turnover and migration. Hence, it would be interesting to determine whether HDAC6 inhibition in p21KD cells has same effect or, contrarily, restores migration. As well, future investigations should focus on understanding how p21 physiologically contributes to tubulin acetylation, and possibly basal HDAC6 inhibition, in untransformed human epithelial cells. Numerous works have demonstrated that Rho activity and actin assembly are involved in microtubule

stabilization in motile cells (Palazzo et al., 2001; Rodriguez et al., 2003; Wen et al., 2004). Reciprocally, dynamic microtubules were shown to mediate Rho activation and actin assembly, especially in motile cells (Broussard et al., 2008; Glaven et al., 1999; Krendel et al., 2002; Kwan and Kirschner, 2005; Zenke et al., 2004). But, whether Rho inactivation in HMECs due to loss of p21 is sufficient per se to destabilize overall microtubule dynamics, particularly at focal adhesion, is still unknown. Similarly, a major issue would be to question whether microtubule destabilization in p21-depleted cells participates to down-regulation of Rho and compromises focal adhesion-associated actin assembly.

In conclusion, we have shown that p21 regulates focal adhesion, stress fiber and microtubule dynamics in untransformed human epithelial cells. These functions correspond to major cytoskeleton factors required for cell adhesion. Thus, their alteration provides a functional explanation for suppression of cell spreading and migration in untransformed p21-depleted epithelial cells. These results further support the idea that CKIs are master regulators of cytoskeleton. Finally, our findings imply that p21 inactivation in epithelial cancers could have a major impact in modulation of cell plasticity associated with invasion and metastatic dissemination.

Materials and methods

Plasmids and siRNA

PAcGFP1-Tubulin vector coding for GFP-α-tubulin was purchased from Clontech. PXN coding sequence was amplified from hTERT-HMECs total cDNA using the forward primer 5'-TAATTGGTACCATGGACGACCTCGACGCCCTGCTGGCGGACTT and the reverse primer 5'-TAACGCAGATCTCTAGCAGAAGAGCTTGAGGAAGCAGTTCTGACAG. PXN CDS was cloned into KpnI/BamHI digested pEGFP-C1 (Clontech). The retroviral GFP-paxillin expressing vector pQC-GPXN was generated by cloning AgeI/BclI digestion product of pGFP-PXN into AgeI/BamHI digested pQCXIN (Clontech).

The pLKO.1 CDKN1A shRNA lentiviral vectors (TRCN0000040123-7) were purchased from Sigma-Aldrich. First nucleotide position of shRNA target on CDKN1A mRNA sequence (NM_000389.3) designate shRNA and their corresponding vectors. Transductions of pLKO.1 sh5 and pLKO.1 sh6

achieved stable p21 knockdown and pLKO.1 sh6. Data from one p21KD model was always confirmed using a second independent p21KD model. Transduction of pLKO.1 NT (non-targeting) (Sigma) was used as control.

Pool of four independent siRNAs (siGENOME SMARTpool, Dharmacon) targeting *SSH1*, *PRKD1* and *ARHGAP19* mRNA was used to transitorily inhibit respectively SSH1L (protein phosphatase slingshot homolog 1)(siSSH1L), PKCμ (siPKCμ) and RhoGAP19 (siGAP19) expression. p21-targeting siRNAs corresponding to sh5 and sh6 targeting sequences (si5 and si6) were purchased from Dharmacon. Pool of 4 independent non-targeting siRNAs (siCONTROL Non-Targeting siRNA Pool #2, siCT, Dharmacon) was used as control in siRNA-mediated knockdown experiments.

Cell culture, transfection and infection

Primary human mammary epithelial cells (HMECs) were obtained from Lonza. Low passage immortalized human mammary epithelial cells (hTMECs, hTERT-transduced HMECs) were provided by R.A. Weinberg (Whitehead Institute, Cambrige, USA). Mortal HMECs and hTMECs-derived cell lines were cultured in MEBM basal medium (Lonza) supplemented with 10 ng/ml human EGF, 5 μg/ml insulin, 0.5 μg/ml hydrocortisone, 0.4% bovine pituitary extract, 50 μg/ml gentamicin and 50 ng/ml amphotericin-B.

Plasmid transfection in hTMECs was performed using FuGENE HD (Roche). Retroviral production was performed in Phoenix Ampho cells (SD 3443, ATCC) and lentiviral production was performed in 293FT cells (Invitrogen) co-transfected by pCMVΔR8.91 (gift from D. Trono, EPFL, Lausanne, Switzerland) and phCMV-G (gift from F.-L. Cosset, ENS, Lyon, France). Stably pAcGFP1-Tubulin-transfected and pQC-GPXN-transduced hTMECs were respectively designated as GT-hMECs and GP-hMECs. Subclones were selected according to optimal fluorescently tagged protein expression, normal 2D mammary epithelial cell morphology and growth.

Cell lines expressing sh5, sh6 and shNT were respectively designated as p21KD5, p21KD6 and NT cells. Cells harboring stable p21 knockdown were generically designated as p21KD cells. Data presentation for one p21KD cell model indicates that similar results were obtained for second independent p21KD model.

Transfection of 10-30 nM siRNAs was performed in hTMECs-derived cell lines using Lipofectamine RNAiMAX (Invitrogen).

Antibodies and reagents

Mouse antibodies against Ku80 (7/Ku80), paxillin (349/Paxillin) and Rac1 (102) were purchased from BD Biosciences. Rabbit anti-SSH1L antibody was purchased from Bethyl Laboratories. Rabbit anti-phospho-serine 978 (pS978) SSH1L was provided by K. Mizuno, Graduate School of Life Sciences, Sendai, Japan. Rabbit antibodies against cofilin, phospho-serine 3 (pS3) cofilin, LIMK1, LIMK2, phospho-threonine 508 LIMK1/phospho-threonine 505 LIMK2 (pT508/5), phosphor-tyrosine 416 (pY416) Src, FAK, phosphor-tyrosine 397 (pY397) FAK, PKCμ, phosphor-serine 744/748 (pS744/8) PKCμ, and mouse antibodies against Src (L4A1) were purchased from Cell Signaling Technology. Mouse antibodies against Cdc42, cyclin B1 (GNS3), p21 (CP36-CP74) and RhoA/B/C (55) were purchased from Millipore. Mouse anti-βII-tubulin (7B9) antibody was purchased from Novus. Mouse antibodies against βI- (SAP.4G5), βIII- (SDL.3D10) and βIV-tubulin (ONS.1A6), total β-tubulin, total α-tubulin, acetylated, tyrosinated and polyglutamylated tubulin were purchased from Sigma. FITC-conjugated monoclonal mouse anti-human α tubulin and TRITC-conjugated polyclonal rabbit anti-mouse Ig antibodies were respectively provided by Sigma and Dako.

TRITC and FITC-conjugated phalloidin, Hoechst 33258, thymidine, deoxycytidine, RNAse, propidium iodide, paclitaxel and mitomycin C were purchased from Sigma. ROCK inhibitor Y-27632 was purchased from Calbiochem. LIMK blocking S3 peptide and its inactive counterpart S3-REV were synthesized by Eurogentec according to following sequences: S3: H2N-MASGVAVSDGVIKVFNRQIKIWFQNRRMKWKK-COOH, S3-REV: H2N-FVKIVGDSVAVGSAMRQIKIWFQNRRMKWKK-COOH, as previously described (Aizawa et al., 2001). Cell permeable exoenzyme C3 transferase was provided by Cytoskeleton. Trypsin neutralizing solution was obtained from Lonza. Oxyrase was purchased from Oxyrase. Tubacin and niltubacin were provided by R. Mazitschek, Massachusetts General Hospital, Boston, USA.

Fluorescent staining microscopy

F-Actin labeling was performed on cells extracted at 37°C in Cytoskeleton Stabilizing Buffer (CSB; 20 mM HEPES, 138 mM KCl, 4 mM MgCl2, 3 mM EGTA) supplemented with 0.1% Triton X-100, 1% BSA, 1 mM ATP and 3 µM phalloidin. After one wash in 0.1% Triton X-100 TBS (TBTS), cells were fixed in 4% PFA/10% sucrose CSB. Cells were then permeabilized in 0.5% Triton X-100 and 1% BSA CSB, blocked in 3% BSA/3% FBS TBST. Finally, cells were stained with 1:100 TRITC-conjugated phalloidin and counterstained with 1 µg/ml Hoechst 33258.

Acetylated-tubulin labeling was realized on cells extracted at room temperature for 1 min in Microtubule Stabilizing Buffer (MTSB; 60mM PIPES pH 6,8, 20 mM HEPES, 1mM MgCl2, 4mM EGTA) supplemented with 0.04% Triton X-100 and 0.25 nM paclitaxel. Cells were fixed in 4% PFA/10% sucrose MTSB, permeabilized in 0.5% Triton X-100 MTSB, blocked in 3% BSA/3% FBS TBST, incubated with 1:1000 anti-acetylated-tubulin mouse antibody and 1:100 TRITC-conjugated polyclonal rabbit anti-mouse Ig antibody, and finally counterstained with Hoechst 33258.

Total α-tubulin labeling was performed on cells extracted at room temperature in MTSB supplemented with 0.04% Triton X-100 and 0.25 nM paclitaxel, fixed in 100% methanol at -20°C, blocked in 3% BSA/3% FBS TBST, incubated with 1:100 FITC-conjugated mouse anti-α-tubulin antibody and counterstained with Hoechst 33258.

Fluorescence microscopy was automated using MetaMorph 7.5.6.0 software and perfomed on a Axioplan 2 imaging device coupled to cooled CCD camera (CoolSNAP HQ monochrome; Photometrics) with 100x/1.4 NA Plan-Apochromat or 63x/1.4 NA Plan-Apochromat objective. F-actin images were acquired as z-series of 0.2 µm-steps, and total fluorescence was quantified on untreated maximum intensity z projection pictures. For stress fibers counting, measure and presentation, maximum intensity z projection pictures were inverted, background subtracted, convolved with a 5x5 kernel and submitted to unsharp mask filter. Microtubule images were acquired as z series, background subtracted convolved for presentation.

Quantitative real-time PCR (qRT-PCR)

qRT-PCR analysis was carried out on LightCycler 2.0 System (Roche Applied Science) as previously described (Ansieau et al., 2008; Vandesompele et al., 2002). Information of primer sequences and

UPL probes (Roche) used for qRT-PCR of *TUBB2A* (NM_001069.2), *TUBB2B* (NM_178012.4), *TUBB3* (NM_006086.2) and *ARHGAP19* (NM_032900.4) mRNAs is available upon request.

Transcriptome analysis

Column-extracted and DNAse-treated total RNAs from 3 independent experiments including untreated and 48 h siCT, si5 and si6 transfected cells were quantified on NanoDrop (Thermo Scientific), quality verified on 2100 Bioanalyzer (Agilent); 1 μg of each total RNA were amplified as cRNA using MessageAmp II aRNA amplification kit (Ambion), dosed and quality verified; 10 μg of each total cRNA were fragmented and hybridized on Codelink Human Whole Genome Microarrays (Applied Microarrays). Arrays were scanned with Scanner Genepix 4000B (Molecular Devices). The results were filtered using Genespring software (Agilent). Only gene exhibiting a fold change over 1.3 related to down- or up-regulation in both si5 and si6 samples relative to siCT sample were considered for analysis. Whole data are available upon request. Untreated samples were used as expression control for siCT samples. IPA software (Ingenuity Systems) and literature-based screen were used to identify genes directly involved in cytoskeleton regulation and sharing modified transcription in p21 knockdown experiments.

Rho, Rac1 and Cdc42 GTPase activity assay

Quantification of Rho, Rac1 and Cdc42 GTPase activity was performed using Rho and Rac1/Cdc42 Activation Assay Kits (Millipore) according to the manufacturer's instructions.

Live cell imaging and analysis

Live cells were visualized on a 37°C heated Zeiss Axiovert 100M microscope automated by MetaMorph 7.5.6.0 software and equipped with a cooled CCD camera (CoolSNAP HQ monochrome; Photometrics). Experiments were performed on cells plated in plastic or glass-bottom dishes (MatTek) maintained on a 37°C heated stage and in a 5% CO2 and humidified atmosphere.

Phase contrast adhesion and migration imaging was performed with a A-Plan 10x/0.25 Ph1 objective. Cell spreading imaging was carried out on 5.10^3 cells/ml solution supplemented with trypsin neutralizing solution (Lonza), 15 min following trypsinization, at 5-min interval, during 24 h. Migration

imaging of individual cells was performed under the same culture procedure, 24 h after plating, and during 90 min. Directional persistence was determined from 8 frames tracks as the ratio of distance to origin relative to total cell path. Wound healing assay was realized on confluent cell monolayer incubated in fresh medium supplemented with 0.25 µg/mL mitomycin C and imaged at 5-min interval. Protrusion dynamics was analyzed under the same culture procedure using at 6-s interval and during 20 min. At least 3 lines-based kymographs per cell were used to evaluate protrusion dynamics parameters (Sidani et al., 2007).

Lamella microtubule imaging was performed with a 100x/1.4 NA Plan-Apochromat or a 63x/1.4 NA Plan-Apochromat objective on cells cultured in phenol-free MEGM containing 5-10 µl/ml oxyrase (Oxyrase, Inc.). Acquisitions were performed from optimal focal planes in lamella, at 3.5-s interval, with a 350-ms exposure and during a minimum of 2.5 min. microtubule plus ends were manually tracked using ImageJ 1.42q software (http://rsb.info.nih.gov/ij/) and MTrackJ plugin (Erik Meijering; http://www.imagescience.org/meijering/software/mtrackj/). For analysis and presentation, image sequences were inverted, processed as stacks and submitted to bleach correction, FFT bandpass filter and contrast enhancing. Distance between plus end and a fixed origin on microtubule body was used to approximate microtubule length changes and velocity between each time point. Only microtubule length changes ≥ 0.4 µm between two consecutive time points were considered as growth or shortening events, while changes < 0.4 µm were considered as pause event. Growth, shortening and pause phases were respectively identified as unique or consecutive growth, shortening and pause events. Mean growth and shortening rates were determined using a custom-written Excel macro (Microsoft) averaging microtubule velocity in each corresponding phase. Total microtubule length change for each phase was calculated as the product of mean growth or shortening rate by total phase duration. Catastrophes (transitions from growth or pause to shortening) and rescues (transitions from shortening to pause or growth) were counted by custom-written Excel macro. Catastrophe frequencies were calculated by dividing the number of catastrophes by the sum of the time spent in growth and pause. Similarly, rescue frequencies were calculated by dividing the number of rescues by the time spent in shortening. Microtubule dynamicity was measured as the total microtubule length grown and shortened relative to the microtubule life span. Mean dynamicity was

calculated for each condition as the average of microtubule dynamicities. For each condition, we analyzed a minimum of 30 microtubules in 10 cells.

Focal adhesion imaging was performed with a 63x/1.4 NA Plan-Apochromat objective using the same conditions. 10 to 13-planes z-series (0.2 μm-steps) per time point were acquired using 300-500 ms exposure. Acquisitions were performed at 40-s interval and during 15-25 min. Final sequences were inverted, background subtracted, bleach corrected, FFT bandpass and unsharp mask filtered. Counting and measure of focal adhesion area were performed on binary converted pictures.

Aknowledgement

We thank Pr. Kensaku Mizuno, Graduate School of Life Sciences (Sendai, Japan), Dr. Ralph Mazitschek (Massachusetts General Hospital, Boston, USA) and ICG (Initiative for Chemical Genetics) - NCI (National Cancer Institute, USA), Dr. Michel Bornens (Institut Curie Paris, France) for providing materials and PLATIM (PLAteau Technique Imagerie/Microcopie, Ecole Normale Supérieure, Lyon, France) for useful microscopy and live cell imaging support. We also thank Pr. Joël Lachuer (ProfileXpert, UMR INSERM U842, Lyon, France) for microarray support, the Centre Commun de Quantimétrie (Lyon, France) and Pr. Diane Braguer and Dr. Stéphane Honoré (UMR INSERM 911, Centre de Recherche en Oncologie Biologique et Oncopharmacologie, Marseille, France) for advices on microtubule dynamics analysis. Benjamin Bouchet is a recipient of a grant from FRM (Fondation pour la Recherche Médicale, France).

References

Abbas, T. and Dutta, A. (2009). p21 in cancer: intricate networks and multiple activities. Nat. Rev. Cancer 9, 400-414.

Aizawa, H., Wakatsuki, S., Ishii, A., Moriyama, K., Sasaki, Y., Ohashi, K., Sekine-Aizawa, Y., Sehara-Fujisawa, A., Mizuno, K., Goshima, Y. et al. (2001). Phosphorylation of cofilin by LIM-kinase is necessary for semaphorin 3A-induced growth cone collapse. Nat. Neurosci. 4, 367-373.

Amano, M., Ito, M., Kimura, K., Fukata, Y., Chihara, K., Nakano, T., Matsuura, Y. and Kaibuchi, K. (1996). Phosphorylation and activation of myosin by Rho-associated kinase (Rho-kinase). J. Biol. Chem. 271, 20246-20249.

Ansieau, S., Bastid, J., Doreau, A., Morel, A. P., Bouchet, B. P., Thomas, C., Fauvet, F., Puisieux, I., Doglioni, C., Piccinin, S. et al. (2008). Induction of EMT by twist proteins as a collateral effect of tumor-promoting inactivation of premature senescence. Cancer Cell 14, 79-89.

Anttila, M. A., Kosma, V. M., Hongxiu, J., Puolakka, J., Juhola, M., Saarikoski, S. and Syrjanen, K. (1999). p21/WAF1 expression as related to p53, cell proliferation and prognosis in epithelial ovarian cancer. Br. J. Cancer 79, 1870-1878.

Arber, S., Barbayannis, F. A., Hanser, H., Schneider, C., Stanyon, C. A., Bernard, O. and Caroni, P. (1998). Regulation of actin dynamics through phosphorylation of cofilin by LIM-kinase. Nature 393, 805-809.

Asada, M., Yamada, T., Ichijo, H., Delia, D., Miyazono, K., Fukumuro, K. and Mizutani, S. (1999). Apoptosis inhibitory activity of cytoplasmic p21(Cip1/WAF1) in monocytic differentiation. EMBO J. 18, 1223-1234.

Balbin, M., Hannon, G. J., Pendas, A. M., Ferrando, A. A., Vizoso, F., Fueyo, A. and Lopez-Otin, C. (1996). Functional analysis of a p21WAF1,CIP1,SDI1 mutant (Arg94 --> Trp) identified in a human breast carcinoma. Evidence that the mutation impairs the ability of p21 to inhibit cyclin-dependent kinases. J. Biol. Chem. 271, 15782-15786.

Besson, A., Assoian, R. K. and Roberts, J. M. (2004a). Regulation of the cytoskeleton: an oncogenic function for CDK inhibitors? Nat. Rev. Cancer 4, 948-955.

Besson, A., Dowdy, S. F. and Roberts, J. M. (2008). CDK inhibitors: cell cycle regulators and beyond. Dev. Cell 14, 159-169.

Besson, A., Gurian-West, M., Schmidt, A., Hall, A. and Roberts, J. M. (2004b). p27Kip1 modulates cell migration through the regulation of RhoA activation. Genes Dev. 18, 862-876.

Broussard, J. A., Webb, D. J. and Kaverina, I. (2008). Asymmetric focal adhesion disassembly in motile cells. Curr. Opin. Cell Biol. 20, 85-90.

Brugarolas, J., Chandrasekaran, C., Gordon, J. I., Beach, D., Jacks, T. and Hannon, G. J. (1995). Radiation-induced cell cycle arrest compromised by p21 deficiency. Nature 377, 552-557.

Caffo, O., Doglioni, C., Veronese, S., Bonzanini, M., Marchetti, A., Buttitta, F., Fina, P., Leek, R., Morelli, L., Palma, P. D. et al. (1996). Prognostic value of p21(WAF1) and p53 expression in breast carcinoma: an immunohistochemical study in 261 patients with long-term follow-up. Clin. Cancer Res. 2, 1591-1599.

Chang, B. D., Watanabe, K., Broude, E. V., Fang, J., Poole, J. C., Kalinichenko, T. V. and Roninson, I. B. (2000). Effects of p21Waf1/Cip1/Sdi1 on cellular gene expression: implications for carcinogenesis, senescence, and age-related diseases. Proc. Natl. Acad. Sci. U. S. A 97, 4291-4296.

Chen, J., Jackson, P. K., Kirschner, M. W. and Dutta, A. (1995). Separate domains of p21 involved in the inhibition of Cdk kinase and PCNA. Nature 374, 386-388.

Choi, C. K., Vicente-Manzanares, M., Zareno, J., Whitmore, L. A., Mogilner, A. and Horwitz, A. R. (2008). Actin and alpha-actinin orchestrate the assembly and maturation of nascent adhesions in a myosin II motor-independent manner. Nat. Cell Biol. 10, 1039-1050.

Coqueret, O. and Gascan, H. (2000). Functional interaction of STAT3 transcription factor with the cell cycle inhibitor p21WAF1/CIP1/SDI1. J. Biol. Chem. 275, 18794-18800.

Debnath, J. and Brugge, J. S. (2005). Modelling glandular epithelial cancers in three-dimensional cultures. Nat. Rev. Cancer 5, 675-688.

Delavaine, L. and La Thangue, N. B. (1999). Control of E2F activity by p21Waf1/Cip1. Oncogene 18, 5381-5392.

Deng, C., Zhang, P., Harper, J. W., Elledge, S. J. and Leder, P. (1995). Mice lacking p21CIP1/WAF1 undergo normal development, but are defective in G1 checkpoint control. Cell 82, 675-684.

Derry, W. B., Wilson, L., Khan, I. A., Luduena, R. F. and Jordan, M. A. (1997). Taxol differentially modulates the dynamics of microtubules assembled from unfractionated and purified beta-tubulin isotypes. Biochemistry 36, 3554-3562.

Duensing, A., Ghanem, L., Steinman, R. A., Liu, Y. and Duensing, S. (2006). p21(Waf1/Cip1) deficiency stimulates centriole overduplication. Cell Cycle 5, 2899-2902.

Efimov, A., Schiefermeier, N., Grigoriev, I., Ohi, R., Brown, M. C., Turner, C. E., Small, J. V. and Kaverina, I. (2008). Paxillin-dependent stimulation of microtubule catastrophes at focal adhesion sites. J. Cell Sci. 121, 196-204.

Eiseler, T., Doppler, H., Yan, I. K., Kitatani, K., Mizuno, K. and Storz, P. (2009). Protein kinase D1 regulates cofilin-mediated F-actin reorganization and cell motility through slingshot. Nat. Cell Biol. 11, 545-556.

el-Deiry, W. S., Tokino, T., Velculescu, V. E., Levy, D. B., Parsons, R., Trent, J. M., Lin, D., Mercer, W. E., Kinzler, K. W. and Vogelstein, B. (1993). WAF1, a potential mediator of p53 tumor suppression. Cell 75, 817-825.

Etienne-Manneville, S. and Hall, A. (2002). Rho GTPases in cell biology. Nature 420, 629-635.

Friedl, P. (2004). Prespecification and plasticity: shifting mechanisms of cell migration. Curr. Opin. Cell Biol. 16, 14-23.

Galmarini, C. M., Bouchet, B. P., Audoynaud, C., Lamblot, C., Falette, N., Bertholon, J., Wang, Q., Beghin, A., Dumontet, C. and Puisieux, A. (2006). A p21/WAF1 mutation favors the appearance of drug resistance to paclitaxel in human noncancerous epithelial mammary cells. Int. J. Cancer 119, 60-66.

Galmarini, C. M., Kamath, K., Vanier-Viornery, A., Hervieu, V., Peiller, E., Falette, N., Puisieux, A., Ann, J. M. and Dumontet, C. (2003). Drug resistance associated with loss of p53 involves extensive alterations in microtubule composition and dynamics. Br. J. Cancer 88, 1793-1799.

Geiger, B., Spatz, J. P. and Bershadsky, A. D. (2009). Environmental sensing through focal adhesions. Nat. Rev. Mol. Cell Biol. 10, 21-33.

Glaven, J. A., Whitehead, I., Bagrodia, S., Kay, R. and Cerione, R. A. (1999). The Dbl-related protein, Lfc, localizes to microtubules and mediates the activation of Rac signaling pathways in cells. J. Biol. Chem. 274, 2279-2285.

Haggarty, S. J., Koeller, K. M., Wong, J. C., Grozinger, C. M. and Schreiber, S. L. (2003). Domain-selective small-molecule inhibitor of histone deacetylase 6 (HDAC6)-mediated tubulin deacetylation. Proc. Natl. Acad. Sci. U. S. A 100, 4389-4394.

Hall, A. (2009). The cytoskeleton and cancer. Cancer Metastasis Rev. 28, 5-14.

Harper, J. W., Adami, G. R., Wei, N., Keyomarsi, K. and Elledge, S. J. (1993). The p21 Cdk-interacting protein Cip1 is a potent inhibitor of G1 cyclin-dependent kinases. Cell 75, 805-816.

Heasman, S. J. and Ridley, A. J. (2008). Mammalian Rho GTPases: new insights into their functions from in vivo studies. Nat. Rev. Mol. Cell Biol. 9, 690-701.

Huang, S., Shu, L., Dilling, M. B., Easton, J., Harwood, F. C., Ichijo, H. and Houghton, P. J. (2003). Sustained activation of the JNK cascade and rapamycin-induced apoptosis are suppressed by p53/p21(Cip1). Mol. Cell 11, 1491-1501.

Hubbert, C., Guardiola, A., Shao, R., Kawaguchi, Y., Ito, A., Nixon, A., Yoshida, M., Wang, X. F. and Yao, T. P. (2002). HDAC6 is a microtubule-associated deacetylase. Nature 417, 455-458.

Huveneers, S. and Danen, E. H. (2009). Adhesion signaling - crosstalk between integrins, Src and Rho. J. Cell Sci. 122, 1059-1069.

Janicke, R. U., Sohn, D., Essmann, F. and Schulze-Osthoff, K. (2007). The multiple battles fought by anti-apoptotic p21. Cell Cycle 6, 407-413.

Jung, P., Menssen, A., Mayr, D. and Hermeking, H. (2008). AP4 encodes a c-MYC-inducible repressor of p21. Proc. Natl. Acad. Sci. U. S. A 105, 15046-15051.

Kaverina, I., Krylyshkina, O. and Small, J. V. (1999). Microtubule targeting of substrate contacts promotes their relaxation and dissociation. J. Cell Biol. 146, 1033-1044.

Kedrin, D., van Rheenen, J., Hernandez, L., Condeelis, J. and Segall, J. E. (2007). Cell motility and cytoskeletal regulation in invasion and metastasis. J. Mammary. Gland. Biol. Neoplasia. 12, 143-152.

Kimura, K., Ito, M., Amano, M., Chihara, K., Fukata, Y., Nakafuku, M., Yamamori, B., Feng, J., Nakano, T., Okawa, K. et al. (1996). Regulation of myosin phosphatase by Rho and Rho-associated kinase (Rho-kinase). Science 273, 245-248.

Kitaura, H., Shinshi, M., Uchikoshi, Y., Ono, T., Iguchi-Ariga, S. M. and Ariga, H. (2000). Reciprocal regulation via protein-protein interaction between c-Myc and p21(cip1/waf1/sdi1) in DNA replication and transcription. J. Biol. Chem. 275, 10477-10483.

Krendel, M., Zenke, F. T. and Bokoch, G. M. (2002). Nucleotide exchange factor GEF-H1 mediates cross-talk between microtubules and the actin cytoskeleton. Nat. Cell Biol. 4, 294-301.

Kwan, K. M. and Kirschner, M. W. (2005). A microtubule-binding Rho-GEF controls cell morphology during convergent extension of Xenopus laevis. Development 132, 4599-4610.

Lacey, K. R., Jackson, P. K. and Stearns, T. (1999). Cyclin-dependent kinase control of centrosome duplication. Proc. Natl. Acad. Sci. U. S. A 96, 2817-2822.

Laukaitis, C. M., Webb, D. J., Donais, K. and Horwitz, A. F. (2001). Differential dynamics of alpha 5 integrin, paxillin, and alpha-actinin during formation and disassembly of adhesions in migrating cells. J. Cell Biol. 153, 1427-1440.

Le, C. C. and Carlier, M. F. (2008). Regulation of actin assembly associated with protrusion and adhesion in cell migration. Physiol Rev. 88, 489-513.

Lee, S. and Helfman, D. M. (2004). Cytoplasmic p21Cip1 is involved in Ras-induced inhibition of the ROCK/LIMK/cofilin pathway. J. Biol. Chem. 279, 1885-1891.

Liu, M., Casimiro, M. C., Wang, C., Shirley, L. A., Jiao, X., Katiyar, S., Ju, X., Li, Z., Yu, Z., Zhou, J. et al. (2009). p21CIP1 attenuates Ras- and c-Myc-dependent breast tumor epithelial mesenchymal transition and cancer stem cell-like gene expression in vivo. Proc. Natl. Acad. Sci. U. S. A 106, 19035-19039.

Lohr, K., Moritz, C., Contente, A. and Dobbelstein, M. (2003). p21/CDKN1A mediates negative regulation of transcription by p53. J. Biol. Chem. 278, 32507-32516.

Lu, X., Toki, T., Konishi, I., Nikaido, T. and Fujii, S. (1998). Expression of p21WAF1/CIP1 in adenocarcinoma of the uterine cervix: a possible immunohistochemical marker of a favorable prognosis. Cancer 82, 2409-2417.

Luo, Y., Hurwitz, J. and Massague, J. (1995). Cell-cycle inhibition by independent CDK and PCNA binding domains in p21Cip1. Nature 375, 159-161.

Macleod, K. F., Sherry, N., Hannon, G., Beach, D., Tokino, T., Kinzler, K., Vogelstein, B. and Jacks, T. (1995). p53-dependent and independent expression of p21 during cell growth, differentiation, and DNA damage. Genes Dev. 9, 935-944.

Maheshwari, G., Wiley, H. S. and Lauffenburger, D. A. (2001). Autocrine epidermal growth factor signaling stimulates directionally persistent mammary epithelial cell migration. J. Cell Biol. 155, 1123-1128.

Martin-Caballero, J., Flores, J. M., Garcia-Palencia, P. and Serrano, M. (2001). Tumor susceptibility of p21(Waf1/Cip1)-deficient mice. Cancer Res. 61, 6234-6238.

Matsuyama, A., Shimazu, T., Sumida, Y., Saito, A., Yoshimatsu, Y., Seigneurin-Berny, D., Osada, H., Komatsu, Y., Nishino, N., Khochbin, S. et al. (2002). In vivo destabilization of dynamic microtubules by HDAC6-mediated deacetylation. EMBO J. 21, 6820-6831.

Mikule, K., Delaval, B., Kaldis, P., Jurcyzk, A., Hergert, P. and Doxsey, S. (2007). Loss of centrosome integrity induces p38-p53-p21-dependent G1-S arrest. Nat. Cell Biol. 9, 160-170.

Mitra, S. K. and Schlaepfer, D. D. (2006). Integrin-regulated FAK-Src signaling in normal and cancer cells. Curr. Opin. Cell Biol. 18, 516-523.

Mogilner, A. and Keren, K. (2009). The shape of motile cells. Curr. Biol. 19, R762-R771.

Mouneimne, G., Soon, L., Desmarais, V., Sidani, M., Song, X., Yip, S. C., Ghosh, M., Eddy, R., Backer, J. M. and Condeelis, J. (2004). Phospholipase C and cofilin are required for carcinoma cell directionality in response to EGF stimulation. J. Cell Biol. 166, 697-708.

Mukherjee, S. and Conrad, S. E. (2005). c-Myc suppresses p21WAF1/CIP1 expression during estrogen signaling and antiestrogen resistance in human breast cancer cells. J. Biol. Chem. 280, 17617-17625.

Nagata-Ohashi, K., Ohta, Y., Goto, K., Chiba, S., Mori, R., Nishita, M., Ohashi, K., Kousaka, K., Iwamatsu, A., Niwa, R. et al. (2004). A pathway of neuregulin-induced activation of cofilin-phosphatase Slingshot and cofilin in lamellipodia. J. Cell Biol. 165, 465-471.

Nishita, M., Tomizawa, C., Yamamoto, M., Horita, Y., Ohashi, K. and Mizuno, K. (2005). Spatial and temporal regulation of cofilin activity by LIM kinase and Slingshot is critical for directional cell migration. J. Cell Biol. 171, 349-359.

Niwa, R., Nagata-Ohashi, K., Takeichi, M., Mizuno, K. and Uemura, T. (2002). Control of actin reorganization by Slingshot, a family of phosphatases that dephosphorylate ADF/cofilin. Cell 108, 233-246.

North, B. J., Marshall, B. L., Borra, M. T., Denu, J. M. and Verdin, E. (2003). The human Sir2 ortholog, SIRT2, is an NAD+-dependent tubulin deacetylase. Mol. Cell 11, 437-444.

Palazzo, A. F., Cook, T. A., Alberts, A. S. and Gundersen, G. G. (2001). mDia mediates Rho-regulated formation and orientation of stable microtubules. Nat. Cell Biol. 3, 723-729.

Palazzo, A. F., Eng, C. H., Schlaepfer, D. D., Marcantonio, E. E. and Gundersen, G. G. (2004). Localized stabilization of microtubules by integrin- and FAK-facilitated Rho signaling. Science 303, 836-839.

Panda, D., Miller, H. P., Banerjee, A., Luduena, R. F. and Wilson, L. (1994). Microtubule dynamics in vitro are regulated by the tubulin isotype composition. Proc. Natl. Acad. Sci. U. S. A 91, 11358-11362.

Pellegrin, S. and Mellor, H. (2007). Actin stress fibres. J. Cell Sci. 120, 3491-3499.

Perkins, N. D. (2002). Not just a CDK inhibitor: regulation of transcription by p21(WAF1/CIP1/SDI1). Cell Cycle 1, 39-41.

Polyak, K., Hamilton, S. R., Vogelstein, B. and Kinzler, K. W. (1996). Early alteration of cell-cycle-regulated gene expression in colorectal neoplasia. Am. J. Pathol. 149, 381-387.

Rodriguez, O. C., Schaefer, A. W., Mandato, C. A., Forscher, P., Bement, W. M. and Waterman-Storer, C. M. (2003). Conserved microtubule-actin interactions in cell movement and morphogenesis. Nat. Cell Biol. 5, 599-609.

Rusan, N. M., Fagerstrom, C. J., Yvon, A. M. and Wadsworth, P. (2001). Cell cycle-dependent changes in microtubule dynamics in living cells expressing green fluorescent protein-alpha tubulin. Mol. Biol. Cell 12, 971-980.

Shim, J., Lee, H., Park, J., Kim, H. and Choi, E. J. (1996). A non-enzymatic p21 protein inhibitor of stress-activated protein kinases. Nature 381, 804-806.

Sidani, M., Wessels, D., Mouneimne, G., Ghosh, M., Goswami, S., Sarmiento, C., Wang, W., Kuhl, S., El-Sibai, M., Backer, J. M. et al. (2007). Cofilin determines the migration behavior and turning frequency of metastatic cancer cells. J. Cell Biol. 179, 777-791.

Srsen, V., Gnadt, N., Dammermann, A. and Merdes, A. (2006). Inhibition of centrosome protein assembly leads to p53-dependent exit from the cell cycle. J. Cell Biol. 174, 625-630.

Suzuki, A., Kawano, H., Hayashida, M., Hayasaki, Y., Tsutomi, Y. and Akahane, K. (2000). Procaspase 3/p21 complex formation to resist fas-mediated cell death is initiated as a result of the phosphorylation of p21 by protein kinase A. Cell Death. Differ. 7, 721-728.

Suzuki, A., Tsutomi, Y., Miura, M. and Akahane, K. (1999). Caspase 3 inactivation to suppress Fas-mediated apoptosis: identification of binding domain with p21 and ILP and inactivation machinery by p21. Oncogene 18, 1239-1244.

Tanaka, H., Yamashita, T., Asada, M., Mizutani, S., Yoshikawa, H. and Tohyama, M. (2002). Cytoplasmic p21(Cip1/WAF1) regulates neurite remodeling by inhibiting Rho-kinase activity. J. Cell Biol. 158, 321-329.

Tarapore, P., Horn, H. F., Tokuyama, Y. and Fukasawa, K. (2001). Direct regulation of the centrosome duplication cycle by the p53-p21Waf1/Cip1 pathway. Oncogene 20, 3173-3184.

Tomar, A. and Schlaepfer, D. D. (2009). Focal adhesion kinase: switching between GAPs and GEFs in the regulation of cell motility. Curr. Opin. Cell Biol. 21, 676-683.

Tran, A. D., Marmo, T. P., Salam, A. A., Che, S., Finkelstein, E., Kabarriti, R., Xenias, H. S., Mazitschek, R., Hubbert, C., Kawaguchi, Y. et al. (2007). HDAC6 deacetylation of tubulin modulates dynamics of cellular adhesions. J. Cell Sci. 120, 1469-1479.

Turner, C. E., Brown, M. C., Perrotta, J. A., Riedy, M. C., Nikolopoulos, S. N., McDonald, A. R., Bagrodia, S., Thomas, S. and Leventhal, P. S. (1999). Paxillin LD4 motif binds PAK and PIX through a novel 95-kD ankyrin repeat, ARF-GAP protein: A role in cytoskeletal remodeling. J. Cell Biol. 145, 851-863.

van de Wetering, M., Sancho, E., Verweij, C., de, L. W., Oving, I., Hurlstone, A., van der Horn, K., Batlle, E., Coudreuse, D., Haramis, A. P. et al. (2002). The beta-catenin/TCF-4 complex imposes a crypt progenitor phenotype on colorectal cancer cells. Cell 111, 241-250.

van Rheenen, J., Song, X., van Roosmalen, W., Cammer, M., Chen, X., Desmarais, V., Yip, S. C., Backer, J. M., Eddy, R. J. and Condeelis, J. S. (2007). EGF-induced PIP2 hydrolysis releases and activates cofilin locally in carcinoma cells. J. Cell Biol. 179, 1247-1259.

Vandesompele, J., De, P. K., Pattyn, F., Poppe, B., Van, R. N., De, P. A. and Speleman, F. (2002). Accurate normalization of real-time quantitative RT-PCR data by geometric averaging of multiple internal control genes. Genome Biol. 3, RESEARCH0034.

Vlachos, P. and Joseph, B. (2009). The Cdk inhibitor p57(Kip2) controls LIM-kinase 1 activity and regulates actin cytoskeleton dynamics. Oncogene 28, 4175-4188.

Wang, W., Eddy, R. and Condeelis, J. (2007). The cofilin pathway in breast cancer invasion and metastasis. Nat. Rev. Cancer 7, 429-440.

Wen, Y., Eng, C. H., Schmoranzer, J., Cabrera-Poch, N., Morris, E. J., Chen, M., Wallar, B. J., Alberts, A. S. and Gundersen, G. G. (2004). EB1 and APC bind to mDia to stabilize microtubules downstream of Rho and promote cell migration. Nat. Cell Biol. 6, 820-830.

Westermann, S. and Weber, K. (2003). Post-translational modifications regulate microtubule function. Nat. Rev. Mol. Cell Biol. 4, 938-947.

Wu, Q., Kirschmeier, P., Hockenberry, T., Yang, T. Y., Brassard, D. L., Wang, L., McClanahan, T., Black, S., Rizzi, G., Musco, M. L. et al. (2002). Transcriptional regulation during p21WAF1/CIP1-induced apoptosis in human ovarian cancer cells. J. Biol. Chem. 277, 36329-36337.

Xiong, Y., Hannon, G. J., Zhang, H., Casso, D., Kobayashi, R. and Beach, D. (1993). p21 is a universal inhibitor of cyclin kinases. Nature 366, 701-704.

Yang, N., Higuchi, O., Ohashi, K., Nagata, K., Wada, A., Kangawa, K., Nishida, E. and Mizuno, K. (1998). Cofilin phosphorylation by LIM-kinase 1 and its role in Rac-mediated actin reorganization. Nature 393, 809-812.

Yilmaz, M. and Christofori, G. (2009). EMT, the cytoskeleton, and cancer cell invasion. Cancer Metastasis Rev. 28, 15-33.

Yokoo, T., Toyoshima, H., Miura, M., Wang, Y., Iida, K. T., Suzuki, H., Sone, H., Shimano, H., Gotoda, T., Nishimori, S. et al. (2003). p57Kip2 regulates actin dynamics by binding and translocating LIM-kinase 1 to the nucleus. J. Biol. Chem. 278, 52919-52923.

Yuan, J., Slice, L. W. and Rozengurt, E. (2001). Activation of protein kinase D by signaling through Rho and the alpha subunit of the heterotrimeric G protein G13. J. Biol. Chem. 276, 38619-38627.

Zamir, E., Katz, M., Posen, Y., Erez, N., Yamada, K. M., Katz, B. Z., Lin, S., Lin, D. C., Bershadsky, A., Kam, Z. et al. (2000). Dynamics and segregation of cell-matrix adhesions in cultured fibroblasts. Nat. Cell Biol. 2, 191-196.

Zaoui, K., Honore, S., Isnardon, D., Braguer, D. and Badache, A. (2008). Memo-RhoA-mDia1 signaling controls microtubules, the actin network, and adhesion site formation in migrating cells. J. Cell Biol. 183, 401-408.

Zenke, F. T., Krendel, M., DerMardirossian, C., King, C. C., Bohl, B. P. and Bokoch, G. M. (2004). p21-activated kinase 1 phosphorylates and regulates 14-3-3 binding to GEF-H1, a microtubule-localized Rho exchange factor. J. Biol. Chem. 279, 18392-18400.

Zhan, J., Easton, J. B., Huang, S., Mishra, A., Xiao, L., Lacy, E. R., Kriwacki, R. W. and Houghton, P. J. (2007). Negative regulation of ASK1 by p21Cip1 involves a small domain that includes Serine 98 that is phosphorylated by ASK1 in vivo. Mol. Cell Biol. 27, 3530-3541.

Zhang, Y., Kwon, S., Yamaguchi, T., Cubizolles, F., Rousseaux, S., Kneissel, M., Cao, C., Li, N., Cheng, H. L., Chua, K. et al. (2008). Mice lacking histone deacetylase 6 have hyperacetylated tubulin but are viable and develop normally. Mol. Cell Biol. 28, 1688-1701.

Zhou, B. P., Liao, Y., Xia, W., Spohn, B., Lee, M. H. and Hung, M. C. (2001). Cytoplasmic localization of p21Cip1/WAF1 by Akt-induced phosphorylation in HER-2/neu-overexpressing cells. Nat. Cell Biol. 3, 245-252.

Zilberman, Y., Ballestrem, C., Carramusa, L., Mazitschek, R., Khochbin, S. and Bershadsky, A. (2009). Regulation of microtubule dynamics by inhibition of the tubulin deacetylase HDAC6. J. Cell Sci. 122, 3531-3541.

Figure Legends

Fig. 1. Depletion of p21 inhibits adhesion in untransformed human mammary epithelial cells. (A) Western blot analysis of p21 in whole lysates from NT, p21KD5 and p21KD6 hTMECs and mortal HMECs. Relative quantification of protein level in triplicate is indicated. Ku80 expression, loading control; molecular mass (kDa). (B) Phase contrast imaging of control (NT) and p21KD (p21KD5, p21KD6) hTMECs. (C) Phase contrast imaging of control (NT) and p21KD (p21KD5, p21KD6) mortal HMECs. (D) Mean cell area measure of NT (n = 30), p21KD5 (n = 30) and p21KD6 (n = 30) hTMECs. (E) Mean cell area measure of NT (n = 50), p21KD5 (n = 50) and p21KD6 (n = 50) HMECs. Decrease percentage is indicated on graph bar. (F) Representative 13-frames montage of time-lapse imaging of NT (green) and p21KD6 (red) cell spreading. Bar, 20 µm. (G) 24 h measure of mean spreading speed in NT (n = 29), p21KD5 (n = 30) and p21KD6 (n = 34) cells. Error bars indicate SEM. **, $P < 0.005$; ***, $P < 0.001$ (Student's *t* test).

Fig. 2. Depletion of p21 suppresses focal adhesions. (A) Live GFP-paxillin imaging in NT and p21KD6 GP-hMECs (upper panels) and binary mask (lower panels). Gray dotted line, cell contour. (B) Mean focal adhesion (FA) count (#) and mean focal adhesion area in NT (13 cells, 629 focal adhesions) and p21KD6 (13 cells, 282 focal adhesions) GP-hMECs. (C) Focal adhesion area distribution in NT (n = 13) and p21KD6 (n = 13) cells. (D) Color-coded focal adhesion dynamics based on live

GFP-paxillin imaging in NT and p21KD6 cells. Yellow arrows indicate neoformed focal adhesions at the leading edge and white arrows indicate sliding focal adhesions at the trailing edge. (E) Focal adhesion assembly frequency in NT (n = 6) and p21KD6 (n = 6) cells. (F) Western blot analysis of pY397 FAK, total FAK, pY416 Src and total Src in whole lysates from NT, p21KD5 and p21KD6 cells. Ku80 expression, loading control; molecular mass (kDa). Bar, 20 μm. Error bar, SEM. *, P < 0.05; ***, P < 0.001; ns, non significant (*t* test).

Fig. 3. Depletion of p21 impedes stress fiber assembly, Rho activity and cofilin phosphorylation. (A) F-actin staining in NT and p21KD cells. (B) Stress fiber quantification in phalloidin-TRITC stained NT (n = 34), p21KD5 (n = 30) and p21KD6 (n = 31) cells. Bar, 20 μm. (C) Total F-actin quantified as total fluorescence of phalloidin-TRITC staining in NT (n = 45), p21KD5 (n = 45) and p21KD6 (n = 44) cells (a.u., arbitrary unit). (D) Quantification of RhoA/B/C (Rho), Rac1 and Cdc42 GTPase activity in NT and p21KD cells. Relative GTPase activity was determined in triplicate as ratio of GTP-bound blot signal relative to total GTPase blot signal in whole cell lysate (a.u.). Representative western blots are presented; black arrow, specific Rac1 signal. Error bar, SD. (E) Western blot analysis of pT508/5 LIMK, total LIMK1 and LIMK2, pS744/8 PKCμ, total PKCμ, pS978 SSH1L, total SSH1L (black arrow, phosphorylated SSH1L; white arrows, hypophosphorylated SSH1L), pS3 cofilin and total cofilin in whole lysates from NT, p21KD5 and p21KD6 hTMECs; western blot analysis of pS3 cofilin in whole lysates from NT, p21KD and p21KD6 HMECs; graph is pS3 cofilin signal relative to total cofilin signal (a.u.). Error bar, SD.

Fig. 4. Cofilin hypophosphorylation due to Rho inactivation is independent of the ROCK-LIMK signaling in HMECs. (A) Western blot analysis of pT508/5 LIMK, total LIMK1, pS3 cofilin, and total cofilin in whole lysates from untreated hTMECs or same cells 12 h treated with Y-27632 (20 μM; control, DMSO) or S3 peptide (40 μg/ml; control, S3-REV peptide). White vertical lines delineate blots from independent gels. (B) Western blot analysis of pS744/8 PKCμ, pS978 SSH1L, total SSH1L, pT508/5 LIMK, pS3 cofilin, GTP-bound Rho and total Rho in whole lysates from untreated hTMECs or same cells treated for 2 or 8 h with C3 transferase (C3 trans, 0.5 μg/ml). Rho GTPase activity was quantified and presented as in (D).

Fig. 5. *ARHGAP19* mRNA is overexpressed in p21-depleted cells and its silencing normalizes Rho activity. (A) Relative *ARHGAP19* mRNA expression in NT, p21KD5 and p21KD6 hTMECs. Error bar, SD from triplicate. Red dotted line, 100% expression in NT cells. (B) Relative *ARHGAP19* mRNA expression in NT GP-hMECs 72 h transfected with control siRNA pool (siCT) and p21KD6 GP-hMECs transfected with control siRNA pool or RhoGAP19-targeted siRNA pool (siGAP19). Red dotted line, 100% expression in NT cells transfected with control siRNA pool. Similar results were obtained in each NT and p21KD6 hTMECs-derived cells. Error bar, SD from triplicate. (C) Quantification of Rho GTPase activity in NT and p21KD6 hTMECs treated as in (B). (D) Western blot analysis of pS744/8 PKCμ, pS978 SSH1L, pY397 FAK, pS3 cofilin in whole lysates from NT and p21KD6 hTMECs treated as in (B). (E) Phase contrast imaging of NT and p21KD6 hTMECs treated as in (B). Black arrows indicate cells with representative morphology. Bar, 100 μm. (F) Live GFP-paxillin imaging in NT and p21KD6 GP-hMECs treated as in (B) (left panels), binary mask (right panels), and mean focal adhesion count (# FA) in same cells (NT+siCT, n = 14; p21KD6+siCT, n = 14; p21KD6+siGAP19, n = 17). Gray dotted line, cell contour. Bar, 10 μm. (G) F-actin staining in NT and p21KD6 hTMECs treated as in (B). Black arrows indicate aberrant F-actin assembly. Bar, 10 μm. Ku80 expression, loading control; molecular mass (kDa). **, $P < 0.005$; ***, $P < 0.001$, ns, non significant (*t* test).

Fig. 6. Depletion of p21 destabilizes microtubules and modifies their composition. (A) Dynamic instability parameters measured in NT (70 microtubules; 14 cells) and p21KD6 GT-hMECs (65 microtubules; 20 cells). Error bar in time percentage graph, 95% confidence interval. Mean dynamicity increase percentage indicated. (B) Immunofluorescence labeling of total α-tubulin (up and middle) and GFP-α-tubulin imaging (low) in NT and p21KD6 cells. Yellow arrows, representative lamella microtubule organization. (C) Western blot analysis of βI- (βI), βII- (βII), βIII- (βIII), βIV- (βIV), total β- (β-tot), acetylated (Ac-tub), polyglutamylated (Glu-tub), tyrosinated (Tyr-tub) and total α-tubulin (α-tot) in whole lysates from NT, p21KD5 and p21KD6 hTMECs; western blot analysis of βII-, βIII-, total β-, acetylated and total α-tubulin in whole lysates from corresponding mortal HMECs. Relative quantification of protein level in triplicate is indicated. (D) Relative *TUBB2A*, *TUBB2B* and *TUBB3*

mRNA expression in NT, p21KD5 and p21KD6 hTMECs. Error bar, SD from triplicate. (E) Immunofluorescence labeling of acetylated tubulin in NT and p21KD6 cells. Gray dotted line, cell contour. Except when specified, error bar is SEM. Bar, 10 μm. *, P < 0.05; **, P < 0.005; ***, P < 0.001 (*t* test).

Fig. 7. HDAC6 inhibition restores microtubule dynamics, focal adhesion and cell spreading in p21-depleted cells. (A) Western blot analysis of acetylated tubulin, pY397 FAK and total FAK in whole lysates from NT GT-hMECs treated 24 h with 0.4 μM niltubacin (NLT) or p21KD6 treated 24 h with 0.4 μM niltubacin or 0.4 μM tubacin (TUB). Relative quantification in triplicate of pY397 FAK signal is indicated. Ku80 expression, loading control. (B) Dynamic instability parameters measured in NT and p21KD6 GT-hMECs treated as in (A) (NT+niltubacin, 43 microtubules, 10 cells; p21KD6+niltubacin, 30 microtubules, 11 cells; p21KD6+tubacin, 30 microtubules, 11 cells). G, growing; S, shortening; CF, catastrophe frequency; RF, rescue frequency. Error bar in time percentage graph, 95% confidence interval. (C) Mean cell area measure of niltubacin treated NT (n = 30) and niltubacin treated (n = 30) or tubacin treated p21KD6 hTMECs (n = 30). (D) Live GFP-paxillin imaging in NT and p21KD6 GP-hMECs treated as in (A) (upper panels) and binary mask (lower panels). Gray dotted line, cell contour. (E) Mean focal adhesion count and mean focal adhesion area in niltubacin treated NT GP-hMECs (13 cells, 612 focal adhesions) and niltubacin treated (14 cells, 299 focal adhesions) or tubacin treated p21KD6 GP-hMECs (13 cells, 491 focal adhesions). Molecular mass (kDa). G, growing; S, shortening; CF, catastrophe frequency; RF, rescue frequency. Except when specified, error bar is SEM. Bar, 10 μm. *, P < 0.05, **, P < 0.005; ***, P < 0.001, ns, non significant (*t* test).

Supplemental material

Fig. S1. Depletion of p21 inhibits 2D migration in untransformed human mammary epithelial cells. (A) Representative 35-min migration tracks obtained from time-lapse recording of NT and p21KD5 cells. Bar, 50 μm. (B) Measure of cell velocity of NT (n = 35), p21KD5 (n = 61), p21KD6 (n = 41) cells based on analysis of 90-min migration tracks. (C) Directional persistence

calculated from 35-min migration tracks in NT (n = 56), p21KD5 (60), p21KD6 (n = 40). (D) Time-lapse imaging of 2D collective migration of NT and p21KD6 during wound healing assay. Bar, 100 µm. Error bars indicate SEM. **, P < 0.005; ***, P < 0.001 (*t* test).

Fig. S2. Depletion of p21 impedes protrusion dynamics. (A) Representative kymographs of lamella edge from phase contrast live recording of NT and p21KD6 hTMECs. Vertical bar, 10 µm; horizontal bar, 1 min 30 s. (B), (C), (D), (E) show respectively persistence, distance, velocity and frequency of protrusion in NT (16 cells, 200 measures) and p21KD6 (39 cells, 174 measures) hTMECs. Fold increase or decrease is eventually indicated. **, P < 0.005; ***, P < 0.001, ns, non significant (*t* test).

Fig. S3. Depletion of PKCµ partially recapitulates cell spreading, focal adhesion, stress fiber and cofilin alterations due to p21 inactivation. (A) Western blot analysis of total PKCµ, pS744/8 PKCµ, pS978 SSH1L, total SSH1L, pT508/5 LIMK, pY397 FAK, total FAK, pS3 cofilin and total cofilin in whole lysate of NT cells 72 h transfected with control siRNA pool (siCT) or PKCµ-targeting siRNA pool (siPKCµ) and p21KD6 cells transfected with control siRNAs. (B) Phase contrast imaging of NT and p21KD6 cells treated as in (A). Bar, 100 µm (left panel) and 50 µm (right panel). (C) Mean cell area measure of NT and p21KD6 cells treated as in (A) (NT+siCT, n = 75; NT+siPKCµ, n = 75; p21KD6+siCT, n = 75). (D) Stress fiber quantification in NT and p21KD6 cells treated as in (H) (NT+siCT, n = 15; NT+siPKCµ, n = 15; p21KD6+siCT, n = 15). (E) Mean focal adhesion (FA) count (#) and mean focal adhesion area in NT and p21KD6 cells treated as in (A) (NT+siCT, 14 cells, 695 focal adhesions; NT+siPKCµ, 14 cells, 404 focal adhesions; p21KD6+siCT, 14 cells, 277 focal adhesions). Ku80 expression, loading control; molecular mass (kDa). Error bar, SEM. **, P < 0.005; ***, P < 0.001, ns, non significant (*t* test).

Fig. S4. Depletion of SSH1L restores phosphorylation of cofilin in p21-depleted cells. (A) Western blot analysis of SSH1L, pS744/7448 PKCµ, pY397 FAK, total FAK, pS3 cofilin in whole lysates from NT hTMECs 72 h transfected with control siRNA pool (siCT) and p21KD6 GP-hMECs transfected with control siRNA pool or SSH1L-targeted siRNA pool (siSSH1L). (B) Mean focal adhesion (FA) count

(#) and mean focal adhesion area in NT cells 72 h transfected with control siRNA pool (10 cells, 520 focal adhesions) and p21KD6 cells transfected with control siRNA pool (10 cells, 251 focal adhesions) or SSH1L-targeted siRNA pool (10 cells, 106 focal adhesions). (C) Phase contrast imaging of NT and p21KD6 hTMECs treated as in (A). Black and white arrows indicate respectively individual and grouped siSSH1L-transfected cells with altered morphology. Bar, 100 μm. (D) F-actin staining in NT and p21KD6 hTMECs treated as in (A). Bar, 20 μm. Ku80 expression, loading control; molecular mass (kDa). ***, $P < 0.001$, ns, non significant (*t* test).

Movie 1. Time-lapse imaging of cell spreading in control and p21KD hTMECs. Phase contrast images were acquired at 5 min interval. Starting point corresponds to 25 min post-trypsinization. Total time is 24 h; movie plays at 13 frames per second. Bar, 20 μm.

Movie 2. Time-lapse imaging of 2D isolated migration in control and p21KD hTMECs. Phase contrast images were acquired at 5 min interval. Tracks represent path of NT (green) and p21KD (red) cell. Total time is 24 h; movie plays at 13 frames per second. Bar, 20 μm.

Movie 3. Time-lapse imaging of focal adhesions in control and p21KD hTMECs. GFP-paxillin images were acquired at 40 s interval. Total time is 14 min and 40 s and movie plays at 13 frames per second. Bar, 10 μm.

Movie 4. Time-lapse imaging of protrusion dynamics in control and p21KD hTMECs. Phase contrast images were acquired at 6 s interval and during 20 min. Movie plays at 65 frames per second. Bar, 20 μm.

Movie 5. Time-lapse imaging of lamella microtubules in control and p21KD hTMECs. GFP-α-tubulin images were acquired at 3.5 s interval. Total time is 5 min and 29 s; movie plays at 13 frames per second. Bar, 5 μm.

Bouchet *et al.* Figure 1

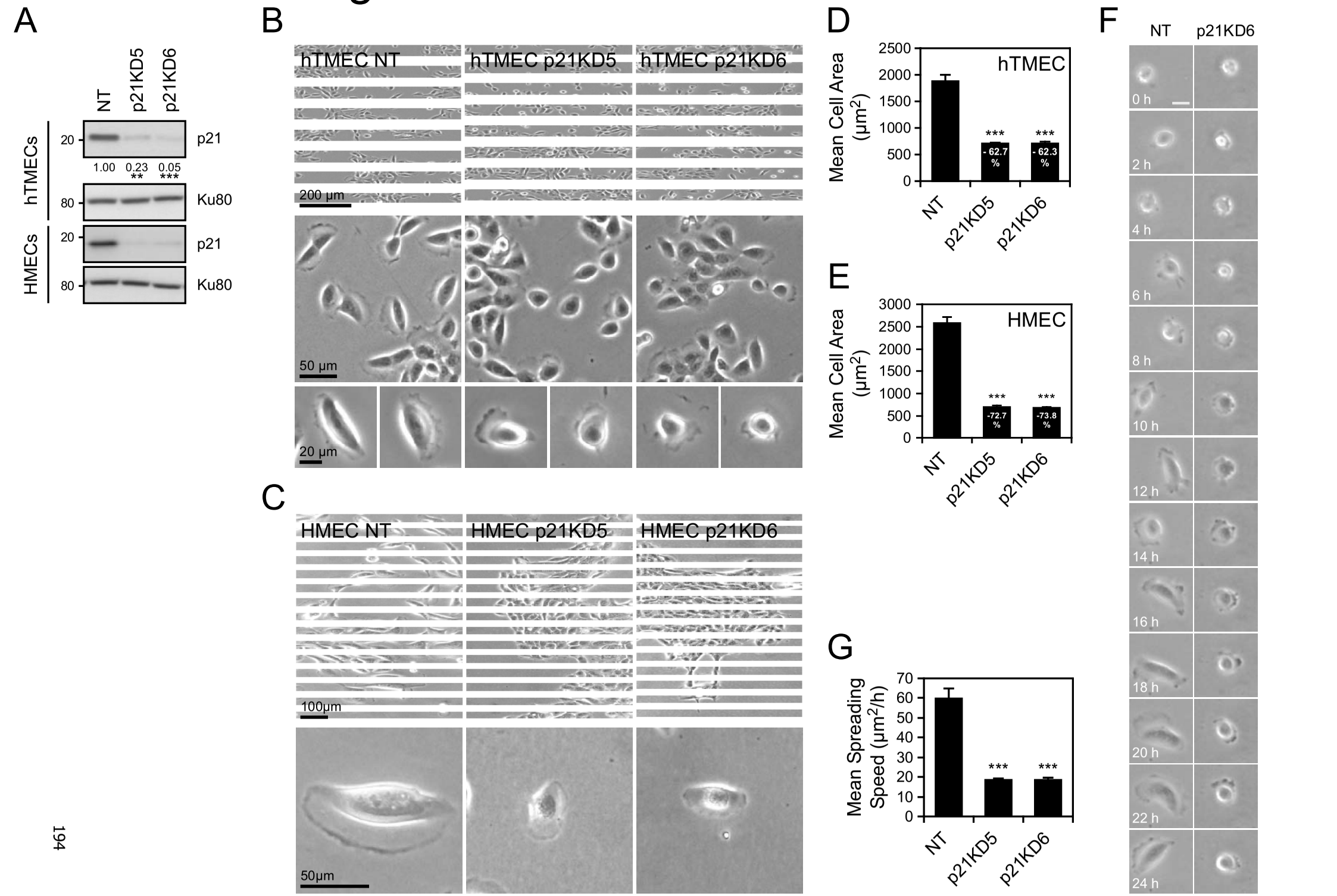

Bouchet *et al.* Figure 2

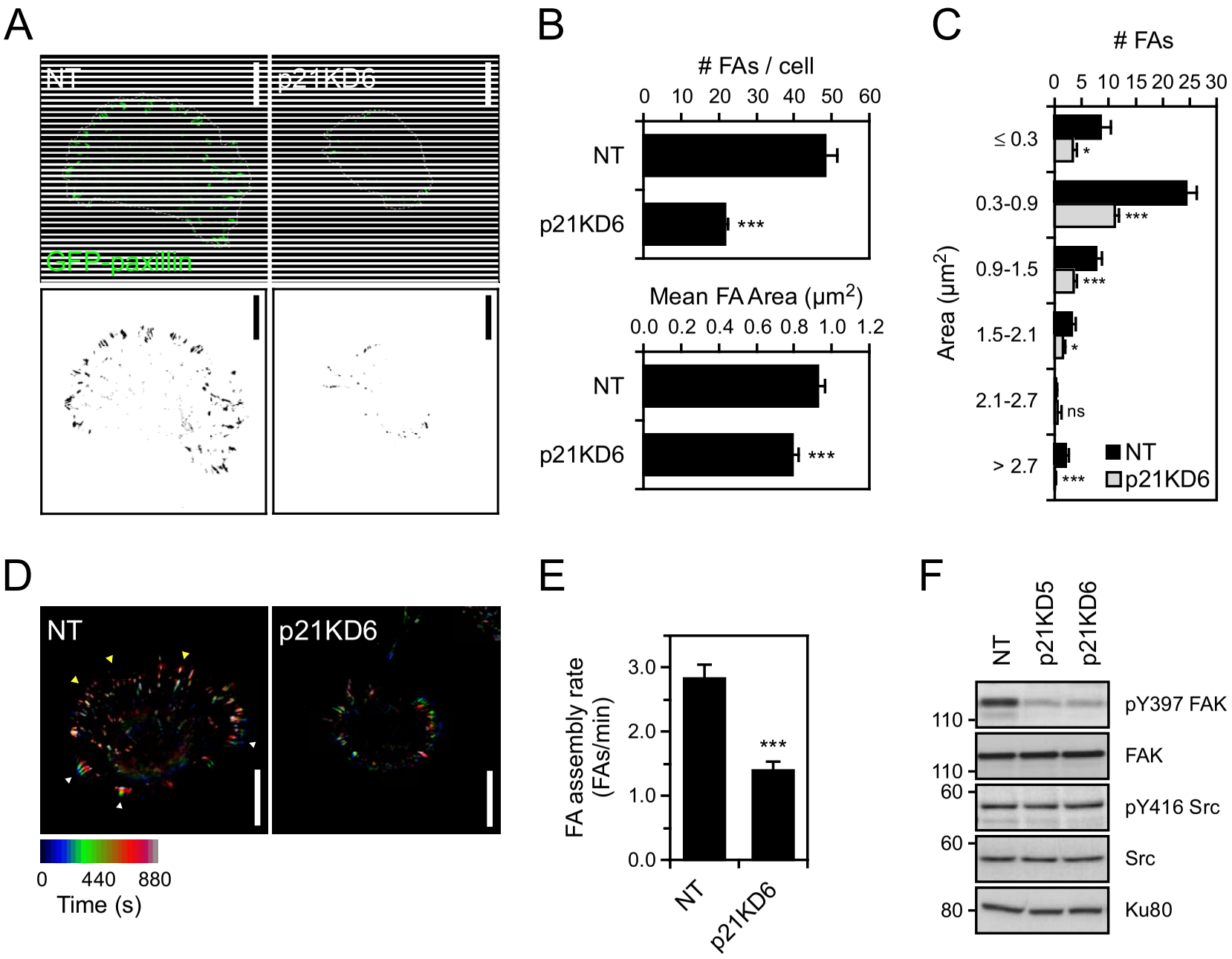

Bouchet *et al.* Figure 3

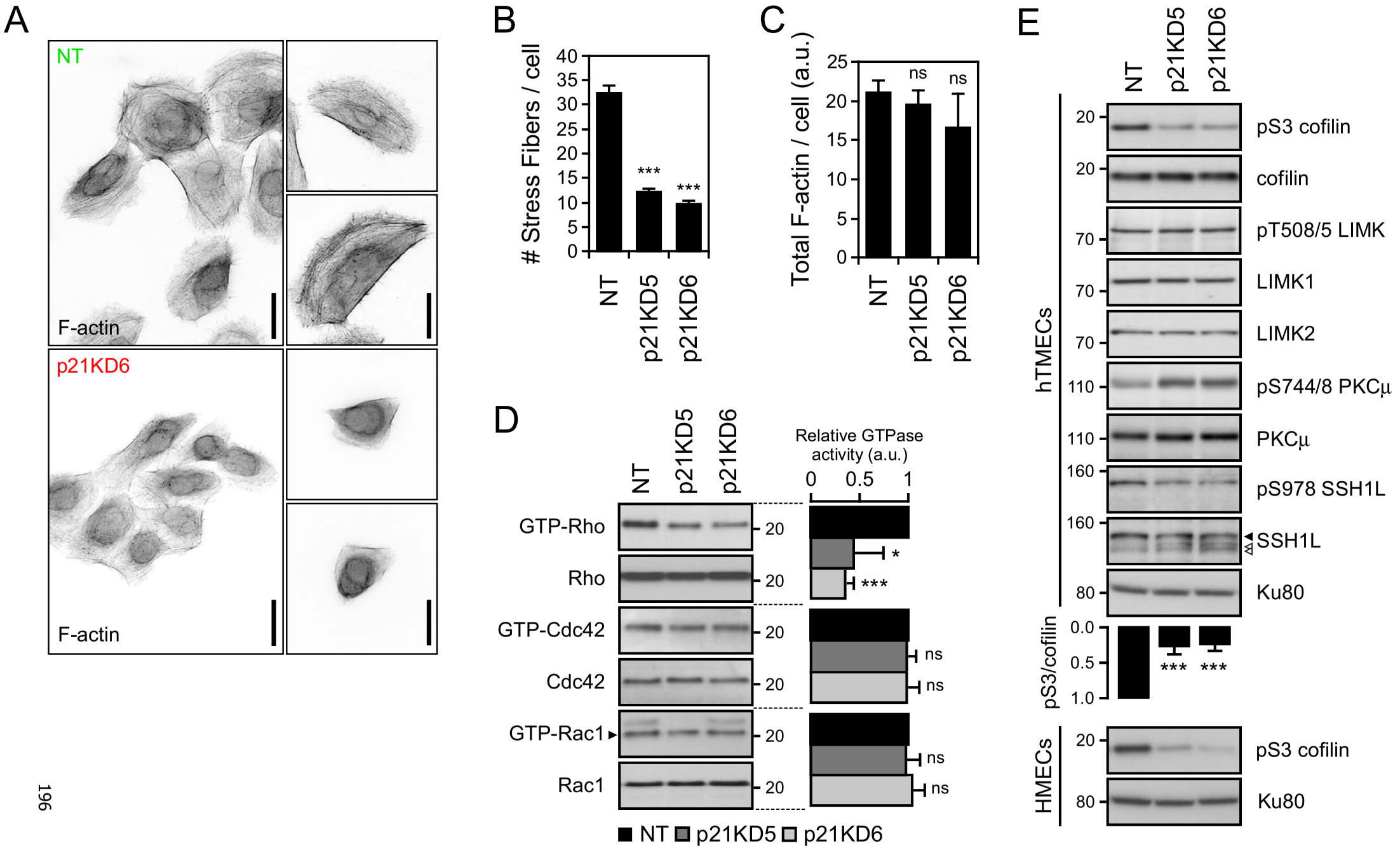

Bouchet *et al.* Figure 4

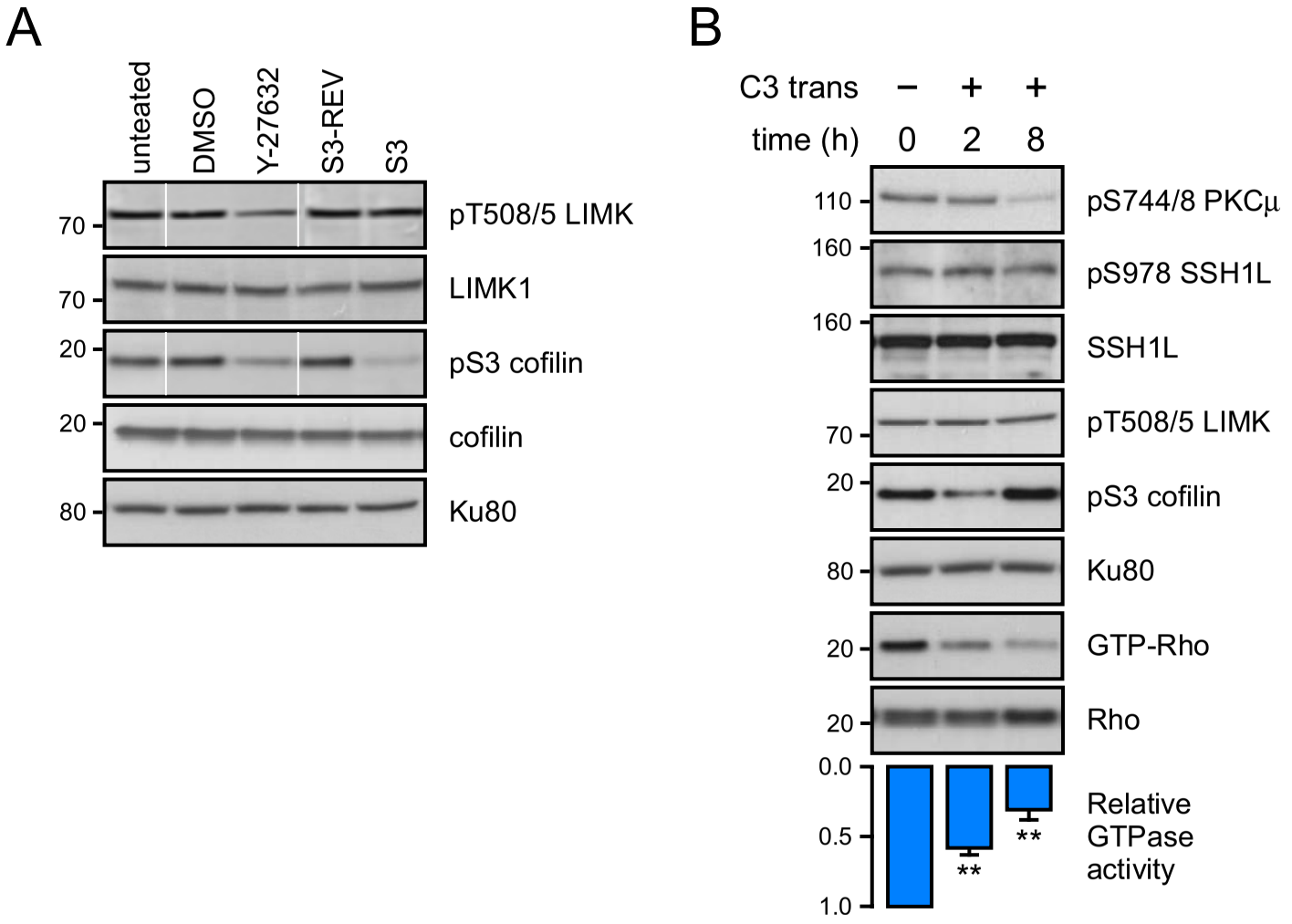

Bouchet *et al.* Figure 5

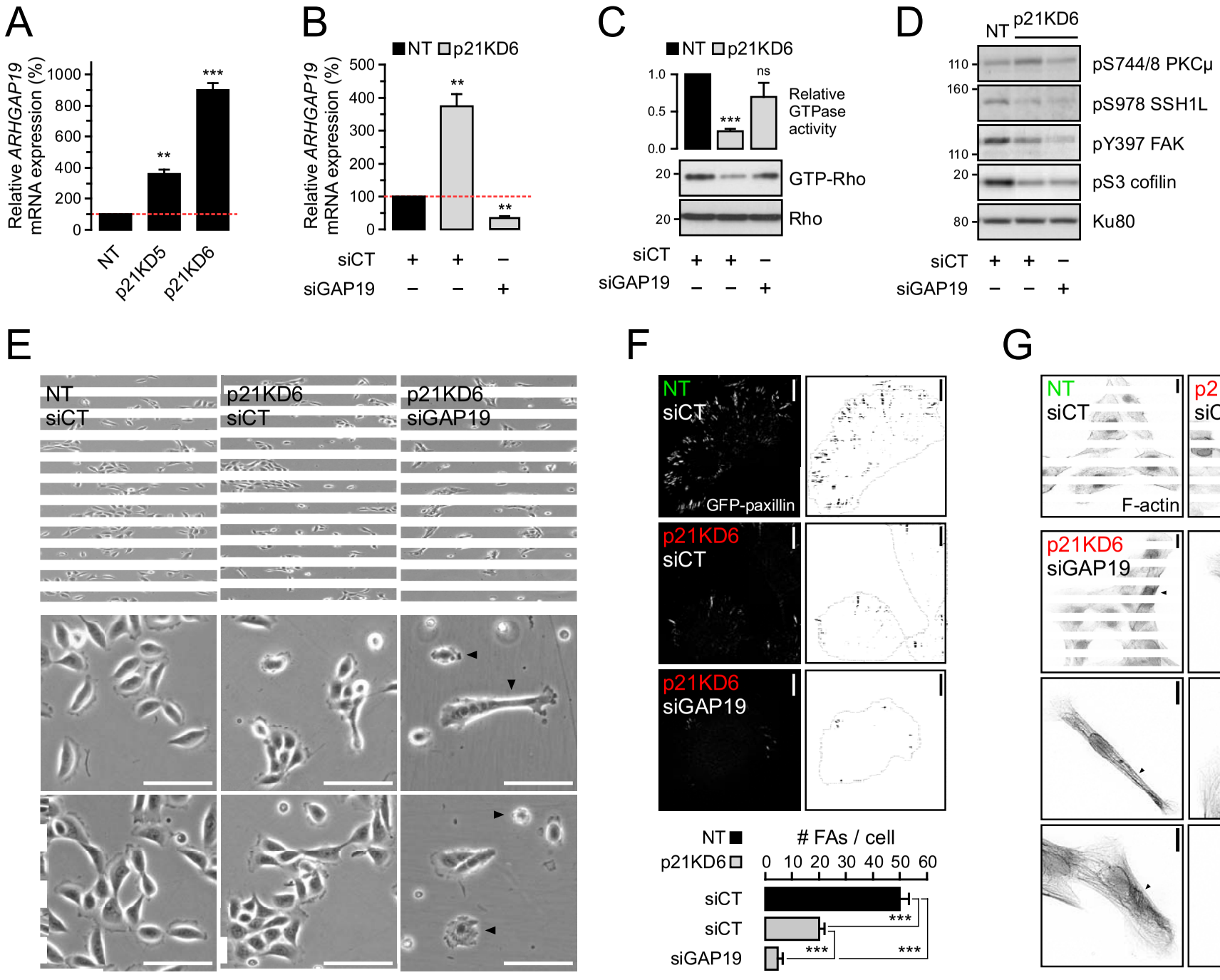

Bouchet *et al.* Figure 6

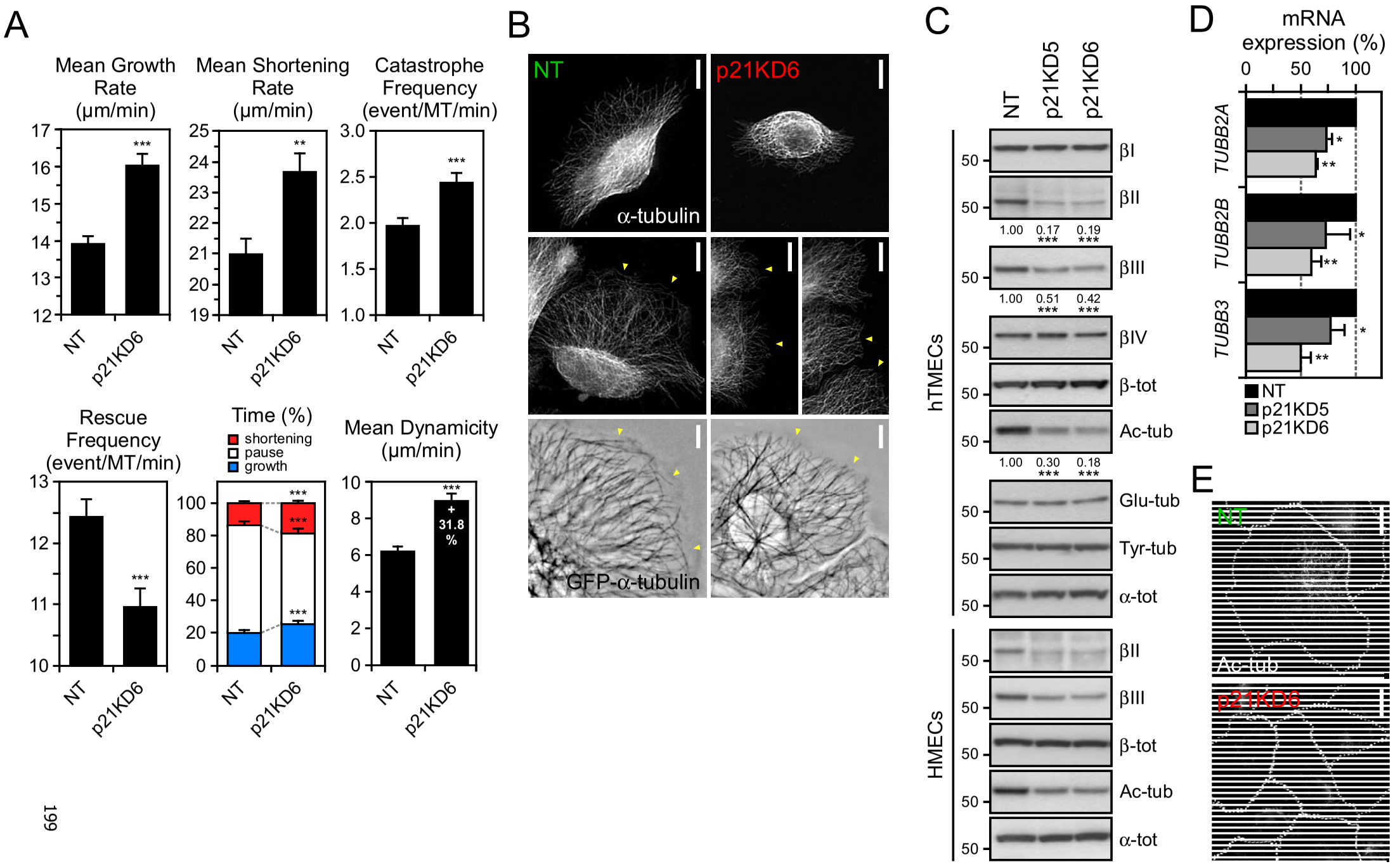

Bouchet *et al.* Figure 7

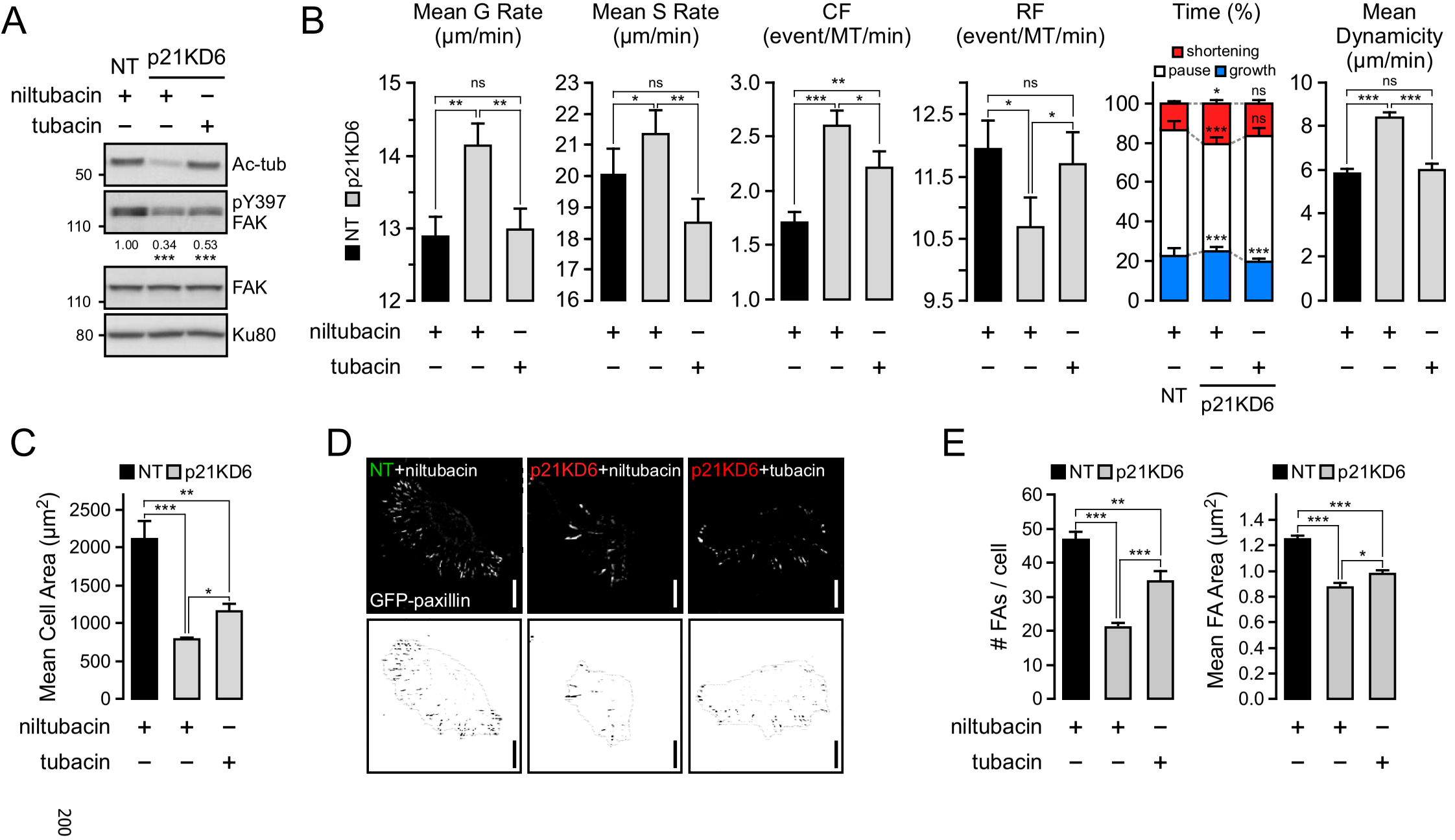

Bouchet *et al.* Figure S1

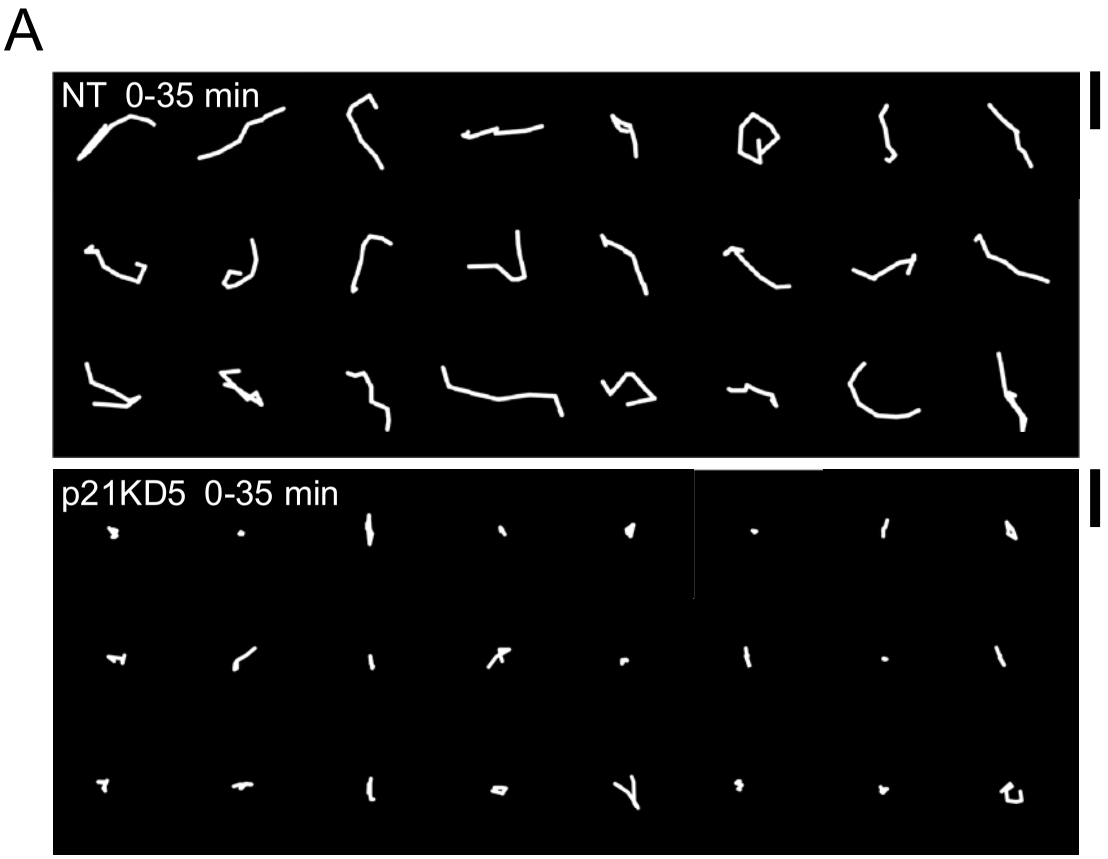

Bouchet *et al.* Figure S2

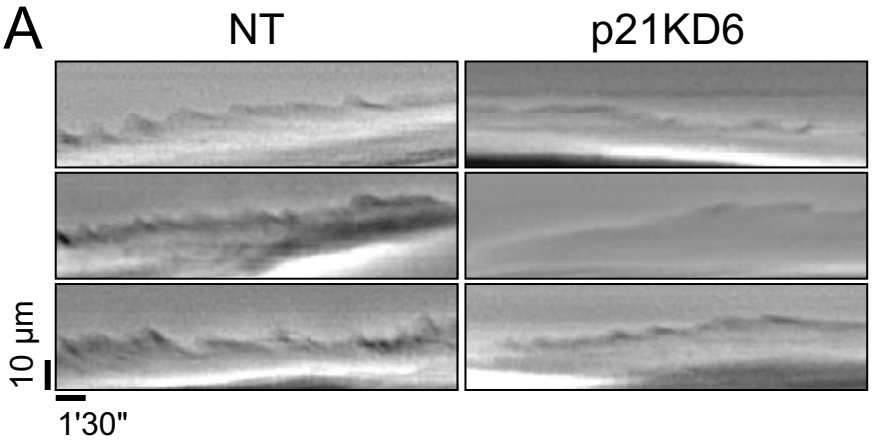

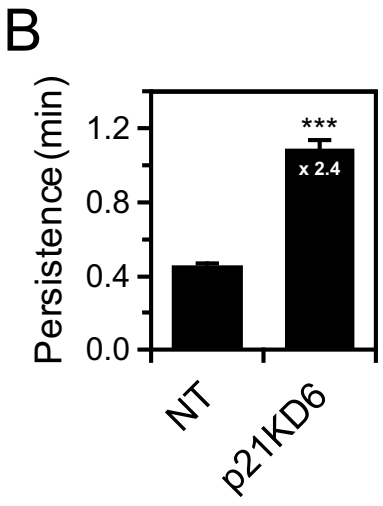

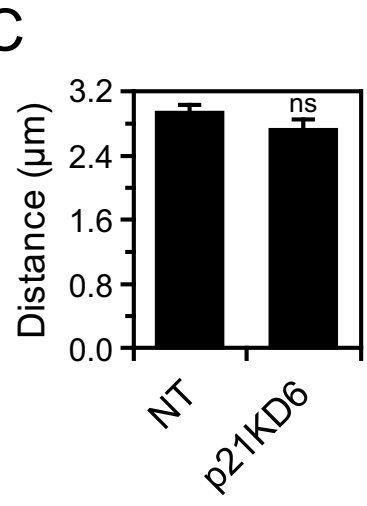

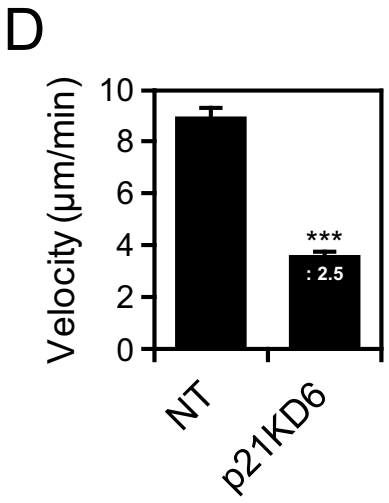

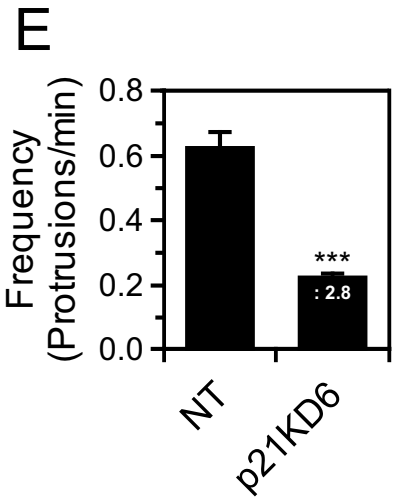

Bouchet *et al.* Figure S3

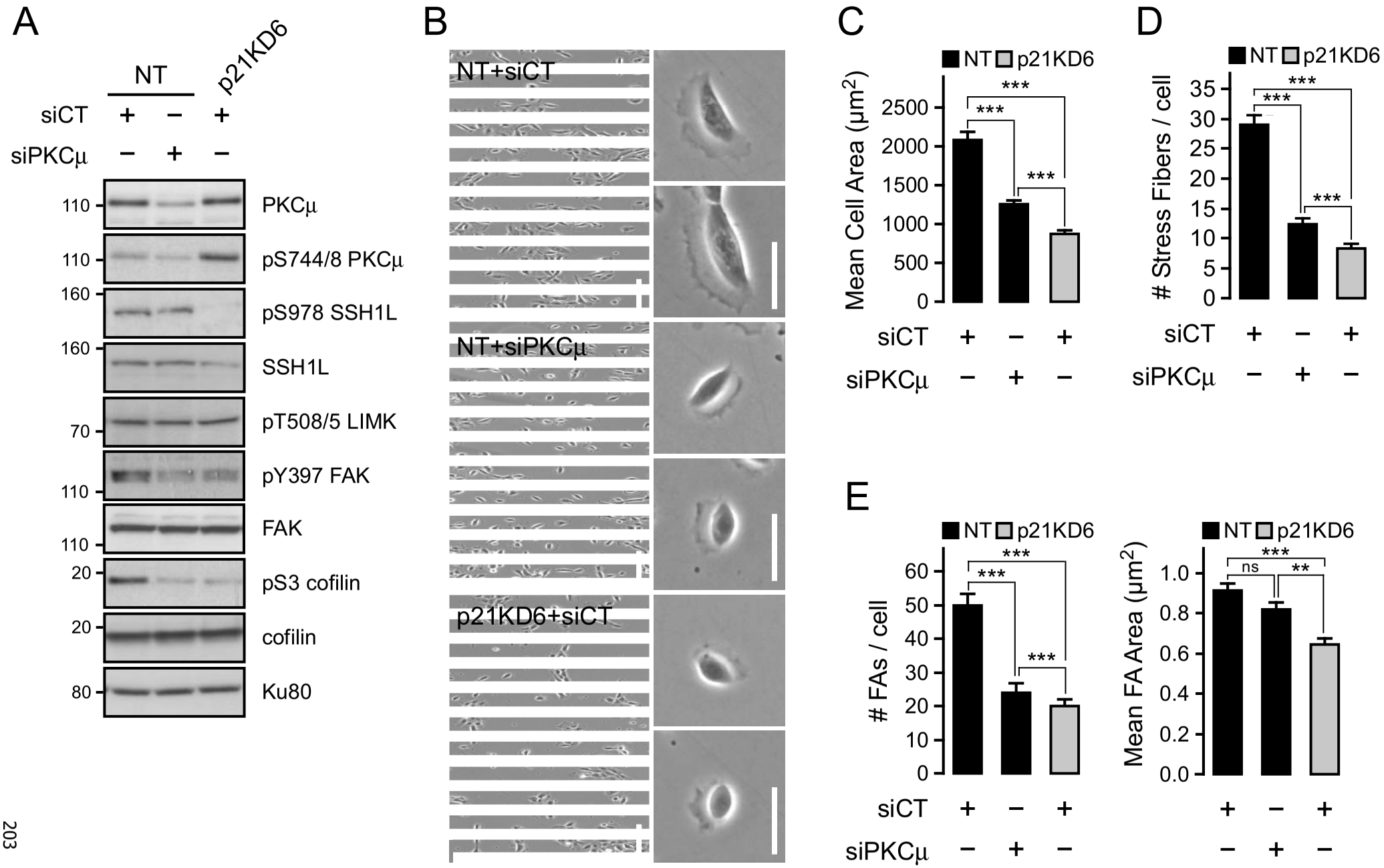

Bouchet *et al.* Figure S4

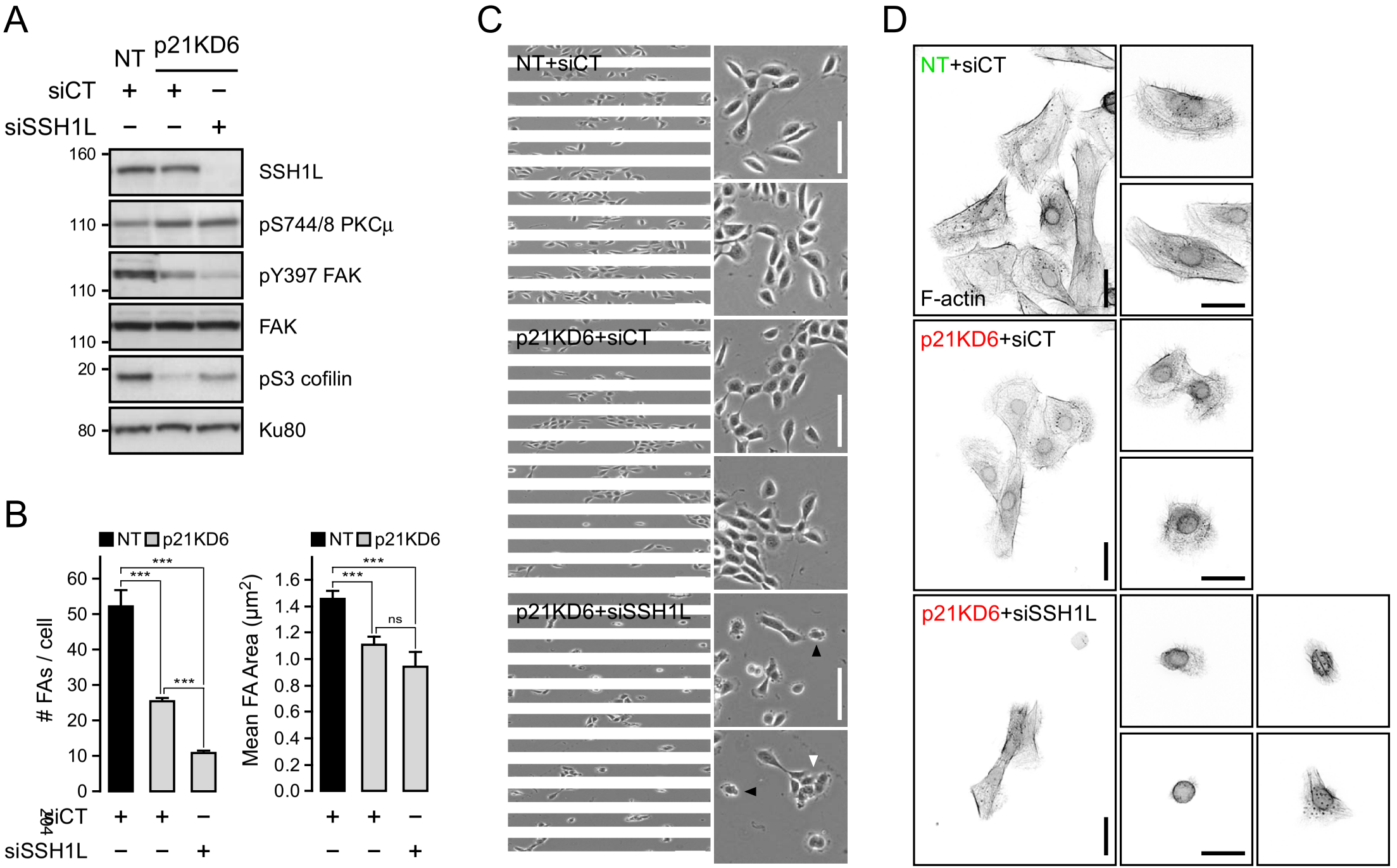

H) ANNEXES

H.1) ANNEXE 1 : MANUSCRIT 2

Promotion of genomic instability by paclitaxel initiates low-efficiency malignant transformation in human mammary epithelial cells

Benjamin Pierre Bouchet[1,2], Béatrice Orsetti[3], Nicole Falette[4], Carole Audoynaud[4], Jacques Bertholon[1,2], Christelle Lamblot[4], Charles Theillet[3], Alain Puisieux[1,2,4] and Carlos María Galmarini[1,3,*]

1 Université Lyon 1, ISPB, Lyon, F-69003, France; Université Lyon 1;IFR62, Lyon, F-69008, France

2 INSERM, U590, Lyon, F-69008, France

3 IRCM, Institut de Recherche en Cancérologie de Montpellier, Montpellier, F-34298, France; INSERM, U896, Montpellier, F-34298, France; Université Montpellier1, Montpellier, F-34298, France ; CRLC Val d'Aurelle Paul Lamarque, Montpellier, F-34298, France

4 Centre LEON BERARD, Unité d'Oncologie Moléculaire, Lyon, F-69373, France

5 Université Lyon 1, UFR de Médecine Lyon-Sud, Oullins, F-69921 France; IFR128, Lyon, F-69365, France; ENS-CNRS, UMR 5239, Oullins, F-69921 France

* C.M. Galmarini current address is PharmaMar, S.A., Colmenar Viejo (Madrid), E-28770 Spain

Correspondence to B. P. Bouchet: bouchetb@lyon.fnclcc.fr; or A. Puisieux : puisieux@lyon.fnclcc

INTRODUCTION

Identification of the driving force of carcinogenesis in humans remains the most controversial issue in cancer research. At one extreme, some investigators have argued that a limited set of genetic alterations suffices to induce human cell transformation and that widespread genomic changes are not required for this process (Elenbaas et al., 2001;Zimonjic et al., 2001). Others have claimed that mutations in critical genes give rise to a mutator phenotype that originates the transformation by favoring mutations of tumor suppressor genes and oncogenes (Loeb et al., 2003;Bielas et al., 2006).

According to this hypothesis, a mutator phenotype can be caused by rare stochastic events involving DNA damage, but can also arise from aberrant gene expression or DNA methylation (Laird and Jaenisch, 1996;Perou et al., 2000;Loeb et al., 2003).

On the other hand, numerous works have suggested that chromosomal instability could be a crucial tumor-initiating process (Ried et al., 1996;Ried et al., 1999;Hollander et al., 1999;Jallepalli et al., 2001;Upender et al., 2004;Weaver et al., 2007). More specifically, it was emphasized that aneuploidy could drive the genomic instability observed in nearly all tumor types by unbalancing expression of thousands genes and consequently triggering autocatalytic genome variation (Upender et al., 2004;Duesberg and Li, 2003). Moreover, many works have described a strong association between genomic instability and acquisition of drug resistance in cancer cells(Roberts et al., 1990;Finette et al., 2000;Kerbel, 1991;Duesberg et al., 2001;Edwards et al., 2003;Snijders et al., 2003;Li et al., 2005).

Currently, whether a limited set of genetic alterations suffices by itself to give rise to a complete malignant transformation in human mammary epithelial cells is still under debate (Zimonjic et al., 2001;Li et al., 2002). We have previously established sub-cell lines (HME1 paclitaxel-surviving populations; PSPs) from the untransformed human mammary epithelial cell line HME1 transiently treated by low-dose paclitaxel (Galmarini et al., 2006). PSPs were found to exhibit an aneuploidy-prone phenotype characterized by a resistance to paclitaxel-induced apoptosis associated with an increased susceptibility to chromosome missegregation (Galmarini et al., 2006;Bouchet et al., 2007). In the present study, we aimed to determine whether genomic instability promoted by low-dose paclitaxel is sufficient to drive malignant transformation in immortalized human mammary epithelial cells. For this purpose, we evaluated genomic instability, multidrug resistance, three-dimensional epithelial organization and spontaneous in vitro transformation in PSPs compared with HME1 and its control clones (CCs). Our results strongly suggest that genomic instability is a low-efficiency but sufficient promoter of in vitro transformation in human mammary epithelial cells.

MATERIAL AND METHODS

Cell culture and reagents

HME1 paclitaxel-surviving populations (PSPs) and control clones (CCs) were established as previously described (Bouchet et al., 2007). HME1 cells and HME1-derived sublines were cultured in

DMEM/Ham's medium supplemented with 0.5 μg/ml hydrocortisone, 10 ng/ml hEGF, 5 μg/ml insulin, 50 μg/ml gentamicin and 10% FBS. Drugs used for the experiments were paclitaxel (Bristol-Myers Squibb, Paris, France), vinorelbine (Pierre Fabre, Castres, France), doxorubicin (Pharmacia, St Quentin, France), vinblastine and gemcitabine (Lilly Laboratories, Saint Cloud, France). Propidium iodide, 3-[4,5-dimethylthiazol-2-yl]-2,5-diphenyl-tetrazolium bromide (MTT) and Hoescht 33258 were purchased from Sigma (St. Quentin Fallavier, France). Matrigel was obtained from Becton Dickinson (USA).

Growth inhibition assay and drug resistance evaluation

Short-term growth inhibition experiments were performed by MTT assays in the presence of paclitaxel, vinblastine, vinorelbine, doxorubicin and gemcitabine as previously described (Galmarini et al., 2001). Mean IC50 values were obtained from resulting dose response curves and calculated as means of three separate experiments, each of which were performed in triplicate. Fold-resistance was determined by calculating the ratio of drugs IC50 in each subline relative to IC50 obtained in HME1 line. Sublines displaying a >2-fold ratio were considered as stably resistant.

Three-dimensional culture of HME1 cells, CCs and PSPs on reconstituted basement membrane

For the establishment of three-dimensional cultures, cells were seeded in precoated glass chamber slides as described previously (Debnath et al., 2003). Briefly, eight-well glass chamber slides were coated with 40 µl.well-1.matrigel. Cell suspension mixed with an equal volume of assay medium containing 4% (v/v) matrigel was then added to the 8-wells chamber slides to yield 5.10^3 cells.well^{-1}. Medium was replaced every 4 days. At day 20, acini were fixed with 4% paraformaldehyde for 10 min at room temperature. Cells were stained with 2 μg.ml^{-1} Hoechst 33258 for 5 min, and an excess of 20 μg.ml^{-1} propidium iodide for 10 minutes to unspecifically stain cytoplasm and allow visualization of cell shape. Pictures of acini were acquired on a confocal laser scanning TCS SP2 microscope (Leica, Le Pecq, France) with a X63 oil-immersion objective. For each field analyzed, final imaging was performed by using ImageJ software and processed as a maximum intensity projection of z-stack of confocal images (interval, 0.7-0.9 μm).

Anchorage-independent growth assay

HME1 cells, CCs and PSPs (2.104 cells.ml^{-1}) were plated in 0.45% low-melting point agarose/growth medium onto 6-well plates with 0.75% agarose underlay. Fresh culture medium (0.5 ml) was added after 1.5 weeks. Colonies were scored after 50 days. Assays were performed in triplicate.

In vivo tumorigenicity assay

Female athymic swiss nude mice (aged 4 weeks at arrival) were from IFFA-CREDO (L'Arbresle, France). Animals were housed in appropriate plastic cages and kept with conventional laboratory-specific animal husbandry procedures. The mice were inspected daily for evaluation of clinical condition while monitoring changes in animal weight twice a week. Animals were euthanized to avoid animal discomfort if clinical conditions may anticipate the potential for animal suffering.

Nude mice were irradiated (400 rad) 4 h prior to injection. Then, HME1, CC1, CC2, CC10 and all PSPs were inoculated subcutaneously at a concentration of 1.107 cells in 0.3 ml (mix of 150 µl of culture media and 150 µl of matrigel). Four mice for each cell line were injected. As positive control, human MCF-7 cells were also injected at the same concentration in two mice. Mice were sacrificed when the tumors reached a diameter of 0.5 cm3 or after 12 months of monitoring.

Metaphase comparative genomic hybridization (mCGH)

DNA was extracted from the HME1, CC and PRC cells using the WizardTM Genomic DNA extraction kit (Promega UK Ltd). Hybridizations were done on Vysis (Downers Grove, IL) normal human metaphases. Genomic DNA labeling and CGH reaction were performed as previously described (Courjal and Theillet, 1997). CGH images were captured on a Zeiss (Le Pecq, France) epifluorescence microscope equipped with a JAI (Glostrup, Denmark) charge-coupled device camera run by Metasystems (Altlussheim, Germany) image analysis software. CGH analysis was done using ISIS 4.4 software (Metasystems).

Array comparative genomic hybridization (aCGH)

We used human Integrachip V2 to establish genomic profiles (IntegraGen SA, Evry, France, http://www.integragen.com). IntegraChip V2 is composed of 3172 bacterial artificial chromosome (BAC) clones including 2862 sequenced clones with a median gap of 1 clone/0.8 Mb. DNA labeling and hybridization, were done as previously described (Orsetti et al., 2006). Arrays were scanned using Axon 4000B scanner (Molecular Devices, CA, USA) and images were analyzed using Genepix 6.0. Extracted values were then normalized, filtered and graphically represented using CAPweb 2.0 (Institut Curie, Paris, France) (http://bioinfo-out.curie.fr/CAPweb). Clones with missing values in over 50% of the samples were discarded. Gains and losses were calculated using CAPweb default parameters (log 2 ratio≤-0.153; log 2 ratio≥0.138). The number of genomic transition sites was determined by the use of the GLAD algorithm (CAPweb 2.0). This number is correlated to the number of regions altered and genomic rearrangements.

Statistical analysis

For each treatment group, the mean and standard deviation was calculated. The differences between groups were tested by the Mann-Whitney U non-parametric test using the statistical package SPSS V10™. The level of significance used in all the analyses was $P<0.05$.

RESULTS

Transient low-dose paclitaxel exposure promotes viable genomic instability in untransformed human mammary epithelial cells

Genomic profiles of the untransformed HME1 line, three representative HME1 control clones (CC1, CC2 and CC10) and all PSPs were analyzed by mCGH. Our analysis confirmed the near-diploid status of HME1 line, with no alteration detected excepting the previously described gain of chromosome 20 (Table 1) (Troester et al., 2004). This genomic gain was consistently observed in all sublines derived from HME1 (Table 1). CC1 and CC2 showed null or very low genomic instability when compared with HME1 (Table I). Of note, CC10 displayed a moderate genomic instability consisting in gains of chromosomes 16p, 19 and 22. In contrast, PSPs presented a wide spectrum of genomic alterations, notably characterized by genomic gains in 85.0% of these HME1-derived sublines (17/20) (Table 1). The highest level of genomic instability was observed in PSP1 and PSP4 (Table 1). These data indicate

that low-dose paclitaxel treatment selectively favors the emergence of viable genomic instability in untransformed human mammary epithelial cells.

Paclitaxel-promoted genomic instability in human mammary epithelial cells is associated with acquisition of multidrug resistance

As a feature of malignant transformation, multidrug resistance was assayed in PSPs compared with HME1 and CCs (Figure 1). We have previously reported that PSPs were globally more resistant to paclitaxel (IC50 for PSPs: 6.5 ± 3.3 nM) than HME1 line (IC50: 3.9 ± 2.5 nM; P=0.02) (Galmarini et al., 2006). A detailed analysis established that PSP1, PSP4, PSP16, PSP21 and PSP43 were stably resistant to paclitaxel. The present analysis showed a significant stable resistance to vinblastine in PSP4, PSP7 and PSP43 (Figure 1). Significant stable resistance was also observed for vinorelbine in PSP1, PSP4 and PSP32 (Figure 1). Similar results were obtained for doxorubicin sensitivity in PSP1, PSP2, PSP3, PSP4, PSP7, PSP9, PSP19, PSP21 and PSP45 compared with HME1 cells (Figure 1). Significant stable resistance to gemcitabine was observed in PSP2 and PSP3 (Figure 1). Of note, CC10 was found to be stably resistant to vinblastine and doxorubicin when compared with HME1 line (Figure 1). Interestingly, the two PSPs that showed most genomic instability, namely PSP1 and PSP4, were highly resistant to paclitaxel and vinorelbine, and to vinblastine and vinorelbine respectively (Table 1, Figure 1). Furthermore, analysis showed that genomic gains were present in 100.0%, 66.7%, 100.0%, 77.8% and 50.0% of PSPs stably resistant to paclitaxel, vinblastine, vinorelbine, gemcitabine and doxorubicin respectively (Table 1, Figure 1).

Paclitaxel-promoted genomic instability in human mammary epithelial cells is associated with aberrant three-dimensional organization

In order to further identify features of malignant epithelial transformation in PSPs, we performed three-dimensional (3D) cultures of these sublines, as well as HME1 cells and CCs, on reconstituted basement membrane (Bissell et al., 1999). After 20 days in 3D culture, single HME1 cells seeded on basement membrane gel formed acinar structures with a hollow lumen, related to normal mammary epithelial organization (Table 1, Figure 2A). Similar patterns of growth in 3D culture were observed for CC1, CC2 and CC10, and for PSP4, PSP9, PSP16, PSP19, PSP32, PSP37 and PSP45 (Table 1). In

contrast, despite a duct-like 3D pattern, 65% of PSPs (13/20) showed a tubular network that was multicellular and devoid of hollow lumen (Table 1, Figure 2B).

Spontaneous *in vitro* transformation of continuous cultures and subclones of genomically unstable human mammary epithelial cells

We firstly submitted HME1 line, PSPs and CCs to anchorage-independent assay. No growth was observed in any plate after 50 days of culture (Table 1). As it was previously shown that hyperplasia or full in vivo tumorigenesis can arise from in vitro untransformed cells, we further investigated the in vivo tumorigenicity of PSPs in immunodeficient mice (Bronson et al., 1997;Shannon et al., 2005). All injected cell lines failed to initiate tumorigenesis in vivo (Table 1). We then decided to investigate if malignant transformation could arise from PSPs in culture conditions that allow spontaneous evolution of genomic instability and identification of resulting phenotypes. For this purpose, continuous culture and limiting dilution subcloning were applied to representative PSPs whose CGH profile showed low (PSP7), moderate (PSP16, PSP45), or pronounced genomic instability (PSP1,PSP4) (Table 1).

We thus cultured PSP1, PSP4, PSP7, PSP16, PSP45, CC2 and HME1 line for 10 population doubling (PD10), and assessed their ability to grow in soft agar (Table 2). Consequently, we found that, in contrast with the early PSP45, PSP45-PD10 subline was able to form colonies in soft agar (Table 2, Fig 3A, B). No colony was found in other PSP-PD10s and PD10 controls. Since chemoresistance is a feature of malignant cells, sensitivity of PSP45-PD10 to paclitaxel was assessed. The paclitaxel IC50 in PSP45-PD10 was 7.3 ± 6.2 nM (Table 2). Although this value corresponds to a 1.7-fold increase of PSP45 paclitaxel IC50 it was not considered as a stable resistance when compared with HME1 cells. Moreover, unlike the early PSP45, when cultured in 3D, PSP45-PD10 organized into a multicellular duct-like pattern that did not show hollow lumen (Figure 3E). Of note, PSP45-PD10 failed to promote tumor formation in vivo.

Further, PSP1, PSP4, PSP7, PSP16, PSP45, and CC2, were submitted to limiting dilution subcloning. Ten subclones (PSP-S) were collected from each PSP, and analyzed for 3D culture patterning and anchorage-independent growth. We then found that PSP4-S2 was able to grow in soft agar, as shown in Figure 3C. However, PSP4-S2 did not form gross individual colonies, but rather small and dispersed subcolonies producing a pseudo-monolayer (Figure 3C, D). No colony was found in other tested PSP

subclones. The paclitaxel IC50 in PSP4-S2 was over 1 μM. Thus, PSP4-S2 displayed a more than 100-fold increase of paclitaxel resistance relatively to its precursor PSP4. Additionally, when culture in 3D, and unlike its precursor, PSP4-S2 organized into a multicellular duct-like pattern that did not show hollow lumen (Figure 3F). Nevertheless, PSP4-S2 failed to promote tumor formation in vivo.

Spontaneous *in vitro* transformation of human mammary epithelial cells is associated with evolving genomic instability

In order to evaluate the status of genomic instability associated with transformation in PSP45 and PSP4, we compared, by aCGH analysis, the pangenomic profiles of PSP45-PD10 and PSP4-S2 with their respective precursors (Figure 4, Supplementary Tables 1-4). As demonstrated by the detection of genomic alterations in PSP4 (34 regions altered) and PSP45 (19 regions altered), our aCGH results were found to be in good agreement with the previous mCGH data (Table 1, Supplementary Tables 1 and 2). Moreover, the number of genomic transition sites were 57 for PSP45, 41 for PSP45-PD10, 56 for PSP4 and 88 for PSP4-S2 indicating a significant difference between PSP4 and PSP4-S2 (P=0.008947).

We further wanted to highlight genomic differences in the couples PSP45/PSP45-PD10 and PSP4 /PSP4-S2. PSP45 and PSP45-PD10 presented 15 common and 8 divergent alteration-containing regions localised on chromosomes 5, 16, 17, 18 and 19 and 20 (Table 3). Alterations in regions on 16p, 17q12, 18p11 and 18q11 were present in PSP45 but not in PSP45-PD10 while a new region on 19q12-q13, an enlarged region on 5q and an increased the level of gain on 20q were specifically seen in PSP45-PD10. PSP4 and PSP4-S2 presented 29 common regions of alteration and 29 different regions present on chromosomes 2, 3, 4, 5, 8p, 10, 12, 13q, 15q, 16, 17p, 18, 19, 21, 22q (Table 4).. Alterations in 2p, 2q11-q23, 3, 5q, 8p12, 12, 15q, 16p, 18p and 22q were observed only in PSP4 while alterations in 2q32-q34, 4, 5p, 10p, 12q13-q15, 13q11-q34, 16, 17p11-p12, 19 and 21 were specifically observed in PSP4-S2. It is of note that alterations on chromosomes 3q26, 6p21, 9q13, 10p12, and 20 are shared by the four samples. Interestingly regions of alteration on chromosome 5q22, 5q23-q33, 16p11-q12, 17q12, 18p11-q11, Xq27 are shared specifically by the two clones PSP4 and PSP45 but were absent of PSP45-PD10 and PSP4-S2 clones. Lastly, PSP45-PD10 and PSP4-S2 did not share any common region of alteration excepting gains and losses common to the four clones.

DISCUSSION

We have previously described the establishment of sub-cell lines (Paclitaxel-Surviving Populations; PSPs) issued from an untransformed human mammary epithelial cell line, HME1, transiently exposed to 10 pM of paclitaxel (Bouchet et al., 2006). Moreover, we recently demonstrated that PSPs were characterized by an aneuploidy-prone phenotype (Bouchet et al., 2007). In the present study, we aimed to investigate genomic instability, multidrug resistance and tumorigenicity in these sublines. Our data showed that the majority of these sublines present higher rates of genomic instability than the original HME1 line and its control clones (CCs). This predominant characteristic in PSPs was found to be associated with aberrant 3D mammary epithelial organization, resistance to paclitaxel, vinblastine, vinorelbine, doxorubicin or gemcitabine, and, in some case, cross-resistance. Further experiments indicated that spontaneous phenotype evolution of these sublines could lead to malignant transformation associated with evolving genomic instability and chemoresistance.

Here we show, by genomic profiling, that viable genomic instability in untransformed human mammary epithelial cells segregates with resistance to transient low-dose paclitaxel treatment. Paclitaxel was shown to be a potent inhibitor of microtubule dynamics, thus modifying functions related to spindle checkpoint (Jordan and Wilson, 2004). Moreover, it was established that conditions that degenerate spindle checkpoint drive mitotic slippage and aneuploidization under paclitaxel treatment (Rieder and Maiato, 2004;Chabalier et al., 2006;Swanton et al., 2007). Lastly, it was demonstrated that genomic destabilization, especially by aneuploidization, was a common feature of paclitaxel resistance in human cancer cells (Roberts et al., 1990;Chabalier et al., 2006;Swanton et al., 2007). Accordingly, our data suggest that tolerance to genomic instability could turn to a selective advantage in untransformed human mammary epithelial cells under transient low-dose paclitaxel exposure. However, the mechanism that led to selection of sublines harboring genomic instability (i.e. PSPs) from HME1 line under low-dose paclitaxel remains unclear. Notably, it is still unknown whether low-dose paclitaxel induced the genomic instability found in PSPs or whether preexisting unstable and resistant cells were selected during the paclitaxel exposure. Of note, our previous results and recent data suggest that low-dose paclitaxel could promote aberrant mitotic slippage and aneuploidization by inhibiting spindle checkpoint and causing viable chromosome missegregation (Ikui et al.,

2005;Galmarini et al., 2006;Bouchet et al., 2007). The resulting phenotypes could be then predisposed to accumulate genomic aberrations. Current investigations in our laboratory aim to address whether low-dose paclitaxel could inactivate spindle checkpoint in genomically stable and untransformed cells, and efficiently produce sublines with viable genomic instability.

Our data also showed that genomic instability and resistance to low-dose paclitaxel is associated with multidrug resistance appearance in human mammary epithelial cells. This is consistent with the numerous works that have reported association between genomic instability and drug resistance in cancer cells (Roberts et al., 1990;Finette et al., 2000;Kerbel, 1991;Wasenius et al., 1997;Duesberg et al., 2001;Edwards et al., 2003;Snijders et al., 2003). Furthermore, recent data strongly suggested that aneuploidy in human cancer cells could drive a sufficient autocatalytic genome variation to generate drug resistant phenotype (Upender et al., 2004;Li et al., 2005). This idea is strengthened by the fact that PSP4-S2 and PSP45-PD10 showed concomitant genomic variation and increased paclitaxel resistance when compared with their respective precursors. Lastly, the present study indicates that combination of genomic instability and multidrug resistance can emerge in untransformed human mammary epithelial cells under the selective pressure of low-dose paclitaxel.

In addition, our results support the idea that genomic instability is a driving force of malignant transformation. Indeed, the majority of PSPs displayed an association between genomic instability and aberrant 3D culture patterning, a well described tumor-associated property (Petersen et al., 1992). Moreover, we show that genomically unstable sublines issued from a low-dose paclitaxel treated untransformed line can spontaneously acquire an in vitro transformed phenotype. Indeed, PSP45-PD10 and PSP4-S2 showed in vitro transformation characterized by anchorage-independent growth and aberrant 3D organization. Since paclitaxel is a non-mutagenic agent, we assume that initiation of transformation in PSPs is unlikely to have been provoked by a paclitaxel-induced oncogenic mutation. Alternatively, we propose that the viable genomic instability promoted by low-dose paclitaxel could be the essential factor of transformation in PSPs. This would be consistent with numerous data pointing out the crucial role of genomic instability in tumorigenesis (Duesberg et al., 1998;Ried et al., 1999;Jallepalli et al., 2001;Upender et al., 2004;Woo and Poon, 2004;Weaver et al., 2007). Besides, the evolving genomic instability and the delay required for completion of in vitro transformation in PSP45 and PSP4 subcultures argue for an autocatalytic and low-efficiency process. This would also be

in accordance with previous works that have documented the long-latency of aneuploidy-driven tumorigenesis (Xu et al., 1999;Zimonjic et al., 2000;Shima et al., 2007;Weaver et al., 2002;Weaver et al., 2007).

Finally, in vitro transformed sublines, i.e. PSP45-PD10 and PSP4-S2, failed to initiate tumorigenesis in vivo. This result seems to indicate that, despite a clear association with in vitro transformation, the genomic instability in these sublines was not sufficient to generate a fully transformed phenotype. Yet, it also fits with the recent characterization of genome destabilization as a low-efficiency, and both oncogenic and oncosuppressor process (Weaver et al., 2007). Of note, further works should address this issue by quantifying spontaneous full transformation emergence in long-term cultured PSPs versus CCs and HME1 line. As well, we can speculate that additional oncogenic or chemical stresses could help to unveil the tumorigenic potential of genomic instability in PSPs.

In conclusion, the present study demonstrates that transient low-dose paclitaxel exposure is sufficient to promote viable genomic instability in untransformed human mammary epithelial cells. Further, our results strongly suggest that genomic instability, in initially untransformed cells, is a gate to multidrug resistance and malignant transformation. This implies that promotion of viable genomic instability in human non-malignant mammary epithelium by low-dose paclitaxel could sensitize untransformed epithelial cells to de novo tumorigenesis.

Table 1. Genomic profile, three-dimensional growth organization, anchorage-independent assay and *in vivo* tumorigenicity of PSPs compared with HME1 cells and CCs.

	mCGH profile		3D-culture pattern	AIA	*In vivo* tumor formation
	Gains	Losses			
HME1	20		Normal duct-like	-	No
CC1	5p12-13, 20		Normal duct-like	-	No
CC2	20		Normal duct-like	-	No
CC10	20	16p, 19, 22	Normal duct-like	-	No
PSP1	5, 7, 12, 15, 20	8q24.2-qter	Multicellular tubular	-	No
PSP2	20, 9q13	9p12-p13, 9q22-qter	Multicellular tubular	-	No
PSP3	20		Multicellular tubular	-	No
PSP4	1q, 5q31-qter, 6, 12, 16, 17, 18, 20	4	Normal duct-like	-	No
PSP6	20		Multicellular tubular	-	No
PSP7	20		Multicellular tubular	-	No
PSP8	5p, 9q13, 16, 20		Multicellular tubular	-	No
PSP9	5, 9q13, 20		Normal duct-like	-	No
PSP16	7, 20		Normal duct-like	-	No
PSP19	9q21.1, 20	16p13-pter	Normal duct-like	-	No
PSP20	9q13, 20		Multicellular tubular	-	No
PSP21	1p34-qter, 9q13-q21.1, 20		Multicellular tubular	-	No
PSP22	9q13-q21.1, 20		Multicellular tubular	-	No
PSP25	7q21-q31, 20		Multicellular tubular	-	No
PSP32	9q13, 20		Normal duct-like	-	No
PSP37	9q13, 20		Normal duct-like	-	No
PSP38	9q13, 19, 20		Multicellular tubular	-	No
PSP43	1q21.1, 9q13, 19q13, 20		Multicellular tubular	-	No
PSP45	7, 20		Normal duct-like	-	No
PSP46	9q13, 20		Multicellular tubular	-	No

mCGH, metaphase Comparative Genomic Hybridization; AIA, anchorage-independent assay; 3D-culture pattern, three-dimensional organization of cells growing on reconstituted basement matrix.

Table 2. *In vitro* transformation of PSPs after continuous culture and subcloning.

Precursor line	Subline	Modification of 3D-culture pattern	AIA	*In vivo* tumor formation[a]	Modified mCGH profile[a]	72h paclitaxel IC_{50} (nM)[a]
PSP45	PSP45-PD10	+	+	-	+	7.3 ± 6.2
PSP4	PSP4-S2	+	+	-	+	> 1000

[a] *In vivo* tumorigenicity assay, CGH and evaluation of paclitaxel sensitivity were only performed in sublines that showed features of *in vitro* transformation on the basis of 3D-culture growth and anchorage-independent assay. AIA, anchorage-independent assay; mCGH, metaphase Comparative Genomic Hybridization.

Table 3. Alteration-containing regions in PSP45 and PSP45-PD10 analyzed by aCGH.

Common alteration-containing regions		Divergent alteration-containing regions			
		Gains		Losses	
Gains	Losses	PSP45	PSP45-PD10	PSP45	PSP45-PD10
5q22	3q26.3	17q12	5q21-5q22	16p11.2	
5q23-5q33	5p15.1	18p11.2	5q34-5q35		
6p21.3	6p21.3-6p21.2	18q11.2	19q12-19q13.4		
7p22-7q35	9p13-9q13		20q11.2		
7q35-7q36	Xq27				
10p12					
16p11.2					
20p11.2-20p11.1					
20q11.2					
20q11.2-20q13.2					

Table 4. Alteration-containing regions in PSP4 and PSP4-S2 analyzed by aCGH.

Common alteration-containing regions		Divergent alteration-containing regions			
		Gains		Losses	
Gains	Losses	PSP4	PSP4-S2	PSP4	PSP4-S2
1q21-1q44	3q26.3	3p24	2p24-2p23	16p11.2	2q32.1-2q34
5p15.3-5p15.1	19p13.1-19p12	3q26.3-3q29	2q11.1-2q23		4p16-4q12
5p15.1-5p13		5q33-5q35	12q13-12q15		4q12-4q27
5p13-5q11.1		8p12	16q23		4q27-4q35
6p25-6p21.3		12p11-12q12	17p11-17p12		5p13
6p21.3-6q12		12q21-12q24.1			10p15-10p12
6q12-6q16		15q22			10p12-10q26
6q16-6q27		15q24			13q11-13q34
8q22		18p13.2-18q23			16p11.2-16q12.1
10p12		22q12			16q12.1-16q21
12p13-12p11.2					19p13-19q12
12q12-12q13					21p11.1-21q22
12q13-12q21					21q22
12q24.1-12q24.3					
14q11.2-14q32					
16p13.3-16p13.2					
16p12-16p11.2					
16q22-16q23					
17p12-17q11.1					
17q21-17q25					
18p11.3					
18p11.3-18p11.2					
20p13-20p11.2					
20p11.2-20q11.1					
20q11.2-20q13.3					
Xp22.3-Xq27					
Xq27-Xq28					

Figure Legends

Figure 1. Resistance profile of CCs and PSPs to five chemotherapeutic agents. Fold resistance was determined as the ratio of IC_{50} value for each cell line relative to IC_{50} in HME1 line. IC_{50} values were obtained from dose-response curves assessed by MTT assay and are means of three separate experiments, each of which were performed in triplicate. Green graph bars correspond to CCs values, orange graph bars correspond to PSPs values. Red line indicates the 2-fold resistance ratio (relative to HME1) that was considered as the stable resistance threshold. PSP4 was found to be over 1250-fold resistant to vinblastine relatively to HME1 line; graph scale cut-off was thus arbitrarily placed at 12-fold resistance ratio.

Figure 2. Three-dimensional organization of PSPs on reconstituted basement membrane. Twenty-days 3D culture of PSPs, CCs and HME1 line were fixe d in 4% paraformaldehyde, and stained with Hoechst 33258 and an excess of propidium in order to visualize cytoplasm. Images were acquired on a confocal microscope and are presented as a maximum intensity projection of z-stacks. **A.** Representative acinus of 3D HME1 culture. Cells are organized in a duct-like pattern showing hollow lumen; this structure is related to normal mammary epithelial organization and consistent with the untransformed status of HME1 line. **B.** Representative acinus of 3D PSP1 culture. The acinar structure is multicellular and forms disorganized aggregate without hollow lumen. Scale bar, 50 μm.

Figure 3. Anchorage-independent growth and three-dimensional organization of PSP sublines issued from continuous culture and subcloning. A, C. Anchorage-independent growth of PSP45-PD10 (**A**) and PSP4-S2 (**C**). **B, D.** Representative pictures of soft-agar PSP45-PD10 (**B**) and PSP4-S2 (**D**) colonies at X20 magnification. **E, F.** Representative confocal imaging of PSP45-PD10 (**E**) and PSP4-S2 (**F**) acini on reconstituted basement membrane. Scale bar, 50 μm.

Figure 4. Pangenomic array CGH profiles of PSP45/PSP45-PD10 and PSP4/PSP-S2 clones. Log2 ratios are plotted in Y axis, each clone is positioned along the genome according to human

genome Hg17 release in X axis. Chromosomes are separated by grey vertical lines. CapWeb default threshold parameters were used and gains are shown in red, losses in green and amplification in blue.

References

Bielas JH, Loeb KR, Rubin BP, True LD, Loeb LA (2006) Human cancers express a mutator phenotype. *Proc Natl Acad Sci U S A* **103** (48): 18238-18242

Bissell MJ, Weaver VM, Lelievre SA, Wang F, Petersen OW, Schmeichel KL (1999) Tissue structure, nuclear organization, and gene expression in normal and malignant breast. *Cancer Res* **59** (7 Suppl): 1757-1763s

Bouchet BP, Bertholon J, Falette N, Audoynaud C, Lamblot C, Puisieux A, Galmarini CM (2007) Paclitaxel resistance in untransformed human mammary epithelial cells is associated with an aneuploidy-prone phenotype. *Br J Cancer* **97** (9): 1218-1224

Bouchet BP, de Fromentel CC, Puisieux A, Galmarini CM (2006) p53 as a target for anti-cancer drug development. *Crit Rev Oncol Hematol* **58** (3): 190-207

Bronson R, Dawe C, Carroll J, Benjamin T (1997) Tumor induction by a transformation-defective polyoma virus mutant blocked in signaling through Shc. *Proc Natl Acad Sci U S A* **94** (15): 7954-7958

Chabalier C, Lamare C, Racca C, Privat M, Valette A, Larminat F (2006) BRCA1 downregulation leads to premature inactivation of spindle checkpoint and confers paclitaxel resistance. *Cell Cycle* **5** (9): 1001-1007

Courjal F, Theillet C (1997) Comparative genomic hybridization analysis of breast tumors with predetermined profiles of DNA amplification. *Cancer Res* **57** (19): 4368-4377

Debnath J, Muthuswamy SK, Brugge JS (2003) Morphogenesis and oncogenesis of MCF-10A mammary epithelial acini grown in three-dimensional basement membrane cultures. *Methods* **30** (3): 256-268

Duesberg P, Li R (2003) Multistep carcinogenesis: a chain reaction of aneuploidizations. *Cell Cycle* **2** (3): 202-210

Duesberg P, Rausch C, Rasnick D, Hehlmann R (1998) Genetic instability of cancer cells is proportional to their degree of aneuploidy. *Proc Natl Acad Sci U S A* **95** (23): 13692-13697

Duesberg P, Stindl R, Hehlmann R (2001) Origin of multidrug resistance in cells with and without multidrug resistance genes: chromosome reassortments catalyzed by aneuploidy. *Proc Natl Acad Sci U S A* **98** (20): 11283-11288

Edwards J, Krishna NS, Witton CJ, Bartlett JM (2003) Gene amplifications associated with the development of hormone-resistant prostate cancer. *Clin Cancer Res* **9** (14): 5271-5281

Elenbaas B, Spirio L, Koerner F, Fleming MD, Zimonjic DB, Donaher JL, Popescu NC, Hahn WC, Weinberg RA (2001) Human breast cancer cells generated by oncogenic transformation of primary mammary epithelial cells. *Genes Dev* **15** (1): 50-65

Finette BA, Homans AC, Albertini RJ (2000) Emergence of genetic instability in children treated for leukemia. *Science* **288** (5465): 514-517

Galmarini CM, Bouchet BP, Audoynaud C, Lamblot C, Falette N, Bertholon J, Wang Q, Beghin A, Dumontet C, Puisieux A (2006) A p21/WAF1 mutation favors the appearance of drug resistance to paclitaxel in human noncancerous epithelial mammary cells. *Int J Cancer* **119** (1): 60-66

Galmarini CM, Falette N, Tabone E, Levrat C, Britten R, Voorzanger-Rousselot N, Roesch-Gateau O, Vanier-Viornery A, Puisieux A, Dumontet C (2001) Inactivation of wild-type p53 by a dominant negative mutant renders MCF-7 cells resistant to tubulin-binding agent cytotoxicity. *Br J Cancer* **85** (6): 902-908

Hollander MC, Sheikh MS, Bulavin DV, Lundgren K, Augeri-Henmueller L, Shehee R, Molinaro TA, Kim KE, Tolosa E, Ashwell JD, Rosenberg MP, Zhan Q, Fernandez-Salguero PM, Morgan WF, Deng CX, Fornace AJ, Jr. (1999) Genomic instability in Gadd45a-deficient mice. *Nat Genet* **23** (2): 176-184

Ikui AE, Yang CP, Matsumoto T, Horwitz SB (2005) Low concentrations of taxol cause mitotic delay followed by premature dissociation of p55CDC from Mad2 and BubR1 and abrogation of the spindle checkpoint, leading to aneuploidy. *Cell Cycle* **4** (10): 1385-1388

Jallepalli PV, Waizenegger IC, Bunz F, Langer S, Speicher MR, Peters JM, Kinzler KW, Vogelstein B, Lengauer C (2001) Securin is required for chromosomal stability in human cells. *Cell* **105** (4): 445-457

Jordan MA, Wilson L (2004) Microtubules as a target for anticancer drugs. *Nat Rev Cancer* **4** (4): 253-265

Kerbel RS (1991) Inhibition of tumor angiogenesis as a strategy to circumvent acquired resistance to anti-cancer therapeutic agents. *Bioessays* **13** (1): 31-36

Laird PW, Jaenisch R (1996) The role of DNA methylation in cancer genetic and epigenetics. *Annu Rev Genet* **30** 441-464

Li R, Hehlman R, Sachs R, Duesberg P (2005) Chromosomal alterations cause the high rates and wide ranges of drug resistance in cancer cells. *Cancer Genet Cytogenet* **163** (1): 44-56

Li R, Rasnick D, Duesberg P (2002) Correspondence re: D. Zimonjic et al., Derivation of human tumor cells in vitro without widespread genomic instability. *Cancer Res* **62** (21): 6345-6348

Loeb LA, Loeb KR, Anderson JP (2003) Multiple mutations and cancer. *Proc Natl Acad Sci U S A* **100** (3): 776-781

Orsetti B, Nugoli M, Cervera N, Lasorsa L, Chuchana P, Rouge C, Ursule L, Nguyen C, Bibeau F, Rodriguez C, Theillet C (2006) Genetic profiling of chromosome 1 in breast cancer: mapping of regions of gains and losses and identification of candidate genes on 1q. *Br J Cancer* **95** (10): 1439-1447

Perou CM, Sorlie T, Eisen MB, van de RM, Jeffrey SS, Rees CA, Pollack JR, Ross DT, Johnsen H, Akslen LA, Fluge O, Pergamenschikov A, Williams C, Zhu SX, Lonning PE, Borresen-Dale AL, Brown PO, Botstein D (2000) Molecular portraits of human breast tumours. *Nature* **406** (6797): 747-752

Petersen OW, Ronnov-Jessen L, Howlett AR, Bissell MJ (1992) Interaction with basement membrane serves to rapidly distinguish growth and differentiation pattern of normal and malignant human breast epithelial cells. *Proc Natl Acad Sci U S A* **89** (19): 9064-9068

Ried T, Heselmeyer-Haddad K, Blegen H, Schrock E, Auer G (1999) Genomic changes defining the genesis, progression, and malignancy potential in solid human tumors: a phenotype/genotype correlation. *Genes Chromosomes Cancer* **25** (3): 195-204

Ried T, Knutzen R, Steinbeck R, Blegen H, Schrock E, Heselmeyer K, du MS, Auer G (1996) Comparative genomic hybridization reveals a specific pattern of chromosomal gains and losses during the genesis of colorectal tumors. *Genes Chromosomes Cancer* **15** (4): 234-245

Rieder CL, Maiato H (2004) Stuck in division or passing through: what happens when cells cannot satisfy the spindle assembly checkpoint. *Dev Cell* **7** (5): 637-651

Roberts JR, Allison DC, Donehower RC, Rowinsky EK (1990) Development of polyploidization in taxol-resistant human leukemia cells in vitro. *Cancer Res* **50** (3): 710-716

Shannon P, Sabha N, Lau N, Kamnasaran D, Gutmann DH, Guha A (2005) Pathological and molecular progression of astrocytomas in a GFAP:12 V-Ha-Ras mouse astrocytoma model. *Am J Pathol* **167** (3): 859-867

Shima N, Alcaraz A, Liachko I, Buske TR, Andrews CA, Munroe RJ, Hartford SA, Tye BK, Schimenti JC (2007) A viable allele of Mcm4 causes chromosome instability and mammary adenocarcinomas in mice. *Nat Genet* **39** (1): 93-98

Snijders AM, Fridlyand J, Mans DA, Segraves R, Jain AN, Pinkel D, Albertson DG (2003) Shaping of tumor and drug-resistant genomes by instability and selection. *Oncogene* **22** (28): 4370-4379

Swanton C, Marani M, Pardo O, Warne PH, Kelly G, Sahai E, Elustondo F, Chang J, Temple J, Ahmed AA, Brenton JD, Downward J, Nicke B (2007) Regulators of mitotic arrest and ceramide metabolism are determinants of sensitivity to paclitaxel and other chemotherapeutic drugs. *Cancer Cell* **11** (6): 498-512

Troester MA, Hoadley KA, Sorlie T, Herbert BS, Borresen-Dale AL, Lonning PE, Shay JW, Kaufmann WK, Perou CM (2004) Cell-type-specific responses to chemotherapeutics in breast cancer 2. *Cancer Res* **64** (12): 4218-4226

Upender MB, Habermann JK, McShane LM, Korn EL, Barrett JC, Difilippantonio MJ, Ried T (2004) Chromosome transfer induced aneuploidy results in complex dysregulation of the cellular transcriptome in immortalized and cancer cells. *Cancer Res* **64** (19): 6941-6949

Wasenius VM, Jekunen A, Monni O, Joensuu H, Aebi S, Howell SB, Knuutila S (1997) Comparative genomic hybridization analysis of chromosomal changes occurring during development of acquired resistance to cisplatin in human ovarian carcinoma cells. *Genes Chromosomes Cancer* **18** (4): 286-291

Weaver BA, Silk AD, Montagna C, Verdier-Pinard P, Cleveland DW (2007) Aneuploidy acts both oncogenically and as a tumor suppressor. *Cancer Cell* **11** (1): 25-36

Weaver Z, Montagna C, Xu X, Howard T, Gadina M, Brodie SG, Deng CX, Ried T (2002) Mammary tumors in mice conditionally mutant for Brca1 exhibit gross genomic instability and centrosome amplification yet display a recurring distribution of genomic imbalances that is similar to human breast cancer. *Oncogene* **21** (33): 5097-5107

Woo RA, Poon RY (2004) Activated oncogenes promote and cooperate with chromosomal instability for neoplastic transformation. *Genes Dev* **18** (11): 1317-1330

Xu X, Wagner KU, Larson D, Weaver Z, Li C, Ried T, Hennighausen L, Wynshaw-Boris A, Deng CX (1999) Conditional mutation of Brca1 in mammary epithelial cells results in blunted ductal morphogenesis and tumour formation. *Nat Genet* **22** (1): 37-43

Zimonjic D, Brooks MW, Popescu N, Weinberg RA, Hahn WC (2001) Derivation of human tumor cells in vitro without widespread genomic instability. *Cancer Res* **61** (24): 8838-8844

Zimonjic DB, Pollock JL, Westervelt P, Popescu NC, Ley TJ (2000) Acquired, nonrandom chromosomal abnormalities associated with the development of acute promyelocytic leukemia in transgenic mice. *Proc Natl Acad Sci U S A* **97** (24): 13306-13311

Bouchet *et al.*
Figure 1

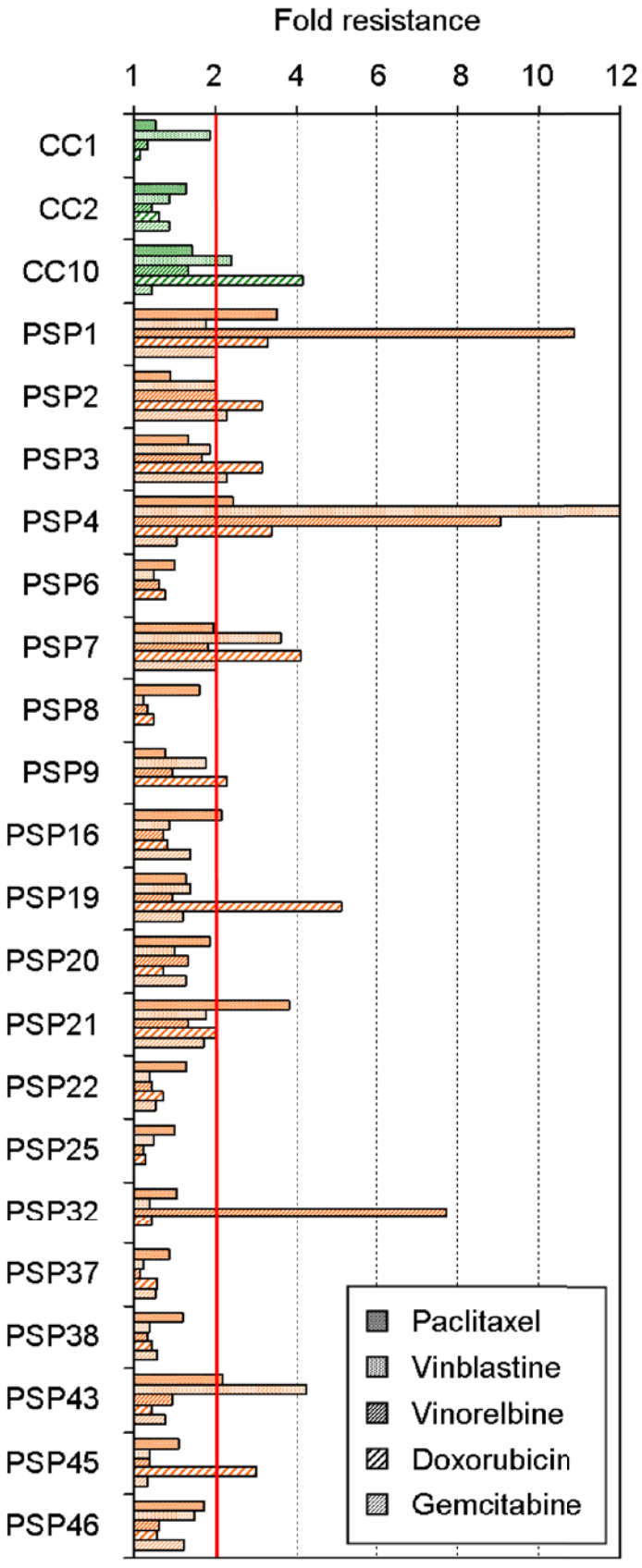

Bouchet *et al.*
Figure 2

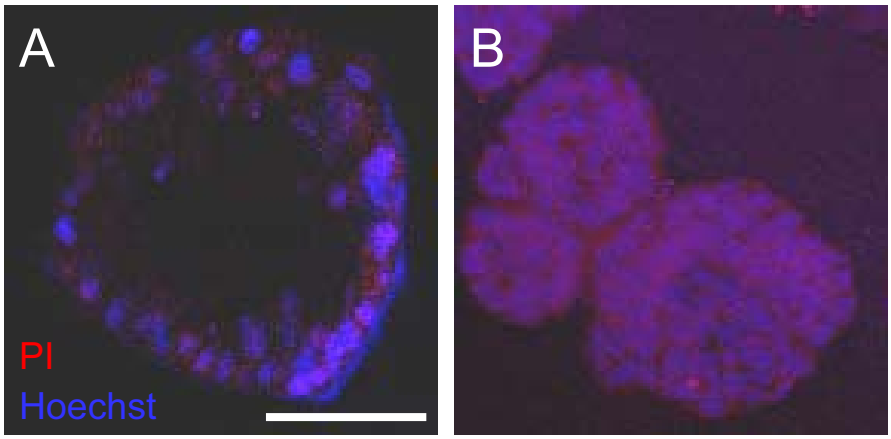

Bouchet *et al.*
Figure 3

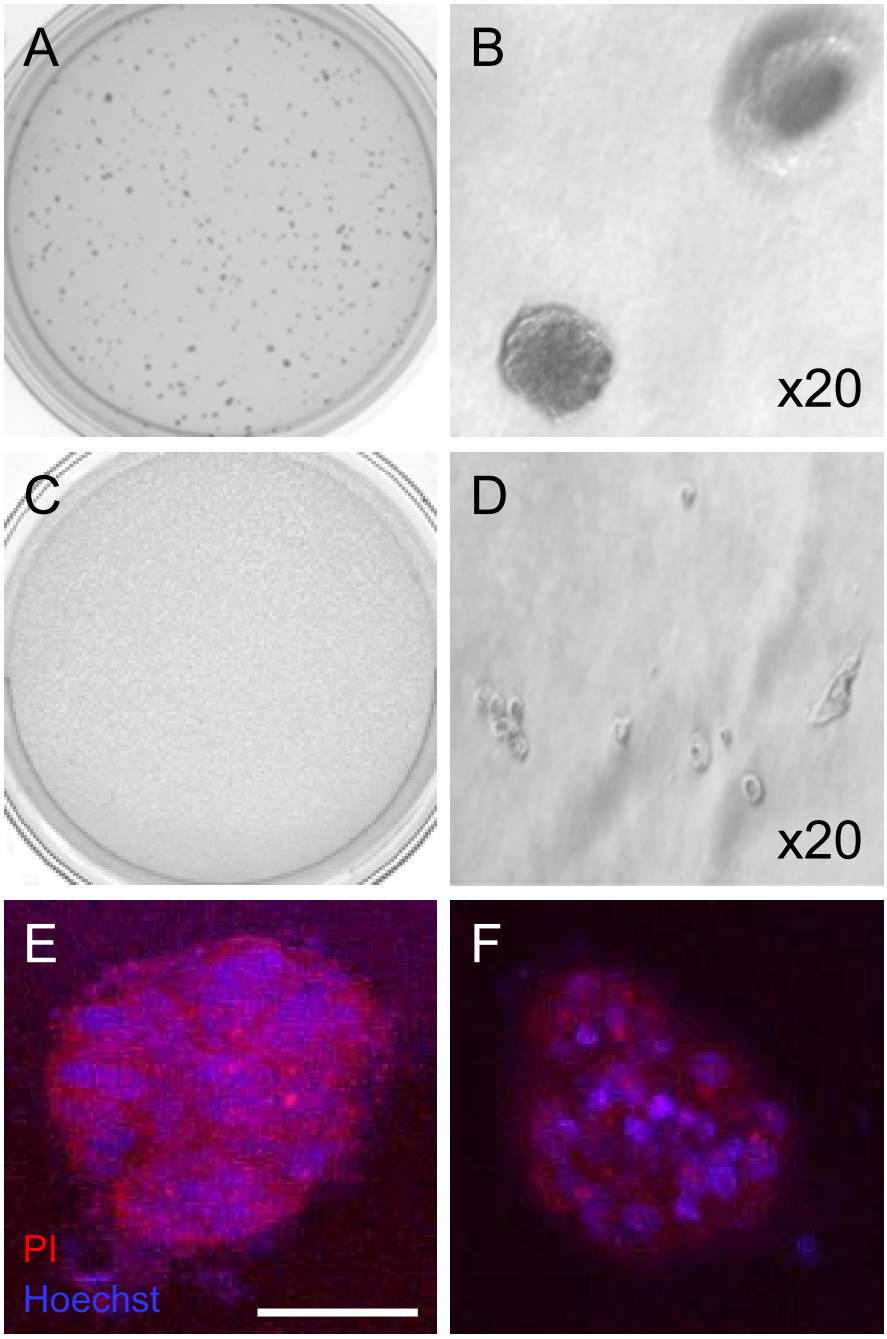

Bouchet *et al.*
Figure 4

A

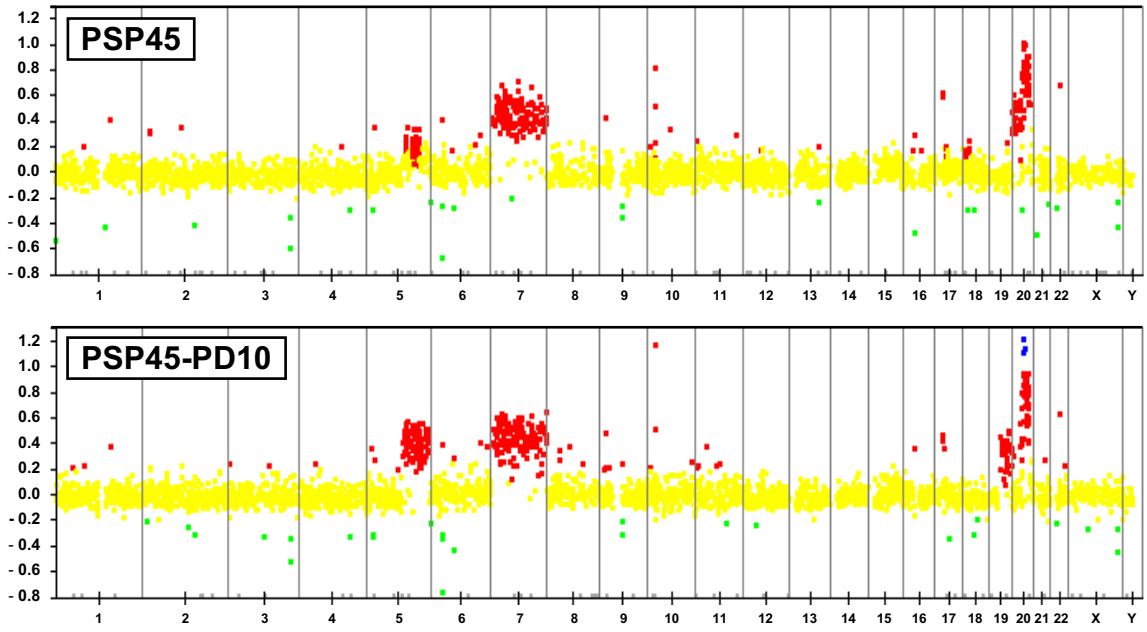

B

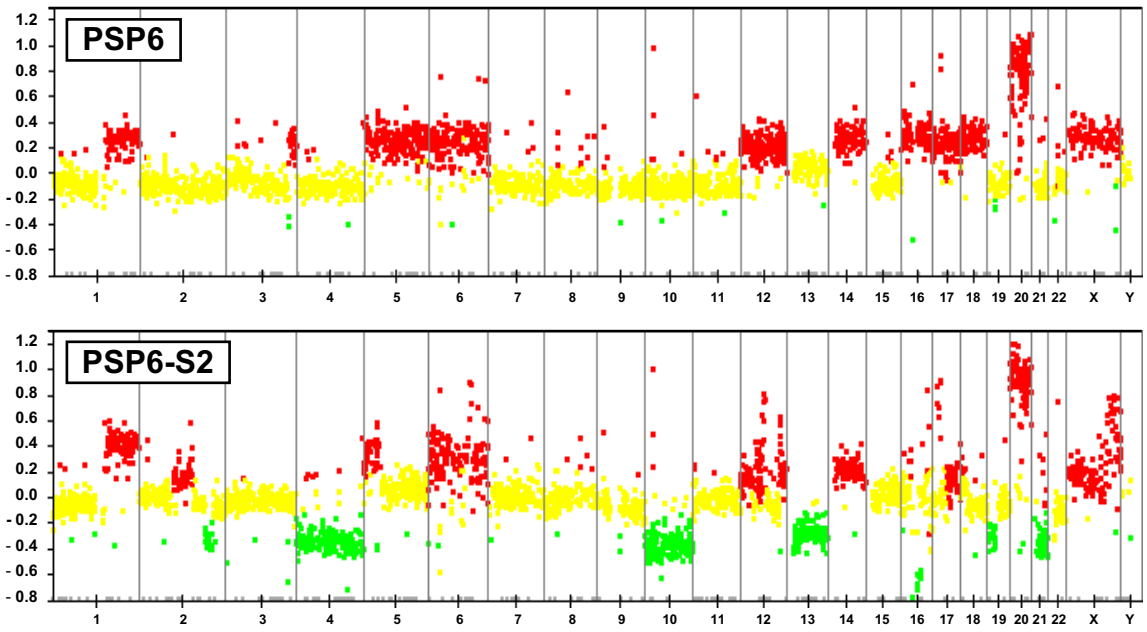

H.2) ANNEXE 2 : PUBLICATIONS

Int. J. Cancer: **119,** 60–66 (2006)

A p21/WAF1 mutation favors the appearance of drug resistance to paclitaxel in human noncancerous epithelial mammary cells

Carlos María Galmarini[1]*, Benjamin Pierre Bouchet[1], Carole Audoynaud[1], Christelle Lamblot[1], Nicole Falette[1], Jacques Bertholon[2], Qing Wang[1], Anne Beghin[2], Charles Dumontet[2] and Alain Puisieux[1]

[1]*Unité d'Oncologie Moléculaire. Centre Léon Bérard, Lyon, France*
[2]*INSERM U590, Centre Léon Bérard, Lyon, France*

We investigated the mechanisms responsible for paclitaxel resistance in HME-1 cells (human mammary epithelial cells immortalized with hTERT). These cells were exposed to paclitaxel (10 pM for 7 days) and 20 cellular surviving populations (PSP) were obtained. PSP demonstrated high levels of resistance to paclitaxel cytotoxicity as compared with HME-1 cells. Activation of *mdr-1* gene expression was observed in 2 PSP. Protein expression analysis using a C-terminal targeted antibody showed that 13 PSP were negative for p21/WAF1 expression after ionizing radiation (6 Gy) or doxorubicin (100 nM) treatment. Sequencing of the 3 exons of the *CDKN1A* gene revealed that 13 PSP contained a point mutation in exon 2. This mutation consisted in a T insertion at codon 104 leading to a premature STOP codon appearance. Mismatch amplification mutation assay and RFLP-PCR confirmed the presence of the mutation in 16 PSP. Western blot using an N-terminal targeted antibody demonstrated that the C-terminal-truncated p21/WAF1 protein (14 kDa) was indeed expressed in the 13 PSP. Our data suggest that p21/WAF1 inactivation may confer a strong resistance to paclitaxel in noncancerous breast epithelial cells harboring a p21/WAF1 mutant.

Key words: paclitaxel; cyclin-dependent kinase inhibitor p21; antineoplastic agent resistance

Paclitaxel is one of the most effective anticancer drugs used in the clinic to treat a variety of solid tumors. In breast cancer patients, administration of paclitaxel in combination or sequentially with other chemotherapy drugs for the treatment of metastatic disease demonstrated to have more anticancer activity than previous nonpaclitaxel chemotherapy regimens.[1] Moreover, recent clinical trials also demonstrated that the use of paclitaxel as adjuvant therapy in early stage breast cancer patients helps to prevent relapse after the initial primary surgical treatment.[2,3]

Despite paclitaxel increasing use, especially in therapy of curable cancers, no data are currently available on its effects on noncancerous human breast epithelial cells. This prompted us to expose hTERT-immortalized human mammary epithelial cells to a stringent selection by this agent in a 7-day drug exposure. We then analyzed the emergence of surviving cells in parallel populations. In contrast to prevalent cellular models of drug resistance derived by multiple stepwise selections, the PSP in our model have experienced a single paclitaxel treatment at concentration levels and time exposure similar than those used in clinical practice. In these experiments, *mdr-1* expression was found to be positive by RT-PCR in 2 of 20 PSP (10%). Given the fact that the *mdr-1*-negative PSP displayed resistance to paclitaxel, we sought to determine whether other alterations existed in these PSP. Our findings indicate that mutations of the *p21/WAF1* gene are involved in resistance to this agent.

Material and methods

Reagents

Paclitaxel was obtained from Bristol-Myers Squibb (Paris, France). Antibodies against C-terminal-p21/WAF1 (SX-118), p53 (DO7) and TRITC-conjugated antimouse antibodies were purchased from DAKO (Glostrup, Denmark). Antibodies against Bax were purchased from Santa Cruz Biotechnology (Santa Cruz, USA). Antibodies against N-terminal p21/WAF1 were purchased from UPSTATE (Waltham, USA). Antibodies against mdm-2 were given by B. Wasylyk. Peroxidase-conjugated secondary antibodies were purchased from Covalab (Oullins, France). Propidium iodide, MTT and Hoescht 33258 were purchased from Sigma (Saint Quentin, France).

Cell lines

HME-1 cells are telomerase-immortalized cells that stably express hTERT. This cell line was given by C. Theillet (Montpellier, France).

Obtention of paclitaxel-surviving populations

One 75-cm^2 tissue culture flask (Corning, NY) was seeded with HME-1 cells at low density (10^6 cells) and allowed to grow to near confluence (~70%). Cell population from this flask was seeded into 20 separate 96-well plates at a concentration of 100 cells per well. The following day, treatment with paclitaxel was begun at a dose of 10 pM. The drug-containing medium was changed every day over a period of 7 days then replaced with drug-free medium. Surviving populations were allowed to grow for 2–3 weeks. Wells containing paclitaxel-surviving populations were harvested, frozen and expanded in drug-free medium for other studies. A control experiment was performed to evaluate the spontaneous development of cell resistance. For this purpose, 18 clones of HME-1 cells (CC) were obtained by limiting dilution (0.1 cell per well) with no exposure to the drug.

To avoid the genetic drift and accumulation of chromosomal aberrations, which are known to occur over time during continuous cell culture, all experiments were performed immediately after the expansion period of HME-1 cells as well as CC and PSP surviving clones.

Growth inhibition assays and cell proliferation assay

Short-term growth inhibition assay was determined in 3 separate experiments, each of which was performed in triplicate using the MTT assay as previously described.[4] Results were expressed as fold-resistance of CC and PSP in comparison to the parental cell line HME-1. Clones displaying a resistant ratio of >2 were considered as stably resistant to paclitaxel.

To examine differences in cell growth of the different cell lines, MTT assay was performed in HME-1, CC and PSP cells seeded at a density of 7×10^3 cells per well into 96-well plate in complete culture media. MTT assay was performed after 72 hr as described

Abbreviations: CC, control clones; CDKN1A/p21/WAF1, cyclin-dependent kinase inhibitor 1A gene; HME-1, human mammary epithelial cells; hTERT, human telomerase reverse transcriptase; *mdr-1,* multidrug resistance-1; MTT, 3-[4,5-dimethylthiazol-2-yl]-2,5-diphenyl-tetrazolium bromide; PCR, polymerase chain reaction; PSP, paclitaxel-surviving populations; RFLP, restriction fragment length polymorphism.

***Correspondence to:** Unité d'Oncologie Moléculaire - Centre Léon Bérard, 28, avenue Laënnec 69373 Lyon CEDEX 08 France.
Fax: +33-4-78-78-28-21. E-mail: fgalma@rockefeller.univ-lyon1.fr
Received 26 September 2005; Accepted 24 November 2005
DOI 10.1002/ijc.21770
Published online 23 January 2006 in Wiley InterScience (www.interscience.wiley.com).

earlier. Results were expressed as percentage of CC and PSP cell proliferation compared to HME-1 cells.

RT-PCR for mdr-1 detection

PCR primers used for *mdr-1* were: for 5′-tcttggcagcaattagaact; rev 5′-cgatttcataagctgctcc. Primers for GAPDH were: for 5′-catccttctccccacacac; rev 5′-agtcccagggctttgatttg. The PCR products of *mdr-1* (326 bp) and GAPDH genes were separated by electrophoresis on a 3 and 10% agarose gel, respectively, and visualized by staining with ethidium bromide.

Northern and Western blots

CDKN1A p21/WAF1 gene expression was analyzed by Northern blot analysis. For this purpose, total RNA was extracted using Tri-Reagent (Sigma), as previously described.[4]

p53, p21/WAF1, mdm-2 and Bax protein expression was determined by Western blot analysis at basal conditions and after γ irradiation (6 Gy) at different time intervals as described previously.[4]

Immunofluorescence and microscopy

Exponentially growing cells were plated on 18-mm microscope glass slides and incubated with doxorubicin (100 nM; 24 hr). Then, cells were fixed in 100% methanol and primary antibodies were added. A TRITC antimouse antibody was used as a secondary antibody for p21/WAF1 staining. DNA was counterstained with 5 μg/ml Hoescht 33258. Coverslips were examined with a Zeiss axioplasm microscope using a Zeiss ×100 1.3 oil-immersion objective.

DNA extraction, PCR amplification and sequence analysis of CDKN1A/p21/WAF1

Genomic DNA was used as a substrate for amplification of the 3 exons of the *CDKN1A/ p21/WAF1* gene by PCR. Exon 1 was amplified with primers: for: 5′-ggcggggcggttgtatatca, rev: 5′-cgcgcacttagagacaccgtgt. Exon 2 was amplified with primers: for: 5′-tagtgtctatccgccgtga, rev: 5′-tctgagaatcctgctcccttaca. Exon 3 was amplified with primers: for: 5′-ctccgccgcgtcctcttct, rev: 5′-gtaccacccagcggacaagtg.

All cell lines were screened for mutations in the *CDKN1A/p21/WAF1* gene. Sequencing was performed with the Bigdye PRISM preready kit (Applied Biosystems, Foster City, CA). Electrophoresis, band visualization and sequence analysis were automatically performed on the ABI 377 automatic sequencer (Applied Biosystems).

Specific PCR for CDKN1A/p21/WAF1 gene mutation

Each DNA sample was subjected to PCR reactions using the following primers: for-5′-tcagttgcctgctctcccagt; rev-5′-catggtcttcctctgctgtcca. The positive identification of the mutated allele was the result of amplification of a 560-bp PCR product. All PCR reactions were performed on a GeneAmp PCR System 9600 from PerkinElmer.

Restriction fragment length polymorphism

A 551-bp fragment was generated by PCR using as sense primer 5′-cagttgcctgctctcccagt, and as antisense primer 5′-ggacccttcagcctgctcc. After purification of the PCR product by centrifugation through a Centricon 30 column, the DNA was digested with the BsmfI restriction enzyme (Biolabs, Beverly), according to the manufacturer's specification.

Results

Selection of paclitaxel-surviving populations

PSP appeared in 16 of 20 plates. The average number of positive wells per plate was 1. Similar experiments were performed with higher concentrations of paclitaxel and no populations were observed in these plates (data not shown). No significant differences in cell growth were observed between HME-1 (100%) and CC (99.3 ± 18%; $p = 1$) or PSP cells (106 ± 36; $p = 0.8$).

Drug sensitivity of HME-1 cells, CC and PSP to different chemotherapeutic agents

We first compared drug sensitivity of PSP against CC and HME-1 cells. Results in Table I shows that PSP were more resistant to paclitaxel (mean ± SD IC_{50} for all PSP: 6.5 ± 3.3) than CC (mean ± SD IC_{50} for all CC: 4.1 ± 1.5; $p = 0.03$) and HME-1 cells (mean ± SD IC_{50}: 3.9 ± 2.5; $p = 0.02$). A more detailed analysis showed that 5 of 20 PSP (PSP1, PSP4, PSP16, PSP21 and PSP43) displayed significant resistance to paclitaxel (more than 2-fold compared to HME-1 cells) ranging from 2.1- to 3.8-fold (Table I). These PSP were considered as stably resistant to paclitaxel.

Expression of the mdr-1 gene and c-erbB2 protein in paclitaxel-surviving populations

Expression of the *mdr-1* gene was evaluated in HME-1, CC and PSP cells using RT-PCR. Only 2 of the 20 PSP expressed the *mdr1* gene (PSP1 and PSP4) (Fig. 1*a*). In reference to c-erbB2, none of the cell lines expressed this protein as detected by immunocytochemistry analysis (data not shown).

Detection of p21/WAF1 protein by western blot and immunofluorescence

We also analyzed the expression of proteins implicated in G2/M cell cycle checkpoint control at baseline and after treatment with γ-irradiation (6 Gy) at different time intervals. In HME-1,

TABLE I – SENSITIVITY PROFILES TO PACLITAXEL AND OCURRENCE OF P21/WAF1 MUTATIONS IN PACLITAXEL-SURVIVING POPULATIONS (PSP)

Cell line	Paclitaxel[1]	p21/WAF1 status	p21/WAF1 expression[2]
HME-1	3.9 ± 2.5	wt[3]	+
CC1	2.1 ± 0.02	wt	+
CC2	5.1 ± 1.3	wt	+
CC3	5.5 ± 2.4	wt	+
CC4	5.8 ± 2.2	wt	+
CC5	6 ± 0.5	wt	+
CC6	5.7 ± 1	wt	+
CC7	2.08 ± 0.1	wt	+
CC8	4.5 ± 0.5	wt	+
CC9	1.7 ± 0.3	wt	+
CC10	5.6 ± 2	wt	+
CC11	5.1 ± 1.1	wt	+
CC12	3.4 ± 1.8	wt	+
CC13	4.7 ± 2.2	wt	+
CC14	3.8 ± 1.7	wt	+
CC15	1.9 ± 0.01	wt	+
CC16	4.3 ± 2.3	wt	+
CC17	2.2 ± 1.2	wt	+
CC18	4.3 ± 0.9	wt	+
PSP1	13.8 ± 10.5	wt	+
PSP2	3.5 ± 1.7	wt	+
PSP3	5.3 ± 4	wt	+
PSP4	9.5 ± 6.7	wt	+
PSP6	4 ± 3.3	Mutated	−
PSP7	7.6 ± 2	wt	+
PSP8	6.4 ± 3.5	wt	+
PSP9	3 ± 0.8	Mutated	−
PSP16	8.4 ± 0.7	Mutated	−
PSP19	5.1 ± 3	Mutated	−
PSP20	7.3 ± 5.9	Mutated	+
PSP21	15 ± 10.5	Mutated	−
PSP22	5 ± 2.3	Mutated	−
PSP25	3.9 ± 1.6	Mutated	−
PSP32	4.1 ± 3.3	Mutated	−
PSP37	3.4 ± 0.9	Mutated	−
PSP38	4.7 ± 1.5	Mutated	−
PSP43	8.5 ± 6	Mutated	−
PSP45	4.2 ± 2.4	wt	−
PSP46	6.8 ± 0.8	Mutated	−

[1]Mean ± SD of IC_{50} values expressed in nM.–[2]Detected by Western blot using an antibody directed against the C-terminal of the protein.–[3]wt: wild-type.

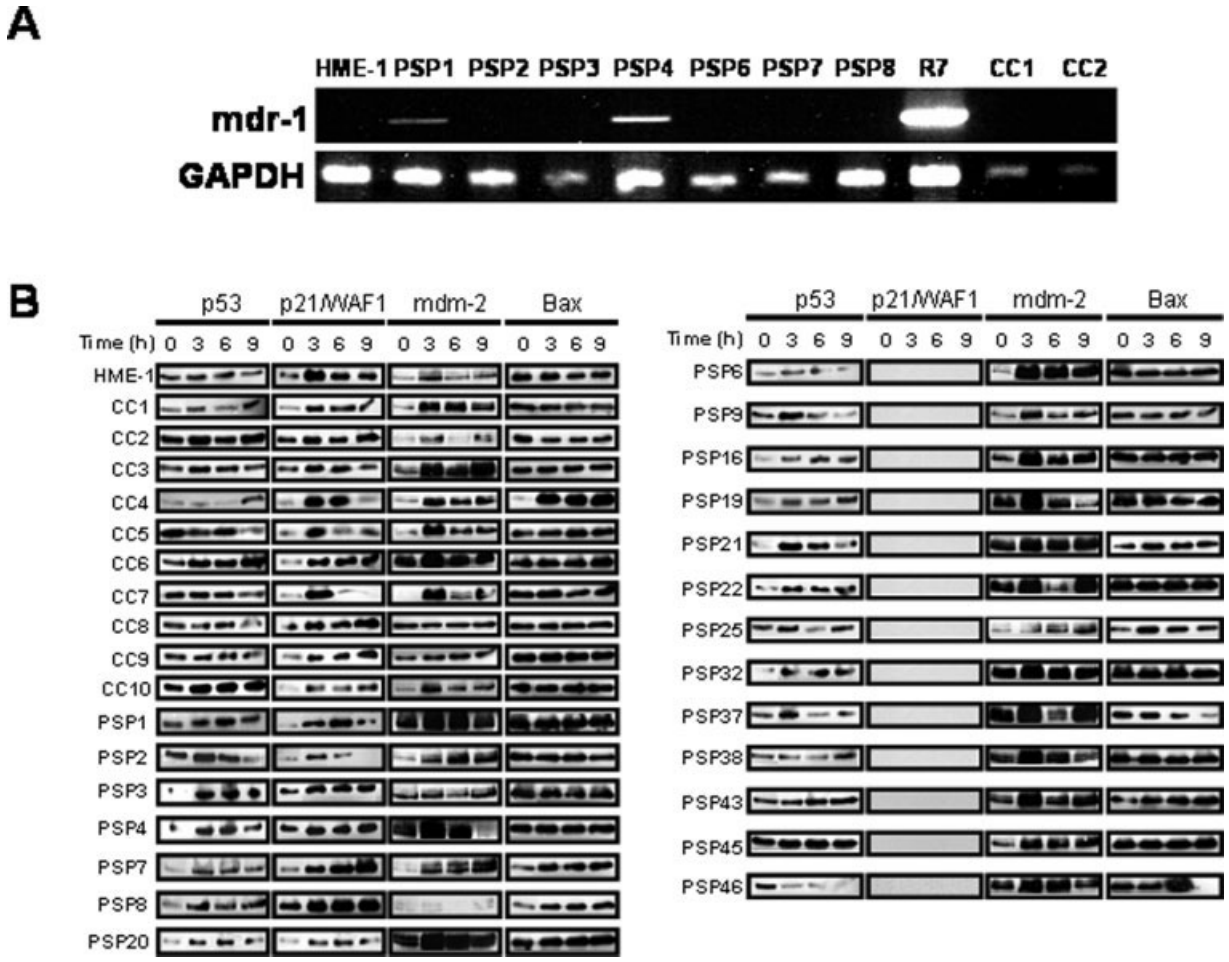

FIGURE 1 – (*a*) Representative gel showing the expression of the *mdr-1* gene by RT-PCR in HME-1 cells, 2 control clones (CC) and 7 paclitaxel-surviving populations (PSP). R7, a P-gp-expressing variant of the K562 cell line, was used as a positive control. (*b*) Protein kinetics of p53 and p53-related proteins (p21/WAF1, Mdm-2 and Bax) in HME-1 cells, CC and 20 PSP after γ irradiation (6 Gy) at different time intervals.

CC and 7 PSP (Fig. 1*b*), we observed p53 and p21/WAF1 accumulation in a time-dependent manner. Other p53-induced proteins (mdm-2 and bax) were also expressed at different levels. In contrast, using an antibody against the C-terminal region of the protein, no p21/WAF1 expression was detected in 13 PSP (Fig. 2*a*).

We then performed indirect immunofluorescence microscopy to assay for the presence of p21/WAF1 after doxorubicin treatment (100 nM). After 24 hr exposure, p21/WAF1 immunoreactivity of a C-terminal antibody was markedly increased in cell nucleus by drug treatment in HME-1 cells (Fig. 2*a*). Similar results were observed after drug treatment of CC and the 7 PSP that expressed p21/WAF1 in Western blot (data not shown). In contrast, no p21/WAF1 detection was observed in 13 PSP after drug treatment confirming the results from Western blots (a representative example of one of these PSP is shown in Fig. 2*a*).

Transcriptional alterations of CDKN1A/p21/WAF1 expression

To detect alterations in the *CDKN1A/p21/WAF1* transcription process, we examined its expression at the RNA level by Northern blot in HME-1, CC and PSP cells (Fig. 2*b*). We observed detectable *CDKN1A/p21/WAF1* RNA expression in almost all cell lines with the exception of PSP45.

CDKN1A/p21/WAF1 mutation analysis

Direct sequence analysis revealed sequence alterations in 13 PSP with respect to the wild-type sequence reported for the *CDKN1A/p21/WAF1* gene (Table I). The *CDKN1A/p21/WAF1* alteration was a T insertion in codon 104 resulting in a premature stop codon in position 127 of exon 2. Of interest, this mutation was present in PSP20 in which p21/WAF1 protein expression was detected using an antibody directed against the C-terminal region. Moreover, PSP45 cells were categorized as wt-*CDKN1A/p21/WAF1* gene. However, these cells did not show detectable levels of the protein by Western blot analysis. All CC expressed wt-*CDKN1A/p21/WAF1*. We also analyzed exons 4–9 of the p53 gene. No missense mutations were detected in HME-1, CC or PSP (data not shown).

Mutated-type allele specific PCR and RFLP-PCR

We then looked for a more sensitive method to detect the *CDKN1A/p21/WAF1* mutation in our cell lines. At first, we performed mutated-type allele specific PCR to discriminate between the wild-type allele of *CDKN1A/p21/WAF1* and the mutant allele. The presence of a given mutated allele could be verified by the presence of a specific band of 560 bp, after performing gel electrophoresis on PCR products. Allele-specific PCR revealed the presence of the mutated-type allele in 16 PSP (Fig. 2*c*). Moreover, the mutated-type allele was detected in PSP7, PSP8 and PSP45. Those PSP were found to carry the wild-type *CDKN1A/p21/WAF1* gene by sequencing analysis. No amplification product was observed when testing for the mutated allele on DNA from HME-1 cells, CC or PSP1, PSP2, PSP3 and PSP4 (Fig. 2*c*).

As the wild-type sequence around codon 104 defines a BsmfI site (recognition sequence GGGAC), which was abolished by the

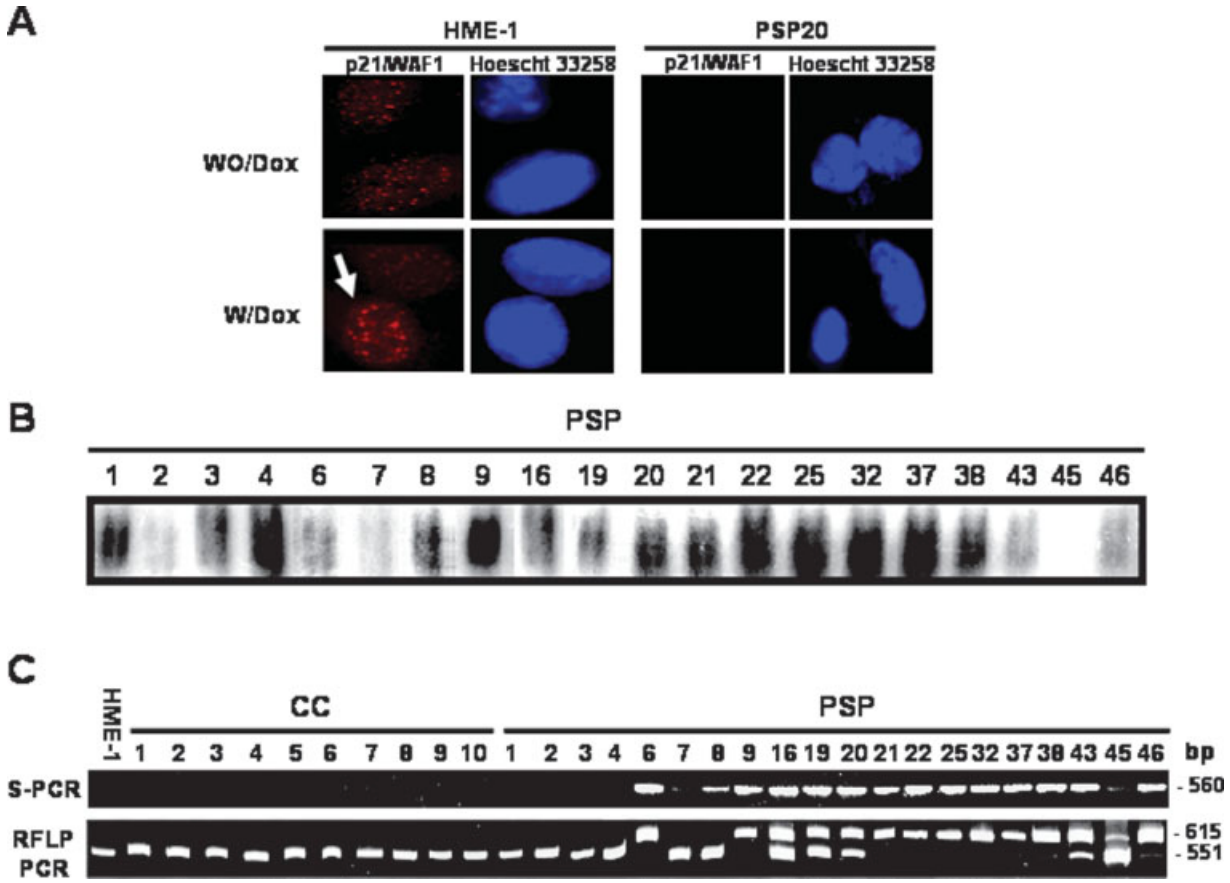

FIGURE 2 – (*a*) Representative examples showing the p21/WAF1 response to doxorubicin (Dox) 100 nM after 24 hr of treatment. Untreated (WO/Dox) or Dox-treated (W/Dox) HME-1 and PSP22 cells were stained with antibodies against C-terminal p21/WAF1 (red, TRITC) and DNA staining (blue, Hoescht 33258). The white arrows indicate the expression of p21/WAF1 in HME-1 cells. (*b*) Northern blotting showing the *CDKN1A/p21/WAF1* RNA levels in paclitaxel-surviving populations (PSP). (*c*) Detection of wild-type and mutated alleles of *CDKN1A/p21/WAF1* using allele-specific PCR (S-PCR) and restriction fragment length polymorphism (RFLP) on isolated DNA from HME-1 cells, CC and PSP cells.

mutation (GGGAC became GTGGA), the presence of the mutation could be tested for by restriction analysis, using BsmfI on a PCR fragment of 615 bp comprising codon 104. Hence, the digestion of the wild-type DNA by BsmfI yielded 1 fragment of 551 bp, that of the mutant DNA 1 uncut fragment of 615 bp, whereas the heterogeneous were recognizable because of the concomitant presence of the 551 and the 615 bp bands. Results shown in Figure 2*c* demonstrated that 7 PSP presented only the uncut 615 bp band indicating the presence of the *CDKN1A/p21/WAF1* mutation. Seven PSP presented both fragments indicating the presence of a heterogeneous state. Finally, 6 PSP as well as HME-1 and CC clones presented only the 551 bp fragment after BsmfI digestion confirming the presence of wild type *CDKN1A/p21/WAF1* gene.

Detection of C-terminal-truncated p21/WAF1 protein by western blot and immunofluorescence

We performed immunoblotting analysis using monoclonal antibodies directed against the N-terminus of the p21/WAF1 protein, which is conserved in the C-terminal-truncated-p21/WAF1 protein (Fig. 3*a*). Expression of a migrating band corresponding to wt-p21/WAF1 protein indicated that the N terminus was intact in HME-1, CC and 12 PSP cells. Interestingly, Western blot analysis revealed also a faster-migrating band protein in 13 PSP. This 14 kDa band corresponding to the C-terminal-truncated-p21/WAF1 protein was detected as a single signal in 7 PSP. Moreover, this band was coexpressed with wt-p21/WAF1 in 6 PSP clones. No p21/WAF1 protein expression was detected in PSP45.

We further examined the intracellular localization of p21/WAF1 and C-terminal-truncated-p21/WAF1 protein using monoclonal antibodies directed against the N-terminus. These experiments were performed in representative examples of the entire population as following: cells expressing wt-p21/WAF1 (HME-1 cells, CC1 and PSP1), cells expressing the C-terminal-truncated-p21/WAF1 (PSP6) or cells expressing no p21/WAF1 cells (PSP45) (Fig. 3*b*). As expected, p21/WAF1 was predominantly localized in the nucleus of HME-1 cells, after treatment with doxorubicin (100 nM). Similar results were observed in CC1 and PSP1 cells (data not shown). In contrast to HME-1 cells, 24 hr after treatment with doxorubicin (100 nM), p21/WAF1 staining did not accumulate in the nucleus and was observed only in the cytoplasm of PSP6. Finally, when examined the intracellular localization in PSP45, p21/WAF1 was virtually absent in these cells after drug treatment.

Detection of the CDKN1A/p21/WAF1 mutation in HME-1 cells

To establish whether the *CDKN1A/p21/WAF1* mutation was present in a minor population of parental HME-1 cells, one 75-cm^2 tissue culture flask was seeded with HME-1 cells at low density and allowed to grow to near confluence (~70%). Then, cells were seeded into 2 separate 96-well plates at a concentration of 100 cells per well and allowed to grow to near confluence. Cells were recovered and specific PCR for *CDKN1A/p21/WAF1* mutation was performed as described in the Material and Methods section. Of 61 propagated colonies, none of them displayed the band corresponding to the 560 bp amplification product. Mutation allele-specific PCR did

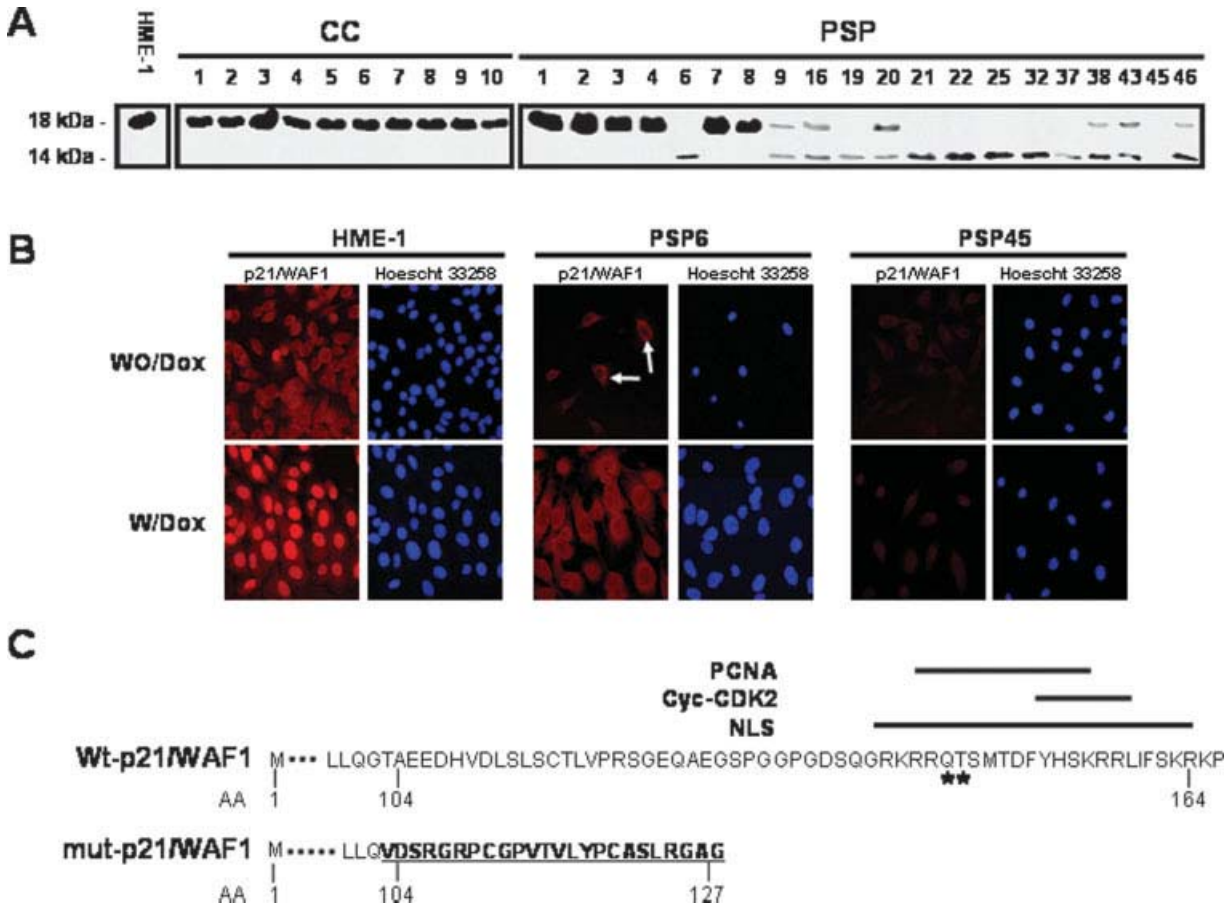

Figure 3 – (*a*) Western blot analysis of p21/WAF1 protein using a monoclonal antibody directed against the N-terminus of the protein. (*b*) Representative examples showing the p21/WAF1 cellular localization before and after treatment with doxorubicin (100 nM; 24 hr). Cells were processed for double immunofluorescence labeling with antibodies against N-terminal region of p21/WAF1 (red, TRITC) and DNA staining (blue, Hoescht 33258). The white arrows indicate the cytoplasmic expression of p21/WAF1 in PSP6 cells. (*c*) Schematic diagrams of wild-type and C-terminal-truncated p21/WAF1 proteins. The positions of the nuclear localization sequence (NLS), PCNA binding region, cyclin binding region and C8 α-subunit of the 20S proteasome are indicated in the wild-type p21/WAF1 sequence. The AKT-phosphorylation sites are represented by **.

not reveal the presence of the mutated-type allele in HME-1 parental cells in any of 61 propagated colonies (data not shown).

Discussion

The present work shows that stringent selection of the immortalized breast epithelial cell line HME-1 with paclitaxel (10 pM) in a 7-day drug exposure results in the establishment of a subset of surviving cell populations bearing a mutation of the *CDKN1A/p21/WAF1* gene (80% of PSP). This mutation favors the appearance of a 14 kDa form that reacts with antibodies raised against the N-terminal region, but not with antibodies raised against the C-terminal region of p21/WAF1. Moreover, the C-terminal-truncated p21/WAF1 protein was distinct from full length p21/WAF1 in the respect that they had different pattern of nuclear–cytoplasm localization.

p21/WAF1, a universal inhibitor of the cyclin-dependent kinases, is a regulator of cellular responses to microtubule damage induced by paclitaxel.[5,6] It is believed that p21/ WAF1 participates directly in the regulation of mitotic exit after microtubule damage induced by paclitaxel, *via* an action on the CDK1/cyclin-B complex.[7,8] Alterations in the expression or function of the p21/WAF1 gene thus may affect response to paclitaxel treatment.

Deletions or mutations of the *p21/WAF1* gene were reported to be rare in human tumors. In breast cancer patients, Balbin reported a tumor-specific alteration in one patient corresponding to a C–T transition in codon 94, which caused the substitution of a tryptophan for an arginine.[9] In another series of 85 primary breast tumors, McKenzie reported 2 primary tumors that contained tumor-specific missense mutations in the *CDKN1A/p21/WAF1* gene.[10] Mutations of *CDKN1A/p21/WAF1* gene have been also reported in human tumor cell lines[11] and in samples of patients with other tumor types.[12–14]

In our study, the p21/WAF1 mutation was characterized by a T insertion in codon 104 resulting in the appearance of a premature stop codon in position 127 of exon 2. As shown in Figure 3*c*, the mutant protein has lost the PCNA binding region (residues 133–164), the weak cyclin-binding region (residues 152–158), the nuclear localization signal (residues 140–156), as well as the Akt-phosphorylation sites (residues 145–146).[15] The C-terminal-truncated protein also showed a replacement of the amino acid sequence from G104 into VDSRGRPCGPVTVLYPCASLRGAG.

Other authors have reported the presence of p21/WAF1 C-terminal mutants in normal and cancer cells. Poon *et al*. and Tchou *et al*. have described a 19 kDa form of p21/WAF1 (p21Δ) in the cytoplasm of UV-irradiated normal diploid fibroblasts and of TPA/phorbol ester-treated Calu-1 and A549 cells.[16,17] This form of p21/WAF1 was probably derived from p21/WAF1 by proteolytic cleavage removing around 10 amino acids from the C-terminus and could not be detected by C-terminal-directed p21/WAF1 antibodies. Similarly to our C-terminal-truncated p21/WAF1 protein, p21Δ localized in the cytoplasm due to insufficient signals

for nuclear localization.[16] Many transformed human cell lines contained the majority of p21/WAF1 in the p21Δ form.[16]

An immediate question was whether the *CDKN1A/p21/WAF1* gene mutation was preexistent in the cell line or whether it was induced by paclitaxel treatment. To address this point, HME-1 parental cells were subjected to a *CDKN1A/p21/WAF1* mutation search. Using a mutation allelle-specific PCR and subcloning of HME-1 cells, we were unable to detect the mutation in the parental cells. This could be due to a lack of sensitivity of this technique. In our opinion, the mutation arose randomly during the history of these cells rather than being induced by paclitaxel exposure. In fact, agents such as paclitaxel are not thought to cause point mutations, and it would be unlikely that this agent would be directly responsible for the 104 codon mutation observed in our PSP. Thus, paclitaxel could select cells with this preexisting mutation.

These results could indicate that p21/WAF1 plays an important role in the cellular response to paclitaxel treatment. In fact, we observed that although the *CDKN1A/p21/WAF1* gene mutation did not confer any cell growth advantage, it conferred a great survival advantage in the presence of paclitaxel. Thus, it is likely to envision C-terminal-truncated p21/WAF1 expression as an intermediate step, which establishes a p21/WAF1 pseudo-null state permissive to "paclitaxel-resistance," which in turn leads to a "fixed drug resistant phenotype" selected after drug treatment. Our results in PSP show a gradual evolution from a wt-p21/WAF1 state to a fully mutated status. Moreover, the intermediary phase observed in some PSP clones, where both the normal and mutated alleles can be detected, could correspond to the evolution from a predominant wt-p21/WAF-1 population to the outgrowth of a predominant C-terminal-truncated p21/WAF1 population. These observations fit with a model of clonal expansion of cells bearing a given set of alterations during drug exposure. These are reminiscent of the conventional thinking about the selection of drug resistant sublines, which dictates that a change found after drug selection directly contributes to the drug resistance phenotype.

Of interest, PSP45 presented another mechanism which resulted in a p21/WAF1-null status. These cells appeared to bear the mutant form of p21/WAF1 as Northern blot and Western blot analyses did not show any signal when screening for the wild-type p21/WAF1 in these cells. However, DNA sequencing revealed only the presence of wild-type alleles. Mutated-type allele-specific PCR and RFLP-PCR confirmed the heterogeneous status of these cells as they detected both wild-type and mutated-type allele. These results indicate that the absence of RNA and protein expression could be caused by reduced expression of the remaining *CDKN1A/p21/WAF1* wild-type allele. In breast cancer cells, the principal mechanisms to explain *CDKN1A/p21/WAF1* gene silencing include *p53* gene mutations, *c-erbB2* gene amplification or epigenetic alterations such as hypermethylation and/or deacetylation of the *CDKN1A/p21/WAF1* gene.[18–20] None of these genetic or epigenetic alterations were presented in PSP45 (data not shown). In this subline, thus, absence of expression of *CDKN1A/p21/WAF1* mRNA and protein could be ascribed to mutations in the gene promoter.

As discussed earlier, the appearance of PSP bearing the *CDKN1A/p21/WAF1* mutation was indicative of a strong growth and selective survival advantage of this mutation during treatment with paclitaxel in breast epithelial nontransformed cells. It was reported that cytoplasmic p21/WAF1 plays an important role in protecting cells against chemical-induced apoptosis. For instance, Asada *et al*. demonstrated that a deletion mutant of p21/WAF1 lacking the nuclear localization signal (ΔNLS-p21/WAF1) also led to an apoptosis-resistant phenotype, mediated by binding to and inhibition of the stress-activated ASK1 activity.[21] However, our growth inhibition assays in the presence of paclitaxel showed that only 3 (15%) of the 13 PSP bearing the C-terminal-truncated p21/WAF1 protein were stably resistant to paclitaxel.

In our experiment, 2 of the 20 paclitaxel-surviving populations displayed increased mRNA levels of the *mdr-1* gene. Both PSP clones expressed wt-*p21/WAF1* gene and were stably resistant to paclitaxel. Thus, overexpression of *mdr-1* gene accounts for 10% of the resistance mechanisms to paclitaxel in this setting. Our data show that short-term exposure to paclitaxel can influence *mdr-1* gene expression and the development of the MDR phenotype in noncancerous breast epithelial cells. The last 5 PSP (25% of surviving populations) showed neither the presence of *p21/WAF1* mutations nor the expression of the *mdr-1* gene. These PSP presented an unstably resistant phenotype to paclitaxel as determined by growth inhibition assay. The growth and selective advantage of these PSP during the selection process could be attributed to other mechanisms of resistance to paclitaxel, such as alterations in the composition and dynamics of microtubules.[22] These alterations were not explored in this work.

In conclusion, the present study demonstrates that paclitaxel selects noncancerous breast epithelial cells harboring a *CDKN1A/p21/WAF1* mutant. It would be of interest to investigate whether the C-terminal-truncated-p21/WAF1 protein described herein expressed different functions than wt-p21/WAF1 and if so, whether these functions could confer a survival advantage to mutant cells after paclitaxel treatment. These experiments are currently being developed in our laboratory. Finally, since paclitaxel is actually used in the adjuvant setting for the treatment of breast cancer, these 20 PSP should be valuable tools to understand the development of paclitaxel resistance phenomena and paclitaxel-induced alterations in noncancerous epithelial breast cancer cells.

References

1. Nabholtz JM, Vannetzel JM, Llory JF, Bouffette P. Advances in the use of taxanes in the adjuvant therapy of breast cancer. Clin Breast Cancer 2003;4:187–92.
2. Erman M, Baltali E, Karaoglu A, Abali H, Engin H, Ozisik Y, Guler N, Altundag K, Tekuzman G, Atahan IL, Onat D, Sayek I. A phase II study on the safety and efficacy of 5-fluorouracil, epirubicin, cyclophosphamide (FEC) followed by paclitaxel in the adjuvant treatment of breast cancer. Cancer Invest 2005;23:215–21.
3. Mamounas EP, Bryant J, Lembersky B, Fehrenbacher L, Sedlacek SM, Fisher B, Wickerham DL, Yothers G, Soran A, Wolmark N. Paclitaxel after doxorubicin plus cyclophosphamide as adjuvant chemotherapy for node-positive breast cancer: results from NSABP B-28. J Clin Oncol 2005;23:3686–96.
4. Galmarini CM, Falette N, Tabone E, Levrat C, Britten R, Voorzanger-Rousselot N, Roesch-Gateau O, Vanier-Viornery A, Puisieux A, Dumontet C. Inactivation of wild-type p53 by a dominant negative mutant renders MCF-7 cells resistant to tubulin-binding agent cytotoxicity. Br J Cancer 2001;85:902–8.
5. Heliez C, Baricault L, Barboule N, Valette A. Paclitaxel increases p21 synthesis and accumulation of its AKT-phosphorylated form in the cytoplasm of cancer cells. Oncogene 2003;22:3260–8.
6. Mantel C, Braun SE, Reid S, Henegariu O, Liu L, Hangoc G, Broxmeyer HE. p21(cip-1/waf-1) deficiency causes deformed nuclear architecture, centriole overduplication, polyploidy, and relaxed microtubule damage checkpoints in human hematopoietic cells. Blood 1999;93:1390–8.
7. Bates S, Ryan KM, Phillips AC, Vousden KH. Cell cycle arrest and DNA endoreduplication following p21Waf1/Cip1 expression. Oncogene 1998;17:1691–703.
8. Barboule N, Chadebech P, Baldin V, Vidal S, Valette A. Involvement of p21 in mitotic exit after paclitaxel treatment in MCF-7 breast adenocarcinoma cell line. Oncogene 1997;15:2867–75.
9. Balbin M, Hannon GJ, Pendas AM, Ferrando AA, Vizoso F, Fueyo A, Lopez-Otin C. Functional analysis of a p21WAF1,CIP1,SDI1 mutant (Arg94–> Trp) identified in a human breast carcinoma. Evidence that the mutation impairs the ability of p21 to inhibit cyclin-dependent kinases. J Biol Chem 1996;271:15782–6.
10. McKenzie KE, Siva A, Maier S, Runnebaum IB, Seshadri R, Sukumar S. Altered WAF1 genes do not play a role in abnormal cell cycle regulation in breast cancers lacking p53 mutations. Clin Cancer Res 1997;3:1669–73.
11. Bhatia K, Fan S, Spangler G, Weintraub M, O'Connor PM, Judde JG, Magrath I. A mutant p21 cyclin-dependent kinase inhibitor isolated from a Burkitt's lymphoma. Cancer Res 1995;55:1431–5.
12. Gao X, Chen YQ, Wu N, Grignon DJ, Sakr W, Porter AT, Honn KV. Somatic mutations of the WAF1/CIP1 gene in primary prostate cancer. Oncogene 1995;11:1395–8.

13. Lacombe L, Orlow I, Silver D, Gerald WL, Fair WR, Reuter VE, Cordon-Cardo C. Analysis of p21WAF1/CIP1 in primary bladder tumors. Oncol Res 1996;8:409–14.
14. Ibrahim SO, Lillehaug JR, Dolphine O, Johnson NW, Warnakulasuriya KA, Vasstrand EN. Mutations of the cell cycle arrest gene p21WAF1, but not the metastasis-inducing gene S100A4, are frequent in oral squamous cell carcinomas from Sudanese toombak dippers and non-snuff-dippers from the Sudan, Scandinavia, USA and UK. Anticancer Res 2002;22:1445–4.
15. Dotto GP p21(WAF1/Cip1): more than a break to the cell cycle? Biochim Biophys Acta1471:M43–56, 2000.
16. Poon RY, Hunter T. Expression of a novel form of p21Cip1/Waf1 in UV-irradiated and transformed cells. Oncogene 1998;16:1333–43.
17. Tchou WW, Rom WN, Tchou-Wong KM. Novel form of p21(WAF1/CIP1/SDI1) protein in phorbol ester-induced G2/M arrest. J Biol Chem 1996;271:29556–60.
18. Slamon DJ, Clark GM, Wong SG, Levin WJ, Ullrich A, McGuire WL. Human breast cancer: correlation of relapse and survival with amplification of the HER-2/neu oncogene. Science 1987;235:177–82.
19. Vogelstein B, Kinzler KW. p53 function and dysfunction. Cell 1992; 70:523–6.
20. Zhou BB, Li H, Yuan J, Kirschner MW. Caspase-dependent activation of cyclin-dependent kinases during Fas-induced apoptosis in Jurkat cells. Proc Natl Acad Sci USA 1998;95:6785–90.
21. Asada M, Yamada T, Ichijo H, Delia D, Miyazono K, Fukumuro K, Mizutani S. Apoptosis inhibitory activity of cytoplasmic p21(Cip1/WAF1) in monocytic differentiation. Embo J 1999;18:1223–34.
22. Galmarini CM, Kamath K, Vanier-Viornery A, Hervieu V, Peiller E, Falette N, Puisieux A, Ann Jordan M, Dumontet C. Drug resistance associated with loss of p53 involves extensive alterations in microtubule composition and dynamics. Br J Cancer 2003;88: 1793–9.

ELSEVIER

Critical Reviews in Oncology/Hematology 58 (2006) 190–207

Critical Reviews in Oncology Hematology

www.elsevier.com/locate/critrevonc

p53 as a target for anti-cancer drug development

Benjamin Pierre Bouchet *, Claude Caron de Fromentel, Alain Puisieux, Carlos María Galmarini

INSERM U590, Centre Léon Bérard, 28 rue Laënnec, 69373 Lyon Cedex 08, France

Accepted 5 October 2005

Contents

Abstract

Loss of p53 function compromises genetic homeostasis in cells exhibiting deregulated DNA replication and/or DNA damage, and prevents normal cytotoxic responses to cancer therapies. Genetic and pharmacological approaches are being developed with the ultimate

* Corresponding author. Tel.: +33 4 78 78 51 25; fax: +33 4 78 78 28 21.
E-mail address: bouchetb@lyon.fnclcc.fr (B.P. Bouchet).

doi:10.1016/j.critrevonc.2005.10.005

goal of restoring or controlling p53 functions in cancer patients. Progress has recently been made in the clinical use of replication-deficient virus carrying *wt-TP53* (Ad5CMV-p53) and/or cancer-selective oncolytic adenoviruses (ONYX-015). These strategies demonstrated clinical activity as monotherapy and were synergistic with traditional chemotherapy agents in the treatment of some types of cancer. In addition, pharmacological methods are under development to either stimulate wild-type p53 protein function, or induce p53 mutant proteins to resume wild-type functions. These methods are based on small chemicals (CP-31388, PRIMA-1), peptides (CDB3) or single-chain Fv antibody fragments corresponding to defined p53 domains. Here, we discuss the mechanisms underlying these approaches and their perspectives for cancer therapy.

Keywords: p53 protein; Apoptosis; Mutation; Prognosis; Gene therapy; ONYX-015

1. Introduction

It is now widely acknowledged that normal cells respond to DNA damage and inappropriate growth signals, such as oncogenic activation, by inducing genetically encoded programs that eliminate inappropriately proliferating cells from the cell cycle, thus protecting multicellular organisms from cancer development. Consequently, in an early phase of tumor development, oncogene-driven hyperproliferation must be associated with evasion of anti-proliferative and cell-death mechanisms that normally limit clonal expansion of somatic cells. In support of this hypothesis, it has been recently shown that precursor lesions of human cancers commonly express markers of a p53-dependent DNA damage response, indicating that early tumorigenesis (before malignant conversion and genomic instability) activates a p53-dependent response that delays or prevents cancer progression [1,2]. Activation of this checkpoint may be due to deregulated DNA replication, including abnormalities in pre-replication complex maturation and stalled or collapsed replication forks, followed by the generation of double-strand breaks. Mutations compromising this checkpoint might thus allow, early in tumorigenesis, cell proliferation, survival, increased genomic instability and tumor progression.

p53, the most frequently mutated gene in human malignancies [3], is found inactivated in approximately 50% of tumors of any location and histological type (generally, point mutations of one allele and deletion of the other allele). This transcription factor is considered as the "guardian of the genome". Present in an inactive form in normal cells, p53 becomes fully functional when activated in response to cell stress (either oncogenic or genotoxic stress). p53 activation leads to the upregulation of various target genes responsible for cell cycle arrest or apoptotic cell death, depending on the cellular environment.

Due to its crucial tumor suppressor activity, *TP53* thus appears to be an appealing target for gene therapy or pharmacological intervention in cancer treatment. In this review, we highlight the current knowledge concerning the different strategies to restore wild-type p53 function and thereby either reverting the malignant phenotype or enhancing drug sensitivity.

2. *TP53* structure and function

The human *TP53* gene spans 20 kb on chromosome band 17p13.1. The gene is composed of 11 exons, the first of which is non-coding [4]. Its promoter does not contain a TATA box but harbors a number of consensus binding sites for common transcription factors, such as Sp1, NF-kappaB or c-Jun. Despite these potential sites for transcriptional regulation, the expression of *TP53* is constitutive and ubiquitous, most of the protein regulation taking place at the post-translational level.

The p53 protein is a nuclear phosphoprotein, composed of 393 amino acids in human (Fig. 1). It has five structural and functional domains: an N-terminal transactivation domain, a proline-rich regulatory domain, a sequence-specific DNA-binding domain, an oligomerization domain and a C-terminal domain involved in the regulation of DNA-binding. In terms of three-dimensional structure, the DNA-binding domain is made of a scaffold of beta-sheets that supports flexible loops and helixes, which are in direct contact with DNA [5]. The most common mutations that occur in cancer alter this structure either by abrogating protein–DNA contacts or by disrupting protein folding (Fig. 1). The p53 protein contains many sites for post-phosphorylation by stress-signalling or growth-signalling kinases (CKI, CKII, Chk2, ATM, ATR, PRKC, JNK, MAPK) and for acetylation by co-activator histone acetyl transferases, such as p300/CBP or pCAF. In most cells, p53 is almost undetectable because it is rapidly ubiquitinated and degradated by the proteasome. The main factor responsible for this constitutive p53 instability is the ubiquitine ligase mdm-2 (OMIM #164785) [6]. However, p53 becomes stabilized and activated in response to many forms of cellular stress, since post-translational modifications usually abrogate the binding of ubiquitine ligases.

Various types of genotoxic and non-genotoxic stresses can lead to p53 activation, including agents that create single or double-strand breaks in DNA (gamma- or UV radiations, free radical damage, inhibitors of topoisomerases), mutagens that form bulky DNA adducts (aflatoxins, benzo(*a*)pyrene, alkylating agents) or agents that block elongation by RNA polymerases. In addition, damage to the mitotic spindle, ribonucleotide depletion, hypoxia, heat shock and exposure to nitric oxide can also induce p53. Induction follows a dif-

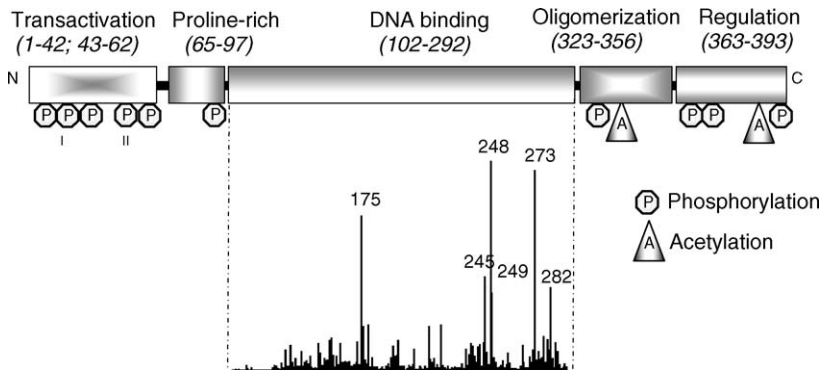

Fig. 1. Structure of the p53 protein. The protein can be divided in five functional domains, the transactivation domain (I and II; aminoacids 1–62), a proline-rich region (aminoacids 65–97), the DNA-binding domain (aminoacids 102–292), the oligomerization domain (aminoacids 323–356) and the regulatory domain (aminoacids 363–393). p53 suffers post-translational modifications, such as phosphorylation (hexagons) and acetylation (triangles), at the N- and C-terminal ends of the molecule. Vertical lines under the DNA-binding domain illustrate the distribution and the prevalence of point mutations found in the *TP53* gene in human tumors. The six most frequently mutated codons ("hotspot" codons) are identified.

ferent time-course, depending upon the nature and intensity of the stress [7–10].

Once activated, p53 can trigger several cellular events via two distinct and parallel pathways, transcription-dependent or transcription-independent. Examples of transcription-independent pathways include binding of p53 to components of the DNA replication/repair machinery, such as the helicases ERCC2 and ERCC3, or the replication protein RPA. Examples of genes transcriptionally regulated by p53 include cell cycle regulators in G1 and in G2 phases (P21/WAF-1, 14-3-3sigma, GADD45), regulators of apoptosis (BAX, CD95/FAS, KILLER/DR5, p53AIP1, PIG3, IGF-BP3, NOXA, PUMA, p53AIF1), genes involved in cellular responses to stress, such as inducible forms of nitric oxide synthase (NOS2) and cyclooxygenase (COX2), and genes involved in DNA repair (O^6MGMT, MSH2) [11,12]. How p53 selects from the set of alternative responses (e.g. choosing between cell cycle arrest or apoptosis) depends upon the nature and the amplitude of the inducing signal, as well as on the cell and tissue type [13]. In this respect, it is important to realize that the two biological responses may co-exist within the same tissue.

3. *TP53* mutations

Somatic *TP53* mutations have been described in almost all types of cancers with a variable prevalence depending on the type of cancer. In cancers of the upper aero-digestive tract (oral, esophageal or bronchial cancers), *TP53* is mutant in up to 75% of the cases of invasive cancers, particularly in smokers who are exposed to mutagens, and the mutation is often detectable in early, pre-neoplastic lesions. In cancers of the lower digestive tract, such as colon cancer, *TP53* mutations are less common at early stages (polyps or adenomas) but become highly prevalent at the adenoma-carcinoma transition. In breast cancers, mutations are detected in about 25% of the cases, but it has been suggested that other mechanisms than mutations may account for inactivation of p53 in a proportion of the cases. Cancers in which *TP53* mutations are infrequent include cancers of the cervix, testicular cancers, neuroblastoma and malignant melanomas, in which the overall *TP53* mutation prevalence is less than 5%. However, in these cancer types, the p53 pathway may be functionally inactivated by viral or cellular oncogenes. As an example, in cervical cancers, the viral antigen E6 of the oncogenic types of Human Papilloma Virus binds to the wild-type p53 protein and induces its rapid degradation, thus effectively bypassing the need of an inactivating mutation to remove p53 protein function [14]. In aggressive neuroblastomas, we showed recently that the bHLH transcription factor twist was overexpressed, leading to an inhibition of the p53-dependent pathway and allowing the survival of N-MYC amplified neuroblastoma cells [15]. Thus, given the central biological function of p53 in the control of proliferation in abnormal or extreme conditions, it can be assumed that deregulation, if not total disruption, of the p53 pathway is one of the hallmarks of cancer cells.

Of all reported *TP53* mutations, 75% are missense and 80% of them are located within the sequence encoding the DNA-binding domain of the protein (Fig. 1). The N-terminus, which contains the transactivation domain, and the C-terminus, which contains regulatory sites, is rarely targeted by mutations (less than 2% of all mutations). In the DNA-binding domain, missense mutations have been reported at almost all residues, but some residues are more frequently mutated than others (Fig. 1), with 30% of the mutations falling at five hotspot codons (175, 245, 248, 273, 282). Four of these codons correspond to arginine residues (175, 248, 273, 282) involved in protein–DNA interactions, either by direct contact with DNA (residues 248 and 273) or by stabilization of the DNA-binding surface (residues 175, 282) [5].

The main functional consequence of *TP53* mutation is the loss of specific DNA-binding and transcriptional activity. However, mutant proteins resulting from missense mutations

differ by their degree of loss of function. Functional assays in yeast and human cells have shown that some mutant proteins retain residual transcriptional activity for a subset of target genes. Indeed, the wild-type p53 protein does not bind equally to the different p53-targeted promoters. For example, the p21/WAF-1 promoter appears to contain binding sites of higher affinity than the BAX promoter [16]. Some mutants, as, for example, arginine to proline at codon 175 (R175P) and arginine to cysteine at codon 181 (R181C), retain the capacity to transactivate WAF1 but are defective for BAX activation and fail to induce apoptosis [17,18]. A recent study showed that a majority of mutants affected in the DNA-binding domain has an impaired transcriptional activity, whereas most of the mutants affected in other regions retain, at least partially, transcriptional activity on various *TP53*-responsive promoters [19].

In addition to loss of function, some *TP53* mutations result in dominant-negative activities and gain of function activities that confer pro-oncogenic properties to p53 mutant proteins. Indeed, several mutants have been shown to interfere with wild-type p53 transactivation, at various degrees [20]. This dominant-negative effect results in the total or partial abrogation of p53 protein function, even if there is still a wild-type protein expressed in the cell. Some mutants are also capable of transactivating or potentiating the transactivation of genes, such as MDR1, EGFR, c-MYC, PCNA, IGF-II or VEGF, which are not transactivated by the wild-type p53 protein and do not necessarily contain p53 binding-sites in their regulatory regions [21]. These "gain of function" properties are associated with growth-promoting phenotypes as well as resistance to anti-cancer drugs.

4. Targeting *TP53* for cancer therapy

Current, experimental approaches that target p53 for cancer treatment include attempts to activate p53 (Table 1) as well as to inactivate p53. These strategies aim to induce apoptosis or to prevent the destruction of normal cells by cytotoxic therapies. On the other hand, in certain cell types, activation of p53 by therapeutic agents may induce cell cycle arrest (and DNA repair) rather than apoptosis, thus resulting in a form of protection of cancer cells against the effects of therapy. Thus, activation of p53 may be seen either as a chemosensitizer or as a chemoprotective mechanism, depending on the cellular context.

Table 1
TP53 as a target for anti-cancer strategies

TP53 activation
(1) Gene therapy to replace *wt-TP53*
TP-53-containing retrovirus
TP-53-containing adenovirus: Ad5CMV-p53
(2) Destruction of wt-p53-deficient cells
Modified adenovirus: ONYX-015
(3) Pharmacological activation
Inhibition of p53/mdm-2 binding: superTIP, nutlins
Direct activation: polyamines
Reactivation of wt-p53 activity in mutant cells: PRIMA-1

5. Gene therapy to restore p53 function

As function of *TP53* is lost in many cancers, it seems reasonable to try to restore p53 function by replacing the mutant gene with a functional wild-type copy. It is believed that restoring of *TP53* function in tumor cells may block tumor development and may sensitize cells to cytotoxic killing, thus improving therapeutic response. One of the most popular approaches to achieve *TP53* restoration is the use of gene therapy. The primary requirement to treat cancer with *TP53*-gene therapy is the necessity for highly efficient delivery of the wild-type *TP53* into tumor cells in vivo. There must also be sufficient expression of functional p53 protein to mediate tumor suppression without affecting normal cells.

5.1. Retrovirus-mediated TP53-gene therapy

Retroviruses are attractive candidates for cancer gene therapy applications because they integrate in a stable form into the genome of infected cells and they require cell division for transduction. Retroviral vectors have therefore been used in the majority of approved gene transfer clinical protocols. It has been demonstrated that retrovirus-mediated gene transfer of the wild-type *TP53* gene into both human lung tumor cell lines and xenograft models could lead to the inhibition of tumor cell growth [22–24].

Based on these results, a phase I clinical trial was undertaken to determine the toxicity of retrovirus-mediated delivery of wild-type *TP53* [25]. Nine patients with non-small cell lung cancer for whom conventional treatments failed were included in the study. A retroviral vector containing the *wt-TP53* gene under control of a beta-actin promoter was injected directly into tumors using bronchoscopic or computed tomography-guided methods. No significant vector-related toxic side effects were reported up to 5 months after treatment, although some complications were experienced that were attributed by the investigators to the procedures used for the administration. Apoptosis was more frequent in post-treatment biopsies than in pretreatment biopsies. Of seven evaluable patients, three exhibited a tumor regression and three showed a stabilization of the disease. However, in spite of the detection of vector sequences by DNA polymerase chain reaction or in situ hybridization in post-treatment biopsies, there was no demonstration of transgene expression. No other study using retroviral vectors containing *wt-TP53* has been published to date. In fact, retroviral vectors have three major drawbacks for use in cancer therapy: they may cause damage to the genome, they may produce high titers of virus and their efficiency of transduction is relatively low especially in non-replicating cells.

5.2. Adenovirus-mediated TP53-gene therapy

A second strategy to *TP53* gene replacement therapy is the use of adenovirus as vectors. Adenoviruses are large, double-stranded DNA viruses that are capable of high transduction efficiency in a wide range of cell types. In contrast with retrovirus, their effect is not limited to actively proliferating cells. Several studies demonstrated that adenovirus serotype 5 administration has a low toxicity profile to humans. In fact, most of adults (85%) have existing antibodies to adenovirus serotype 5, but less than 15% of exposed patients become clinically symptomatic [26]. Moreover, because they do not integrate into the genome, there is no risk of insertional mutagenesis. For example, in the 1960s, oral adenoviral vaccines were given to thousands of military recruits without increase in cancer risk [27].

5.2.1. Ad5CMV-p53

Ad5CMV-p53 (Advexin® INTROGEN Therapeutics Inc.; Gendicine® Shenzhen SiBiono GeneTch Co. Ltd.) is a recombinant E1-deleted serotype 5 adenoviral vector encoding *TP53*. The generation and identification of this adenovirus vector expressing p53 was initially performed more than 10 years ago, by Zhang et al. [28]. In in vitro studies, Ad5CMV-p53 has demonstrated its efficiency for the expression of a functional wild-type p53 protein and the inhibition of cell-growth as well as a synergistic enhancement of the cytotoxicity of anti-cancer drugs in different cellular models [29–32]. Experiments in animal models confirmed the therapeutic effect of Ad5CMV-p53 in vivo. These studies also confirmed that the risk of insertion of the p53 DNA into the host cell genome is very low and is not increased when cells are exposed to conventional treatments used in cancer therapy. Since then, the use of Ad5CMV-p53 in the clinical has raised major interests.

Clinical studies showed that intratumoral injection of Ad5CMV-p53 resulted in vector-specific *wt-TP53* RNA expression into tumor tissues in patients with various tumor types and showed its ability to selectively kill cancer cells [33–35] (Table 2). These trials also demonstrated that Ad5CMV-p53 was safe and well tolerated with minimal adverse reactions. This minimal toxicity indicates that Ad5CMV-p53 has a high therapeutic index that may allow it to be used in combination with other conventional treatments, such as chemotherapy and/or radiation therapy.

5.2.2. Non-small cell lung cancer (NSCLC)

A first phase I dose-escalation study administering Ad5CMV-p53 as monotherapy was carried out in 15 patients with incurable disease harboring *TP53* mutations [33]. Intratumoral treatment was performed at four different dose levels either by bronchoscopic intratumoral injection or by CT-guided percutaneous injection of the vector solution. Successful transfer of *wt-TP53* was achieved only with higher vector doses. Transient local disease control by a single intratumoral injection of the vector solution was observed in four of six successfully transduced patients. No clinically significant toxicity was observed.

A second phase I study evaluated intratumoral injections of Ad5CMV-p53 in doses ranging from 10^6 to 10^{11} plaque-forming units (PFU) in 28 patients with progressive disease [36]. A total of 84 doses of Ad5CMV-p53 were delivered, with 56 of these doses as repeated injections (up to six injections given monthly). The presence of adenoviral vector DNA in post-treatment biopsy specimens was demonstrated in 18 of 21 of evaluable patients. Therapeutic activity in 25 evaluable patients included partial responses in two patients and disease stabilization (range, 2–14 months) in 16 patients. The remaining seven patients exhibited disease progression. Vector related toxicity was minimal and consisted principally of fevers and pain at the site of injections. The maximum tolerated dose (MTD) was not reached. Because of the low toxicity, 10 patients at the end of the study were able to be treated as outpatients rather than as inpatients. A subset of patients ($n = 12$) included in this phase I dose escalation trial received intralesional administration of Ad5CMV-p53 via bronchoscopic injection [37]. Six of the 12 patients had significant improvement in airway obstruction and 3 patients showed partial response. This report demonstrated that Ad5CMV-p53 can be safely administrated by bronchoscopic injection into endobronchial NSCLC.

In a third phase I study ($n = 25$), Ad5CMV-p53 was delivered into the bronchial passages via repeated instillations [38]. The initial dose was 2×10^9 viral particles (vp) per dose

Table 2
Principal clinical trials using Ad5CMV-p53 for the treatment of cancer

Author	Disease	Trial	*N*	Dose[a]	Route	OR[b]	Main toxicity	Ref.
Swisher	NSCLC	Phase I	28	10^6–10^{11}	IT	2	Fever, pain at site of injections	[36]
Carbone	NSCLC	Phase I	25	2×10^9–5×10^{11}	BI	2	Fever, hypoxia, dispnea	[38]
Schuler	NSCLC	Phase II	25	7.5×10^{12} plus chemotherapy	IT	13	Flu-like syndrome, nausea, fatigue	[40]
Swisher	NSCLC	Phase II	19	3×10^{11}–3×10^{12} plus radiotherapy	IT	12	Fever and chills	[41]
Clayman	HNSCC	Phase I	17	10^6–10^{11}	IT	2	Fever, pain at site of injections, edema	[42]
Buller	Ovary	Phase I	17	7.5×10^{10}–7.5×10^{12}	i.p.	8	Fever, hypotension, abdominal complaints	[48]
Kuball	Bladder	Phase I	11	7.5×10^{11}–7.5×10^{13}	II	ND	Urethral and vesical burning, fatigue	[53]
Cristofanilli	Breast	Phase II	9	2.5×10^{12} plus chemotherapy	IT	9	Fatigue, fever	[55]

[a] Doses are expressed in PFU/dose.
[b] OR: overall responses; NSCLC: non-small cell lung cancer; HNSCC: head and neck squamous cell cancer; IT: intratumoral; BI: bronchial instillation; i.p.: intraperitoneal; II: intravesical instillation.

up to 14 cycles of therapy and this was escalated in 10-fold dose increments. The maximum planned dose of 2×10^{12} vp was tolerated, but one of the four patients at this dose level experienced grade 4 pulmonary toxicity and another died about 1 month after his second cycle. A cohort of 10 patients was therefore treated at the recommended phase II dose of 5×10^{11} vp. At this dose, no greater than grade 3 toxicity was observed. The most frequent toxicity was fever, and the significant toxicities were all hypoxia and dyspnea as expected. Of the 24 evaluable patients, 1 demonstrated an objective radiographic partial response, 1 showed a pathologic response in the treated lobe, 17 showed stable disease and 7 showed progressive disease 4 weeks after starting therapy. The drug was well tolerated and subjectively improved breathing was noted in many patients.

Ad5CMV-p53 clinical activity was also evaluated in combination with either chemical or radiation-based therapies by Nemunaitis et al. [39]. In this phase I study, 24 patients with advanced NSCLC and abnormal p53 function were administered intravenous cisplatin 80 mg/m^2 on day 1 and Ad5CMV-p53 on day 4 (doses ranging from 10^6 to 10^{11} PFU) for a total of up to six courses (28 days per course). Transient fever related to vector injection was developed in eight of 24 patients. Of 23 assessable patients, 2 patients achieved a partial response and 17 patients achieved a stable disease. In biopsy samples, an increase of a mean apoptotic index from 0.01 to 0.044 ($P = 0.011$) was detected. Intratumor transgene mRNA was identified in 43% of assessable patients. This study showed that intratumoral injection with Ad5CMV-p53 in combination with cisplatin seems to be well tolerated and to be clinically active.

In a multicenter phase II study, 25 incurable NSCLC patients received a combination of intratumoral injection of Ad5CMV-p53 (7.5×10^{12} PFU; day 1) with carboplatin (area under the curve, 6; day 1) plus paclitaxel (175 mg/m^2, day 1) or cisplatin (100 mg/m^2, day 1) plus vinorelbine (25 mg/m^2, days 1, 8, 15 and 22) [40]. In the group treated with carboplatin plus paclitaxel, no additional benefit could be found in lesions treated with Ad5CMV-p53 therapy. In contrast, the group treated with cisplatin plus vinorelbine exhibited a difference in the local effect from gene therapy combined with chemotherapy, which was most pronounced after the second and third cycles. This study suggested some additional local effects from Ad5CMV-p53 treatment on the background of a less than optimal response to systemic chemotherapy. In contrast, Ad5CMV-p53 therapy does not appear to provide an additional benefit, if the overall response to systemic chemotherapy is optimal. Finally, combinatorial approach did not generate the additional toxicity associated with platinum compounds.

Finally, a phase II study evaluated Ad5CMV-p53 combined with radiation therapy in 19 non-metastatic patients who were not eligible for chemoradiation or surgery. Ad5CMV-p53 was injected intratumorally (doses from 3×10^{11} to 3×10^{12} viral particles) on days 1, 18 and 32 in conjunction with conventional radiation therapy (60 Gy) over 6 weeks [41]. The most common adverse events were grade 1 or 2 fevers and chills. Ad5CMV-p53 did not appear to increase the side effects caused by radiation treatment. Of the 19 patients, 12 (63%) had complete or partial responses at the injection site 3 months after completing the treatment. Responses were pathologically confirmed by biopsies. Further randomized trials are expected to follow on these results.

5.2.3. Head and neck cancer

A phase I clinical trial with Ad5CMV-p53 showed data on 17 evaluable patients with incurable recurrent local or regionally metastatic tumors [42]. Patients received multiple intratumoral injections of Ad5CMV-p53 with doses from 10^6 up to 10^{11} PFU. Two patients showed objective tumor regressions of greater than 50% and six patients showed stable disease for up to 3.5 months. Progressive disease was observed in nine patients. One resectable patient presented a complete pathologic response. No dose-limiting toxicity or serious adverse events were noted.

In phase II studies, 150 patients have been treated in three coordinated trials, which evaluated various dosage levels and schedules of Ad5CMV-p53 for safety, tolerance and efficacy [43]. Ad5CMV-p53 was injected intratumorally daily in a schedule of 1, 3 consecutive or 6 bi-consecutive days (dose range of 10^9–10^{11} PFU/day) every 4 weeks (one cycle) in patients with recurrent or refractory disease and unresectable tumors. Complete response was achieved in 7 patients, partial response in 10 and stable disease in 29. There has been no toxic death. Related adverse events included self-limited fever and chills and injection site pain.

The data presented in phase I/II safety studies, along with the pharmacokinetic profile, showed a lack of toxicity at therapeutically active doses upon intratumoral administration of Ad5CMV-p53 in 226 patients with head and neck cancer [44,45]. Treatment tolerability was highly acceptable, with no related toxic death. The most frequent related adverse events were fever, chills, flu-like syndrome and pain at the injection site graded mild-to-moderate. The most frequent related serious adverse events were infection and haemorrhage [45]. In 190 patients, Ad5CMV-p53 treatment showed no evidence of horizontal transmission of the vector to household contacts of treated patients. No replication-competent adenovirus outbreaks were detected and Ad5CMV-p53 was shown to be genetically stable. Viable virus was recovered from all body fluids examined in treated patients [45]. Ad5CMV-p53 is currently being evaluated in an international phase III study of patients with head and neck cancer. In this trial, Ad5CMV-p53 is given by direct tumor injection allowing for better transduction and evaluation of delivery.

In October 2003, Ad5CMV-p53 (Gendicine®, Shenzhen SiBiono GeneTch Co. Ltd.) obtained a drug license for head and neck squamous cell carcinoma (HNSCC) from the State Food and Drug Administration of China and became the world's first commercial gene therapy drug for cancer [46]. In the phase I studies, 12 patients with advanced laryngocarcinoma were treated with Ad5CMV-p53 [47]. Locoregional

intratumor injection was conducted every day for a total of 10 injections (doses ranging from 10^{10} to 10^{12} vp). These studies demonstrated that Ad5CMV-p53 therapy was safe at doses up to 10^{12} vp with an early indication of clinical benefits. All patients were free of relapse between 36 and 42 months after Ad5CMV-p53 administration, even though the standard recurrent rate after tumor resection for patients with advanced laryngocarcinoma is approximately of 30% at 36 months. In a multi-center, randomized and placebo controlled phase II study, intratumor injections of Ad5CMV-p53 (10^{12} vp/dose/week for a total of 8 weeks) were administered alone ($n = 45$) or in combination with radiation therapy (70 Gy/8 weeks) to advanced HNSCC patients [47]. The results revealed that Ad5CMV-p53 gene therapy is safe and efficacious as compared to radiation therapy alone. Side effects were mainly self-limited fever (I/II grade) occurring in approximately 31% patients. Complete regression was achieved in 29 patients (64.7%) in the combinatory group against 9 of the radiotherapy group (20%).

5.2.4. Ovarian cancer

A phase I trial evaluated monotherapy with Ad5CMV-p53 in 17 heavily pretreated recurrent patients [48]. Ad5CMV-p53 was administered i.p. as a single dose escalated from 7.5×10^{10} to 7.5×10^{12} PFU. Vector-specific transgene expression in tumor was documented by rt-PCR in cells from both ascitic fluid and tissue biopsies at doses as low as 7.5×10^{10} PFU/single dose. The maximum tolerated dose (MTD) was not established. Likewise, no dose-limiting toxicity resulted from the delivery of 236 doses of Ad5CMV-p53. Fever, hypotension abdominal complaints, nausea and vomiting were the most common adverse events. CA125 responses, defined as a greater than 50% decrement in serum CA125 from baseline, were documented in 8 of 16 women who completed three cycles. There were no objective responses documented by computed tomography scan. On the contrary, the best CT responses were three cases of stable disease. Long-term follow up showed that the median survival for single-dose administration of Ad5CMV-p53 was of 5 months [49].

A second phase I study administered Ad5CMV-p53 i.p. to 17 patients with heavily pretreated metastatic epithelial ovarian cancer [50]. The compound was given daily for 5 days every 3 weeks at doses ranging from 3×10^{10} to 3×10^{12} PFU. No dose-limiting toxicities were observed. Common toxicities were abdominal pain, fever, myalgias and chills. One patient had grade 3 edema and headache. There were no hematological toxicities. Of 11 evaluable patients, 6 had stable disease after four courses of therapy and 5 patients progressed after two courses of therapy.

When administered as combinatory chemotherapy, the administration of multiple cycles of Ad5CMV-p53 (i.p.) with gemcitabine showed a synergistic effect to treat recurrent disease [51]. Another study also showed that, in heavily pretreated recurrent ovarian cancer, combination of Ad5CMV-p53 with platinum-based chemotherapy had significant clinical activity [49].

5.2.5. Other tumors

Phase I studies were also conducted in other tumor types. In recurrent glioblastoma patients, Lang et al. reported that intratumoral injection of Ad5CMV-p53 (doses ranging from 3×10^{10} to 3×10^{12} PFU) was associated with minimal toxicity and resulted in transfer of the *TP53* gene and expression of a functionally active p53 protein [52]. However, with the bolus injection method used in this trial, the distribution of Ad5CMV-p53 was limited to a short distance from the injection site.

In patients suffering from bladder cancer, Ad5CMV-p53 was administrated on day 1 as a single intratumoral injection (7.5×10^{11} PFU) at cystoscopy or as a single intravesical instillation at three dose levels (7.5×10^{11} to 7.5×10^{13} PFU) [53]. Specific transgene expression was detected in tissues from seven of eight assessable patients treated with intravesical instillation of Ad5CMV-p53 but in none of three assessable patients treated with intratumoral injection. In this study, side effects were local and of transient nature and the dose-limiting toxicity was not reached. Another phase I data on Ad5CMV-p53 in the treatment of locally advanced bladder cancer have shown intravesical instillation (up to 10^{12} vp daily for 4 days) to be safe and well tolerated [54]. Asymptomatic shallow mucosal ulcerations were seen only in one patient and mostly resolved by day 28. Two patients were clinically disease free 23 months after treatment, while seven patients progressed after 2 months.

In 12 locally advanced breast cancer patients, intratumoral injection of Ad5CMV-p53 (2.5×10^{12} vp on days 1 and 2 of a 21-day cycle) was administered combined with docetaxel (75 mg/m^2 i.v.; day 1), doxorubicin (50 mg/m^2 i.v.; day 1) and prophylactic G-CSF [55]. After 66 delivered cycles, toxicity was mainly fatigue and fever. One patient showed neutropenic infection. Objective clinical responses were observed in 90% of patients; however, almost all patients had residual pathologic foci of disease in the breast.

In a phase I/II trial in eight patients with advanced esophageal cancer, tumors were locally injected with Ad5CMV-p53 twice weekly for 2–5 months [56]. Of seven evaluable patients, only one had progressive disease. The drug was well tolerated, with pain and mild fever noted. Similar results were reported by Dummer et al. in patients with metastatic melanoma ($N = 5$) [34].

5.2.6. Problems related to the use of Ad5CMV-p53

For Ad5CMV-p53, heterogeneity or indeed lack of expression of receptors (CAR) and co-receptors (integrin $\alpha v\beta 3$ and $\alpha v\beta 5$ classes) in tumors could be implicated in the poor efficiency of infectivity by the vector [57]. This infection efficiency can be also impeded by the presence of adenovirus-neutralising antibodies. The inadequacy of p53 gene therapy to induce cell growth inhibition with a potentially disabled downstream p53 pathway could be another explanation for resistance to Ad5CMV-p53. Zeimet and Marth suggested that epigenetic deregulation or the dominant-negative effect of mutant p53 could contribute to this process, i.e. the p53 func-

tional inactivation [57]. Interestingly, while these alternative p53 inactivation mechanisms lead to resistance to Ad5CMV-p53 in tumor cells, ONYX-015 therapy takes advantage of this p53 inactivated status and it is efficient with an apparent non-selective oncolytic activity in some tumors where p53 wild-type is expressed.

6. Killing p53-deficient cells with modified adenoviruses

The use of E1B-defective adenoviruses represents an extremely promising approach to take advantage of *TP53* status as a basis for cancer therapy. This approach is essentially different from "replacement" gene therapy. Indeed, it does not involve transfer of a *TP53* gene into cells, but requires the introduction of genetically modified viruses that will take advantage of dysfunctional p53 in cancer cells to selectively kill them.

DNA tumor viruses, such as adenoviruses infect quiescent cells and induce them to enter the S phase of the cell cycle so that viral DNA replication can proceed. The adenovirus E1A protein, which binds pRB, p300 and other related proteins, is largely responsible for this forced entry into S phase. The E1B region of the viral genome encodes a 55 kDa protein (E1B 55K) that binds and inactivates p53 in infected cells. This binding is essential to virus replication, possibly because E1A induces p53-dependent apoptosis [58]. Thus, an adenovirus deficient for the E1B protein may replicate only in cells that are deficient for p53 function. This should allow selectivity for tumor cells with mutated p53 and spare normal cells.

6.1. ONYX-015

The delta 1520 (dl1520; ONYX-015) virus is a human group C mutant adenovirus that contains a 827 bp deletion in the E1B region and a point mutation at codon 2022 that generates a stop codon preventing expression of a truncated protein from residual portions of the deleted gene. ONYX-015 can replicate in both tumor and non-cancer cells that lack functional p53, showing a cytopathic effect for tissues expressing an abnormal *TP53* gene, without damaging normal tissue (Fig. 2).

In in vitro experiments ONYX-015 has been shown to kill cervical carcinoma cells, colon carcinoma cells, glioblastoma cells and pancreatic adenocarcinoma cells lacking functional p53 with an efficiency comparable with that of wild-type adenovirus [59,60]. It was also demonstrated that this virus caused a significant reduction in tumor size of human p53-deficient xenografts in nude mice [60–62]. Treatment with ONYX-015 could also sensitize p53-deficient cancer cells radiotherapy [63,64]. From animal studies, it appears that ONYX-015 efficacy is independent of the route of administration. Tumor cytotoxicity is enhanced when divided multiple doses are used and when conventional chemotherapy agents are administered prior to or concurrent with ONYX-015.

Questions surrounding ONYX-015 regarding its mechanism of action and selectivity for p53-deficient cells remain unanswered. Indeed, several reports have indicated that both wild-type adenovirus (wt-Ad5) and ONYX-015 replicate in various cells irrespective of their p53 status [65,66]. Such data are generally inconsistent with the proposed model for selective destruction of tumor cells by ONYX-015. Furthermore, in clinical trials, drug treatment induced objective responses in tumors with mutant or *wt-TP53* without substantial damage to normal tissue. A study by Ries et al. provides a mechanistic basis for this phenomenon [67]. This study demonstrated that ONYX-015-induced cell lysis can occur in cells with *wt-TP53* if mutations affecting other genes in the p53 pathway are present, effectively rendering the cell p53-deficient. However, the detailed mechanism of cell selectivity is still a matter of debate [65,68]. Hann and Balmain have analyzed ONYX-015 replication in primary human epithelial

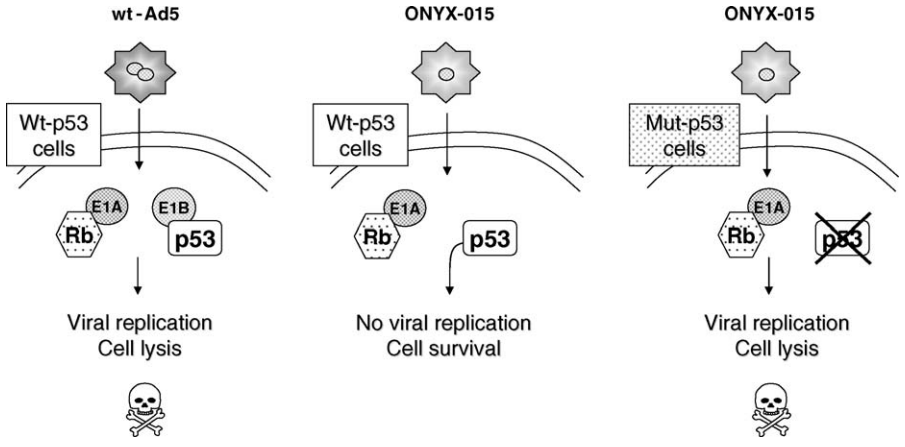

Fig. 2. Principle of ONYX-015-based therapy. Replication of a wild-type adenovirus (wt-Ad) in normal cells results in cell lysis. In contrast, ONYX-015 (E1B-deleted adenovirus) cannot replicate in normal cells due to the suppressive effect of wild-type p53, thus cells survive to the infection. However, in p53-deficient cells, the defective virus can replicate inducing cell lysis.

cells expressing either dominant-negative or gain-of-function mutant *TP53* genes [69]. Of all mutant alleles examined, only mutant R248W (that has lost its DNA-binding activity but retains a global conformation close to that of wt-p53) could significantly facilitate ONYX-015 replication. Hsieh et al. also showed that by binding to functional p53 protein, the Hepatitis B virus X protein could render liver cells more susceptible to infection with a E1B-deleted adenovirus [70]. Therefore, the nature of *TP53* mutation and the presence of HBV in cancer cells may affect the lytic properties of the recombinant virus in tumor cells.

To date, most trials have used intratumoral injection to deliver ONYX-015 into tumors. Recent phase I studies have also addressed feasibility of harmless ways to deliver the viral particles, such as i.p., i.a. and i.v. administration either alone or in combination with chemotherapy and/or immunotherapy [71–75]. Another recent trial has assessed the feasibility of topical administration of ONYX-015 as a mouthwash in patients with premalignant dysplastic lesions of the oral mucosa [73]. All these studies have demonstrated good tolerability at maximum administered dosages (10^{13} PFU) without reaching the dose-limiting toxicity (DLT). The most commonly reported toxicities were flu-like symptom and injection-site pain being. Toxicity appears to be related to route of administration. The virus is actually dispensed in saline. Alternative carriers have been investigated in preclinical trials, with higher rates of infectivity shown using 1% lignocaine or 200 IU/ml hyaluronidase.

Like other adenoviruses, ONYX-015 is presumably cleared by immune mechanisms, although this has not been studied extensively. Exposure to ONYX-015 induces neutralizing-antibody production irrespective of route of administration but this does not appear to inhibit efficacy or interfere with future dosing [72,76,77]. Circulating ONYX-015 genome has been detected up to 10 days after injection into patients with head and neck cancer. Moreover, Wadler et al. noticed that the recombinant virus was not only present but capable of replicating in tumor cells up to 1 week after injection [78].

ONYX-015 appears to have activity against some cancers, especially when combined with conventional cytotoxic chemotherapy (Table 3). Employing it injection with chemotherapy has led to sustained responses.

6.2. Head and neck cancer

In a phase I study in patients with recurrent and refractory disease, ONYX-015 was administered by a single intratumoral injection (doses from 10^7 to 10^{11} PFU) to a total of 22 patients [76,79]. Treatment was well tolerated, with the main toxicity being grade 1/2 flu-like symptoms. Two patients did experience mild pain on injection site, and this was related to the volume of the injected solution. The pain resolved within 1 h and rarely required any further analgesia. Using conventional response criteria, no objective responses were observed. However, magnetic resonance imaging scans were suggestive of tumor necrosis at the site of viral injection in five patients. Of these five cases, four had mutant p53 tumors with response duration lasting from 4 to 12 weeks. Safety data showed that no virus was detected in either blood samples or the injection site and oropharyngeal swabs, suggesting that virus shedding was not a major issue.

Two phase II studies were initiated in patients with recurrent and refractory disease, one using ONYX-015 as monotherapy and the second in combination with standard chemotherapy (cisplatin and 5-FU). The first study was initiated in 40 patients with recurrent and refractory tumors [80]. Patients received intratumoral injections of ONYX-015 (10^{10} PFU/day) for either 5 consecutive days (standard regimen; $n = 30$) or twice daily for 2 consecutive weeks (hyperfractionated regimen; $n = 10$) during a 21-day cycle. Treatment-related toxicity included mild to moderate fever (67% overall) and injection site pain (47% on the standard regimen, 80% on the hyperfractionated regimen). Standard treatment resulted in 14% partial to complete regression, 41% stable disease and 45% progressive disease rates. Hyperfractionated treatment resulted in 10% complete response, 62% stable disease and 29% progressive disease rates. The per-

Table 3
Principal clinical trials using ONYX-015 for the treatment of cancer

Author	Primary site	Trial	*N*	Dose[a]	Route	OR[b]	Main toxicity	Ref
Ganly	HNSCC	Phase I	22	10^7–10^{11}	IT	0	Fever, pain at site of injections	[76]
Nemunaitis	HNSCC	Phase II	40	SR: 10^{10} d1–5; HR: 10^{10} d1–15	IT	SR: 4; HR: 1	Fever, pain at site of injections	[43]
Khuri	HNSCC	Phase II	37	SR: 10^{10} d1–5 plus chemotherapy	IT	19	pain at site of injections, mucositis	[81]
Reid	Colon	Phase II	35	2×10^8–2×10^{12} days 1 and 8 (two cycles)	i.a.	2	Fever, rigors, fatigue	[77]
Makower	Liver	Phase II	19	6×10^9–3×10^{11}	IT	1	Fever, hepatic toxicicity, anemia	[84]
Mulvihill	Pancreas	Phase I	23	10^8–10^{11}	IT	0	Pancreatitis	[85]
Hecht	Pancreas	Phase II	21	2×10^8–10^{11} plus chemotherapy	IT	2	Pancreatitis, sepsis, duodenal perforation	[86]
Vasey	Ovary	Phase I	16	10^9–10^{11}	i.p.	0	Abdominal pain, diarrhea	[74]
Galanis	Sarcoma	Phase I	6	10^9–10^{10} days 1–5 plus chemotherapy	IT	1	Anorexia, fatigue, myalgia, rigors	[89]

[a] Doses are expressed in PFU/dose.
[b] OR: overall responses; HNSCC: head and neck squamous cell cancer; SR: standard regimen; HR: hyperfractionated regimen; IT: intratumoral; i.a.: intra-arterial; i.p.: intraperitoneal.

sistent viral detection observed in two patients 10 days after the last injection suggested that a viral replicative process was ongoing, although it did not persist since none of the samples tested showed evidence of circulating viral genome more than 17 days after the last injection.

The most promising data have emerged from the second phase II study combining ONYX-015 with cytotoxic chemotherapy [81]. This trial enrolled 37 patients with recurrent and refractory squamous cell carcinoma. Patients were treated with intratumoral injections of ONYX-015 (10^{10} PFU/day; days 1–5) with i.v. cisplatin (80 mg/m^2 intravenously over 4 h; day 1) and 5-fluorouracil (800–1000 mg/m^2 continuous infusion per day; days 1–5). Treatment caused an overall response rate of 63% with eight (27%) complete responses. There was no correlation between response and *TP53* gene status. By 6 months, none of the responding tumors had progressed, whereas all non-injected tumors treated with chemotherapy alone had progressed. The toxic effects that occurred were acceptable. The most common adverse events related to ONYX-015 were injection site pain and mucous membrane disorder. Of these two, 29% were grade 3 and 11% were grade 4. No treatment-related deaths occurred. Tumor biopsies obtained after treatment showed tumor-selective viral replication and necrosis induction. In this study, ONYX-015 combined with cisplatin and 5-FU was active as a method of local control in most patients. Whether this enhanced local control would be translated into a survival advantage remains to be confirmed by phase III trials.

6.3. Gastrointestinal cancers

ONYX-015 was also administrated in phase I/II studies to patients with liver metastatic gastrointestinal cancer, principally of colorectal origin [75,77,82]. In this study, the compound was infused into the hepatic artery (doses of 2×10^8–2×10^{12} vp; days 1 and 8 for two cycles). Of the 35 enrolled patients, 7 were treated in a dose-escalation phase and 28 were treated with the highest dose level in combination with i.v. 5-fluorouracil and folinic acid (Mayo regimen given every 4–5 weeks starting on day 2). Patients without evidence of disease progression were permitted to have up to eight treatments with ONYX-015 combined with 5-FU/folinic acid. No dose-limiting toxicity, maximally tolerated dose or treatment-emergent clinical hepatotoxicity was identified. Mild to moderate fever, rigors and fatigue were the most common adverse events. The median survival was 12 months among a population of patients with extensive prior therapy [77]. A more detailed and recent report focused on the patients treated with ONYX-015 who had failed prior therapy with 5-FU/folinic acid showed that despite the extensive prior therapy, the median survival of these patients was 10.7 months, 46% were alive at 1 year and two patients (8%) had partial responses [82]. Viral genomes were detected in the blood of patients 2–9 days following infusion of ONYX-015 despite high levels of neutralizing antibody.

A second phase II trial reported the results of ONYX-015 in 18 patients with refractory metastatic colorectal cancer [83]. ONYX-015 was administered i.v. at a dose of 2×10^{12} vp every 2 weeks. Common toxicities included flu-like symptoms, nausea and emesis. Seven patients were assessed as having stable disease after 2 months of treatment, whereas two patients were considered to have stable disease after 4 months. Detectable circulating ONYX-015 DNA was identified in 36% of patients 72 h after last infusion, which was suggestive of ongoing viral replication.

Another phase II trial was recently conducted in 19 unresectable patients with hepatobiliary tumors, who underwent intralesional ONYX-015 injection (doses of 6×10^9 or 10^{10} PFU/lesion up to a total dose of 3×10^{10} PFU) [84]. Serious toxicities (>grade 2) were uncommon and included hepatic toxicity (three patients), anemia (one patient), infection (one patient) and cardiac toxicity (one patient, atrial fibrillation). Of 16 evaluable patients, 1 had a partial response, 1 had prolonged disease stabilization and 8 had a reduction of tumor markers superior to 50%. Viral shedding was confined to bile (two of two patients) and ascites (four of four patients).

Mulvihill et al. carried out a phase I dose escalation study of ONYX-015 in 23 patients with unresectable pancreatic cancer [85]. ONYX-015 (doses of 10^8 PFU up to 10^{11} PFU) was administered via CT-guided injection or intraoperative injection into pancreatic primary tumors every 4 weeks until tumor progression. Although a mild, transient pancreatitis was noted in one patient, injection was generally well-tolerated. Maximally tolerated doses and dose-limiting toxicities were not reached. Viral replication was not documented. No objective responses were demonstrated.

In addition, synergistic or additive efficacy of ONYX-015 and chemotherapy has been documented in locally advanced pancreatic cancer clinical trials. In a study enrolling 21 patients, ONYX-015 was combined with gemcitabine [86]. Patients underwent eight sessions of ONYX-015 (2×10^8 or 10^{11} vp/treatment) delivered by endoscopic-ultrasound-guided injection into the primary pancreatic tumor over 8 weeks. Gemcitabine was delivered at doses of 1 g/m^2 for the last 4 weeks. This trial reported two patients with sepsis, one patient with an asymptomatic fluid collection after injection and two patients with duodenal perforations. The authors believe that these events were related to injection technique rather than the agents used. No clinical pancreatitis occurred despite mild, transient elevations in lipase in a minority of patients. After combination therapy, 2 patients had partial regressions of the injected tumor, 2 had minor responses, 6 had stable disease and 11 had progressive disease or had to go off study because of treatment toxicity.

6.4. Other cancers

In patients with ovarian cancer, ONYX-015 i.p. was administered to 16 women with recurrent/refractory ovarian

cancer in a phase I trial [74]. Patients received 35 cycles (median, two cycles) of ONYX-015 delivered on days 1–5 in four dose cohorts: 10^9, 10^{10}, 3×10^{10} and 10^{11} PFU. The most common significant toxicities related to virus administration were flu-like symptoms, emesis and abdominal pain. One patient in the second cohort developed grade 3 abdominal pain and diarrhea, which was dose-limiting. The maximum-tolerated dose was not reached at 10^{11} PFU, and at this dose level patients did not experience significant toxicity. There was no clear-cut evidence of clinical or radiologic response in any patient. One hypothesis to explain the failure of ONYX-015-based oncolytic effect in ovarian cancers may be the lack of expression of coxsakie/adenovirus receptors (CAR) and integrin co-receptors on the surface of ovarian tumor cells [67,87,88]. Indeed, attachment of adenoviruses to the target cell surface is mediated through CAR and integrin co-receptor, and thus CAR deficiency may be a biological basis of resistance to adenovirus-based therapies.

In six patients with advanced sarcomas, ONYX-015 was administered in combination with chemotherapy [89]. ONYX-015 (10^9–10^{10} PFU/dose; days 1–5) was injected intratumorally in liver ($n = 4$) or chest wall masses ($n = 2$) in combination with MAP (mitomycin-C, doxorubicin, cisplatin). ONYX-015 was very well tolerated with only minor toxicities attributed to virus alone being grade 1 fever or grades 1–2 pain at the injection site. The toxicities related to both ONYX-015 and MAP chemotherapy were also mild and consisted mainly of anorexia, fatigue, myalgia and rigors. Dose-limiting toxicity was not encountered. There was evidence of anti-tumor activity in one out of six patients. Adenoviral replication was detected in two out of six patient biopsies on day 5 of the first cycle.

In 10 patients with advanced carcinoma metastatic to the lung, results of a phase I dose-escalation study of ONYX-015 gave some evidence of the drug concentrating in malignant tissue following its i.v. administration at dose levels between 2×10^{10} and 2×10^{13} PFU (administrated weekly within 21-day cycles) [80]. No dose-limiting toxicity was identified. Mild to moderate fever, rigors and a dose-dependent transient transaminitis were the most common adverse events. Intravenous infusion allowed detectable intratumoral viral replication. These results were confirmed in other clinical trials of ONYX-015 administered in combination with chemotherapy or interleukin-2 [72]. Clinical data was also obtained in a phase I study in five patients with breast cancer after administration of ONYX-015 (intratumorally; 10^9 PFU/dose). In two of the five patients, adenovirus, tumor necrosis and neutralizing antibodies were detected. No toxicities were reported except one complaint of chest pains. No clinical response was detected in the two patients [90].

6.5. Oral dysplasias

As dysplastic lesions of the oral epithelium are known precursors of oral cancer and as significant proportion of these lesions have functional defects in p53 response pathways, Rudin et al. administrated ONYX-015 as a mouthwash to patients with clinically apparent and histologically dysplastic lesions of the oral mucosa [73]. A total of 22 patients (19 assessable patients) were enrolled onto the study. Patients rinsed and 'held' for 30 min a 15 m solution of ONYX-015. Cohorts of patients were treated on three different sequentially tested regimens. Cohort 1 ($n = 7$) consisted of patients who were administered ONYX-015 10^{10} PFU daily for 5 days, with cycles repeated every 4 weeks for a maximum of 12 cycles. Cohort 2 ($n = 12$) were administered a similar dose-intensity, receiving once-weekly administration of ONYX-015 10^{10} PFU for 24 weeks. Patients in cohort 3 received ONYX-015 10^{11} PFU daily for 5 days, followed by weekly administration over the next 5 weeks. This 6-week block was repeated in weeks 7–12.

Histologic resolution of dysplasia was seen in 7 (37%) of 19 patients, and the grade of dysplasia improved in 1 additional patient. The majority of responses were transient. The mouthwash was well tolerated without any grade-3 toxicities. Only one of seven patients demonstrated an increase in circulating anti-adenoviral antibody titer while on therapy. Histological response correlated with a decrease in p53 positivity over time. Viral replication was confirmed in two of three lesions examined. This approach to cancer prevention was tolerable, feasible and has demonstrable activity. Future development could include other premalignant lesions, such as cervical dysplasias or Barrett's esophagus.

6.6. Problems related to the use of ONYX-015

Similarly to Ad5CMV-p53, heterogeneity or indeed lack of expression of receptors (CAR) and co-receptors (integrin $\alpha v\beta 3$ and $\alpha v\beta 5$ classes) in tumors could be implicated in the poor efficiency of infectivity by ONYX-015 [57]. In addition, many tumors cells fail to support ONYX-015 oncolytic replication. In contrast to permissive tumor cell lines, refractory tumor cells infected with ONYX-015 failed to shut down cellular protein synthesis in the absence of E1B-55K. When a heat shock is applied, resistant cells are sensitized to the cytolytic activity of this agent [91]. It is well established that heat shock proteins are commonly upregulated in tumor cells. Therefore, the induction of a heat shock response by the use of pharmacological inducers of a heat shock response (e.g. benzoquinoid ansamycins) or by local hyperthermia could represent a promising strategy to improve ONYX-015 efficiency in cancer therapy.

7. Pharmacological modulation of p53 protein functions

Conceivably, modulation of wt-p53 can exert different, if not opposite, effects depending on the target cells and the clinical context. In tumor cells with *wt-TP53* gene, increasing the

activity of p53 may help to increase the response to therapy and to eliminate these cells. In contrast, in non-tumor cells, it is possible that increasing p53 protein function may activate a physiological, "guardian-of-the-genome" effect that contributes to the protection against the toxic effects of cancer treatment. However, the opposite hypothesis is also under investigation: in non-tumor cells, it may be beneficial to transiently switch off p53 function to suppress the apoptotic response induced by therapeutic agents, and therefore protect against secondary effects.

7.1. p53 activation

The most direct mechanism for inducing an accumulation of wild-type p53 is to disrupt its negative regulation by mdm-2. This protein is transcriptionally activated by the binding of p53 to a p53-responsive element within the mdm-2 gene. Mdm-2 then binds to the N-terminus of p53, thereby preventing p53 from interacting with the transcriptional machinery and inducing its degradation by the proteasome. In 1997, Bottger et al. designed a synthetic mdm-2-binding miniprotein that specifically targets the p53-binding site [92]. This was achieved by expressing a mdm-2-binding peptide within the active site loop of the bacterial thioredoxin protein. This new protein, designated SuperTIP (Thioredoxin Insert Protein), was shown to compete with mdm-2 for binding to p53 and to activate p53-dependent transcription, leading to nuclear accumulation of p53 and cell cycle arrest.

More recently, Vassilev et al. identified a family of synthetic compounds, the nutlins [93]. These molecules can potently displace p53 from the p53-binding pocket on mdm-2. As predicted, the compounds effectively trigger p53 activation, cell-cycle arrest and apoptosis in tumor cells that retain normal p53, but are inactive in tumors that have mutant p53. When applied to normal cells they induce growth arrest but not apoptosis, and the growth arrest is reversible when the compounds are washed away. In animal xenograft models, nutlins controlled the growth of tumors without apparent toxicity to the normal tissue. Other approaches to inhibit the p53–mdm-2 interaction using synthetic molecules have also been proposed [94].

Another potentially interesting biochemical pathway that may activate p53 involves polyamines. These molecules are essential regulators of cell growth through multiple mechanisms that are still largely unknown. Synthetic polyamines analogs have been shown to activate p53 function in a number of cultured cell lines [95,96]. In agreement with this hypothesis, a chemical inhibitor of ornithine decarboxylase, DFMO (alpha-difluoromethylornithine), also induced p53 protein accumulation [97]. It has been proposed that these effects are due to increased levels of p53 mRNA. These results suggest that polyamines may play a role in the control of p53 protein conformation and activity. Further experiments are needed to determine whether using polyamines may be a clinically achievable approach to modulate p53 function.

7.2. p53 inhibitors

Pifithrin is a synthetic compound that blocks p53 expression at the transcriptional level (Fig. 3) [98]. This compound rescues wt-p53 cells from apoptotic death induced by irradiation and various cytotoxic drugs including doxorubicin, etoposide, paclitaxel and ara-C [98]. Thus, pifithrin may be used to reduce the side effects of radiation therapy or chemotherapy in patients with human cancers. Recent articles essentially reported successful administration of pifithrin in animal models as a protector against secondary effects of drugs, rather than as a cytotoxic therapeutic molecule [99–102]. However, pifithrin could act as an activator of the p53 pathway promoting doxorubicin-induced apoptosis in mouse epidermal JB6 C141 cells [103].

7.3. Re-activation of wt-p53 activity in mutant p53

Mutant p53 proteins differ from each other by their biological properties. While some mutants have totally lost wild-type p53 function, some other mutations are not associated with irreversible loss of wild-type activity. The key biochemical activity of p53 that is altered by mutation is the sequence-specific DNA-binding. This activity is regulated by two C-terminal domains, which specify protein oligomerization (residues 325–363) and negative control of DNA-binding (residues 363–393) (Fig. 1). Inhibition of the latter domain is crucial for high-affinity binding to DNA. Several experimental studies have shown that it is possible to target this domain specifically with peptides or proteins

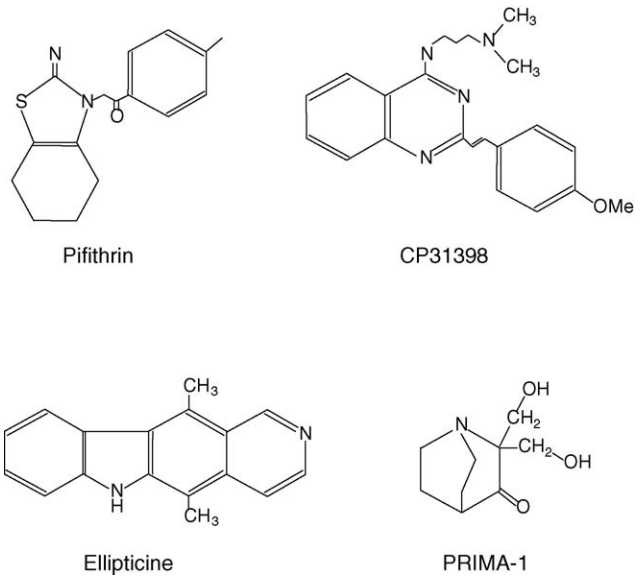

Fig. 3. Small molecules used for targeting wild-type or mutant p53. Pifithrin is a synthetic compound that blocks p53 expression at the transcriptional level. CP31398 is a small molecule that is able to stabilize the p53 core domain. Ellepticine has the ability to restore mutant p53 transcription function. Finally, PRIMA-1 is able to restore the DNA-binding property of a wide range of mutant p53 proteins.

that neutralize the negative regulation exerted by the extreme C-terminus.

Single chain antibody fragments (scFvs) are polypeptides derived from monoclonal antibodies, in which the variable light and heavy chains are connected via a flexible linker. For example, the stable association of scFV421 and scFv11D3 (generated from the mouse PAb421 and 11D3 monoclonal antibodies) with p53 efficiently restored the DNA-binding activity of some mutants in vitro [104]. In human tumor cells, these scFvs showed ability to partially restore the transcriptional activity of mutant p53. Using a similar approach, Govorko et al. have constructed an scFv antibody gene library generated from a mouse immunized with an epitope, which is cryptic in wild-type p53 but exposed in a wide range of mutants. They isolated a scFv, ME1, bound to mutant p53 but not to wild-type p53 [105]. This type of molecules belongs to a new family of potential therapeutic agents, termed "trabodies" (transcription-activating-antibodies).

Several small chemicals have been developed that stabilize the folding of the DNA-binding domain of p53, and thus limit the functional consequences of common *TP53* mutations. For example, a family of short molecules containing two hydrophobic groups bridged by a linker has recently been developed, that can bind within the DNA-binding domain of p53 and stabilize its structure by providing additional rigidity. These compounds protect wild-type p53 from denaturation by thermal stress and partially restore the capacity of several mutants to react with antibodies specific for the wild-type form of p53. When added to cultured cells expressing mutant p53, these chemicals can stimulate the transcription of a p53-dependent reporter gene. Furthermore, one of these chemicals, CP-31398, has been shown to inhibit the growth of small xenografts of human tumor cell lines into nude mice, at doses which did not induce significant adverse effects (Fig. 3) [106]. These preliminary results need to be further confirmed in other preclinical studies.

Other small chemicals with preferential anti-proliferative activity towards cells that carry mutant *TP53* were developed. These compounds were shown to induce the expression of p53-target genes, such as p21/WAF-1 and BAX, in cells expressing mutant *TP53* but not in *TP53*-null cells, suggesting that their activity is based on the rescue of mutant p53 proteins. An example of these compounds is the 9-hydroxyellipticine (9-HE), which was shown to cause induction of apoptosis in the G1 phase of the cell cycle in cell lines expressing a mutant p53 protein (Fig. 3) [107]. Another example is PRIMA-1, which is able to restore the DNA-binding property of a wide range of mutant p53 in vitro, including most common "hotspots" mutants (Fig. 3). Treatment of mutant *TP53*-expressing cells with PRIMA-1 results in the activation of several p53-target genes [108,109]. In contrast, *wt-TP53*-expressing cells do not exhibit any p53 stabilization or induction of p53-target genes upon treatment with PRIMA-1. Furthermore, PRIMA-1 is able to induce apoptosis in cells expressing p53 mutant, but not in cells with a wild-type p53. Pilot in vivo experiments using SCID mice bearing xenografts of human tumor cells have shown that PRIMA-1 exerted a mutant p53-dependent anti-tumor effect without any apparent toxic side effect [108,109]. The mechanism by which PRIMA-1 acts on mutant p53 is still unknown.

With the mutant p53 rescuing strategy, the great challenge lies in the fact that the target may be viewed as not one protein, but many, because of the wide spectrum of tumor-associated p53 mutations [110]. Thus, further investigations are needed to precise the way they act at the molecular level but also to optimize their structures and to perform clinical trials.

8. Other strategies

8.1. Use of vaccinia vectors

Several studies have reported success in using viral vectors derived from the vaccinia virus as candidates for delivering *TP53* gene for therapy. Timiryasova et al. have analyzed the effect of local injection of a recombinant p53-expressing vaccinia vector in nude mice bearing implanted glioma cells [111,112]. Injection of the viral vector induced a major oncolytic effect, probably due to p53-mediated cell apoptosis. This effect was increased when injection was accompanied by radiotherapy [112]. No overt signs of toxicity were observed. In another study, Chen et al. have proposed that combination therapy with vaccinia-mediated *TP53* and cytokine genes (such as interleukin-2 and interleukin-12) may offer prospect for synergistic anti-tumor response [113].

8.2. Viral delivery of chimeric TP53 constructs

Conseiller et al. have built a chimera tumor suppressor, CTS1, based on a *wt-TP53* in which the NH_2- and COOH-terminal domains have been substituted with heterologous sequences [114]. The rationale for replacing these two domains is that they both play roles in p53 protein inactivation, either through mdm-2-dependent degradation (N-terminus) or through allosteric regulation of DNA-binding (C-terminus). CTS1 was obtained by fusion of the VP16 activation domain, and of an optimized leucine-zipper domain, respectively, at the N- and C-termini of the p53 core domain (amino acids 75–325). The chimera was found to have a constitutive, p53-like activity in suppressing cell growth and inducing apoptosis. This activity was resistant to inactivation by mdm-2 as well as to dominant-negative inhibition by mutant p53.

Adenovirus-mediated transfer of CTS1 in tumor cell lines showed that the chimera was significantly more efficient than the same vector containing wild-type p53 [115]. In fact, the chimera induced prolonged expression of p53 and showed a higher inhibition of tumor growth [114]. These results were confirmed in vivo in pre-established tumor developed

in nude mice [114,115]. In another study, Naumann et al. have evaluated CTS1 gene transfer therapy for malignant glioma [116]. They reported that an adenovirus encoding CTS1 induced growth arrest and loss of viability in all glioma cell lines examined in synergy with irradiation. Thus, CTS1 gene transfer is a promising strategy for somatic gene therapy.

8.3. Non-viral strategies

Several different, non-viral strategies are presently being examined for their ability to deliver wild-type p53 expression plasmid in vivo and to mediate effective anti-tumor responses. Direct DNA injection and cationic lipid-mediated gene transfer are primary examples. Although generally less efficient than the viral systems described above in actual delivery of the transgene to target cells, the advantages of such non-viral approaches include an apparent tolerance by the immune system, and reduced concerns over safety issues, such as containment.

A phase I trial evaluated the effect of intratumoral injection of a "naked" *wt-TP53* expression plasmid in patients with either primary or secondary liver tumors [117]. This approach has shown only limited effects, as investigators were unable to detect exogenously introduced *wt-TP53* within injected tumors. Some degree of response was, however, noted in patients with primary liver tumors compared with patients with liver metastasis. A more promising non-viral delivery approach uses cationic liposomes, in complex with plasmid DNA carrying the transgene of interest, which can be efficiently endocytozed by mammalian cells [118]. The main advantages of lipid-mediated gene transfer are that the process is relatively non-toxic and non-immunogenic. Injection of a liposome-p53 complex in the tail of nude mice inoculated with breast carcinomas cells resulted in a reduction of tumor size in over 50% of treated animals. Xu et al. also used a cationic immunoliposome system, directed by a lipid-tagged scFv against the human transferrin receptor, as a transfer system to mediate *TP53*-gene therapy [119]. When combined with docetaxel, this treatment was found to significantly improve the survival of mice carrying metastatic human breast cancer cells. Nevertheless, the extremely low yield of this lipid-tagged scFv is a major drawback for further use in therapy [120].

Liposomes may permit multiple administrations and systemic delivery of wild-type p53 gene, which is likely to be necessary for the successful treatment of metastatic tumors. Ramesh et al. described an improved extruded *N*-[1-(2,3-dioleoyloxy)]-*N*,*N*,*N*-trimethylammonium propane methylsulphate:cholesterol (DOTAP:chol) cationic liposome that efficiently delivered *TP53* and *FHIT* (Fragile HIstidine Triad gene) to localized human primary lung cancers and to experimental disseminated metastases in a mice lung cancer model [121]. Transgene expression was observed in 25% of tumor cells per tumor in primary tumors and 10% in disseminated tumors. DOTAP:chol–*TP53* and –*FHIT* complex suppressed significantly both primary and metastatic lung tumor growth. Multiple treatments revealed a 2.5-fold increase in gene expression and increased therapeutic efficacy compared to single treatment. Moreover, liposome-*p53* DNA complex treatment led to prolonged survival. However, this approach has not yet been evaluated in clinical trials.

Other original approaches have been evaluated to deliver directly *TP53* gene or p53 protein into cells. Matsubara et al. have evaluated the efficacy of electroporation-mediated incorporation of *wt-TP53* DNA [122]. Electric pulses were delivered to nude mice carrying human esophageal cancer xenografts after they were injected a *wt-TP53*-expressing plasmid: the growth of tumors was then suppressed, and simultaneous administration of chemotherapy produced a synergistic therapeutic effect. It has been also possible to directly deliver the p53 protein into cells using membrane-permeable peptides as carriers [123]. The p53 protein fused to poly-arginine peptides could penetrate human oral cancer cells harboring *TP53* mutation, and lead to induction of p21/WAF-1, inhibition of proliferation and enhancement of cisplatin-dependent induction of apoptosis. Nevertheless, these approaches need further evaluation before application in human clinical trials.

However, one could consider that non-viral systems remain far to give transfection rates as effective as those performed by viral vectors. Indeed, according to Zeimet and Marth, the fact that "for millions of years the main job of viruses has been to penetrate cellular systems [. . .]" argues for this comparison between the efficiency of viral and non-viral vectors [57].

9. Perspectives and future challenges

Given their central role in the control of life and death of cells exposed to DNA-damage, *TP53* and the p53 protein are attractive targets for therapeutic approaches that may be added to current protocols. A first approach is to restore or increase p53 function in cancer cells. These cells would then become more susceptible to killing by radio- or chemotherapy. This is the aim of most current *TP53*-based gene therapy approaches. In this sense, the use of replication-deficient virus carrying *wt-TP53* (Ad5CMV-p53) and/or cancer-selective oncolytic adenoviruses (ONYX-015) represents a novel cancer treatment platform. Both strategies resulted in a safe anti-cancer therapy. Therapeutic effect was obtained in combination with chemotherapy and/or radiotherapy. Moreover, its promise is in cases where conventional anti-cancer treatments have failed to provoke a therapeutic effect. The approach represented by these compounds is currently in advanced clinical trials and is most likely to become the first, p53-based therapy to reach the bedside.

However, different questions surrounding Ad5CMV-p53 or ONYX-015 administration in the clinical setting remain unanswered. For example, the applicability of it adminis-

tration is limited by tumor location, physician expertise and accessible technology. For localized tumors, delivery of these compounds is currently performed by intratumoral injection with good tolerability and clinical activity. However, for various advanced cancers these compounds would have to be delivered intravenously and the different published studies have demonstrated tolerability of the treatment but with limited efficacy. Also the basic problem of viral cancer-targeting specificity remains. Cancer- and/or tissue-specific modifications of viral coat proteins might change vector tropism and increase the selectivity of cancer targeting and would also reduce toxicity. Similarly, new generation of replicative viral vectors, placing the expression of therapeutics genes under the control of tumor-specific promoters or transcriptional control regions represents a new field of investigation. Indeed, as shown in preclinical studies, this strategy confers tumor specificity, which in turn could represent a new rational basis for the *TP53* gene therapy [124–126]. A final problem to be solved is the fact that prolonged exposure to Ad5CMV-p53 or ONYX-015 could lead to a stronger immunological response. Overcoming this limitation may be an important and rewarding technological task.

A second approach is to modulate p53 functions in normal cells in order to induce protective responses. This is illustrated in several pharmacological approaches using small molecules to activate or inhibit p53 functions. On the basis of current preclinical studies, several small molecules targeting p53 may find their way into clinical practice within the next few years. However, many of the current versions of the available lead compounds are active at only very high concentrations, incompatible with their pharmacological use. Therefore, these compounds need to be optimized to develop molecules with the appropriate pharmacological properties.

Reviewers

Hervé Bonnefoi, Professor, Département de Gynécologie et d'Obstétrique, Unité d'Oncogynécologie Médicale, Hôpitaux Universitaires de Genève, Boulevard de la Cluse 30, CH-1211 Genève 14, Switzerland.

Jack A. Roth, M.D., F.A.C.S., The University of Texas MD Anderson Cancer Center, Professor and Chairman, Bud Johnson Clinical, Distinguished Chair, Department of Thoracic & Cardiovascular Surgery, Professor of Molecular & Cellular Oncology, Director, W.M. Keck Center for Cancer Gene Therapy, 1515 Holcombe Boulevard, Houston, TX 77030-4009, USA.

David Malkin, M.D., F.R.C.P. (C), F.A.A.P., Professor of Pediatrics and Medical Biophysics, Director, Cancer Genetics Program, Staff Oncologist, Division of Hematology/Oncology, Senior Scientist, Cancer Research Program, Research Institute, The Hospital for Sick Children, University of Toronto, 555 University Ave., Toronto, Ont., Canada M5G 1X8.

References

[1] Bartkova J, Horejsi Z, Koed K, et al. DNA damage response as a candidate anti-cancer barrier in early human tumorigenesis. Nature 2005;434:864–70.
[2] Gorgoulis VG, Vassiliou LV, Karakaidos P, et al. Activation of the DNA damage checkpoint and genomic instability in human precancerous lesions. Nature 2005;434:907–13.
[3] Olivier M, Eeles R, Hollstein M, Khan MA, Harris CC, Hainaut P. The IARC TP53 database: new online mutation analysis and recommendations to users. Hum Mutat 2002;19:607–14.
[4] Szymanska K, Hainaut P. TP53 and mutations in human cancer. Acta Biochim Pol 2003;50:231–8.
[5] Cho Y, Gorina S, Jeffrey PD, Pavletich NP. Crystal structure of a p53 tumor suppressor-DNA complex: understanding tumorigenic mutations. Science 1994;265:346–55.
[6] Momand J, Zambetti GP, Olson DC, George D, Levine AJ. The mdm-2 oncogene product forms a complex with the p53 protein and inhibits p53-mediated transactivation. Cell 1992;69:1237–45.
[7] Galmarini CM, Kamath K, Vanier-Viornery A, et al. Drug resistance associated with loss of p53 involves extensive alterations in microtubule composition and dynamics. Br J Cancer 2003;88:1793–9.
[8] Galmarini CM, Falette N, Tabone E, et al. Inactivation of wild-type p53 by a dominant negative mutant renders MCF-7 cells resistant to tubulin-binding agent cytotoxicity. Br J Cancer 2001;85:902–8.
[9] Pluquet O, Hainaut P. Genotoxic and non-genotoxic pathways of p53 induction. Cancer Lett 2001;174:1–15.
[10] Vogelstein B, Lane D, Levine AJ. Surfing the p53 network. Nature 2000;408:307–10.
[11] Hussain SP, Hofseth LJ, Harris CC. Radical causes of cancer. Nat Rev Cancer 2003;3:276–85.
[12] Tokino T, Nakamura Y. The role of p53-target genes in human cancer. Crit Rev Oncol Hematol 2000;33:1–6.
[13] Oren M. Decision making by p53: life, death and cancer. Cell Death Differ 2003;10:431–42.
[14] Scheffner M, Werness BA, Huibregtse JM, Levine AJ, Howley PM. The E6 oncoprotein encoded by human papillomavirus types 16 and 18 promotes the degradation of p53. Cell 1990;63:1129–36.
[15] Valsesia-Wittmann S, Magdeleine M, Dupasquier S, et al. Oncogenic cooperation between H-Twist and N-Myc overrides failsafe programs in cancer cells. Cancer Cell 2004;6:625–30.
[16] Flaman JM, Robert V, Lenglet S, Moreau V, Iggo R, Frebourg T. Identification of human p53 mutations with differential effects on the BAX and p21 promoters using functional assays in yeast. Oncogene 1998;16:1369–72.
[17] Ludwig RL, Bates S, Vousden KH. Differential activation of target cellular promoters by p53 mutants with impaired apoptotic function. Mol Cell Biol 1996;16:4952–60.
[18] Smith PD, Crossland S, Parker G, et al. Novel p53 mutants selected in BRCA-associated tumours which dissociate transformation suppression from other wild-type p53 functions. Oncogene 1999;18:2451–9.
[19] Kato S, Han SY, Liu W, et al. Understanding the function-structure and function-mutation relationships of p53 tumor suppressor protein by high-resolution missense mutation analysis. Proc Natl Acad Sci USA 2003;100:8424–9.
[20] Brachmann RK, Vidal M, Boeke JD. Dominant-negative p53 mutations selected in yeast hit cancer hot spots. Proc Natl Acad Sci USA 1996;93:4091–5.

[21] Cadwell C, Zambetti GP. The effects of wild-type p53 tumor suppressor activity and mutant p53 gain-of-function on cell growth. Gene 2001;277:15–30.
[22] Cai DW, Mukhopadhyay T, Liu Y, Fujiwara T, Roth JA. Stable expression of the wild-type p53 gene in human lung cancer cells after retrovirus-mediated gene transfer. Hum Gene Ther 1993;4:617–24.
[23] Fujiwara T, Grimm EA, Mukhopadhyay T, Cai DW, Owen-Schaub LB, Roth JA. A retroviral wild-type p53 expression vector penetrates human lung cancer spheroids and inhibits growth by inducing apoptosis. Cancer Res 1993;53:4129–33.
[24] Runnebaum IB, Wang S, Kreienberg R. Retrovirally mediated wild-type p53 restores S-phase modulation without inducing WAF1 mRNA in breast carcinoma cells containing mutant p53. J Cell Biochem 1995;59:537–44.
[25] Roth JA, Nguyen D, Lawrence DD, et al. Retrovirus-mediated wild-type p53 gene transfer to tumors of patients with lung cancer. Nat Med 1996;2:985–91.
[26] Brandt CD, Kim HW, Vargosko AJ, et al. Infections in 18,000 infants and children in a controlled study of respiratory tract disease. I. Adenovirus pathogenicity in relation to serologic type and illness syndrome. Am J Epidemiol 1969;90:484–500.
[27] Takafuji ET, Gaydos JC, Allen RG, Top Jr FH. Simultaneous administration of live, enteric-coated adenovirus types 4, 7 and 21 vaccines: safety and immunogenicity. J Infect Dis 1979;140:48–53.
[28] Zhang WW, Fang X, Branch CD, Mazur W, French BA, Roth JA. Generation and identification of recombinant adenovirus by liposome-mediated transfection and PCR analysis. Biotechniques 1993;15:868–72.
[29] Eastham JA, Grafton W, Martin CM, Williams BJ. Suppression of primary tumor growth and the progression to metastasis with p53 adenovirus in human prostate cancer. J Urol 2000;164:814–9.
[30] Giuliano M, Catalano A, Strizzi L, Vianale G, Capogrossi M, Procopio A. Adenovirus-mediated wild-type p53 overexpression reverts tumourigenicity of human mesothelioma cells. Int J Mol Med 2000;5:591–6.
[31] Inoue A, Narumi K, Matsubara N, et al. Administration of wild-type p53 adenoviral vector synergistically enhances the cytotoxicity of anti-cancer drugs in human lung cancer cells irrespective of the status of p53 gene. Cancer Lett 2000;157:105–12.
[32] Putzer BM, Bramson JL, Addison CL, et al. Combination therapy with interleukin-2 and wild-type p53 expressed by adenoviral vectors potentiates tumor regression in a murine model of breast cancer. Hum Gene Ther 1998;9:707–18.
[33] Schuler M, Rochlitz C, Horowitz JA, et al. A phase I study of adenovirus-mediated wild-type p53 gene transfer in patients with advanced non-small cell lung cancer. Hum Gene Ther 1998;9:2075–82.
[34] Dummer R, Bergh J, Karlsson Y, et al. Biological activity and safety of adenoviral vector-expressed wild-type p53 after intratumoral injection in melanoma and breast cancer patients with p53-overexpressing tumors. Cancer Gene Ther 2000;7:1069–76.
[35] INGN 201: Ad-p53, Ad5CMV-p53, Adenoviral p53, INGN 101, p53 gene therapy–Introgen, RPR/INGN 201. BioDrugs 2003;17: 216–22.
[36] Swisher SG, Roth JA, Nemunaitis J, et al. Adenovirus-mediated p53 gene transfer in advanced non-small-cell lung cancer. J Natl Cancer Inst 1999;91:763–71.
[37] Weill D, Mack M, Roth J, et al. Adenoviral-mediated p53 gene transfer to non-small cell lung cancer through endobronchial injection. Chest 2000;118:966–70.
[38] Carbone DP, Adak S, Schiller J, et al. Adenovirus p53 administered by bronchoalveolar lavage in patients with bronchioalveolar cell lung carcinoma (BAC). Proc Am Soc Clin Oncol 2003;22:2494.
[39] Nemunaitis J, Swisher SG, Timmons T, et al. Adenovirus-mediated p53 gene transfer in sequence with cisplatin to tumors of patients with non-small-cell lung cancer. J Clin Oncol 2000;18:609–22.
[40] Schuler M, Herrmann R, De Greve JL, et al. Adenovirus-mediated wild-type p53 gene transfer in patients receiving chemotherapy for advanced non-small-cell lung cancer: results of a multicenter phase II study. J Clin Oncol 2001;19:1750–8.
[41] Swisher SG, Roth JA, Komaki R, et al. Induction of p53-regulated genes and tumor regression in lung cancer patients after intratumoral delivery of adenoviral p53 (INGN 201) and radiation therapy. Clin Cancer Res 2003;9:93–101.
[42] Clayman GL, el-Naggar AK, Lippman SM, et al. Adenovirus-mediated p53 gene transfer in patients with advanced recurrent head and neck squamous cell carcinoma. J Clin Oncol 1998;16:2221–32.
[43] Nemunaitis J, Carol BL, Costenla-Figueiras M, Yver A, Lyndah D. Three phase II trials of intratumoral injection with a replication-deficient adenovirus carrying the p53 gene (Ad5CMV-P53) in patients with recurrent/refractory head and neck cancer. Proc Am Soc Clin Oncol 1999;18:1661.
[44] Yver A, Dreiling L, Mohanty S, et al. Tolerance and safety of rpr/ingn 201, an adeno-viral vector containing a p53 gene, administered intratumorally in 309 patients with advanced cancer enrolled in phase I and II studies world-wide. Proc Am Soc Clin Oncol 1999;18:1806.
[45] Yver A, Gautier E, Saulnier P, Walsh V, Duprey S, Escudier B. Clinical biosafety, distribution, genetic stability and potential for transmission of adenoviral vector for gene transfer (therapy): data from 190 subjects treated intra-tumorally with rpr/ingn 201 (Ad5CMV-p53). Proc Am Soc Clin Oncol 2001;20:1046.
[46] Pearson S, Jia H, Kandachi K. China approves first gene therapy. Nat Biotechnol 2004;22:3–4.
[47] Peng Z, Han D, Zhang S, et al. Clinical evaluation of safety and efficacy of intratumoral administration of a recombinant adenoviral-p53 anticancer agent (Genkaxin®). Mol Ther 2003;7:S422–3.
[48] Buller RE, Runnebaum IB, Karlan BY, et al. A phase I/II trial of rAd/p53 (SCH 58500) gene replacement in recurrent ovarian cancer. Cancer Gene Ther 2002;9:553–66.
[49] Buller RE, Shahin MS, Horowitz JA, et al. Long term follow-up of patients with recurrent ovarian cancer after Ad p53 gene replacement with SCH 58500. Cancer Gene Ther 2002;9:567–72.
[50] Wolf JK, Bodurka DC, Gano JB, et al. A phase I study of Adp53 (INGN 201; ADVEXIN) for patients with platinum- and paclitaxel-resistant epithelial ovarian cancer. Gynecol Oncol 2004;94: 442–8.
[51] Wen SF, Mahavni V, Quijano E, et al. Assessment of p53 gene transfer and biological activities in a clinical study of adenovirus-p53 gene therapy for recurrent ovarian cancer. Cancer Gene Ther 2003;10:224–38.
[52] Lang FF, Bruner JM, Fuller GN, et al. Phase I trial of adenovirus-mediated p53 gene therapy for recurrent glioma: biological and clinical results. J Clin Oncol 2003;21:2508–18.
[53] Kuball J, Wen SF, Leissner J, et al. Successful adenovirus-mediated wild-type p53 gene transfer in patients with bladder cancer by intravesical vector instillation. J Clin Oncol 2002;20:957–65.
[54] Pagliaro LC, Keyhani A, Liu B, et al. Gene therapy in bladder cancer: phase I results with Ad5CMV-p53 (RPR/INGN 201). Proc Am Soc Clin Oncol 2001;20:799.
[55] Cristofanilli M, Khrisnamurthy S, Guerra L, et al. Ad5CMV-p53 combined with docetaxel (T) and doxorubicin (D) as induction chemotherapy (IC) for patients with locally advanced breast cancer (LABC): preliminary report of safety and efficacy. Proc Am Soc Clin Oncol 2003;22:967.
[56] Ochiai T, Matsubara H, Shimada H. A phase I/II trial of adenoviral p53 gene therapy (INGN 201) for esophageal squamous cell carcinoma. Proc Am Soc Clin Oncol 2003;22:877.
[57] Zeimet AG, Marth C. Why did p53 gene therapy fail in ovarian cancer? Lancet Oncol 2003;4:415–22.
[58] Teodoro JG, Shore GC, Branton PE. Adenovirus E1A proteins induce apoptosis by both p53-dependent and p53-independent mechanisms. Oncogene 1995;11:467–74.

[59] Bischoff JR, Kirn DH, Williams A, et al. An adenovirus mutant that replicates selectively in p53-deficient human tumor cells. Science 1996;274:373–6.
[60] Heise C, Sampson-Johannes A, Williams A, McCormick F, Von Hoff DD, Kirn DH. ONYX-015, an E1B gene-attenuated adenovirus, causes tumor-specific cytolysis and antitumoral efficacy that can be augmented by standard chemotherapeutic agents. Nat Med 1997;3:639–45.
[61] Milas M, Yu D, Lang A, et al. Adenovirus-mediated p53 gene therapy inhibits human sarcoma tumorigenicity. Cancer Gene Ther 2000;7:422–9.
[62] Miyake H, Hara I, Hara S, Arakawa S, Kamidono S. Synergistic chemosensitization and inhibition of tumor growth and metastasis by adenovirus-mediated P53 gene transfer in human bladder cancer model. Urology 2000;56:332–6.
[63] Geoerger B, Grill J, Opolon P, et al. Potentiation of radiation therapy by the oncolytic adenovirus dl1520 (ONYX-015) in human malignant glioma xenografts. Br J Cancer 2003;89:577–84.
[64] Portella G, Pacelli R, Libertini S, et al. ONYX-015 enhances radiation-induced death of human anaplastic thyroid carcinoma cells. J Clin Endocrinol Metab 2003;88:5027–32.
[65] Hall AR, Dix BR, O'Carroll SJ, Braithwaite AW. p53-dependent cell death/apoptosis is required for a productive adenovirus infection. Nat Med 1998;4:1068–72.
[66] Steegenga WT, Riteco N, Bos JL. Infectivity and expression of the early adenovirus proteins are important regulators of wild-type and DeltaE1B adenovirus replication in human cells. Oncogene 1999;18:5032–43.
[67] Ries SJ, Brandts CH, Chung AS, et al. Loss of p14ARF in tumor cells facilitates replication of the adenovirus mutant dl1520 (ONYX-015). Nat Med 2000;6:1128–33.
[68] Edwards SJ, Dix BR, Myers CJ, et al. Evidence that replication of the antitumor adenovirus ONYX-015 is not controlled by the p53 and p14(ARF) tumor suppressor genes. J Virol 2002;76:12483–90.
[69] Hann B, Balmain A. Replication of an E1B 55-kilodalton protein-deficient adenovirus (ONYX-015) is restored by gain-of-function rather than loss-of-function p53 mutants. J Virol 2003;77:11588–95.
[70] Hsieh JL, Wu CL, Lee CH, Shiau AL. Hepatitis B virus X protein sensitizes hepatocellular carcinoma cells to cytolysis induced by E1B-deleted adenovirus through the disruption of p53 function. Clin Cancer Res 2003;9:338–45.
[71] Nemunaitis J, Ganly I, Khuri F, et al. Selective replication and oncolysis in p53 mutant tumors with ONYX-015, an E1B-55kD gene-deleted adenovirus, in patients with advanced head and neck cancer: a phase II trial. Cancer Res 2000;60:6359–66.
[72] Nemunaitis J, Cunningham C, Tong AW, et al. Pilot trial of intravenous infusion of a replication-selective adenovirus (ONYX-015) in combination with chemotherapy or IL-2 treatment in refractory cancer patients. Cancer Gene Ther 2003;10:341–52.
[73] Rudin CM, Cohen EE, Papadimitrakopoulou VA, et al. An attenuated adenovirus, ONYX-015, as mouthwash therapy for premalignant oral dysplasia. J Clin Oncol 2003;21:4546–52.
[74] Vasey PA, Shulman LN, Campos S, et al. Phase I trial of intraperitoneal injection of the E1B-55-kd-gene-deleted adenovirus ONYX-015 (dl1520) given on days 1 through 5 every 3 weeks in patients with recurrent/refractory epithelial ovarian cancer. J Clin Oncol 2002;20:1562–9.
[75] Sze DY, Freeman SM, Slonim SM, et al. Dr. Gary J. Becker Young Investigator Award: intraarterial adenovirus for metastatic gastrointestinal cancer: activity, radiographic response, and survival. J Vasc Interv Radiol 2003;14:279–90.
[76] Ganly I, Kirn D, Eckhardt G, et al. A phase I study of ONYX-015, an E1B attenuated adenovirus, administered intratumorally to patients with recurrent head and neck cancer. Clin Cancer Res 2000;6:798–806.
[77] Reid T, Galanis E, Abbruzzese J, et al. Intra-arterial administration of a replication-selective adenovirus (dl1520) in patients with colorectal carcinoma metastatic to the liver: a phase I trial. Gene Ther 2001;8:1618–26.
[78] Wadler S, Yu B, Tan JY, et al. Persistent replication of the modified chimeric adenovirus ONYX-015 in both tumor and stromal cells from a patient with gall bladder carcinoma implants. Clin Cancer Res 2003;9:33–43.
[79] Kirn D, Nemunaitis J, Ganly I, et al. A phase II trial of intratumoral injection with an e1b-deleted adenovirus, onyx-015, in patients with recurrent, refractory head and neck cancer. Proc Am Soc Clin Oncol 1998;17:1509.
[80] Nemunaitis J, Cunningham C, Buchanan A, et al. Intravenous infusion of a replication-selective adenovirus (ONYX-015) in cancer patients: safety, feasibility and biological activity. Gene Ther 2001;8:746–59.
[81] Khuri FR, Nemunaitis J, Ganly I, et al. A controlled trial of intratumoral ONYX-015, a selectively-replicating adenovirus, in combination with cisplatin and 5-fluorouracil in patients with recurrent head and neck cancer. Nat Med 2000;6:879–85.
[82] Reid TR, Freeman S, Post L, McCormick F, Sze DY. Effects of ONYX-015 among metastatic colorectal cancer patients that have failed prior treatment with 5-FU/leucovorin. Cancer Gene Ther 2005.
[83] Hamid O, Varterasian ML, Wadler S, et al. Phase II trial of intravenous CI-1042 in patients with metastatic colorectal cancer. J Clin Oncol 2003;21:1498–504.
[84] Makower D, Rozenblit A, Kaufman H, et al. Phase II clinical trial of intralesional administration of the oncolytic adenovirus ONYX-015 in patients with hepatobiliary tumors with correlative p53 studies. Clin Cancer Res 2003;9:693–702.
[85] Mulvihill S, Warren R, Venook A, et al. Safety and feasibility of injection with an E1B-55 kDa gene-deleted, replication-selective adenovirus (ONYX-015) into primary carcinomas of the pancreas: a phase I trial. Gene Ther 2001;8:308–15.
[86] Hecht JR, Bedford R, Abbruzzese JL, et al. A phase I/II trial of intratumoral endoscopic ultrasound injection of ONYX-015 with intravenous gemcitabine in unresectable pancreatic carcinoma. Clin Cancer Res 2003;9:555–61.
[87] Bruning A, Kohler T, Quist S, et al. Adenoviral transduction efficiency of ovarian cancer cells can be limited by loss of integrin beta3 subunit expression and increased by reconstitution of integrin alphavbeta3. Hum Gene Ther 2001;12:391–9.
[88] Zeimet AG, Muller-Holzner E, Schuler A, et al. Determination of molecules regulating gene delivery using adenoviral vectors in ovarian carcinomas. Gene Ther 2002;9:1093–100.
[89] Galanis E, Okuno SH, Nascimento AG, et al. Phase I–II trial of ONYX-015 in combination with MAP chemotherapy in patients with advanced sarcomas. Gene Ther 2005;12:437–45.
[90] Kenzer MC, Randlev B, Valente N, Kaplan E, Tripathy D. Intratumoral administration of ONYX-015 virus in breast cancer. Proc Am Soc Clin Oncol 2002;21:1903.
[91] O'Shea CC, Soria C, Bagus B, McCormick F. Heat shock phenocopies E1B-55K late functions and selectively sensitizes refractory tumor cells to ONYX-015 oncolytic viral therapy. Cancer Cell 2005;8:61–74.
[92] Bottger A, Bottger V, Sparks A, Liu WL, Howard SF, Lane DP. Design of a synthetic mdm-2-binding mini protein that activates the p53 response in vivo. Curr Biol 1997;7:860–9.
[93] Vassilev LT, Vu BT, Graves B, et al. In vivo activation of the p53 pathway by small-molecule antagonists of mdm2. Science 2004;303:844–8.
[94] Klein C, Vassilev LT. Targeting the p53–mdm2 interaction to treat cancer. Br J Cancer 2004;91:1415–9.
[95] Kramer DL, Vujcic S, Diegelman P, White C, Black JD, Porter CW. Polyamine analogue-mediated cell cycle responses in human

melanoma cells involves the p53, p21, Rb regulatory pathway. Biochem Soc Trans 1998;26:609–14.
[96] Kramer DL, Vujcic S, Diegelman P, et al. Polyamine analogue induction of the p53-p21WAF1/CIP1-Rb pathway and G1 arrest in human melanoma cells. Cancer Res 1999;59:1278–86.
[97] Ray RM, Zimmerman BJ, McCormack SA, Patel TB, Johnson LR. Polyamine depletion arrests cell cycle and induces inhibitors p21(Waf1/Cip1), p27(Kip1), and p53 in IEC-6 cells. Am J Physiol 1999;276:C684–91.
[98] Komarov PG, Komarova EA, Kondratov RV, et al. A chemical inhibitor of p53 that protects mice from the side effects of cancer therapy. Science 1999;285:1733–7.
[99] Komarova EA, Neznanov N, Komarov PG, Chernov MV, Wang K, Gudkov AV. p53 inhibitor pifithrin alpha can suppress heat shock and glucocorticoid signaling pathways. J Biol Chem 2003;278:15465–8.
[100] Schafer T, Scheuer C, Roemer K, Menger MD, Vollmar B. Inhibition of p53 protects liver tissue against endotoxin-induced apoptotic and necrotic cell death. Faseb J 2003;17:660–7.
[101] Vollmar B, El-Gibaly AM, Scheuer C, Strik MW, Bruch HP, Menger MD. Acceleration of cutaneous wound healing by transient p53 inhibition. Lab Invest 2002;82:1063–71.
[102] Zhang M, Liu W, Ding D, Salvi R. Pifithrin-alpha suppresses p53 and protects cochlear and vestibular hair cells from cisplatin-induced apoptosis. Neuroscience 2003;120:191–205.
[103] Kaji A, Zhang Y, Nomura M, et al. Pifithrin-alpha promotes p53-mediated apoptosis in JB6 cells. Mol Carcinog 2003;37:138–48.
[104] Caron de Fromentel C, Gruel N, Venot C, et al. Restoration of transcriptional activity of p53 mutants in human tumour cells by intracellular expression of anti-p53 single chain Fv fragments. Oncogene 1999;18:551–7.
[105] Govorko D, Cohen G, Solomon B. Single-chain antibody against the common epitope of mutant p53: isolation and intracytosolic expression in mammalian cells. J Immunol Methods 2001;258:169–81.
[106] Foster BA, Coffey HA, Morin MJ, Rastinejad F. Pharmacological rescue of mutant p53 conformation and function. Science 1999;286:2507–10.
[107] Weinstein JN, Myers TG, O'Connor PM, et al. An information-intensive approach to the molecular pharmacology of cancer. Science 1997;275:343–9.
[108] Bykov VJ, Issaeva N, Shilov A, et al. Restoration of the tumor suppressor function to mutant p53 by a low-molecular-weight compound. Nat Med 2002;8:282–8.
[109] Bykov VJ, Issaeva N, Selivanova G, Wiman KG. Mutant p53-dependent growth suppression distinguishes PRIMA-1 from known anticancer drugs: a statistical analysis of information in the National Cancer Institute database. Carcinogenesis 2002;23:2011–8.
[110] Bykov VJ, Selivanova G, Wiman KG. Small molecules that reactivate mutant p53. Eur J Cancer 2003;39:1828–34.
[111] Gridley DS, Andres ML, Li J, Timiryasova T, Chen B, Fodor I. Evaluation of radiation effects against C6 glioma in combination with vaccinia virus-p53 gene therapy. Int J Oncol 1998;13:1093–8.
[112] Timiryasova TM, Gridley DS, Chen B, et al. Radiation enhances the anti-tumor effects of vaccinia-p53 gene therapy in glioma. Technol Cancer Res Treat 2003;2:223–35.
[113] Chen B, Timiryasova TM, Andres ML, et al. Evaluation of combined vaccinia virus-mediated antitumor gene therapy with p53, IL-2, and IL-12 in a glioma model. Cancer Gene Ther 2000;7:1437–47.
[114] Conseiller E, Debussche L, Landais D, et al. CTS1: a p53-derived chimeric tumor suppressor gene with enhanced in vitro apoptotic properties. J Clin Invest 1998;101:120–7.
[115] Bougeret C, Virone-Oddos A, Adeline E, et al. Cancer gene therapy mediated by CTS1, a p53 derivative: advantage over wild-type p53 in growth inhibition of human tumors overexpressing mdm2. Cancer Gene Ther 2000;7:789–98.
[116] Naumann U, Kugler S, Wolburg H, et al. Chimeric tumor suppressor 1, a p53-derived chimeric tumor suppressor gene, kills p53 mutant and p53 wild-type glioma cells in synergy with irradiation and CD95 ligand. Cancer Res 2001;61:5833–42.
[117] Habib NA, Ding SF, el-Masry R, et al. Preliminary report: the short-term effects of direct p53 DNA injection in primary hepatocellular carcinomas. Cancer Detect Prev 1996;20:103–7.
[118] Lesoon-Wood LA, Kim WH, Kleinman HK, Weintraub BD, Mixson AJ. Systemic gene therapy with p53 reduces growth and metastases of a malignant human breast cancer in nude mice. Hum Gene Ther 1995;6:395–405.
[119] Xu L, Tang WH, Huang CC, et al. Systemic p53 gene therapy of cancer with immunolipoplexes targeted by anti-transferrin receptor scFv. Mol Med 2001;7:723–34.
[120] Xu L, Huang CC, Huang W, et al. Systemic tumor-targeted gene delivery by anti-transferrin receptor scFv-immunoliposomes. Mol Cancer Ther 2002;1:337–46.
[121] Ramesh R, Saeki T, Templeton NS, et al. Successful treatment of primary and disseminated human lung cancers by systemic delivery of tumor suppressor genes using an improved liposome vector. Mol Ther 2001;3:337–50.
[122] Matsubara H, Maeda T, Gunji Y, et al. Combinatory anti-tumor effects of electroporation-mediated chemotherapy and wild-type p53 gene transfer to human esophageal cancer cells. Int J Oncol 2001;18:825–9.
[123] Takenobu T, Tomizawa K, Matsushita M, et al. Development of p53 protein transduction therapy using membrane-permeable peptides and the application to oral cancer cells. Mol Cancer Ther 2002;1:1043–9.
[124] Casado E, Nettelbeck DM, Gomez-Navarro J, et al. Transcriptional targeting for ovarian cancer gene therapy. Gynecol Oncol 2001;82:229–37.
[125] Uchino J, Takayama K, Harada A, et al. Infectivity enhanced, hTERT promoter-based conditionally replicative adenoviruses are useful for SCLC treatment. Cancer Gene Ther 2005;12:737–48.
[126] Kazhdan I, Long L, Montellano R, Cavazos DA, Marciniak RA. Targeted gene therapy for breast cancer with truncated Bid. Cancer Gene Ther 2005.

Biography

Benjamin P. Bouchet is a Doctor of Pharmacy from the Claude Bernard University of Lyon, France. He is a Ph.D. student at the INSERM 590 unit located at the Léon Bérard Center, Cancer Institute, Lyon. His work is supported by the Fondation pour la Recherche Médicale.

FORMATION SFC

Bull Cancer 2006 ; hors série : 145-53

p53 comme cible thérapeutique pour le développement de médicaments anticancéreux

p53 as a therapeutic target for the development of anticancer drugs

Benjamin Pierre Bouchet
Claude Caron de Fromentel
Carlos María Galmarini
Alain Puisieux

Inserm U590, Centre Léon Bérard,
28 rue Laennec, 69373 Lyon Cedex 08
<puisieux@lyon.fnclcc.fr>

Résumé. La perte de la fonction oncosuppressive de la protéine p53 constitue un événement déterminant au cours de la progression tumorale. Aussi, de nombreuses approches à visée thérapeutique ont été développées dans le but de rétablir ou de contrôler les fonctions de p53 dans les cellules cancéreuses. L'utilisation d'adénovirus permettant le transfert du gène sauvage *TP53* (Ad5CMV-p53) et d'adénovirus oncolytiques spécifiques des tissus tumoraux (Onyx015) a démontré une activité prometteuse en monothérapie et une action synergique avec les chimiothérapies conventionnelles pour le traitement de certains types de cancer. De même, des stratégies pharmacologiques visant soit à stimuler les fonctions de la forme sauvage de p53 (p53 *wild type*), soit à rétablir certaines des fonctions normales de p53 en ciblant les formes mutantes sont en cours de développement. Ces stratégies reposent sur l'utilisation de petits composés chimiques (CP31388, Prima1), de peptides (CDB3) ou de fragments variables de chaînes d'immunoglobulines (scFvs) ciblant des domaines définis de p53. Nous décrivons ici sommairement ces différentes approches et présentons certains résultats obtenus en clinique. Les perspectives offertes par ces nouvelles stratégies thérapeutiques sont discutées. ▲

Mots clés : protéine oncosuppressive p53, apoptose, mutation, thérapie génique, thérapeutique ciblée

Abstract. *Loss of p53 oncosuppressive functions represents a major event during tumoral progression. Several therapeutic approaches aiming the restoration or the control of p53 function in tumor cells have been developed. The use of adenoviruses for wild type TP53 transfer (Ad5CMV-p53) or tumor-specific oncolytic adenoviruses (ONYX-015) has demonstrated promising activity as a monotherapy as well as in association with conventional chemotherapeutic drugs, with a synergistic action in the treatment of some types of cancer. In addition, pharmacological methods are under development to either stimulate wild-type p53 protein function, or rescue p53 mutant proteins to recover wild-type functions. These methods are based on small chemicals (CP-31388, PRIMA-1), peptides (CDB3) or single-chain Fv antibody fragments corresponding to defined p53 domains. Here, we describe the mechanisms underlying these approaches and some of the clinical trials which have tested these approaches. The therapeutic perspectives of the p53 targeting for drug development are also discussed.* ▲

Key words: *p53 tumor suppressor, apoptosis, mutation, gene therapy, targeted therapy*

Dans les cellules normales, les processus de réplication de l'ADN et de division cellulaire font l'objet d'une régulation très fine afin de prévenir une prolifération anormale et une perte de la stabilité génétique qui pourraient provoquer, ou accompagner, une transformation maligne. L'activation des points de contrôle du cycle cellulaire permet de bloquer transitoirement celui-ci pour réparer des altérations génétiques mineures ou, en présence d'altérations plus importantes, d'enclencher des processus plus coercitifs, tels que l'arrêt définitif du cycle cellulaire (sénescence) ou la mort cellulaire par apoptose. La sénescence et l'apoptose constituent donc des « systèmes de surveillance » très efficaces pour limiter l'expansion de cellules potentiellement délétères pour l'organisme [1-3]. La protéine oncosuppressive p53 est un acteur clé de ces processus de sauvegarde. Du fait de son inactivation récurrente dans le processus de cancérogenèse, le gène (*TP53*) et la protéine p53 apparaissent comme des cibles privilégiées pour des approches de thérapie génique ou pour une intervention pharmacologique à visée thérapeutique. Nous présenterons ici l'état actuel des connaissances concernant les différentes stratégies qui visent soit à rétablir les fonctions oncosuppressives de p53 sauvage, soit à augmenter la chimiosensibilité des cellules tumorales.

TP53 : structure et fonction

Le gène humain *TP53* est localisé au niveau de la région chromosomique 17p13.1. Il est composé de 11 exons, le premier étant non codant. L'expression de p53 est constitutive et ubiquitaire et sa régulation fonctionnelle semble essentiellement être de nature post-traductionnelle.

p53 est une phosphoprotéine nucléaire de 393 acides aminés qui agit comme facteur de transcription (*figure 1*). Elle est composée de cinq domaines structuraux et fonctionnels : un domaine N-terminal de transactivation, un domaine de régulation riche en proline, un domaine de liaison à l'ADN, un domaine d'oligomérisation et un domaine C-terminal impliqué dans la régulation de la liaison de p53 à l'ADN. Au plan structural, le domaine de liaison à l'ADN est composé d'une armature de feuillets β qui supportent un ensemble de boucles et d'hélices flexibles en contact direct avec l'ADN. Les mutations de *TP53* les plus fréquemment observées dans les cancers affectent le repliement de la protéine ou son interaction directe avec les sillons de la molécule d'ADN et abrogent l'interaction ADN-protéine (*figure 1*). p53 contient de nombreux sites de phosphorylation, cibles de kinases impliquées dans les voies de signalisation qui contrôlent la prolifération cellulaire (CKI, CKII, Chk2, ATM, ATR, PRKC, JNK, MAPK) et des sites d'acétylation par des coactivateurs du type histone acétyl-transférase (HAT), tels p300-CBP ou pCAF. Dans les cellules normales, la protéine p53 présente une forte instabilité du fait de sa rapide ubiquitinylation et de sa dégradation par le protéasome. Le facteur principalement responsable de cette instabilité constitutive de p53 est l'ubiquitine ligase mdm2 (Omim #164785). Les modifications post-traductionnelles, opérées en réponse à divers stress, vont stabiliser et activer p53 en abrogeant sa liaison à mdm2.

Une fois activée, suite à un stress de type oncogénique ou génotoxique, p53 enclenche une réponse cellulaire empruntant deux voies distinctes et parallèles : la voie dépendante et la voie indépendante de la transcription. Cette dernière comprend l'interaction de p53 avec des composants de la machinerie de réplication/réparation de l'ADN, tels que les hélicases ERCC2 et ERCC3 ou la *replication protein A* (RPA). Parmi les gènes régulés transcriptionnellement par p53 figurent notamment des régulateurs importants du cycle cellulaire en phases G1 et G2 (p21/WAF1, 14-3-3σ, GADD45), des régulateurs de l'apoptose (Bax, CD95-FAS, killer-DR5, p53AIP1, PIG3, IGF-BP3, Noxa, Puma, p53AIF1, survivine), ainsi qu'un certain nombre d'autres gènes impliqués dans la réponse aux stress (hypoxie). La décision entre les différentes réponses potentiellement déclenchées par p53 va dépendre autant de la nature et de l'amplitude du stimulus que du type cellulaire et histologique. Il faut donc noter que deux réponses biologiques distinctes peuvent coexister dans le même tissu.

Mutations de *TP53*

La mutation du gène *TP53* est l'événement le plus fréquent dans les cancers humains (www.p53.iarc/fr). Souvent de type faux-sens, la mutation d'un allèle est généralement associée à la délétion de l'autre allèle (perte d'hétérozygotie) dans la cellule cancéreuse, conduisant à une perte d'activité. Les mutations somatiques de *TP53* ont ainsi été observées dans tous les types de tumeur, mais avec une fréquence variable. Dans les carcinomes invasifs des voies aérodigestives supérieures (cancers ORL, œsophagiens et bronchiques), *TP53* est muté dans plus de 75 % des cas. Bien qu'à une fréquence plus faible, la mutation peut être observée dès le stade de la lésion prénéoplasique. Dans les cancers des voies digestives inférieures, tels que les cancers colorectaux, les mutations de *TP53* sont observées dans environ 60 % des cas et apparaissent le plus souvent lors de la transition adénome-carcinome. Dans les cancers du sein, les mutations sont détectées dans environ 25 % des cas. Les cancers du col de l'utérus, des testicules, les neuroblastomes et les mélanomes malins représentent une catégorie de cancers dans lesquels les mutations de *TP53* sont rares (fréquence des mutations < 5 %). Cependant, dans ces types de cancer, la voie de signalisation p53 peut être rendue déficiente par l'activation d'oncogènes viraux ou cellulaires. On peut citer, à titre d'exemple, la dégradation et l'inactivation de p53 par l'antigène E6 du virus du papillome (*human papillomavirus*, HPV), associé aux cancers du col de l'utérus. Nous avons également montré récemment que le facteur de transcription Twist1 était surexprimé dans

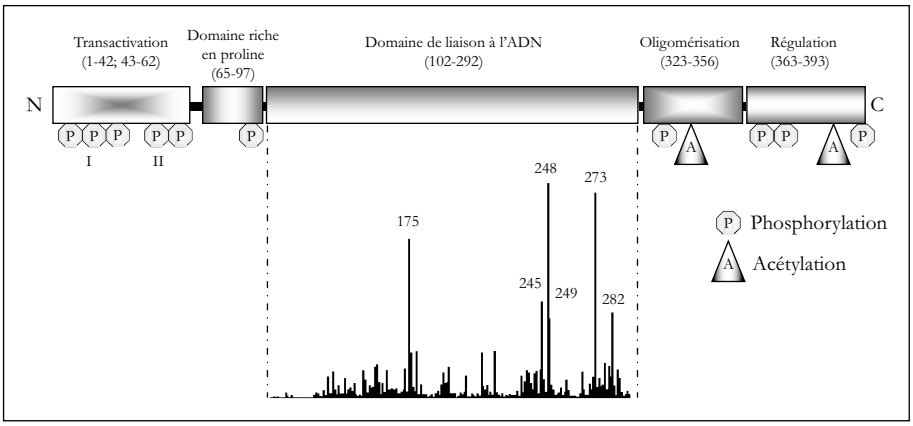

Figure 1. Structure de la protéine p53. La protéine p53 est composée de cinq domaines fonctionnels : le domaine de transactivation (I et II, acides aminés 1-62), une région régulatrice riche en proline (acides aminés 65-97), un domaine de liaison à l'ADN (acides aminés 102-292), un domaine d'oligomérisation (acides aminés 323-356) et un domaine C-terminal de régulation (acides aminés 363-393). p53 subit des modifications post-traductionnelles, telles que des phosphorylations (hexagones) et des acétylations (triangles), au niveau des régions N et C-terminales. Le diagramme sous le domaine de liaison à l'ADN illustre la distribution et la prévalence des mutations ponctuelles du gène *TP53* dans les tumeurs humaines. Les six codons les plus fréquemment mutés (« points chauds ») sont indiqués.

les neuroblastomes agressifs et que ce processus conduisait à l'inactivation de la voie p53 en favorisant ainsi la survie des cellules de neuroblastomes présentant une amplification de l'oncogène N-*myc* [4]. Il est donc probable que p53 est inactivée dans la plupart des tumeurs humaines, soit par altération génétique, soit par inactivation fonctionnelle.

Parmi toutes les mutations de *TP53* rapportées, 75 % sont des mutations faux-sens, la grande majorité d'entre elles étant localisées dans la région correspondant au domaine de liaison à l'ADN de la protéine (*figure 1*). La partie N-terminale, qui contient le domaine de transactivation, et la partie C-terminale, où sont localisés les principaux sites de régulation, sont rarement affectées (moins de 5 % des cas). Au sein du domaine de liaison à l'ADN, tous les résidus semblent constituer des cibles potentielles de mutations. Cependant, il existe des mutations *hot-spots* ou « points chauds de mutations » (codons 175, 245, 248, 273 et 282) qui sont le siège de près de 30 % des mutations observées. Quatre de ces codons correspondent à des résidus arginine (175, 248, 273 et 282) impliqués dans l'interaction protéine-ADN, soit par contact direct (248, 273), soit par stabilisation de l'interface protéine-ADN (175, 282).

La conséquence fonctionnelle principale de la mutation de *TP53* est la perte de la liaison spécifique à l'ADN et de l'activité transcriptionnelle de la protéine. Cependant, les formes mutantes issues de mutations faux-sens sont caractérisées par des degrés d'altération fonctionnelle différents. Des tests fonctionnels chez la levure et dans des lignées cellulaires humaines ont ainsi démontré que certaines protéines mutantes conservaient une activité transcriptionnelle résiduelle pour quelques gènes cibles. En effet, p53 sauvage possède une affinité différente en fonction du promoteur ciblé. Par exemple, le promoteur de *p21-WAF1* semble contenir des sites de plus grande affinité pour p53 que celui de *BAX*. Ainsi, les mutants R175P et R181C transactivent le gène *p21-WAF1* mais non le gène *BAX*, d'où une inhibition partielle du processus d'apoptose. Outre la simple perte de fonction, certaines mutations de *TP53* peuvent conduire à l'expression de protéines présentant des activités dominantes négatives ou à un gain de fonction conférant à la protéine mutante des propriétés pro-oncogéniques. Certaines protéines mutantes peuvent, par exemple, interférer avec p53 sauvage pour la transactivation. En cas d'absence de perte d'hétérozygotie, ces effets dominants négatifs sont à l'origine d'une abrogation, totale ou partielle, des fonctions de p53 sauvage endogène. Certains mutants sont également capables de transactiver ou de favoriser la transactivation de gènes tels que *MDR1*, *EGFR*, c-*MYC*, *PCNA*, *IGF-II*, ou *VEGF* qui ne constituent pas des cibles transcriptionnelles de p53 sauvage. Les formes mutantes présentant un gain de fonction ou une fonction dominante négative sont souvent observées dans des tumeurs agressives et chimiorésistantes [5].

TP53 comme cible thérapeutique

Parmi les approches ciblant p53 pour le traitement du cancer, les stratégies développées visent soit à activer p53, soit à l'inactiver, et ce afin d'induire respectivement l'apoptose ou la protection des cellules normales contre les thérapies cytotoxiques. À ce titre, il est important de noter que, dans certains types cellulaires, l'activation de p53 déclenche préférentiellement l'arrêt du cycle (et la réparation de l'ADN) et participe ainsi à une forme de protection des cellules tumorales contre les effets thérapeutiques cytotoxiques. En conséquence, l'activation de p53 peut être considérée, en fonction du contexte et du type cellulaire, soit comme un processus chimiosensibilisateur, soit comme un mécanisme chimioprotecteur.

Approches de thérapie génique visant à restaurer les fonctions de p53

Du fait de la grande fréquence de mutations de *TP53*, l'approche consistant à restaurer des fonctions de p53 par l'introduction d'une copie normale du gène sauvage est vite apparue comme logique et pertinente. Elle a pour objectif de bloquer le développement tumoral et, éventuellement, de sensibiliser les cellules malignes aux composés cytotoxiques, augmentant ainsi la réponse thérapeutique. La principale difficulté d'une telle approche de thérapie génique est liée à l'efficacité, voire à la spécificité, de la vectorisation.

• *Approches de thérapie génique par utilisation de rétrovirus*

En tant que vecteurs de thérapie génique, les rétrovirus présentent l'intérêt théorique d'intégrer de façon stable le génome des cellules infectées. La division cellulaire est nécessaire à leur transduction, ce qui les rend particulièrement attractifs pour une approche anticancéreuse. Plusieurs équipes ont ainsi montré que l'utilisation de vecteurs rétroviraux permettant l'expression de *TP53* sauvage conduisait à une inhibition significative de la croissance des cellules tumorales dans le cadre d'approches précliniques.

Sur la base de ces observations, une étude clinique de phase I a été réalisée pour déterminer la toxicité de l'introduction de *TP53* par rétrovirus [6]. Neuf patients présentant un cancer du poumon non à petites cellules, chez lesquels les traitements conventionnels avaient échoué, ont été inclus dans cette étude. Un vecteur rétroviral contenant *TP53* sauvage sous le contrôle du promoteur de la β-actine a fait l'objet d'une injection directement dans les tumeurs (intratumorale) par une méthode bronchoscopique ou guidée par tomographie et assistée par ordinateur. Aucun effet secondaire toxique majeur n'a été rapporté, avec un recul de 5 mois après le traitement. Les biopsies effectuées après traitement présentaient un index apoptotique plus élevé que celui observé avant le traitement. Sur 7 patients pouvant être évalués, 3 ont présenté une régression tumorale et 3 une stabilisation de la maladie. Cependant, en dépit de la détection des séquences du vecteur par ADN polymérase ou hybridation *in situ* dans les biopsies post-traitement, l'expression du transgène n'a pas été démontrée.

• *Approches de thérapie génique par utilisation d'adénovirus*

Les adénovirus sont des virus à ADN double brin présentant une haute efficacité de transduction dans un grand nombre de types cellulaires. Contrairement aux rétrovirus, leur effet n'est pas limité aux cellules en cours de prolifération. De nombreuses études ont démontré que l'administration d'un adénovirus du sérotype 5 présentait une faible toxicité chez l'humain. En effet, la plupart des adultes (85 %) présentent des anticorps dirigés contre les adénovirus du sérotype 5, mais moins de 15 % des patients exposés présentent des symptômes relatifs à cette infection. Enfin, contrairement au mode d'action des

rétrovirus, l'absence d'intégration génomique permet d'écarter tout risque de mutagenèse insertionnelle dans les cellules infectées.

L'Ad5CMV-p53 (Advexin®, Introgen Therapeutics Inc. ; Gendicine®, Shenzhen SiBiono GeneTch Co. Ltd) est un adénovirus du sérotype 5 dont le génome est amputé de la région E1 et qui code pour la protéine p53 sauvage sous le contrôle du promoteur CMV (cytomégalovirus). Des études *in vitro* ont montré qu'il permettait d'induire une expression efficace de la protéine p53 sauvage et fonctionnelle, inhibant ainsi la croissance cellulaire et potentialisant l'effet cytotoxique de molécules anticancéreuses dans différents modèles cellulaires. Des expériences réalisées dans des modèles animaux ont confirmé le potentiel thérapeutique de l'Ad5CMV-p53 *in vivo*. Ces études ont également confirmé que le risque que *TP53* transduit s'intègre dans le génome de l'hôte était négligeable et qu'il n'était pas augmenté par l'usage des traitements conventionnels en thérapie anticancéreuse. Depuis ces premières études, l'intérêt pour cette approche n'a cessé de croître, donnant lieu à de nombreuses évaluations cliniques [7]. La mise en place d'études précliniques a permis de montrer que l'injection intratumorale d'Ad5CMV-p53 était à l'origine d'une mort spécifique des cellules tumorales. Ces essais ont aussi démontré que l'Ad5CMV-p53 était dépourvu de nocivité et bien toléré, avec des réactions secondaires minimes. Cette faible toxicité fait de lui un composé présentant un index thérapeutique élevé, pouvant être utilisé en combinaison avec d'autres traitements conventionnels tels que la chimiothérapie et/ou la radiothérapie.

– *Ad5CMV-p53 et cancer du poumon non à petites cellules (non small cell lung cancer, NSCLC)*. Une première étude de phase I a été réalisée par administration (injection bronchoscopique ou percutanée guidée par tomographie) d'Ad5CMV-p53 par paliers de doses, en monothérapie, chez 15 patients présentant un NSCLC avec mutations de *TP53*. Le transfert du gène n'a été efficace qu'à de hautes doses de vecteur. Une stabilisation locale et transitoire de la maladie a cependant été observée après une seule injection intratumorale chez 4 patients sur 6 présentant une transduction significative du transgène. Aucune toxicité majeure n'a été observée. Une seconde étude de phase I a évalué l'effet d'injections multiples d'Ad5CMV-p53 à des doses comprises entre 10^6 et 10^{11} PFU (*plaque-forming unit*) chez 28 patients atteints d'une maladie évolutive. L'ADN de l'adénovirus a été détecté dans les biopsies de 18 patients sur 21 testés. L'activité thérapeutique, évaluée chez 25 patients, s'est manifestée sous la forme d'une réponse partielle chez 2 patients et d'une stabilisation (entre 2 et 4 mois) chez 16 ; les 7 autres patients ont présenté une progression de la maladie. Les effets secondaires du vecteur ont consisté essentiellement en des douleurs au site d'injection et en une fièvre modérée. La dose maximale tolérée n'a pas été évaluée. Dans une troisième étude de phase I, l'Ad5CMV-p53 a été administré dans les bronches des patients (n = 25) par instillations répétées. La concentration initiale était de 2.10^9 vp (*viral particles*) par dose, selon 14 cycles de thérapie et l'administration échelonnée en doses croissantes par puissances de 10 vp. La dose maximale tolérée a été évaluée à 2.10^{12} vp. Un patient a présenté à cette dose une toxicité pulmonaire de grade 4 tandis qu'un autre est décédé 1 mois après son second cycle de thérapie. Une cohorte de 10 patients a été traitée, en phase II par 5.10^{11} vp/dose. À cette concentration, aucune toxicité supérieure au grade 3 n'a été observée. Des effets secondaires modérés, à titre d'hypoxie, de dyspnées et de fièvre, ont été observés. Sur les 24 patients évaluables, 1 patient a montré une réponse partielle en radiographie, 1 a présenté une réponse pathologique au niveau du lobe traité, 17 ont montré une stabilisation de la maladie et 7 ont présenté une maladie évolutive 4 semaines après le début de la thérapie. L'Ad5CMV-p53 a également été évalué en association, soit à une chimiothérapie, soit à une radiothérapie, par l'équipe de Nemunaitis [8], dans le cadre d'une étude de phase I. Avec des injections intraveineuses de cisplatine, elle était bien tolérée et présentait une certaine efficacité. Dans une étude multicentrique de phase II, chez 25 patients incurables présentant un NSCLC, l'Ad5CMV-p53 injecté en intratumoral a été évalué seul ou associé à des chimiothérapies carboplatine et paclitaxel. Les patients du groupe traité par l'association ont présenté un effet local contrairement à ceux traités par l'Ad5CMV-p53 seul. Néanmoins, dans des conditions optimales de chimiothérapie, l'utilisation d'Ad5CMV-p53 ne semblait pas présenter de bénéfice additionnel. Enfin, une étude de phase II a évalué la combinaison de l'Ad5CMV-p53 avec la radiothérapie chez 19 patients non métastatiques mais non sélectionnables pour la chimioradiation ou la chirurgie. Sur ces 19 patients, 12 (63 %) ont présenté une réponse partielle ou complète au niveau du site d'injection, 3 mois après l'arrêt du traitement. Les réponses cliniques étaient associées à une réponse histologique évaluée après biopsie.

– *Ad5CMV-p53 et cancer de la tête et du cou*. L'Ad5CMV-p53 a également montré une activité dans les cancers de la tête et du cou, au cours de divers essais de phases I et II que nous ne détaillerons pas ici. Il est important cependant de souligner que, en octobre 2003, sous le nom de spécialité Gendicine® (Shenzhen SiBiono GeneTch Co. Ltd), il a reçu une autorisation de mise sur le marché par la SFDA (State Food and Drug Administration of China), avec une indication dans le carcinome à cellules squameuses de la tête et du cou (*head and neck squamous cell carcinoma*, HNSCC) et est ainsi devenu le premier médicament de thérapie génique pour le traitement du cancer [9]. Dans une étude de phase I, 12 patients présentant un laryngocarcinome ont reçu 10 injections intratumorales. Aucun n'a présenté de rechute entre 36 et 42 mois après le traitement. Une étude multicentrique de phase II, randomisée avec placebo, a été réalisée par injection intratumorale de l'Ad5CMCV-p53 (10^{12} vp/dose par semaine pendant 8 semaines) seule ou en association avec une radiothérapie (70 grays/8 semaines), chez des patients présentant un HNSCC avancé (n = 45) [7]. L'innocuité de ce traitement et l'efficacité de l'association Ad5CMCV-p53 et radiothérapie, en comparaison à la radiothérapie seule, ont été démontrées. Les effets secondaires se sont limités à des fièvres (grades I-II) chez 31 % des patients. Une rémission complète a été observée chez 65 % des patients du groupe traité par la combinaison Ad5CMV-p53 et radiothérapie contre seulement 20 % dans le groupe traité par la radiothérapie seule.

– *Ad5CMV-p53 et autres types tumoraux*. Dans les cancers ovariens, la thérapie génique par administration d'Ad5CMV-p53 n'a pas montré d'efficacité potentiellement exploitable en clinique [10], tandis que, dans les glioblastomes, les cancers de la vessie, les cancers du sein, les cancers œsophagiens et les mélanomes, elle a montré une activité faible à modérée.

– *Problèmes spécifiques à l'utilisation de l'Ad5CMV-p53*. L'hétérogénéité, voire la perte d'expression, des récepteurs

pour l'adénovirus de sérotype 5 (*coxsackie-adenovirus receptor*, CAR) et des corécepteurs (intégrines de classes αvβ3 et αvβ5) dans les tumeurs peut être à l'origine d'une faible infectivité [10]. Celle-ci peut être également due à des anticorps anti-Ad5 dans les ascites tumorales. Par ailleurs, l'efficacité d'une approche de thérapie génique de ce type peut être diminuée par l'existence d'altérations d'effecteurs ou de modulateurs endogènes de p53, de dérégulations d'ordre épigénétique ou de la présence d'une forme dominante négative de p53, contribuant à une inactivation fonctionnelle du transgène *TP53*.

Lyse des cellules déficientes pour p53 par un adénovirus modifié

L'utilisation d'un adénovirus déficient pour la protéine virale E1B représente une approche originale qui exploite le statut de p53 dans les cellules cancéreuses. Cette approche est différente de la thérapie génique de « remplacement ». En effet, elle n'implique pas le transfert de p53 dans les cellules mais repose sur l'introduction d'un virus génétiquement modifié utilisant la perte de fonctionnalité de p53 pour tuer spécifiquement les cellules tumorales.

• *Onyx015*

La réplication et l'activité lytique des adénovirus de type sauvage nécessitent le détournement de la synthèse protéique des cellules infectées. Ces processus reposent sur l'inactivation des points de contrôle dépendant des voies de signalisation de la protéine Rb (protéine du rétinoblastome) et de p53, respectivement par les protéines virales E1A et E1B. L'adénovirus delta 1520 (dl1520, Onyx015, Onyx Pharmaceuticals) a été génétiquement modifié afin qu'il n'exprime pas la protéine E1B 55KDa. De ce fait, il ne peut pas neutraliser p53 au cours de l'infection et, tout au moins en théorie, peut donc se répliquer uniquement dans les cellules p53-déficientes. Il exerce ainsi un effet lytique sur les tissus présentant une altération de p53, sans affecter les tissus « normaux » exprimant p53 (*figure 2*).

Des expériences *in vitro* ont montré que l'Onyx015 pouvait provoquer la mort de cellules tumorales déficientes pour p53, avec une efficacité comparable à celle observée avec un adénovirus non modifié [7]. Il a été également démontré que ce virus provoquait une réduction significative de la masse tumorale dans des modèles de xénogreffes chez la souris *nude*. Par ailleurs, le traitement par l'Onyx015 sensibilise les cellules tumorales déficientes pour p53 à la radiothérapie. Des études chez l'animal ont montré que l'efficacité de l'Onyx015 était indépendante du mode d'administration. L'efficacité semble, par ailleurs, accrue par l'utilisation de doses fractionnées et par l'administration de la chimiothérapie conventionnelle avant plutôt qu'après ou concomitamment à l'Onyx015.

Il subsiste cependant des questions non élucidées concernant le mode d'action de l'Onyx015 et, en particulier, sur sa supposée spécificité pour les cellules p53-déficientes. En effet, de nombreux travaux expérimentaux montrent que l'Onyx015, comme l'Ad5CMV-p53, est capable de se répliquer dans divers types cellulaires, indépendamment du statut (sauvage ou muté) du gène *TP53*. Ces données apparaissent donc en contradiction avec le modèle de destruction sélective des cellules tumorales. De plus, différents essais cliniques ont montré que le traitement par l'Onyx015 induisait une réponse objective à la fois dans des tissus tumoraux p53-déficients et dans des tissus tumoraux exprimant p53 sauvage, sans pour autant endommager les tissus normaux. Une étude du groupe de Ries fournit une hypothèse rationnelle à cette observation [11]. Elle suggère en effet que la lyse par l'Onyx015 peut avoir lieu dans des cellules exprimant p53 sauvage, si certains de ses effecteurs sont altérés, provoquant ainsi une inactivation de la voie contrôlée par p53. Cependant, le mécanisme détaillé de la sélectivité de l'Onyx015 demeure un sujet controversé. Hann et Balmain ont analysé la réplication de l'Onyx015 dans des cellules épithéliales humaines exprimant un dominant négatif de *TP53* ou un mutant présentant un gain de fonction [7]. Parmi tous les allèles analysés, seul le mutant R248W (dépourvu d'activité de liaison à l'ADN, mais conservant une conformation globale proche de p53 sauvage) facilite significativement la réplication de l'Onyx015. Ainsi, la nature de la mutation de *TP53* pourrait affecter les propriétés lytiques de l'Onyx015.

Dans la plupart des essais cliniques, l'Onyx015 est administré par injection intratumorale. Certaines études récentes de phase I ont démontré la faisabilité et l'innocuité d'autres modes d'administration de types injections intrapéritonéales, intraartérielles ou intraveineuses, seules ou en association avec une chimiothérapie et/ou à une radiothérapie. Un autre essai clinique récent a testé la faisabilité d'une administration topique de l'Onyx015 par des bains de bouche, chez des patients présentant des lésions dysplasiques prémalignes de la muqueuse orale. Toutes ces études ont montré une bonne tolérance des patients vis-à-vis de l'Onyx015, à des doses maximales administrées (10^{13} PFU) sans provoquer de toxicité dose-limite. Les effets secondaires les plus fréquemment décrits sont des symptômes pseudo grippaux et des douleurs au site d'injection. La toxicité semble liée spécifiquement au mode d'administration. Des *carriers* alternatifs ont fait l'objet d'études précliniques montrant des taux élevés d'infectivité en utilisant de la lignocaïne à 1 % ou de la hyaluronidase à 200 UI/ml.

• *Problèmes spécifiques à l'utilisation de l'Onyx015*

Comme avec l'Ad5CMV-p53, l'hétérogénéité ou la perte des récepteurs et corécepteurs dans les tumeurs peut être impliquée dans la diminution de l'infectivité de l'Onyx015. Par ailleurs, de nombreuses tumeurs sont résistantes à la réplication oncolytique de l'Onyx015. Contrairement aux lignées cellulaires tumorales permissives, les lignées tumorales réfractaires infectées par l'Onyx015 semblent présenter une résistance à l'inhibition de la synthèse protéique, en l'absence de la protéine E1B. Or, ce mécanisme participe normalement à la réplication oncolytique. Cependant, l'application d'un choc thermique sensibilise ces cellules à l'activité cytolytique de l'adénovirus [12]. Les protéines de choc thermique (*heat shock proteins*, Hsp) étant surexprimées dans de nombreux cancers, l'utilisation d'inducteurs pharmacologiques de la réponse au choc thermique (de type ansamycines benzoquinoïdes) ou l'induction d'une hyperthermie locale pourrait permettre d'améliorer l'efficacité de l'Onyx015.

Autres stratégies de thérapie génique

• *Utilisation du virus de la vaccine*

Plusieurs études précliniques ont utilisé des vecteurs viraux dérivés du virus de la vaccine pour délivrer *TP53* à des fins de thérapie génique. Des résultats intéressants ont été rapportés, en particulier en termes d'activité oncolytique, mais ils nécessitent d'être confirmés avant d'envisager des essais cliniques.

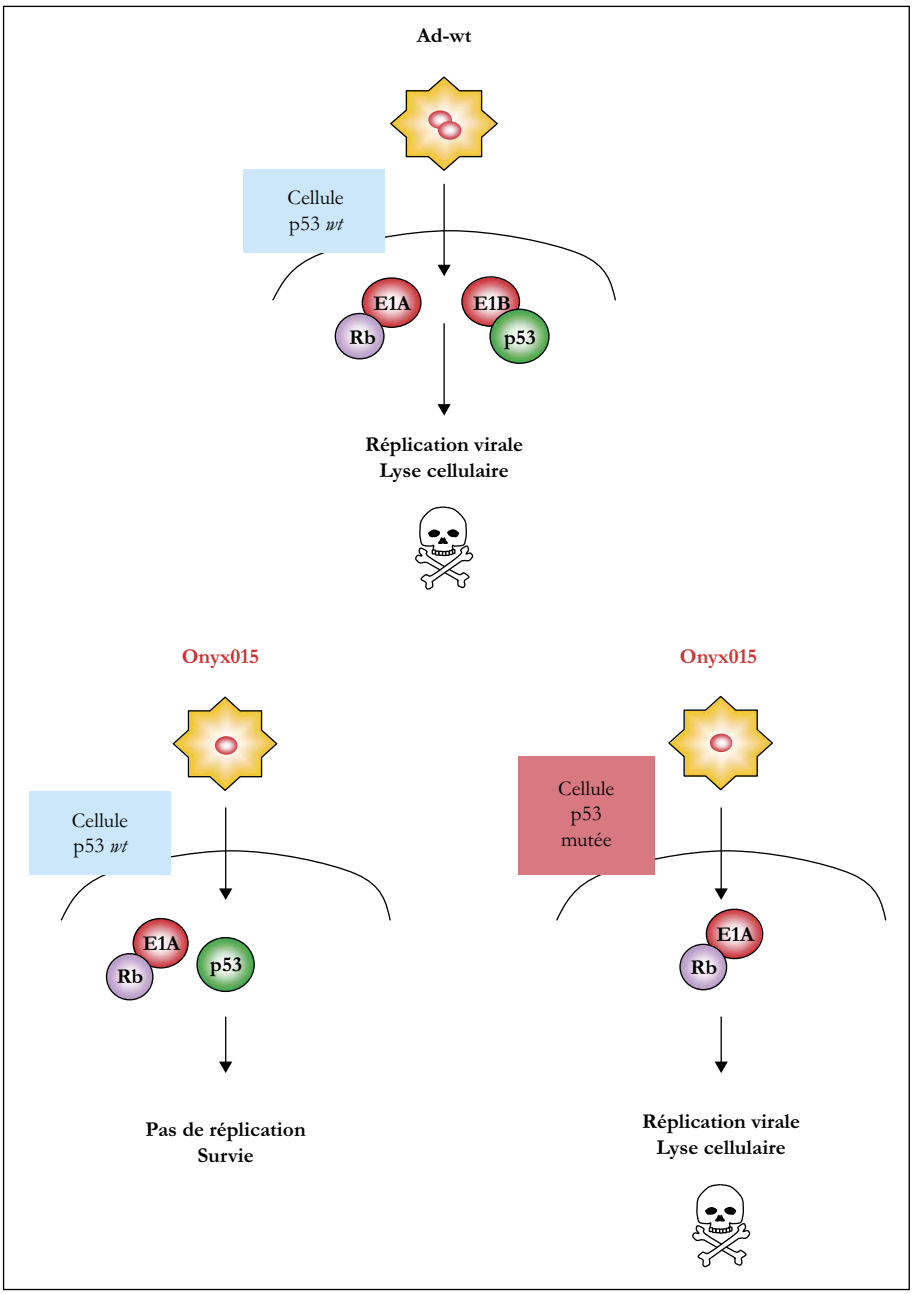

Figure 2. Principe de la thérapie par l'Onyx015. La réplication d'un adénovirus sauvage (Ad-*wt*) dans une cellule normale provoque une lyse cellulaire. L'Onyx015 (dans lequel E1B est délétée) est incapable de se répliquer dans une cellule normale, du fait de l'effet suppressif de p53 sauvage (p53 wt). En revanche, dans une cellule déficiente pour p53, le virus peut se répliquer et induire la lyse cellulaire.

• *Transduction virale de constructions chimériques de TP53*

L'équipe d'Emmanuel Conseiller a construit, en 1998, une chimère suppressive de tumeur, CTS1 (*chimeric tumor suppressor* 1), fondée sur la structure de p53 sauvage dans laquelle les domaines N et C-terminaux ont été substitués par des séquences hétérologues [13]. Cette substitution a été réalisée dans le but de supprimer la régulation négative exercée par ces deux domaines sur p53 à travers, respectivement, la dégradation dépendante de mdm2 et la régulation allostérique de la liaison à l'ADN. Cette protéine chimère semble présenter une activité similaire à celle de p53, et constitutive pour la suppression de la croissance et l'induction de l'apoptose. Cette activité n'est altérée ni par le rôle physiologique de mdm2, ni par l'expression d'une protéine p53 mutante dominante négative.

Le transfert adénoviral de *CTS1* a montré qu'il était plus efficace que celui de p53 sauvage avec le même vecteur. La chimère induit une expression prolongée de p53 et exerce ainsi une activité majeure de suppression de la croissance tumorale.

• *Stratégies non virales*

Un certain nombre d'études utilisant des stratégies non virales pour introduire un plasmide exprimant *TP53* ont été réalisées. Nous ne les détaillerons pas ici. On peut néanmoins

citer l'injection directe du gène *TP53* « nu », l'utilisation de liposomes ou l'électroporation. Les avantages de ces techniques sont leur faible immunogénicité et l'innocuité des excipients utilisés. De façon générale, les stratégies non virales sont cependant encore loin de permettre des taux de transduction aussi efficaces que ceux obtenus avec les vecteurs viraux.

Modulation pharmacologique des fonctions de p53

La modulation des fonctions de p53 peut présenter différents bénéfices, en fonction des cellules ciblées et du contexte clinique. Dans le cadre d'une réflexion théorique, on peut en effet envisager une activation pharmacologique de p53 sauvage ou la réactivation d'une forme mutante inactive de p53 dans les cellules tumorales pour potentialiser la réponse à la thérapie et conduire à la mort cellulaire. On peut également envisager d'inactiver les fonctions de p53 dans les cellules normales pour inhiber la réponse apoptotique induite par les agents thérapeutiques et les protéger ainsi contre les effets toxiques de la thérapie.

• *Activation des fonctions oncosuppressives de p53*

Le mécanisme le plus direct pour induire l'accumulation de p53 sauvage est d'empêcher sa régulation négative par mdm2. Cette protéine est transcriptionnellement activée par p53 grâce à des éléments de réponse situés dans son promoteur. La protéine mdm2 est une E3-ligase capable de se lier à la partie N-terminale de p53, inhibant ainsi son activité transcriptionnelle, et d'induire sa dégradation par le protéasome après ubiquitinylation. En 1997, Bottger a réalisé une miniprotéine synthétique liant mdm2 et ciblant spécifiquement le site de liaison à p53 [7]. Cette miniprotéine correspond à l'insertion d'un peptide au niveau du site actif de la protéine virale thiorédoxine. Nommée superTIP (*thioredoxin insert protein*), elle entre en compétition avec mdm2 pour la liaison à p53, conduisant ainsi à l'accumulation nucléaire de p53, activant la transcription p53-dépendante et provoquant l'arrêt du cycle cellulaire.

Plus récemment, l'équipe de Vassilev a identifié une famille de composés synthétiques, appelés nutlines, qui semblent pouvoir exclure p53 de sa poche de liaison à mdm2 [14]. Comme attendu, ces composés activent p53 et induisent un arrêt du cycle cellulaire et l'apoptose dans les cellules tumorales présentant une p53 sauvage. En revanche, les nutlines sont inactives dans les tumeurs où p53 est mutée. Dans les cellules normales, elles provoquent un arrêt de croissance mais non l'apoptose, cet arrêt de croissance étant réversible quand les composés sont éliminés. Dans des modèles de xénogreffes, elles ont montré qu'elles pouvaient contrôler la croissance des tumeurs, sans toxicité apparente pour les tissus normaux. D'autres approches ont été depuis proposées pour inhiber l'interaction p53-mdm2.

Une voie biochimique potentiellement intéressante pour l'activation de p53 est celle des polyamines. Ces molécules sont des régulateurs essentiels de la croissance cellulaire à travers divers mécanismes encore mal compris. Des analogues synthétiques des polyamines semblent pouvoir activer les fonctions de p53 dans un certain nombre de types cellulaires [7]. Il semblerait que les polyamines jouent un rôle dans le contrôle de la conformation de p53 et dans son activité mais des travaux seront nécessaires pour préciser leur mécanisme d'action et déterminer si elles peuvent à l'avenir être utilisées en clinique pour moduler les fonctions de p53.

• *Inhibiteurs de p53*

La pifithrine (*figure 3*) est un composé synthétique qui bloque l'expression de p53 au niveau transcriptionnel [15]. Il inhibe l'apoptose induite par irradiation ou traitement par la doxorubicine, l'étoposide, le paclitaxel ou l'ara-C, dans des cellules exprimant une p53 sauvage. La pifithrine pourrait donc être utilisée pour réduire les effets secondaires de la radiothérapie ou de la chimiothérapie. Il a en effet été montré que son administration dans des modèles animaux protégeait contre les effets secondaires de composés cytotoxiques. Néanmoins, des travaux récents ont montré qu'elle pouvait aussi promouvoir l'apoptose induite par la doxorubicine des cellules épidermiques JB6C141 de souris.

• *Réactivation des fonctions de p53 dans des tumeurs exprimant une forme mutante de TP53*

Comme indiqué précédemment, les protéines mutantes de p53 diffèrent entre elles par leurs propriétés biologiques. Tandis que certains mutants semblent dépourvus de façon définitive des fonctions oncosuppressives de p53, d'autres ne présentent qu'une perte partielle et/ou réversible. L'activité biochimique majeure qui est inactivée par mutation est la liaison spécifique à l'ADN. Cette activité est régulée par deux domaines C-terminaux responsables de l'oligomérisation (résidus 325-363) et du contrôle négatif de la liaison à l'ADN (résidus 363-393). L'inhibition de ce dernier est cruciale pour une liaison de haute affinité à l'ADN. De nombreuses études montrent qu'il est possible de cibler ce domaine spécifiquement avec des peptides ou des protéines, afin de rétablir la capacité de liaison.

Les fragments variables d'anticorps simple chaîne (*single chain antibody fragments variable*, scFvs) sont des polypeptides dérivés d'anticorps monoclonaux dans lesquels les chaînes variables légères et lourdes sont reliées par un *linker* (pont d'acides aminés) flexible. Par exemple, la capacité d'association stable de scFv421 et scFv11D3 (générés à partir des

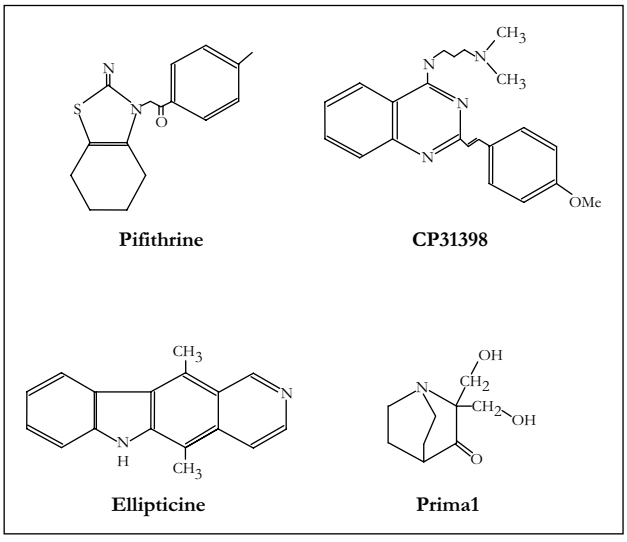

Figure 3. Petites molécules utilisées pour cibler p53 sauvage ou mutée. La pifithrine est un composé synthétique qui bloque l'expression de p53 au niveau transcriptionnel. CP31398 est une petite molécule capable de stabiliser le domaine central de p53. L'ellipticine permet de restaurer les fonctions transcriptionnelles de p53 dans des cellules exprimant une p53 mutée. Prima1 est capable de rétablir la propriété de liaison spécifique à l'ADN de protéines p53 mutantes.

anticorps monoclonaux de souris PAb421 et 11D3) avec p53 permet de restaurer efficacement l'activité de liaison à l'ADN de certains mutants *in vitro* [16]. Dans les cellules tumorales, ces scFvs sont donc capables de restaurer partiellement l'activité transcriptionnelle d'une protéine p53 mutée. En utilisant une approche similaire, Govorko et son équipe ont construit une librairie de scFvs à partir de souris immunisées par un épitope cryptique dans p53 sauvage mais exposé dans un grand nombre de formes mutantes. Le scFv ME1 a ainsi été isolé pour sa liaison spécifique à p53 mutée. Ces molécules représentent une nouvelle famille d'agents thérapeutiques anticancéreux potentiels, appelés les *trabodies* (*transcription-activating antibodies*).

De nombreuses petites molécules chimiques ont été développées pour stabiliser la structure du domaine de liaison à l'ADN de p53, limitant ainsi les conséquences fonctionnelles des mutations de *TP53* les plus fréquentes. À titre d'exemple, il a été récemment développé une famille de molécules contenant deux groupements hydrophobes reliés par un *linker*, capables d'interagir avec le domaine de liaison à l'ADN de p53 et de stabiliser sa structure. Ces composés protègent les protéines p53 sauvages contre la dénaturation thermique et restaurent partiellement la capacité de certains mutants à réagir avec des anticorps spécifiques de p53 sauvage. Ces composés peuvent également stimuler la transcription dépendante de p53 d'un gène rapporteur dans des cellules exprimant une p53 mutée. De plus, l'un de ces composés, le CP31398 (*figure 3*), semble pouvoir inhiber la croissance de petites xénogreffes de lignées tumorales humaines chez la souris *nude* à des doses ne provoquant pas d'effets secondaires. De la même manière, un peptide de 9 résidus nommé CDB3 semble, selon le même principe que pour le CP31398, agir comme une protéine chaperon et secourir p53 de sa forme mutante. Ces études préliminaires nécessitent cependant d'être confirmées par de nouvelles études précliniques. Par ailleurs, d'autres composés chimiques ont été développés, capables d'induire l'expression de gènes cibles de p53, tels que *p21/WAF1* ou *BAX*, dans des cellules exprimant une

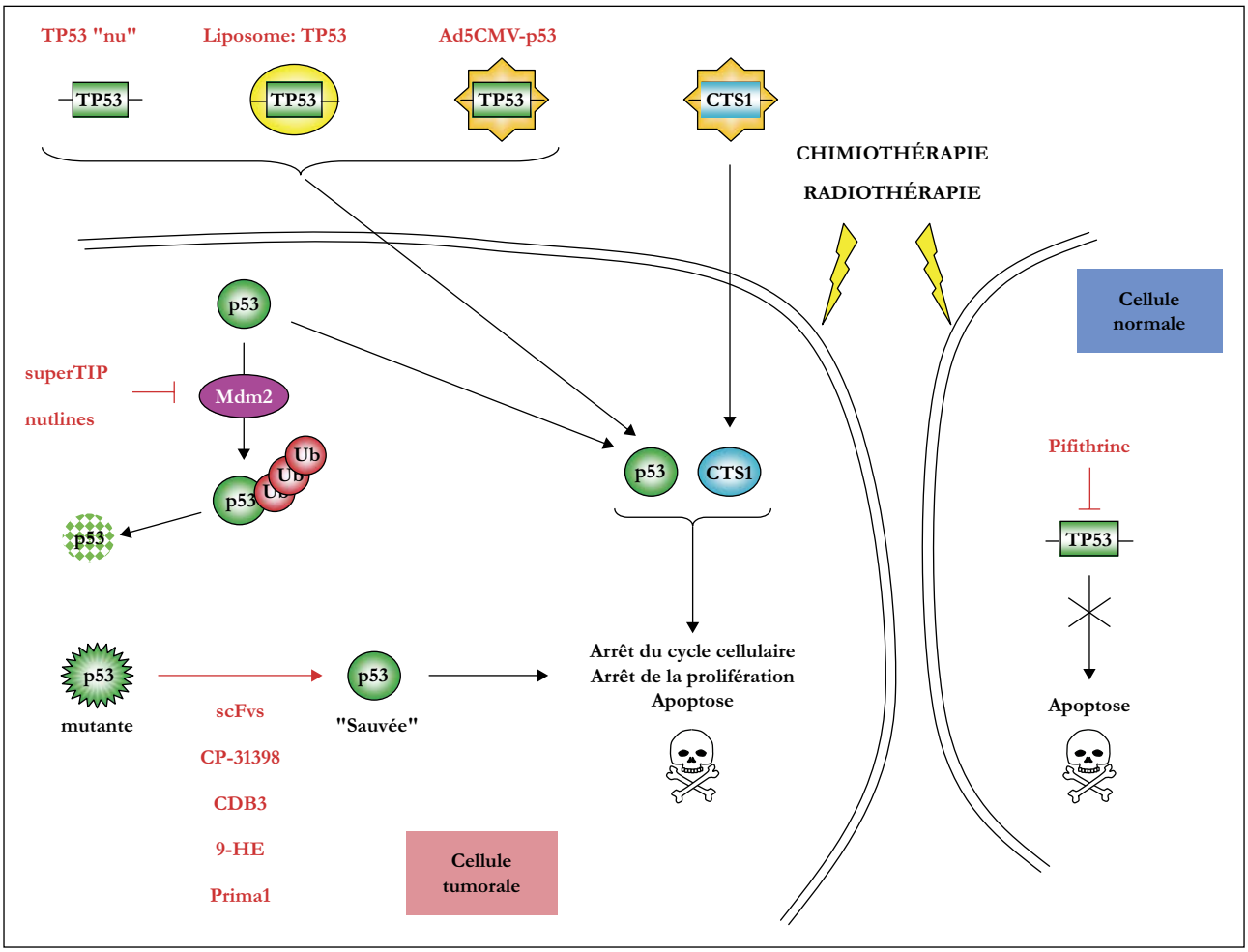

Figure 4. Stratégies thérapeutiques agissant sur les fonctions de p53. La protéine p53 sauvage peut être réexprimée dans les cellules tumorales pour restaurer ses fonctions oncosuppressives. Différentes approches ont été développées : injection intratumorale de *TP53* « nu », introduction de liposomes complexés avec des plasmides codant pour *TP53* (liposome : *TP53*), infection par l'adénovirus de sérotype 5 exprimant *TP53* sous le contrôle d'un promoteur CMV (Ad5CMV-p53), infection par un adénovirus exprimant le suppresseur de tumeur chimérique CTS1 (*chimeric tumor suppressor 1*) récapitulant, de façon constitutive, les fonctions oncosuppressives de p53. La liaison avec mdm2 peut être inhibée pour stabiliser p53 en empêchant son ubiquitinylation (Ub) (superTIP, nutlines). Les formes mutantes de p53 peuvent subir un « sauvetage » fonctionnel (scFvs ou *single chain fragments variable*), CP31398, CDB3, hydroxyellipticine 9 (9HE), Prima1. Enfin, la pifithrine peut être utilisée dans les cellules normales pour les protéger des effets toxiques des radiothérapies et chimiothérapies conventionnelles, en inhibant l'expression de p53.

p53 mutée, mais non dans des cellules dépourvues de p53. Cela suggère que leur activité repose également sur le « sauvetage » des protéines p53 mutantes. Parmi ces composés, la 9-hydroxyellipticine (9HE) est capable d'induire l'apoptose en phase G1 du cycle, dans des lignées cellulaires exprimant une p53 mutée [7]. Prima 1 est un autre exemple de molécule capable de restaurer les propriétés de liaison à l'ADN pour un grand nombre de mutants p53, *in vitro*, incluant les protéines mutées au niveau des « points chauds ». Le traitement de cellules exprimant une forme mutée de p53 par Prima 1 provoque l'activation des gènes cibles de p53 [17]. Au contraire, les cellules exprimant une protéine p53 sauvage et traitées par Prima 1 ne semblent pas montrer de stabilisation de la protéine ni d'induction de gènes cibles de p53. Des expériences menées par Bykov *et al.* [17], et utilisant des souris SCID porteuses de xénogreffes de cellules tumorales, ont montré que Prima 1 exerce une activité antitumorale dépendante de la mutation de p53 et sans effets toxiques notoires. Son mécanisme d'action reste à identifier (*figure 3*).

Perspectives

Du fait de leur rôle central dans le contrôle de la vie et de la mort des cellules exposées aux agents génotoxiques, la protéine p53 et son gène *TP53* demeurent des cibles attractives pour le développement d'approches thérapeutiques.
Une première approche a consisté à restaurer ou à potentialiser les fonctions de p53 dans les cellules tumorales (*figure 4*). Ces cellules deviennent alors plus sensibles à la cytotoxicité de la radiothérapie et de la chimiothérapie. Ces chimio et radiosensibilisations restent actuellement l'objectif principal de la plupart des stratégies ciblant *TP53* dans les cancers. En ce sens, les virus déficients pour la réplication et contenant *TP53* sauvage (Ad5CMV-p53) et/ou les adénovirus oncolytiques tumorosélectifs (Onyx015) représentent des outils prometteurs. Cependant, de nombreuses questions concernant l'utilisation de l'Ad5CMV-p53 et de l'Onyx015 restent encore en suspens. En particulier, le mode d'administration et la vectorisation sont des problèmes dont l'approche demeure délicate. Dans les tumeurs localisées, le transfert de ces composés est en général réalisé par injection intratumorale avec une bonne tolérance et une activité clinique évidente. Alors que, dans la majorité des cas de cancer, une administration intraveineuse serait nécessaire, différentes publications montrent que l'utilisation de cette voie diminue de façon considérable l'efficacité du traitement. De même, la spécificité tumorale des vecteurs utilisés reste matière à débat. Des modifications tumorospécifiques ou histospécifiques des protéines de l'enveloppe pourraient, tout en réduisant les effets secondaires, augmenter la sélectivité des vecteurs. Dans la même optique, les nouvelles générations de vecteurs, plaçant l'expression de transgènes thérapeutiques sous le contrôle de promoteurs ou de régions régulatrices tumorospécifiques, représentent un champ d'investigation tout à fait prometteur. L'intérêt de ce type de stratégie est démontré par des études précliniques, ce qui laisse envisager une nouvelle base rationnelle pour la thérapie génique ciblant *TP53* [18]. Enfin, l'immunogénicité des vecteurs adénoviraux reste un problème important à résoudre pour le développement de la thérapie génique. Une seconde approche consiste en la modulation pharmacologique des fonctions de p53 dans les cellules normales afin d'induire un effet protecteur. Sur la base d'études cliniques récentes, plusieurs molécules pourraient à terme trouver leur place dans l'arsenal thérapeutique anticancéreux. La nécessité d'utiliser de fortes doses pour l'obtention d'un effet protecteur reste cependant aujourd'hui un frein significatif à leur utilisation. ▼

RÉFÉRENCES

1. Lowe SW, Cepero E, Evan G. Intrinsic tumour suppression. *Nature* 2004 ; 432 : 307-15.

2. Bartkova J, Horejsi Z, Koed K, *et al.* DNA damage response as a candidate anti-cancer barrier in early human tumorigenesis. *Nature* 2005 ; 434 : 864-70.

3. Gorgoulis VG, Vassiliou LV, Karakaidos P, *et al.* Activation of the DNA damage checkpoint and genomic instability in human precancerous lesions. *Nature* 2005 ; 434 : 907-13.

4. Valsesia-Wittmann S, Magdeleine M, Dupasquier S, *et al.* Oncogenic cooperation between H-Twist and N-Myc overrides failsafe programs in cancer cells. *Cancer Cell* 2004 ; 6 : 625-30.

5. Galmarini CM, Falette N, Tabone E, *et al.* Inactivation of wild-type p53 by a dominant negative mutant renders MCF-7 cells resistant to tubulin-binding agent cytotoxicity. *Br J Cancer* 2001 ; 85 : 902-8.

6. Roth JA, Nguyen D, Lawrence DD, *et al.* Retrovirus-mediated wild-type p53 gene transfer to tumors of patients with lung cancer. *Nat Med* 1996 ; 2 : 985-91.

7. Bouchet BP, Caron de Fromentel C, Puisieux A, Galmarini CM. p53 as a target for anticancer drug development. *Crit Rev Oncol Hematol* (*sous-presse*).

8. Nemunaitis J, Swisher SG, Timmons T, *et al.* Adenovirus-mediated p53 gene transfer in sequence with cisplatin to tumors of patients with non-small-cell lung cancer. *J Clin Oncol* 2000 ; 18 : 609-22.

9. Pearson S, Jia H, Kandachi K. China approves first gene therapy. *Nat Biotechnol* 2004 ; 22 : 3-4.

10. Zeimet AG, Marth C. Why did p53 gene therapy fail in ovarian cancer? *Lancet Oncol* 2003 ; 4 : 415-22.

11. Ries SJ, Brandts CH, Chung AS, *et al.* Loss of $p14^{ARF}$ in tumor cells facilitates replication of the adenovirus mutant dl1520 (Onyx-015). *Nat Med* 2000 ; 6 : 1128-33.

12. O'Shea CC, Soria C, Bagus B, McCormick F. Heat shock phenocopies E1B-55K late functions and selectively sensitizes refractory tumor cells to Onyx-015 oncolytic viral therapy. *Cancer Cell* 2005 ; 8 : 61-74.

13. Conseiller E, Debussche L, Landais D, *et al.* CTS1 : a p53-derived chimeric tumor suppressor gene with enhanced in vitro apoptotic properties. *J Clin Invest* 1998 ; 101 : 120-7.

14. Vassilev LT, Vu BT, Graves B, *et al.* In vivo activation of the p53 pathway by small-molecule antagonists of MDM2. *Science* 2004 ; 303 : 844-8.

15. Komarov PG, Komarova EA, Kondratov RV, *et al.* A chemical inhibitor of p53 that protects mice from the side effects of cancer therapy. *Science* 1999 ; 285 : 1733-7.

16. Caron de Fromentel C, Gruel N, Venot C, *et al.* Restoration of transcriptional activity of p53 mutants in human tumour cells by intracellular expression of anti-p53 single chain Fv fragments. *Oncogene* 1999 ; 18 : 551-7.

17. Bykov VJ, Issaeva N, Shilov A, *et al.* Restoration of the tumor suppressor function to mutant p53 by a low-molecular-weight compound. *Nat Med* 2002 ; 8 : 282-8.

18. Kazhdan I, Long L, Montellano R, Cavazos DA, Marciniak RA. Targeted gene therapy for breast cancer with truncated Bid. *Cancer Gene Ther* 2005 ; [Epub ahead of print].

[Cancer Biology & Therapy 6:3, 377-382; March 2007]; ©2007 Landes Bioscience

Research Paper

Weekly Administration of Paclitaxel Induces Long-Term Aneugenicity in Nude Mice

Carlos M. Galmarini[1,*]
Benjamin P. Bouchet[2]
Nicole Falette[2]
Liliana Vila[3]
Christelle Lamblot[2]
Carole Audoynaud[2]
Jacques Bertholon[2]
Alain Puisieux[2]

[1]Université Claude Bernard Lyon 1 CNRS UMR 5239; Lyon, France

[2]Unité d'Oncologie Moléculaire; Centre Léon Bérard; Lyon, France

[3]Service d'Hématologie; Hôpital Edouard Herriot; Lyon, France

*Correspondence to: Carlos M. Galmarini; EA 3737 "Pathologie des Cellules Lymphoïdes"; UFR de Médecin Lyon-Sud; Centre Hospitalier Lyon-Sud; 165, Chemin du Grand Revoyet; Pierre-Bénite 69495 France; Tel.: +33.4.26.23.59.43; Fax: +.33.4.78.86.43.55; Email: carlos.galmarini@recherche.univ-lyon1.fr

Original manuscript submitted: 09/08/06
Manuscript accepted: 12/13/06

Previously published online as a *Cancer Biology & Therapy* E-publication: http://www.landesbioscience.com/journals/cc/abstract.php?id=3713

KEY WORDS

paclitaxel, drug toxicity, aneugens, micronuclei, micronucleus test

ABBREVIATIONS

MNE	micronucleated erythrocytes
MN	micronuclei
PB	peripheral blood
AO	acridine orange
BM	bone marrow
STA group	short-term analysis group
LTA group	long-term analysis group
AML	acute myeloid leukaemia
MDS	myelodisplastic syndrome
ALL	acute lymphoid leukaemia

ACKNOWLEDGEMENTS

Benjamin Bouchet is a recipient of a "Foundation pour la Recherche Medicale" grant.

ABSTRACT

We investigated the potential in vivo aneugenic effects associated with paclitaxel treatment. For this purpose, we treated female nude mice with paclitaxel using doses equivalent to those used in weekly schedules at the clinical level (three cycles of 30 mg/kg/week for three consecutive weeks followed by one resting week). We then evaluated the frequencies of micronucleated erythrocytes (MNE) in peripheral blood using the acridine orange micronucleus assay. The frequency of MNE was evaluated after 24 h and 168 h of administration of the last dose of each paclitaxel cycle (STA mice group) as well as after one year of the first dose of treatment (LTA mice group). We also analyzed the cytology of peripheral blood and bone marrows obtained from these mice at each time period. In the STA mice group, three cycles of paclitaxel induced a 2.4-fold increase in MNE frequencies compared to the control group ($p < 0.01$). This effect was observed after 24 h of the last dose of each chemotherapy cycle and persisted at least for 168 h. In the LTA mice group, paclitaxel-treated mice presented a 1.8-fold increase in the MNE frequency ($p = 0.01$) indicating that paclitaxel-induced MNE increase lasted for at least one year. Although the appearance of micronuclei in erythrocytes and granulocytes in peripheral blood and bone marrow cytological smears, there was no evidence of myeloproliferative disease. The present data therefore indicate an aneugenic potential of paclitaxel for humans, which should be considered in the risk-benefit analysis of its increasing clinical use.

INTRODUCTION

Paclitaxel (Taxol®) is a chemotherapeutic agent extracted from the bark of Taxus brevifolia (pacific yew).[1] In tumor cell lines, its cytotoxicity involves two independent phenomena depending on drug concentrations: at nanomolar range, paclitaxel suppresses microtubule dynamics inducing the appearance of lagging chromosomes and micronuclei formation.[2] At micromolar range, paclitaxel induces the formation of parallel microtubule bundles during interphase and abnormal spindle asters during mitosis.[3,4] Both effects induce cell cycle blockage in the G_2 or M phase and cause cell death.[5,6]

In the clinical practice, paclitaxel is among the most important agents available used for the treatment of a broad range of human cancers.[4] This drug exerts an important antitumor activity against several advanced, refractory, or metastatic human neoplasias such as ovarian, breast and non-small cell lung cancers.[7-9] Moreover, interesting results in terms of clinical outcome after administration of paclitaxel as an adjuvant chemotherapeutic agent have been reported, particularly in breast and lung cancers.[10-13]

Despite paclitaxel's increasing use at the clinical level, especially for the therapy of curable cancers, very few data are currently available on its potential genotoxicity on normal human cells. Nevertheless, paclitaxel belongs to the spindle inhibitors that are well-known aneugenic agents.[14-16] Aneuploidy is actually known to have a possible involvement in the emergence and progression of cancers.[17-19] In this sense, different clinical studies have reported the occurrence of secondary malignancies (especially acute leukemias) in patients treated with paclitaxel-based chemotherapy.[12,20,21] In these studies, paclitaxel was administered in combination to other chemotherapeutic agents (e.g., cyclophosphamide, etoposide, etc.) that are well-know inducers of aneugenicity.[22-25] Whether clinical administration of paclitaxel could also induce aneugenicity is not known.

Thus, increasing clinical use of taxol, coupled to its mode of antitumor action, suggest that its carcinogenic potential for humans should also be considered. However, few in vivo studies were designed to evaluate the frequency and severity of chromosomal damage following treatment with this agent.[26,27] This prompted us to investigate the potential in

vivo genotoxic effects associated with paclitaxel administration. For this purpose, we treated nude mice with doses of paclitaxel equivalent to those used in weekly schedules at the clinical level.[28-32] We then evaluated the frequencies of micronuclei (MN) in peripheral blood (PB) erythrocytes from paclitaxel-treated mice using the acridine orange (AO) micronucleus assay and analyzed the cytology of PB and bone marrows smears (BM) obtained from these mice.[33-35]

MATERIAL AND METHODS

Chemicals. Paclitaxel was purchased from Bristol Myers Squibb. Acridine orange was purchased from Sigma.

Animals. Female athymic swiss nude mice (aged four weeks at arrival) were obtained from IFFA-CREDO (L'Arbresle, France). Animals were housed in appropriate plastic cages and kept with conventional laboratory-specific animal husbandry procedures (e.g., appropriate room temperature, humidity, light cycle, etc.). Access to food and water was not restricted. The mice were inspected daily for evaluation of clinical condition while monitoring changes in animal weight twice a week. Animals were euthanized to avoid animal discomfort if clinical conditions may anticipate the potential for animal suffering.

The mice were acclimated to the laboratory environment and examined prior to initiation of the study to ensure that they appeared healthy. Experiments were performed at 8 weeks old (average weight: 23 g) where bone marrow is expected to be actively dividing.[35]

Mice treatment. Thirty-nine mice were assigned at random to three different groups: the short-term analysis (STA) group (n = 18), the long-term analysis (LTA) group (n = 12) and the control group (n = 9; untreated animals). Each animal of the STA and LTA groups received paclitaxel at a total dose of 30 mg/kg/week (equivalent to human dose of 100 mg/m2) for three consecutive weeks followed by one resting week. Paclitaxel was injected i.p. in appropriate volumes. Initial drug toxicity studies were performed at these doses and no major toxicities were observed (weight loss <10%).

In the STA group, mice received one (n = 6), two (n = 6) or three (n = 6) chemotherapy cycles. All mice in the LTA group received three chemotherapy cycles. There was no significant difference in toxicity between treatment groups.

Mice euthanasia. Animals of the STA group were killed periodically by cervical dislocation 24 h (n = 3) and 168 h (n = 3) after the last administration of paclitaxel in cycles 1–3. One mice of the control group was euthanized at the same time. Animals of the LTA group were followed for 1 year from the date of first paclitaxel injection before being euthanized. At that time, the last three mice of the control group were also killed.

Peripheral blood and bone-marrow collection. Blood and bone marrow samples were harvested according to the schedule described below. Blood samples were collected via intracardiac puncture under anesthesia (i.p. injection of ketamine 90 mg/kg and xylazine hydrochloride 10 mg/kg). An aliquout of heart puncture blood specimens from each animal were smeared onto clean microscope slides, allowed to air-dry, then fixed with absolute methanol for 3 min and stained with May Grundwald Giemsa.

For bone marrow collection, mice were killed under anesthesia by cervical dislocation and one usable femur was excised, skin and muscle tissue were trimmed, and both ends of the bone tips were severed with bone snips. Bone marrow was flushed out from the channel into a tube with RPMI medium supplemented with fetal calf serum 20%. An aliquot of bone marrow material was smeared

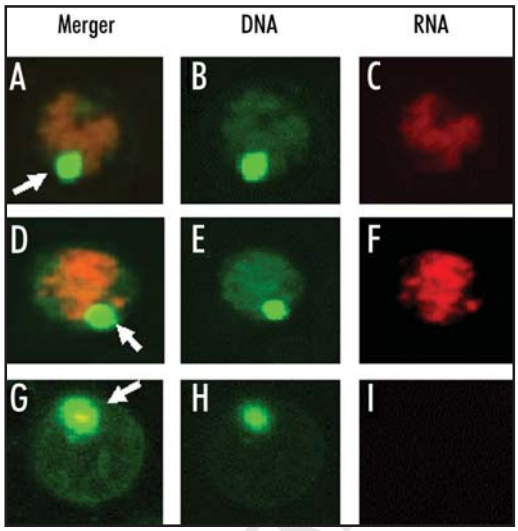

Figure 1. Photomicrographs showing an example of peripheral blood micronuclei in a nude mice treated by paclitaxel. The animal received one cycle of paclitaxel at a total dose of 30 mg/kg/week for three consecutive weeks and was killed 24 after the last dose of paclitaxel. Blood sample was collected and dropped in the centre of an acridine orange-coated slide. Paclitaxel treatment leads to micronuclei formation (white arrows); micronuclei were round or oval in shape and emitted green fluorescence. (A, D and G) merge images; (B, E and H) DNA staining; (C, F and I) RNA staining.

on clean slides. Slides were stained for cytological analysis in a routine fashion with May-Grünwald Giemsa technique using a Haemastain automatic staining machine, coverslipped using Permount, blind coded, and used for data collection.

Acridine orange staining procedure. Preparations of AO-coated glass slides and peripheral blood cells were performed as described previously.[25,35,36] Briefly, AO was dissolved in distilled water at a concentration of 1 mg/ml. Ten microliters of this solution was placed on a pre-heated (about 70°C) cleaned glass slide, and spread by moving a glass rod back and forth over it, then air-dried. The AO-coated glass slides were stored in a dry location until used at room temperature.[36]

Collected blood (10 µl) was dropped in the centre of an acridine orange-coated slide, covered with a 24 mm x 50 mm coverslip, and stored in a deep freezer until analysis as described earlier.[36] Two slides per mice were performed. Before scoring, slides were allowed to stand overnight to allow cells to settle and to maximize staining. Specimens were evaluated with the aid of a Zeiss fluorescent microscope (x100) equipped with blue excitation and 515–530 nm barrier filters.

Data collection, analysis and interpretation. Criteria for scoring MN in blood samples using acridine orange-coated slides are described in detail by Krishna and Sato.[33,35] In repeated dosing regimens as used in our experiments, micronuclei in blood samples could be detected either in polychromatic or normochromatic erythrocytes (MNE).[35] Thus, to accomplish micronuclei scoring, 10,000 total erythrocytes per smear were inspected and the number of micronucleated polychromatic and mature erythrochytes was recorded. Results were expressed as percentage of micronucleated cells related to total mature erythrocytes.

Statistical analysis. The differences between groups were tested by the Mann-Whitney U non-parametric test using the statistical package SPSS V10™. The level of significance used in all the analyses was $p < 0.05$.

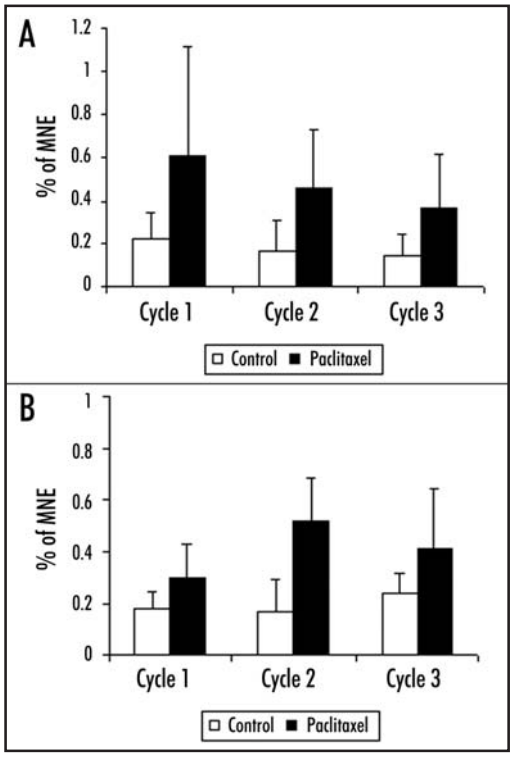

Figure 2. Percentage of micronucleated cells in control and paclitaxel-treated mice after each treatment cycle. Micronucleated erythrocytes were counted after 24 h (A) and 168 h (B) of the last dose of each chemotherapy cycle.

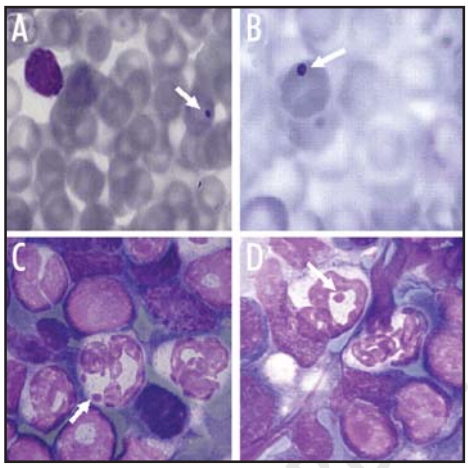

Figure 3. Photomicrographs of peripheral blood (PB) and bone marrow (BM) smears from female swiss nude mice that had received treatment with paclitaxel. (A and B) showed the presence of micronucleated erythrocytes in peripheral blood smears (original magnification, ×200). (C and D) showed the presence of micronuclei in segmented granulocytes in bone marrow (original magnification, ×200). PB and BM samples were smeared onto clean microscope slides, allowed to air-dry, then fixed with absolute methanol for 3 min and stained with May-Gründwald Giemsa. White arrows indicate micronuclei.

RESULTS

Detection of micronucleated erythrocytes using the AO method. We investigated if paclitaxel could induce MN in animal models by using the AO method. As shown in Figure 1, micronuclei were bright green stained, presented a round or oval shape, and a size that represented no more than 20% of total cell surface; thus, they were readily distinguished from artefacts such as staining particles. Micronuclei were detected either in polychromatic erythrocytes emitting also a red fluorescence (RNA and polysaccharide-containing reticulum structures) (Fig. 1A–F) and normochromatic erythrocytes emitting almost no fluorescence or only a dim outline (Fig. 1G–I).

Induction of MNE in the STA group. Short-term analysis compared the frequencies of MNE after 24 h and 168 h of administration of the last dose of each paclitaxel cycle (Fig. 2). A global analysis performed after finished the three chemotherapy cycles showed that the mean MNE frequency in the control group was 0.19 ± 0.1%, in agreement with results previously found by other authors.[37-39] The mean MNE frequency in the STA paclitaxel treated group was 0.46 ± 0.3%. Statistical analysis showed a significant increase in the frequency of MNE in the STA paclitaxel treated group compared to the control group ($p < 0.01$).

We then investigated the frequencies of MNE only after 24 h of administration of the last dose of each treatment cycle (Fig. 2A). The mean MNE frequency in the control group was 0.17 ± 0.1% while the mean MNE frequency in the STA paclitaxel treated group was 0.5 ± 0.4%. Statistical analysis showed a significant increase in the frequency of MNE in the STA paclitaxel treated group compared to the control group ($p < 0.01$). The induction of MNE by paclitaxel treatment was also observed in blood samples obtained after 168 h of administration of the last dose of each treatment (Fig. 2B). The mean MNE frequency in the control group was 0.19 ± 0.04% while the mean MNE frequency in the STA paclitaxel treated group was 0.41 ± 0.11%. Statistical analysis showed a significant increase in the frequency of MNE in the STA paclitaxel treated group compared to the control group ($p < 0.01$).

When analysing after each individual chemotherapy cycle, frequencies of MNE in the 24 h control group were 0.22 ± 0.1, 0.16 ± 0.1 and 0.14 ± 0.1, for cycle 1, cycle 2 and cycle 3, respectively. The frequencies of MNE after 24 h of the last dose of paclitaxel were 0.6 ± 0.5, 0.4 ± 0.2 and 0.3 ± 0.2, for cycle 1, cycle 2 and cycle 3, respectively. Results showed that paclitaxel induced a 2.7-, 2.8- and 2.5-fold increase of MNE after each treatment cycle compared to control group, respectively. Statistical analysis showed that MNE frequencies significantly increased after 24 h of the last dose of each paclitaxel cycle (cycle 1: $p = 0.03$; Cycle 2: $p = 0.01$; Cycle 3: $p = 0.01$).

When analysing after each individual chemotherapy cycle, frequencies of MNE in the 168 h control group were 0.18 ± 0.07, 0.16 ± 0.07 and 0.24 ± 0.1, for cycles 1, 2 and 3, respectively. The frequencies of MNE after 168 h of the last dose of paclitaxel were 0.3 ± 0.13, 0.52 ± 0.16 and 0.4 ± 0.23, for cycle 1, cycle 2 and cycle 3, respectively. At that time, paclitaxel induces a 1.6-, 3.1- and 1.6-fold increase of MNE after each treatment cycle compared to control group, respectively. Statistical analysis showed that MNE frequencies significantly increased after 168 h of the last dose of each paclitaxel cycle (cycle 1: $p = 0.03$; Cycle 2: $p < 0.01$; Cycle 3: $p = 0.08$).

Induction of MNE in long-term assays. We then analyzed the MNE frequency in the LTA mice group. In this group, mice were treated with three cycles of paclitaxel and MNE were counted after one year of the first dose of treatment. As observed in Table 1, paclitaxel-treated mice presented a 1.8-fold increase in the MNE frequency (0.3 ± 0.02) compared to the control group (0.16 ± 0.08). These results indicated that paclitaxel-induced MNE increase lasted for at least one year ($p < 0.01$).

Table 1 **Frequencies of micronucleated-erythrocytes after 1 year (LTA group) of intraperitoneal treatment with paclitaxel**

Group	N	Mean % of MN*	SD
Control	3	0.16	0.08
Paclitaxel-treated mice†	12	0.30	0.02

*MN, micronuclei; SD, standard deviation. †Mice received three cycles of paditaxel (90 mg/kg) and were lasted for one year before euthanasia.

Histological examination of bone marrow and peripheral blood smears in non-treated and paclitaxel-treated mice. Representative PB and BM histological smears of both untreated and paclitaxel-treated mice in the STA and LTA groups are illustrated in Figure 3. Cytological analysis revealed the presence of MNE in PB smears (Fig. 3A and B). Furthermore, micronuclei were also detected in granulocytes (mostly neutrophils) (Fig. 3C and D). However, there was no cytological evidence of myeloproliferative disease in any of the analyzed smears.

DISCUSSION

Our results indicate that administration of three cycles of paclitaxel to nude mice induces the appearance of MNE in peripheral blood samples. This effect was observed after 24 h of the last dose of each chemotherapy cycle and persisted at least for 168 h. Moreover, the increase in MNE lasted for one year after treatment. To our knowledge, this is the first study demonstrating that paclitaxel administrated at multiple doses is a strong in vivo aneugenic agent. The genetic toxicity of paclitaxel described here was observed at concentrations similar to those used in clinical practice.[28-32] The present data therefore indicate a carcinogenic potential of paclitaxel for humans, which should be considered in the risk-benefit analysis of its increasing clinical use.

The genetic toxicity of DNA-damaging agents is well-established in in vivo animal models.[22,26,36] In contrast, only two studies described the genotoxic activity of paclitaxel in animals. The first study showed that a single i.p. injection of paclitaxel (50 mg/kg) in CBA mice (9-weeks old) induced an increase in MNE in BM at 24 h and 48 h sampling times.[26] The second study demonstrated that the frequency of MNE in BM increased 24 h and 36 h after administration of paclitaxel (10 μg/kg) in swiss albino mice.[40] Such effects have been associated with an aneugenic mechanism associated with metaphase spindle disturbance by paclitaxel.[26,41] Moreover, as paclitaxel injury favours the appearance of antiapoptotic mechanisms in early erythroid progenitors (BFU-E), these mechanisms may be involved in the appearance of MNE in PB. Using in vitro semisolid cultures of BFU-E from paclitaxel-treated mice, Juaristi and colleagues found that BFU-E increased the expression of proteins associated with the antiapoptotic response in paclitaxel-surviving cells. These mechanisms may avoid a greater damage on erythropoietic progenitors, and at the same time, may induce erythropoietic survival necessary for the recovery of the size and composition of the red cell compartment even if erythrocytes are altered, as MNE.[42]

In vitro, the genotoxic activity of paclitaxel was mostly studied by using the cytokinesis-blocked micronuclei assay. On human lymphocytes, Digue et al. observed that paclitaxel treatment induced an increase in binucleated micronucleated cell rates confirming the strong in vitro aneugenic potential of this drug.[27] Similarly, Jagetia et al. also observed that paclitaxel was a strong inducer of MN in the chinese hamster lung V79 cell line.[40] However, Hei et al. failed to demonstrate the genotoxic activity of paclitaxel in the C3H 10T1/2 mouse embryo fibroblast cell line.[43]

The aneugenic effects of paclitaxel can easily be compared to those induced by other tubulin-binding agents such as vinca alkaloids. Different studies demonstrated that vinblastine,[44-46] vincristine,[47,48] and vindesine[49] increased the frequency of MNE from the blood. Vinca alkaloids are known to be essentially aneugenic compounds despite a slightly different mechanism of action compare to taxanes. At μM levels, vinca alkaloids act by inducing microtubule disassembly; however, it is important to note that at nM levels, taxanes and vinca alkaloids act similarly by inhibiting microtubule dynamics.[50] On the other hand, higher doses of vinblastine and vincristine resulted in a dose-dependent increase in the frequency of MNE and could induce a long lasting aneugenic effect, probably related to the accumulation of vinca alkaloids that are either free or associated to tubulin[44,45] . The dose response relationship of paclitaxel with MNE frequencies was not determined in our study and thus these experiments are needed.

The aneugenic effect of paclitaxel is a consequence of abnormalities in the distribution of chromosomes during the cell division in those affected cells that manage to complete cell division and survive.[26,41,51] In fact, during anaphase, loss of individual chromosomes as a result of paclitaxel-induced defects in attachment to the spindle apparatus or in movement of chromosomes relative to the poles should mainly lead to numerous MN observed after drug treatment. Erythrocytes are particularly well suited for evaluating MN events since erythroblast precursors are rapidly dividing cells that expel their nucleus after mitosis, making MN-associated chromosomes relatively simple to detect.[25,36,52] An interaction between paclitaxel and centrosomes could also explain a considerable amount of the micronuclei due to the appearance of multipolar mitosis.[27] All these actions induce the formation of aneuploid daughter cells.[27]

The consequences of this effect may be important and could potentially lead to carcinogenesis, and hence to the appearance of a secondary neoplasm linked to the treatment, as was already demonstrated for clastogenic antineoplastic agents, even if the risk of secondary neoplasm seems to be weak with spindle inhibitors.[16,41] In fact, Duesberg et al. have recently emphasized the “aneuploidy first” hypothesis.[19,53] According to this view, a carcinogen "initiates" carcinogenesis by generating aneuploid cells. Aneuploidy then initiates autocatalytic karyotype variations, which generate new lethal, pre-neoplastic and eventually neoplastic karyotypes. The autocatalytic karyotype evolution would thus explain the transformation of an "initiated" pre-neoplastic into a neoplastic cell.

Nevertheless, we did not observe any evidence of the presence of myeloproliferative syndromes in PB or BM smears in treated mice.[54] This may be due to the low number of mice included in the LTA group and to the period of latency of only one year after treatment. However, we observed alterations in erythrocytes and granulocytes in PB and BM smears. These results are in accordance with Juneja et al. that reported transient morphologic abnormalities in neutrophils of patients treated with taxanes.[55]

At the clinical level, different studies reported the appearance of secondary myeloproliferative syndromes after chemotherapeutic treatments including taxanes. A first study by Mamounas et al. reported that addition of paclitaxel to an adjuvant combination of doxorubicin and cyclophsophamide (AC) increase the risk of appearance of secondary acute myeloid leukaemia (AML) or myelodysplastic

syndrome (MDS) in patients with operable breast cancer.[12] This study (NSABP B-28; n = 3060) showed that from the eight cases of reported AML/MDS, 6 occurred in the AC/paclitaxel arm. The interval from first chemotherapy to the development of the AML/MDS ranged from 9 months to 46 months. A second study by Martin et al. also reported that addition of docetaxel to adjuvant AC induces the appearance of secondary AML compared to a AC plus 5-FU combination (FAC) in node-positive breast cancer patients (n = 1491).[56] After five years of follow-up, AML developed in two patients in the TAC group and one patient in the FAC group. A third study by Henderson et al. reported the incidence of secondary AML/MDS and acute lymphoid leukaemia (ALL) in women with node-positive operable breast cancer (n = 3,121).[20] However, this study found no significant differences in the incidences of secondary malignancies between the AC plus paclitaxel group and the AC group. The AC plus paclitaxel arm presented four cases of AML and four cases of MDS while the AC arm showed six cases of AML, two cases of MDS, and one case of ALL. Other authors presented case reports relating taxane therapy with the appearance of myeloproliferative syndromes.[21,23]

Whether paclitaxel co-administration potentiates the well-known genotoxic activity of alkylating agents and topoisomerase-II inhibitors in these clinical studies is not known. Paclitaxel should mimic the situation observed after clinical administration of vincristine. This agent was observed to induce MNE in mice experiments.[47,48] Moreover, this drug is an active component of polychemotherapy schedules known to induce secondary malignancies.[24,45] However, a direct relationship between vincristine administration and increased incidence of secondary malignancies was never found. Here, we demonstrate that MNE frequencies were increased after paclitaxel treatment compared to the control group. It should be interesting to perform similar studies using polychemotherapy including paclitaxel, alkylating agents and topoisomerase-II inhibitors.

In summary, our results suggest a carcinogenic potential for taxol in vivo that should be considered when administrated in the adjuvant treatment setting. In fact, the anti-mitotic activity of taxol that leads to its clinical efficacy carries with it a mechanistically related ability to disturb the integrity of the genome. Confirmation of the aneugenic potential of paclitaxel on peripheral blood sample series from cancer patients treated with weekly paclitaxel is clearly warranted. We believe this is important because as cancer therapy improves and survival is increased, secondary malignancies will become an increasingly important issue.

References

1. Schiff PB, Horwitz SB. Taxol stabilizes microtubules in mouse fibroblast cells. Proc Natl Acad Sci USA 1980; 77:1561-5.
2. Jordan MA, Toso RJ, Thrower D, Wilson L. Mechanism of mitotic block and inhibition of cell proliferation by taxol at low concentrations. Proc Natl Acad Sci USA 1993; 90:9552-6.
3. Manfredi JJ, Horwitz SB. Taxol: an antimitotic agent with a new mechanism of action. Pharmacol Ther 1984; 25:83-125.
4. Rowinsky EK, Cazenave LA, Donehower RC. Taxol: a novel investigational antimicrotubule agent. J Natl Cancer Inst 1990; 82:1247-59.
5. Moos PJ, Fitzpatrick FA. Taxane-mediated gene induction is independent of microtubule stabilization: induction of transcription regulators and enzymes that modulate inflammation and apoptosis. Proc Natl Acad Sci USA 1998; 95:3896-901.
6. Shen SC, Huang TS, Jee SH, Kuo ML. Taxol-induced p34cdc2 kinase activation and apoptosis inhibited by 12-O-tetradecanoylphorbol-13-acetate in human breast MCF-7 carcinoma cells. Cell Growth Differ 1998; 9:23-9.
7. McGuire WP, Hoskins WJ, Brady MF, Kucera PR, Partridge EE, Look KY, Clarke-Pearson DL, Davidson M. Cyclophosphamide and cisplatin versus paclitaxel and cisplatin: a phase III randomized trial in patients with suboptimal stage III/IV ovarian cancer (from the Gynecologic Oncology Group). Semin Oncol 1996; 23:40-7.
8. Holmes FA, Walters RS, Theriault RL, Forman AD, Newton LK, Raber MN, Buzdar AU, Frye DK, Hortobagyi GN. Phase II trial of taxol, an active drug in the treatment of metastatic breast cancer. J Natl Cancer Inst 1991; 83:1797-805.
9. Chang AY, Kim K, Glick J, Anderson T, Karp D, Johnson D. Phase II study of taxol, merbarone, and piroxantrone in stage IV non-small-cell lung cancer: The Eastern Cooperative Oncology Group Results. J Natl Cancer Inst 1993; 85:388-94.
10. O'Leary J, Volm M, Wasserheit C, Muggia F. Taxanes in adjuvant and neoadjuvant therapies for breast cancer. Oncology (Williston Park) 1998; 12:23-7.
11. Erman M, Baltali E, Karaoglu A, Abali H, Engin H, Ozisik Y, Guler N, Altundag K, Tekuzman G, Atahan IL, Onat D, Sayek I. A phase II study on the safety and efficacy of 5-fluorouracil, epirubicin, cyclophosphamide (FEC) followed by paclitaxel in the adjuvant treatment of breast cancer. Cancer Invest 2005; 23:215-21.
12. Mamounas EP, Bryant J, Lembersky B, Fehrenbacher L, Sedlacek SM, Fisher B, Wickerham DL, Yothers G, Soran A, Wolmark N. Paclitaxel after doxorubicin plus cyclophosphamide as adjuvant chemotherapy for node-positive breast cancer: results from NSABP B-28. J Clin Oncol 2005; 23:3686-96.
13. Bradley JD, Paulus R, Graham MV, Ettinger DS, Johnstone DW, Pilepich MV, Machtay M, Komaki R, Atkins J, Curran WJ. Phase II trial of postoperative adjuvant paclitaxel/carboplatin and thoracic radiotherapy in resected stage II and IIIA non-small-cell lung cancer: promising long-term results of the Radiation Therapy Oncology Group—RTOG 9705. J Clin Oncol 2005; 23:3480-7.
14. Surralles J, Xamena N, Creus A, Marcos R. The suitability of the micronucleus assay in human lymphocytes as a new biomarker of excision repair. Mutat Res 1995; 342:43-59.
15. Huber R, Salassidis K, Kulka U, Braselmann H, Bauchinger M. Detection of centromeres in vinblastine- and radiation-induced micronuclei of human lymphocytes using FISH with an alpha satellite pancentromeric DNA probe. Environ Mol Mutagen 1996; 27:105-9.
16. Sgura A, Antoccia A, Ramirez MJ, Marcos R, Tanzarella C, Degrassi F. Micronuclei, centromere-positive micronuclei and chromosome nondisjunction in cytokinesis blocked human lymphocytes following mitomycin C or vincristine treatment. Mutat Res 1997; 392:97-107.
17. Hecht F,Hecht BK. Incidence Etiol 1987; 9-49.
18. Oshimura M, Barrett JC. Chemically induced aneuploidy in mammalian cells: mechanisms and biological significance in cancer. Environ Mutagen 1986; 8:129-59.
19. Duesberg P, Rasnick D. Aneuploidy, the somatic mutation that makes cancer a species of its own. Cell Motil Cytoskeleton 2000; 47:81-107.
20. Henderson IC, Berry DA, Demetri GD, Cirrincione CT, Goldstein LJ, Martino S, Ingle JN, Cooper MR, Hayes DF, Tkaczuk KH, Fleming G, Holland JF, Duggan DB, Carpenter JT, Frei E, III, Schilsky RL, Wood WC, Muss HB, Norton L. Improved outcomes from adding sequential Paclitaxel but not from escalating Doxorubicin dose in an adjuvant chemotherapy regimen for patients with node-positive primary breast cancer. J Clin Oncol 2003; 21:976-83.
21. Seymour JF, Juneja SK, Campbell LJ, Ellims PH, Estey EH, Prince HM. Secondary acute myeloid leukemia with inv(16): report of two cases following paclitaxel-containing chemotherapy and review of the role of intensified ara-C therapy. Leukemia 1999; 13:1735-40.
22. Shelby MD, Zeiger E. Activity of human carcinogens in the Salmonella and rodent bone-marrow cytogenetics tests. Mutat Res 1990; 234:257-61.
23. Dissing M, Le Beau MM, Pedersen-Bjergaard J. Inversion of chromosome 16 and uncommon rearrangements of the CBFB and MYH11 genes in therapy-related acute myeloid leukemia: rare events related to DNA-topoisomerase II inhibitors? J Clin Oncol 1998; 16:1890-6.
24. Josting A, Wiedenmann S, Franklin J, May M, Sieber M, Wolf J, Engert A, Diehl V. Secondary myeloid leukemia and myelodysplastic syndromes in patients treated for Hodgkin's disease: a report from the German Hodgkin's Lymphoma Study Group. J Clin Oncol 2003; 21:3440-6.
25. Macgregor JT, Wehr CM, Gould DH. Clastogen-induced micronuclei in peripheral blood erythrocytes: the basis of an improved micronucleus test. Environ Mutagen 1980; 2:509-14.
26. Tinwell H, Ashby J. Genetic toxicity and potential carcinogenicity of taxol. Carcinogenesis 1994; 15:1499-501.
27. Digue L, Orsiere T, De MM, Mattei MG, Depetris D, Duffaud F, Favre R, Botta A. Evaluation of the genotoxic activity of paclitaxel by the in vitro micronucleus test in combination with fluorescent in situ hybridization of a DNA centromeric probe and the alkaline single cell gel electrophoresis technique (comet assay) in human T-lymphocytes. Environ Mol Mutagen 1999; 34:269-78.
28. Green MC, Buzdar AU, Smith T, Ibrahim NK, Valero V, Rosales MF, Cristofanilli M, Booser DJ, Pusztai L, Rivera E, Theriault RL, Carter C, Frye D, Hunt KK, Symmans WF, Strom EA, Sahin AA, Sikov W, Hortobagyi GN. Weekly paclitaxel improves pathologic complete remission in operable breast cancer when compared with paclitaxel once every 3 weeks. J Clin Oncol 2005; 23:5983-92.
29. bu-Rustum NR, Aghajanian C, Barakat RR, Fennelly D, Shapiro F, Spriggs D. Salvage weekly paclitaxel in recurrent ovarian cancer. Semin Oncol 1997; 24:S15.
30. Clavarezza M, Del ML, Venturini M. Taxane-containing chemotherapy in the treatment of early breast cancer patients. Ann Oncol 2006; 17 Suppl 7:vii22-vii26.
31. Eniu A, Palmieri FM, Perez EA. Weekly administration of docetaxel and paclitaxel in metastatic or advanced breast cancer. Oncologist 2005; 10:665-85.
32. Markman M, Blessing J, Rubin SC, Connor J, Hanjani P, Waggoner S. Phase II trial of weekly paclitaxel (80 mg/m2) in platinum and paclitaxel-resistant ovarian and primary peritoneal cancers: a Gynecologic Oncology Group study. Gynecol Oncol 2006; 101:436-40.
33. Sato SI, Tomita I. Short-term screening method for the prediction of carcinogenicity of chemical substances: current status and problems of an in vivo rodent micronucleus assay. J Health Sci 2001; 47:1-8.
34. Hayashi M, Sofuni T, Ishidate M, Jr. An application of Acridine Orange fluorescent staining to the micronucleus test. Mutat Res 1983; 120:241-7.

35. Krishna G, Hayashi M. In vivo rodent micronucleus assay: protocol, conduct and data interpretation. Mutat Res 2000; 455:155-66.
36. Hayashi M, Morita T, Kodama Y, Sofuni T, Ishidate M, Jr. The micronucleus assay with mouse peripheral blood reticulocytes using acridine orange-coated slides. Mutat Res 1990; 245:245-9.
37. Salamone MF, Mavournin KH. Bone marrow micronucleus assay: a review of the mouse stocks used and their published mean spontaneous micronucleus frequencies. Environ Mol Mutagen 1994; 23:239-73.
38. Hamada S, Yamasaki KI, Nakanishi S, Omori T, Serikawa T, Hayashi M. Evaluation of the general suitability of the rat for the micronucleus assay: the effect of cyclophosphamide in 14 strains. Mutat Res 2001; 495:127-34.
39. Dertinger SD, Camphausen K, Macgregor JT, Bishop ME, Torous DK, Avlasevich S, Cairns S, Tometsko CR, Menard C, Muanza T, Chen Y, Miller RK, Cederbrant K, Sandelin K, Ponten I, Bolcsfoldi G. Three-color labeling method for flow cytometric measurement of cytogenetic damage in rodent and human blood. Environ Mol Mutagen 2004; 44:427-35.
40. Jagetia GC, Nayak V. Treatment of mice with a novel antineoplastic agent taxol before irradiation increases the frequency of micronuclei in the bone marrow. Mutat Res 1996; 349:219-27.
41. Adler ID. Synopsis of the in vivo results obtained with the 10 known or suspected aneugens tested in the CEC collaborative study. Mutat Res 1993; 287:131-7.
42. Juaristi JA, Aguirre MV, Carmuega RJ, Romero-Benitez M, Alvarez MA, Brandan NC. Hematotoxicity induced by paclitaxel: in vitro and in vivo assays during normal murine hematopoietic recovery. Methods Find Exp Clin Pharmacol 2001; 23:161-7.
43. Hei TK, Hall EJ. Taxol, radiation, and oncogenic transformation. Cancer Res 1993; 53:1368-72.
44. Jagetia GC, Jacob PS. Vinblastine treatment induces dose-dependent increases in the frequency of micronuclei in mouse bone marrow. Mutat Res 1992; 280:87-92.
45. Morales-Ramirez P, Vallarino-Kelly T, Cruz-Vallejo V. Kinetics of micronucleated polychromatic erythrocyte (MN-PCE) induction in vivo by aneuploidogens. Mutat Res 2004; 565:79-87.
46. Udroiu I, Ieradi LA, Cristaldi M, Tanzarella C. Detection of clastogenic and aneugenic damage in newborn rats. Environ Mol Mutagen 2006; 47:320-4.
47. Krishna G, Fiedler R, Theiss JC. Simultaneous evaluation of clastogenicity, aneugenicity and toxicity in the mouse micronucleus assay using immunofluorescence. Mutat Res 1992; 282:159-67.
48. Ohuchida A, Furukawa A, Kondo Y, Ono T, Nito S. Micronucleus test with vincristine administered by intraperitoneal injection and oral gavage. Mutat Res 1989; 223:395-8.
49. Jagetia GC, Jyothi P. Enhancement of micronuclei frequency by vindesine in mouse bone marrow. Mutat Res 1997; 388:1-5.
50. Jordan MA, Wilson L. Microtubules as a target for anticancer drugs. Nat Rev Cancer 2004; 4:253-65.
51. Thierens H, Vral A, Morthier R, Aousalah B, De RL. Cytogenetic monitoring of hospital workers occupationally exposed to ionizing radiation using the micronucleus centromere assay. Mutagenesis 2000; 15:245-9.
52. Protocol recommended by the CSGMT/JEMS.MMS for the short-term mouse peripheral blood micronucleus test. The Collaborative Study Group for the Micronucleus Test (CSGMT) (CSGMT/JEMS.MMS, The Mammalian Mutagenesis Study Group of the Environmental Mutagen Society of Japan). Mutagenesis 1995; 10:153-9.
53. Duesberg P, Rasnick D, Li R, Winters L, Rausch C, Hehlmann R. How aneuploidy may cause cancer and genetic instability. Anticancer Res 1999; 19:4887-906.
54. Kogan SC, Ward JM, Anver MR, Berman JJ, Brayton C, Cardiff RD, Carter JS, de Coronado S, Downing JR, Fredrickson TN, Haines DC, Harris AW, Harris NL, Hiai H, Jaffe ES, MacLennan IC, Pandolfi PP, Pattengale PK, Perkins AS, Simpson RM, Tuttle MS, Wong JF, Morse HC, III. Bethesda proposals for classification of nonlymphoid hematopoietic neoplasms in mice. Blood 2002; 100:238-45.
55. Juneja SK, Matthews JP, Luzinat R, Fan Y, Michael M, Rischin D, Millward MJ, Toner GC. Association of acquired Pelger-Huet anomaly with taxoid therapy. Br J Haematol 1996; 93:139-41.
56. Martin M, Pienkowski T, Mackey J, Pawlicki M, Guastalla JP, Weaver C, Tomiak E, Al-Tweigeri T, Chap L, Juhos E, Guevin R, Howell A, Fornander T, Hainsworth J, Coleman R, Vinholes J, Modiano M, Pinter T, Tang SC, Colwell B, Prady C, Provencher L, Walde D, Rodriguez-Lescure A, Hugh J, Loret C, Rupin M, Blitz S, Jacobs P, Murawsky M, Riva A, Vogel C. Adjuvant docetaxel for node-positive breast cancer. N Engl J Med 2005; 352:2302-13.

British Journal of Cancer (2007) 97, 1218 – 1224

www.bjcancer.com

Paclitaxel resistance in untransformed human mammary epithelial cells is associated with an aneuploidy-prone phenotype

BP Bouchet*[,1,2,3,4], J Bertholon[1,2,4], N Falette[5], C Audoynaud[5], C Lamblot[5], A Puisieux[1,2,3,5,4] and CM Galmarini[1,6,7,8]

[1]Université de Lyon, Lyon, F-69622, France; [2]Université Lyon 1, ISPB, Lyon, F-69003, France; [3]INSERM, U590, Lyon, F-69008, France; [4]IFR 62, Lyon, F-69008, France; [5]Centre LEON-BERARD, Oncologie Moléculaire, Lyon, F-69373, France; [6]Université Lyon 1, UFR de Médecine Lyon-Sud, Oullins, F-69921, France; [7]CNRS, UMR 5239, Oullins, F-69921, France; [8]IFR 128, Lyon, F-69365, France

Despite its increasing clinical use, almost no data are currently available about paclitaxel effects on non-cancerous mammary epithelial cells. We have previously established paclitaxel-resistant sub-cell lines (paclitaxel-surviving populations, PSPs; $n = 20$), and sensitive controls (control clones, CCs; $n = 10$), from the untransformed human mammary epithelial cell line HME1. In this study, we aimed to establish whether paclitaxel resistance was associated with a modified sensitivity to paclitaxel-induced aneuploidy. For this purpose, we analysed basal and paclitaxel-induced chromosome missegregation, apoptosis and aberrant spindle multipolarisation as well as microtubular network composition for each subline. PSP sublines showed higher basal and paclitaxel-induced chromosome missegregation than the CC sublines. This phenomenon was associated with resistance to paclitaxel-induced apoptosis. No significant difference in paclitaxel-induced spindle pole abnormalities between CC and PSP sublines was found. Besides, we showed that a majority of PSPs display a constitutively disrupted microtubular network composition due to aberrant tubulin expression and post-translational modifications. These results clearly indicate that paclitaxel resistance in untransformed human mammary epithelial cells is related to an increased susceptibility to acquire aneuploidy in response to this agent. The consequences of these paclitaxel-associated alterations could be deleterious as they can potentially trigger tumorigenesis.
British Journal of Cancer (2007) **97,** 1218 – 1224. doi:10.1038/sj.bjc.6603936 www.bjcancer.com
Published online 30 October 2007

Keywords: paclitaxel; drug resistance; aneuploidy; chromosomal instability; micronuclei; microtubule

Cytotoxicity is a desirable consequence of cancer chemotherapy. In most tumour cells, induction of genotoxic damage by anticancer agents favours cell death (Colella *et al*, 1999; Branch *et al*, 2000). However, increased genetic damages could also have adverse consequences if the affected cells are not malignant. In fact, it has been previously shown that genetic instability, characterised by an abnormal number of chromosomes, is associated with secondary malignancies. Thus, consideration of the potential aneugenicity of chemotherapy to humans is a necessary adjunct to its clinical use.

Paclitaxel is a chemotherapeutic agent that is frequently used in several human cancers, including lung, ovarian and breast cancer. Several previous works have addressed the aneugenic potential of this agent in various *in vitro* and *in vivo* models (Tinwell and Ashby, 1994; Jagetia and Adiga, 1995; Jagetia and Nayak, 1996; Digue *et al*, 1999; Galmarini *et al*, 2007). However, despite its increasing use, almost no data are currently available concerning its effects in normal human mammary epithelial cells. In a precedent work, we described that sub-cell lines of untransformed human mammary epithelial cells (HME1) were able to survive to a 1-week paclitaxel treatment (paclitaxel-surviving populations, PSPs) (Galmarini *et al*, 2006). In most of these sublines, the emergence of a transitory or stable drug resistance phenotype was related to the inactivation of p21/WAF1 protein.

In this study, we sought to determine whether paclitaxel resistance could be related to a modified sensitivity to paclitaxel aneugenicity. For this purpose, we firstly assayed whether paclitaxel treatment of PSPs and control clones (CCs) sublines induced alterations typically associated to aneuploidy appearance (chromosome missegregation and apoptosis defect). We secondly analysed the constitutive microtubular network composition and the aberrant spindle multipolarisation process after paclitaxel exposure in these sublines as potential causes for differential effect of paclitaxel on chromosomal stability. Our results show that paclitaxel resistance in untransformed mammary epithelial cells, characterised by an apoptosis defect, is associated with an aneuploidy-prone phenotype.

*Correspondence: Dr BP Bouchet, Unité INSERM 590 – Oncogenèse et Progression Tumorale, Centre LEON-BERARD, 28, rue Laënnec, 69373 LYON Cedex 08, France;
E-mail: bouchetb@lyon.fnclcc.fr
Received 17 May 2007; revised 18 July 2007; accepted 18 July 2007; published online 30 October 2007

MATERIALS AND METHODS

Reagents

Paclitaxel was obtained from Bristol-Myers Squibb (Paris, France). Cytochalasin-B and Hoechst 33258 were purchased from Sigma

(St Quentin Fallavier, France). Mouse fluorescein isothiocyanate (FITC)-conjugated anti-human α-tubulin, mouse anti-human γ-tubulin and rabbit tetramethylrhodamine isothiocyanate (TRITC)-conjugated anti-mouse IgG antibodies were purchased from DAKO (Glostrup, Denmark). Antibodies against α-tubulin (B-5-1-2), acetylated tubulin (6-11B-1), tyrosinated tubulin (Tub-1A2), β-tubulin (Tub 2.1) and β-actin (AC-15) were purchased from Sigma (St Quentin Fallavier, France); antibodies against class IV β-tubulin isotype were purchased from Biogenex (San Ramon, CA, USA). Class III β-tubulin isotype (TUJ1 clone) was kindly provided by Anthony Frankfurter (University of Virginia, Charlottesville, VA, USA).

Obtention of PSPs

HME1 cells were purchased from ATCC collection (hTERT-HME1, telomerase-immortalised human mammary epithelial cells that stably express the telomerase catalytic subunit, hTERT). Paclitaxel-surviving populations were obtained from HME1 cells as reported previously (Galmarini *et al*, 2006). Briefly, HME1 cells were seeded onto 20 separate 96-well plates at a concentration of 100 cells/well. The following day, treatment with paclitaxel started at a dose of 10 pM over a period of 7 days. Paclitaxel-surviving Populations were allowed to grow for 2–3 weeks in paclitaxel-free culture medium. Wells containing PSPs were harvested, frozen and expanded in drug-free medium for experimental studies. As a control, 10 clones of HME1 cells (CCs) were obtained by limiting dilution (0.1 cell/well) with no exposure to the drug.

Cytokinesis-block micronucleus assay

CC and PSP cells were seeded at a concentration of 10^6 cells ml^{-1}. Paclitaxel was added at two different concentrations (1 and 20 nM). After 6 h of paclitaxel treatment, cytochalasin-B (5 μg ml^{-1}) was added and cells were incubated at 37°C for 24 h and then fixed in 100% methanol. DNA was counterstained with Hoechst 33258 (5 μg ml^{-1}). Coverslips were examined with an Axioplan microscope (Carl Zeiss, Sartrouville, France) using a Zeiss ×100 1.3 oil-immersion objective. Pictures were acquired by using a confocal laser scanning TCS SP2 microscope (Leica, Le Pecq, France) and a ×63 oil-immersion objective. The main nucleus and micronuclei showed bright blue fluorescence (Figure 1B). The micronucleation index was determined for each subline by the use of two independent cytokinesis-block micronucleus (CBMN) assays. Each assay consisted in two micronuclei scoring in a minimum of 200 binucleated cells per experimental condition (total score on 400 cells). Criteria for scoring micronuclei in binucleated cells in the CBMN assay were described in detail by Fenech (2000). After 24 h of single cytochalasin-B treatment, the mean frequency of binucleated cells in CC and PSP were 55.1 and 60.1%, respectively.

Western blots

Protein expression was determined by Western blot analysis in CC and PSP cells at basal conditions as described previously (Galmarini *et al*, 2001). Horizontal scanning was performed on Western blots by acquisition into Adobe Photoshop software (Apple, Cupertino, CA, USA).

Apoptosis detection

Apoptotic index was calculated as the percentage of cells showing apoptotic morphology revealed by 5 μg ml^{-1} Hoechst 33258 (Sigma, St Quentin Fallavier, France) staining of nuclei, after 72 h paclitaxel treatment (1 or 20 nM) or without treatment. For each experimental condition, a minimum of 200 cells per subline were analysed. Apoptosis was also evaluated in cytochalasin-B-treated cells, with or without 30 h paclitaxel treatment. For each independent CBMN assay, a minimum of 300 cells were analysed.

Double-immunofluorescence staining

CC and PSP were grown on glass coverslips and treated for 24 h with paclitaxel at two different dose levels: 1 and 20 nM. To assay mitotic spindle pole impairments, cells were fixed with 4% paraformaldehyde and then permeabilised with 1% Triton X-100 in phosphate-buffered saline (PBS). After incubation with a blocking solution (5% bovine serum albumin (BSA) in PBS) for 30 min, cells were incubated with primary mouse anti-human γ-tubulin antibody diluted 1/1000 for 1 h at 37°C in a humid chamber. After three washes with a PBS/BSA1% solution, cells were incubated for 30 min with a TRITC-conjugated goat

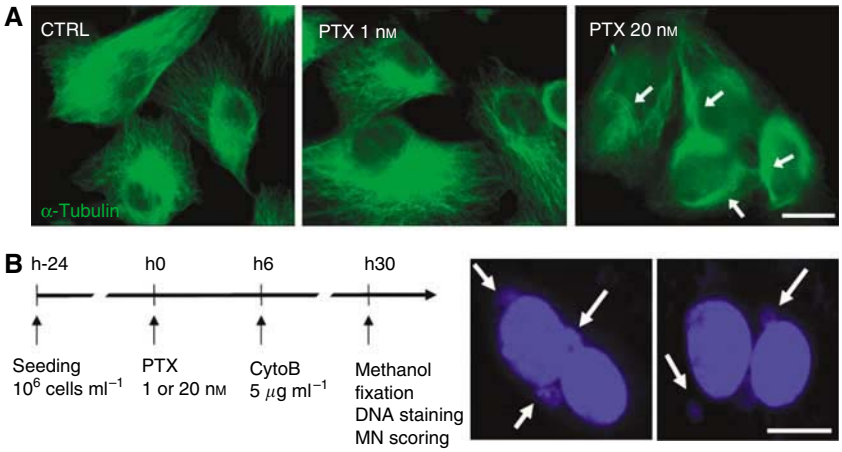

Figure 1 Effect of 1 and 20 nM paclitaxel on microtubular network and chromosome segregation in untransformed human mammary epithelial cells. (**A**) Immunostaining of α-tubulin (green) in untreated (CTRL), 1 and 20 nM paclitaxel-treated (PTX 1 and 20 nM) HME1 cells. White arrows indicate microtubule bundles. Scale bar, 10 μm. (**B**) Micronucleus detection in paclitaxel-treated PSP and CC cells by CBMN assay. Briefly, 10^6 cells ml^{-1} were seeded 24 h before paclitaxel (PTX) treatment (24 h). Cytochalasin-B (CytoB) at 5 μg ml^{-1} was added in culture media 6 h after the beginning of paclitaxel exposure (6 h). After 30 h of paclitaxel treatment, cells were fixed by methanol, DNA was stained with Hoechst 33258 and binucleated cells with micronuclei (MN) were scored. White arrows indicate micronuclei in binucleated cytokinesis-blocked HME1 cells treated by 1 nM paclitaxel. Scale bar, 10 μm. CBMN, cytokinesis-block micronucleus.

anti-mouse IgG secondary antibody. Then cells were incubated with a FITC-conjugated mouse anti-human-α-tubulin diluted 1/100. Finally, DNA was counterstained by the addition of Hoechst 33258 (1 $\mu g\,ml^{-1}$) for 5 min. Cells were observed with a Zeiss Axioplan microscope using a Zeiss ×100 1.3 oil-immersion objective. The spindle pole abnormalities were scored in a minimum of 300 mitotic cells per subline and for each condition (baseline, 1 and 20 nM paclitaxel).

Time-lapse imaging

We established HME1 cell line expressing histone H2B-GFP (H2B-GFP) by stably transfecting hTERT-HME1 cells with plasmid pBOS-H2BGFP (BD Biosciences, Erembodegem, Belgium) under blasticidin selection (5 $\mu g\,ml^{-1}$). Exponentially growing cells were plated on six-well culture plate and incubated with paclitaxel (1 nM for 24 h). Images were acquired on a Zeiss Axiovert photomicroscope with a PowerShot G5 Digital Camera (Canon, Courbevoie, France) under 37°C heated atmosphere. Together with the fluorescent images, transmitted light (differential interference contrast optics) images were acquired. Data were analysed using the Image J software.

Statistical analysis

The differences between groups were tested by the Mann–Whitney *U* non-parametric test using the statistical package SPSS V10™. The level of significance used in all the analyses was $P<0.05$.

RESULTS

Paclitaxel induces persistent chromosome missegregation in PSP but not in CC sublines

To evaluate the chromosome segregation process after paclitaxel treatment in CC and PSP sublines, we performed CBMN assays. These assays were carried out without the use of specific markers of chromosomes, and thus estimated the global missegregation process but did not specify associated chromosome aberrations (for example, nucleoplasmic bridges, chromosome non-disjunction and breakage). We decided to test effects of 1 and 20 nM paclitaxel on chromosome segregation, as these two doses were previously found to be the paclitaxel IC_{20} and IC_{80} in HME1 cell line (Galmarini *et al*, 2006). Moreover, these doses act differentially to induce cell death in untransformed mammary cells. As shown in Figure 1A, 1 nM paclitaxel did not cause massive disorganisation of microtubule network, whereas 20 nM paclitaxel induced microtubule bundles in HME1 cells.

At baseline conditions, none of the CCs presented binucleated cells with micronuclei (Figure 1B; Table 1). In contrast, PSPs showed basal micronucleation (mean frequency of binucleated cells with micronuclei = 4.9%). This increased frequency was due to four PSPs (PSP2, PSP4, PSP6 and PSP21; ranging from 16.7 to 40%) showing high basal micronucleation (Supplementary Table 1). Hence, some PSP sublines present constitutive chromosome aberrations compared with the sensitive CC sublines.

At dose of paclitaxel 1 nM, 60% (6/10) of CCs showed micronucleation in binucleated cells (Supplementary Table 1) with a mean frequency of 1.1% (ranging from 0 to 4.1%). Paclitaxel at the same dose also increased the frequency of micronucleation in PSPs. After this treatment, 80% of PSPs (16/20) showed binucleated cells with micronuclei; the mean frequency of micronucleation was 4.9% (range: 0–14.6%) (Table 1 and Supplementary Table 1). Strikingly, the four PSPs that shared a high basal micronucleation (PSP2, PSP4, PSP6 and PSP21) showed a decreased micronucleation after 1 nM paclitaxel exposure.

After 20 nM paclitaxel exposure, massive cell death induced in CC sublines during the CBMN assay did not permit to score micronucleation in binucleated cells (Table 1, Supplementary Table 1). In contrast, at the same time point, 80% of PSP (16/20) sublines presented binucleated cells with micronuclei after drug treatment (Supplementary Table 1). Besides, the mean frequency of micronucleation in PSP binucleated cells was 42.5% (Table 1).

PSP sublines are resistant to paclitaxel-induced apoptosis

We sought to determine if the increased paclitaxel-induced chromosome aberrations observed in PSPs was associated with a defect of paclitaxel-induced cell death. For this purpose, we treated all sublines with this agent at doses of 1 and 20 nM, for 72 h, and we evaluated the apoptotic index (Table 1). In CC cells, paclitaxel treatment induced apoptosis in a dose-dependent manner (1 nM: 3.5%; 20 nM: 62.6%). Similarly, PSPs showed a dose-dependent paclitaxel-induced apoptosis; however, apoptotic index was significantly lower in PSP than in CC sublines (1 nM: 1.2%, $P<0.05$; 20 nM: 34.5%, $P<0.001$).

To establish a correlation between cell death and micronucleation in CCs and PSPs, we counted apoptosis in those slides used for micronucleation counting by CBMN assay. Notably, a similar significant apoptotic tendency than that observed after 72 h was already observed in PSP compared with CC sublines after 30 h of combined 20 nM paclitaxel-cytochalasin-B treatment (CC: 45.1%, PSP: 35.4%, $P<0.05$; Supplementary Figure 1). This result was corroborated by the observation of a significantly lower binucleation in CC compared with PSP sublines, after 20 nM paclitaxel treatment, indicative of an increased cell death and/or cell-cycle delay in these sublines (CC: 1.0%, PSP: 6.0%, $P<0.01$; Supplementary Table 2). When performing a more detailed analysis, we observed that 'unstable' PSP sublines (U-PSP), namely those that showed constitutive chromosome segregation defect (PSP2, PSP4, PSP6 and PSP21; Table 1), exhibited significantly more apoptosis than stable PSP sublines (S-PSP) when analysed after combined 1 nM paclitaxel-cytochalasin-B treatment (U-PSP: 13.2%, S-PSP: 4.1%, $P<0.05$; Supplementary Figure 1).

Table 1 Micronucleation, apoptosis and spindle pole status in CC and PSP sublines after paclitaxel treatment

	MN-BN[a]			Apoptosis[b]			Spindle pole status[c]					
							Control		Paclitaxel 1 nM		Paclitaxel 20 nM	
	Control	Paclitaxel 1 nM	Paclitaxel 20 nM	Control	Paclitaxel 1 nM	Paclitaxel 20 nM	SP = 2	SP > 2	SP = 2	SP > 2	SP = 2	SP > 2
CC	0.0	1.1	ND	0.2	3.5	62.6	95.5	4.5	86.0	13.9	26.8	73.2
PSP	4.9	4.9*	42.5	0.5	1.2*	34.5***	95.1	4.9	92.7	7.3	14.8	85.2

PSP, paclitaxel-surviving population. [a]Percentage of binucleated cells showing micronucleation; values represent mean percentage of micronucleated cells in CC ($n=10$) and PSP subline ($n=20$) groups. [b]Percentage of cells showing apoptotic morphology; values represent mean percentage of apoptotic cells in CC ($n=10$) and PSP subline ($n=20$) groups. [c]Percentage of mitotic cells with 2 (SP = 2) or more spindle poles (SP > 2); values represent mean percentage of each category in CC ($n=10$) and PSP subline ($n=20$) groups. *$P<0.05$, ***$P<0.001$, comparison between CC and PSP values. ND, not determined.

PSP sublines display constitutive disruptions of the microtubular network composition

Numerous authors suggested that alterations of microtubule dynamics could lead to chromosome missegregation and aneuploidy (ter Haar *et al*, 1996; Sorger *et al*, 1997; Rosa *et al*, 2006). Moreover, it is well established that composition of microtubule network – particularly tubulin isotype expression and tubulin post-translational modifications – closely influences microtubule dynamics and resistance to paclitaxel (Ohta *et al*, 1994; Kavallaris *et al*, 1997; Ranganathan *et al*, 1998; Carles *et al*, 1999; Banerjee, 2002). For this reason, we decided to investigate the microtubular network composition in PSP compared with CC sublines. We thus analysed the expression of total α- and total β-tubulin, acetylated- and tyrosinated-α-tubulin, and class III and class IV β-tubulin. In the CC, total α- and total β-tubulin were uniformly expressed (Figure 2). The levels of protein expression of acetylated α-tubulin and tyrosinated α-tubulin were unchanged between the different CCs; however, the levels of protein expression of acetylated α-tubulin were low compared with those observed for tyrosinated α-tubulin. Class III and class IV β-tubulins were similarly expressed in the CCs.

In the PSPs, total α-tubulin expression was expressed in similar levels in all the sublines. However, total β-tubulin protein content was highly altered in several PSP sublines including PSP1, PSP7, PSP16, PSP19, PSP43 and PSP45 (Figure 2). Indeed, these sublines presented a decreased expression of total β-tubulin compared with CCs and other PSPs. When analysing the expression of acetylated α-tubulin, we observed that protein levels were different between the different sublines, with higher contents of acetylated tubulin protein in PSP1, PSP2, PSP3, PSP4, PSP19, PSP21, PSP32 and PSP45. In these PSPs, compared with the CCs, the acetylated α-tubulin was found to be overexpressed. These variations in protein expression were not observed for tyrosinated α-tubulin. Compared with CCs, the amounts of class III β-tubulin were greatly decreased in PSP1, PSP16, PSP19, PSP20, PSP38 and PSP43. In contrast PSP2, PSP4, PSP22, PSP25 and PSP32 presented higher levels of class III β-tubulin than those observed in CC sublines. Finally, the amounts of class IV β-tubulin showed to be highly decreased in PSP1, PSP2 and PSP4. These data indicate that the majority of PSP sublines exhibit a disrupted microtubular network when compared with sensitive sublines.

PSP and CC sublines undergo dose-dependent aberrant spindle multipolarisation after paclitaxel treatment

We aimed to verify whether chromosome missegregation process observed in PSPs could be associated to aberrant mitotic spindle polarisation. For this purpose, we evaluated the spindle pole status by double-immunofluorescence staining of α-tubulin and γ-tubulin in untreated and paclitaxel-treated (1 and 20 nM) PSP sublines compared with CC sublines (Figure 3A, Table 1). Percentage of normal bipolar and multipolar mitoses was determined as described in Material and Methods.

At baseline, the vast majority of mitoses in CC sublines were normal, with almost all cells showing a bipolar spindle (Table 1). When treated with paclitaxel, the CC cells revealed a dose-dependent increase of mitotic multipolarisation (1 nM: 13.9%; 20 nM: 73.2%). Similarly, at baseline, most of PSPs had normal mitoses with 95.1% of cells showing a bipolar spindle (Table 1). When treated with paclitaxel, PSPs displayed a mean percentage of multipolar mitoses of 7.3 and 85.2% after 1 and 20 nM paclitaxel exposure, respectively. In this sublines group, the percentage of mitoses with more than two poles also increased in a dose-dependent manner (Table 1). Notably, compared with CCs, PSPs seemed to show less mitotic multipolarisation after 1 nM paclitaxel treatment; in contrast, PSP sublines seemed to show more mitotic multipolarisation after 20 nM; however, these differences were not statistically significant ($P > 0.05$).

To confirm that the previously observed paclitaxel-associated spindle multipolarisation in fixed samples were not due to methodological artifacts, we evaluated the real-time effects of paclitaxel in the HME1 cell line stably expressing a histone H2B-green fluorescent protein (GFP). Expression of this fusion protein allows sensitive analysis of chromosome dynamics as these structures are fluorescently labelled in living cells (Kanda *et al*, 1998). The cell divisions observed in the control situation (Figure 3B) were highly comparable with our observations in fixed samples. This implies that the intensity of the lamp beam did not cause significant cell-cycle arrest and predominantly allowed mitoses to occur normally.

Mitotic progression was analysed on real time in 1 nM paclitaxel-treated cells ($n = 10$) compared with untreated cells ($n = 10$) (Figure 3B–C). Untreated cells generally, completed metaphase–telophase progression in approximately 25 min (Figure 3B). In contrast, most of the 1 nM paclitaxel-treated cells showed delayed mitosis and aborted telophase, especially in cells in which appearance of multipolar spindle was observed (Figure 3C). After paclitaxel exposure, most of the recorded multipolarised mitoses led to initial metaphase arrest or aborted telophase followed by irreversible metaphase-like arrest characterised by unaligned chromosomes (Figure 3C and data not shown).

DISCUSSION

In a precedent work, we have shown that paclitaxel-resistant sublines (PSPs) can be established from an untransformed human mammary epithelial cell line (Galmarini *et al*, 2006). In this study, we aimed to further investigate the response of these drug-resistant

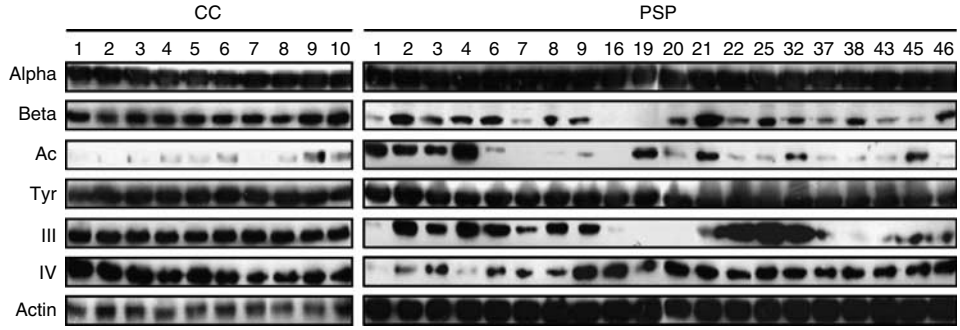

Figure 2 Microtubular network composition in CC and PSP sublines. Expression of total α-tubulin (*Alpha*), β-tubulin (*Beta*), acetylated α-tubulin (*Ac*), tyrosinated α-tubulin (*Tyr*), class III β-tubulin (*III*), class IV β-tubulin (*IV*) and β-actin (*Actin*) were analysed by Western blot in whole-cell lysates of exponentially growing cells from CC (1–10) and PSP (1–46) sublines. CC, control clone; PSP, paclitaxel-surviving population.

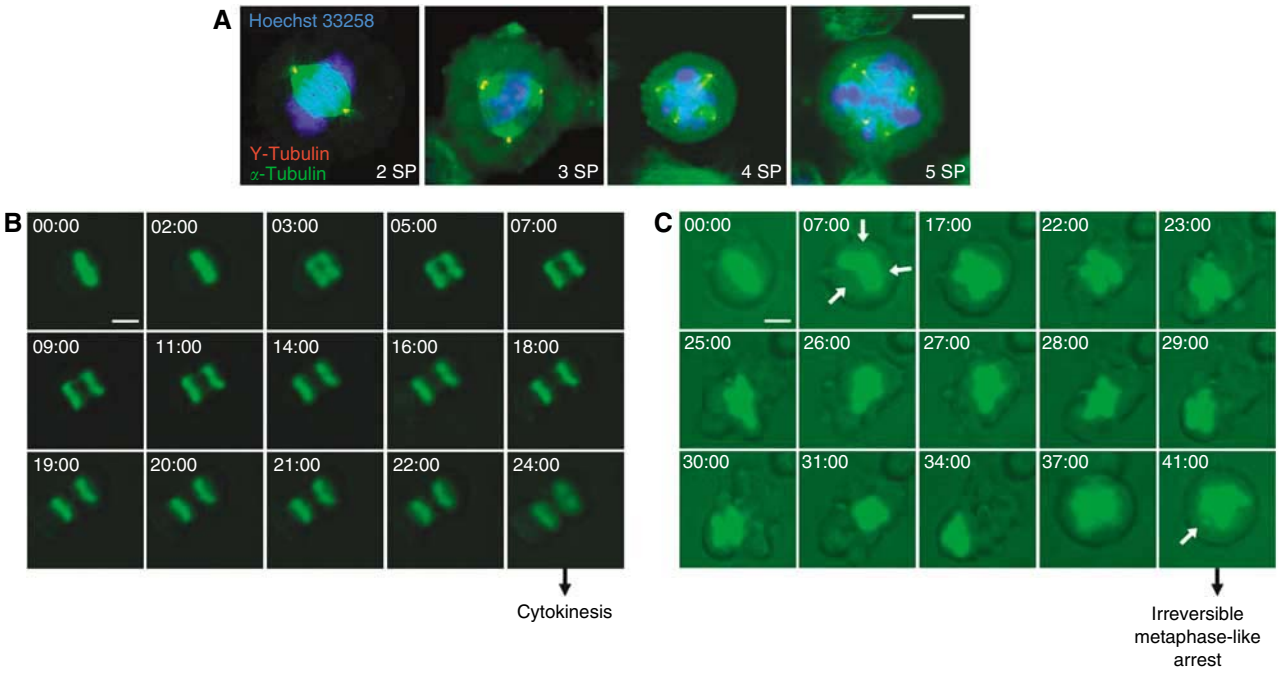

Figure 3 Spindle pole aberrations in untransformed human mammary epithelial cells after paclitaxel treatment. (**A**) Double-immunofluorescence staining was performed to detect γ-tubulin (red) and α-tubulin (green). DNA was counterstained with Hoechst 33258 (blue). Panels show representative mitotic figures of CC cells with two (2SP), three (3SP), four (4SP) or five (5SP) spindle poles. Scale bar, 10 μm. (**B**) Representative time-lapse imaging of chromosomes in an untreated H2B-GFP expressing HME1 cell during metaphase–telophase transition. As indicated, cytokinesis was completed 24 min after metaphase (24:00). (**C**) Representative time-lapse imaging of chromosomes in a 1 nM paclitaxel-treated H2B-GFP expressing HME1 cell during metaphase–telophase transition. White arrows on 07:00 panel indicate the tripolar spindle orientation. Of note, 41 min (41:00) after metaphase, cell failed to enter telophase and irreversibly arrested in a metaphase-like arrest showing unaligned chromosome (white arrow). Time, mm : ss normalised to metaphase equals 00 : 00. Scale bar, 10 μm.

untransformed cells to paclitaxel. For this purpose, we evaluated the effects of this agent on mitotic chromosome segregation, as well as apoptotic response of PSP sublines compared with control-sensitive sublines (CCs). Our results clearly indicate that paclitaxel-resistant untransformed human mammary epithelial cells have an increased susceptibility to develop aneuploidy in response to this agent. Our data also suggest that disruption of microtubular network, a well-known paclitaxel-resistant mechanism, could contribute to this aneuploidy-prone phenotype.

Our *in vitro* experiments showed that after paclitaxel treatment, PSP sublines presented more paclitaxel-induced chromosome missegregation than paclitaxel-sensitive sublines. Furthermore, our results suggest that the lower level of micronucleation observed in paclitaxel-treated CC sublines could be explained by a rapid cell death onset that eliminates CC cells displaying dose-dependent chromosome aberrations. Given the fact that this would be consistent with their sensitive status, further kinetic investigation of apoptotic response to paclitaxel in these sublines will be needed to ascertain this issue (Galmarini *et al*, 2006). Additionally, PSPs also showed lower paclitaxel-induced apoptotic levels, consistent with their previously described resistant status (Galmarini *et al*, 2006). The combination of apoptosis defect with chromosome missegregation have been extensively described as a driving force responsible for aneuploidy in tumour cells (Hollander *et al*, 1999; Jallepalli and Lengauer, 2001; Rajagopalan and Lengauer, 2004; Weaver *et al*, 2007). Thus, our results strongly suggest that paclitaxel-resistant untransformed mammary cells are characterised by an aneuploidy-prone response to paclitaxel treatment. To our knowledge, this is the first study identifying the increased susceptibility to aneuploidisation in untransformed human mammary epithelial cells as an advantage under paclitaxel treatment.

Of note, four PSP sublines (PSP2, PSP4, PSP6 and PSP21) showed a substantially increased level of constitutive chromosome missegregation as shown by an increased level of micronuclei at baseline. Strikingly, these four PSPs presented a diminished level of chromosome missegregation after 1 nM paclitaxel treatment. Moreover, we found that these 'unstable' PSPs underwent significantly more apoptosis than 'stable' PSP sublines after short-term 1 nM paclitaxel treatment (CBMN assays, 30 h). All these results suggest a rapid elimination of cells in response to overmassive chromosome aberrations. Our data would be in accordance with recent works that indicate that high level of aneuploidy leads to cell lethality and/or could avoid stable selection of phenotype with growth advantage (Weaver *et al*, 2007). However, additional investigations will be necessary to specify cell death response in paclitaxel-resistant untransformed mammary cells.

Our data also revealed that aneuploidy-prone phenotype in untransformed mammary cells could be, at least in part, driven by alterations in the composition of microtubular network. Indeed, the majority of PSPs presented constitutive altered levels of total β-tubulin protein content, acetylated α-tubulin and/or class III β-tubulin. The link between aberrant modifications of microtubule dynamics and paclitaxel resistance was yet established in paclitaxel-resistant cells through identification of alterations in tubulin isotype expression and/or post-translational modifications. Indeed, several groups have described association of increased expression of total β-tubulin, class III β-tubulin and/or acetylated α-tubulin with paclitaxel resistance (Ohta *et al*, 1994; Kavallaris *et al*, 1997; Ranganathan *et al*, 1998; Carles *et al*, 1999; Banerjee, 2002). Furthermore, several studies have demonstrated that microtubule defects, such as changes in the expression of tubulins or mutations in the tubulins genes, can lead to chromosome missegregation (ter Haar *et al*, 1996; Sorger *et al*,

1997; Asakawa *et al*, 2006; Rosa *et al*, 2006). Thus, it is conceivable that cells that exhibit paclitaxel resistance related to aberrant tubulin expression would also show an increased susceptibility to chromosome missegregation, as that observed in PSP sublines. Notably, the diversity of tubulin alterations in PSP sublines did not permit to identify specific tubulin patterns inducing drug resistance, but rather an association between globally imbalanced tubulin ratios and paclitaxel-induced chromosome missegregation susceptibility. Additionally, it remains unclear how these different modified tubulin ratios affect the stability of microtubules in PSPs and their sensitivity to paclitaxel. However, our results indicate that, in paclitaxel-resistant untransformed human mammary epithelial cells, association of microtubular network disruption with apoptosis defect could greatly contribute to trigger aneuploidy in response to paclitaxel. As various processes could associate microtubule defects and paclitaxel resistance, further studies should ascertain mechanisms that impede microtubule-related cell death initiation in PSP sublines (Davis and Johnson, 1999; Nuydens *et al*, 2000; Mollinedo and Gajate, 2003). Of note, an other interesting issue would consist in determining whether modified tubulin expressions have been initially selected in HME1 cells because of their paclitaxel-resistance properties or whether they result from paclitaxel-induced aberrant but viable phenotypes.

Finally, even if our data show a dose-dependent increase of spindle multipolarisation, associated with aberrant chromosomes behaviour in both PSP and CC sublines after paclitaxel treatment, no significant difference concerning this process was found between the two sublines group. We cannot exclude that differences could be detected at different post-paclitaxel treatment times of analysis. Hence, further kinetic studies will be necessary to specify the response to paclitaxel in regard to spindle pole abnormalities in PSP sublines.

Recent works claimed that high rates of drug resistance in cancer cells are caused by aneuploidy-catalysed generation of resistance-specific aneusomies (Li *et al*, 2005; Duesberg *et al*, 2007). Hence, we speculate that plasticity of chromosomal patrimony in PSPs could be linked to their ability to escape from paclitaxel-induced apoptosis. Indeed, our results show that these sublines are prone to acquire karyotype modifications. The resulting massive gene dosage modifications could explain their predisposition to acquire paclitaxel resistance. In contrast, cells that retain chromosomal stability, unable to adapt to paclitaxel-induced chromosome aberrations, would undergo efficient apoptosis. Other previous works prompt us to envisage that paclitaxel doses that could trigger moderate aneuploidy could also efficiently promote the acquisition of a resistant phenotype (Weaver *et al*, 2007). Thus, further investigations should aim to precise interrelations between drug-resistance appearance and aneuploidisation in untransformed cells.

In summary, our results strongly indicate that paclitaxel resistance in untransformed human mammary epithelial cells is associated with the emergence of chromosome missegregation and disrupted microtubular network. In addition, these non-cancerous cells are deficient for paclitaxel-induced apoptosis and thus, characterised by an aneuploidy-prone phenotype related to paclitaxel treatment. The consequences of these paclitaxel effects in non-tumour cells could be deleterious as the potentially resulting chromosomal instability could promote tumorigenesis hence the appearance of a secondary neoplasm linked to paclitaxel treatment.

ACKNOWLEDGEMENTS

Benjamin P Bouchet is a recipient of a grant from the Fondation pour la Recherche Médicale.

Supplementary Information accompanies the paper on British Journal of Cancer website (http://www.nature.com/bjc)

REFERENCES

Asakawa K, Kume K, Kanai M, Goshima T, Miyahara K, Dhut S, Tee WW, Hirata D, Toda T (2006) The V260I mutation in fission yeast alpha-tubulin Atb2 affects microtubule dynamics and EB1-Mal3 localization and activates the Bub1 branch of the spindle checkpoint. *Mol Biol Cell* **17:** 1421 – 1435

Banerjee A (2002) Increased levels of tyrosinated alpha-, beta(III)-, and beta(IV)-tubulin isotypes in paclitaxel-resistant MCF-7 breast cancer cells. *Biochem Biophys Res Commun* **293:** 598 – 601

Branch P, Masson M, Aquilina G, Bignami M, Karran P (2000) Spontaneous development of drug resistance: mismatch repair and p53 defects in resistance to cisplatin in human tumor cells. *Oncogene* **19:** 3138 – 3145

Carles G, Braguer D, Dumontet C, Bourgarel V, Goncalves A, Sarrazin M, Rognoni JB, Briand C (1999) Differentiation of human colon cancer cells changes the expression of beta-tubulin isotypes and MAPs. *Br J Cancer* **80:** 1162 – 1168

Colella G, Marchini S, D'Incalci M, Brown R, Broggini M (1999) Mismatch repair deficiency is associated with resistance to DNA minor groove alkylating agents. *Br J Cancer* **80:** 338 – 343

Davis PK, Johnson GV (1999) The microtubule binding of Tau and high molecular weight Tau in apoptotic PC12 cells is impaired because of altered phosphorylation. *J Biol Chem* **274:** 35686 – 35692

Digue L, Orsiere T, De MM, Mattei MG, Depetris D, Duffaud F, Favre R, Botta A (1999) Evaluation of the genotoxic activity of paclitaxel by the *in vitro* micronucleus test in combination with fluorescent *in situ* hybridization of a DNA centromeric probe and the alkaline single cell gel electrophoresis technique (comet assay) in human T-lymphocytes. *Environ Mol Mutagen* **34:** 269 – 278

Duesberg P, Li R, Sachs R, Fabarius A, Upender MB, Hehlmann R (2007) Cancer drug resistance: the central role of the karyotype. *Drug Resist Updat* **10:** 51 – 58

Fenech M (2000) The *in vitro* micronucleus technique. *Mutat Res* **455:** 81 – 95

Galmarini CM, Bouchet BP, Audoynaud C, Lamblot C, Falette N, Bertholon J, Wang Q, Beghin A, Dumontet C, Puisieux A (2006) A p21/WAF1 mutation favors the appearance of drug resistance to paclitaxel in human noncancerous epithelial mammary cells. *Int J Cancer* **119:** 60 – 66

Galmarini CM, Bouchet BP, Falette N, Vila L, Lamblot C, Audoynaud C, Bertholon J, Puisieux A (2007) Weekly administration of paclitaxel induces long-term aneugenicity in nude mice. *Cancer Biol Ther* **6**(3)**:** 377 – 382

Galmarini CM, Falette N, Tabone E, Levrat C, Britten R, Voorzanger-Rousselot N, Roesch-Gateau O, Vanier-Viornery A, Puisieux A, Dumontet C (2001) Inactivation of wild-type p53 by a dominant negative mutant renders MCF-7 cells resistant to tubulin-binding agent cytotoxicity. *Br J Cancer* **85:** 902 – 908

Hollander MC, Sheikh MS, Bulavin DV, Lundgren K, Augeri-Henmueller L, Shehee R, Molinaro TA, Kim KE, Tolosa E, Ashwell JD, Rosenberg MP, Zhan Q, Fernandez-Salguero PM, Morgan WF, Deng CX, Fornace Jr AJ (1999) Genomic instability in Gadd45a-deficient mice. *Nat Genet* **23:** 176 – 184

Jagetia GC, Adiga SK (1995) Influence of various concentrations of taxol on cell survival, micronuclei induction, and LDH activity in cultured V79 cells. *Cancer Lett* **96:** 195 – 200

Jagetia GC, Nayak V (1996) Treatment of mice with a novel antineoplastic agent taxol before irradiation increases the frequency of micronuclei in the bone marrow. *Mutat Res* **349:** 219 – 227

Jallepalli PV, Lengauer C (2001) Chromosome segregation and cancer: cutting through the mystery. *Nat Rev Cancer* **1:** 109 – 117

Kanda T, Sullivan KF, Wahl GM (1998) Histone – GFP fusion protein enables sensitive analysis of chromosome dynamics in living mammalian cells. *Curr Biol* **8:** 377 – 385

Kavallaris M, Kuo DY, Burkhart CA, Regl DL, Norris MD, Haber M, Horwitz SB (1997) Taxol-resistant epithelial ovarian tumors are associated with altered expression of specific beta-tubulin isotypes. *J Clin Invest* **100:** 1282 – 1293

Li R, Hehlman R, Sachs R, Duesberg P (2005) Chromosomal alterations cause the high rates and wide ranges of drug resistance in cancer cells. *Cancer Genet Cytogenet* **163:** 44 – 56

Mollinedo F, Gajate C (2003) Microtubules, microtubule-interfering agents and apoptosis. *Apoptosis* **8:** 413 – 450

Nuydens R, Dispersyn G, Van Den KG, de Jong M, Connors R, Ramaekers F, Borgers M, Geerts H (2000) Bcl-2 protects against apoptosis-related microtubule alterations in neuronal cells. *Apoptosis* **5:** 43 – 51

Ohta S, Nishio K, Kubota N, Ohmori T, Funayama Y, Ohira T, Nakajima H, Adachi M, Saijo N (1994) Characterization of a taxol-resistant human small-cell lung cancer cell line. *Jpn J Cancer Res* **85:** 290 – 297

Rajagopalan H, Lengauer C (2004) Aneuploidy and cancer. *Nature* **432:** 338 – 341

Ranganathan S, Benetatos CA, Colarusso PJ, Dexter DW, Hudes GR (1998) Altered beta-tubulin isotype expression in paclitaxel-resistant human prostate carcinoma cells. *Br J Cancer* **77:** 562 – 566

Rosa J, Canovas P, Islam A, Altieri DC, Doxsey SJ (2006) Survivin modulates microtubule dynamics and nucleation throughout the cell cycle. *Mol Biol Cell* **17:** 1483 – 1493

Sorger PK, Dobles M, Tournebize R, Hyman AA (1997) Coupling cell division and cell death to microtubule dynamics. *Curr Opin Cell Biol* **9:** 807 – 814

ter Haar E, Day BW, Rosenkranz HS (1996) Direct tubulin polymerization perturbation contributes significantly to the induction of micronuclei *in vivo*. *Mutat Res* **350:** 331 – 337

Tinwell H, Ashby J (1994) Genetic toxicity and potential carcinogenicity of taxol. *Carcinogenesis* **15:** 1499 – 1501

Weaver BA, Silk AD, Montagna C, Verdier-Pinard P, Cleveland DW (2007) Aneuploidy acts both oncogenically and as a tumor suppressor. *Cancer Cell* **11:** 25 – 36

Supplementary Table 1. Micronucleation, apoptosis and spindle poles status in CC and PSP sublines after paclitaxel treatment.

	MN-BN[a]			Apoptosis[b]			Spindle Poles Status[c]					
							Control		Paclitaxel 1 nM		Paclitaxel 20 nM	
	Control	Paclitaxel 1 nM	Paclitaxel 20 nM	Control	Paclitaxel 1 nM	Paclitaxel 20 nM	SP=2	SP>2	SP=2	SP>2	SP=2	SP>2
CC1	0.0	1.6 ↗[d]	ND	0.5	5.5 ↗	60.4 ↗	96.4	3.6	95.8	4.2	64.3	35.7
CC2	0.0	0.0 -	ND	0.0	6.0 ↗	57.0 ↗	95.5	4.5	90.0	10.0	50.0	50.0
CC3	0.0	1.6 ↗	ND	1.0	2.0 ↗	60.0 ↗	96.1	3.9	92.5	7.1	1.5	98.5
CC4	0.0	4.1 ↗	ND	0.0	8.0 ↗	64.0 ↗	93.8	6.2	62.9	37.1	1.6	98.4
CC5	0.0	1.3 ↗	ND	0.0	1.8 ↗	69.7 ↗	90.0	10.0	77.8	22.2	63.3	36.7
CC6	0.0	1.1 ↗	ND	0.0	0.4 ↗	64.9 ↗	96.8	3.2	84.3	15.7	2.0	98.0
CC7	0.0	0.0 -	ND	0.0	7.5 ↗	47.3 ↗	98.6	1.4	97.9	2.1	32.1	67.9
CC8	0.0	0.0 -	ND	0.0	1.8 ↗	65.4 ↗	95.4	4.6	73.9	26.1	1.8	98.2
CC9	0.0	0.0 -	ND	0.0	1.8 ↗	64.0 ↗	95.2	4.8	93.9	6.3	27.2	72.8
CC10	0.0	1.7 ↗	ND	0.0	0.5 ↗	73.1 ↗	97.5	2.5	91.2	8.8	23.8	76.2
PSP1	0.0	3.9 ↗	21.4 ↗[e]	0.5	0.0 ↘	31.7 ↗	97.8	2.2	96.0	4.0	5.0	95.0
PSP2	40.0	1.0 ↘	11.8 ↗	1.5	1.9 ↗	39.1 ↗	93.7	6.3	91.4	8.6	16.7	83.3
PSP3	0.0	0.8 ↗	22.2 ↗	0.0	8.6 ↗	49.3 ↗	95.0	5.0	76.1	23.9	4.8	95.2
PSP4	16.7	9.9 ↘	28.6 ↗	1.0	0.5 ↘	27.1 ↗	97.0	3.0	94.9	5.1	21.6	78.4
PSP6	16.7	10.8 ↘	35.0 ↗	0.5	2.7 ↗	49.8 ↗	94.4	5.6	84.6	15.4	7.6	92.4
PSP7	0.0	2.0 ↗	50.0 ↗	0.0	0.5 ↗	52.4 ↗	99.0	1.0	97.9	2.1	2.6	97.4
PSP8	0.0	9.5 ↗	100.0 ↗	0.0	0.0 -	26.8 ↗	98.6	1.4	97.9	2.1	0.0	100.0
PSP9	0.0	13.4 ↗	60.0 ↗	0.0	0.0 -	47.3 ↗	95.9	4.1	100.0	0.0	32.8	67.2
PSP16	0.0	0.0 -	50.0 ↗	0.0	0.0 -	32.7 ↗	95.4	4.6	90.1	9.9	7.3	92.7
PSP19	0.0	0.0 -	42.9 ↗	0.0	1.9 ↗	29.7 ↗	91.6	8.4	96.1	3.9	12.0	88.0
PSP20	0.0	5.9 ↗	75.0 ↗	0.0	0.0 -	24.8 ↗	93.1	5.2	91.3	8.7	37.2	62.8
PSP21	25.0	4.4 ↘	20.0 ↗	1.0	0.0 ↘	33.8 ↗	92.0	8.0	92.7	7.3	17.4	82.6
PSP22	0.0	14.6 ↗	0.0 ↘	0.0	0.5 ↗	50.5 ↗	95.5	4.5	96.2	3.8	36.9	63.1
PSP25	0.0	4.6 ↗	100.0 ↗	0.0	2.0 ↗	27.5 ↗	92.1	7.9	90.5	9.5	11.1	88.9
PSP32	0.0	9.8 ↗	100.0 ↗	0.0	0.0 -	35.8 ↗	97.7	2.3	98.5	1.5	6.7	93.3
PSP37	0.0	0.0 -	33.3 ↗	0.0	2.5 ↗	24.8 ↗	96.0	4.0	94.0	6.0	33.3	66.7
PSP38	0.0	2.0 ↗	100.0 ↗	2.0	0.0 ↘	12.8 ↗	96.0	4.0	85.9	14.1	17.2	82.8
PSP43	0.0	0.0 -	0.0 -	1.0	2.2 ↗	25.9 ↗	92.4	7.6	93.0	7.0	4.2	95.8
PSP45	0.0	3.0 ↗	0.0 ↘	1.0	0.0 ↘	43.8 ↗	88.7	11.3	89.9	10.1	2.7	97.3
PSP46	0.0	2.6 ↗	0.0 ↘	1.0	0.0 ↘	24.4 ↗	99.3	0.7	97.7	2.3	18.3	81.7

[a] percentage of binucleated cells showing micronucleation in CC and PSP sublines.

[b] percentage of cells showing apoptotic morphology in CC and PSP sublines.

[c] percentage of mitotic cells with 2 (SP=2) or more spindle poles (SP>2) in CC and PSP sublines.

[d] arrows in “Paclitaxel 1 nM” columns means increased (↗), decreased (↘) or unchanged (-) value in 1 nM paclitaxel treated sublines compared with untreated sublines.

[e] arrows in “Paclitaxel 20 nM” columns means increased (↗), decreased (↘) or unchanged (-) value in 20 nM paclitaxel treated sublines compared with 1 nM paclitaxel treated sublines.

ND, not determined.

Supplementary Table 2. Frequency of binucleated cells in cytochalasin-B treated CC and PSP sublines with or without paclitaxel treatment.

	BN[a]		
	Control + CytoB	Paclitaxel 1 nM + CytoB	Paclitaxel 20 nM + CytoB
CC1	64.2	62.3	0.5
CC2	46.5	29.7	1.5
CC3	44.2	29.0	1.4
CC4	52.6	35.4	0.5
CC5	62.2	37.3	0.0
CC6	33.3	42.9	0.5
CC7	57.4	15.8	0.5
CC8	49.5	37.6	3.0
CC9	58.0	62.4	0.5
CC10	75.6	54.9	0.5
CC-Mean[b]	**54.4**	**40.7**	**1.0**
PSP1	79.2	87.9	7.0
PSP2	60.3	50.7	8.5
PSP3	64.0	59.7	8.8
PSP4	49.4	59.5	10.4
PSP6	66.7	44.8	9.6
PSP7	67.8	48.3	3.0
PSP8	66.8	36.8	3.5
PSP9	53.7	32.1	2.5
PSP16	55.9	43.7	4.0
PSP19	64.2	55.3	9.9
PSP20	71.0	54.4	7.7
PSP21	45.6	22.0	7.4
PSP22	60.1	23.9	3.8
PSP25	71.6	59.8	1.0
PSP32	69.7	53.1	1.5
PSP37	65.7	32.4	4.4
PSP38	62.4	45.7	1.0
PSP43	60.4	46.8	0.5
PSP45	58.2	32.4	24.8
PSP46	69.6	53.7	0.5
PSP-Mean[c]	**63.1**	**47.1**	**6.0****

[a] percentage of binucleated cells in CC and PSP sublines.

[b] mean percentage of binucleated cells in CC sublines group.

[c] mean percentage of binucleated cells in PSP sublines group.

CytoB: cytochalasin-B

***P*<0.01, comparison between CC-Mean and PSP-Mean values.

Supplementary Figure 1. Apoptosis in cytochalasin-B treated CC and PSP sublines with or without paclitaxel. A. Percentage of apoptosis (% Apoptosis) in untreated (CTRL), 1 nM or 20 nM paclitaxel (PTX 1 nM, PTX 20 nM) treated CC (n=10) or PSP (n=20) sublines submitted to CBMN assay. **B.** Percentage of apoptosis (% Apoptosis) in "stable" (S-PSP: PSP1, PSP3, PSP7, PSP8, PSP9, PSP16, PSP19, PSP20, PSP22, PSP25, PSP32, PSP37, PSP38, PSP43, PSP45, PSP46. n=16) and "unstable" (U-PSP: PSP2, PSP4, PSP6, PSP21. n=4) PSP sublines submitted to CBMN assay after 1 nM paclitaxel treatment. *P* value determined by Mann-Whitney U non-parametric test; A: comparison between CC and PSP values, B: comparison between S-PSP and U-PSP values. NS: non significant.

Supplementary Figure 1

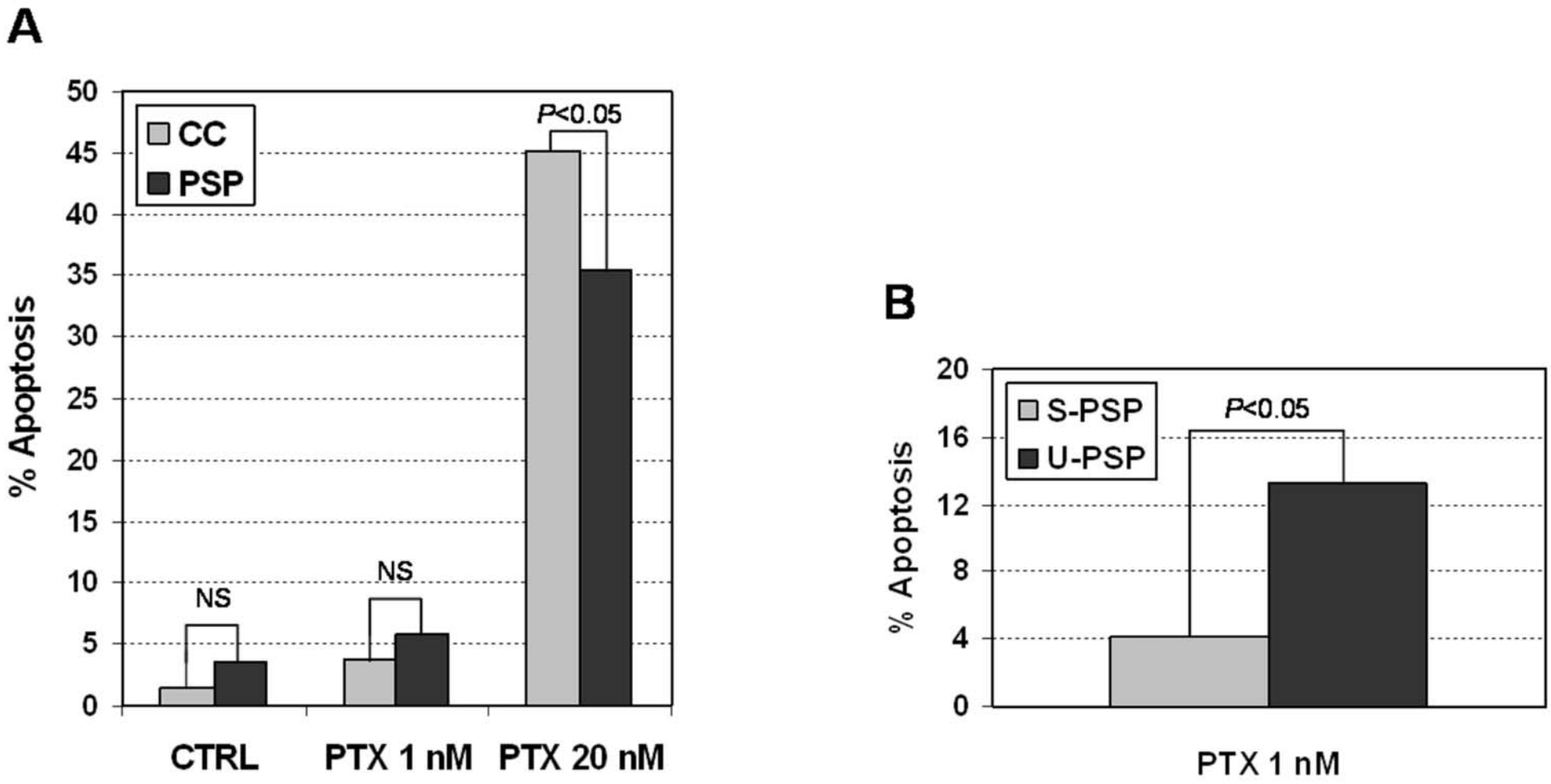

Cancer Cell
Article

Induction of EMT by Twist Proteins as a Collateral Effect of Tumor-Promoting Inactivation of Premature Senescence

Stéphane Ansieau,[1] Jeremy Bastid,[1,2,6] Agnès Doreau,[1,6] Anne-Pierre Morel,[3,6] Benjamin P. Bouchet,[1,2] Clémence Thomas,[1,2] Frédérique Fauvet,[3] Isabelle Puisieux,[1] Claudio Doglioni,[4] Sara Piccinin,[5] Roberta Maestro,[5] Thibault Voeltzel,[1] Abdelkader Selmi,[1,2] Sandrine Valsesia-Wittmann,[1] Claude Caron de Fromentel,[1] and Alain Puisieux[1,2,3,*]
[1]Inserm, U590, Lyon, F-69008, France
[2]Université de Lyon, Lyon 1, Institut des Sciences Pharmaceutiques et Biologiques, Lyon, F-69008, France
[3]Centre Léon Bérard, FNCLCC, Laboratoire de Recherche Translationnelle, Lyon, F-69008, France
[4]Belluno City Hospital, Belluno, I-32100, Italy
[5]CRO IRCCS, Aviano National Cancer Institute, Aviano, I-33081, Italy
[6]These authors contributed equally to this work
*Correspondence: puisieux@lyon.fnclcc.fr
DOI 10.1016/j.ccr.2008.06.005

SUMMARY

Twist1 and Twist2 are major regulators of embryogenesis. Twist1 has been shown to favor the metastatic dissemination of cancer cells through its ability to induce an epithelial-mesenchymal transition (EMT). Here, we show that a large fraction of human cancers overexpress Twist1 and/or Twist2. Both proteins override oncogene-induced premature senescence by abrogating key regulators of the p53- and Rb-dependent pathways. Twist1 and Twist2 cooperate with Ras to transform mouse embryonic fibroblasts. Interestingly, in epithelial cells, the oncogenic cooperation between Twist proteins and activated mitogenic oncoproteins, such as Ras or ErbB2, leads to complete EMT. These findings suggest an unanticipated direct link between early escape from failsafe programs and the acquisition of invasive features by cancer cells.

INTRODUCTION

Twist proteins are highly conserved basic helix-loop-helix (bHLH) transcription factors that have important regulatory functions during embryogenesis. In *Drosophila*, the ancestral Twist protein (named DTwist) is crucial for proper gastrulation and mesoderm formation (Simpson, 1983; Thisse et al., 1987). In mammals, two Twist-like proteins, Twist1 and Twist2, share high structural homology (Li et al., 1995; Wolf et al., 1991). Gene deletion experiments have shown that *TWIST1* is required for closure of the neural tube during mouse development (Chen and Behringer, 1995), while *TWIST2* knockout mice display elevated expression of proinflammatory cytokines causing perinatal death (Sosic et al., 2003). Interestingly, this phenotype is also found in individuals doubly heterozygous for *TWIST1* and *TWIST2* alleles, reflecting some functional redundancy (Bialek et al., 2004). While Twist proteins are only expressed in a subset of mesodermally and ectodermally derived tissues, *TWIST1* is overexpressed in various human solid tumors including numerous types of carcinomas as well as sarcomas, gliomas, neuroblastomas, and melanomas (Yang et al., 2004; Kwok et al., 2005; Mironchik et al., 2005; Zhang et al., 2007; Ohuchida et al., 2007; Entz-Werle et al., 2005; Elias et al., 2005; Valsesia-Wittmann et al., 2004; Hoek et al., 2004). The role of Twist1 in tumor progression has been convincingly associated with the metastatic process (Yang et al., 2004). Exogenous overexpression

SIGNIFICANCE

Because cells are frequently subjected to abnormal growth signals, multicellular organisms develop two major safeguard programs, senescence and apoptosis, that can eliminate potentially deleterious cells at early stages of tumor development. The mechanisms by which precancer cells escape these protective barriers remain to be determined. Herein, we identify Twist proteins as decisive early drivers of tumorigenesis. Indeed, Twist1 and Twist2 abrogated oncogene-induced senescence by inhibiting key regulators of this safeguard program. Strikingly, this deleterious effect was associated with complete epithelial-mesenchymal transition (EMT), a process associated with the acquisition of invasive potential. These observations suggest that some metastatic capabilities of cancer cells can be acquired during malignant conversion as a side effect of the inactivation of primary failsafe mechanisms.

of Twist1 increases the invasive and metastatic abilities of human cancer cells by promoting the downregulation of E-cadherin and the induction of an epithelial-mesenchymal transition (EMT) (Yang et al., 2004; Kwok et al., 2005; Mironchik et al., 2005). EMT, which was first recognized as a feature of embryogenesis, converts epithelial cells into mesenchymal cells and promotes cell motility through profound disruption of cell-cell junctions and extensive reorganization of the actin cytoskeleton (Hay, 1995).

The results presented herein indicate that *TWIST2*, similarly to *TWIST1*, is overexpressed in a large variety of human primary tumors and cancer cell lines. We next demonstrate that both Twist1 and Twist2 inhibit premature senescence in cancer cells, a process identified as an initial barrier to tumor development. Indeed, senescence occurs in vivo in precancerous lesions in response to aberrant mitogenic signaling, and its inactivation is required for progression toward malignancy (Chen et al., 2005; Michaloglou et al., 2005; Collado et al., 2005). We further show that this property allows Twist proteins to cooperate with mitogenic oncoproteins, resulting in full transformation of murine cells. Interestingly, in human epithelial cells, escape from premature senescence mediated by Twist1 or Twist2 is associated with complete EMT. Altogether, these findings suggest an as yet undescribed link between early escape from failsafe programs and acquisition of metastatic features.

RESULTS

Twist1 and Twist2 Override Oncogene-Induced Senescence in Murine and Human Cancer Cells

Twist1 has been shown to play a major role in breast cancer progression by promoting EMT and favoring the metastatic process (Yang et al., 2004). To further evaluate the role of both Twist proteins in carcinoma progression, we first took advantage of the MMTV-*ErbB2/Neu* transgenic mouse model (unactivated rat *ErbB2/Neu* gene under the transcriptional control of the mouse mammary tumor virus promoter/enhancer). *ERBB2* is a major oncogene involved in human breast tumorigenesis, and this mouse model is considered to be an appropriate tool for deciphering the molecular pathways involved in breast cancer progression. After a long latency, which is believed to represent the time required for mammary epithelial cells to acquire additional cooperative events, MMTV-*ErbB2/Neu* transgenic mice stochastically develop focal mammary tumors that can eventually metastasize to the lungs (Guy et al., 1992). Analysis of *TWIST1* and *TWIST2* expression in twenty independent spontaneous mammary tumors demonstrated a frequent activation of the *TWIST2* gene (Figure 1). Indeed, whereas *TWIST1* expression levels remained weak in all tumors, *TWIST2* was significantly upregulated ($p < 0.0001$) in 12 of them (60%), suggesting that Twist2 might be involved in tumor progression.

In an initial approach to define potential Twist2 oncogenic functions, cancer cell lines derived from either *TWIST2*-positive or -negative tumors from MMTV-*ErbB2/Neu* transgenic mice were established, and the consequences of *TWIST2* depletion by RNA interference were evaluated. Surprisingly, knockdown of *TWIST2* in *TWIST2*-expressing cell lines invariably triggered cellular senescence characterized by flattened cytoplasm, G1 growth arrest, senescence-associated β-galactosidase

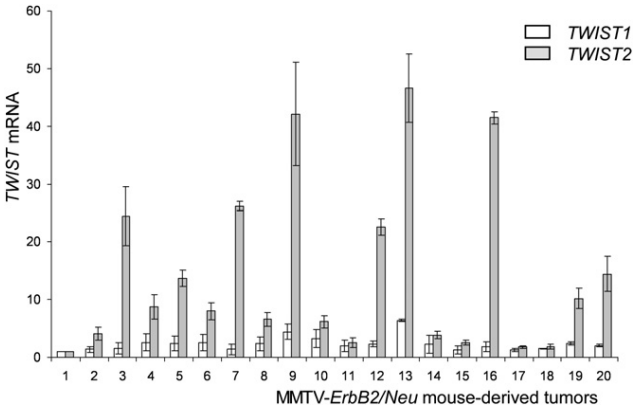

Figure 1. *TWIST2* Is Overexpressed in MMTV-*ErbB2/Neu*-Derived Mammary Tumors

TWIST1 and *TWIST2* gene expression in spontaneous tumors developed in MMTV-*ErbB2/Neu* transgenic mice as assessed by quantitative RT-PCR. Error bars represent mean ± SD of triplicate experiments.

(SA-β-gal) activity, and induction of the de novo marker of cellular senescence *DEC1* (Qian et al., 2008; Collado et al., 2005) (Figure 2). Similar results were obtained using two independent *TWIST2* shRNA sequences. As expected, these two shRNAs had no effect on *TWIST2*-negative cell lines, thus demonstrating the specificity of the observation.

As aberrant activation of ErbB2 in mammary epithelial cells triggers a premature senescence response (Trost et al., 2005), our observations suggested that Twist2 induction might override oncogene-induced senescence in vivo. This property was not limited to murine cells. In fact, *TWIST2* but also *TWIST1* depletion promoted senescence in human melanoma and breast cancer cell lines (Figure 3), linking Twist1 and Twist2 to the inactivation of this failsafe program.

TWIST1 and *TWIST2* Are Frequently Overexpressed in Human Cancers

Whereas the overexpression of *TWIST1* has already been described in a large variety of tumors, the status of *TWIST2* in malignancies remains largely unknown. We thus measured *TWIST1* and *TWIST2* mRNA levels in a wide range of human tumors (n = 148) and human tumor-derived cell lines (n = 64) encompassing eight different cancer types (Figure 4A; see also Figure S1 available online). Overall, *TWIST1* and *TWIST2* were significantly upregulated in primary tumor cells ($p = 0.002$ and $p = 0.04$, respectively) and in cancer cell lines ($p < 0.0001$ and $p = 0.0042$, respectively) compared to their normal counterparts. As shown in Figure 4A, *TWIST1* and *TWIST2* overexpression was particularly frequent in melanoma samples. Melanomas are malignant proliferation of cutaneous melanocytes that can develop from benign nevi. Premature senescence is a major safeguard mechanism preventing the progression from nevi to melanomas (Michaloglou et al., 2005). Although generally harboring activating mutations in the B-Raf oncoprotein (a major effector of Ras), nevi typically remain in a growth-arrested state for decades. Peeper and collaborators have demonstrated that cells within nevi display characteristic features of senescence (including expression of $p16^{Ink4a}$) and are growth arrested, whereas in

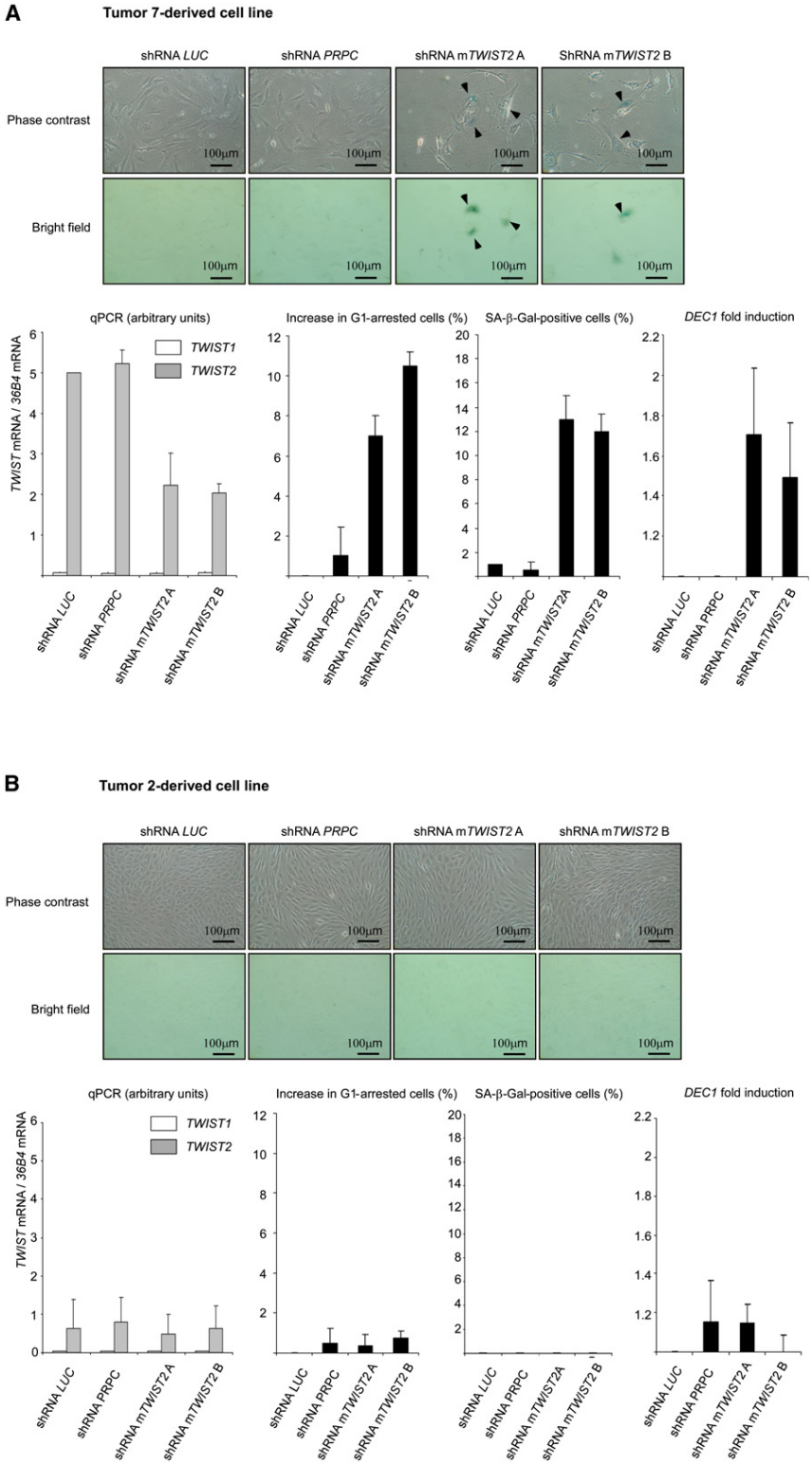

Figure 2. *TWIST2* Depletion Induces Senescence in MMTV-*ErbB2*/*Neu*-Derived Tumor Cells

Cells derived from MMTV-*ErbB2*/*Neu* transgenic mouse tumors either overexpressing *TWIST2* (tumor 7-derived cell line, [A]) or with no endogenous expression of *TWIST2* (tumor 2-derived cell line, [B]) were transiently infected with retroviral constructs expressing either shRNAs directed against the murine *TWIST2* gene (shRNA m*TWIST2* A and shRNA m*TWIST2* B) or shRNAs directed against the *luciferase* gene (shRNA *LUC*) or the prion pRpC protein (shRNA *PRPC*) as controls.

Upper panels: representative photomicrographs of cells obtained by phase-contrast microscopy and of SA-β-galactosidase staining observed in bright field.

Lower panels: *TWIST1* and *TWIST2* expression levels as assessed by real-time quantitative RT-PCR (qPCR; relative mRNA levels are indicated), % of increase in G1-arrested cells, % of SA-β-galactosidase (SA-β-Gal)-positive cells, and fold induction of the senescence marker *DEC1* are shown. Error bars represent mean ± SD of triplicate experiments.

melanoma, senescence is absent and cells proliferate (Michaloglou et al., 2005). Based on these observations, we evaluated Twist1 and p16^{Ink4a} expression using immunohistochemistry in a series of 12 melanocytic nevi and 10 melanomas. (Of note, there is no reliable antibody against Twist2 currently available.) Strikingly, all nevi contained p16^{Ink4a}-expressing cells (50%–100% positive cells in 8 out of 12 cases), whereas no Twist1-expressing cells were observed. In contrast, high levels of Twist1 were detected in 5 out of 10 cases of melanoma. Consistent with a role of Twist1 in the inhibition of premature senescence, p16^{Ink4a} immunoreactivity was either undetectable or low in these samples, with an exclusive pattern when compared with Twist1 immunoreactivity (Figure 4B).

Twist1 and Twist2 Cooperate with Activated Ras for Malignant Transformation and Disrupt Both p53 and Rb Tumor Suppressor Pathways

The induction of premature senescence following constitutive activation of the Ras/Raf mitogenic pathway is particularly well documented (Serrano et al., 1997). To further study the biological effects of Twist1 and Twist2, standard cooperation assays were performed in primary murine embryonic fibroblasts (MEFs) using an activated form of H-Ras (H-Ras^{V12}). As expected, MEFs infected only with H-Ras^{V12} immediately stopped growing and underwent senescence characterized by flattened cytoplasm, induction of SA-β-gal activity, and G1 growth arrest (data not shown). In contrast, cells sequentially infected with H-Ras^{V12} and either Twist1

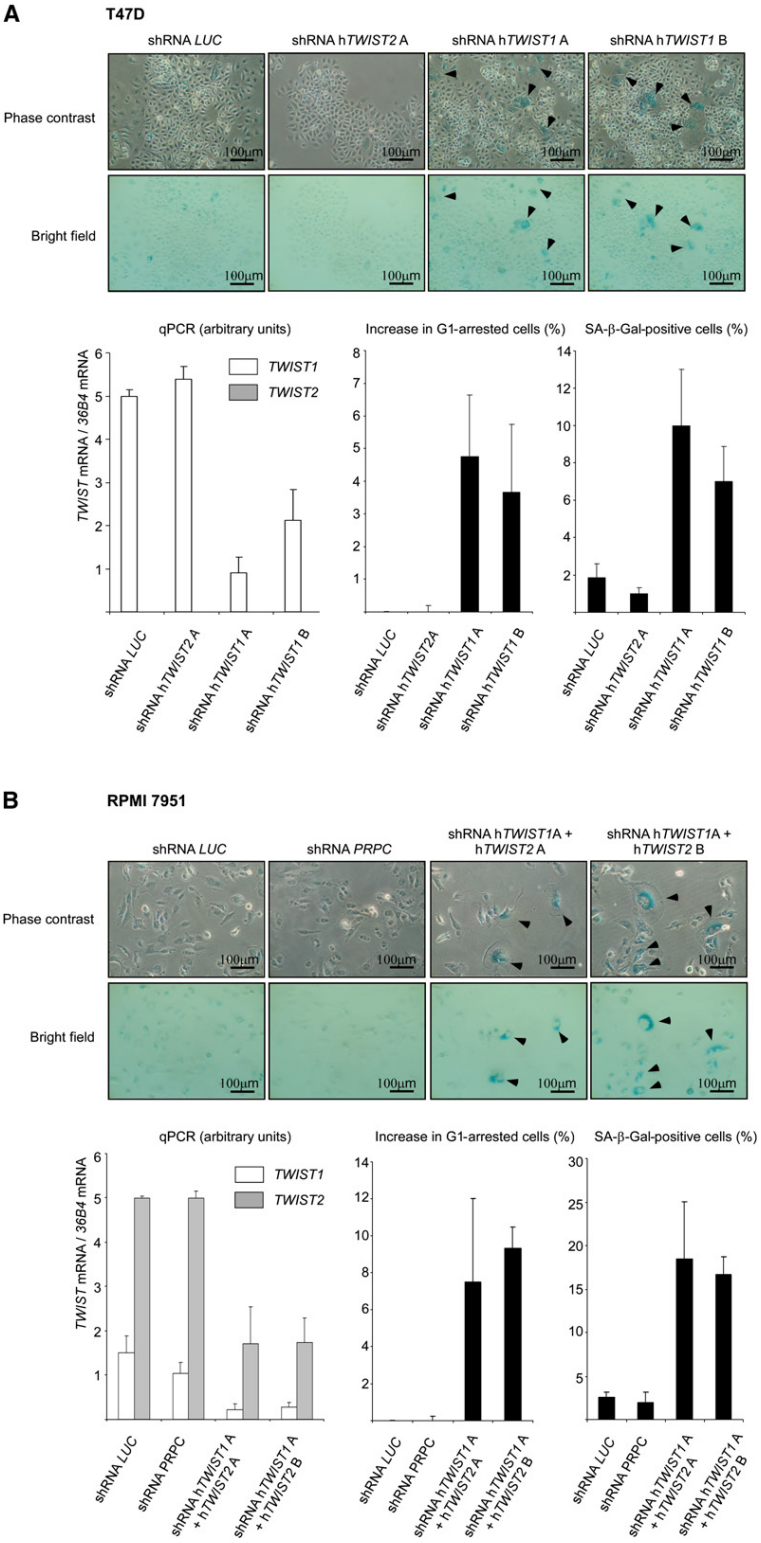

Figure 3. *TWIST1* and/or *TWIST2* Depletion Induces Senescence in Human Breast Cancer and Melanoma Cell Lines

T47D (human breast cancer cell line carrying four copies of *ERBB2*; [A]) and RPMI 7951 (human melanoma cell line carrying a mutant B-Raf^{V600E}; [B]) cells were doubly infected with lentiviral constructs expressing either shRNA directed against the human *TWIST1* (shRNA h*TWIST1* A and shRNA h*TWIST1* B) or *TWIST2* (shRNA h*TWIST2* A and shRNA h*TWIST2* B) genes as indicated or shRNAs directed against the *luciferase* gene (shRNA *LUC*) or the prion pRpC protein (shRNA *PRPC*) as controls.

Upper panels: representative photomicrographs of cells obtained by phase-contrast microscopy and of SA-β-galactosidase staining observed in bright field.

Lower panels: *TWIST1* and *TWIST2* expression levels as assessed by real-time qPCR (relative mRNA levels are indicated), % of increase in G1-arrested cells, and % of SA-β-Gal-positive cells are shown. Error bars represent mean ± SD of triplicate experiments.

transformation such as loss of contact inhibition, growth in soft agar, and high tumorigenic potential as demonstrated after subcutaneous grafting into athymic *nude* mice (Figures 5B–5D; Figure S2). Although the time required for tumor growth varied slightly, clonogenic and tumorigenic capabilities were observed even in the presence of relatively low levels of ectopic Ras and/or Twist expression (data not shown). Upon histological examination, expanding xenografts displayed all of the features of aggressive sarcomas, with high levels of aberrant mitosis, anisokaryosis, and major angiogenic activity, further demonstrating a potent oncogenic cooperation between Twist proteins and Ras (Figure 5). Of note, although Twist proteins have been shown to regulate proinflammatory cytokine gene expression (Sosic et al., 2003), microarray analysis of MEFs and transformed MEFs did not show striking differences in expression of chemokines, interleukins, and their receptors (Table S1).

The p53 and Rb tumor suppressor pathways are known to play a pivotal role in the onset of premature senescence (Serrano et al., 1996). To further investigate the mechanisms by which Twist proteins inhibit oncogene-induced failsafe programs, we compared the endogenous expression of p16^{Ink4a}, ARF, p53, and p21^{Cip1} in MEFs infected with H-Ras^{V12} alone or in combination with Twist1 or Twist2 retroviral expression constructs. As shown in Figure 6A, Twist1 or Twist2 expression was sufficient to completely abrogate p16^{Ink4a} and p21^{Cip1} induction by activated Ras without downregulating ARF and p53 levels. Identical inhibitory effects were observed in cell lines either generated through the MEF transformation assays (Ras + Twist1, Ras + Twist2) or derived from tumors induced in athymic *nude* mice (Figure 6A). To confirm that Twist per se was sufficient to abrogate p16^{Ink4A} and p21^{Cip1} activation, we

or Twist2 continued proliferating (Figure 5A) and could be maintained in culture for months. MEFs overexpressing both H-Ras^{V12} and Twist1 or Twist2 exhibited hallmarks of malignant

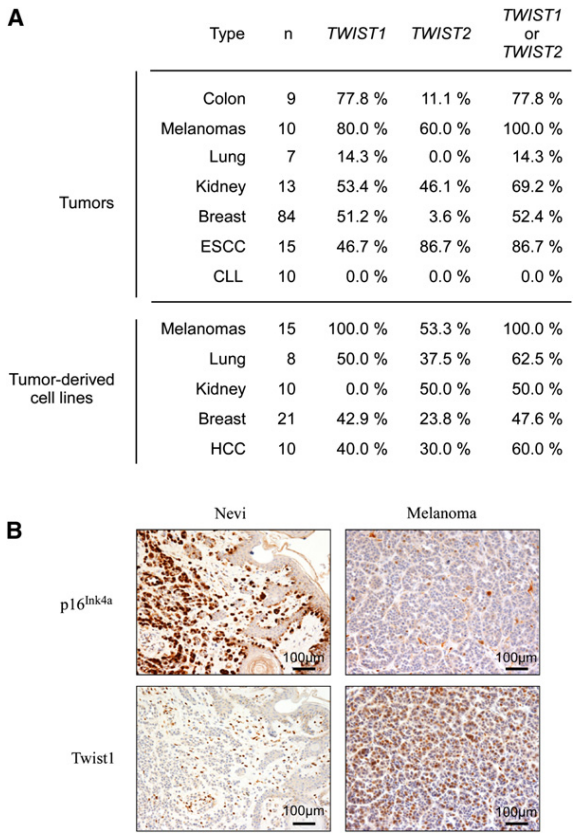

Figure 4. *TWIST1* and *TWIST2* Genes Are Overexpressed in Various Human Tumors and Tumor-Derived Cell Lines

(A) *TWIST1* and *TWIST2* gene expression was assessed by TaqMan real-time quantitative PCR analysis. Expression was compared with that of healthy tissue or normal cell counterparts. Percentages of samples harboring an overexpression of *TWIST1* or *TWIST2* genes (>2-fold) are shown. (More information is available in Figure S1 and the Supplemental Experimental Procedures.) ESCC, esophageal squamous cell carcinoma; CLL, chronic lymphoid leukemia; HCC, hepatocellular carcinoma.

(B) Immunohistochemical analysis of $p16^{Ink4a}$ and Twist1 protein levels in human nevi and melanomas. Brownish dots detected in the cytoplasm of nevus cells are melanin granules. The dark brown cells in nevi are fibroblasts revealing that dermal fibroblasts are reactive for Twist1.

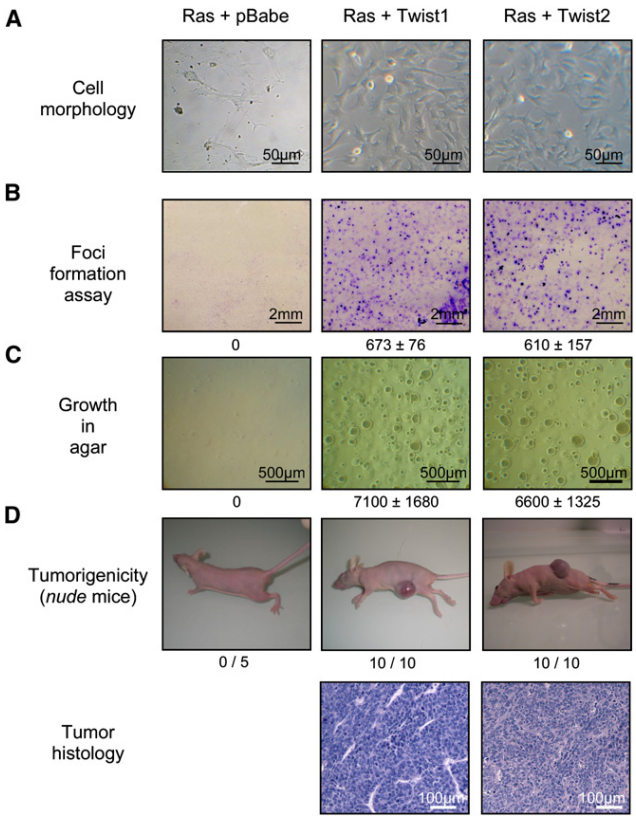

Figure 5. Twist Proteins Cooperate with Ras in MEF Transformation

Primary murine embryonic fibroblasts (MEFs) were sequentially infected with a retroviral vector encoding $H\text{-}Ras^{V12}$ (Ras) and a retroviral vector encoding Twist1, Twist2, or an empty vector (pBabe) as a control.

(A) Ras-infected cells underwent senescence, whereas Ras + Twist-infected cells are immortalized.

(B) Foci formation assays indicating that Ras + Twist-infected MEFs have lost cell contact inhibition. Foci numbers (for 3×10^3 cells) ± SD of triplicate experiments are indicated.

(C) Ras + Twist-infected MEFs grow on soft agar. Colony numbers (for 2×10^5 cells) ± SD of triplicate experiments are indicated.

(D) MEFs infected with Ras alone or with Ras + Twist1 or Twist2 were subcutaneously grafted into irradiated Swiss *nude* mice. Ras + Twist-transformed MEFs are tumorigenic. The number of mice developing tumors is indicated. The tumors display characteristics of aggressiveness (including high mitotic index and high vascular density).

knocked down *TWIST1* expression using RNA interference in Ras + Twist1-transformed MEFs. As shown in Figure 6B, inhibition of *TWIST1* expression led to a significant reinduction of the expression of both cyclin-dependent kinase inhibitors. Nevertheless, this reinduction was not sufficient to trigger senescence, which might be due to residual ectopic Twist1. To gain insight into the mechanisms underlying the regulatory roles of Twist proteins, the effect of Twist1 and Twist2 on the $p16^{INK4A}$ and $p21^{CIP1}$ genes was assessed in reporter assays. Consistent with the protein expression profile observed, Twist1 and Twist2 inhibited $p16^{INK4A}$ and $p21^{CIP1}$ promoter activation by $H\text{-}Ras^{V12}$ and p53 (Figures 6C and 6D). Although the molecular mechanisms involved in this effect are still under investigation, preliminary experiments suggest that the ability of Twist proteins to prevent the Ras-mediated activation of $p16^{INK4A}$ might be associated with their ability to interact with the Ras effector Ets2 (Figure S3).

Twist1 and Twist2 Overcome Premature Senescence and Cooperate Further with Mitogenic Oncoproteins to Promote EMT and Invasiveness

The ability of Twist1 and Twist2 to overcome oncogene-induced senescence was confirmed in a variety of human cells including primary mammary epithelial cells (HMECs) (Figure 7), IMR90 and MRC5 diploid fibroblasts (Figure S4), and immortalized BJ primary fibroblasts expressing an inducible version of $H\text{-}Ras^{V12}$ (data not shown). In all cases, expression of Twist1 or Twist2 completely abolished premature senescence induced by the activated mitogenic oncoprotein. We thereby confirmed that Twist1 or Twist2 overexpression was sufficient to override this crucial primary safeguard mechanism, thus providing a rationale for the observed oncogenic cooperation. Intriguingly, experiments with HMECs revealed a second level of cooperation. As

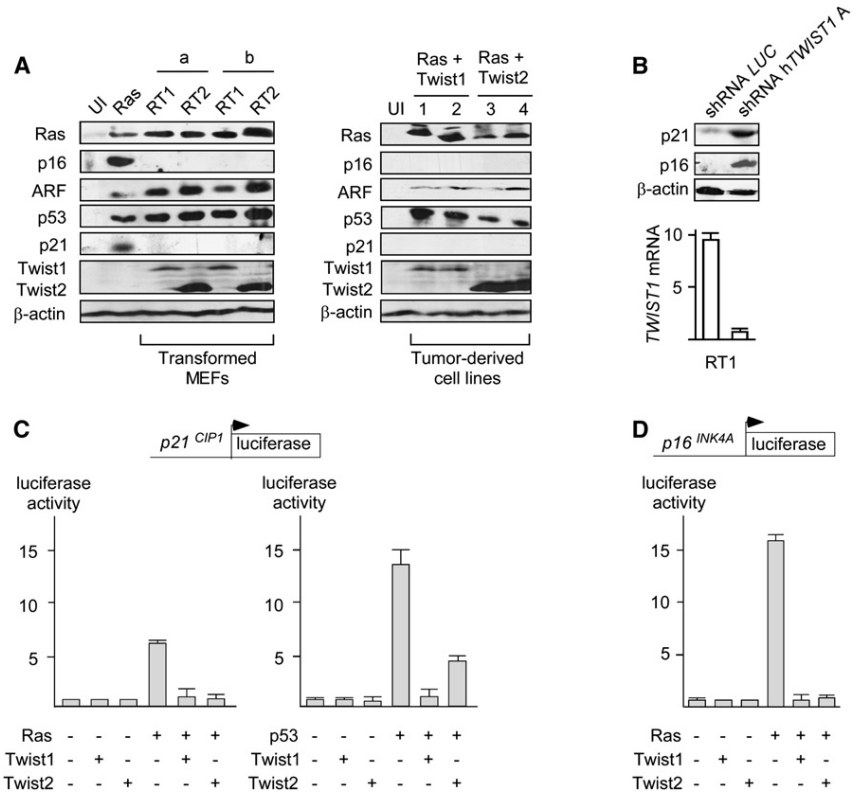

Figure 6. Effects of Twist1 and Twist2 Overexpression on Key Regulators of the p53 and Rb Signaling Pathways in Murine and Human Cells

(A) Western blots of cell lysates. Ras, $p16^{Ink4a}$, ARF, p53, $p21^{Cip1}$, Twist1, and Twist2 protein levels are shown as indicated. Left panel: cell lysates from uninfected (UI) MEFs, MEFs transiently infected with a H-Ras^{V12} (Ras) retroviral expression construct, and transformation assay-derived cell lines coexpressing H-Ras^{V12} and Twist1 (RT1) or H-Ras^{V12} and Twist2 (RT2). "a" and "b" represent two independent infection experiments. Right panel: cell lysates from uninfected MEFs or from murine tumor-derived cell lines coexpressing H-Ras^{V12} and Twist1 or H-Ras^{V12} and Twist2 as indicated.

(B) Cell lysates from cell lines coexpressing H-Ras^{V12} and Twist1 infected with a shRNA directed against the *TWIST1* gene (shRNA *TWIST1* A) or the *luciferase* gene (shRNA *LUC*). Inhibition of *TWIST1*, as assessed by real-time qPCR (relative mRNA levels are shown), is associated with the restoration of $p16^{Ink4a}$ and $p21^{Cip1}$ protein expression.

(C and D) Twist1 and Twist2 act as transcriptional repressors of both $p16^{INK4A}$ and $p21^{CIP1}$ genes. E1A-immortalized MEFs were transiently cotransfected with H-Ras^{V12}, p53, Twist1, and Twist2 expression constructs as indicated, along with the human $p21^{CIP1}$ (C) and $p16^{INK4A}$ (D) promoters. Relative luciferase activity is shown.

Error bars represent mean ± SD of triplicate experiments.

shown in earlier studies (Yang et al., 2004), ectopic expression of Twist1 alone in HMECs triggered several features of EMT (Figure 7). However, Twist1-mediated EMT was only partial as demonstrated by the observed cellular morphology, the significant but incomplete decrease of the E-cadherin epithelial marker, and the modest increase of the vimentin mesenchymal marker (Figures 7A and 7B). Of note, a similar effect was also observed with Twist2. In contrast, expression of both Twist1 (or Twist2) and H-Ras^{V12} (or ErbB2) triggered a total loss of E-cadherin, an increase in vimentin expression (Figure 7 and data not shown), and a concomitant acquisition of invasive properties (Figure 7C). A cooperative effect between Twist and mitogenic oncoproteins on the acquisition of mesenchymal features and invasive properties was also observed in Ras-transformed mammary epithelial MCF10A cells (MCF10A cells retrovirally infected by Ras^{V12}, MCF10A pLX Ras^{V12}) (Figure S5) (Konishi et al., 2007).

Because the role of Twist1 in the induction of EMT was originally demonstrated in polarized Madin-Darby canine kidney (MDCK) epithelial cells (Yang et al., 2004), we next examined the effects of Twist1 or Twist2 in the presence or absence of H-Ras^{V12} in these cells. In line with previous observations, overexpression of Twist1 or Twist2 alone was sufficient to trigger some morphological features of EMT, including a fibroblastic morphology, associated with a significant decrease of epithelial markers and increase of mesenchymal protein levels. Nevertheless, as demonstrated by the additional reduction of epithelial markers and further increase of mesenchymal protein expression, complete EMT required the presence of H-Ras^{V12}, confirming the cooperative effect (Figure 8). The mechanisms underlying this observation remain unknown. EMT is regulated by an elaborate interplay of signaling pathways. However, it is noteworthy that oncogenic Ras has been shown to cooperate with TGF-β to induce EMT (Oft et al., 1996) and that TGF-β is believed to act through the induction of several transcription repressors, including Twist1 (Kang and Massague, 2004).

Taken together, our results highlight an unexpected double-barreled oncogenic cooperation between Twist proteins and mitogenic oncoproteins such as Ras and ErbB2. On one hand, Twist1 or Twist2 allows cancer cells to override premature senescence, and on the other hand, concomitant activation of Twist and mitogenic signaling promotes complete EMT, thereby facilitating invasion and metastasis.

DISCUSSION

Aberrant cell proliferation and malignant transformation induced by some oncogenes are restrained by cellular senescence (Serrano et al., 1997). First considered as a cell culture artifact, premature senescence was recently confirmed in vivo as an early barrier against tumor progression (Bartkova et al., 2005; Chen et al., 2005; Gorgoulis et al., 2005; Collado et al., 2005). Indeed, it occurs in many different precancerous tissues in both humans and mice but is absent in malignant tumors, suggesting that its inactivation is a general requirement for full-blown cancer progression. However, the mechanisms allowing premalignant cells to bypass this primary failsafe program remain

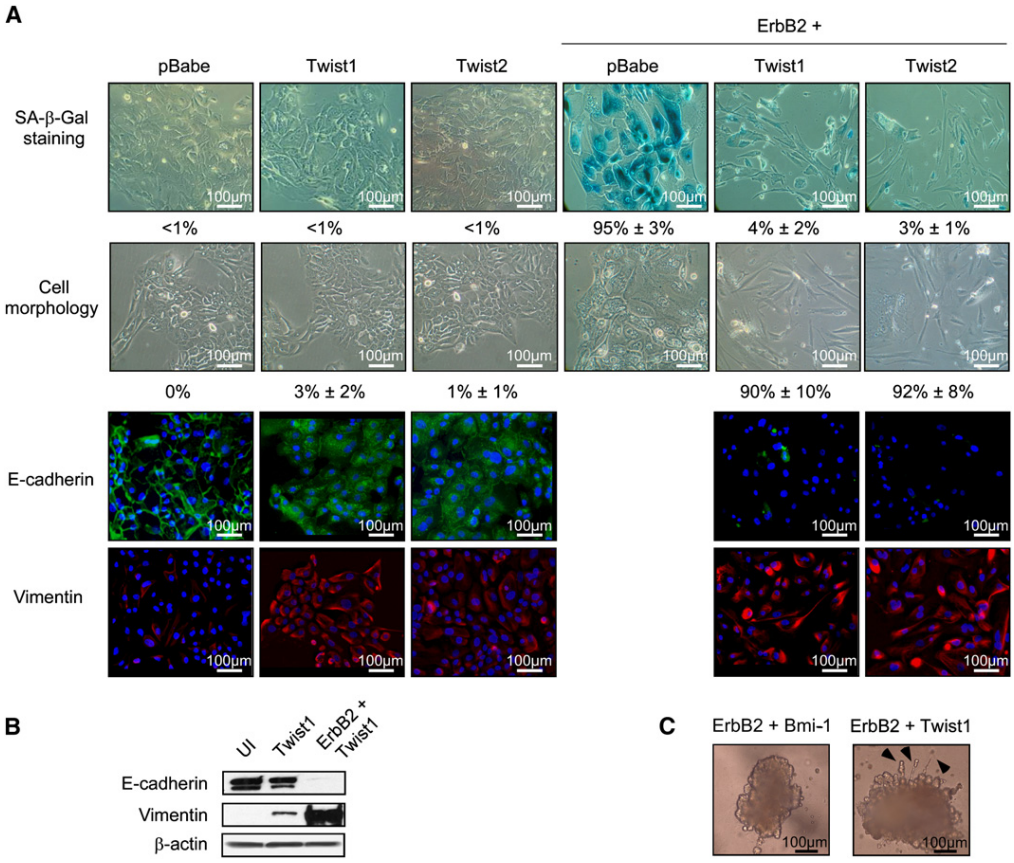

Figure 7. Twist-Dependent Failsafe Program Escape in Human Mammary Epithelial Cells Is Associated with Complete EMT and Acquisition of Invasive Properties

(A) Human mammary epithelial cells (HMECs) were infected with Twist1 or Twist2 retroviral expression constructs (left three columns) or sequentially infected with ErbB2 and Twist1 or Twist2 retroviral expression constructs (right three columns) as indicated. First row: representative photomicrographs of SA-β-Gal staining. Percentages of SA-β-Gal-positive cells (±SD of triplicate experiments) are indicated. Second row: phase-contrast microscopy showing cell morphology. Percentages of fibroblastic cells (±SD of triplicate experiments) are indicated. Third and fourth rows: E-cadherin (epithelial marker) and vimentin (mesenchymal marker) expression analysis by immunofluorescence. Nuclei were counterstained using Hoechst.

(B) Expression of E-cadherin and vimentin proteins in the same cells was analyzed by western blotting.

(C) Comparison by Matrigel invasion assay of the invasive properties of HMEC cells sequentially infected with ErbB2 and either Bmi-1 or Twist1 retroviral expression constructs as indicated. Bmi-1 was used as a control due to its ability to override oncogene-induced senescence.

largely unknown. Our results show that Twist1 and Twist2, two important regulators of embryogenesis, are frequently activated in human cancer cells and that their induction is sufficient to override oncogene-induced senescence in both murine and human cells by inhibiting both the p53 and Rb tumor suppressor pathways. In line with these observations, Twist proteins cooperate with Ras to transform MEFs, further demonstrating their oncogenic properties. At least in vitro, the Twist1 and Twist2 oncogenic activities appear to rely largely upon the inhibition of premature senescence. Indeed, in conditions where Ras activation does not trigger senescence, e.g. targeted knockin of a mutant *K-Ras* gene in immortalized MCF10A breast cells, no Twist-dependent transforming activity as assessed by soft agar assay (Figure S6) could be observed. Of note, MCF10A is a nontumorigenic but immortal HMEC cell line displaying a rearrangement and a deletion affecting the *INK4/ARF* locus that lead to a homozygous loss of the $p16^{INK4A}$, *ARF*, and $p15^{INK4B}$ genes (Cowell et al., 2005).

The role of Twist proteins in the inhibition of premature senescence is concordant with previous studies that reported the induction of Twist1 expression during the progression toward malignant stages in several cancer types including prostate, bladder, and pancreatic lesions (Kwok et al., 2005; Zhang et al., 2007; Ohuchida et al., 2007). The inverse correlation between $p16^{Ink4a}$ and Twist1 protein levels in nevi and melanoma samples also supports the role of Twist proteins as negative modulators of $p16^{INK4A}$ and as crucial inhibitors of oncogene-induced senescence in human cancer cells. As we have previously demonstrated that Twist1 and Twist2 are able to inhibit Myc-induced apoptosis in vitro and in vivo (Maestro et al., 1999; Valsesia-Wittmann et al., 2004), Twist proteins appear to act as general inhibitors of oncogene-induced safeguard programs. Noticeably, in response to activated Ras, Twist1 and Twist2 appear to act by downregulating the cyclin-dependent kinase inhibitors $p16^{Ink4a}$ and $p21^{Cip1}$ without affecting ARF levels, whereas ARF is a crucial Twist target in response to aberrant

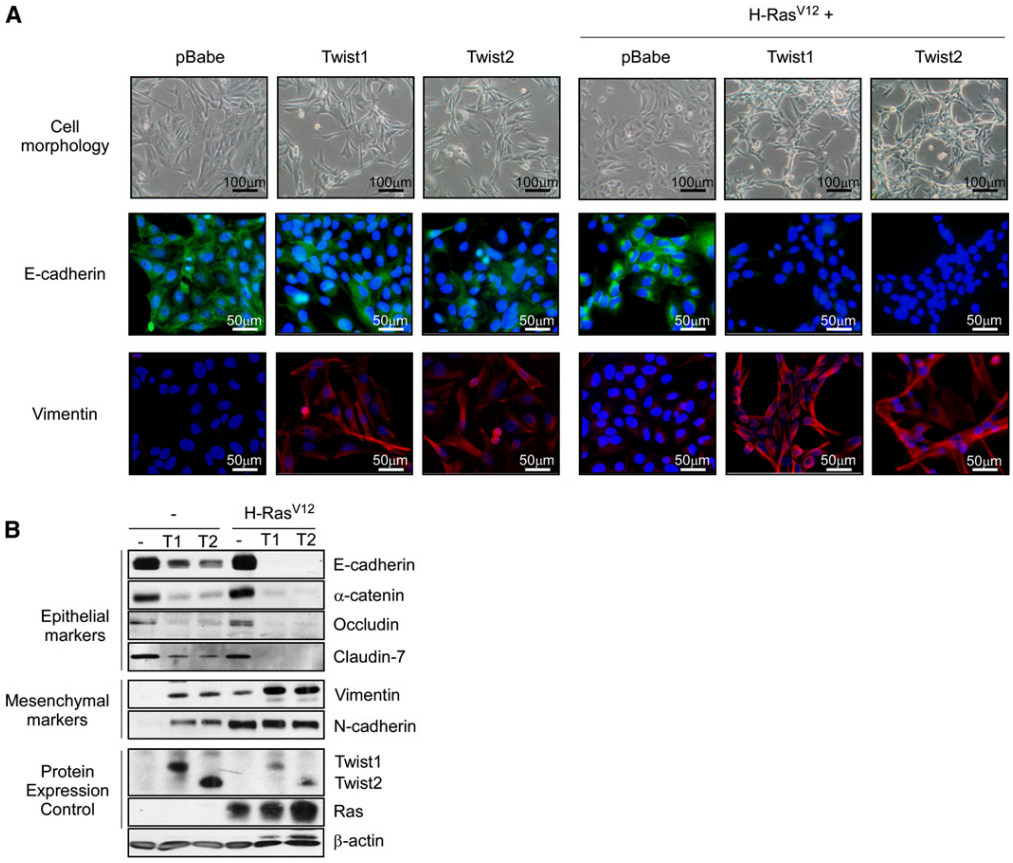

Figure 8. Twist Proteins Cooperate with Ras to Induce Complete EMT in MDCK Cells

Madin-Darby canine kidney (MDCK) cells were infected with Twist1 or Twist2 retroviral expression constructs (left three columns) or sequentially infected with H-Ras^{V12} and Twist1 or Twist2 retroviral expression constructs (right three columns) as indicated.

(A) First row: representative photomicrographs of cells obtained by phase-contrast microscopy. Second and third rows: E-cadherin and vimentin expression analysis by immunofluorescence. Nuclei were counterstained with Hoechst.

(B) Expression analysis of epithelial and mesenchymal markers, Twist1, Twist2, and Ras proteins by western blotting.

Myc activation (Maestro et al., 1999; Valsesia-Wittmann et al., 2004). Although the underlying mechanisms remain to be determined, the differential effect on *ARF* gene expression has been confirmed in reporter assays (data not shown).

Escape from oncogene-induced senescence and apoptosis being a general prerequisite for malignant conversion, our observations suggest that Twist1 and Twist2 are early drivers of tumor progression and provide a rationale for the high frequency of *TWIST1* and *TWIST2* overexpression in a large variety of human tumors. Furthermore, these findings shed new light on the role of Twist proteins in EMT and metastasis. Several groups have previously reported that high Twist1 expression promotes EMT and correlates with tumor invasion and metastasis in a variety of human cancers (Yang et al., 2004; Mironchik et al., 2005; Kang and Massague, 2004). Overall, our data show that in cells with aberrant mitogenic signaling, Twist1 or Twist2 reactivation overrides primary safeguard mechanisms to trigger cell transformation and, as a side effect, promotes EMT in cooperation with mitogenic oncoproteins, favoring invasiveness. In conditions where the mitogenic activation does not trigger senescence (due either to low levels of oncoprotein or to alternative mechanisms leading to a deregulation of safeguard programs), Twist1 and Twist2 do not display major transforming capabilities but still cooperate with activated oncoproteins in promoting EMT (Figures S5 and S6).

A prevailing model proposes that transcription factors involved in EMT promotion, such as Twist1, Snail, and Slug, are induced in rare cancer cells residing at the invasive edge of advanced carcinomas in response to signals released by the activated stroma (Scheel et al., 2007). According to this model, *TWIST1* induction will not provide any growth advantage within the primary tumor and will specifically favor cell dissemination, particularly the steps of motility and invasiveness. Based on our observations, we propose an alternative model in which, in the presence of aberrant mitogenic signaling, reactivation of the developmental proteins Twist1 and Twist2 promotes the transition from a premalignant to a malignant stage by inactivation of innate failsafe programs. Due to the cooperative effect of Twist1 or Twist2 and mitogenic factors on EMT promotion, this model predicts that most of the cancer cells within the primary tumor will be responsive to EMT-inducing signals from

the microenvironment, highly increasing the risk of metastatic dissemination.

Challenging the classical view of metastasis as the final step of tumor progression, recent observations further support the notion that early transformed cells are capable of dissemination. Specifically, Klein and colleagues have reported that disseminated cancer cells in the bone marrow of breast cancer patients exhibit different and fewer alterations than their matched primary tumors (Schmidt-Kittler et al., 2003; Schardt et al., 2005). By using BALB/c mice transgenic for the activated rat *ErbB2/Neu* gene, the same group recently demonstrated that dissemination of epithelial cells begins shortly after expression of the oncogenic transgene, as early as the stage of atypical hyperplastic lesion (Husemann et al., 2008). Strikingly, unlike both normal mammary glands and the invasion front of advanced tumors, these early lesions are characterized by a significant overexpression of *TWIST1* (of note, *TWIST2* expression was not examined by these authors). Although further work is warranted to confirm these observations in human cancers, these and our findings support the hypothesis that reactivation of Twist proteins in vivo promotes malignant conversion concomitantly with metastatic dissemination.

EXPERIMENTAL PROCEDURES

Constructs

N-terminally FLAG-tagged human Twist1, Twist2, and H-Ras^{V12} proteins were expressed from the pBabe, pCI-neo, or pcDNA3 expression vectors (Promega). The human *ERBB2* cDNA was subcloned into the pBabe retroviral expression vector.

Human *ARF*, *p16^{INK4A}*, and *p21^{CIP1}* luciferase reporter constructs have been described previously (Linggi et al., 2002; Hara et al., 1996; el-Deiry et al., 1993). The H-Ras^{V12} pBabe and the Bmi-1 pBabe expression constructs were generous gifts from the laboratories of Robert A. Weinberg and Goberdhan P. Dimri.

shRNAs directed against the human *TWIST1* gene (shRNA h*TWIST1* A, 5′-GCTGAGCAAGATTCAGACC-3′ [Yang et al., 2004]; shRNA h*TWIST1* B, 5′-GTACATCGACTTCCTCTAC-3′), the human *TWIST2* gene (shRNA h*TWIST2* A, 5′-GCAAGAAGTCGAGCGAAGA-3′; shRNA h*TWIST2* B, 5′-GCTGAGCAAGATCCAGACG-3′), and the murine *TWIST2* gene (shRNA m*TWIST2* A, 5′-GCAAGAAATCGAGCGAAGA-3′; shRNA m*TWIST2* B, 5′-GCTCAGCAAGATCCAGACG-3′) and control shRNAs directed against the *luciferase* GL3 gene (shRNA *LUC*, 5′-CTTACGCTGAGTACTTCGA-3′) and the prion pRpC protein (shRNA *PRPC*, 5′-TGAGCAGGCCCATCATACA-3′) were subcloned into the pRETRO-SUPER and the lentiviral pLVTHM expression vectors.

Cell Culture and Retroviral Infection

Primary MEFs (derived from C57BL/6 × DBA2 F1 mice), E1A-immortalized MEFs, transformed MEF cell lines, and tumor-derived cell lines were maintained in DMEM supplemented with 10% fetal bovine serum, 1% penicillin/streptomycin, 1 mM HEPES (GIBCO), and 0.1 mM nonessential amino acids. RPMI 7951, T47D, MDCK, MCF10A, and HMEC cell lines were grown as recommended by the American Type Culture Collection (ATCC).

Plt-E and Plt-A producer cells were used to generate retroviral stocks. 3 × 10^6 Plt-E (-A) cells were transfected by calcium phosphate precipitation with 10 μg of retroviral vector and then placed after 24 hr in 5 ml of fresh medium for viral production. Forty-eight hours after transfection, the supernatant was collected, filtered (0.45 μm, Millipore), and supplemented with 4 μg/ml of polybrene (Sigma). The viral stock was placed in contact with 1 × 10^6 MEFs (or 2.5 × 10^5 human cells) for 3 hr, and infected cells were selected after 24 hr with appropriate antibiotics. Cooperation assays were performed by sequential infections using Ras- or ErbB2-expressing constructs and Twist1, Twist2, or empty (pBabe) expression constructs, spaced by a 48 hr period of time. Foci formation and growth on agar were assessed as described in Petrenko et al. (2003). *TWIST1* and/or *TWIST2* depletion experiments were performed by a double 48 hr-spaced infection of cells with retroviral or lentiviral shRNA expression virus using Plt-E or 293T cells as packaging cell lines.

Real-Time qRT-PCR

SYBR green quantitative PCR (Figure 1, Figure 2, Figure 3, and Figure 6) was performed using *36B4* as an internal control gene. Trans-species primer pairs were 5′-GCAGGACGTGTCCAGCTC-3′ and 5′-CTGGCTCTTCCTCGCTGTT-3′ for *TWIST1*, 5′-GCAAGAAGTCGAGCGAAGAT-3′ and 5′-GCTCTGCAGCTCCTCGAA-3′ for *TWIST2*, 5′-GGCGGGGAATAAAACGGAGCGA-3′ and 5′-CCTCACGGGCACAAGTCTGGAA-3′ for *DEC1* (Collado et al., 2005), and 5′-GCTGATGGGCAAGAACACCA-3′ and 5′-CCGGATGTGAGGCAGCAGTT-3′ for *36B4*.

The TaqMan quantitative PCR method used to analyze *TWIST* expression in human primary tumors and tumor-derived cell lines is described in detail in the Supplemental Experimental Procedures.

Human Tumor Samples

Human tissue samples were obtained from the Centre de Ressources Biologiques (Centre Léon Bérard, French agreement number DC-2008-99) after approval by the Comité de Protection des Personnes Lyon Est and by the institutional review board and ethics committee of Centre Léon Bérard, with fully informed patient consent.

Reporter Assays

3 × 10^5 E1A-immortalized MEFs were cotransfected with 1.5 μg of reporter construct, 0.5 μg of expression vector, and 0.3 μg of internal pRL-TK-luc construct (Promega) using jetPEI transfectant (Q-Biogen). Twenty-four hours after transfection, luciferase activity was monitored using the Dual-Luciferase Reporter Assay System (Promega) and a luminometer (Luminoskan Ascent, Labsystem).

Mouse Xenografts

Animal maintenance and experiments were carried out in accordance with the animal care guidelines of the European Union and with French laws and were validated by the Comité Régional d'Ethique Animale CNRS Rhône-Alpes. Six-week-old female athymic Swiss nude mice (Charles River Laboratories) were subcutaneously grafted in the left flank with 1 × 10^5 Ras + Twist1 or Twist2 retrovirally infected MEFs. Tumor growth was monitored twice a week with calipers at the site of injection. Animals were allowed to form tumors up to 1.5 cm in diameter, at which point they were euthanized. Each tumor was dissected and either fixed in formaldehyde and processed for histopathologic examination or used for protein or RNA extraction.

Immunoblot Analysis

Cell lysates were prepared in RIPA buffer. Protein expression was examined by western blotting using rabbit anti-mouse p16^{Ink4a} M-156 and anti-human p16^{Ink4a} H-156 (Tebu-bio), anti-mouse p21^{Cip1} C-19 (Tebu-bio), anti-Ras C-20 (Tebu-bio), anti-mouse ARF Ab80 (Abcam), anti-human ARF Ab1 (Neo-Markers), anti-mouse p53 CM5 (Novocastra), and anti-Claudin-7 (Zymed) polyclonal antibodies and mouse anti-human p21^{Cip1} SX118 (Dako), anti-β-actin AC15 (Sigma), anti-FLAG M2 (Stratagene), anti-E-cadherin, anti-N-cadherin, anti-α-catenin, anti-ZO-1 (BD Biosciences), anti-vimentin V9 (Dako), and anti-occludin (Zymed) monoclonal antibodies for primary detection. Horseradish peroxidase-conjugated donkey anti-rabbit or sheep anti-mouse antibodies (Amersham) were used as secondary antibodies. Western blots were revealed using an ECL Detection Kit (Amersham).

Characterization of Senescent Cells

SA-β-Galactosidase Staining

Cells were fixed in 3% formaldehyde, washed three times with PBS, and incubated at 37°C for 12 hr in buffer containing 40 mM sodium phosphate (pH 6), 5 mM $K_4Fe(CN)_6$, 5 mM $K_3Fe(CN)_6$, 150 mM NaCl, 2 mM $MgCl_2$, and 1 mg/ml X-Gal.

Flow Cytometry Analysis

Trypsinized cells were washed in PBS, fixed in cold 70% ethanol/PBS for 30 min, washed, and incubated for 1 hr in 1 ml PBS containing 0.1 mg/ml RNase A and 20 mg/ml propidium iodide. Cell-cycle profiles were then

determined using a FACSCalibur flow cytometer (BD Biosciences), and data were analyzed using CellQuest software.

Immunofluorescence Analysis

Cells were seeded onto glass coverslips 24 hr prior to treatments. Cells were fixed with 4% formaldehyde for 10 min, permeabilized with 0.1% Triton X-100 for 20 min at room temperature, saturated for 30 min with 10% FCS in PBS, washed in PBS, incubated overnight at 4°C with monoclonal anti-E-cadherin (BD Biosciences) or anti-vimentin V9 (Dako) antibodies, and then incubated for 1 hr with FITC- or TRITC-conjugated rabbit anti-mouse antibodies (Dako). Cells were counterstained with 2 μg/ml Hoechst (33258, Sigma). Coverslips were then mounted with Fluoromount-G (Southern Biotech).

Immunohistochemistry

Routine formalin-fixed and paraffin-embedded excision biopsies of a series of melanocytic neoplasms (including 12 nevi and 10 melanomas) were analyzed. Immunohistochemistry was performed on 5 μm tissue sections. All specimens were immunostained with a non-biotin detection system (Bond Polymer Refine, Leica Microsystems), with diaminobenzidine development. Heat-induced antigen retrieval was performed using Tris-EDTA buffer (pH 9.0) in a water bath at 95°C for 30 min. Monoclonal anti-$p16^{Ink4a}$ (clone JC8, NeoMarkers) and anti-Twist1 (clone Twist2C1a, Biomatrix) antibodies were used. Stainings were performed with an automatic immunostainer (Bond System, Leica Microsystems).

Matrigel Invasion Assays

Matrigel (BD Biosciences) was added to the wells of an eight-well Labtek chamber in a volume of 300 μl/well. A Matrigel plug of about 1 mm diameter was removed. The hole was successively filed with 1×10^5 cells and 100 μl of Matrigel. Appropriate growth medium was added on top. Cultures were analyzed for up to 4 days. Areas of migration were visualized using an Olympus IX50 (NA 0.075). Samples were performed in duplicate.

ACCESSION NUMBERS

Microarray data have been entered into the NCBI Gene Expression Omnibus (http://www.ncbi.nlm.nih.gov/geo/) with the accession number GSE11756.

SUPPLEMENTAL DATA

The Supplemental Data include Supplemental Experimental Procedures, Supplemental References, six figures, and one table and can be found with this article online at http://www.cancercell.org/cgi/content/full/14/1/79/DC1/.

ACKNOWLEDGMENTS

The authors thank Isabelle Treilleux and Jean-Philippe Michot (Anatomy-Cytopathology Unit, Centre Léon Bérard); Joël Lachuer (ProfileExpert, Bron, France); and Gaël Grelier, Carole Audoynaud, Claire Ciancia, Fanny Courbis-Poncet, and Isabelle Durand for technical assistance. We also thank Eric Tabone (Centre de Ressources Biologiques, Centre Léon Bérard), Elisabeth Brambilla, and Jean Tanitakis for providing tumor samples; Gordon Peters and Takahiro Maeda for providing the luciferase reporter constructs; Patrizia Casalini for providing the *ErbB2* expression vector; R.A. Weinberg for providing the $H\text{-}Ras^{V12}$ retroviral expression construct; G.P. Dimri for providing the Bmi-1 retroviral expression construct; and Ben Ho Park for providing the MCF10A-derived cell lines. The authors extend special thanks to Patrick Mehlen and Raphaël Rousseau for scientific discussions.

This work was supported by grants from the Institut National du Cancer, the Association pour la Recherche contre le Cancer (ARC), the Ligue Nationale contre le Cancer, the Comités de l'Ain et du Rhône, and the Breast Cancer Research Foundation. R.M. is supported by the Italian Association for Cancer Research (AIRC).

Received: October 10, 2007
Revised: May 9, 2008
Accepted: June 11, 2008
Published: July 7, 2008

REFERENCES

Bartkova, J., Horejsi, Z., Koed, K., Kramer, A., Tort, F., Zieger, K., Guldberg, P., Sehested, M., Nesland, J.M., Lukas, C., et al. (2005). DNA damage response as a candidate anti-cancer barrier in early human tumorigenesis. Nature *434*, 864–870.

Bialek, P., Kern, B., Yang, X., Schrock, M., Sosic, D., Hong, N., Wu, H., Yu, K., Ornitz, D.M., Olson, E.N., et al. (2004). A twist code determines the onset of osteoblast differentiation. Dev. Cell *6*, 423–435.

Chen, Z., Trotman, L.C., Shaffer, D., Lin, H.K., Dotan, Z.A., Niki, M., Koutcher, J.A., Scher, H.I., Ludwig, T., Gerald, W., et al. (2005). Crucial role of p53-dependent cellular senescence in suppression of Pten-deficient tumorigenesis. Nature *436*, 725–730.

Chen, Z.F., and Behringer, R.R. (1995). twist is required in head mesenchyme for cranial neural tube morphogenesis. Genes Dev. *9*, 686–699.

Collado, M., Gil, J., Efeyan, A., Guerra, C., Schuhmacher, A.J., Barradas, M., Benguria, A., Zaballos, A., Flores, J.M., Barbacid, M., et al. (2005). Tumour biology: senescence in premalignant tumours. Nature *436*, 642.

Cowell, J.K., Laduca, J., Rossi, M.R., Burkhardt, T., Nowak, N.J., and Matsui, S. (2005). Molecular characterization of the t(3;9) associated with immortalization in the MCF10A cell line. Cancer Genet. Cytogenet. *163*, 23–29.

el-Deiry, W.S., Tokino, T., Velculescu, V.E., Levy, D.B., Parsons, R., Trent, J.M., Lin, D., Mercer, W.E., Kinzler, K.W., and Vogelstein, B. (1993). WAF1, a potential mediator of p53 tumor suppression. Cell *75*, 817–825.

Elias, M.C., Tozer, K.R., Silber, J.R., Mikheeva, S., Deng, M., Morrison, R.S., Manning, T.C., Silbergeld, D.L., Glackin, C.A., Reh, T.A., and Rostomily, R.C. (2005). TWIST is expressed in human gliomas and promotes invasion. Neoplasia *7*, 824–837.

Entz-Werle, N., Stoetzel, C., Berard-Marec, P., Kalifa, C., Brugiere, L., Pacquement, H., Schmitt, C., Tabone, M.D., Gentet, J.C., Quillet, R., et al. (2005). Frequent genomic abnormalities at TWIST in human pediatric osteosarcomas. Int. J. Cancer *117*, 349–355.

Gorgoulis, V.G., Vassiliou, L.V., Karakaidos, P., Zacharatos, P., Kotsinas, A., Liloglou, T., Venere, M., DiTullio, R.A., Jr., Kastrinakis, N.G., Levy, B., et al. (2005). Activation of the DNA damage checkpoint and genomic instability in human precancerous lesions. Nature *434*, 907–913.

Guy, C.T., Webster, M.A., Schaller, M., Parsons, T.J., Cardiff, R.D., and Muller, W.J. (1992). Expression of the neu protooncogene in the mammary epithelium of transgenic mice induces metastatic disease. Proc. Natl. Acad. Sci. USA *89*, 10578–10582.

Hara, E., Smith, R., Parry, D., Tahara, H., Stone, S., and Peters, G. (1996). Regulation of p16CDKN2 expression and its implications for cell immortalization and senescence. Mol. Cell. Biol. *16*, 859–867.

Hay, E.D. (1995). An overview of epithelio-mesenchymal transformation. Acta Anat. (Basel) *154*, 8–20.

Hoek, K., Rimm, D.L., Williams, K.R., Zhao, H., Ariyan, S., Lin, A., Kluger, H.M., Berger, A.J., Cheng, E., Trombetta, E.S., et al. (2004). Expression profiling reveals novel pathways in the transformation of melanocytes to melanomas. Cancer Res. *64*, 5270–5282.

Husemann, Y., Geigl, J.B., Schubert, F., Musiani, P., Meyer, M., Burghart, E., Forni, G., Eils, R., Fehm, T., Riethmuller, G., and Klein, C.A. (2008). Systemic spread is an early step in breast cancer. Cancer Cell *13*, 58–68.

Kang, Y., and Massague, J. (2004). Epithelial-mesenchymal transitions: twist in development and metastasis. Cell *118*, 277–279.

Konishi, H., Karakas, B., Abukhdeir, A.M., Lauring, J., Gustin, J.P., Garay, J.P., Konishi, Y., Gallmeier, E., Bachman, K.E., and Park, B.H. (2007). Knock-in of mutant K-ras in nontumorigenic human epithelial cells as a new model for studying K-ras mediated transformation. Cancer Res. *67*, 8460–8467.

Kwok, W.K., Ling, M.T., Lee, T.W., Lau, T.C., Zhou, C., Zhang, X., Chua, C.W., Chan, K.W., Chan, F.L., Glackin, C., et al. (2005). Up-regulation of TWIST in prostate cancer and its implication as a therapeutic target. Cancer Res. *65*, 5153–5162.

Li, L., Cserjesi, P., and Olson, E.N. (1995). Dermo-1: a novel twist-related bHLH protein expressed in the developing dermis. Dev. Biol. *172*, 280–292.

Linggi, B., Muller-Tidow, C., van de Locht, L., Hu, M., Nip, J., Serve, H., Berdel, W.E., van der Reijden, B., Quelle, D.E., Rowley, J.D., et al. (2002). The t(8;21) fusion protein, AML1 ETO, specifically represses the transcription of the p14(ARF) tumor suppressor in acute myeloid leukemia. Nat. Med. *8*, 743–750.

Maestro, R., Dei Tos, A.P., Hamamori, Y., Krasnokutsky, S., Sartorelli, V., Kedes, L., Doglioni, C., Beach, D.H., and Hannon, G.J. (1999). Twist is a potential oncogene that inhibits apoptosis. Genes Dev. *13*, 2207–2217.

Michaloglou, C., Vredeveld, L.C., Soengas, M.S., Denoyelle, C., Kuilman, T., van der Horst, C.M., Majoor, D.M., Shay, J.W., Mooi, W.J., and Peeper, D.S. (2005). BRAFE600-associated senescence-like cell cycle arrest of human naevi. Nature *436*, 720–724.

Mironchik, Y., Winnard, P.T., Jr., Vesuna, F., Kato, Y., Wildes, F., Pathak, A.P., Kominsky, S., Artemov, D., Bhujwalla, Z., Van, D.P., et al. (2005). Twist overexpression induces in vivo angiogenesis and correlates with chromosomal instability in breast cancer. Cancer Res. *65*, 10801–10809.

Oft, M., Peli, J., Rudaz, C., Schwarz, H., Beug, H., and Reichmann, E. (1996). TGF-beta1 and Ha-Ras collaborate in modulating the phenotypic plasticity and invasiveness of epithelial tumor cells. Genes Dev. *10*, 2462–2477.

Ohuchida, K., Mizumoto, K., Ohhashi, S., Yamaguchi, H., Konomi, H., Nagai, E., Yamaguchi, K., Tsuneyoshi, M., and Tanaka, M. (2007). Twist, a novel oncogene, is upregulated in pancreatic cancer: clinical implication of Twist expression in pancreatic juice. Int. J. Cancer *120*, 1634–1640.

Petrenko, O., Zaika, A., and Moll, U.M. (2003). deltaNp73 facilitates cell immortalization and cooperates with oncogenic Ras in cellular transformation in vivo. Mol. Cell. Biol. *23*, 5540–5555.

Qian, Y., Zhang, J., Yan, B., and Chen, X. (2008). DEC1, a basic helix-loop-helix transcription factor and a novel target gene of the p53 family, mediates p53-dependent premature senescence. J. Biol. Chem. *283*, 2896–2905.

Schardt, J.A., Meyer, M., Hartmann, C.H., Schubert, F., Schmidt-Kittler, O., Fuhrmann, C., Polzer, B., Petronio, M., Eils, R., and Klein, C.A. (2005). Genomic analysis of single cytokeratin-positive cells from bone marrow reveals early mutational events in breast cancer. Cancer Cell *8*, 227–239.

Scheel, C., Onder, T., Karnoub, A., and Weinberg, R.A. (2007). Adaptation versus selection: the origins of metastatic behavior. Cancer Res. *67*, 11476–11479.

Schmidt-Kittler, O., Ragg, T., Daskalakis, A., Granzow, M., Ahr, A., Blankenstein, T.J., Kaufmann, M., Diebold, J., Arnholdt, H., Muller, P., et al. (2003). From latent disseminated cells to overt metastasis: genetic analysis of systemic breast cancer progression. Proc. Natl. Acad. Sci. USA *100*, 7737–7742.

Serrano, M., Lee, H., Chin, L., Cordon-Cardo, C., Beach, D., and DePinho, R.A. (1996). Role of the INK4a locus in tumor suppression and cell mortality. Cell *85*, 27–37.

Serrano, M., Lin, A.W., McCurrach, M.E., Beach, D., and Lowe, S.W. (1997). Oncogenic ras provokes premature cell senescence associated with accumulation of p53 and p16INK4a. Cell *88*, 593–602.

Simpson, P. (1983). Maternal-zygotic gene interactions during formation of the dorsoventral pattern in Drosophila embryos. Genetics *105*, 615–632.

Sosic, D., Richardson, J.A., Yu, K., Ornitz, D.M., and Olson, E.N. (2003). Twist regulates cytokine gene expression through a negative feedback loop that represses NF-kappaB activity. Cell *112*, 169–180.

Thisse, B., el Messal, M., and Perrin-Schmitt, F. (1987). The twist gene: isolation of a Drosophila zygotic gene necessary for the establishment of dorsoventral pattern. Nucleic Acids Res. *15*, 3439–3453.

Trost, T.M., Lausch, E.U., Fees, S.A., Schmitt, S., Enklaar, T., Reutzel, D., Brixel, L.R., Schmidtke, P., Maringer, M., Schiffer, I.B., et al. (2005). Premature senescence is a primary fail-safe mechanism of ERBB2-driven tumorigenesis in breast carcinoma cells. Cancer Res. *65*, 840–849.

Valsesia-Wittmann, S., Magdeleine, M., Dupasquier, S., Garin, E., Jallas, A.C., Combaret, V., Krause, A., Leissner, P., and Puisieux, A. (2004). Oncogenic cooperation between H-Twist and N-Myc overrides failsafe programs in cancer cells. Cancer Cell *6*, 625–630.

Wolf, C., Thisse, C., Stoetzel, C., Thisse, B., Gerlinger, P., and Perrin-Schmitt, F. (1991). The M-twist gene of Mus is expressed in subsets of mesodermal cells and is closely related to the Xenopus X-twi and the Drosophila twist genes. Dev. Biol. *143*, 363–373.

Yang, J., Mani, S.A., Donaher, J.L., Ramaswamy, S., Itzykson, R.A., Come, C., Savagner, P., Gitelman, I., Richardson, A., and Weinberg, R.A. (2004). Twist, a master regulator of morphogenesis, plays an essential role in tumor metastasis. Cell *117*, 927–939.

Zhang, Z., Xie, D., Li, X., Wong, Y.C., Xin, D., Guan, X.Y., Chua, C.W., Leung, S.C., Na, Y., and Wang, X. (2007). Significance of TWIST expression and its association with E-cadherin in bladder cancer. Hum. Pathol. *38*, 598–606.

Cancer Cell, Volume *14*

Supplemental Data

Article

Induction of EMT by Twist Proteins as a Collateral Effect of Tumor-Promoting Inactivation of Premature Senescence

Stéphane Ansieau, Jeremy Bastid, Agnès Doreau, Anne-Pierre Morel, Benjamin P. Bouchet, Clémence Thomas, Frédérique Fauvet, Isabelle Puisieux, Claudio Doglioni, Sara Piccinin, Roberta Maestro, Thibault Voeltzel, Abdelkader Selmi, Sandrine Valsesia-Wittmann, Claude Caron de Fromentel, and Alain Puisieux

Supplemental Experimental Procedures

Constructs

The human Ets2 cDNA, generously provided by the laboratory of D. Stehelin (IBL, Lille, France), was subcloned into the pCI-neo expression vector.

Immunoprecipitation

$3x10^6$ 293T cells were transiently transfected with 5 μg FLAG-Twist and Ets2 expression constructs. 36h post-transfection, cells were harvested, lysed in a 250 mM NaCl, 50 mM Tris pH8, 1mM EDTA, 0.5% NP40 extraction buffer, sonicated and cleared by centrifugation. Lysates were incubated 2h at room temperature with 1 μg of the monoclonal anti-FLAG M2 antibody (Stratagene) or 1 μg of the rabbit polyclonal anti-Ets2 antibody C-20 (TEBU sc-351). Lysates were next incubated with protein A Sepharose (GE Healthcare). After extensive washes in binding buffer, beads were resuspended in Laemmli buffer, boiled and loaded on SDS-PAGE. Ectopically expressed and immunoprecipitated proteins (Co-IP) were examined by western blotting using the rabbit polyclonal anti-Ets2 C-20 and the mouse monoclonal anti-FLAG M2 antibodies.

TWIST Expression Analysis in Human Primary Tumors and Tumor-Derived Cell Lines (see Figure S1)

TaqMan quantitative PCR analysis was carried out on a LightCycler 2.0 System (Roche Applied Science). PCR mixtures contained LightCycler TaqMan mix, 200 nM primers and 1.67μl of template cDNA in a 6.67μl reaction volume. Housekeeping genes (*ACTB*, *ATP6AP1*, *CFL1*, *GAPDH*, *GUSB*, *HPRT1*, *PGK1*, *PPIB*, *TBP*, *TFRC*, *TUBA1C* and *UBB*), used for normalization of target mRNA expression in each sample type, were selected by systematic geNorm analysis as previously described (Vandesompele et al., 2002). Real-time PCR intron-spanning assays were designed using the ProbeFinder software (Roche Applied Science). Sequences of primers and probes are listed below:

Gene	NCBI RefSeq		Primer Sequence	Universal Probe Library
ACTB	NM_001101.2	Forward	ATTGGCAATGAGCGGTTC	#11
		Reverse	GGATGCCACAGGACTCCAT	
ATP6AP1	NM_001183.4	Forward	TGCAGCTCTCTACCTACTTAGATCC	#1
		Reverse	CTGTGAAATCCTCAATGCTCAG	
CFL1	NM_005507.2	Forward	GTGCCCTCTCCTTTTCGTTT	#5
		Reverse	TTGAACACCTTGATGACACCAT	
GAPDH	NM_002046.3	Forward	AGCCACATCGCTCAGACAC	#60
		Reverse	GCCCAATACGACCAAATCC	
GUSB	NM_000181.2	Forward	CGCCCTGCCTATCTGTATTC	#57
		Reverse	TCCCCACAGGGAGTGTGTAG	
HPRT1	NM_000194.1	Forward	TGACCTTGATTTATTTTGCATACC	#73
		Reverse	CGAGCAAGACGTTCAGTCCT	
PGK1	NM_000291.2	Forward	CTGTGGCTTCTGGCATACCT	#42
		Reverse	CTTGCTGCTTTCAGGACCA	
PPIB	NM_000942.4	Forward	ACTTCACCAGGGGAGATGG	#20
		Reverse	AGCCGTTGGTGTCTTTGC	
TUBA1C	NM_032704.2	Forward	CCCCTTCAAGTTCTAGTCATGC	#58
		Reverse	CATTGCCAATCTGGACACC	
UBB	NM_018955.2	Forward	AGGATCCTGGTATCCGCTAAC	#39
		Reverse	TCACATTTTCGATGGTGTCACT	
TWIST1	NM_000474.3	Forward	GGCTCAGCTACGCCTTCTC	#88
		Reverse	CCTTCTCTGGAAACAATGACATCT	
TWIST2	BC 033168	Forward	CATGTCCGCCTCCCACTA	#10
		Reverse	GCATCATTCAGAATCTCCTCCT	

TWIST expression in tumors was compared with normal tissues provided by the Biologic Resource Center of the Léon Bérard Center and/or commercial RNA (Clontech). An average between independent sources was used as a reference (indicated as Norm-Mean). *TWIST* expression in breast tumors and melanomas was normalized using human mammary epithelial cells (HMEC) and three independent sources of normal human melanocytes (MHN-mean) respectively as references.

Supplemental References

Vandesompele, J., De Preter, K., Pattyn, F., Poppe, B., Van Roy, N., De Paepe, A., Speleman, F., (2002). Accurate normalization of real-time quantitative RT-PCR data by geometric averaging of multiple internal control genes. Genome Biol. *18*, 3.

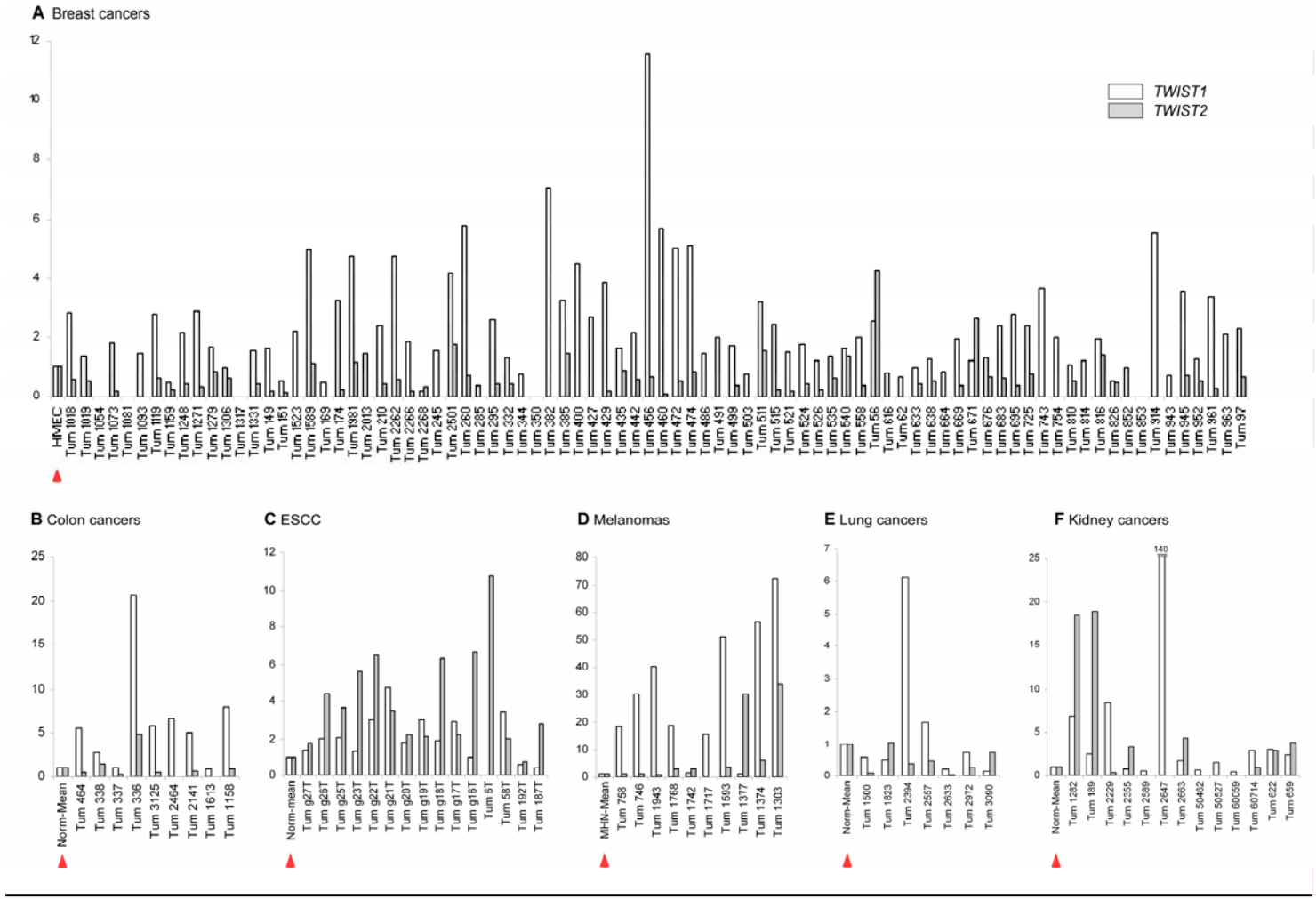

Figure S1. *TWIST1/2* Expression Levels in Human Tumors

*TWIST1*and *TWIST2* expression were assessed by qPCR and compared with that of healthy tissues or normal cell counterparts (indicated with an arrow). Relative amounts of *TWIST1* and *TWIST2* RNA expressed in breast cancers (A), colon cancers (B), esophageal squamous cell carcinomas (ESCC) (C), melanomas (D), lung cancers (E), and kidney cancers (F) are shown.

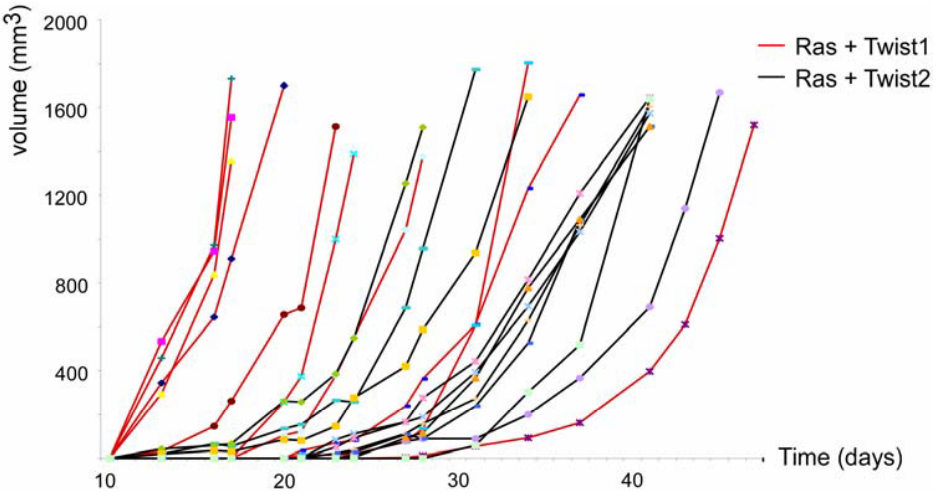

Figure S2. Xenograft Monitoring in *nude* Mice

1×10^5 cells were injected in irradiated six weeks old female *nude* mice and tumor size measured every three days.

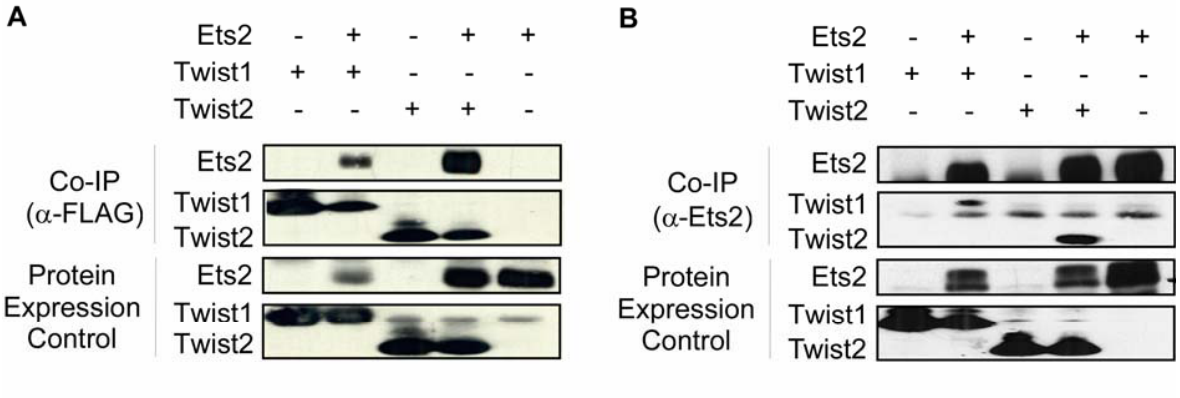

Figure S3. Twist and Ets2 Proteins Coimmunoprecipitate

293T cells were transiently transfected with FLAG-Twist and Ets2 expression constructs as indicated. Twist and Ets2 proteins were respectively immunoprecipitated using the anti-FLAG M2 (A) or the anti-Ets2 C20 antibody (B). Ectopically and immunoprecipitated (Co-IP) protein expression was examined by western blotting.

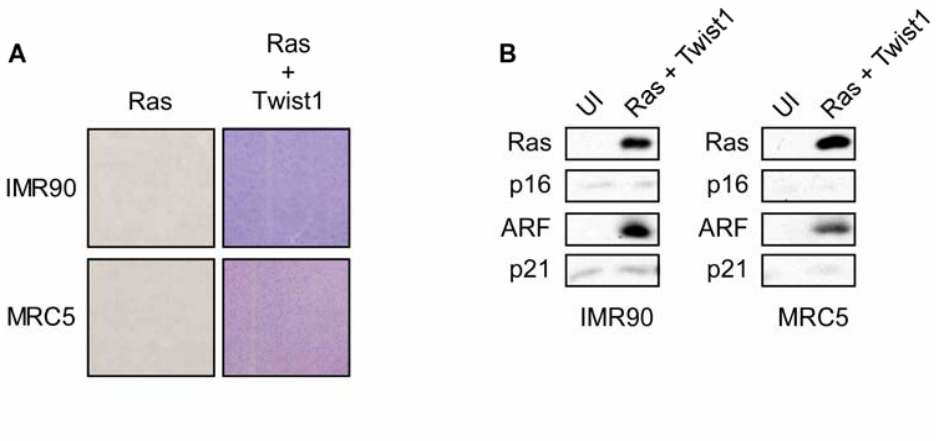

Figure S4. Twist1 Overrides Oncogene-Induced Senescence in Human Cells

(A) IMR90 and MRC5 human diploid fibroblasts were sequentially infected with H-Ras^{V12} and Twist1 retroviral expression constructs, as indicated. Cells were fixed and stained with crystal violet four weeks after infection.

(B) Expression analysis of Ras, p16^{Ink4a}, ARF, and p21^{Cip1} in IMR90 (left panel) or MRC5 (right panel) uninfected (UI) or infected with both H-Ras^{V12} and Twist1 retroviral constructs.

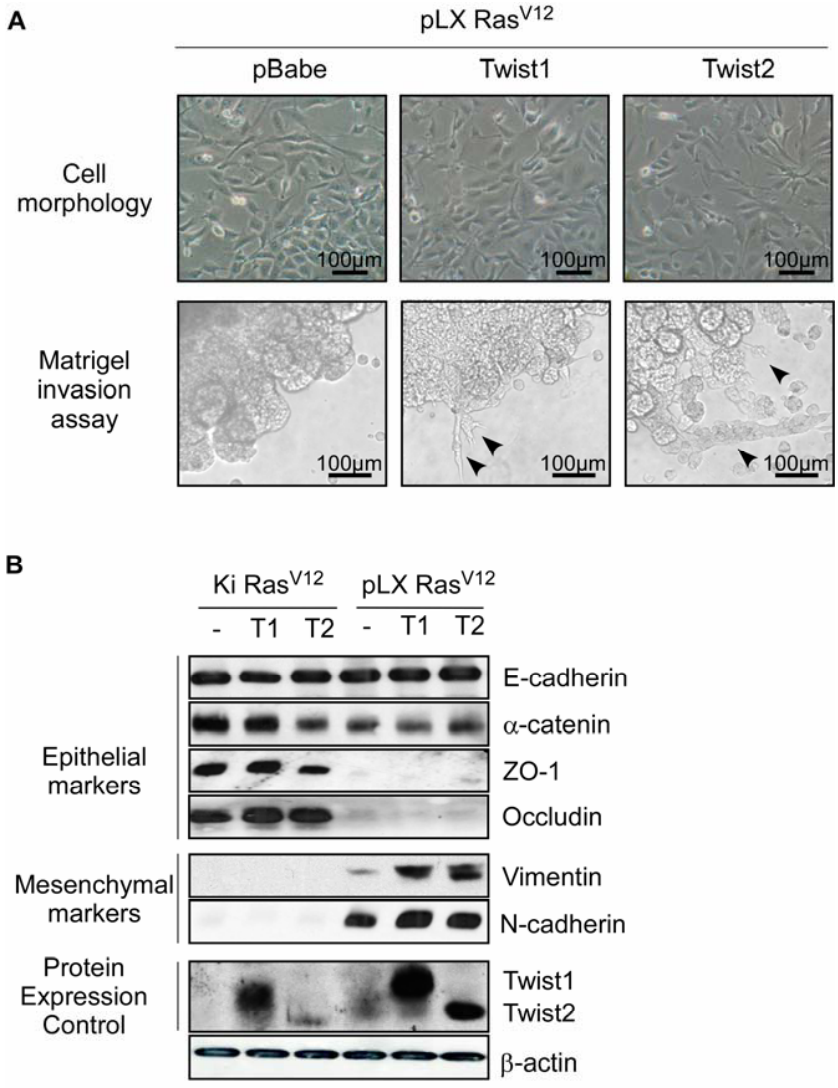

Figure S5. Twist1 or Twist2 and Ras Proteins Cooperate to Confer Invasive Capabilities to MCF10A Cells

(A) Human mammary epithelial cells MCF10A retrovirally infected with an activated version of K-Ras (pLX Ras^{V12}, Konishi et al., 2007) were sequentially infected with Twist1 or Twist2 retroviral expression constructs, or the empty pBabe vector as a control.

Upper panel: representative photomicrographs of cells obtained by phase-contrast microscopy. Lower panel: Matrigel invasion assay.

(B) Expression analysis of epithelial, mesenchymal markers and Twist proteins by western-blotting. Expression of the same markers was examined in MCF10A cells expressing a knocked-in activated version of K-Ras (Ki Ras^{V12}, Konishi et al., 2007) infected with Twist1 (T1) or Twist2 (T2) retroviral expression constructs or the empty pBabe vector (-) as a control, as indicated.

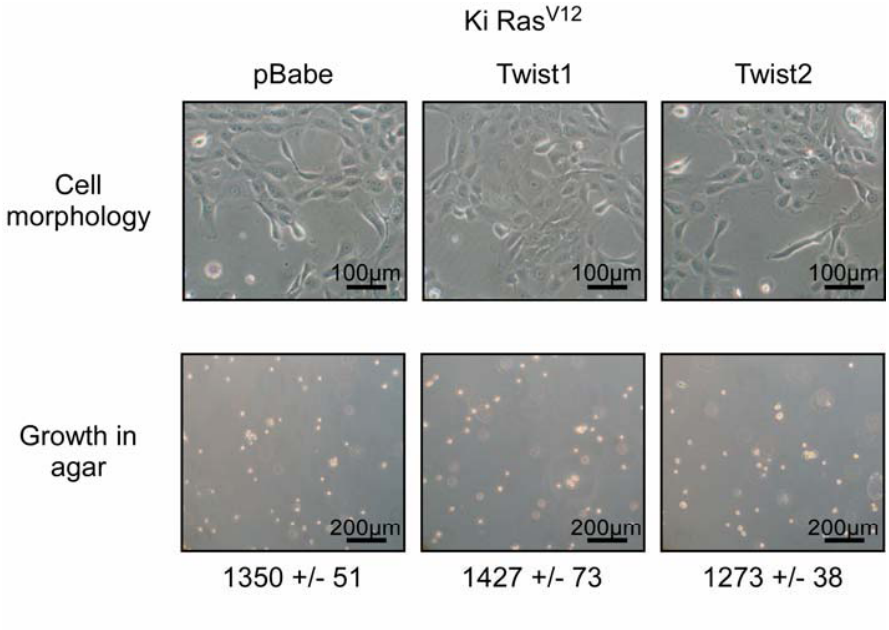

Figure S6. Twist1 and Twist2 Oncogenic Activities Rely upon the Inhibition of Premature Senescence

Targeted knock-in of a mutant K-Ras in immortalized MCF10A breast cells (Ki Ras^{V12}) does not trigger senescence, and confers limited features of transformation (Konishi et al., 2007). These cells were infected with Twist1 or Twist2 retroviral expression constructs, or the empty pBabe vector as a control.

Upper panel: representative photomicrographs of cells obtained by phase-contrast microscopy.

Lower panel: growth in soft agar. Colonies numbers (for 2×10^5 cells) +/- SD of triplicates are indicated.

Table S1. Gene Expression Analysis of Interleukins, Interleukin receptors, Chemokines, and Chemokine Receptors in MEF Cells and MEF Cells Sequentially Infected with Ras^{V12} and Twist Retroviral Expression Constructs

Gene expression profiles were performed by ProfileXpert (Lyon). Briefly, RNA were prepared using the RNeasy mini kit (Qiagen), amplified and biotine-labelled using the Message Amp kit version II (Ambion) and hybridized to Codelink DNA chips (CodeLink UniSet Mouse 20K I Bioarray, GE Healthcare). Hybridization, washes and revelation were performed using the Codelink Epression Assay Reagent kit (GE Healthcare).

Ras + T1: MEF cells sequentially infected with H-Ras^{V12} and Twist1 retroviral expression constructs; Ras + T2: MEF cells sequentially infected with H-Ras^{V12} and Twist2 retroviral expression constructs.

The SNAIL family member SCRATCH1 is not expressed in human tumors

JÉRÉMY BASTID[1-3*], BENJAMIN PIERRE BOUCHET[1-3*], CLAIRE CIANCIA[1-3], JULIE POURCHET[1,2], CAROLE AUDOYNAUD[2], GAËL GRELIER[1,2], ALAIN PUISIEUX[1-3] and STÉPHANE ANSIEAU[1,2]

[1]Inserm U590; [2]Centre Léon Bérard, Lyon; [3]Université de Lyon, Lyon 1, ISPB, F-69008, France

Received June 12, 2009; Accepted August 20, 2009

DOI: 10.3892/or_00000000

Abstract. The SNAIL and SLUG transcription factors play important roles in embryogenesis owing to their anti-apoptotic properties and their ability to promote morphogenetic changes by inducing epithelial-mesenchymal transitions (EMT). These characteristics provide many of the proteins in these families with oncogenic and pro-metastatic capabilities when reactivated in cancers. The SCRATCH subgroup of the SNAIL superfamily, including SCRATCH1 and SCRATCH2, display distinct embryonic functions and diverge early in evolution. Despite the described overexpression of *SCRT1* (encoding for SCRATCH1) in a small subset of human lung cancers, there is little data supporting a role of SCRATCH proteins in tumorigenesis. To further explore this possibility, we assessed *SNAI1* (SNAIL), *SNAI2* (SLUG) and *SCRT1* (SCRATCH1) expression in a wide panel of human and murine tumors encompassing 151 primary tumors and 6 different cancer types, including melanomas and multiple different carcinomas. Whereas *SNAI1* and *SNAI2* are widely expressed in human and murine tumors, our results reveal that *SCRT1* transcripts are undetectable in nearly all of the examined tumors suggesting that SCRATCH1 plays a minor role, if any, in tumorigenesis. Our data therefore suggest that oncogenic properties are not shared by all SNAIL superfamily members but instead are specifically allotted to the SNAIL subgroup supporting the conclusions that SNAIL and SCRATCH subgroups are functionally divergent and strengthening the hypothesis that the oncogenic potential of SNAIL and SLUG proteins relies on the hijacking of their embryonic functions.

Introduction

The epithelial-mesenchymal transition (EMT) is a trans-differentiation process that switches a polarized epithelial phenotype into a highly motile fibroblastoid or mesenchymal phenotype. Required for morphogenetic movements during the embryonic development, EMT is also suggested to play an important role in promoting cancer cell dissemination (1,2). Additionally, we and others have shown that EMT was associated with the acquisition of stem-like properties (3,4) and with the inhibition of inherent primary failsafe programs (5), suggesting a major role during primary tumor growth. In light of its emerging role in tumor progression, signaling pathways regulating EMT induction have been deeply investigated, highlighting a prevalent role of various developmental gene regulators including the SNAIL transcription factor superfamily (6,7).

SNAIL superfamily members share a highly conserved carboxy-terminal DNA binding domain encompassing four to six zinc fingers, as well as an N-terminal repression domain, known as the SNAG domain (6). Through these two structures, SNAIL proteins specifically bind to E-box responsive elements and by recruiting the corepressor CtBP inhibit their target genes (8,9). The SNAIL superfamily encompasses five members, organized into two evolutionary and functionally distinct subgroups, namely the SNAIL subgroup, encompassing the SNAIL (*SNAI1*), SLUG (*SNAI2*) and SMUC (*SNAI3*) proteins, and the SCRATCH subgroup, encompassing the two SCRATCH1 (*SCRT1*) and SCRATCH2 (*SCRT2*) proteins (10,11). SNAIL and SLUG, the two most studied members of the family, are essential for neural crest and mesoderm formation in mouse and chick embryos, respectively (10-13). Downstream the CSF/c-kit signaling pathway, SLUG was also found to be a determinant for spermatogenesis, melanocyte development and hematopoietic progenitor cell survival (7). Down-regulation of *SNAI2* expression is thus associated with various pigmentation disorders such as the Waardenburg syndrome and piebaldism, as well as human congenital anemia (14). Inversely, *SNAI2* overexpression has been described in a large spectrum of human cancers including leukemia, esophageal carcinomas and mesotheliomas (14), wherein the *SNAI2* encompassing region is frequently amplified (14). *SNAI2* is expressed in human breast tumors (14), but normal mammary epithelial cells also display high levels of *SNAI2* (15), therefore rendering the role of SLUG in breast tumorigenesis less clear. *SNAI1* is also overexpressed in a wide panel of cancers including breast, colon and gastric cancers, hepatocellular carcinomas, melanomas and synovial sarcomas within which

Correspondence to: Professor Alain Puisieux or Dr Stéphane Ansieau, Centre Léon Bérard, 28 rue Laennec, F-69008, France
E-mail: puisieux@lyon.fnclcc.fr
E-mail: ansieau@lyon.fnclcc.fr

*Contributed equally

Key words: SNAIL transcription factors, SCRATCH, tumorigenesis, epithelial-mesenchymal transition

Table I. Sequences of primers and probes.

	NCBI RefSeq	Primer sequence	Universal Probe (Taqman) Library
ACTB	NM_001101.2	Forward: attggcaatgagcggttc Reverse: ggatgccacaggactccat	#11
ATP6AP1	NM_001183.4	Forward: tgcagctctctacctacttagatcc Reverse: ctgtgaaatcctcaatgctcag	#1
CFL1	NM_005507.2	Forward: gtgccctctccttttcgttt Reverse: ttgaacaccttgatgacaccat	#5
GAPDH	NM_002046.3	Forward: agccacatcgctcagacac Reverse: gcccaatacgaccaaatcc	#60
GUSB	NM_000181.2	Forward: cgccctgcctatctgtattc Reverse: tccccacagggagtgtgtag	#57
HPRT1	NM_000194.1	Forward: tgaccttgatttattttgcatacc Reverse: cgagcaagacgttcagtcct	#73
PGK1	NM_000291.2	Forward: ctgtggcttctggcatacct Reverse: cttgctgctttcaggacca	#42
PPIB	NM_000942.4	Forward: acttcaccaggggagatgg Reverse: agccgttggtgtctttgc	#20
TUBA1C	NM_032704.2	Forward: ccccttcaagttctagtcatgc Reverse: cattgccaatctggacacc	#58
UBB	NM_018955.2	Forward: aggatcctggtatccgctaac Reverse: tcacattttcgatggtgtcact	#39
SNAI1	NM_005985	Forward: gctgcaggactctaatccaga Reverse: atctccggaggtgggatg	#11
SNAI2	NM_003068	Forward: tggttgcttcaaggacacat Reverse: gttgcagtgagggcaagaa	#7
SCRT1	NM_031309.4	Forward: tcaaacttgacgcgttctcttcgg Reverse: agtcgctgaggtacccttttatcgt	None

it is invariably associated with dedifferentiation and invasiness (16-23). Additionally, SNAIL was shown to be required for tumor growth and metastatic properties of human breast and mouse skin carcinoma cell lines (24,25) and associated with recurrence of breast tumors (26). Reactivation of each of *SNAI1* or *SNAI2* genes has been associated with the acquisition of invasive properties due to their ability to induce an EMT (7,27). Interestingly, SNAIL stabilization by TNF-α through NF-κB activity was recently shown as a primary mechanism by which tumor-associated macrophages (TAMs) might promote tumor cell motility (28). Their anti-apoptotic properties might also contribute to their oncogenic potential. Indeed, SNAIL expression in MDCK epithelial cells induces an EMT associated with resistance to serum-deprivation or TNF-α-induced apoptosis (27). SLUG was also shown in hematopoietic precursor cells to function downstream p53 as a critical switch that prevents their apoptosis by antagonizing the transactivation of *PUMA* gene (*BBC3*) by p53 (29).

Despite their sequence homology (around 60% identity with SLUG and SNAIL C-terminal zinc-fingers), SCRATCH proteins functionally diverge from SNAIL and SLUG. In *Drosophila*, *Scrt* is exclusively expressed in dividing neuronal precursors and persists in post-mitotic neurons (30). Similarly, in the mouse, *Scrt1* is only expressed in neural tissues and in the adult nervous system (31). Expression of *Scrt2* during mouse development is even more restricted to cells that appear to be migrating radially to the neocortex and the hippocampus and in the cortical subventricular zone that gives rise to glial cells. Its expression progressively decreases, to be virtually undetectable in the adult brain (32). In light of these divergences and knowing that the SCRATCH proteins constitute an evolutionary distinct subgroup of the SNAIL superfamily (10,11), we sought to investigate whether tumor promoting properties are shared by all SNAIL superfamily members or rather restricted to the SNAIL subgroup. The detection of *SCRT1* transcripts in a small subset of lung

carcinomas (31) and the anti-apoptotic properties of the *C. elegans* SCRATCH ortholog Ces-1 (33) argue in favor of a role of SCRATCH proteins in tumorigenesis. To further explore this hypothesis, we assessed the expression of genes from each subgroup, namely *SCRT1*, *SNAI1* and *SNAI2* in a wide panel of human and murine primary tumors. Our results first confirmed the reactivation of *SNAI1* and *SNAI2* in multiple human cancers. In contrast, with the exception of a handful of breast tumors, we failed to detect *SCRT1* transcripts in any of the carcinomas and melanomas examined therefore excluding a preponderant role in human cancers. Further analyses of murine mammary tumors from the MMTV-*ERBB2*/*Neu* mouse model strengthened the conclusion that SCRATCH1 is unlikely to play a role in tumorigenesis. Overall, these results suggest that oncogenic properties are specifically allotted to the SNAIL subgroup of the SNAIL superfamily.

Materials and methods

mRNA extraction and reverse transcription. Total mRNA was extracted using TriReagent® (Sigma) and Phase Lock Gel® (Eppendorf) according to the instructions of the manufacturer. mRNA (1 μg) was reverse transcribed using the First-strand cDNA Synthesis® (Amersham Bioscience/GE Healthcare).

Gene expression analysis in human primary tumors. Taqman quantitative PCR analysis was carried out on a LightCycler® 2.0 System (Roche Applied Science) at least in triplicates. Housekeeping genes (*ACTB*, *ATP6AP1*, *CFL1*, *GAPDH*, *GUSB*, *HPRT1*, *PGK1*, *PPIB*, *TBP*, *TFRC*, *TUBA1C* and *UBB*) were used for normalization of target mRNA expression in each sample type. They were selected by systematic geNorm analysis as previously described (34). Real-time specific intron-spanning PCR assays were designed using the ProbeFinder software (Roche Applied Science). Transcription was compared with normal tissues provided by the Biologic Resource Center of the Centre Léon Bérard and/or commercial RNA (Clontech). An average between independent sources was used as a reference (indicated as Norm-Mean) in lung, kidney, colon and ESCC tumors. In breast tumors and melanomas, expression was normalized using human mammary epithelial cells (indicated as Norm) and three independent sources of normal human melanocytes (Melanocyte-mean) respectively as references.

SCRT1 transcription was assessed by SYBR green quantitative PCR. Expression was compared with an average between independent sources in kidney and colon cancers. No *SCRT1* expression was detected in ESCC, lung tumors and melanomas as well as their normal counterparts. As no *SCRT1* transcript was expressed in normal mammary epithelial cells, relative expression of SCRT1 in breast tumors is displayed in arbitrary units.

Sequences of primers and probes are listed in Table I.

Gene expression analysis in MMTV-ErbB2/Neu transgenic mice-derived tumors. SYBR green quantitative PCR was performed using *Rplp0* (encoding for 36B4) as an internal control gene. Relative expression is displayed in arbitrary units. Sequences of specific murine primer pairs are listed in Table II.

Table II. Sequences of specific murine primer pairs.

	NCBI RefSeq	Primer sequence
RplpO	NM_007475	Forward: gctgatgggcaagaacacca Reverse: ccggatgtgaggcagcagtt
Snai1	NM_011427	Forward: caccctcatctgggactctc Reverse: gcttttgccactgtcctcat
Snai2	NM_011415	Forward: cagctccactccactctcct Reverse: tgaaccactgtgatccttgg
Scrt1	NM_130893	Forward: agacctcgacagctcctacg Reverse: ccccacgtagtcactgaggta

Results

In order to evaluate the role of the SNAIL family transcription factor SCRATCH1 in tumorigenesis, *SNAI1*, *SNAI2* and *SCRT1* expression was assessed by qRT-PCR in 132 human primary tumors encompassing 6 different cancer types and 19 murine primary mammary tumors. Accurate expression analysis was performed using the Taqman or SYBRgreen technology and a combination of 12 housekeeping genes selected by systematic geNorm analysis (34).

SNAI1 and SNAI2 are widely expressed in human primary tumors. Confirming previous work (35), *SNAI1* was found to be overexpressed (at least twice the expression of the corresponding normal tissue, dashed line) with high frequencies in breast tumors (overexpression: 97%, 0- to 72-fold, n=78; Fig. 1a) regardless of the subtype examined (*in situ* carcinoma, invasive ductal carcinomas or invasive lobular carcinomas), strengthening the hypothesis of its crucial role in breast tumorigenesis. *SNAI2* was not overexpressed in breast cancers compared to normal human mammary epithelial cells (overexpression: 0%, 0.1- to 1.8-fold, n=78; Fig. 1a). However, analysis of relative amount of *SNAI2* mRNA confirmed that both normal human mammary epithelial cells and breast tumors in fact display high *SNAI2* expression (Fig. 1a, inset graph) (15). In accordance with previous work, expression of *SNAI1* and *SNAI2* was increased in a significant proportion of esophageal squamous cell carcinomas (overexpression: 73%, 0.8- to 4.2-fold for *SNAI1*, and 80%, 0.9- to 5.4-fold for *SNAI2*, n=15, respectively; Fig. 2a) (36) and *SNAI1* was found to be overexpressed in melanomas (overexpression: 60%, 0- to 212-fold, n=10; Fig. 2c, left graph) (23,36). *SNAI2* transcripts are detectable at a similar high rate in both melanocytes and melanomas (Fig. 2c, right graph), wherein it was suggested to genetically program melanomas to metastasize (37). We additionally confirmed *SNAI1* and revealed the previously undescribed *SNAI2* overexpression in colon (overexpression: 44%, 0.5- to 8.2-fold for *SNAI1*, and 33%, 0.4- to 28.9-fold for *SNAI2*, n=9; Fig. 2d) and kidney cancers

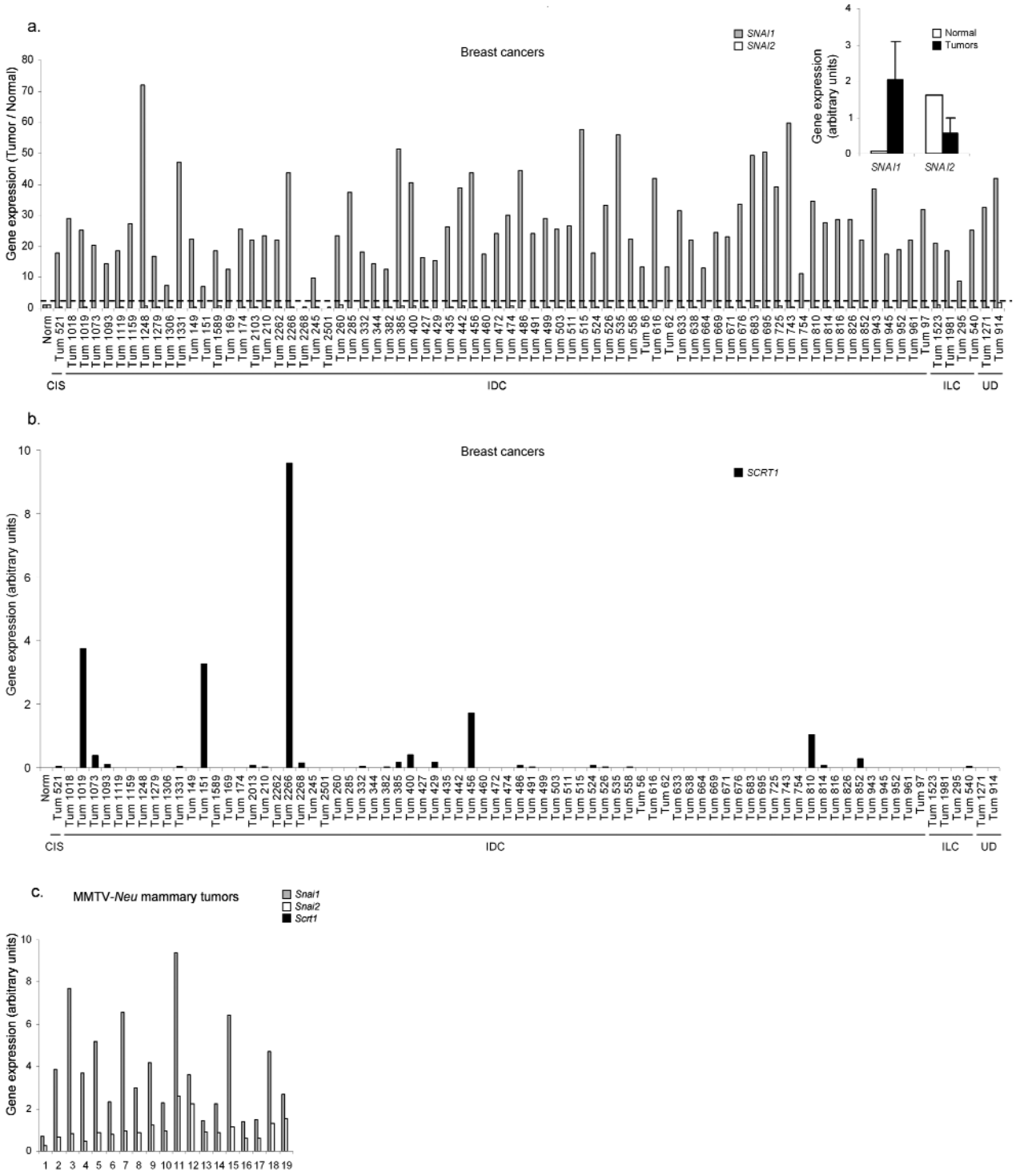

Figure 1. Expression analysis of SNAIL family genes in human and murine breast tumors. (a) *SNAI1* and *SNAI2* transcription was assessed by qRT-PCR in human breast tumors and normalized using normal human mammary epithelial cells. Relative amounts of transcripts are shown. CIS, carcinoma *in situ*; IDC, invasive ductal carcinomas; ILC, invasive lobular carcinomas; UD, undefined. Inset graph displays relative amounts of *SNAI1* and *SNAI2* mRNA to the normalizer genes in human mammary epithelial cells (Normal) and breast tumors (Tumors). (b) *SCRT1* transcription was assessed by qRT-PCR in human breast tumors and human mammary epithelial cells. Relative amounts of *SCRT1* mRNA to the normalizer genes are shown. CIS, carcinoma *in situ*; IDC, invasive ductal carcinomas; ILC, invasive lobular carcinomas; UD, undefined. Of note, as *SCRT1* could not be detected in normal epithelial cells, expression is thus displayed in arbitrary units. (c) Murine *Snai1*, *Snai2* and *Scrt1* transcription was assessed by qRT-PCR in MMTV-*ERBB2*/*Neu* transgenic mice-derived mammary tumors. Relative amounts of mRNA to the normalizer gene are shown.

(overexpression: 62%, 0.3- to 19.9-fold for *SNAI1*, and 38%, 0.1- to 41.6-fold, for *SNAI2*, n=13; Fig. 2e). Finally, both genes were found transcriptionally inactive in lung tumors (Fig. 2b).

SCRT1 is not expressed in human carcinomas and melanomas. *SCRT1* mRNA was undetectable in ESCC, lung carcinomas, melanomas as well as in the corresponding normal tissues of origin (Fig. 2a-c) and was barely detectable in colon and

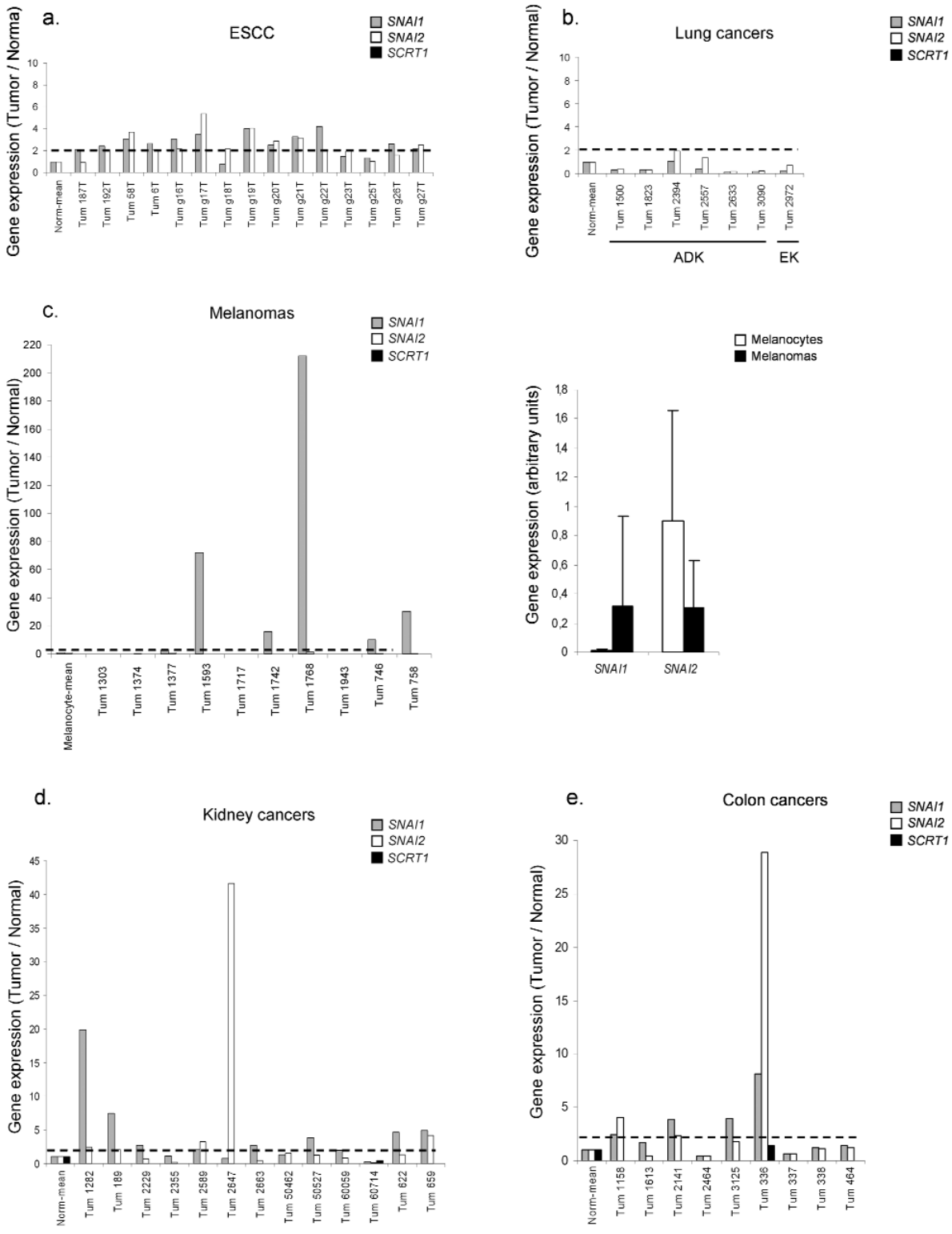

Figure 2. Expression analysis of Snail family genes in human tumors. (a-f) *SNAI1*, *SNAI2* and *SCRT1* transcription in (a) esophageal squamous cell carcinoma (ESCC), (b) lung cancers; ADK, adenocarcinomas; EK, epidermoid carcinomas, (c) melanomas, (d) kidney cancers and (e) colon cancers was assessed by qRT-PCR and normalized with that of healthy tissues or normal cell counterparts (Norm). Of note, *SCRT1* could not be amplified in normal esophageal squamous epithelium, normal lung and melanocytes and the corresponding tumors. Inset graph in (c) (right) displays relative amounts of *SNAI1* and *SNAI2* mRNA to the normalizer genes in melanocytes and melanomas.

kidney cancer specimens (Fig. 2d and e). In breast cancers, *SCRT1* mRNA was mainly undetectable although *SCRT1* mRNA could be amplified in 5 out of 78 tumor samples (Fig. 1b). Because of the limited and overall low expression of *SCRT1* in human breast tumors, we therefore speculated that SCRATCH1 must have a minor role, if any, in breast carcinogenesis. To substantiate our conclusion, we next assessed *Snai1*, *Snai2* and *Scrt1* expression in 19 freshly

isolated murine mammary tumors derived from an MMTV-*ERBB2/Neu* mouse transgenic model (expressing the *ERBB2/Neu* proto-oncogene under the control of the MMTV promoter) (38). In accordance with our results in human breast tumors, *Snai1* and *Snai2* transcripts were found to be expressed in MMTV-*ERBB2/Neu* mouse derived tumors (Fig. 1c). However, no expression of *Scrt1* could be detected in these tumors, again supporting the idea that SCRATCH1 does not play a role in breast carcinogenesis.

Discussion

The SNAIL and SLUG transcription factors are believed to promote cancer progression through their ability to promote EMT and to protect cells from apoptosis, properties reminiscent to their embryonic functions (6). Despite their evolutionary and functional divergence (10,11), several observations supported the hypothesis that oncogenic potential could also be allotted to the SCRATCH subgroup of the family. Indeed, *SCRT1* transcripts were detected in a small subset of lung carcinomas (31). Additionally, *C. elegans* SCRATCH ortholog Ces-1, likewise SNAIL and SLUG, was shown to display anti-apoptotic properties (33). To further explore this hypothesis, we investigated the expression of the Snail family related gene *SCRT1*, *SNAI1* and *SNAI2* in a wide panel of human tumors as well as in murine mammary tumors. Our results clearly established that, whereas *SNAI1* and *SNAI2* are widely overexpressed in many human cancers, *SCRT1* transcripts remained undetectable in most human cancers examined. Of note, we failed to detect *SCRT1* transcription in a set of lung adenocarcinomas and epidermoid carcinomas (Fig. 2a), strengthening the exclusivity of its previously described expression in small cell lung carcinomas with neuroendocrine (NE) features (31). As *SCRT1* is implicated in the maintenance of NE features, one can however assume that its expression in small cell lung carcinomas with NE features reflects the NE phenotype of these cells rather than a role in lung carcinogenesis.

It is noteworthy that *SCRT1* expression was detectable in a small subset of breast human cancers (5 out of 78; Fig. 1b) and in a limited number of human breast tumor cell lines (2 out of 15; data not shown). These data suggest that SCRATCH1 is unlikely to play a role in breast tumorigenesis. The rare expression observed in some breast tumors could rather reflect the presence of NE cells where SCRATCH1 is known to be functional (31); a hypothesis requiring further confirmation. However, using the Oncomine multiple array comparison software (www.oncomine.org), we found that *SCRT1* mRNA is not enriched in tumors with NE features and does not take part of the neuroendocrine signature.

The lack of detectable *SCRT1* expression in the large panel of human tumors examined is likely to exclude a role of SCRATCH1 in carcinogenesis and melanomagenesis. As phylogenetic and embryonic expression analysis demonstrated that SCRATCH (SCRATCH1 and SCRATCH2) and SNAIL (SNAIL, SLUG and SMUC) proteins constitute evolutionary and functionally distinct subgroups (10), one could presume that only the hijacking of SNAIL subgroup functions may provide cancer cells with a selective advantage. However, as a neuronal specific network might be essential for reactivating *SCRT1* expression, a specific role in promoting neuronal-derived tumorigenesis could not be excluded. Further investigations, including domain-swap chimera experiments, are warranted to definitively clarify the point.

Acknowledgements

The authors thank George Hinkal for his help in manuscript preparation and scientific discussions. We also thank Eric Tabone (Centre de Ressources Biologiques, Centre Léon Bérard, Lyon, France) and Elisabeth Brambilla for providing tumor samples. This study was supported by the Ligue Contre le Cancer (Comité du Rhône et Comité de l'Ain). BPB is a recipient of a scholarship from the Fondation pour la Recherche Médicale (FRM).

References

1. Lee JM, Dedhar S, Kalluri R and Thompson EW: The epithelial-mesenchymal transition: new insights in signaling, development, and disease. J Cell Biol 172: 973-981, 2006.
2. Thiery JP: Epithelial-mesenchymal transitions in tumour progression. Nat Rev Cancer 2: 442-454, 2002.
3. Mani SA, Guo W, Liao MJ, *et al*: The epithelial-mesenchymal transition generates cells with properties of stem cells. Cell 133: 704-715, 2008.
4. Morel AP, Lievre M, Thomas C, Hinkal G, Ansieau S and Puisieux A: Generation of breast cancer stem cells through epithelial-mesenchymal transition. PLoS one 3: e2888, 2008.
5. Ansieau S, Bastid J, Doreau A, *et al*: Induction of EMT by twist proteins as a collateral effect of tumor-promoting inactivation of premature senescence. Cancer Cell 14: 79-89, 2008.
6. Nieto MA: The snail superfamily of zinc-finger transcription factors. Nat Rev Mol Cell Biol 3: 155-166, 2002.
7. Peinado H, Olmeda D and Cano A: Snail, Zeb and bHLH factors in tumour progression: an alliance against the epithelial phenotype? Nat Rev Cancer 7: 415-428, 2007.
8. Grimes HL, Chan TO, Zweidler-McKay PA, Tong B and Tsichlis PN: The Gfi-1 proto-oncoprotein contains a novel transcriptional repressor domain, SNAG, and inhibits G1 arrest induced by interleukin-2 withdrawal. Mol Cell Biol 16: 6263-6272, 1996.
9. Nibu Y, Zhang H, Bajor E, Barolo S, Small S and Levine M: dCtBP mediates transcriptional repression by Knirps, Kruppel and Snail in the *Drosophila* embryo. EMBO J 17: 7009-7020, 1998.
10. Barrallo-Gimeno A and Nieto MA: Evolutionary history of the Snail/Scratch superfamily. Trends Genet (In press).
11. Barrallo-Gimeno A and Nieto MA: The Snail genes as inducers of cell movement and survival: implications in development and cancer. Development 132: 3151-3161, 2005.
12. Nieto MA, Sargent MG, Wilkinson DG and Cooke J: Control of cell behavior during vertebrate development by Slug, a zinc finger gene. Science 264: 835-839, 1994.
13. Carver EA, Jiang R, Lan Y, Oram KF and Gridley T: The mouse snail gene encodes a key regulator of the epithelial-mesenchymal transition. Mol Cell Biol 21: 8184-8188, 2001.
14. Cobaleda C, Perez-Caro M, Vicente-Duenas C and Sanchez-Garcia I: Function of the zinc-finger transcription factor SNAI2 in cancer and development. Annu Rev Genet 41: 41-61, 2007.
15. Come C, Arnoux V, Bibeau F and Savagner P: Roles of the transcription factors snail and slug during mammary morphogenesis and breast carcinoma progression. J Mammary Gland Biol Neoplasia 9: 183-193, 2004.
16. Blanco MJ, Moreno-Bueno G, Sarrio D, Locascio A, Cano A, Palacios J and Nieto MA: Correlation of Snail expression with histological grade and lymph node status in breast carcinomas. Oncogene 21: 3241-3246, 2002.
17. Elloul S, Elstrand MB, Nesland JM, *et al*: Snail, Slug, and Smad-interacting protein 1 as novel parameters of disease aggressiveness in metastatic ovarian and breast carcinoma. Cancer 103: 1631-1643, 2005.
18. Rosivatz E, Becker I, Specht K, *et al*: Differential expression of the epithelial-mesenchymal transition regulators snail, SIP1, and twist in gastric cancer. Am J Pathol 161: 1881-1891, 2002.

19. Sugimachi K, Tanaka S, Kameyama T, *et al*: Transcriptional repressor snail and progression of human hepatocellular carcinoma. Clin Cancer Res 9: 2657-2664, 2003.
20. Miyoshi A, Kitajima Y, Kido S, Shimonishi T, Matsuyama S, Kitahara K and Miyazaki K: Snail accelerates cancer invasion by upregulating MMP expression and is associated with poor prognosis of hepatocellular carcinoma. Br J Cancer 92: 252-258, 2005.
21. Palmer HG, Larriba MJ, Garcia JM, *et al*: The transcription factor SNAIL represses vitamin D receptor expression and responsiveness in human colon cancer. Nat Med 10: 917-919, 2004.
22. Saito T, Oda Y, Kawaguchi K, *et al*: E-cadherin mutation and Snail overexpression as alternative mechanisms of E-cadherin inactivation in synovial sarcoma. Oncogene 23: 8629-8638, 2004.
23. Poser I, Dominguez D, De Herreros AG, Varnai A, Buettner R and Bosserhoff AK: Loss of E-cadherin expression in melanoma cells involves up-regulation of the transcriptional repressor Snail. J Biol Chem 276: 24661-24666, 2001.
24. Olmeda D, Montes A, Moreno-Bueno G, Flores JM, Portillo F and Cano A: Snai1 and Snai2 collaborate on tumor growth and metastasis properties of mouse skin carcinoma cell lines. Oncogene 27: 4690-4701, 2008.
25. Olmeda D, Moreno-Bueno G, Flores JM, Fabra A, Portillo F and Cano A: SNAI1 is required for tumor growth and lymph node metastasis of human breast carcinoma MDA-MB-231 cells. Cancer Res 67: 11721-11731, 2007.
26. Moody SE, Perez D, Pan TC, *et al*: The transcriptional repressor Snail promotes mammary tumor recurrence. Cancer Cell 8: 197-209, 2005.
27. Vega S, Morales AV, Ocana OH, Valdes F, Fabregat I and Nieto MA: Snail blocks the cell cycle and confers resistance to cell death. Genes Dev 18: 1131-1143, 2004.
28. Wu Y, Deng J, Rychahou PG, Qiu S, Evers BM and Zhou BP: Stabilization of snail by NF-kappaB is required for inflammation-induced cell migration and invasion. Cancer Cell 15: 416-428, 2009.
29. Wu WS, Heinrichs S, Xu D, Garrison SP, Zambetti GP, Adams JM and Look AT: Slug antagonizes p53-mediated apoptosis of hematopoietic progenitors by repressing puma. Cell 123: 641-653, 2005.
30. Roark M, Sturtevant MA, Emery J, Vaessin H, Grell E and Bier E: scratch, a pan-neural gene encoding a zinc finger protein related to snail, promotes neuronal development. Genes Dev 9: 2384-2398, 1995.
31. Nakakura EK, Watkins DN, Schuebel KE, Sriuranpong V, Borges MW, Nelkin BD and Ball DW: Mammalian scratch: a neural-specific Snail family transcriptional repressor. Proc Natl Acad Sci USA 98: 4010-4015, 2001.
32. Marin F and Nieto MA: The expression of Scratch genes in the developing and adult brain. Dev Dyn 235: 2586-2591, 2006.
33. Metzstein MM and Horvitz HR: The C. elegans cell death specification gene ces-1 encodes a snail family zinc finger protein. Mol Cell 4: 309-319, 1999.
34. Vandesompele J, De Preter K, Pattyn F, Poppe B, van Roy N, De Paepe A and Speleman F: Accurate normalization of real-time quantitative RT-PCR data by geometric averaging of multiple internal control genes. Genome Biol 18: 3, 2002
35. Come C, Magnino F, Bibeau F, De Santa BP, Becker KF, Theillet C and Savagner P: Snail and slug play distinct roles during breast carcinoma progression. Clin Cancer Res 12: 5395-5402, 2006.
36. Uchikado Y, Natsugoe S, Okumura H, Setoyama T, Matsumoto M, Ishigami S and Aikou T: Slug expression in the E-cadherin preserved tumors is related to prognosis in patients with esophageal squamous cell carcinoma. Clin Cancer Res 11: 1174-1180, 2005.
37. Gupta PB, Kuperwasser C, Brunet JP, *et al*: The melanocyte differentiation program predisposes to metastasis after neoplastic transformation. Nat Genet 37: 1047-1054, 2005.
38. Guy CT, Webster MA, Schaller M, Parsons TJ, Cardiff RD and Muller WJ: Expression of the neu protooncogene in the mammary epithelium of transgenic mice induces metastatic disease. Proc Natl Acad Sci USA 89: 10578-10582, 1992.